Development of Elderly Posture Male and Female Finite Element Neck Models and Assessment of Tissue-Level Response Under Impact Loading

by

Miguel Angel Corrales Fabre

A thesis
presented to the University of Waterloo
in fulfillment of the
thesis requirement for the degree of
Master of Applied Science
in
Mechanical Engineering

Waterloo, Ontario, Canada, 2020

©Miguel Angel Corrales Fabre 2020

Author's Declaration

I hereby declare that I am the sole author of this thesis. This is a true copy of the thesis, including any required final revisions, as accepted by my examiners.

I understand that my thesis may be made electronically available to the public.

Abstract

The growing elderly population and their increased incidence of injury calls for strategies to protect this at-risk population. The effects of ageing include a change in posture, biological material properties, and bone morphology relative to a younger population. These changes may contribute to the increased rates and severities of injuries observed in the elderly population in car crash scenarios but requires further investigation. Finite element human body models (HBMs) have been used as a design tool in automotive, sports, and defence applications to understand the biomechanical response of humans and to test and develop protective technologies. HBMs enable the investigation of changes that may occur with ageing and to assess the resulting response at the tissue level to aid in an improved understanding of injury risk.

Specific to the neck, the lordosis of the cervical spine increases with age. It has been proposed that the overall neck posture influences the response of the soft tissue under impact loading. Given that the neck region serves as the connection between the head and the thorax, the kinematic response might change with a change in the neck posture, and therefore, the likelihood of injury may change with increased cervical lordosis associated with age. Importantly, the effect of age has not been extensively studied using HBMs in the neck region.

In this study, male and female aged neck models were developed from existing young neck models. The aged neck models included the average increase in lordosis of the cervical spine and an increase in the facet joint angles associated with ageing. Available literature was used to define a posture for each model to represent an average 75-year-old 5^{th} percentile female and 50^{th} percentile male, and a new methodology to reposture the models was developed. In addition, the cervical capsular joint cartilage geometry was improved based on the literature. The young head and neck models were accurately repostured to represent average 75 YO subjects. Importantly, with the reposturing methodology developed in this study, the aged neck models demonstrated comparable mesh quality to the young models.

The young and aged neck models were simulated in frontal (2g to 15g), lateral (4g to 7g), and rear (7g) impact scenarios and assessed using head kinematics, the capsular ligament (CL) distraction expressed as a nominal strain, and the changes in the intervertebral disc (IVD) space expressed as a nominal strain. The kinematic responses were compared between young and aged models and between male and female models. In this study, it was found that the model head kinematics were not sensitive to the morphological changes in the neck. However, a sensitivity to the age-related lordosis changes was identified at the tissue level within the models. Importantly, in the rear impact, the female models predicted higher CL strains than those

of the male model, and the predicted strains in the aged female neck model were higher than those in the young female model, in agreement with findings in the literature. In contrast, the aged female model generally predicted less IVD space strain and less CL strain relative to the young female model in the frontal and lateral impacts. In general, the aged male neck model predicted higher IVD space strain, and higher or similar CL strain compared to the young model. The variation in predicted results with age were attributed, in part, to the subject-specific nature of the models. In particular, the subject-specific male neck was longer than that of the average population. In the present study, it was shown that global metrics, such as head kinematics, may not be sensitive to changes in posture, whereas specific soft tissue responses could be more informative in terms of detecting changes in response and may be more relevant to the prediction of injury risk. It is recommended that future research incorporate the effects of ageing on the material properties within the neck models. The developed aged models provide a basis for assessing the effect of aged posture on response and may inform safety system design and optimization for the elderly population in the future.

Acknowledgements

I am most grateful to my mentor and thesis supervisor, Prof. Duane Cronin, for giving me the chance to pursue my degree in his research group doing really cool stuff I never imagined I would be doing. For being always approachable, understanding, remarkably committed and a great role model. Thanks for the freedom, guidance, patience, and long hours of dedication to my research and personal well being. Thanks for all the travel and publication opportunities in several conferences and journals.

Special thanks to Skye Malcom, Chin-Hsu, Maika Katagiri, John Combest, and Daniel Kim for listening to me at least every month and for their valuable feedback and advice. To Honda R&D Americas, FCA Canada and GM Canada for their financial support and extensive technical feedback throughout my thesis program. I am also pleased to thank the Global Human Body Models Consortium (GHBMC) for the leadership, technical advice, access to the FE models, and financial support.

Thanks to the University of Waterloo, Canada, the Natural Sciences and Engineering Research Council, Canada (NSERC), the Consejo Nacional de Ciencia y Tecnologia, Mexico (CONACyT), and the Fundacion Mexicana para la Educacion, la Tecnologia y la Ciencia, Mexico (FUNED) for the financial support.

To my fellow students at the Impact Mechanics and Material Characterization Group, thanks for making the workspace an interesting place to be. Special thanks to Donata Gierczycka and Jeff Barker for their technical support and companionship in the research trips. Special thanks to my roommates for the unmentionable. Thanks to my friends who have helped me, and continue to do so, to exacerbate my curiosity and enjoy my life in amazing ways.

Finally, thanks to my family for the unconditional support throughout my life. To my grandmother and uncle for being role models and encourage me with their example to push my goals further.

Table of Contents

List of Abbreviations

GHBMC: Global Human Body Model Consortium

WAD: Whiplash associated disorders

FE: Finite element

HBM: Human Body Model

NM: Neck model

YO: Years old

M50: GHBMC 50th percentile male finite element detailed neck model version 5.0

F05: GHBMC 5th percentile female finite element detailed neck model version 5.0

$M50_{26YO}$: M50 model with the capsular joint cartilage geometry updated

$F05_{26YO}$: F05 model with the capsular joint cartilage geometry updated

$M50_{75YO}$: Based on the $M50_{26YO}$. Neck model that represents a 75-years-old 50th percentile male subject

$F05_{75YO}$: Based on the $F5_{26YO}$. Neck model that represents a 75-years-old 5th percentile female subject

CL: Capsular ligament

IVD: Intervertebral disc

UCS: Upper cervical spine

LCS: Lower cervical spine

BD: Vertebral body depth

AF: Annulus fibrosus

NP: Nucleus pulposus

CCJ: Cervical capsular joints

ANSUR: Anthropometric Survey of US Army Personnel

NHANES: National Health and Nutrition Examination Survey

JARDA: Japanese anthropometric reference data

BMI: Body mass index

SD: Standard deviation

CSP: Cervical Spine Posture predictor model

FBP: Full Body Posture predictor model

CT: Computed tomography

CII: Crash induced injuries

CSP_M: Cervical Spine Posture predictor model with the anthropometrics of the $M50_{26YO}$ model

CSP_{M26YO}: CSP_M with the adjusted eight to match the $M50_{26YO}$ middle arch cord length

CSP_{F26YO}: Cervical Spine Posture predictor model with the anthropometrics of the $F05_{26YO}$ model

FBP_{M26YO}: Full Body Posture predictor model with the anthropometrics of the $M50_{26YO}$ with the eight adjusted

FBP_{F26YO}: Full Body Posture predictor model with the anthropometrics of the $F05_{26YO}$

PMHS: Postmortem human subjects

List of Figures

List of Tables

Chapter 1: Introduction

1.1 Motivation

It has been found that the elderly have an increased incidence of injury and mortality (Heinrich et al., 2017; Kahane J, 2013), and an increased incidence of hard tissue fracture in the lower cervical spine (Lomoschitz et al., 2002) in traffic accidents. The potential causes include exposure to different loading conditions in a car crash, changes in the neck tissue material properties (Trajkovski et al., 2014), postural changes (Park et al., 2016a) and morphological changes such as bone remodelling (Hadjidakis and Androulakis, 2006; Parenteau et al., 2014). Specifically, with increasing age, the cervical spine undergoes an increase in lordosis (Klinich et al., 2004) as a consequence of an increased kyphosis of the thoracic spine (Boyle et al., 2002; Fon et al., 1980) and the necessity to maintain head angle during common tasks. In addition, with increasing age, the cervical spine undergoes a number of morphological changes (Parenteau et al., 2014), and the effect of those changes on the kinematic response has not been investigated in the context of the age-related changes. Notably, the inter-subject variability in the bone morphology increases with increasing age (Parenteau et al., 2014; Klinich et al., 2004). Understanding the musculoskeletal kinematics that differs between the elderly and the young population during an injurious event is of importance to prevent specific motions that can lead to injury in the aged sector of the population.

In addition to the increased incidence of injury in the elderly, small stature females (5^{th} percentile female) occupants demonstrated a higher incidence of injury in car crash events (Bose et al., 2011) when compared to the mid-size male (50^{th} percentile male). It has been reported that females have a higher risk of whiplash-associated disorders (WAD) compared to males (Carlsson, 2012). In general, automotive compliance tests have looked at the young 50^{th} percentile male and the young 5^{th} percentile female with the intent of covering a wide range of body anthropometrics (Mertz et al., 1989). Therefore, the effect of age on anthropometrics is of interest in the context of automotive safety. In addition, common safety equipment, such as reactive head restraints, are more effective for males than females (Kullgren et al., 2013), suggesting that there is a need for an improved understanding of how to protect subjects with statures and anthropometrics outside the 50^{th} percentile male. An understanding of the differences between sexes, anthropometrics, and age groups is of importance to better protect at-risk groups in the population.

Detailed human body models (HBMs) have been developed for design purposes and increased safety, mainly in the automotive industry. Detailed HBMs have been developed to target relevant anthropometric

groups (e.g. 5th percentile female and 50th percentile male) and postures (e.g. driving and pedestrian). Existing HBMs can form the basis for the development of new models that represent different anthropometric groups (Hu et al., 2019) or postures (B. Frechede et al., 2006) that fall into the categories of repositioning, morphing and reposturing. A simulation-based method, referred to as repositioning further on, has been used (e.g. positioning in a sled or vehicle environment) to change the posture of the HBM while maintaining the resulting strains and stress in the tissues (Boakye-Yiadom and Cronin, 2018). However, this technique is generally limited to a small change in posture. Morphing tools have also been used to modify HBM by defining the target coordinates of all the nodes (Hu et al., 2019). The morphing method could be problematic on detailed models where a large number of nodes are involved in the morphing process. On the other hand, non-physics-based morphing methods, referred to as reposturing further on, has been used to modify the nodal coordinates of the models in a strain-free state to achieve a new posture. Recently, a simple-simulation reposturing tool (PIPER, PIPER project, EU) has been developed (Beillas et al., 2015) to reposture (no stress-strain field retained) HBMs without the need of defining transformation rules for all the nodes, as in the morphing methods, and reducing the simulation time with respect to the full-simulation method using a finite element solver. Importantly, the target posture is defined using the position of the hard tissue, and a set of mesh quality enhancement tools (Janak et al., 2018) has been integrated into the PIPER framework. The ability to accurately reaching the target posture while maintaining mesh quality in detailed HBMs is distinctive of the PIPER software.

Research on the age-related change in tissue response using such FE models requires modifications to represent an aged subject, including changes in posture, tissue morphology, and biological material properties. Limited investigations regarding the effect of posture in the neck have been undertaken (B Fréchède et al., 2006) using simplified neck models (Fréchède et al., 2005) but not in the context of the ageing process. With regard to the elderly population in general, only limited HBM investigations have been undertaken. A 65 YO mid-size male was developed (Schoell et al. 2015) with an emphasis on the thorax, abdomen, and lower extremities, excluding any changes in the neck region associated with ageing, to investigate thorax response in crash scenarios. Other body regions or specific tissues have been considered; for example, Huang et al., 2018 develop a 70 years old (YO) femur and tibia with a detailed knee joint model and perform a series of simulations. The developed 70 YO lower extremity model response was compared to that of a 30 YO model, and it was found that the aged model failed at lower displacements and had lower resultant forces at failure than the 30 YO model, demonstrating the importance of ageing effects on injury risk. Given the limited attention to the neck region in aged persons

and the higher potential for injury associated with increased age, detailed human neck models that consider an aged posture and geometry may inform human safety research and improvements to protect the geriatric population.

1.2 Research Objectives and Approach

The overall goal of this research was to develop a 75 years old 50^{th} percentile male and 5^{th} percentile female neck models and to assess the effect of age on the head kinematic and tissue response. This study focused on changes in geometry but did not consider the effect of changing material properties with age.

The first objective of the present study aimed to quantify the changes in the cervical posture and hard tissue morphology that are associated with the ageing process and quantify the differences between sexes using the existing literature.

Secondly, a methodology to reposition detailed human body models while retaining mesh quality at the tissue level was developed. The method was developed by quantifying the postures reported in the literature, defining a target cervical spine posture for the aged models, and applying a new hybrid reposturing method to achieve an aged posture. Two aged models were created from existing young FE neck models. The first NM represented an average 75 YO 50^{th} percentile male subject ($M50_{75YO}$), developed from a young average stature male model ($M50_{26YO}$). The second NM represented an average of 75 YO 5^{th} percentile female subject ($F05_{75YO}$) developed from an existing small stature female model ($F05_{26YO}$).

The third objective was to identify potential factors that may be associated with increased response and potential increased injury risk, considering the postural and morphological changes in the neck attributed to increased age. Specifically, the responses of young and aged male and female models will be compared in frontal, lateral and rear impacts to assess the effect of age and sex on head kinematics and tissue-level distractions to understand the potential for injury risk.

1.3 Thesis Organization

Chapter two introduces the relevant literature. First, an overview of the neck anatomy is presented. Then, the postural and morphological changes associated with age are summarized from the existing literature. A brief overview of finite element models with emphasis on human neck models follows, and, finally, the common methods of repositioning, morphing and reposturing human body models methods will be presented.

Chapter three firstly introduces a geometrical update of the capsular cartilage required to improve the FE model biofidelity in general. Hence, the methods and results of the cartilage update are presented as part of the methods chapter to establish the baseline young neck models. Secondly, the neck reposturing methods developed in this research are described. Beginning with the validation of the posture of the baseline models using anthropometric studies, this was a critical step in order to define an aged posture based on the existing young posture male and female neck models. The development of a coupled methodology to reposition human body models, including a commercial CAD software and an available HBM repositioning tool, is introduced after with emphasis on the accuracy and mesh quality of the final posture. Finally, the evaluation of the aged neck models is described.

Chapter four presents the results and first comparing the young male to the aged male, then the young female to the aged female, and finally, the effect of ageing in the male models was compared against the effect of ageing in the female models.

Chapter five presents a discussion with an emphasis on the intra-sex differences in the context of the tissue response difference associated to the ageing process.

Finally, chapter six summarizes the findings and highlights the conclusions of the present study. Limitations and recommendations will then be discussed, and future work is proposed.

Chapter 2: Background

A summary of the structurally relevant anatomical features within the neck will be presented. A literature review of the anatomical changes associated with age was undertaken and then summarized, along with an overview of contemporary finite element neck models. Existing methods to re-posture FE models (i.e. simulation-based, morphing, repositioning, and re-posturing), including finite element neck models, are presented. Finally, the experimental data used to previously validate the FE neck models will be described, as it will be used as the loading conditions to evaluate the models developed in the present study.

2.1 Anatomy and Physiology of the Neck

Anatomy is the study of the structure of living things with regards to their composition; it aims to describe the structure of the living. The definition of anatomical terms of planes and directions (Figure 1) enables clear and consistent communication regarding anatomical descriptions. Within the neck, the anatomical directions (Figure 1) help to locate tissues, usually with respect to the cervical spine.

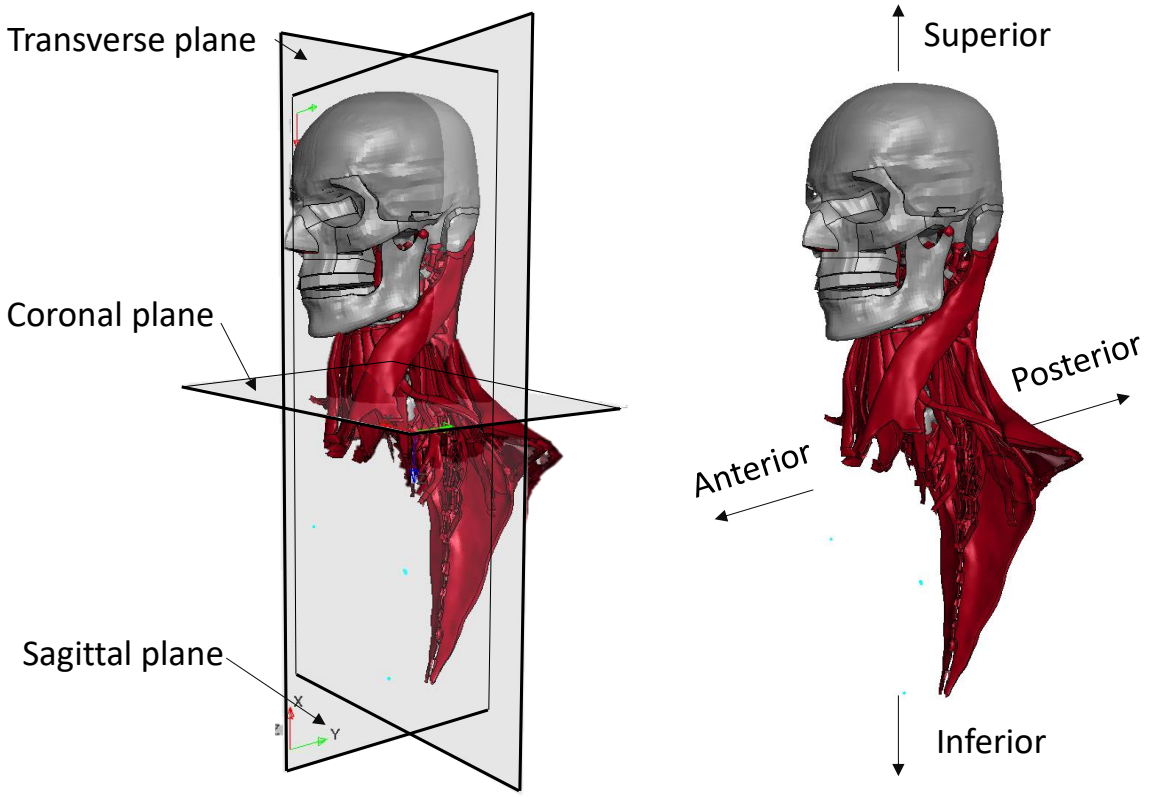

Figure 1: Anatomical planes and directions for the human neck demonstrating the coronal, sagittal, and transverse planes, and the anterior-posterior and superior-inferior directions.

Anatomical terms to describe movements (Figure 2) have also been established amongst the physiology community and health practitioners. Specific to the neck, the range of motion of the head can be described with extension-flexion, axial rotation, and lateral bending (Figure 2).

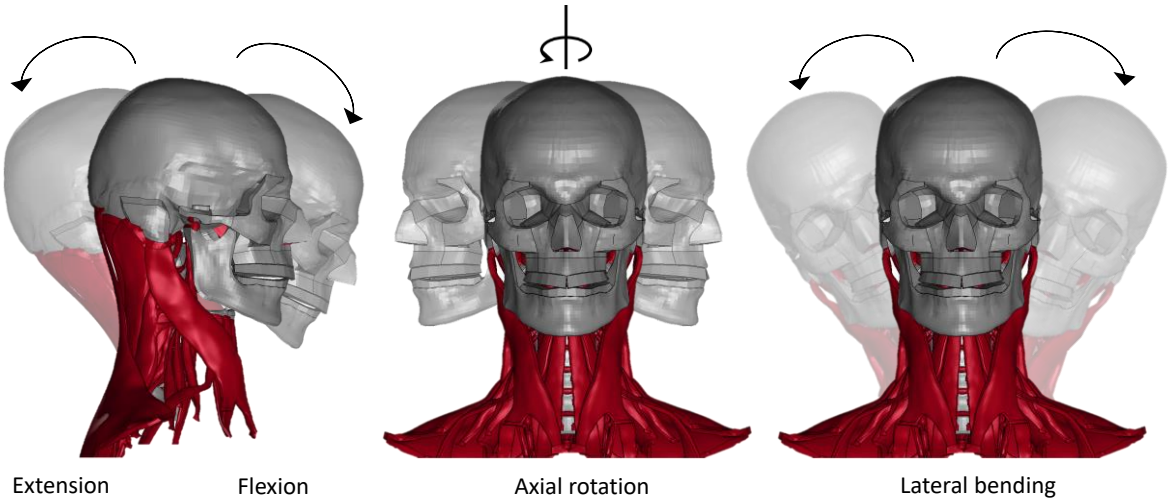

Figure 2: Anatomical terms for movement in the neck: flexion/extension [left], axial rotation [middle], lateral bending [right].

The neck connects the head to the thorax and serves as a support providing stability for the head while providing a large head range of motion (Bogduk and Mercer, 2000). The neck includes structurally relevant tissues and non-structural tissues. The structurally relevant tissues include the ligamentous spine (vertebrae, ligaments, cartilage, and intervertebral discs), the musculature and the skin and adipose tissue (Figure 3). The non-structural tissues include, amongst others, the spinal cord and nerve roots, trachea and the arteries and veins. The neck connects to the head and at the first cervical vertebra interface and the occipital condyles and to the thorax at the first thoracic vertebra interface and the seventh cervical vertebra with some muscles extending through the thorax region.

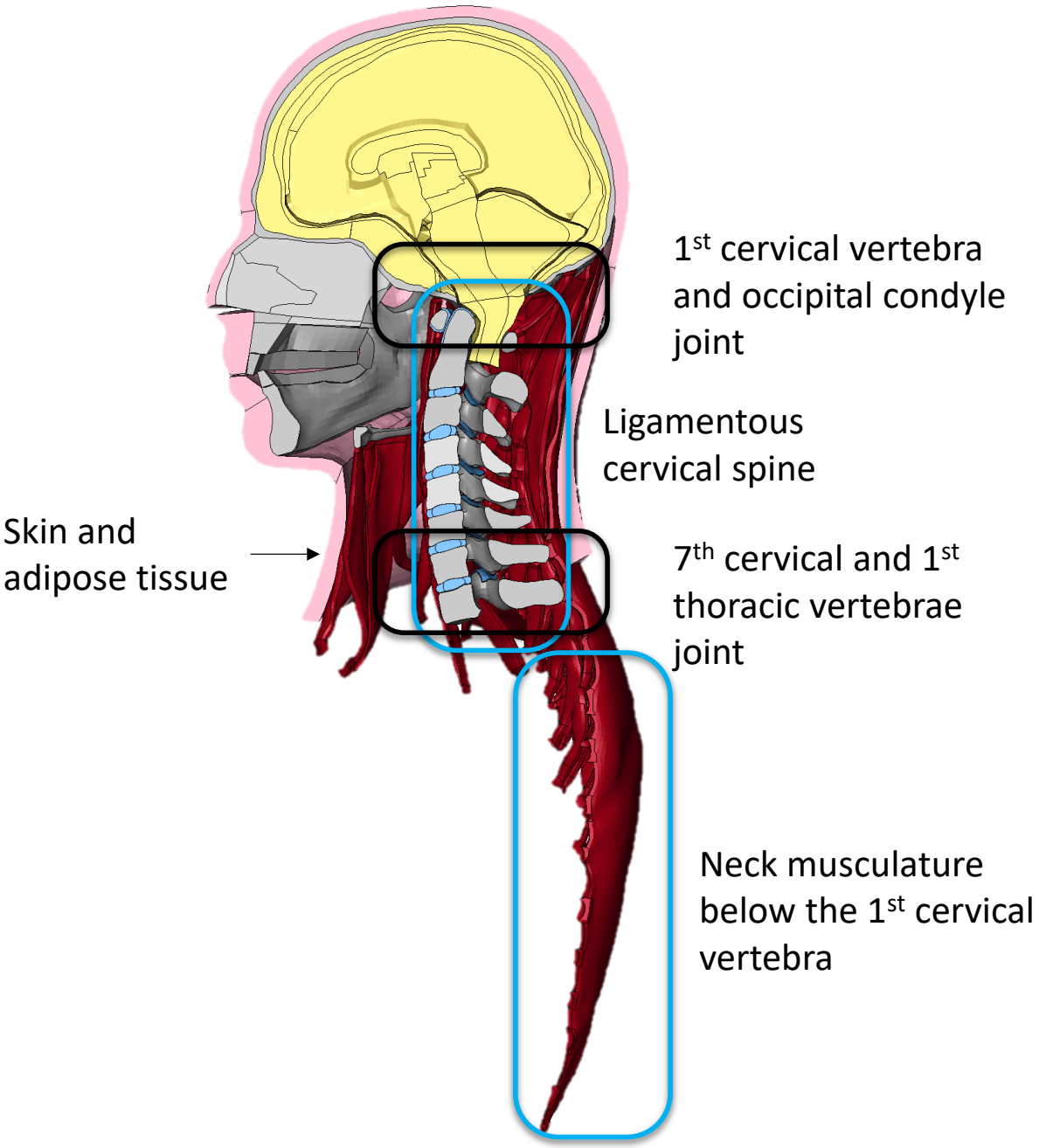

Figure 3: Sagittal view of the neck, demonstrating the superior and inferior ends of the neck region, ligamentous spine, neck musculature (red) and skin and adipose tissue (pink).

2.1.1 Tissues in the Ligamentous Cervical Spine

The ligamentous cervical spine (Manohar M Panjabi et al., 1991; Manohar M. Panjabi et al., 1991b) comprises seven cervical vertebrae, the joints (capsular joint and intervertebral joint), and ligaments between them (Figure 4). The ligamentous spine is commonly divided into the upper cervical spine (UCS), including the first and second cervical vertebra (C1-C2) and the lower cervical spine (LCS), including the third to the seventh cervical vertebra (C3-C7). This separation of the ligamentous spine is due to the morphological differences between those cervical levels and the range of motion enabled at each level.

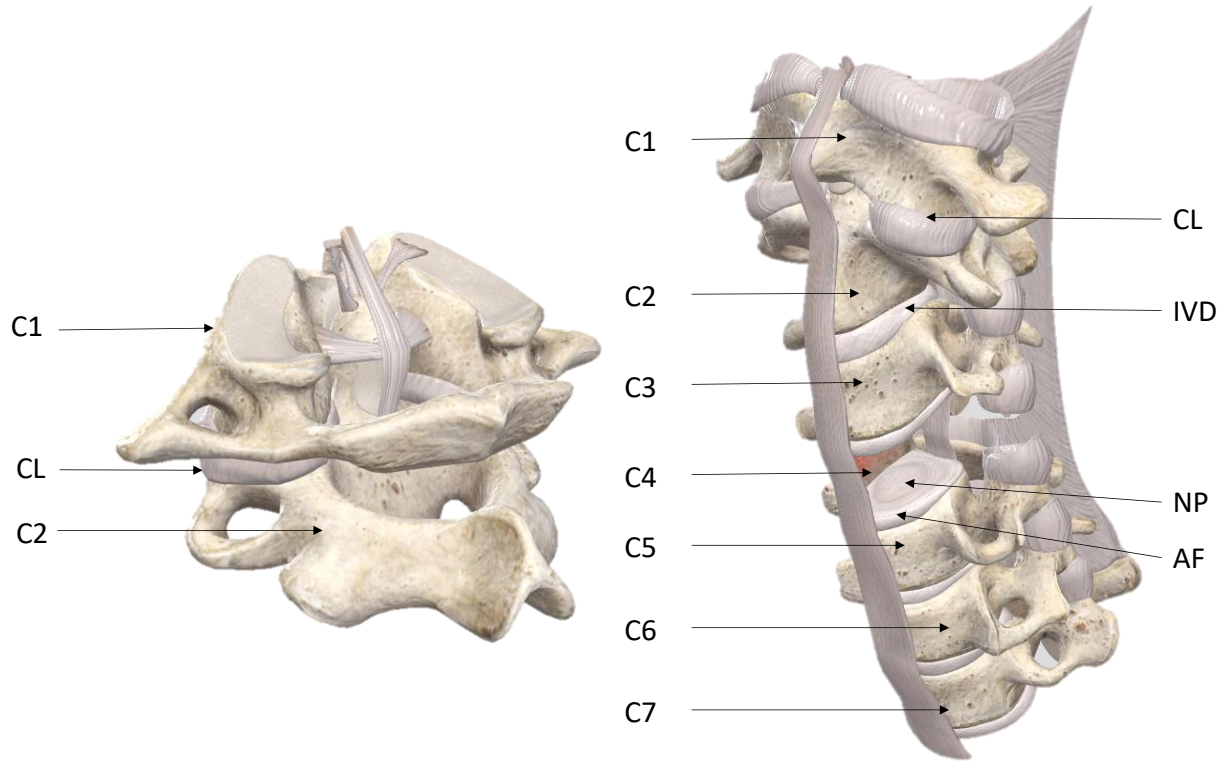

Figure 4: Upper and lower cervical spine with tissues associated with injury and pain response (Image courtesy of Complete Anatomy).

The vertebrae comprises an external layer of cortical bone surrounding the porous trabecular bone (Cowin, 2001) and serves as an anchorage for the muscles. The vertebrae morphology and the connective tissue arrangement of the LCS are constructed to mainly facilitate flexion-extension range of motion in

contrast with the UCS, which also provides a high degree of axial rotation. The UCS (Figure 4) includes the atlas (C1) and the axis (C2), with odontoid serving as a pin-like mechanism that allows for a wide range of motion in axial rotation. The vertebra dimensions are often described, amongst others, by the body depth (BD), and the facet angle (Θ) (Figure 5) (Parenteau et al., 2014).

The intervertebral discs serve as load support and limit the range of motion (Humzah and Soames, 1988). The LCS includes five intervertebral discs (IVD), starting between C2 and C3, up to C6 and C7. The IVD (Figure 5) comprises the annulus fibrosus (AF) embedded in a ground substance and the nucleus pulposus (NP). The IVD serves as structural support in all modes of loading (e.g. tension-compression). The IVD geometry is described, amongst others, with IVD height defined as the distance between two adjacent vertebral endplates in the IVD foramen (Pooni et al., 1986).

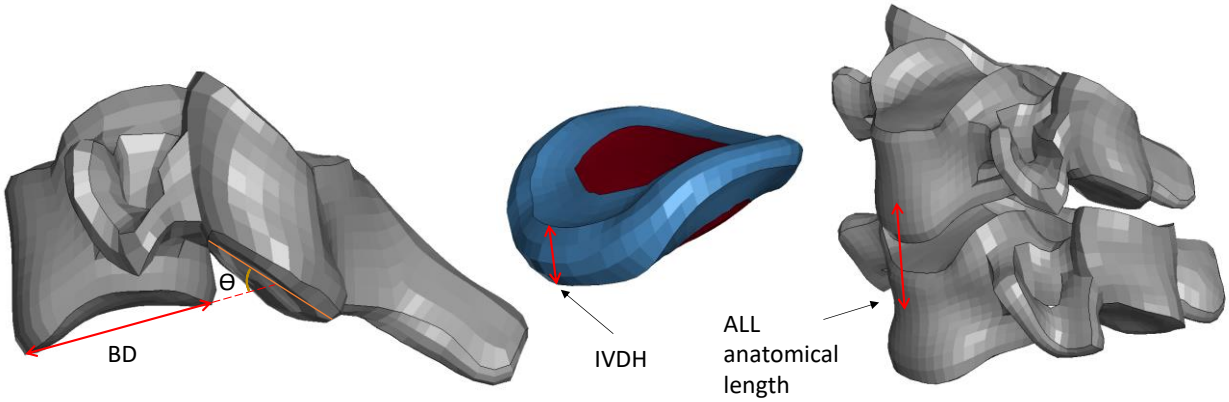

Figure 5: Side view of the 5th cervical vertebra showing the vertebral body depth (BD) and the facet angle (Θ). Isometric view of the intervertebral disc showing the intervertebral disc height (IVDH). Isometric view of a segment C45 demonstrating an exemplar of the insertion points of the anterior longitudinal ligament used to define the anatomical length (ALL).

The ligaments constrain the range of motion of the cervical spine (Takeshita et al., 2004) with a cable-like structure that does not transmit loads in compression. In the lower cervical spine, five distinct ligaments (capsular, anterior, posterior, interspinous ligament and the ligamentum flavum) connect the adjacent vertebra, and each one of them is commonly loaded in specific motions; for example, the ligaments on the anterior aspect of the cervical spine are expected to be loaded in extension in contrast with the those in the posterior side that are expected to be loaded in flexion. However, the capsular ligament (CL) ring-like

geometry allows for the load to be transmitted in both loading modes (flexion and extension). The ligament length is described as the distance between the insertion points in the bony structures that are attached to (Pearson et al., 2004). In the upper cervical spine, the ligaments include the alar, cruciate, capsular, interspinous and membrane ligaments.

The cervical capsular joints (CCJ) serve as a kinematic guide to the vertebrae as well as load support (Jaumard et al., 2011). The cervical capsular joints (Figures 6), together with the IVD, serve as a joint between the vertebrae in the cervical spine. Each vertebra in the cervical spine has four articular facets (superior and inferior, left and right) comprising a layer of cortical bone and a layer of capsular cartilage. The capsular ligament (CL, Figure 4) encapsulates the joint and contains the synovial fluid that serves as a lubricant for the joint. Each CCJ also includes two CCJ meniscuses (Figure 6) that enhance joint congruity and stability. Around the periphery of the facets, the capsular ligament is attached, connecting the inferior facet of the superior vertebra and the superior facet of the inferior vertebra (DM, VM, Figure 6). The CCJ cartilage is nonlinearly distributed along the cortical bone facet with the maximum thickness close to the geometrical mid-point of the articular surface and a gradual thinning towards the CCJ periphery (Womack et al., 2008). An important parameter used to describe the CCJ is the facet angle with respect to the vertebral body (Parenteau et al., 2014), as it drives, in part, the facet joint kinematics. It has been shown that the capsular joint plays a significant role in the kinetic and kinematic response of the ligamentous cervical spine (John et al., 2018) and has been implicated as a source of pain in whiplash-associated disorders (WAD) (Cavanaugh, 2006; Quinn and Winkelstein, 2007).

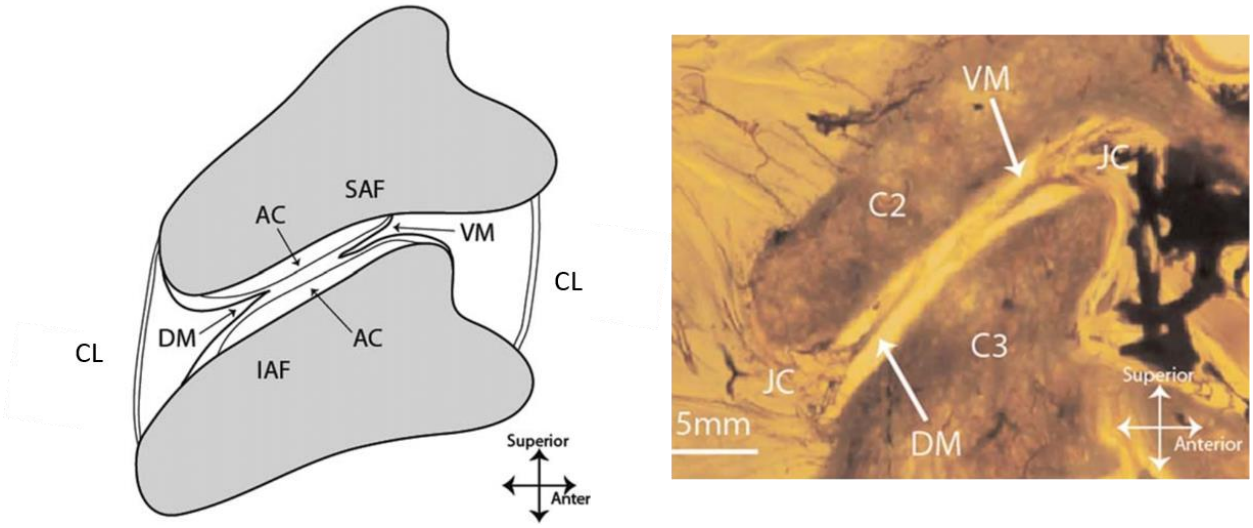

Figure 6: Schematic of the cervical capsular joint (left) showing the cartilage (AC) attached to the superior articular facet (SAF) and to the inferior articular facet (IAF), the capsular ligament (CL), articular cartilage (AC), the Ventral meniscus (VM) and the Dorsal meniscus (DM). On the right, plastination of cross-section cervical capsular joint showing the VM and DM in the joint capsule (JC). (Taken from Farrell et al., 2015 Creative Commons Attribution-NonCommercial-NoDerivs 3.0 Unported (CC BY-NCND3.0) Licence (http://creativecommons.org/licenses/by-nc-nd/3.0/)).

2.1.2 Neck Musculature

The ligamentous cervical spine serves as support and anchor to the neck muscles, comprising 27 muscle pairs, which are symmetric about the sagittal plane. Muscles, together with the nervous system, serve as static equilibrium control and dynamic movement actuators and control of the head (Knaub and Myers, 1998). Skeletal muscles attach, in general, to two bones through tendons with the insertion at the bone that has the maximum movement when the muscle is activated, and the origin at the opposite end. The muscles in the neck are usually divided into six groups: Hyoid muscles, anterior muscles, lateral muscles, suboccipital muscles, back muscles, and vertebral muscles. Muscles usually work in antagonistic pairs, with the agonist muscle providing the force to move the attached bone while the antagonist muscle applies an opposing force (cocontraction) to act as a motion controller. In neck flexion and extension, the anteriorly located (flexors) and posteriorly located (extensors) muscles act as an antagonistic pair (Figure 7 and 8). From the mechanics perspective, muscles have a passive response and an active response. The active response is a cognitive response to external stimuli, while the passive response is independent of

the external environment. Muscle activation is controlled by the nervous system and is subjected to lag (activation time) driven by the voluntary and reactive response of the subject. Muscle activation has been characterized by a curve with three regions, the activation onset (delay), the activation region and the deactivation or relaxation region (Happee, 1994).

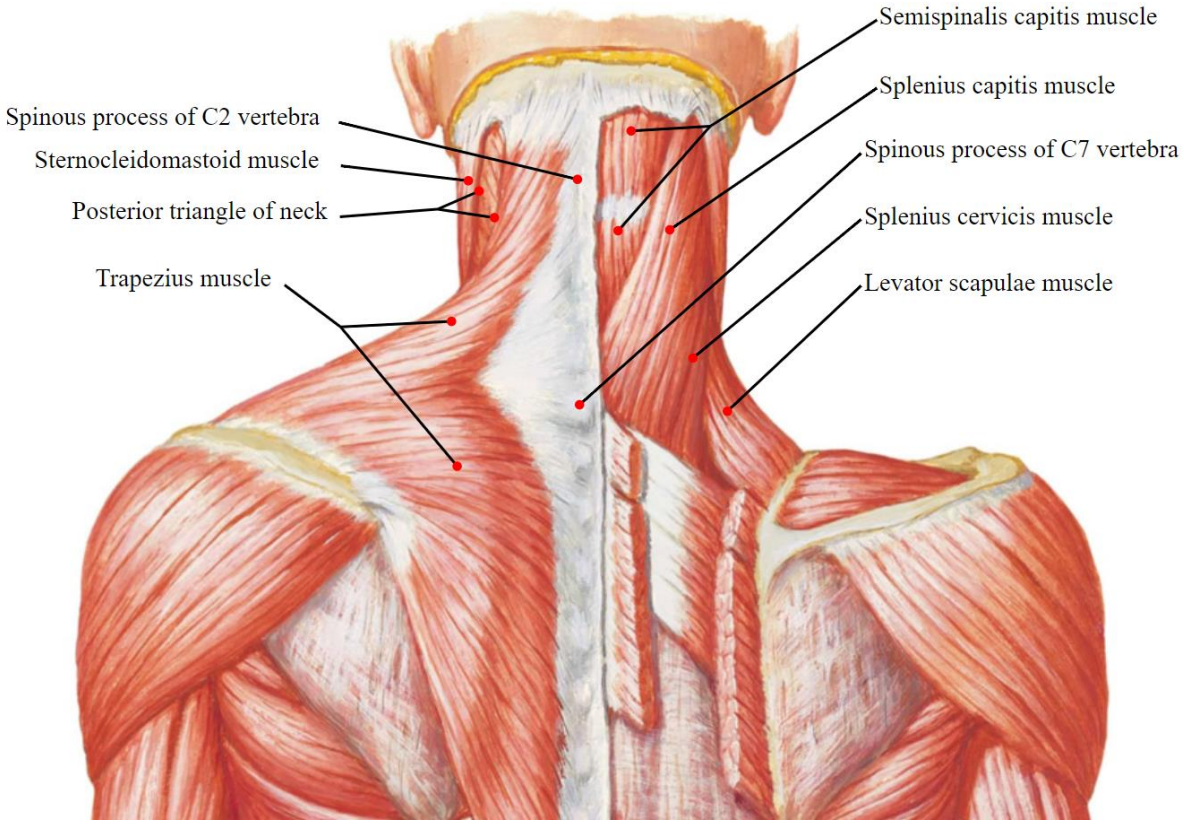

Figure 7: Posterior neck muscles. Activated in neck extension (extensors).

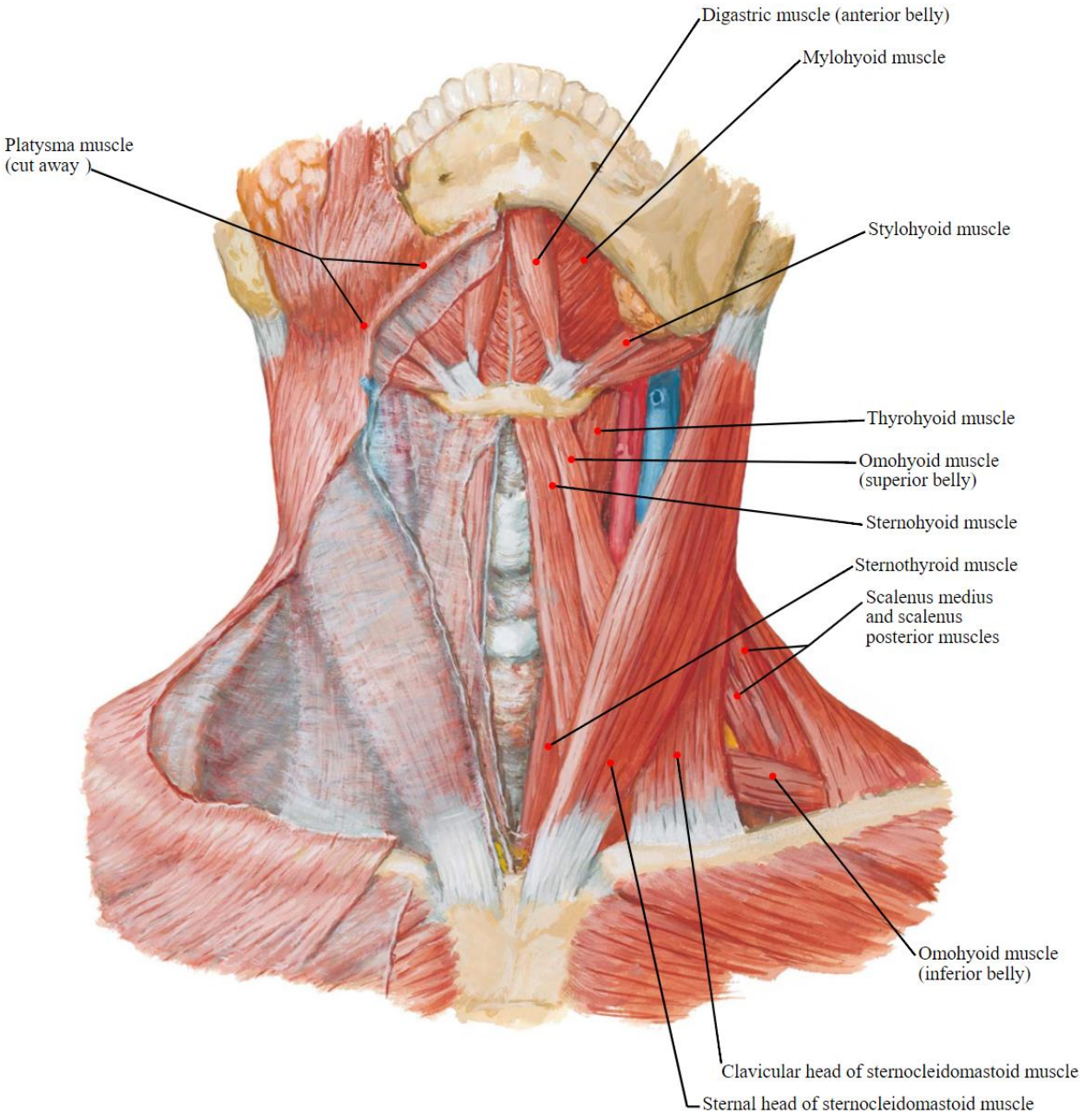

Figure 8: Anterior neck muscles. Activated in neck flexion (flexors).

2.2 Anthropometric and Posture Changes with Increasing Age

General anthropometrics used for mechanical design will be reviewed. Then, anthropometric studies specific to the neck will be described in the context of the ageing population. Finally, tissue level anthropometrics studies will be reviewed and discussed with an emphasis on the differences between the young and the elderly population.

Anthropometrics refers to the measurements of human features (e.g. stature, age, and weight). Statistical anthropometric studies within a community are useful for identifying target populations, understanding variability, and quantifying human anatomy changes over time periods (Gordon et al., 2014, 1989; Schneider et al., 1983). Humans can be measured in many ways, and engineers have identified relevant measurements with regards to the effect on the mechanical response of the human body in the context of injury biomechanics. As with any statistical analysis, the sample size is of importance. A number of large data sets exist, to name a few; The "Anthropometric Survey of US Army Personnel" (ANSUR) (Gordon et al., 2014, 1989) and the National Health and Nutrition Examination Survey (NHANES) in the United States of America, and the "Japanese anthropometric reference data" (JARDA 2001) (HOSOYA and N, 2002) in Japan.

Anthropometrics can be global (e.g. stature, body mass index and age), regional (e.g. neck length, neck circumference and neck curvature) and local (e.g. vertebral body depth and capsular facet angle). For research and design purposes, humans are often distinct according to their relevant anthropometrics. Common global anthropometrics used to differentiate human sizes is their stature and mass (Carlsson et al., 2014). With the intent of covering a broad spectrum of the population, four anthropometric groups (Table 1) based on stature and weight were proposed (Schneider et al., 1983) based on a population pool between 18 and 74 years old (Table 1).

Table 1: Anthropometric groups defined for male and female (Schneider et al., 1983).

Anthropometric group	Stature (cm)	Weight (kg)	Mean age (years)
Small female (5th percentile)	148.6 – 153.7	44.1 – 48.6	36
Mid-size female (50th percentile)	160.0 – 163.8	59.5 – 65.9	40.3
Mid-size male (50th percentile)	172.7 – 177.8	73.6 – 80.5	36.2

Large male (95th percentile)	185.4 – 189.2	98.6 – 109.1	34.1

Subjects from three different anthropometric groups were selected (5th percentile female, 50th percentile male and 95th percentile male), and regional anthropometrics (Table 2) were measured, including the neck region dimensions (Schneider et al., 1983). The neck region was characterized using seven measurements: the anterior length, the width in the mid and lower parts, the depth in the mid and lower parts and circumference in the mid and lower parts. Neck length was defined as the length between the most anterior-inferior location (tip) of the chin and the suprasternal landmark in the frontal plane. The neck width was defined as the length between the most lateral ends of the neck at the estimated midpoint and lower end of the neck length. The neck depth was defined as the posterior-anterior length perpendicular to the neck axis at the estimated midpoint and lower end of the neck length. The neck circumference was defined as the circumference perpendicular to the neck axis at the estimated midpoint and lower end of the neck length (Table 2) (Schneider et al., 1983).

Table 2: Regional anthropometrics. Mean values and standard deviation (SD) (Schneider et al., 1983).

	Neck length (SD)	Neck width (cm)		Neck depth (cm)		Neck circumference (cm)	
	Anterior (SD)	Mid (SD)	Lower (SD)	Mid (SD)	Lower (SD)	Mid (SD)	Lower (SD)
5th percentile female	8.1 (1.24)	9.1 (0.58)	10.4 (1.18)	9.0 (0.48)	9.3 (1.1)	30.4 (1.54)	32.2 (1.32)
50th percentile male	8.5 (1.46)	11.4 (0.62)	12.2 (0.67)	11.5 (0.65)	11.5 (1.03)	38.3 (1.45)	39.3 (1.65)
95th percentile male	9.8 (1.14)	12.6 (0.78)	13.6 (0.82)	12.6 (0.64)	13.1 (1.32)	42.1 (1.95)	43.3 (1.7)

In recent studies, more detailed anthropometrics, such as the neck curvature, have been added to the commonly studied parameters. Notably, the age of the subjects has been reported and included as a variable in statistical analysis. In the neck region, cervical lordosis increases, higher inferior and superior Bezier angles (Figure 9a), with age (Klinich et al., 2012, 2004) as a consequence of a thoracic kyphosis

increase and the need for maintaining the head angle. In a study (Klinich et al., 2012), specific vertebrae landmarks (Figure 9b) of 177 radiographs of subjects in a seated position with a variety of anthropometrics (Table 3) were digitized. The inferior and superior Bezier angles were reported (Klinich et al., 2004) (Figure 9a).

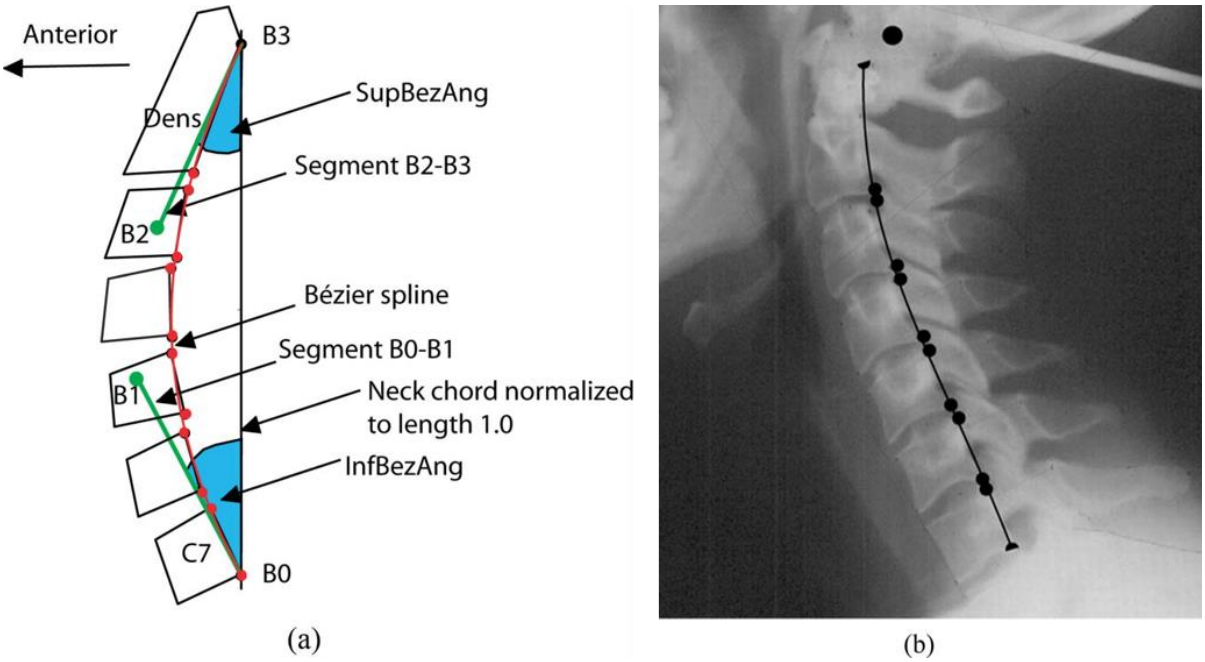

Figure 9: Bezier angles of the cervical spine (Klinich et al., 2012). Superior Bezier angle ladled as "SupBezAng" and inferior Bezier angle labeled as "InfBezAng". Taken from Klinich et al., 2012.

Table 3: Summary of relevant literature reporting posture in terms of age.

Study	N (+18 YO)	N by sex	Age groups (YO)	Results
Park et al., 2016b	90	47 F, 43 M	20 to 88	Coordinates of the center of the eye, tragion, C7/T1, T12/L1, and L5/S1
Klinich et al., 2012, 2004	177	93 F, 84 M	18-24, 35-44, 62-74	Bezier angles

Reed and Jones, 2017	140	79 F, 61 M	18 to 74	Individual vertebrae positions
Parenteau et al., 2014	425	250 F, 175 M	18-29, 30-44, 45-59, 60+	Vertebral body depth, Facet angle, Spinal canal diameter

Recent anthropometrical studies have shown that the overall spine posture change with age (Park et al., 2016b) towards a more forward head position and an increased thoracic and cervical curvature. Ninety subjects with a wide variety of anthropometrics were measured (Table 3) in a driving position. A set of equations were derived from the measurements to predict the location of the tragion, eyeball, C7-T1 joint, T12-L1 joint, pelvis and inferior extremities in terms of seat position and anthropometrics, including age and sex. This set of equations is referred to as the Full Body Posture Predictor (FBP) further on (Figure 10).

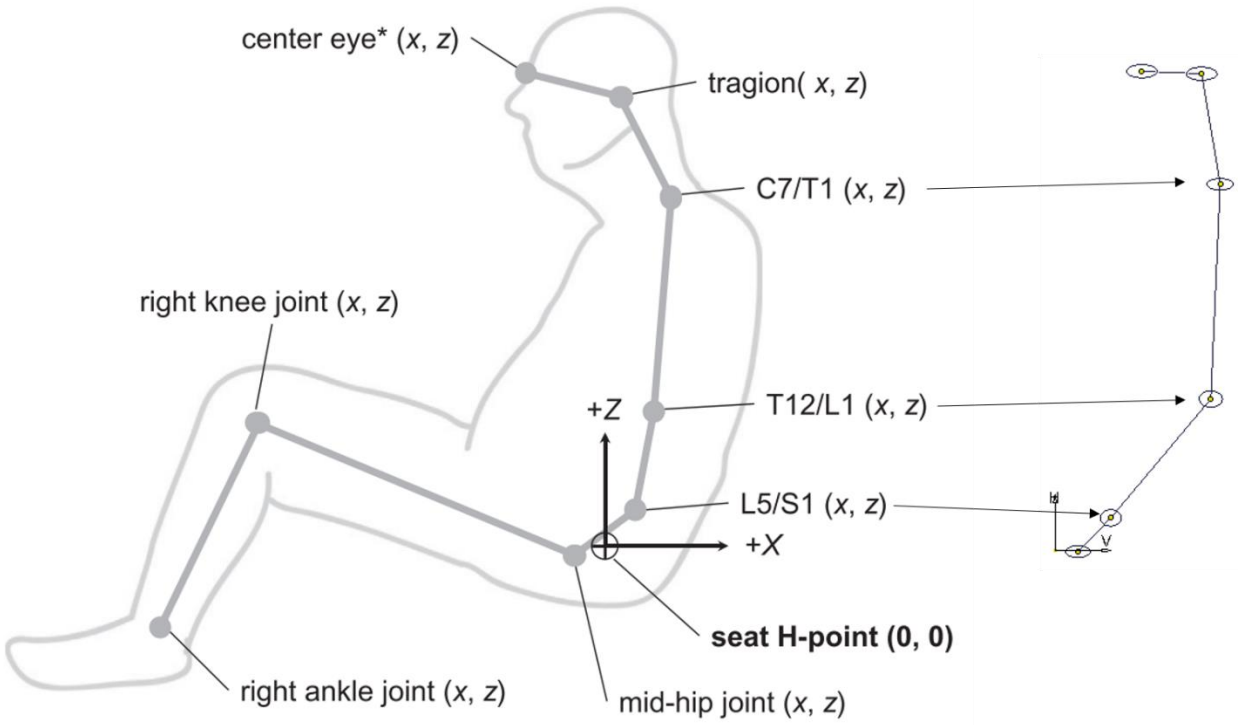

Figure 10: Full body posture predictor (FBP) on the left (taken from Park et al., 2016b) and the CAD representation on the right.

A python script described as a Cervical Spine Predictor (CSP) was developed (Reed and Jones, 2017) (Figure 11) based on the radiographs digitized in Klinich et al., 2012 to predict the vertebral positions in terms of sex, age, stature and seated stature.

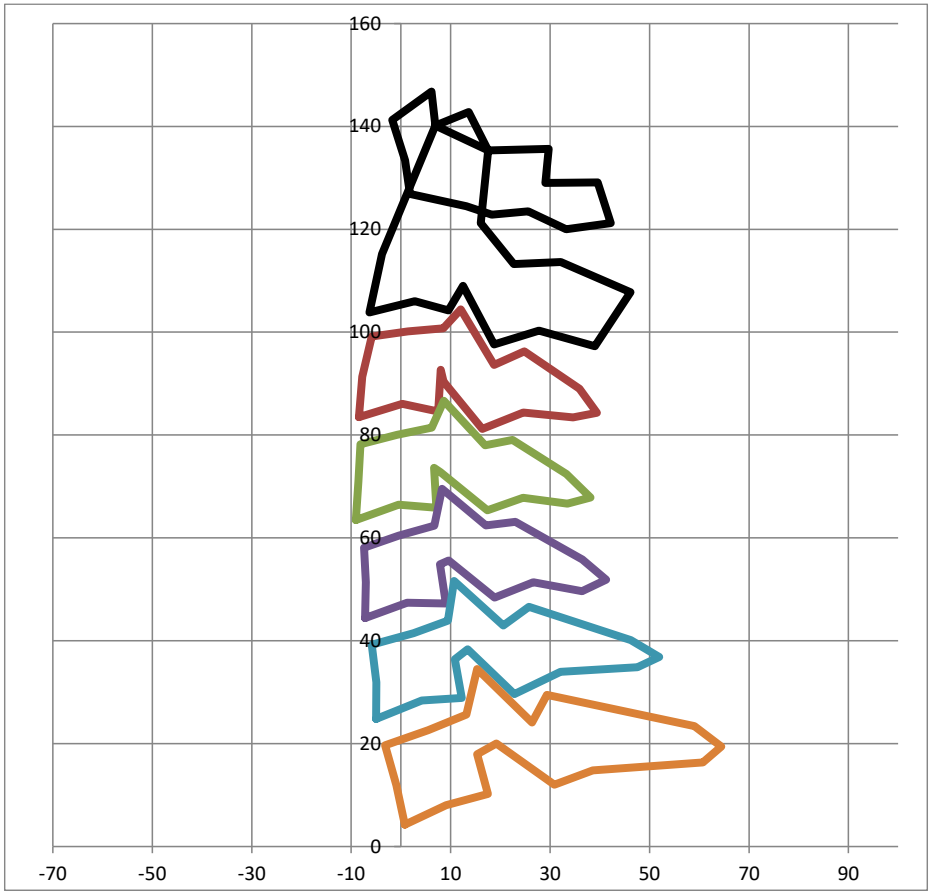

Figure 11: Cervical spine predictor (CSP) for the posture of a 50th percentile 26 YO male (Reed and Jones, 2017).

It was found that cervical lordosis increased in general with age. For small stature females, the change in the superior Bezier angle with age was more prominent than that in the average size male (Figure 11). It is important to note that in the CSP (Reed and Jones, 2017), the mass, age, stature, and seated stature are inputs of the predictor. In contrast, the values reported in Klinich et al., 2012 were separated by sex, age group (young: 18-24 YO, mid-aged: 35-44 YO and older: 62-74 YO) and size group (small, medium, and tall).

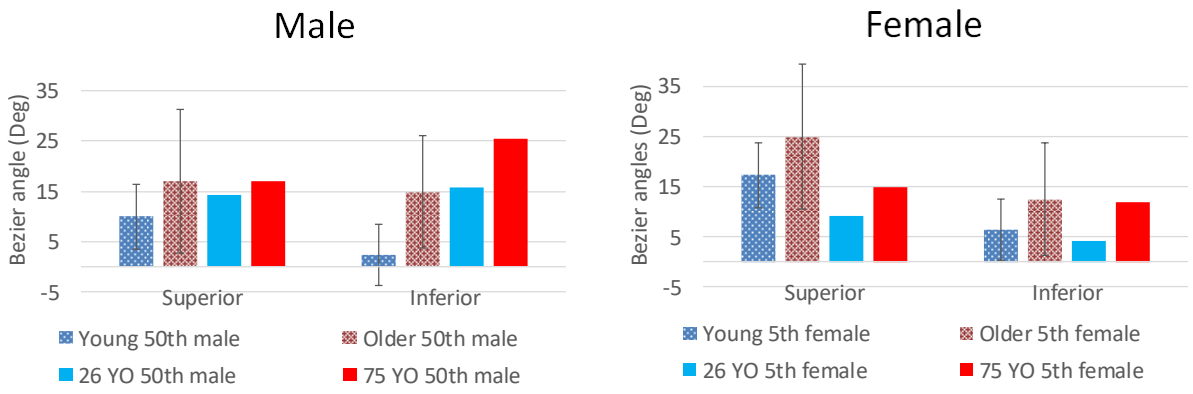

Figure 12: Bezier angles reported for young and old populations. Literature data (Klinich et al., 2012) in patterned bars (young: 18-24 YO and older: 62-74 YO) and CSP predictions (Reed and Jones, 2017) in solid bars.

At the vertebral level, Parenteau et al., 2014 measured the body depth, facet angle and spinal cord canal depth (Figure 13) of 425 subjects of different age groups and sex using computed tomography (CT) scans. It was found that the facet angle changes due to ageing (Figure 14) were statistically significant. Previous anthropometric studies focused on quantifying the cervical vertebra (Gilad and Nissan, 1986; Panjabi et al., 1991a; Panjabi et al., 1993; Przybylski et al., 1998; Yoganandan et al., 2003); however, age or sex dependency was not reported, and the sample size was small relative to the most recent studies (Parenteau et al., 2014; Reed and Jones, 2017).

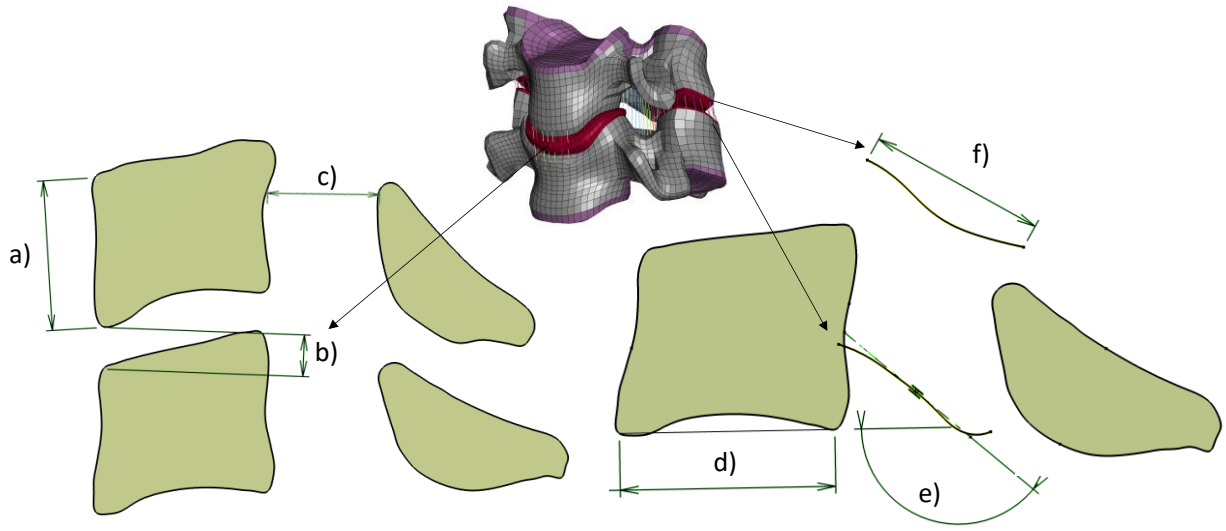

Figure 13: Cross-section in the sagittal plane of the segment C45 demonstrating: a) Vertebral body height, b) IVD space, c) spinal cord canal depth, d) Vertebral body depth, e) Facet angle, f) Facet depth.

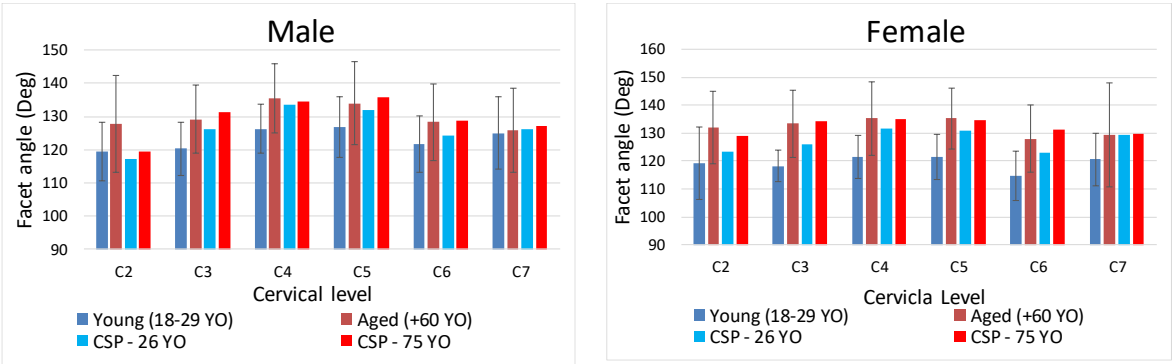

Figure 14: Facet angle change for young and aged subjects reported by Parenteau et al., 2014 (patterned bars) and CSP (solid bars).

2.3 Finite Element Human Body Models

Since the 1970's, numerous computational models of the human body have been developed (Yang et al., 2018) with the intent of understanding response in impact scenarios and to predict the potential for injury risk. Initially, simple spring-mass systems were used to create multi-body human models focused on the

prediction of the kinematic response of the hard tissues. However, multi-body models lack the ability to evaluate stresses and strains of various tissues, which is critical in predicting injury at the tissue level. More recently, detailed HBM finite element models have been developed in the context of automotive safety and used mainly for the design of safety systems such as airbags and seatbelts (Pyttel et al., 2007). FE models require inputs (geometry, material properties and boundary conditions) that are relevant to the problem being investigated and, when validated under representative loadings, have the ability to inform engineers about the kinematic and kinetic response in impact scenarios, as well as local level metrics (e.g. local strains) and failure modes. Many of these quantities are challenging or not possible to measure simultaneously using current experimental methods. Human body FE models (HBMs) have been developed to predict body kinematics under loading conditions, mainly in car crash scenarios (Gayzik et al., 2011; Iwamoto et al., 2015; Östh et al., 2017a). Early HBMs (Yang et al., 1998) were validated under a limited set of loading conditions using simple geometry and lacking some tissues (e.g. capsular cartilage). More recently, detailed HBMs have been developed based on subject-specific CT data of living subjects (Gayzik et al., 2011), corresponding to a specific age and anthropometric group geometry (e.g. 26 YO for the GHBMC M50, Table 3). Such HBMs were developed with the intent of representing anthropometric groups considered in automotive safety compliance testing.

2.3.1 Finite Element Models of the Neck

The neck region has been identified as an essential contributor to the head kinematics under loading and to head motion control and support in a resting position. In addition, the association of whiplash-associated disorders (WAD) and high and low severity crash induced injuries (CII) to tissues in the neck has encouraged the development of advanced neck models. Therefore, a number of neck models (NM) have been developed over the years with increasing levels of detail, validation extent and different purposes (Deng et al., 1999; Fice and Cronin, 2012; Fréchède et al., 2005; Ivancic et al., 2005; Kitagawa et al., 2008, 2006; Langlois et al., 2006; Meyer et al., 2004; Ng et al., 2003; Stemper et al., 2005; Zhang et al., 2008). Initially, neck models were developed to predict gross kinematics (e.g. head kinematics). More recently, NMs have been developed with the intent of predicting response and the potential for injury at the tissue level, which increases the level of complexity when compared to the earlier developments. Detailed full neck models that include the vertebrae, ligaments, IVD, cervical capsular cartilage and musculature have been developed and validated under a wide range of validation cases and anatomic levels. Multi-level validation has been performed with the purpose of predicting head and neck

kinematic response under dynamic omnidirectional loading and crash-induced injuries (Fice et al., 2011; Östh et al., 2017b; Yang, 2017).

Panzer et al., 2011 (Figure 14) develop a detailed 50th percentile male neck model (UW neck model) with the intent of developing a full head and neck model detailed enough to predict head and neck response and quantify the effect of active musculature on the potential for the neck injury. The geometry of the vertebrae was based on a model previously developed (Deng et al., 1999) from an average human data set, while the soft tissue geometry was based on the available literature. The vertebrae were modelled with hexahedral elements for the trabecular bone and shell elements for the cortical bone. The ligaments were represented with 1D nonlinear rate-dependent tension-only spring elements (Figure 15). The IVD included the annulus fibrosus ground substance and nucleus pulpousus with hexahedral elements and a set of layers of shell elements to represent the annulus fibrosus fibre matrix. The cervical capsular joint was constructed including the cervical capsular cartilage with hexahedral elements, the capsular ligament with beam elements and a simple volume-pressure airbag model for the synovial fluid. The muscles were modelled with Hill-type 1D elements to represent 25 muscle pairs in the cervical spine (Figure 15). The UW neck model has been used to investigate load sharing at the motion segment level and to study neck kinematics and tissue response in frontal impacts of various severities (Panzer et al., 2011). In addition, Fice et al., 2011 investigated the ligament distraction in rear impact as means to predict pain response associated with WAD. However, the UW model lacked a full three-dimensional representation of the passive muscle tissue, adipose tissue, and skin.

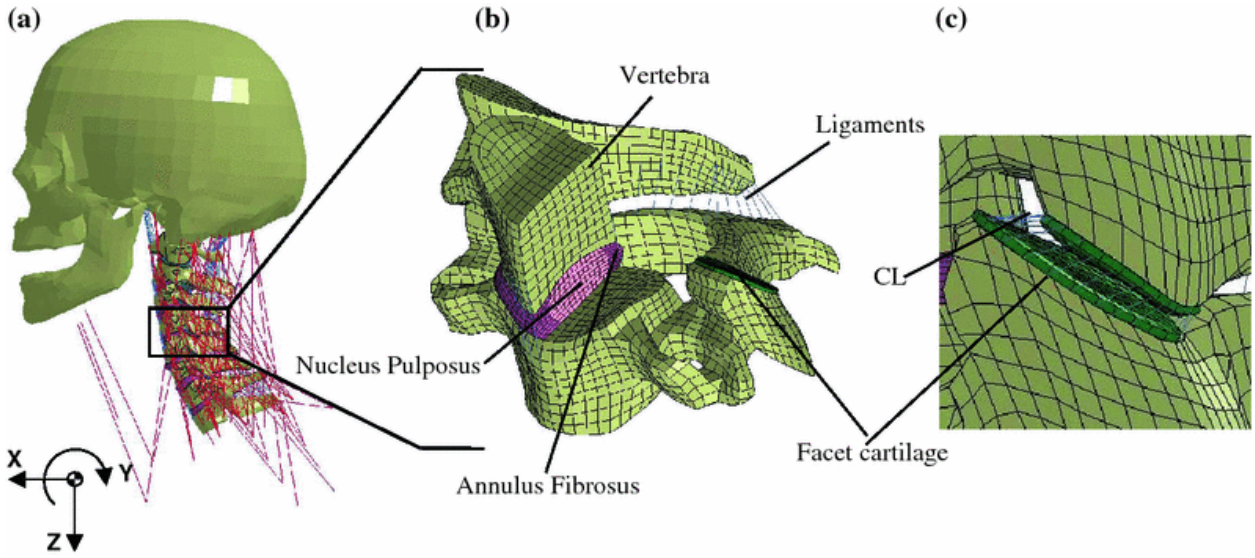

Figure 15: 50th percentile male neck model developed for frontal (Panzer et al., 2011) and rear impact conditions (Fice et al., 2011). Taken from Fice et al., 2011.

The ViVa neck model developed by Östh et al., 2017b (Figure 16), represents a 50th percentile female subject with similar construction to Fice et al., 2011 in the neck region. The cervical capsular cartilage, muscles and IVD were similarly constructed. However, Östh et al., 2017b used tetrahedral and triangular elements to represent the vertebrae. Shell elements for the ligaments lacked representation of the synovial fluid but included the trachea, skin, and neck flesh (Figure 16). Although still in development, the ViVa model has been compared to volunteer experimental data in rear impact at full-body level (Östh et al., 2017b), and a variety of muscle activation technics were developed and compared at the full neck level (Putra et al., 2019)

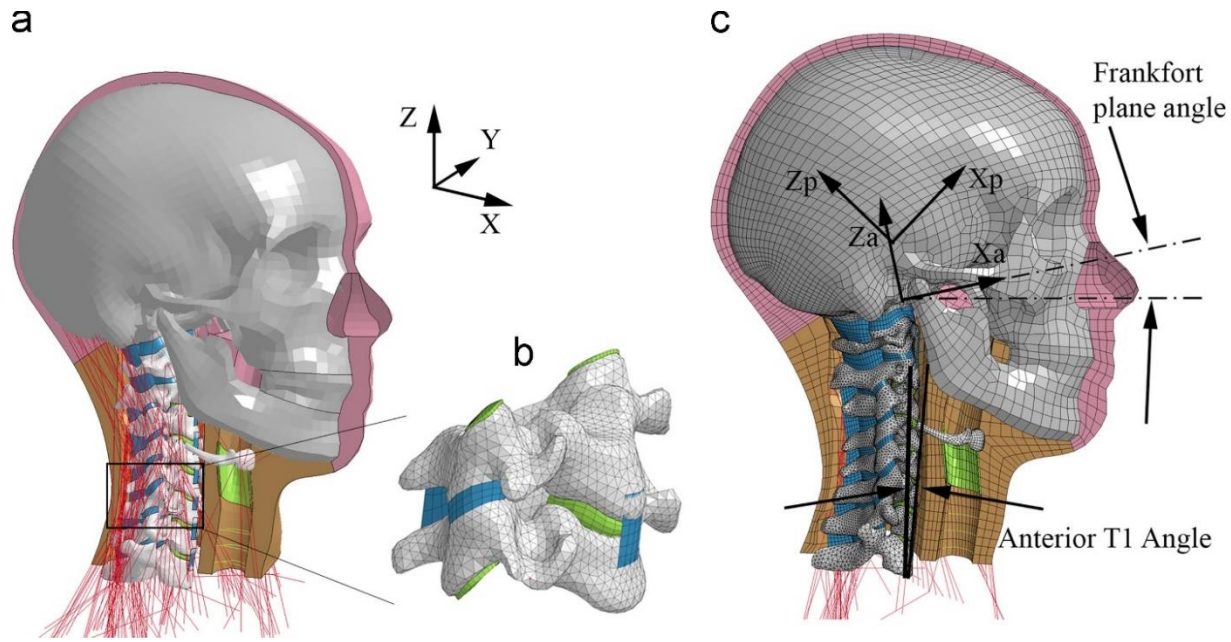

Figure 16: 50th percentile female neck model developed with a focus on rear impact (Östh et al., 2017b).

2.3.2 The GHBMC M50 and F05 Neck Models

The GHBMC neck models (Barker and Cronin, 2020) include a 50th percentile young (26 YO) male (M50) and 5th percentile young (26 YO) female (F05) (Figure 17). This NM was geometrically based on computed tomography and magnetic resonance imagining of specific subjects within their anthropometric group with regards to stature and weight. The male subject was 26 years old, weighed 78 kg, was 174.9 cm tall, and had a body mass index of 25.7, while the female subject was 24 years old, weighed 48.1 kg, was 149.9 cm tall, and had a body mass index of 21.4. The selected subjects fall within the ranges defined for their respective anthropometric group at full-body level (Schneider et al., 1983) (Table 1). However, at the neck level (Table 3), the male subject had a longer neck length and a straighter neck curvature than the average population (Reed and Jones, 2017).

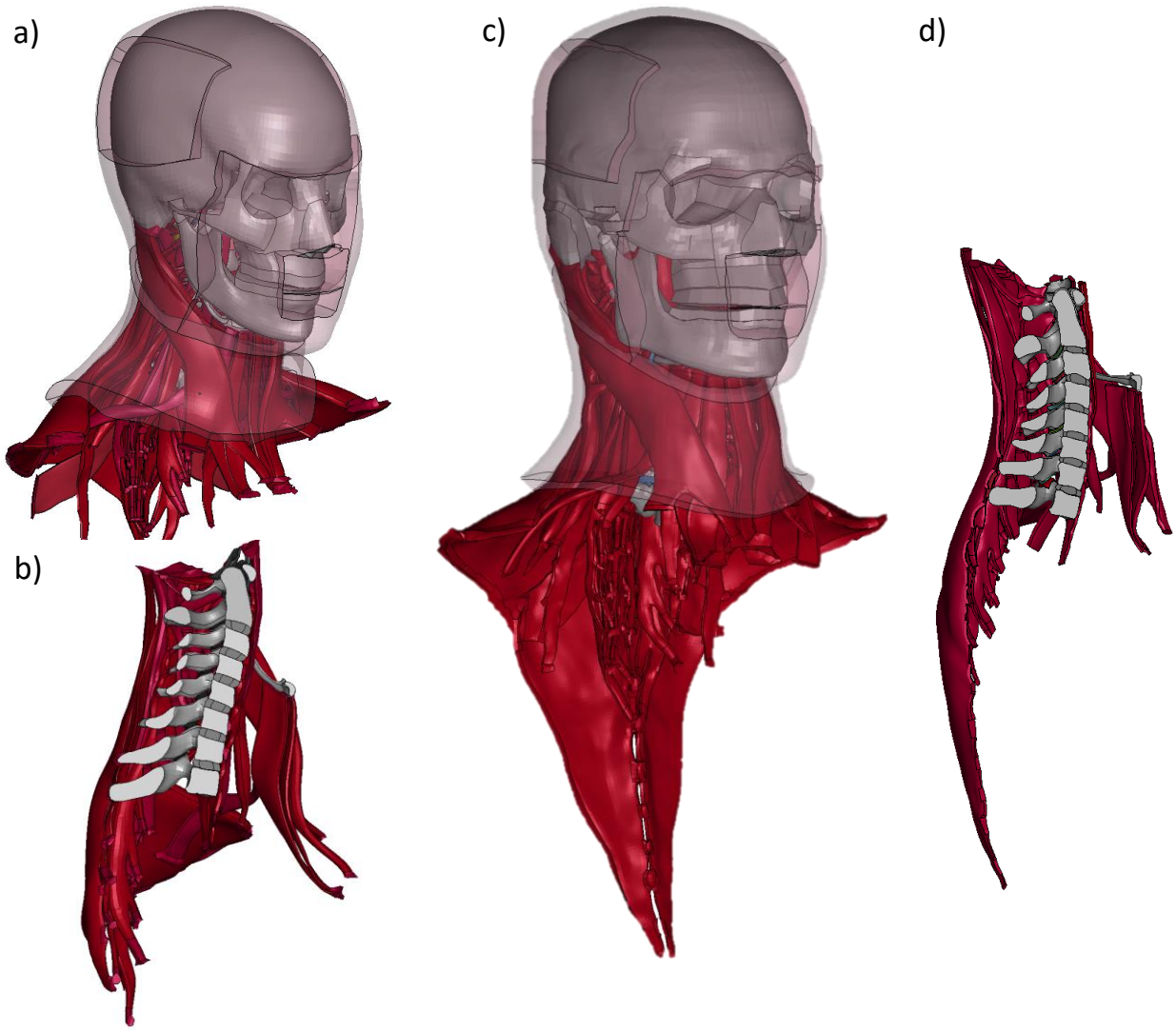

Figure 17: GHBMC neck models. a) F05 head and neck, b) F05 neck sagittal view, c) M50 head and neck, and d) M50 neck sagittal view. Cross-sections and orthogonal views not to scale.

The GHBMC M50 neck model has been previously validated (Barker et al., 2017; Barker and Cronin, 2020) at various levels (segment, ligamentous spine and full neck level), including approximately 60 validation cases under various loading modes. The validation cases will be described at the end of this section. The full GHBMC M50 head and neck model with skin and flesh includes 508,708 nodes and 293,264 elements (81,939 shells, 4402 beams, 206,684 solid) while the F05 has 423,246 nodes and 200,927 elements (35,232 shell, 4,206 beam, 161,489 solid). The neck model incorporates all structural

tissues with representative constitutive models and material properties, which are summarized in Table 4. Prediction of catastrophic failure related to crash induced injuries has been implemented in the GHBMC neck models in the form of element erosion for bone and ligament fracture and a contact algorithm with failure for the IVD avulsion. In addition to the catastrophic injury prediction in the GHBMC neck model, sub-catastrophic injury can be inferred by monitoring the distraction of the tissues associated with the pain response. Within the neck, capsular ligament (CL) distraction (Cavanaugh, 2006; Quinn and Winkelstein, 2007) and intervertebral disc (IVD) lesions have been associated with the potential for pain response (Curatolo et al., 2011; Yoganandan et al., 2001).

Table 4: GHBMC material models, mesh type, numerical implementation of the failure criteria and material properties references.

Material	Material model	Mesh	Failure criteria	Reference
Passive Muscles	Ogden Hyperelastic	Solid elements	NA	(Davis et al., 2003; Hedenstierna et al., 2008)
Active Muscle	Muscle	Axial elements		(Winters, 1995, 1990; Winters and Stark, 1988, 1985)
Flesh	Simplified Rubber/Foam	Solid elements		(Yamada, 1970)
Skin	Viscoelastic	Shell elements		
Cortical bone	Isotropic elastic plastic	Shell elements	Equivalent-plastic-strain-based element erosion	(McElhaney, 1966; Reilly et al., 1974)
Cancellous bone	Isotropic elastic-plastic	Solid elements		(Keaveny et al., 2001; Lindahl, 1976)
Vertebral body endplate	Isotropic elastic-plastic	Shell elements	NA	(Denozière and Ku, 2006; Panzer and Cronin, 2009)

Ligament	Non-linear tension-only strain-rate dependent	Axial elements	Displacement-based progressive element erosion	(Mattucci et al., 2012) (Mattucci and Cronin, 2015)
Facet cartilage	General viscoelastic	Solid elements	NA	(DiSilvestro and Suh, 2001)
IVD Nucleus	Fluid	Solid elements	Tied interface criterion based on critical stress	(Yang and Kish, 1988)
IVD annulus fibrosus ground substance	Hill foam	Solid elements		(Fujita et al., 1997) (Kasra et al., 2004)
IVD annulus fibrosus fibers	Orthotropic elastic Third-order polynomial	Shell elements five double-stacked layers	NA	(Ebara et al., 1996; Holzapfel et al., 2005; Skaggs et al., 1994)

With respect to the hard tissue, the vertebrae were represented by quadrilateral shell elements and hexahedral elements for the cortical bone and trabecular bone, respectively (Figure 18). Bone failure was included in both trabecular and cortical bone using element erosion based on an equivalent plastic strain (DeWit and Cronin, 2012). The capsular facet included hexahedral elements representing the capsular cartilage with a constant thickness.

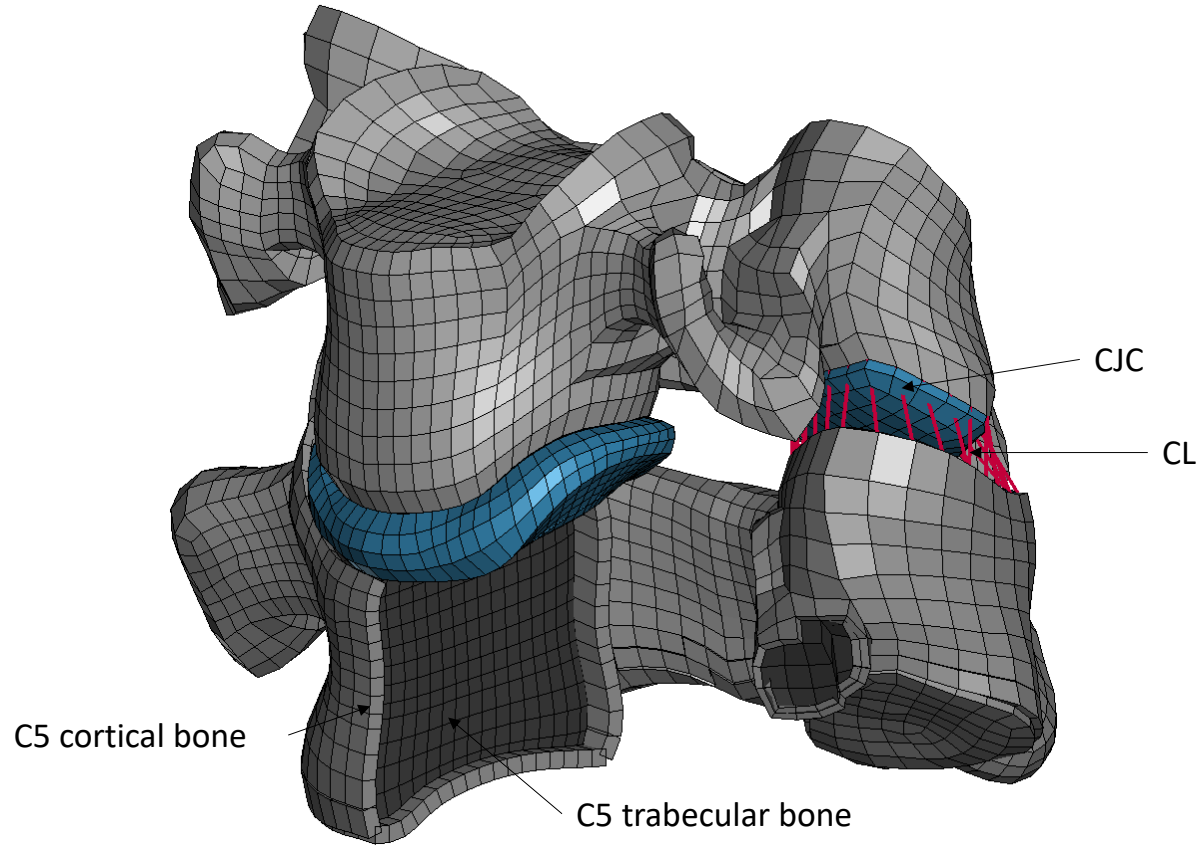

Figure 18: C45 motion segment model from the M50 neck model. Demonstrating the cortical and trabecular bone, capsular joint cartilage (CJC) and capsular ligament (CL).

The IVD annulus fibrosus (AF) was modelled as a set of concentric rings of quadrilateral shell elements and hexahedral elements to model the AF ground substance, and the nucleus pulposus (Figure 19). Disc avulsion was included in the model using a tied interface with failure at a critical stress (DeWit and Cronin, 2012).

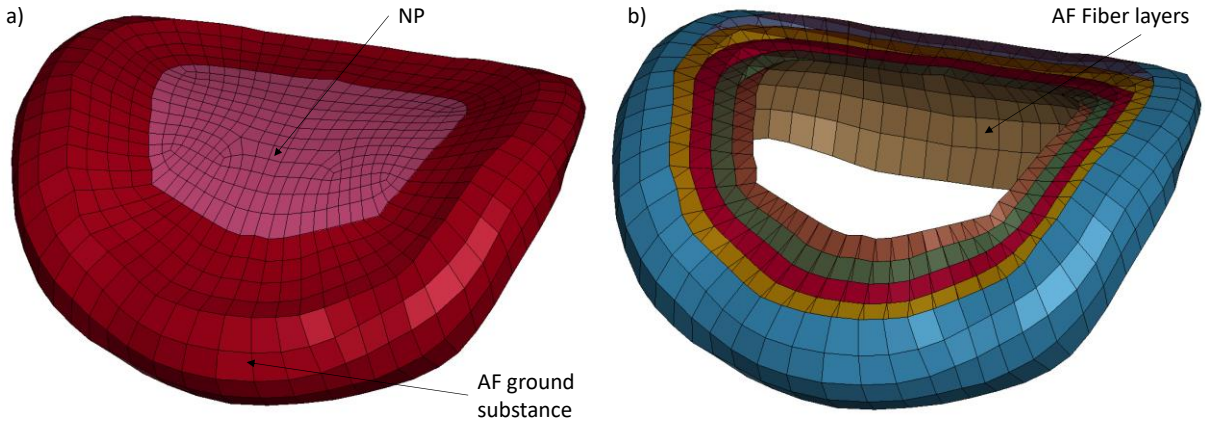

Figure 19: Intervertebral disc (IVD) of the segment C45 of the M50 model. The nucleus pulposus (NP) and annulus fibrosus (AF) ground substance was represented with solid elements, and the AF fibre layers were represented with shell elements.

The ligaments were represented with 1D uniaxial tension-only elements. Each ligament group was represented with a number of 1D uniaxial tension-only elements (ranging from 7 in the ALL to 28 in the CL) with a displacement-based failure criterion (DeWit and Cronin, 2012). Using multiple elements for the representation of the ligaments allowed for load distribution and enable the progressive failure observed in the experimental data (Mattucci et al., 2012). The ligaments in the LCS (Figure 20b) and UCS (Figure 20a) differed as per their anatomical description and were positioned based on available literature.

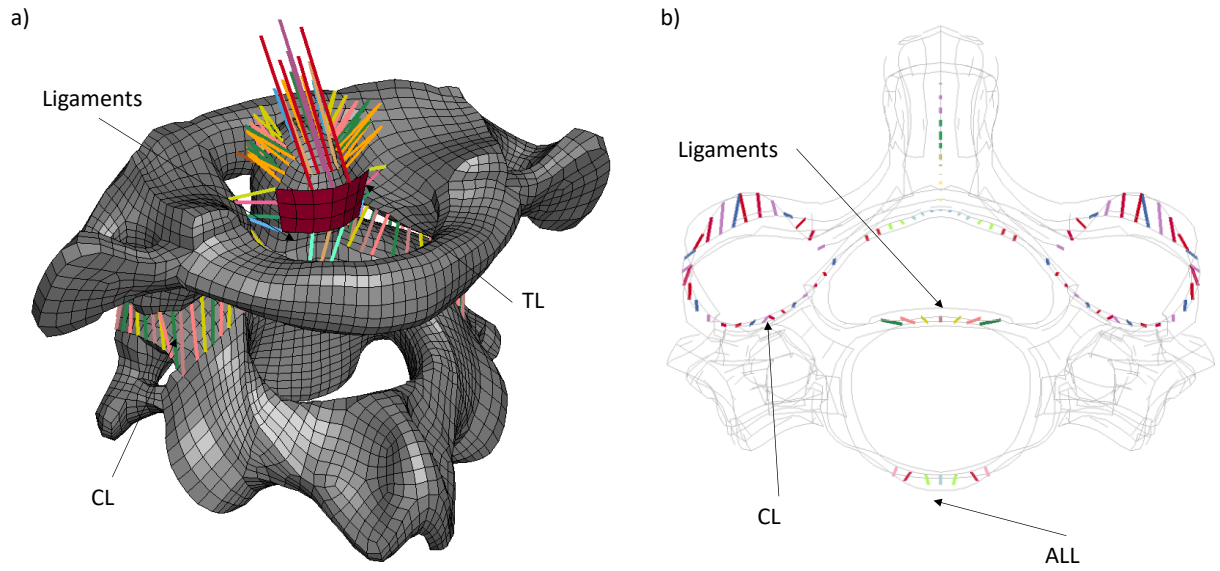

Figure 20: Ligaments in the a) isometric view of the upper cervical spine (UCS) and b) top view with edges only of segment C45 in the lower cervical spine (LCS).

In contrast with the previously described neck models (Östh et al., 2016; Panzer et al., 2011), the GHBMC model (Barker and Cronin, 2020) represents the passive muscles with hexahedral elements (Figure 21a) and the active muscles with hill-type beam elements (Figure 21b) using a hybrid approach. The active muscle representation is attached to the active muscle representation by node-sharing. Similarly, the active and passive muscles are attached to the bones through node-sharing. The activation strategy (Correia et al., 2020a) groups the muscles in flexors and extensors and was optimized for human volunteer data over a range of frontal impact severities (2g to 15g).

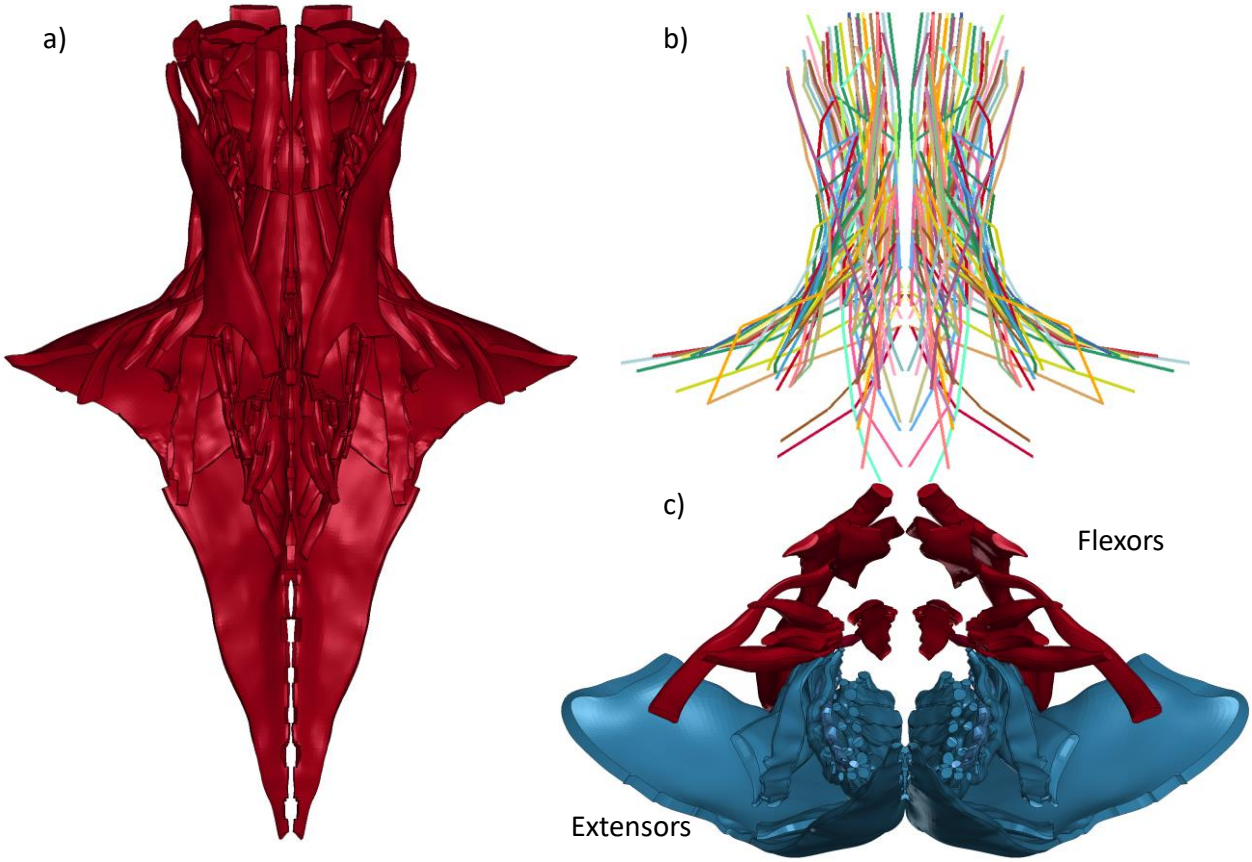

Figure 21: $M50_{26YO}$ neck muscles. a) Frontal view of the passive neck muscles, b) frontal view of the active neck muscles, and c) bottom view of the flexors (red) and extensors (blue) passive neck muscles.

The skin and adipose tissue are represented with quadrilateral shell elements and hexahedral elements, respectively (Figure 22).

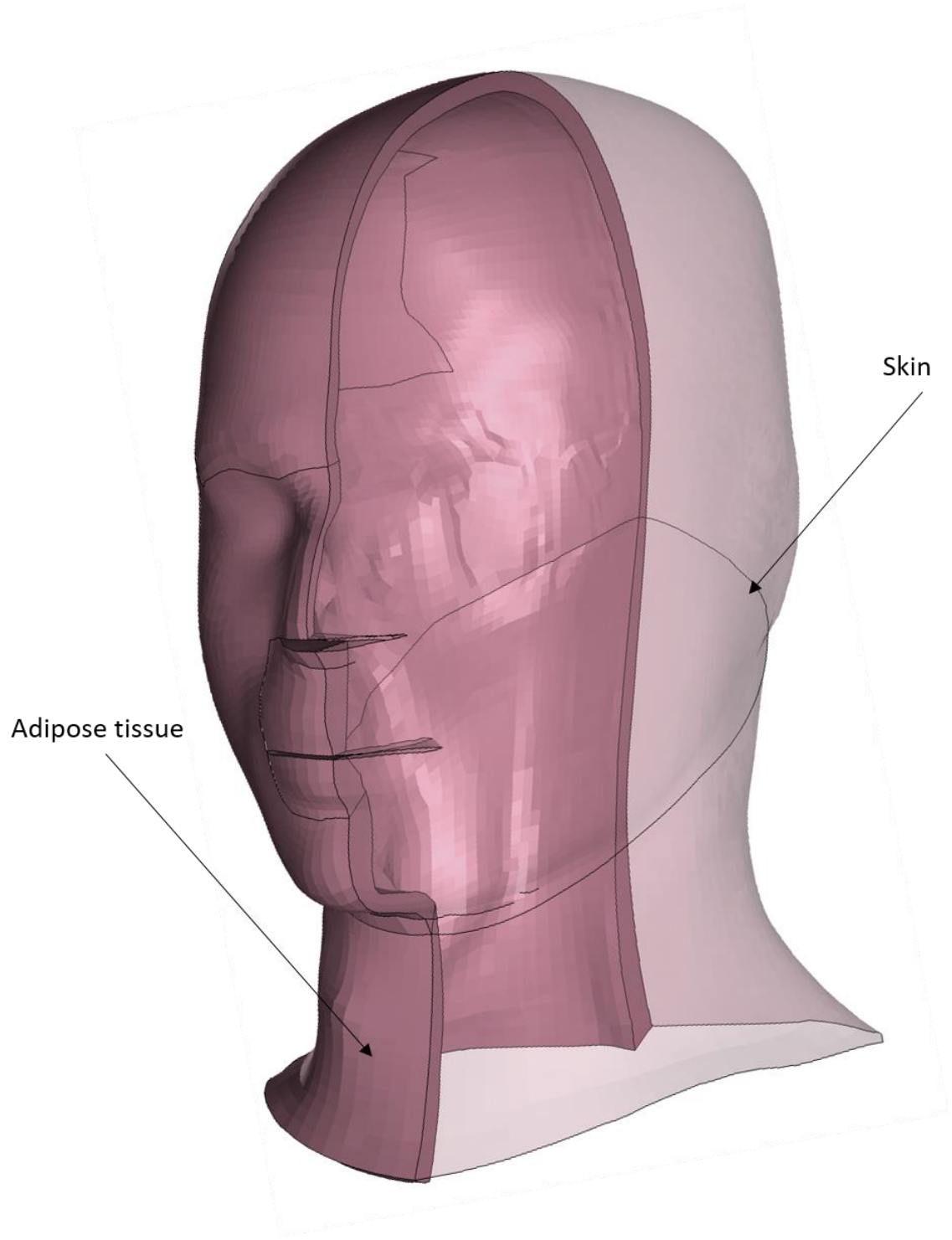

Figure 22: Adipose tissue represented with hexahedral elements (solid pink) and skin represented with shell elements (transparent pink).

Element quality in FE models is critical to minimize numerical error in the solution, where poor element quality can negatively affect the model response (Burkhart et al., 2013). High element quality refers to the 3D elements being cubes with equal lengths on all sides and 90-degree angles at all corners, and 2D elements being squares. Different element quality criteria exist to quantify the deviation of the elements from their ideal shapes, which are often used as rigorous thresholds for model development. The element aspect ratio describes how different the maximum length of an element is from the minimum length; for example, an aspect ratio of one means that the edges of the element are of the same length. The Jacobian describes the volume distortion of an element from the ideal shape (perfect cube) and is represented by the determinant of the Jacobian matrix, which defines the mapping of the element vertices of an ideal element (Jacobian of 1) to the element of interest (Knupp, 2002). Usually, a Jacobian greater than 0.3 for the majority of the elements (99% of the elements) is acceptable. A Jacobian lower than zero implies that the volume of an element is negative, which results in an error when assembling the model in most commercial FE solvers. Biological tissues exhibit rounded irregular shapes that are prone to generating poor mesh quality; therefore, significant efforts by the community of human body model developers aim towards developing meshing techniques that result in a high mesh quality. For the GHBMC neck models used in the present study, an aspect ratio of less than 6.0 for shells and 8.0 for solids and a Jacobian greater than 0.4 for shells and 0.3 for solids were used as element quality thresholds in the model development (Schwartz et al., 2015). In addition, a mesh resolution (mesh size) appropriate to describe the intended mechanical behaviour (Burkhart et al., 2013) and minimize numerical error is required.

2.4 Finite Element Model Verification and Validation

Finite element model verification is the process where the material models and numerical implementations of the numerous components of the model of interest are verified to behave as expected, given the underlying mathematical model and solution (Schwer, 2006). In addition, an essential step in the development of FE models is the validation of the model through objective comparison to independent experimental data. Independent experimental data is the data that has not been used to populate the constitutive model or numerical implementation in any way (Schwer, 2006). The cross-correlation and corridor methods (CORA, pdb, Germany) offer an objective way two compare the model response (comparison curve) to the experimental data (reference curve). The level of correlation is calculated as a value between 0 and 1, where 1 means perfect correlation and 0 means no correlation. The cross-correlation method is divided into three components (V, G and P). The V component compares the

shape of the curves, the G component compares the areas under each curve, and the P component describes the amount of shift applied to the comparison curve to obtain the highest rating. When the reference curve is coupled with corridors, often available in experimental data, the corridor method can be used to quantify the deviation of the comparison curve with respect to the experimental curves.

2.4.1 GHBMC Neck Model Verification and Validation

The GHBMC neck model has been verified at the tissue level; for example, individual tissues were verified against experimental testing (Barker et al., 2017). Single element simulations have been performed for each material implementation in the GHBMC neck models to confirm that the response is in agreement with the experimental data, including the hourglass controls and dapping coefficients commonly used to achieve model stability.

The validation cases of the GHBMC neck model can be described as hierarchical in nature. The smallest repeating structural unit is the motion segment. Therefore, the model has been validated at the segment level under quasi-static flexion, extension, lateral bending and axial rotation, and at dynamic rates in flexion and extension (Barker et al., 2017). The ligamentous spine was validated at the tissue level in rear impact (Barker and Cronin, 2020) using cadaveric data. At the full neck level, the model was validated using in a rear impact using cadaveric full neck experimental data; therefore, no muscle activation was included in this validation step (Barker and Cronin, 2020). In addition, in a frontal and lateral impact using volunteer data, with muscle activation included, the GHBMC neck model was validated using the cross-correlation and corridor method (Table 5) (Barker and Cronin, 2020; Correia et al., 2020).

Table 5: Validation cases summary

Level	Loading	Severity	Assessment level	Outcome
Full neck	Frontal	2 to 15g	Head kinematics	CORA Rating of 0.737
	Lateral	4 to 7g	Head kinematics	CORA Rating of 0.65
	Rear	7g	Head kinematics	CORA Rating of 0.76
Ligamentous spine	Frontal	8g	Ligament and IVD strain	Within one SD of the experimental response
	Rear	8g	Ligament and IVD strain	Within one SD of the experimental response
	Tension	Quasi-static	Ligament and IVD strain	Within one SD of the experimental response
	Axial rotation	Quasi-static	Ligament and IVD strain	Within one SD of the experimental response
Motion segment	Dynamic flexion	Up to failure	Resultant rotation	CORA Rating of 0.65
	Quasi-static flexion	Range of motion	Resultant rotation	CORA Rating of 0.82
	Dynamic extension	Up to failure	Resultant rotation	CORA Rating of 0.69
	Quasi-static extension	Range of motion	Resultant rotation	CORA Rating of 0.86
	Quasi-static lateral bending	Range of motion	Resultant rotation	Within one SD of the experimental response
	Quasi-static axial rotation	Range of motion	Resultant rotation	Higher than the experimental response

Specifically for the validation cases used in the present thesis, at the segment level, the segment models (Barker et al., 2017) were loaded in extension-flexion, lateral bending and axial rotation. The segment models were loaded by applying a rotational moment to the superior endplate of the superior vertebra while the inferior endplate of the inferior vertebra was fixed. The first layer of elements was modelled as rigid to mimic the fixture used in the experiments (Figure 23). The resultant angular displacement at the

superior endplate of the vertebra was monitored and compared to the experimental data (Camacho et al., 1997; Moroney et al., 1988; Nightingale et al., 2007a; Panjabi et al., 1991; Wheeldon et al., 2006).

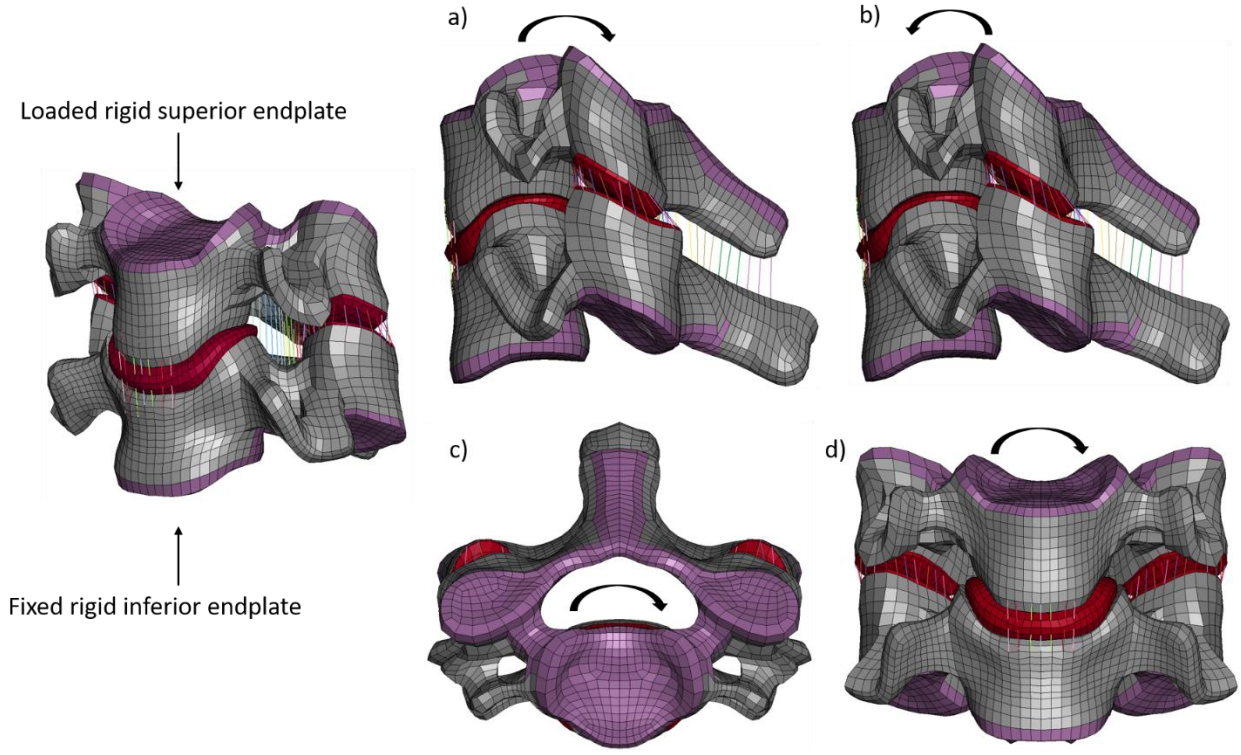

Figure 23: Motion segment validation cases; a) extension, b) flexion, c) axial rotation, and d) lateral bending.

At the full neck, and specific to the present study, the GHBMC model was validated against volunteer experimental data (Wismans et al., 1987; Wismans and Spenny, 1983) for frontal and lateral impact and cadaveric data (Deng et al., 2000) for the rear impact. The frontal and lateral impacts were modelled using experiments of living humans seated in a sled and subjected to acceleration pulses ranging from 2 g to 15 g. The reported T1 kinematics where applied to the T1 vertebra in the models, and the tendons at the inferior tips of the muscle ends and the last layer of flesh and skin were fixed to the T1 motion (Figure 24). Then, the head kinematics were monitored and compared to the experimental data using the cross-

correlation method.

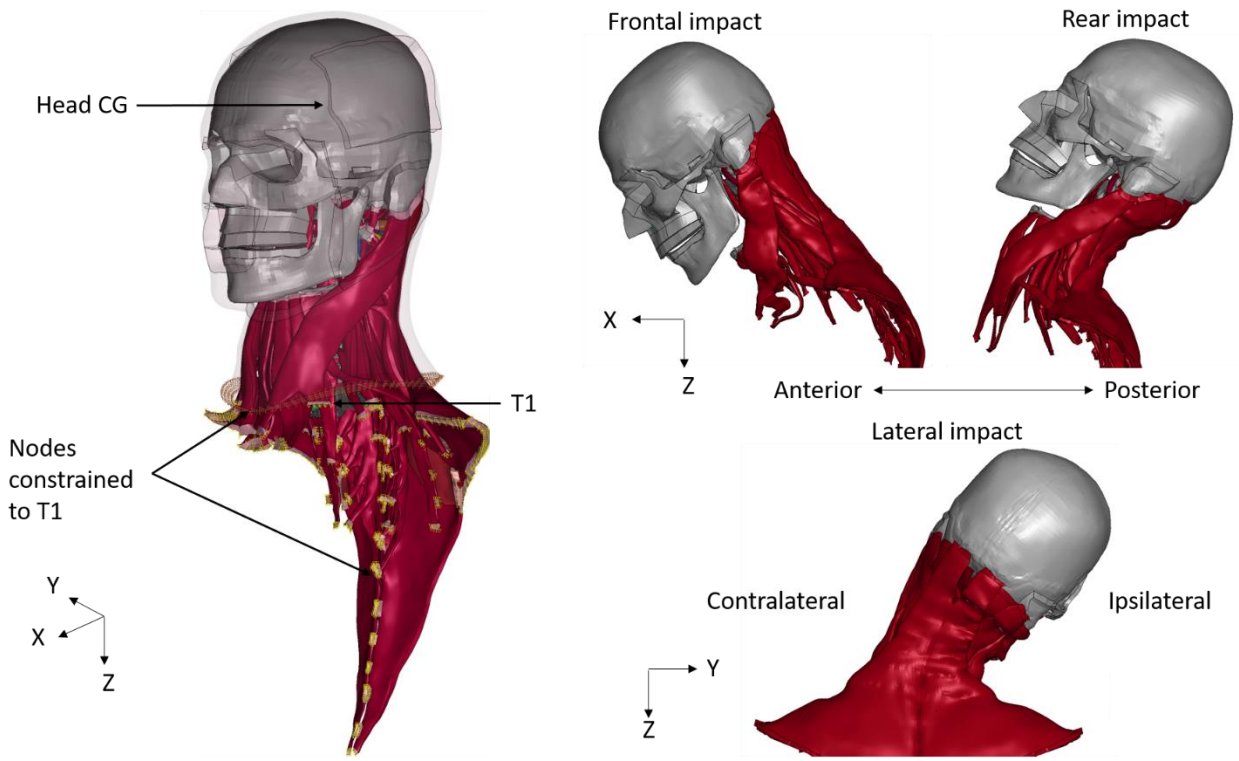

Figure 24: M50 full neck boundary conditions in frontal, rear and lateral impact scenarios.

2.4.2 Reposturing and Morphing Detailed Human Body Models

Human body models represent a specific subject or anthropometric group, usually in a seated or erect position. For example, the detailed GHBMC models used in this study represent a specific 26-year-old male subject and a 24-years-old female subject in a seated position. However, to study the effects of the postural changes associated with age (Reed and Jones, 2017), the models have to be modified (repostured) to represent their aged posture (cervical curvature) in a driving position. In simplified models with kinematic joints (Schwartz et al., 2015), it can be relatively straightforward to repostured the model while maintaining mesh quality, owing to the lack of complex mesh of the soft tissues. However, detailed models (Barker and Cronin, 2020) present challenges in terms of target definition and final mesh quality (Janak et al., 2018). There are several methods to modify detailed models; a FE simulation-based technique, referred as repositioning further on, can be used in the resultant stress-strain field is required (e.g. out of neutral posture), if the stress-strain field is not of interest, a morphing package can be used to

modify the nodal coordinates of the model, however, the target generation can be challenging to define and the interaction with the surrounding tissues can be difficult to describe. With both the repositioning and morphing approach, the mesh quality could be challenging to maintain in the modified model.

To study different anthropomorphic groups using the existing HBMs, researchers have developed morphing methodologies in custom codes (Zhang et al., 2017). In addition to postural changes, bone morphology variations have been investigated in parametric studies by morphing the hard tissue to the desired shape (John et al., 2019) using a commercial package. Boyle et al., 2019 studied the response of a simplified HBM in a reclined seat during frontal crashes using the morphing and reposturing method by Zhang et al., 2017. Hu et al., 2019 evaluated 100 different models incorporating variation in the ribcage, tibia, femur, and external body surface using the GHBMC simplified model (M50-OS v1.8.4) also using the method by Zhang et al., 2017. Using a morphing method, John et al., 2019 did a parametric study to investigate the relationship between vertebrae geometry (disk height, body depth, and global segmental size) and segmental kinematics in rear impact by morphing the vertebrae of a simplified head and neck model (John et al., 2017). The mesh quality before and after the morphing was not reported.

Recently, a light-simulation (computationally cheap while compromising accuracy) approach, without retaining the stress-strain state and no need to define targets for every node, has been developed and implemented towards human body model repositioning. This approach will be referred to as reposturing (new neutral posture) (Beillas and Berthet, 2017). The reposturing method has been implemented in the publicly available open source tool (PIPER, PIPER project, EU) (Janak et al., 2018) developed with the intent of merging the efforts of morphing and reposturing human body models amongst the academic and industrial community. PIPER is meant to link another open source tool (SOFA, National Institute for Research in Digital Science and Technology, France) focused on soft tissue simulation applicable to the medical field and FE models. Using PIPER, reposturing requires model-specific metadata, which is meant mainly to differentiate soft tissues from hard tissues and to define landmarks in the hard tissue entities. The landmarks, usually three per bone, served as targets for the reposturing process. Importantly, the reposturing approach has been coupled with mesh enhancement tools (Janak et al., 2018) that allow for the retention of the mesh quality of the HBMs.

Posture validation is a challenge when investigating the effect of biofidelic new postures; recent posture predictor tools (e.g. CSP and FBP) provide researchers with the required data to define biofidelic postures

to use as a target in the reposturing process. Maintaining mesh quality after the reposturing process at the soft tissue level can be challenging and is often not reported in detail in morphing studies (Hu et al., 2019). To address this challenge, under the PIPER framework, a set of mesh repair tools was developed in such a way that the output model can be repaired to have the same mesh quality as the input model if the metadata is well defined.

Chapter 3: Methods

With the aim of understanding the implications of an aged posture on the global kinematic and local tissue level responses of a 50th percentile male and a 5th percentile female, two models were developed. The first represented a 75-year-old (YO) mid-size male ($M50_{75YO}$), and the second representing a 75 YO small stature female ($F05_{75YO}$). The developed models were assessed in frontal, rear and lateral impacts, and the global kinematic response and local soft tissue response were compared to those of the young models.

3.1 Cartilage Geometry Enhancement and Young Model Validation

Prior to undertaking the study of the aged models, the literature review identified a limitation in the current young models with respect to the facet joint geometry. The facet joint geometry has been identified as a critical component that affects the motion segment kinematics (John et al., 2018). An accurate representation of the facet joint cartilage was considered important due to the potential effect in capsular ligament strain and cervical facet kinematics, which have been implicated as a potential source of pain in whiplash-associated disorders (WAD). In the original GHBMC models, the shape and thickness of the capsular joint cartilage were simplified such that the facet joint gap was overrepresented, leading to an inaccurate interaction at the interface of the adjacent vertebra. In the young baseline models (M50 v5.0 and F05 v5.0), the CJC geometry was idealized by an extrusion of the underlying facet hard tissue with a constant thickness (average of 0.7 mm) (Figure 25). To address this limitation, the geometry of the cervical joint cartilage (CJC) was updated to represent the maximum thickness and thickness distribution reported in the literature (Womack et al., 2008) for both M50 and F05 neck models. The models with the updated CJC geometry ($M50_{26YO}$ and $F05_{26YO}$) were subjected to the same validation cases to the baseline M50 and F05 models.

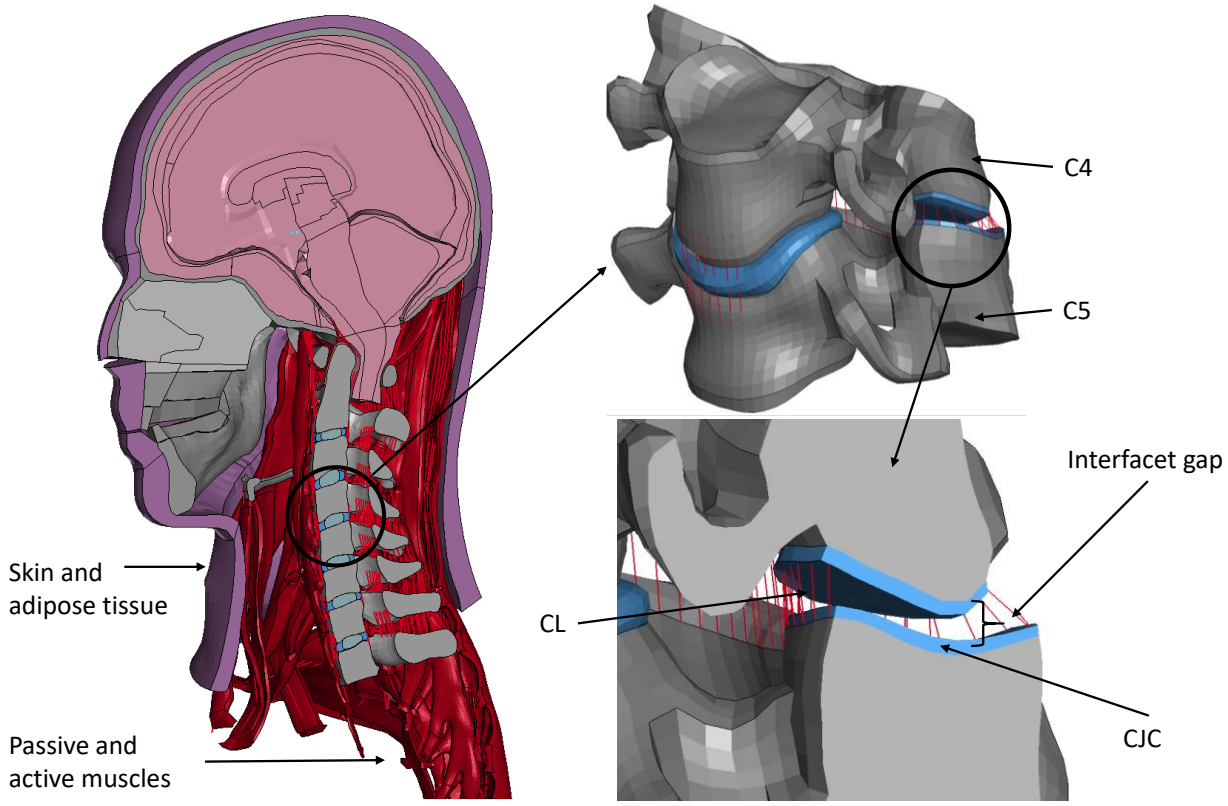

Figure 25: Capsular cartilage demonstrating constant thickness and the interfacet gap in the M50 model (C45 motion segment shown).

The constant cartilage thickness in the M50 and F05 neck models led to an average interfacet gap of 1.4 mm. A recent study (Womack et al., 2008) identified varying thicknesses of the CJC within the joint. Imaging data of post mortem human subjects (PMHS) suggests that the facet gap should be close to zero in the lower cervical spine (Farrell et al., 2015). In addition, facet pressure mapping studies suggest that an interfacet gap is formed in physiologic neck flexion (Jaumard et al., 2011).

Recent numerical studies with regards to the CJC shape suggested that the cartilage surfaces can play a substantial role in the mechanics of the neck (Womack et al., 2011). Importantly, the equation

$$t = t_{max}\left[\cos\left(\frac{\pi\frac{r}{r_p}}{2}\right)\right]^k \quad (1)$$

that describes the non-linear distribution of the CJC thickness, t, as a function of the maximum CJC thickness was developed. Where t_{max} is the maximum cartilage thickness measured, $\frac{r}{r_p}$ the location in the capsular facet, and k shape coefficient (Womack et al., 2008). The variables t_{max} and k were found independently for each cervical level (C2 to C7). It was found that the maximum CJC thickness was close to the geometrical centroid of the capsular facet with a gradual thinning moving towards the periphery (Womack et al., 2008).

To improve the biofidelity of the models at the tissue level, the cartilage surface of the capsular joint was enhanced to account for the distribution of the cartilage thickness observed in the human cervical spine (Figure 26).

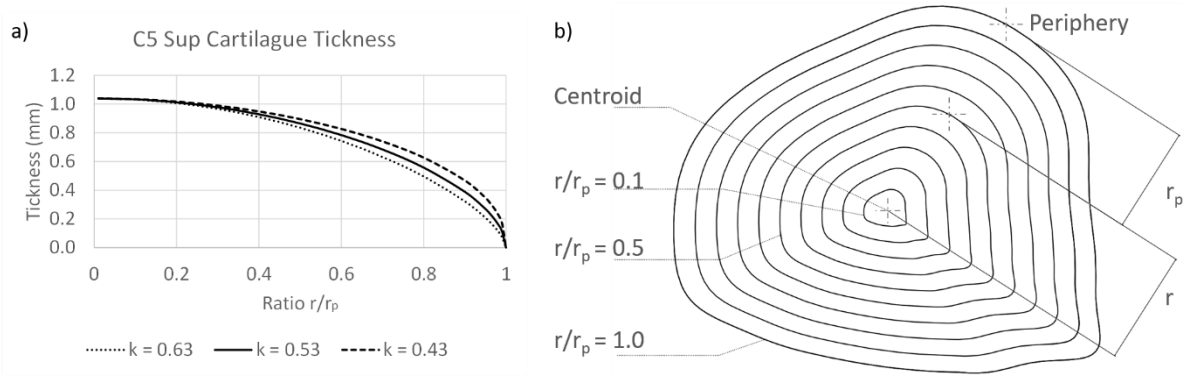

Figure 26: a) Exemplary C5 cartilage thickness (mm) profile normalized to the hard tissue surface with varying k values and b) top view of the superior C5 cartilage.

The non-linear function of the cartilage thickness normalized to the underlying hard tissue surface was defined in the literature (Equation 1). The equation was defined as a function of the ratio of the radius of the point of interest with respect to the centroid and the periphery (r/rp) where t is the thickness at the point of interest, t_{max} is the maximum thickness, r the radius to the centroid and rp the radius to the periphery. Hence, the updated surfaces of the capsular facets of the M50 and F05 models were constructed, and the centroid was calculated using commercial CAD software (CATIA V5, Dassault Systems, France). The cartilage thickness was defined in function of the facet surface and the location with respect to the centroid and periphery (r/rp). The maximum cartilage thickness and k values used per vertebra were taken from the literature (W. Womack et al., 2008) and summarized in table 6.

Table 6: Maximum cartilage thickness and k values used for the cartilage thickness definition.

	Superior cartilage		Inferior cartilage	
Level	k	t_{max} (mm)	k	t_{max} (mm)
C3	0.48	1.14	0.57	0.99
C4	0.58	1.13	0.50	1.05
C5	0.53	1.04	0.55	1.14
C6	0.44	0.97	0.47	0.94
C7	0.49	1.14	0.36	0.89

New surfaces that represent the cartilage thickness distribution in function of the hard tissue surface were generated using the calculated cartilage thickness and used to project the existing nodes of the capsular cartilage in the FE model. The cross-section of the final cartilage geometry is presented in table 7.

Table 7: Cross-sections of the cervical capsular joints in the original model (M50) and the updated CJC geometry ($M50_{26YO}$).

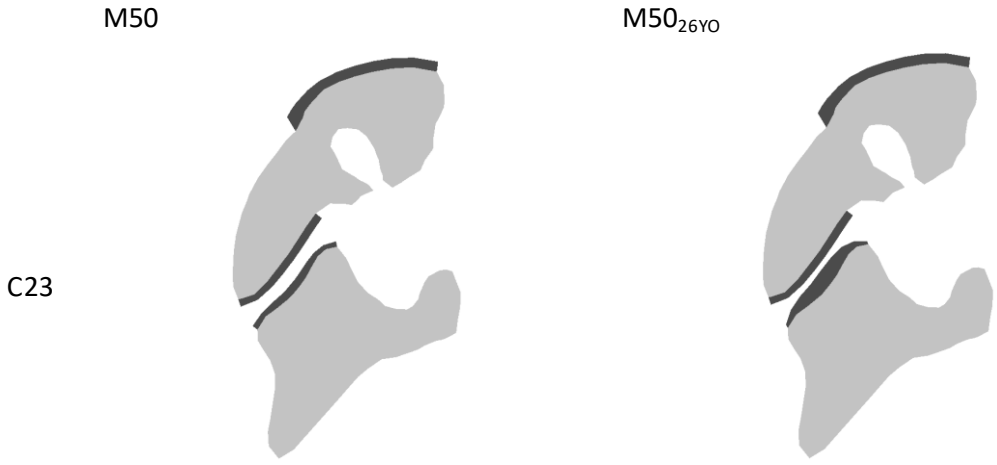

C34

C45

C56

C67

C7T1

The mesh quality of the enhanced cartilage was assessed and found to be within the common mesh quality requirements of the GHBMC models, including element warpage (<50 deg), aspect ratio (<8), skew (<70 deg), and Jacobian (>0.4).

3.1.1 Motion Segment and Whole Neck Validation of the GHBMC Neck Models with the Updated Cartilage Geometry

The original M50 neck model was previously validated at the full neck (Barker and Cronin, 2020) and the motion segment level (Barker et al., 2017) with the constant thickness cartilage. The neck model validation cases were repeated with the updated cartilage geometry ($M50_{26YO}$) at the segment (C2-C3 to C7-T1) (Barker et al., 2017) and the full neck level to assess the effect of this change on model performance (Barker and Cronin, 2020). The motion segment models were extracted from the full neck model with the updated CJC ($M50_{26YO}$) for evaluation in a quasi-static range of motion (extension, flexion, axial rotation, and lateral bending) and high dynamic rate up to failure in flexion and extension. The model response was then compared to the corresponding experimental data in a range of motion and traumatic loading (Camacho et al., 1997; Moroney et al., 1988; Nightingale et al., 2007; Panjabi et al., 2001; Wheeldon et al., 2006). The reduction of the interfacet gap leads to an increased segment stiffness in extension loading due to interaction of the facet surfaces. In contrast, minor effects in flexion, lateral bending and axial rotation were observed due to the modest interaction between the facet surfaces in those load cases when compared to the extension loading (Figure 27). The CORA ratings generally increased in dynamic and quasistatic flexion-extension loading (Table 8). The rest of the results of the segment level validation process can be found in Appendix 1.

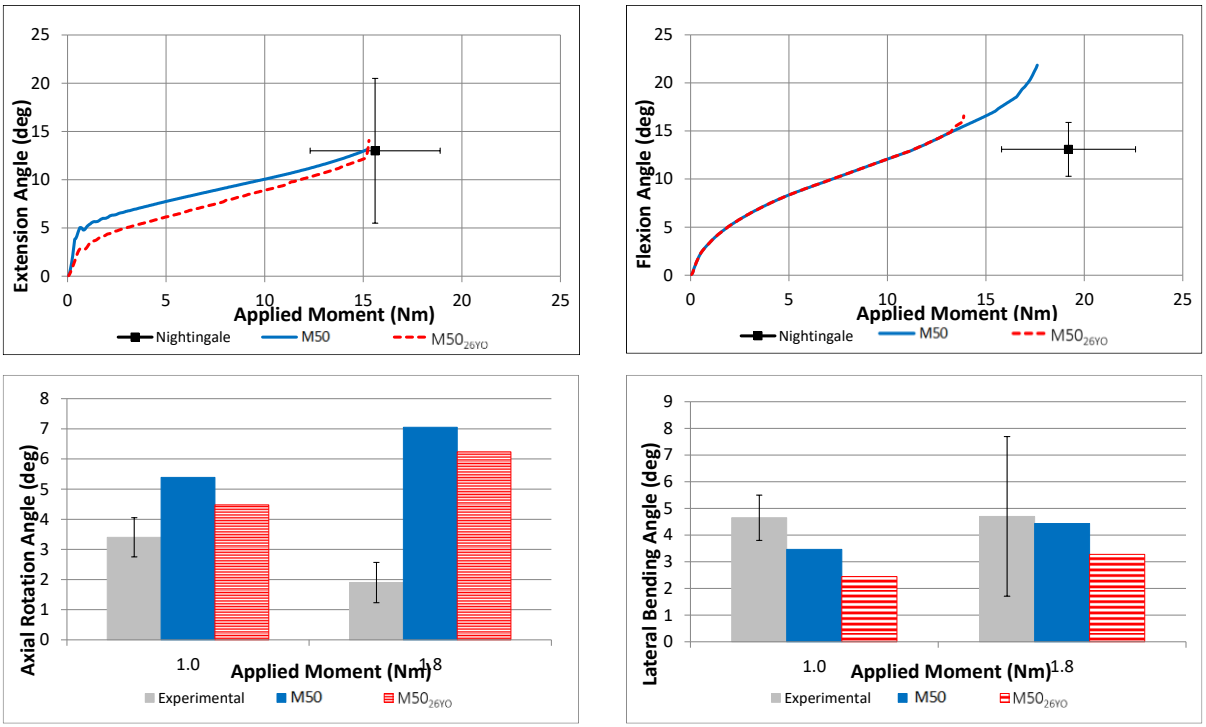

Figure 27: Segment level response of an exemplary segment C45 in traumatic extension and flexion (Nightingale et al., 2007a) and at a range of motion in axial rotation and lateral bending (Moroney et al., 1988; Panjabi et al., 2001).

Table 8: CORA ratings for the segment level validation of the updated cervical capsular joint cartilage in dynamic and quasistatic flexion and extension loading.

Segment level validation			CORA Rating		
Loading	Severity	Assessment level	M50	$M50_{26YO}$	% of difference
Dynamic flexion	Up to failure	Resultant rotation	0.57	0.56	-2%
Quasi-static flexion	Range of motion	Resultant rotation	0.59	0.65	10%

Dynamic extension	Up to failure	Resultant rotation	0.67	0.71	6%
Quasi-static extension	Range of motion	Resultant rotation	0.57	0.62	9%

The full neck models with the CJC enhancement ($M50_{26YO}$ and $F05_{26YO}$) were compared against volunteer experimental data in frontal and lateral impacts following previously reported methods (Barker and Cronin, 2020). Head CG kinematics of the $M50_{26YO}$ and $F05_{26YO}$ models were monitored and compared to the corresponding experimental data. CORA ratings were calculated to objectively assess the model performance against the experimental data and compared to the ratings obtained by the baseline M50 and F05.

At the full neck level, the cartilage update did not affect the head kinematics (Figure 25). The CORA ratings were 0.98 (strong similarity) on average with the lowest rating, 0.92, corresponding to the linear acceleration in the Z direction in the rear impact. The rest of the results of the full neck validation process can be found in Appendix 2.

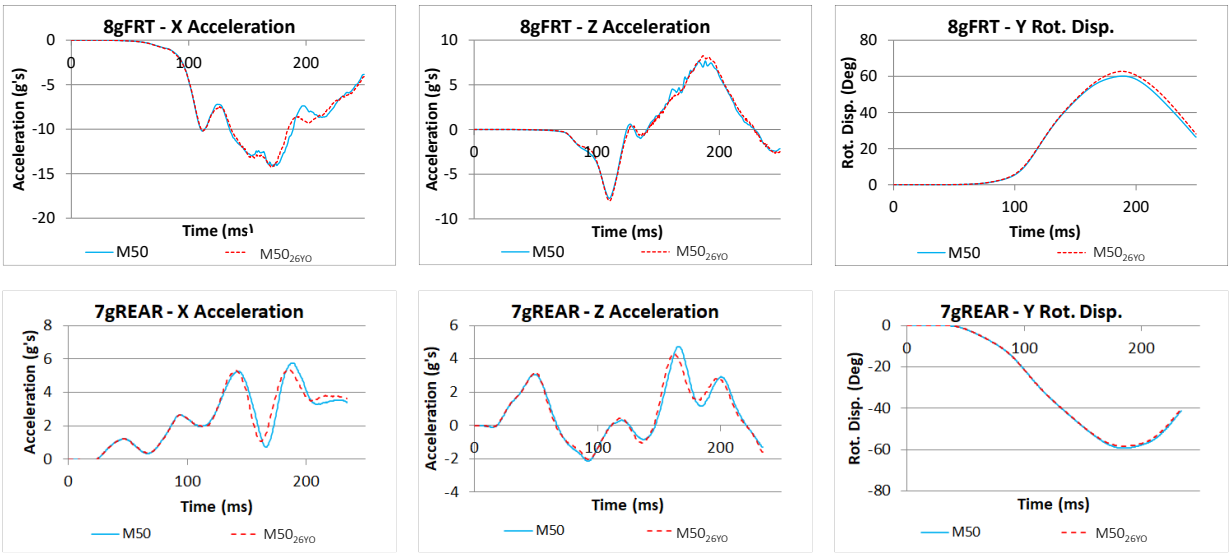

Figure 28: Head kinematics for and exemplary frontal (top) and rear (bottom) impact scenarios.

3.2 Reposturing and Morphing a Young Human Neck Finite Element Model to an Aged Posture

In the present study, a hybrid approach for reposturing the neck models was proposed, using both a CAD package and a reposturing tool. The PIPER reposturing tool (Beillas et al., 2015) allows the user to define the target posture based on a light simulation (Pre-Pos module) prior to the reposturing simulation (Fine-Pos); however, in the repositioning environment, there is no functionality that allows for a literature-based posture definition as no other database can be imported to the environment. Therefore, a CAD package was introduced to define the aged target posture. A CAD assembly representing the HBMs cervical spine where the literature that could be integrated with other literature data and used to define the new posture was developed. In addition to the reposturing process, the CAD assembly was used to compare the young posture to the literature data. Importantly, the CAD assembly enabled measurements that are challenging (e.g. facet angle) or not possible (e.g. Bezier angles) to retrieve in the reposturing tool or in a finite element pre-processing tool.

The posture and the facet angle of the young neck models with updated CJC ($M50_{26YO}$ and $F05_{26YO}$) were compared to the literature, and then, the geometrical targets for the aged models ($M50_{75YO}$ and $F05_{75YO}$) were subsequently defined in a CAD environment based on literature. The aged posture then would be imported to PIPER through landmarks, determining the position of the vertebrae and skull. Then, the reposturing simulation and mesh smoothing process inside PIPER was performed. Both the $M50_{26YO}$ and $F05_{26YO}$ models were repostured to account for the average change in posture associated with age and morphed to account for the morphological changes of the vertebrae associated with the ageing process resulting in the $M50_{75YO}$ and $F05_{75YO}$ models. The mesh quality was assessed using a post-processor package (Hypermesh, Altair Engineering Inc.) using the mesh quality requirements of the production model. The reposturing methodology is outlined in Figure 29.

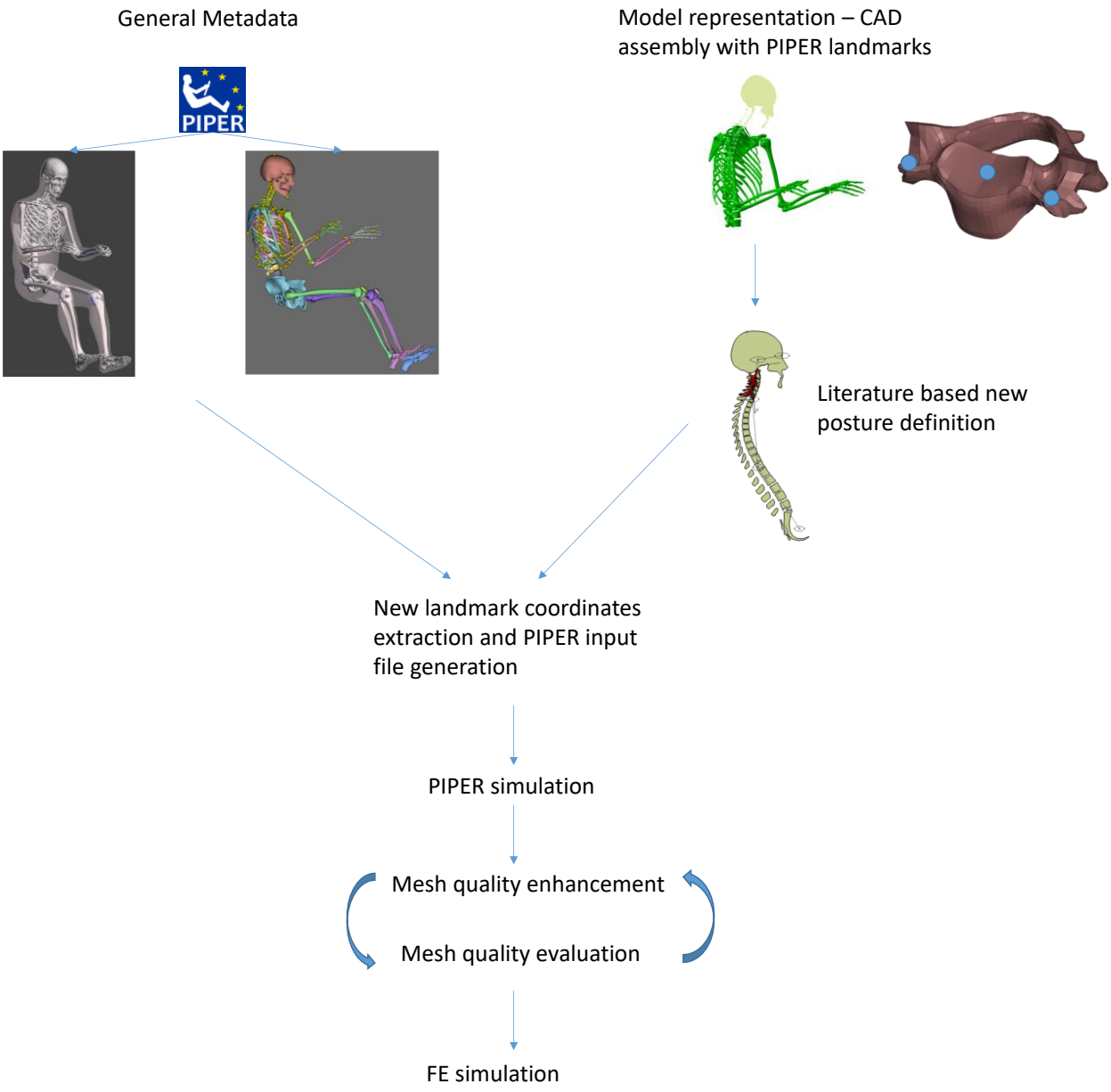

Figure 29: Reposturing methodology using a CAD software, PIPER, a finite element preprocessor and a script environment.

3.2.1 Geometric Description of Hard Tissue Positions Using CAD Software

A set of 3D CAD assemblies that represented the vertebrae of the $M50_{26YO}$ and $F05_{26YO}$ models were developed to compare the young posture reported in the literature with the posture of the $M50_{26YO}$ and $F05_{26YO}$ models. To develop the CAD assembly for each model, the midsagittal nodes were extracted from the FE neck models and imported into CATIA V5. The nodes were used to create splines to define a surface representing the sagittal plane of each vertebral body (Figure 30b) and the landmarks of the skull and vertebra that were used as targets for the reposturing (Figure 30c). The landmarks were selected based on commonly used skull and vertebrae landmarks. For the skull, the inferior corner of the eye cavity, the superior apex of the head, and the tragion were selected similar to other anthropometric studies (Park et al., 2016b; Reed and Jones, 2017). The tragion is a geometrical feature in the soft tissue of the ear close to the ear canal. However, there is no representation of the ear in the M50 or F05 models; therefore, the location of the tragion was estimated using bony structures. The zygon and the superior apex of the head where used as per superimposition studies relating skeletal geometrical features to external soft tissue geometrical features (Damas et al., 2020). An individual part (*.CATPart) was created for each vertebra and the skull. The individual vertebra and skull parts (Figure 30b) were imported into an assembly (*.CATProduct) (Figure 30a), where they could rotate and translate as rigid bodies.

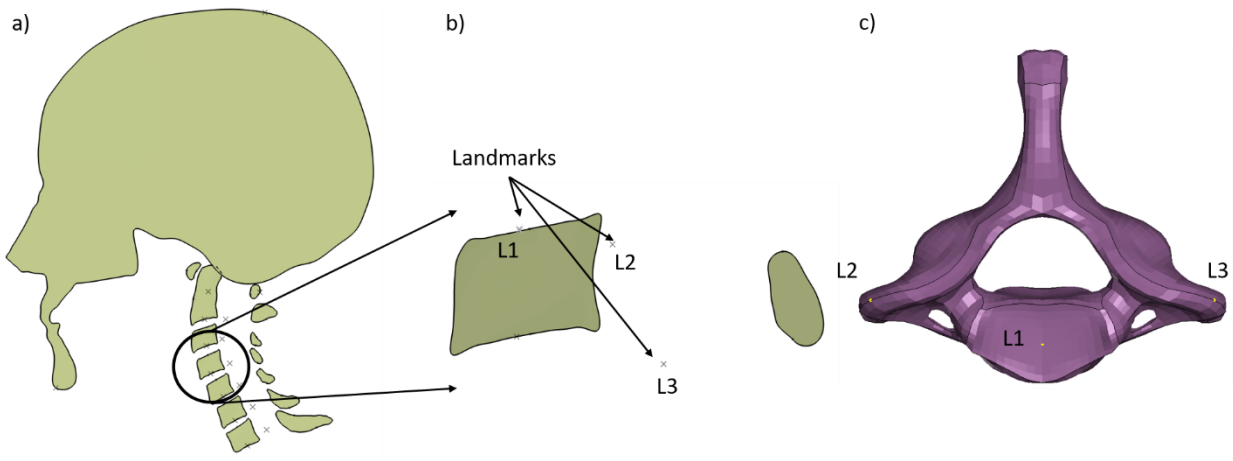

Figure 30: Exemplar $F05_{26YO}$ CAD assembly. a) CAD assembly, b) C4 vertebra sagittal plane representation including PIPER landmarks, and c) the corresponding location of the landmarks in the FE model that were used for the reposturing target. The same method was used in the $M50_{26YO}$ model.

3.2.2 $M50_{26YO}$ and $F05_{26YO}$ Model Postures Compared to Anthropometric Data

First, the posture of the $F05_{26YO}$ and $M50_{26YO}$ was compared to the literature (Park et al., 2016a; Reed and Jones, 2017) to identify if their posture was a representation of a 26 YO subjects of their respective anthropometrics. The posture of the $M50_{26YO}$ and $F05_{26YO}$ models were compared to the CSP using as inputs for the CSP the anthropometrics of each model ($M50_{26YO}$ and $F05_{26YO}$) (for the male 78 kg of weight, 174.9 cm in stature, and BMI of 25.7 and for the female, 48.1 kg of weight, 149.9 cm in stature, and BMI of 21.4); the CSP outputs the coordinates of the corners of the vertebral bodies, facet corners and spinous process corner with respect the superior corner of the first thoracic vertebra. For visualization purposes, a CATIA V5 VBA code was developed to create a surface that represented the vertebrae outline dimensions and locations in the sagittal plane, according to the CSP (Figure 30). The young male (78 kg of weight, 174.9 cm in stature, and BMI of 25.7) posture predicted by the CSP (CSP_M) and FBP (FBP_M) was compared with the posture of the $M50_{26YO}$ model. It was found that the neck middle chord length of the $M50_{26YO}$ model was higher by 10.8% and straighter (6.3% smaller inferior and superior Bezier angles) than the average of the population used to develop the CSP and FBP (Figure 31).

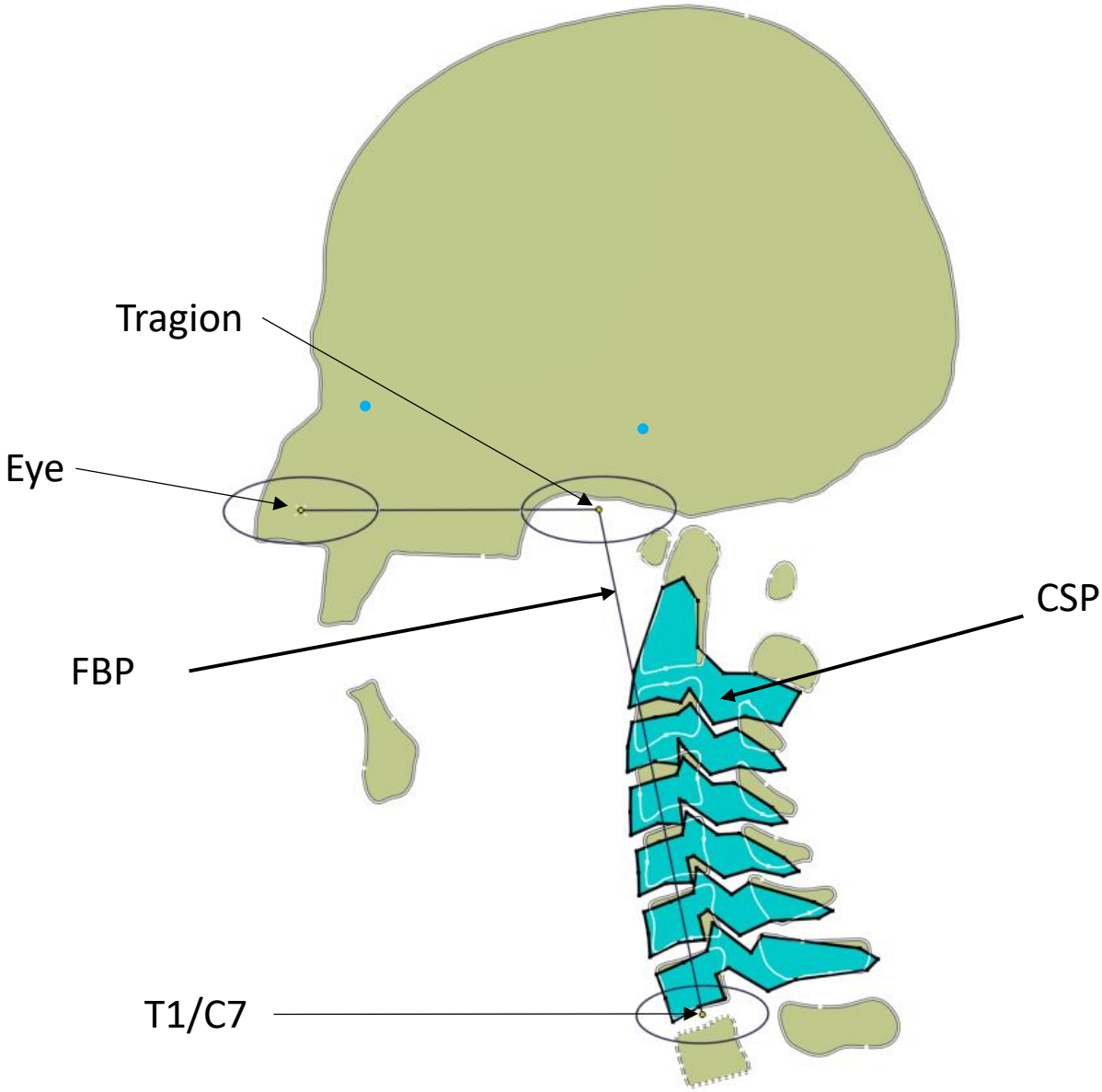

Figure 31: Comparison of the $M50_{26YO}$ (yellow surface) to the CSP_M (blue surface) (Reed and Jones, 2017) and FBP_M (black lines) (Park et al., 2016b). Model eye and tragion positions indicated by bright blue solid dots.

To be able to define an aged posture based on the young posture using the CSP, a representation of the $M50_{26YO}$ cervical spine using the CSP with 26 YO as one of the inputs was needed (CSP_{M26YO}). It was

found that increasing the stature in the CSP by 5.5% (183.6 cm stature) (CSP_{M26YO}) resulted in a neck length similar to the subject-specific M50 model matching the middle chord length of the $M50_{26YO}$ model. The stature in the CSP_{M26YO}, 183.6 cm, was below the stature range of a 95th percentile male (185.4 to 189.2 cm) and above the stature range of a 50th percentile male (172.7 to 177.8 cm). Both models, $M50_{26YO}$ and CSP_{M26YO}, were then compared to the full-body posture predictor (FBP_{M26YO}) by Park et al., 2016b, with a stature increased 5.5% and found to be within one standard deviation of the predicted posture (FBP_{M26YO}) (Figure 32). The process for the small stature female was similar to the male model. The young female posture of the CSP_{F26YO} and FBP_{F26YO} was overlaid with the $F05_{26YO}$ hard tissue positions in the CAD software and was found to be within one standard deviation of the FBP_{F26YO} predicted posture of a small stature female 0.3% smaller than the middle chord length predicted by the CSP_{F26YO}.

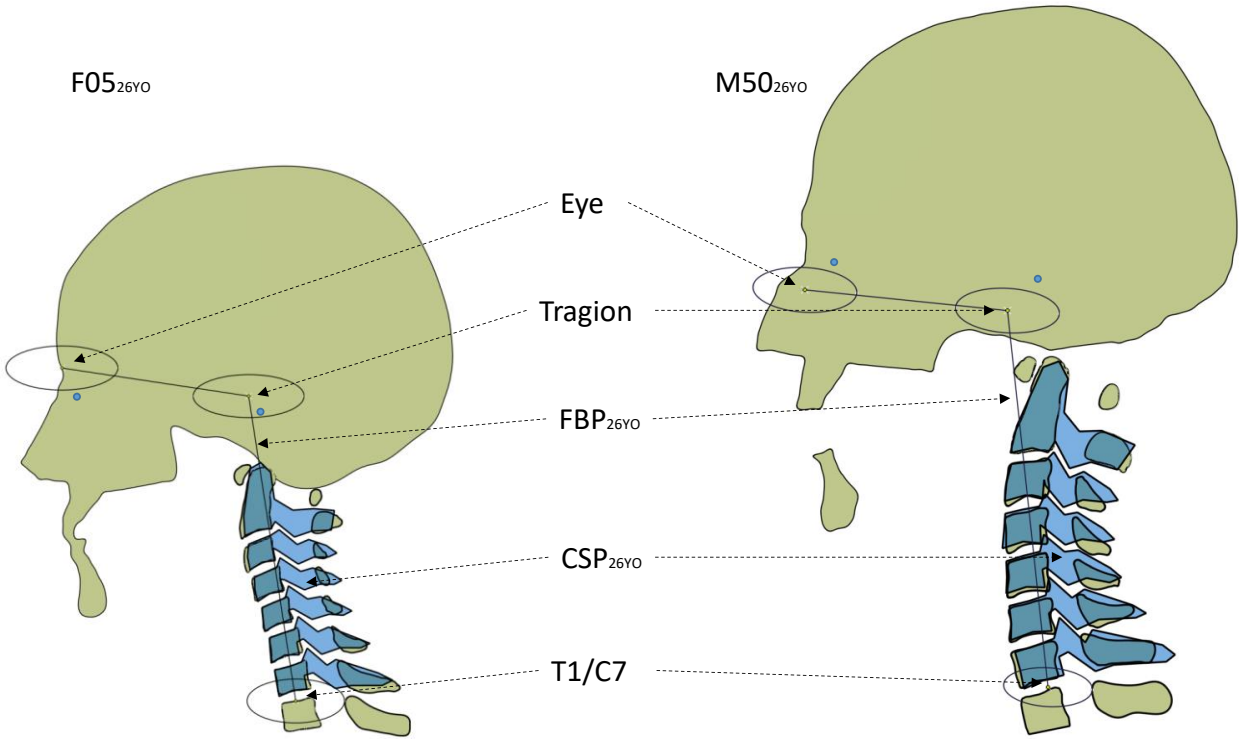

Figure 32: Comparison of the $F05_{26YO}$ and $M50_{26YO}$ with the CSP_{M26YO} (adjusted to match the $M50_{26YO}$ middle cord length), CSP_{F26YO}, FBP_{M26YO} and FBP_{F26YO}, respectively. Model eye and tragion positions indicated by bright blue solid dots.

3.2.3 Aged Posture Definition Based on Anthropometric Data

The aged posture was defined by increasing the age in the CSP (CSP_{M26YO} and CSP_{F26YO}) to 75 YO for both the male and female models, generally resulting in an increased lordosis in the spine (CSP_{M75YO} and CSP_{F75YO}), representing the an average curvature for the aged population. The increase in lordosis was higher for the $F05_{26YO}$ than for the $M50_{26YO}$. In the CAD assembly, the vertebrae were translated and rotated to match the at the superior corners of the CSP (CSP_{M75YO} and CSP_{F75YO}) vertebrae (Figure 33). The capsular facets were included in the CAD assembly and used to check for collision (surfaces intersecting each other) using the product collision tool (CATIA V5) prior to the PIPER simulation. With the increased lordosis, the facet surfaces of adjacent vertebra slide relative one to another, making it challenging to achieve a congruent vertebral position at all segment levels. In addition, checking for collisions prior to the PIPER simulation allowed to turn off the "bone collision" option in PIPER, improving stability during the reposturing process.

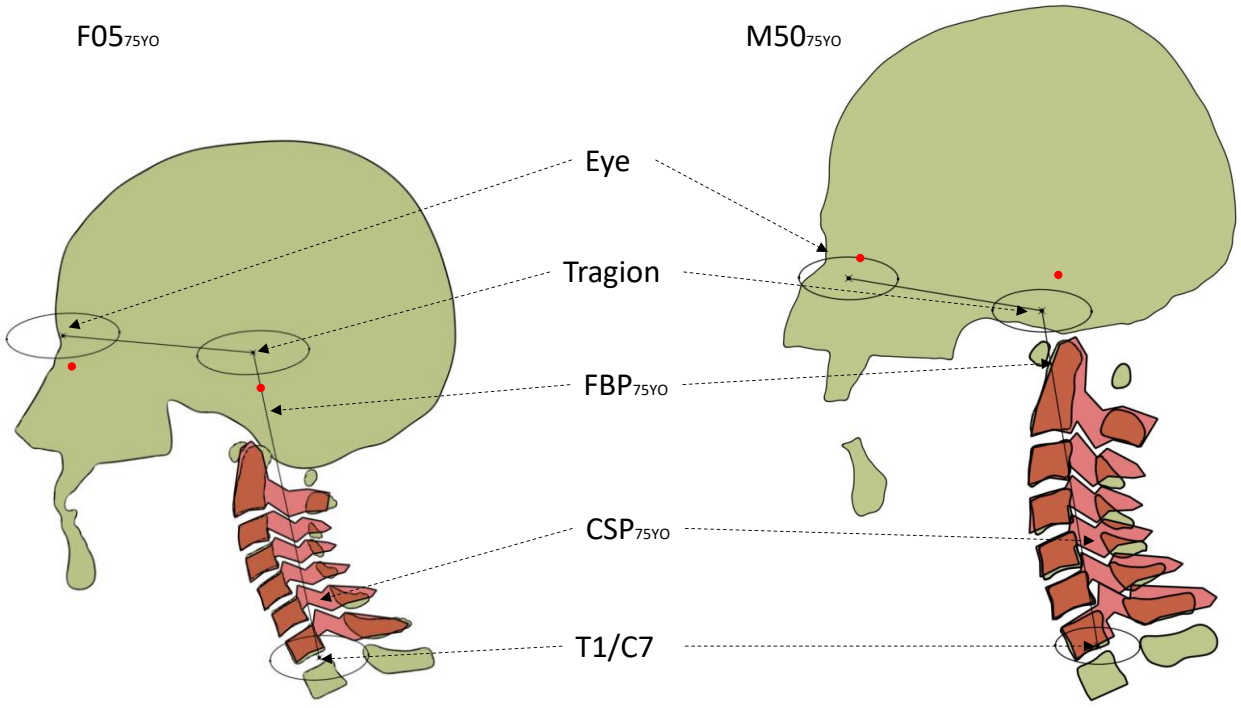

Figure 33: Comparison of the posture defined for the $F05_{75YO}$ and $M50_{75YO}$ to the CSP_{75YO} and the FBP_{75YO}. Model eye and tragion in solid red dots.

After the manual repositioning of the vertebrae in the CAD assembly, the landmarks needed for the PIPER reposturing were extracted as the target landmarks for the aged posture. Then, the input file for PIPER with the target coordinates was created. PIPER requires a full-body model to perform any reposturing process; hence, the model-specific PIPER metadata was developed in detail for the neck region, while a simplified definition was developed for the rest of the body for both female and male models. The detailed neck metadata includes three landmarks per hard tissue entity, that is, two at the transverse processes and one at the mid-point of the superior endplate for the vertebrae and one at the chin, one at the back and one at the top of the head for the skull (Figure 34). Shell envelopes with consistent normal directions pointing outwards were defined for each hard tissue and skin entity in PIPER, since inconsistent normal orientation would lead to an unstable reposturing simulation.

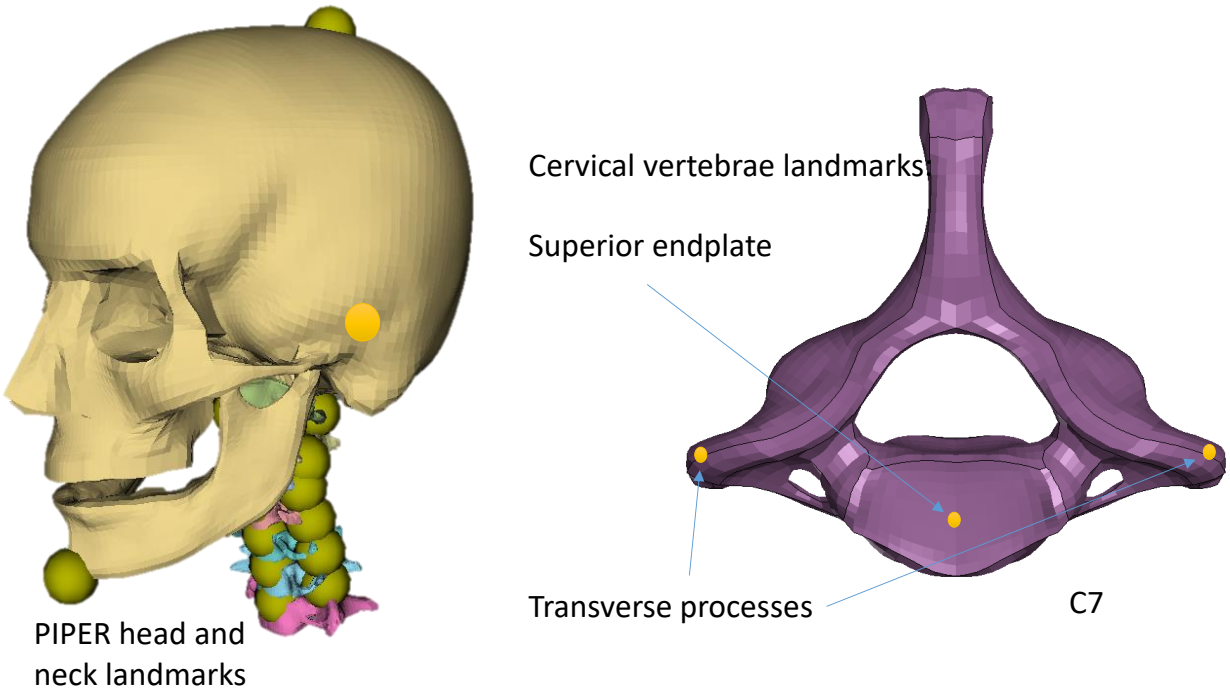

Figure 34: PIPER landmarks (yellow circles) used for the neck repositioning. Left: head and neck landmarks in the PIPER environment. Right: 7th cervical vertebra in a pre-processor environment with the landmarks used trough the cervical spine (C1 to C7).

3.2.4 Aged Posture Implementation – From Young to Aged Posture and Morphology

The models were repositioned in the Fine-Pos module within the PIPER software, with a time step of 1 ms with bone collision turned off to improve stability and reduce computation time. It was acceptable to ignore bone collision in the repositioning simulation since the posture definition in CAD was verified against capsular facet collision, and the path of the bony entities did not overlap during the repositioning. The final vertebral positions were achieved within 0.9 microns of the input targets defined using the CSP and, therefore, acceptable. It is worth noting that if the standard PIPER methodology of reposturing (defining the posture in the Pre-Pos module and reposturing in the Fine-Pos module) was used, the output posture could lead to positional differences greater than one millimetre, causing instabilities in the reposturing simulation and bone interpenetration.

Immediately after reposturing the hard tissues, it was found that 23% of the soft tissue elements violated the mesh quality requirements for the GHBMC models; hence, the PIPER smoothing tools were used to smooth the soft tissue meshes separately, following the repositioning. The model was segmented into three groups, which exhibited similar mesh quality issues. That is, passive musculature (negative jacobian), tendons (warpage angle), and intervertebral discs (penetration with the adjacent vertebral bodies and warpage angle). The mesh smoothing required multiple iterations using the "moving average," "kringing interpolation," and "smooth surface" tools inside the PIPER environment. The repostured and smoothed models were imported into a pre-processor (Hypermesh, Altair Engineering Inc.) to check the minimum warpage angle, Jacobian and aspect ratio. If the mesh quality was found outside the thresholds, another smoothing iteration was performed. The final smoothed model met the GHBMC mesh quality requirements (less than 0.99% of the elements violating the thresholds), as was the case for the original GHBMC models.

3.2.5 Facet Angle Morphing

Following the reposturing of the $M50_{26YO}$ and $F05_{26YO}$ models, morphological changes associated with age in the hard tissue were investigated. Specifically, the facet joint angle was quantified in the $M50_{26YO}$ and $F05_{26YO}$ models, and a target facet angle correspondent to an aged subject was defined based on literature data (Parenteau et al., 2014) due to the importance of the facet joints to the capsular ligament deformation and facet joint kinematics (John et al., 2018). Then, the facet angle was modified to account for the increased facet angle associated with age in both male and female models (Figure 35). The previously described cartilage geometry was used with no modifications as the facet surface itself was not modified.

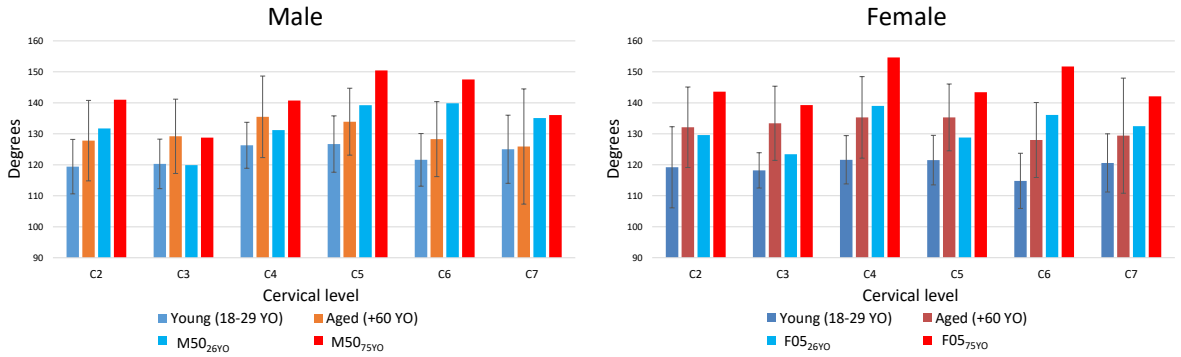

Figure 35: Literature facet joint angle of young and aged population (Parenteau et al., 2014) and the F05$_{26YO}$, F05$_{75YO}$, M50$_{26YO}$, and M50$_{75YO}$ models.

Firstly, the facet angle of each young vertebra, within each model, was measured on a local XY plane (Figure 36) through the centroid of the facet projected to the sagittal plane to be coincident with the middle plane of the vertebral bodies (Figure 36), similar to the method used to measure the facet angle in the literature. The facet angle of the M50$_{26YO}$ was within one standard deviation of the anthropometric data in the C3, C4, and C7 vertebrae and outside for the other segments. Similarly, the F05$_{26YO}$ model was within one standard deviation of the anthropometric data only in the C2, C3, and C4 vertebrae.

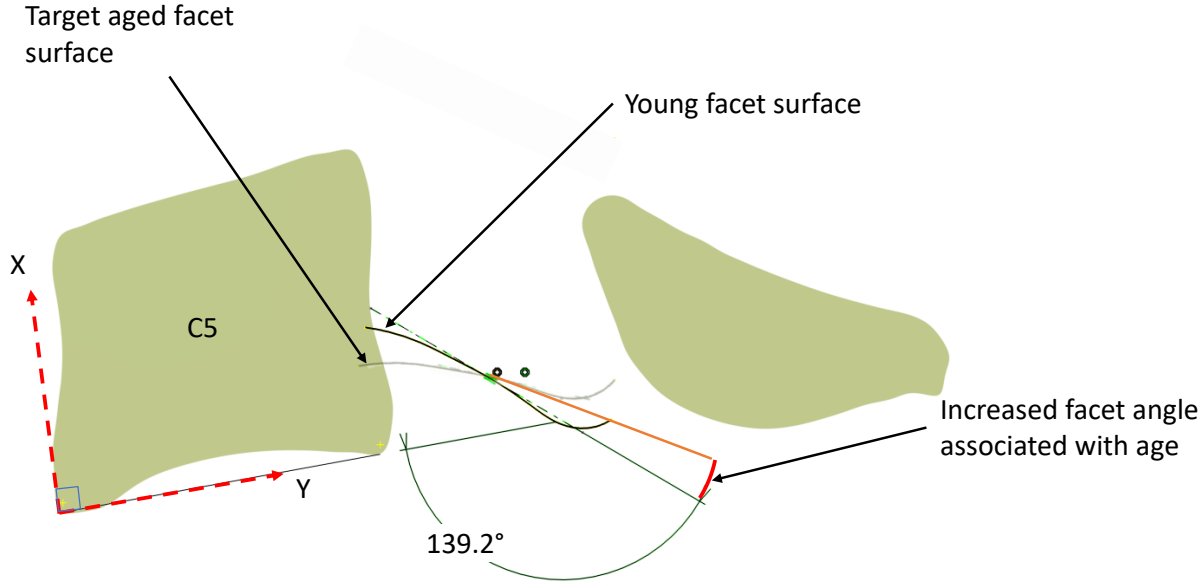

Figure 36: Exemplar fifth cervical vertebra (C5) of the $M50_{26YO}$ model. Measurement of the facet angle.

The target aged facet angle to be applied to the $M50_{75YO}$ and $F05_{75YO}$ models was calculated by applying the percentage of change reported in the literature (Parenteau et al., 2014) to each cervical level (Figure 35) to the $M50_{26YO}$ and $F05_{26YO}$ models. The vertebrae that had a facet angle outside one standard deviation from the anthropometric data in the young models were also outside one standard deviation for the aged models and within two standard deviations. The facet pillars were morphed using the Fine-Pos PIPER module using the capsular cartilage as the control solid for the transformation. Hard tissue properties (rigid bodies) were assigned to the facet cartilage elements, while soft tissue properties were assigned to the capsular pillars. Then, the cartilage was rotated as a whole to the required aged facet angle. The resulting model had poor element aspect ratios in the facet pillars, and the tetrahedral elements representing the tendons were inverted (negative jacobian). To address this, the facet pillars and surrounding soft tissues were smoothed using the PIPER smoothing tools. The final models meet the mesh quality requirements.

3.3 FE Neck Model Load Cases and Assessment

Four neck models were assessed in this study: $M50_{26YO}$, $F05_{26YO}$, $M50_{75YO}$ and $F05_{75YO}$. The neck models were evaluated under 2g to 15g frontal impact loading, 7g to 4g lateral and 7g rear. The hard tissue failure implementation in the model was based on plastic strain; therefore, the vertebrae was modelled as a deformable solid despite of the relatively small strain expected when compared to the sift tissue. Ligament failure was included as element erosion based maximum tensile deformation and IVD avulsion as tiebreak contact based on maximum shear and normal stress.

Head kinematics were monitored considering the main relevant axis for each loading condition; for the frontal and rear impacts, the X and Y linear accelerations and the Y rotational acceleration were included. For the lateral impacts, the Y and Z linear accelerations and the X rotational acceleration were included.

In addition to head kinematics, the soft tissue responses were monitored. The CL distraction and the change in the IVD space were tracked during the simulations and expressed as nominal strains. In the frontal and rear impact conditions, the CL nominal strain was measured as the change in length of a CL

beam element in the anterior aspect, and one CL beam in the posterior aspect of the capsular facet (Location A and B in Figure 37) divided over the anatomical length. Similarly, the IVD space nominal strain was measured as the change in length of the IVD space in the most anterior and posterior aspects of adjacent vertebral bodies (Location C and D Figure 37).

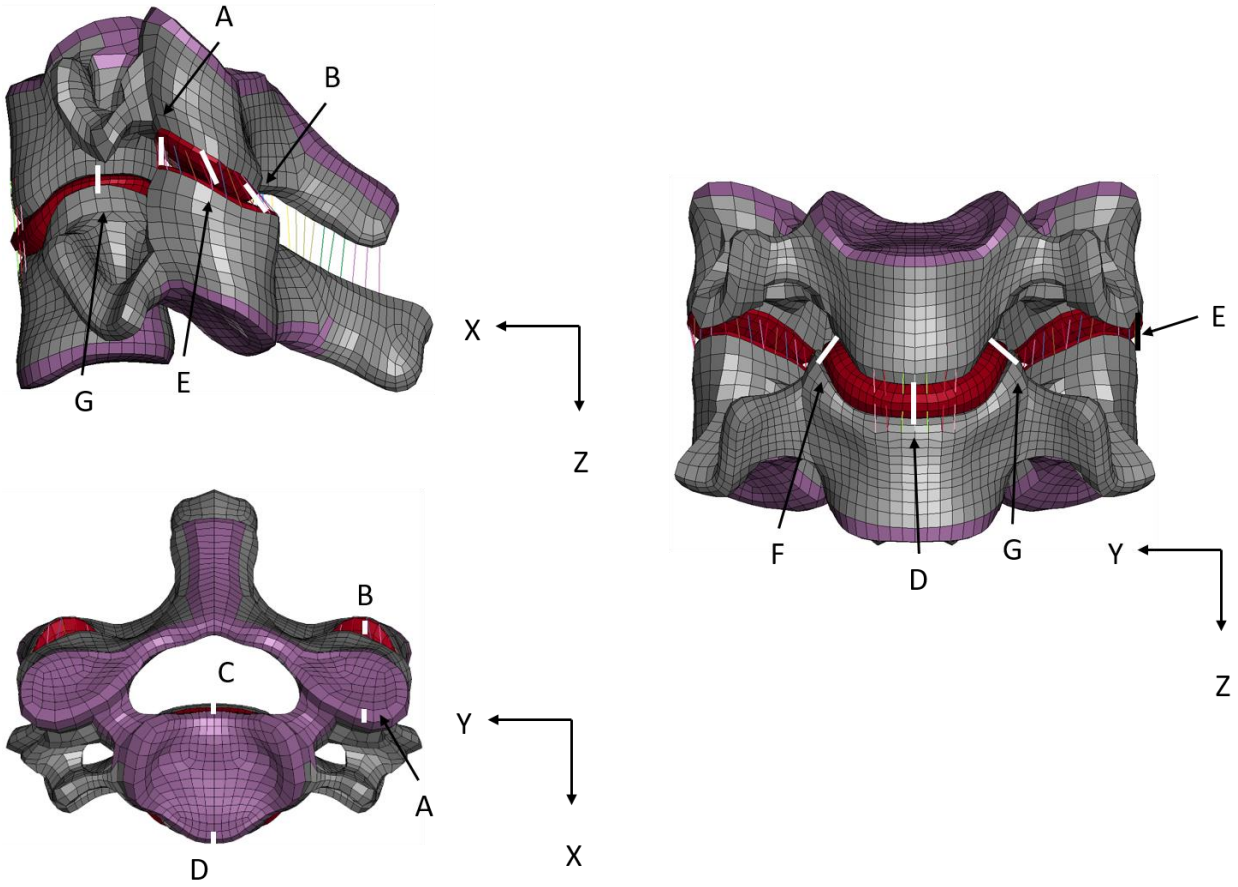

Figure 37: Measurement of the CL and IVD space strain. Location A: Anterior aspect of the capsular facet used to calculate the CL strain in a rear impact. Location B: Posterior aspect of the capsular facet used to calculate the CL strain in the frontal impact. Location C: Posterior IVD used for the IVD space strain in the frontal impact. Location D: Anterior IVD location used for IVD space strain in the rear impact. Location E: Contralateral aspect of the capsular facet was used to calculate the CL strain in the lateral impacts. Location F: Ipsilateral IVD location was used to measure the IVD space strain in the lateral impact. Location G: Contralateral IVD location was used to measure the IVD space strain in the lateral impacts.

The soft tissue responses, measured as strain, have been assessed at different levels. First, the maximum values of the CL strain were averaged across all impact severities (2 to 15g in frontal and 4g to 7g in lateral) and segment levels (C23 to C45 in frontal, lateral and rear). Similarly, the maximum values of IVD space strain have been averaged across the impact severities and segment levels in frontal and lateral, while in the rear impact, an average of all segment levels will be presented. Then, the average results of the aged models ($M50_{75YO}$ and $F05_{75YO}$) were compared against those of the young models ($M50_{26YO}$ and $F05_{26YO}$). Finally, the soft tissue results at individual levels and impact severities will be presented.

Chapter 4: Results

In this chapter, a comparison of the geometry of the young ($M50_{26YO}$ and $F05_{26YO}$) models to the aged ($M50_{75YO}$ and $F05_{75YO}$) models is presented. Critical to model performance and validation is achieving a high level of mesh quality, so this was checked for each model. The results of the finite element simulations (frontal 2g to 15g, lateral 4g to 7g, and rear 7g impacts) are presented for the male models ($M50_{26YO}$ and $M50_{75YO}$) and then female models ($F05_{26YO}$ and $F05_{75YO}$) to investigate changes in neck posture with ageing. Lastly, the effects of an aged posture are compared between the male and female models.

4.1 Finite Element Mesh Quality and Geometry of the Aged Neck Models

The mesh quality of the aged neck models ($M50_{75YO}$ and $F05_{75YO}$) was evaluated using a commercial finite element post-processor. The mesh quality was found to be within the acceptable thresholds of the commercial GHBMC detailed model family (Corrales and Cronin, 2019). The thresholds include no more than 1% of the elements having an aspect ratio greater than 8, and 100% of the elements having a Jacobian smaller than 0.3.

The repositioned locations of the vertebrae were within 0.01 mm of the target aged posture (Section 3.2). The increased lordosis associated with age led to an increased inferior and superior Bezier angles in both the male and female models (Figure 38). The increase in lordosis was evident in the female model with a 551% higher inferior Bezier angle (from 2.2° for the young to 14.3° for the aged) and 43% higher superior Bezier angle (from 15° for the young to 21.3° for the aged) when compared to the male model (204% for the inferior Bezier angle and 51% for the superior Bezier angle).

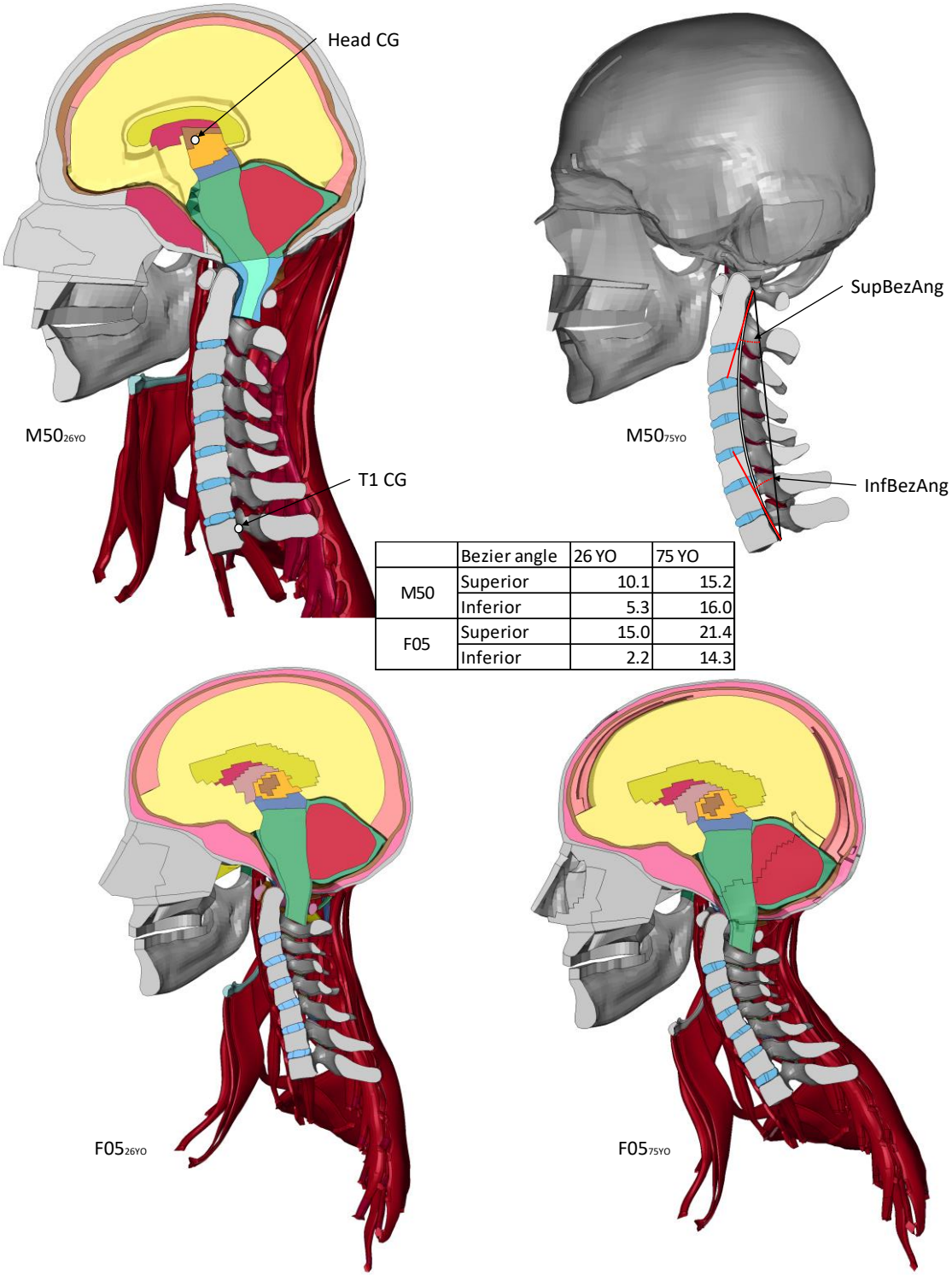

	Bezier angle	26 YO	75 YO
M50	Superior	10.1	15.2
	Inferior	5.3	16.0
F05	Superior	15.0	21.4
	Inferior	2.2	14.3

Figure 38: F05$_{26YO}$, M50$_{26YO}$, F05$_{75YO}$ and M50$_{75YO}$ head and neck models, showing the change in lordosis associated with age and the corresponding Bezier angles.

One consequence of the increased cervical curvature was an increased intervertebral disc foramen height at the anterior aspect and decreased in the posterior aspect for both the $M50_{75YO}$ and $F05_{75YO}$ models (Figure 39). For the $M50_{75YO}$ model, the IVD height was increased by 5% in the anterior aspect and reduced by 9% in the posterior aspect. Similarly, for the $F05_{75YO}$, the IVD foramen height was increased by 2% in the anterior aspect and reduced by 12% in the posterior aspect.

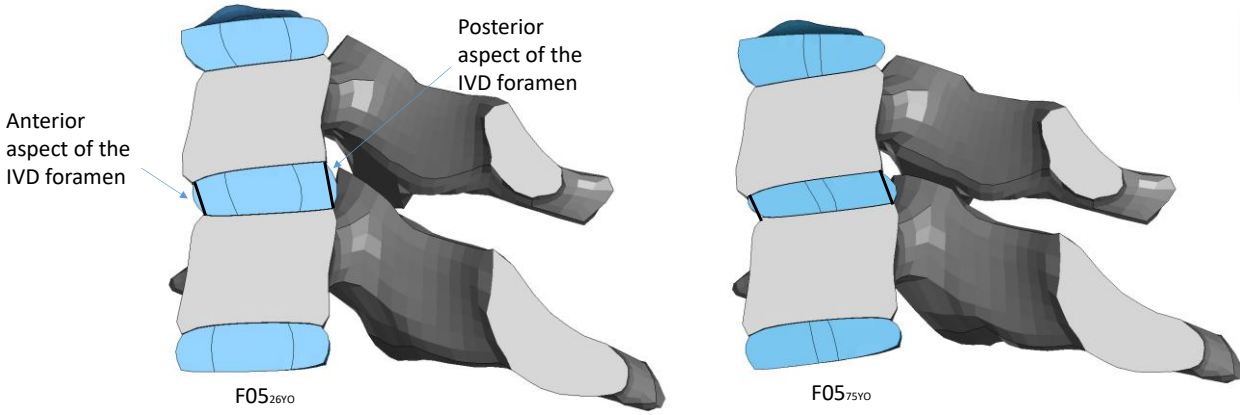

Figure 39: IVD height measurement in the $F05_{26YO}$ (left) and $F05_{75YO}$ (right) C45 segment.

It has been identified that the head position changes with age (Park et al., 2016b) as a result of the combined effect of the increased cervical spine lordosis and the need to maintain head angle (line of sight) for everyday tasks. With respect to the center of gravity of T1, the center of gravity of the head (Figure 37) of the $M50_{75YO}$ was located 22.3 mm anterior and 4.2 mm inferior to the head CG of the $M50_{26YO}$. The $F05_{75YO}$ head CG was located 30.2 mm anterior and 7.6 mm inferior to that of the $F05_{26YO}$ model head CG.

4.2 Aged $M50_{75YO}$ and Young $M50_{26YO}$ Male Finite Element Neck Model Comparison

The $M50_{75YO}$ and $M50_{26YO}$ models were compared in frontal, lateral and rear impacts based on cross-correlation (CORA) of the head kinematics between the two models, with the aim to identify trends and quantify the effect of change in posture associated with ageing on head kinematics. Exemplar responses are presented in this section, and the complete set of simulation data is reported in Appendix 3 for the male models.

4.2.1 $M50_{26YO}$ and $M50_{75YO}$ Male FE Model Head Kinematic Response Comparison

The cross-correlation ratings obtained by comparing the $M50_{26YO}$ to the $M50_{75YO}$ head kinematics varied depending on the impact severity in frontal impact (Figure 40). Specifically, with an increasing impact severity in the frontal impacts, the cross-correlation rating generally increased, corresponding to a more similar response between the young and aged male models. In contrast, in the lateral impact cross-correlation rating decreased with increasing impact severity for lateral impacts. The highest correlation for all scenarios was in the 7g rear impact (0.97); however, only one impact case was investigated, so trends could not be assessed. Importantly, the interpretation of the cross-correlation ratings has been suggested as "excellent" for the range of ratings 0.86 to 1.00 (Cesari et al., 2001), suggesting a strong similarity of the $M50_{26YO}$ to the $M50_{75YO}$ across all impact cases.

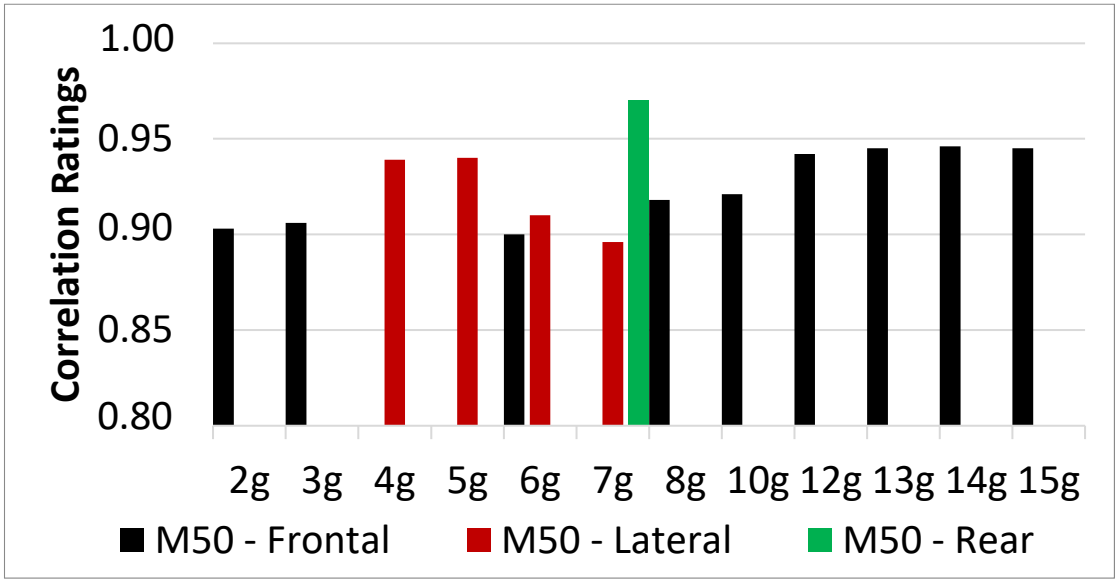

Figure 40: Correlation ratings between the $M50_{26YO}$ and $M50_{75YO}$ male neck models in frontal, lateral and rear impacts. Values close to 1 indicate a strong similarity between the kinematic response of the models.

In the frontal impacts from 2g to 6g (Figure 41), the head kinematics slightly differ between the $M50_{26YO}$ and the $M50_{75YO}$. The main difference was observed in the higher acceleration peaks in the X and Z axis and lower rotational acceleration peaks in the Y-axis.

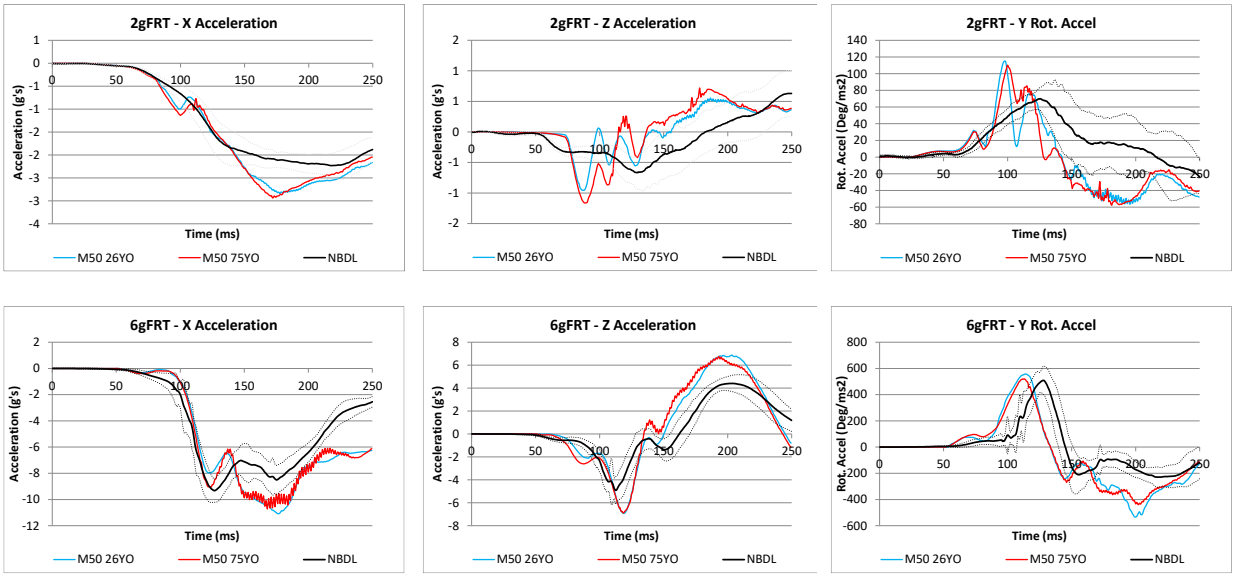

Figure 41: Head kinematic response of the male models in 2g and 6g frontal impacts.

The neck models included a hard tissue failure criterion based on element erosion (equivalent-plastic-strain-based) to predict trabecular and cortical bone failure in the vertebra. Hard tissue failure occurred at C6 in the $M50_{75YO}$ model for all the high-severity frontal impacts (from 8g to 15g), resulting in a spike in acceleration, which was visible in the head kinematic responses (Figure 42). In general, increased impact severity resulted in hard tissue fractures occurring earlier in time. At the higher severities, 8g to 15g, the head kinematic response of the $M50_{75YO}$ model was close to that of the $M50_{26YO}$ model until hard tissue failure occurred.

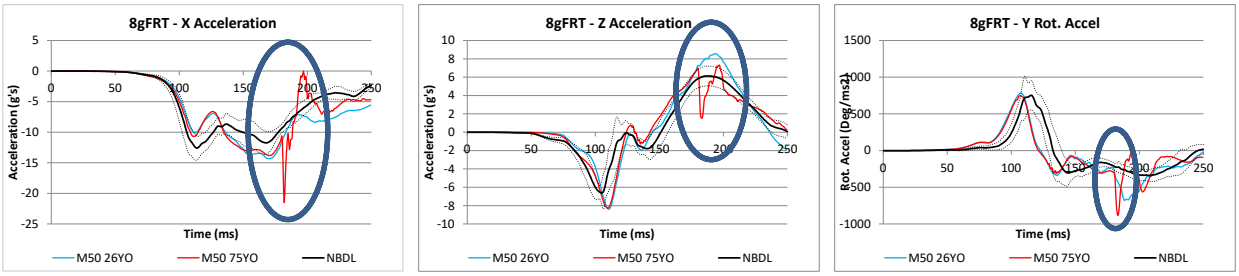

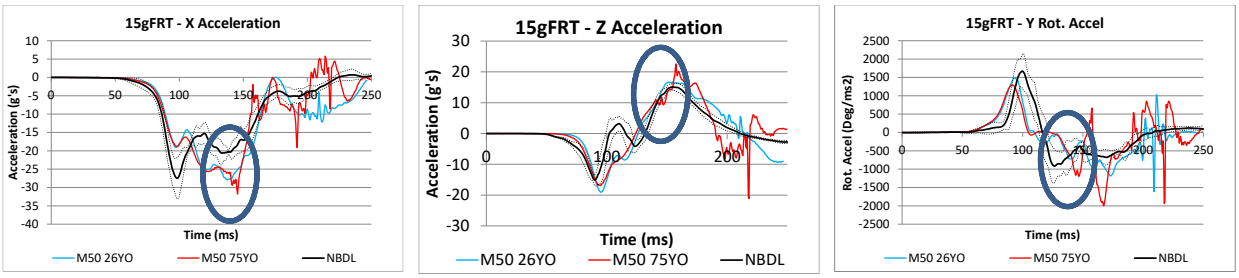

Figure 42: Head kinematic response of the male models in 8g and 15g frontal impacts.

In lateral impacts (4g, 5g, 6g and 7g), generally, the head kinematic cross-correlation ratings between the $M50_{26YO}$ and $M50_{75YO}$ models decrease with increasing impact severity attributed mainly to the differences in the rotational acceleration in the X-axis. In the Y-axis, the head acceleration response of the $M50_{75YO}$ model exhibited higher acceleration peaks than that of the $M50_{26YO}$ (Figure 43).

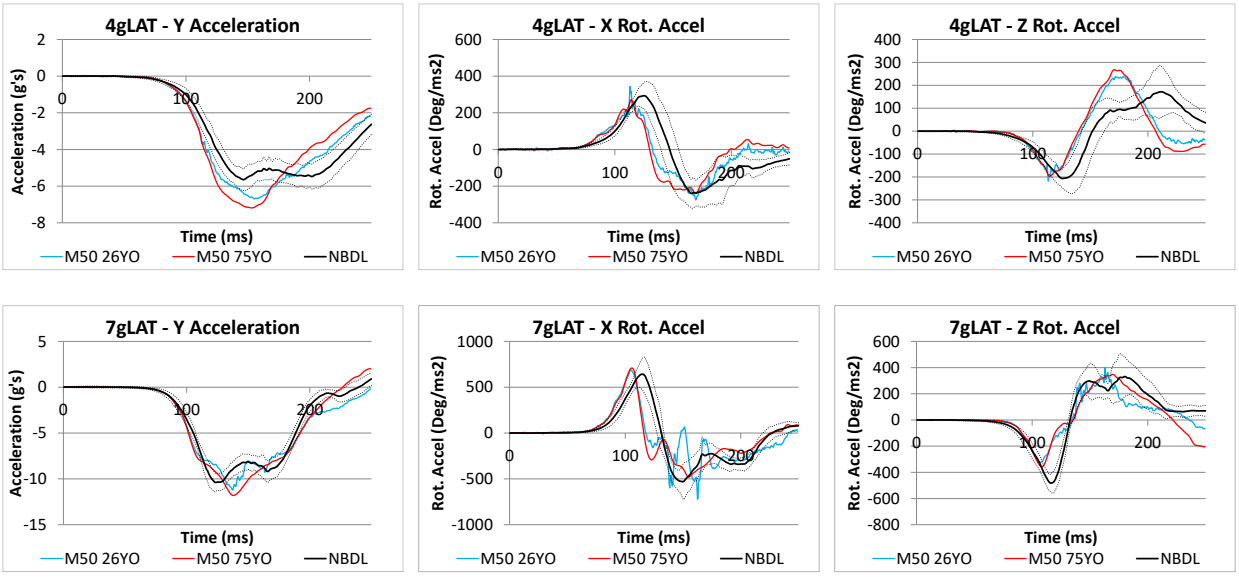

Figure 43: Head kinematic response of the male models in 4g and 7g lateral impacts.

In the 7g rear impact, the $M50_{75YO}$ had higher X and Z linear accelerations and lower Y rotational accelerations; however, the differences in head kinematics between the $M50_{75YO}$ and $M50_{26YO}$ were modest (Figure 44).

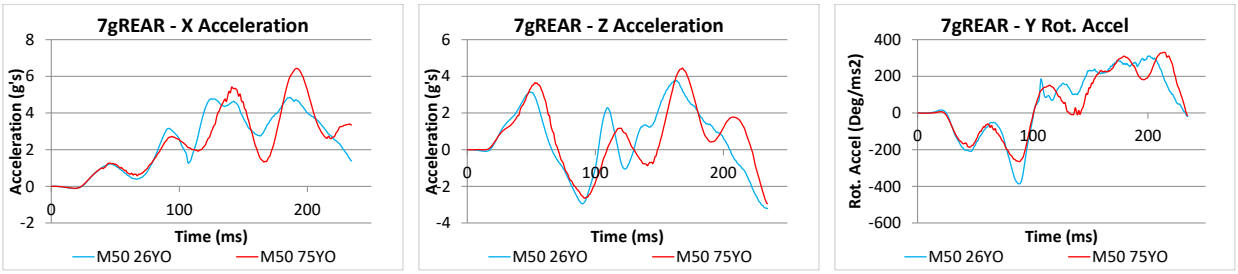

Figure 44: Head kinematic response of the male models for a 7g rear impact.

4.2.1 Aged and Young Male FE Neck Model Soft Tissue Response

In the frontal impacts, when averaging the soft tissue response at all the segment levels (C23 to C67) and impact severities (2g to 15g), the $M50_{75YO}$ model predicted 2% more CL strain and 11% more IVD space strain than the strains predicted by the $M50_{26YO}$. In contrast, in the rear impact, the $M50_{75YO}$ model predicted less CL and IVD space strain (1% and 7% less strain, respectively) than that of the $M50_{26YO}$. In the lateral impacts, the $M50_{75YO}$ model predicted more CL strain (9% more) while less IVD space strain (4% less) than the $M50_{26YO}$ (Figure 45). Although averaging all segment levels and impact severities obscures some of the local differences, the averages serve to condense a large amount of information and ease the comparison between the young and aged models.

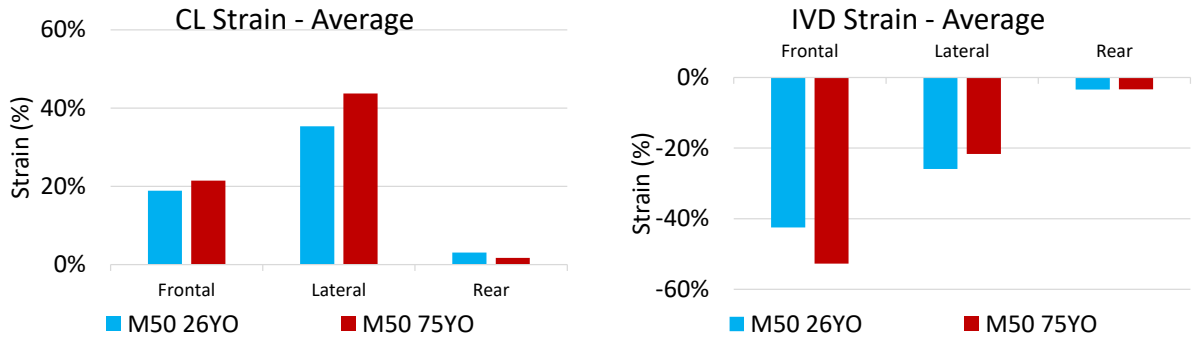

Figure 45: Male model average CL and IVD space strain for frontal, lateral and rear impacts.

Considering the response at the individual cervical levels for frontal impact, the $M50_{75YO}$ predicted 3% less CL strain than that of the $M50_{26YO}$ at the 2g frontal impact (Figure 46). In contrast, for the 8g and 15g frontal impacts, the $M50_{75YO}$ predicted more CL strain on average than the $M50_{26YO}$ model. In particular,

at the C23 and C67 levels, the $M50_{75YO}$ model predicted 32% more CL strain than that of the $M50_{26YO}$. Regarding the IVD space strain, the M5075YO model predicted more IVD space strain across all impact severities and segment levels (Figure 46).

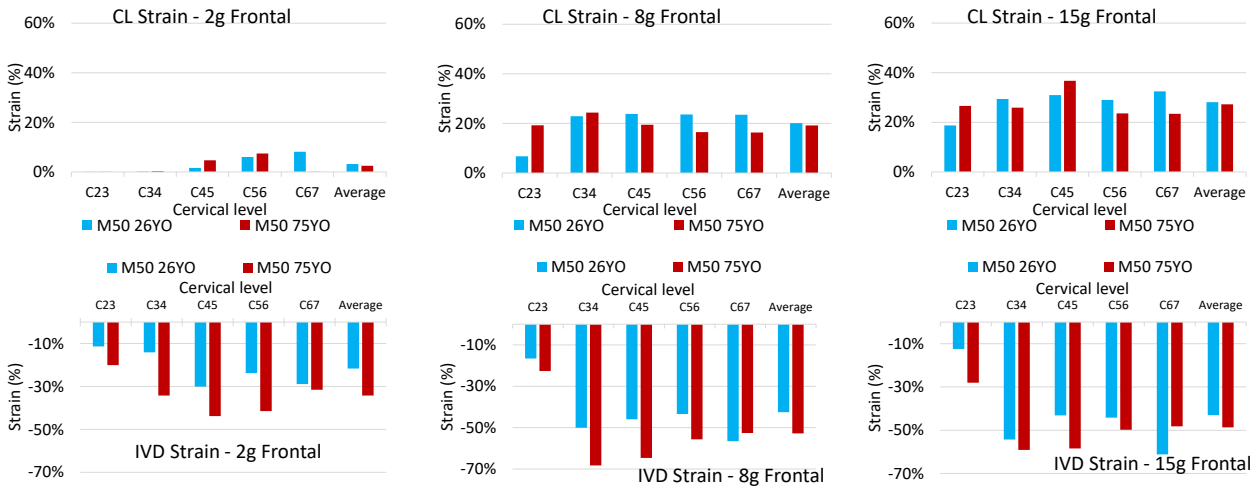

Figure 46: $M50_{75YO}$ and $M50_{26YO}$ capsular ligament (CL) and intervertebral disc (IVD) strain in the 2g, 8g, and 15g frontal impacts.

In lateral impacts, the $M50_{75YO}$ model predicted 4% less for the 4g impact and 12% more CL strain at the 7g impact than that of the $M50_{26YO}$ model (Figure 47). However, in both impact severities, the $M50_{75YO}$ model predicted 16% more CL strain on average at the segment C23 than the $M50_{26YO}$ model did. Concerning the IVD space strain, the $M50_{75YO}$ model predicted less IVD space strain for both the 4g and 7g lateral impacts (2% and 4%, respectively) than that of the $M50_{26YO}$ model.

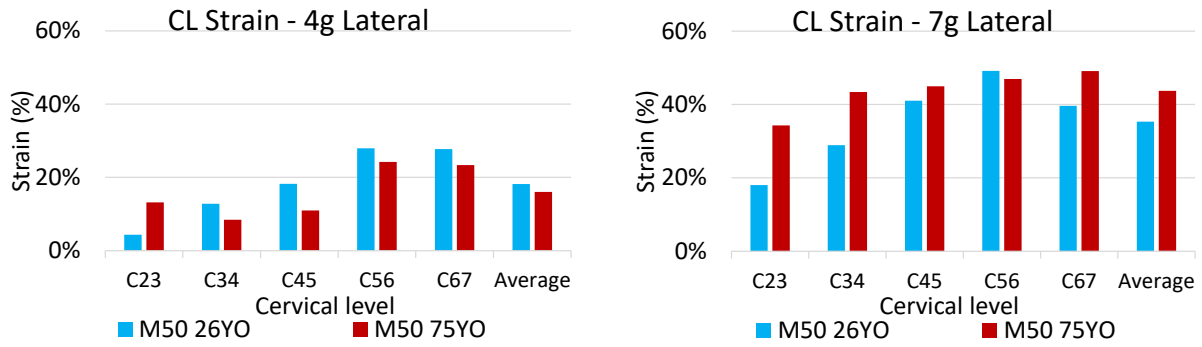

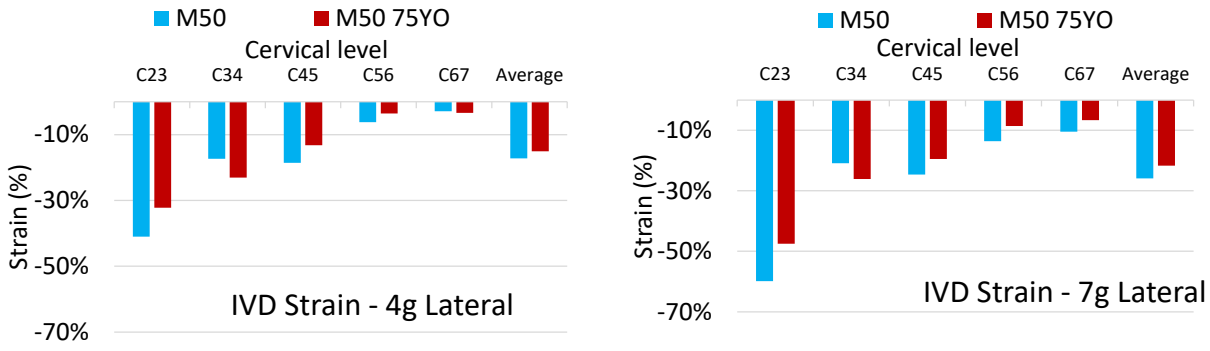

Figure 47: $M50_{75YO}$ and $M50_{26YO}$ CL and IVD space strain for the 4g and 7g lateral impacts.

In the rear impact, the $M50_{75YO}$ model predicted less CL and IVD space strain at all spinal levels (Figure 48).

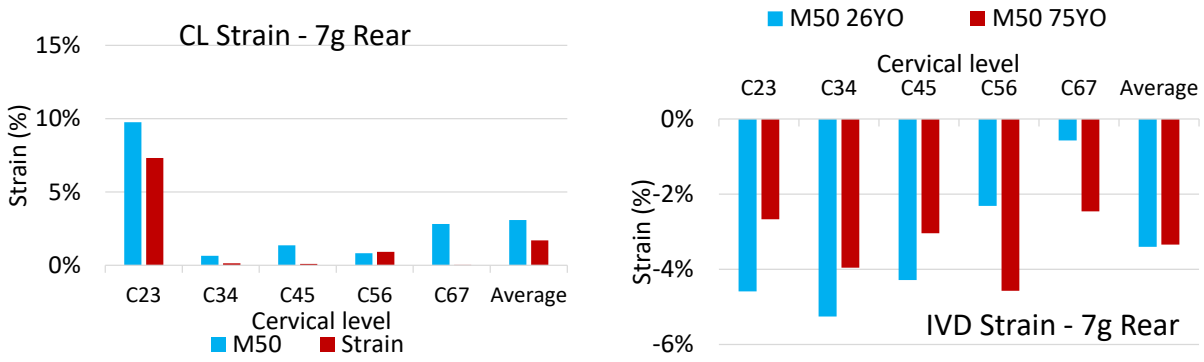

Figure 48: $M50_{75YO}$ and $M50_{26YO}$ capsular ligament (CL) and intervertebral disc (IVD) strain for the 7g rear impact.

4.3 Aged Female Finite Element Neck Model Comparison to Young Model and Experimental Data

The $F05_{26YO}$ and $F05_{75YO}$ models were loaded using the same boundary conditions as the $M50_{75YO}$ and $M50_{26YO}$ models (frontal, lateral and rear impacts). The head kinematics were tracked, and a cross-correlation based comparison was performed to identify trends and quantify the effect of change in posture associated with ageing on head kinematics. The complete set of simulation data is presented in Appendix 3.

4.3.1 $F05_{26YO}$ and $F05_{75YO}$ Male FE Model Head Kinematic Response Comparison

The cross-correlation ratings in the frontal, lateral and rear impacts obtained by comparing the head kinematics of the $F05_{26YO}$ to the $F05_{75YO}$ were similar across all the impact severities. The average of all cross-correlation ratings in the frontal impacts was 0.92, with the lowest rating being in the 2g frontal impact and the highest at 15g frontal impact. The lateral impacts had the lowest cross-correlation ratings on average, with the lowest rating for the 6g impact and the highest rating for the 4g impact. For the lateral impacts (5g to 7g), the cross-correlation rating demonstrated a "good" correlation (good correlation defined within the range 0.65 to 0.85) while all the other impact cases demonstrated an "excellent" correlation (Cesari et al., 2001). The 7g rear impact had the highest rating of all impact directions for the female models (Figure 49). The cross-correlation ratings demonstrated a "good" to "excellent" correlation between the $F05_{26YO}$ and the $F05_{75YO}$ suggesting a strong similarity between models across all impact cases.

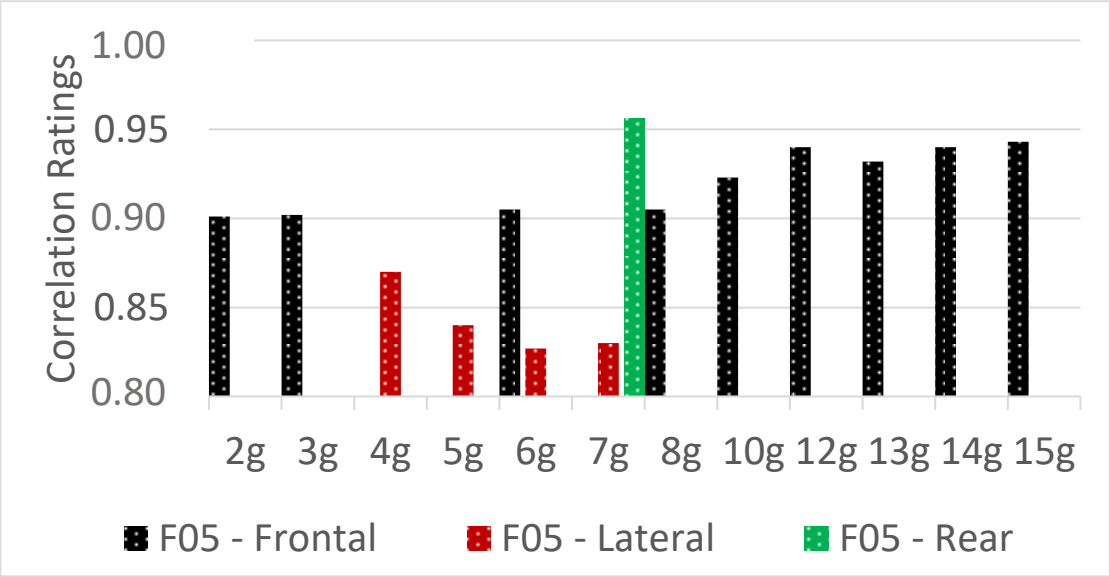

Figure 49: Correlation ratings for the young compared against the aged female neck models in frontal, lateral and rear impacts.

At low severity (2g) frontal impacts, the $F05_{26YO}$ and $F05_{75YO}$ models had similar head kinematics (Table 37). With increasing severity (6g to 15g), the differences between $F05_{26YO}$ and $F05_{75YO}$ models in the linear acceleration in the Z and X directions increased, with the $F05_{26YO}$ model predicting higher linear and rotational acceleration peaks (Figure 50).

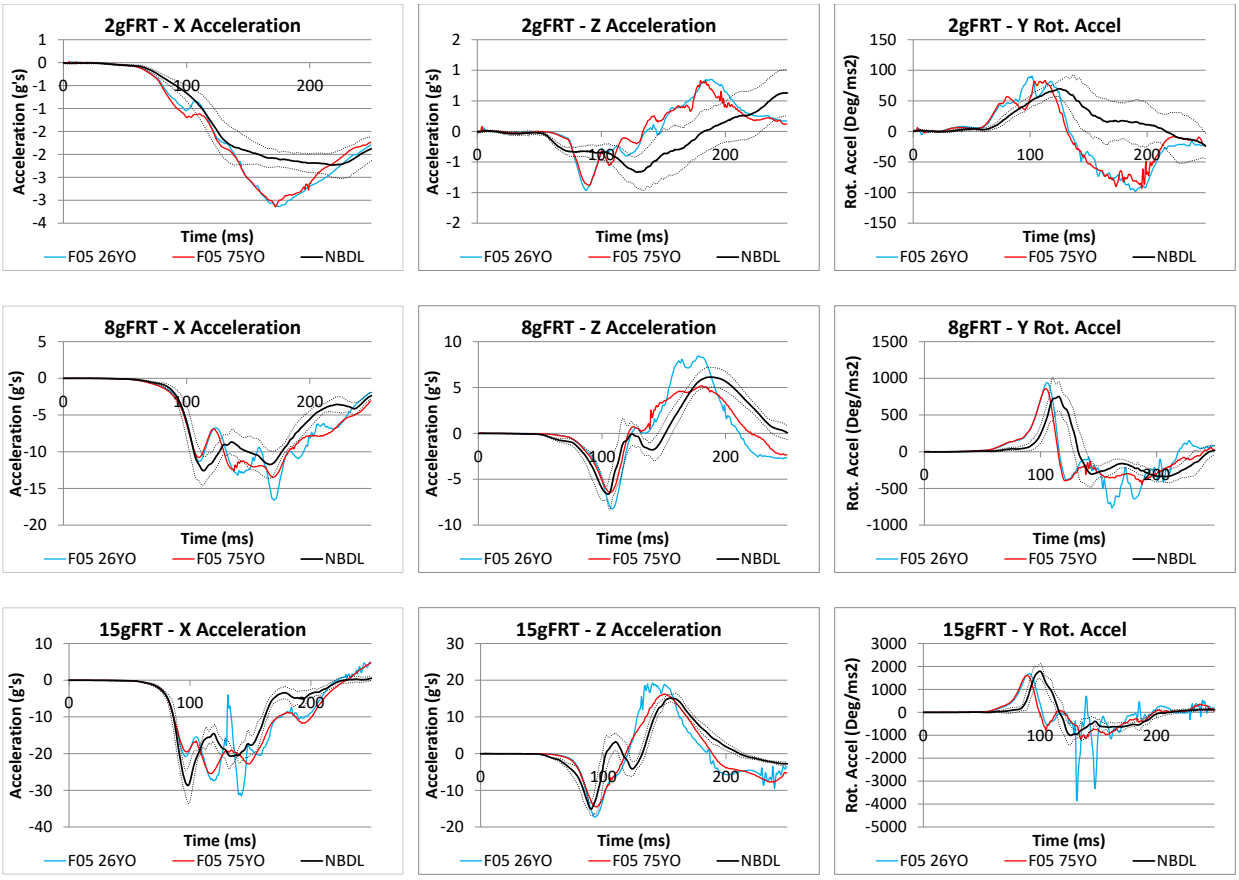

Figure 50: Head kinematics of the female young and aged models in frontal impacts.

In lateral impacts, the head kinematic response of the $F05_{26YO}$ model was similar to the one of the $F05_{75YO}$ (Figure 51). The main differences were observed in the rotational acceleration in the Z-axis.

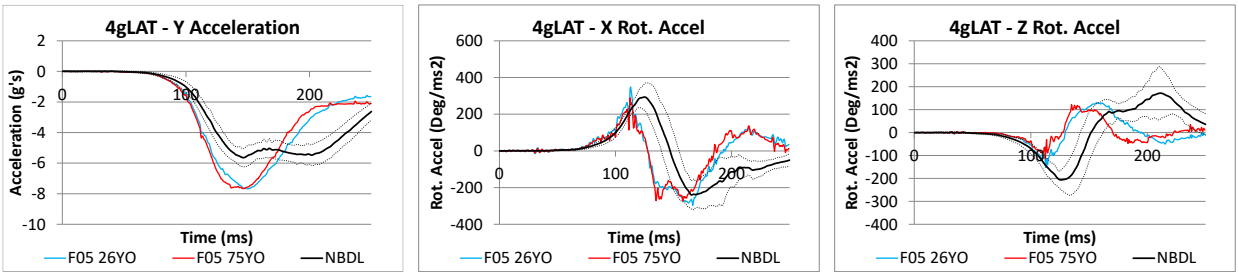

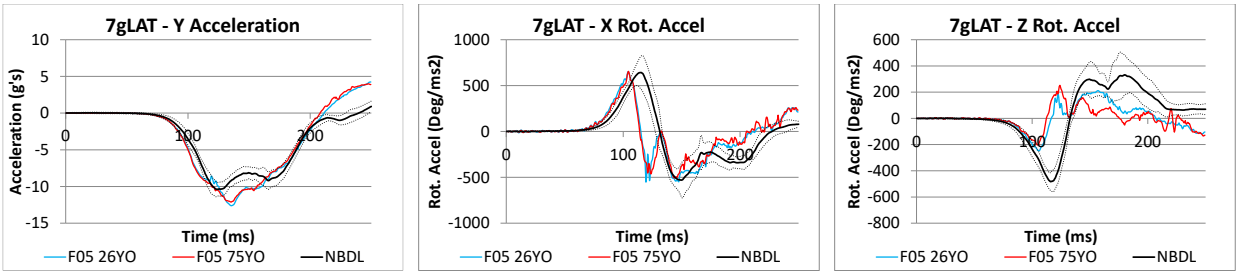

Figure 51: Female models in lateral impact head kinematics.

In the 7g rear impact, the $F05_{75YO}$ model predicted higher linear acceleration peaks in the Z-axis than that of the $F05_{26YO}$. In contrast, the linear and rotational accelerations in the X and Y axis, respectively, the response of both $F05_{75YO}$ and $F05_{26YO}$ models was similar (Figure 52).

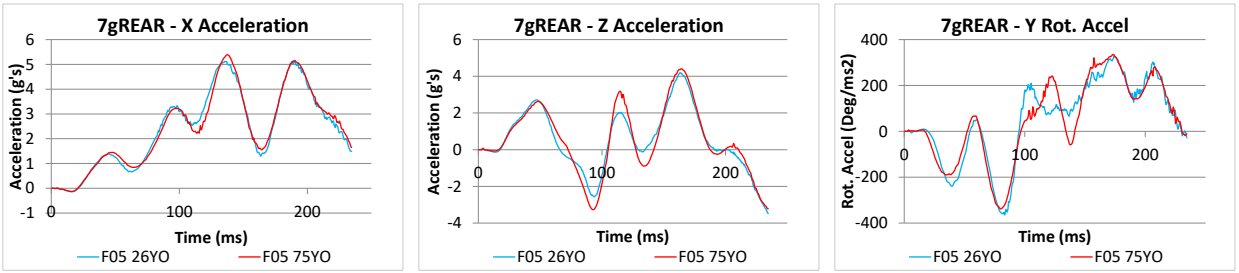

Figure 52: Female models in rear impact head kinematics.

4.3.2 Aged and Young Female FE Neck Models Soft Tissue Response

The $F05_{75YO}$ model predicted less CL and IVD space strain on average in all impact directions except for the rear impact, where the $F05_{75YO}$ model predicted 6% more CL strain than that of the $F05_{26YO}$ model (Figure 53). Although averaging all segment levels and impact severities obscured some of the local differences, the averages served to condense a large amount of information for comparison between the male and female models. Specific values will be reported in the following sections.

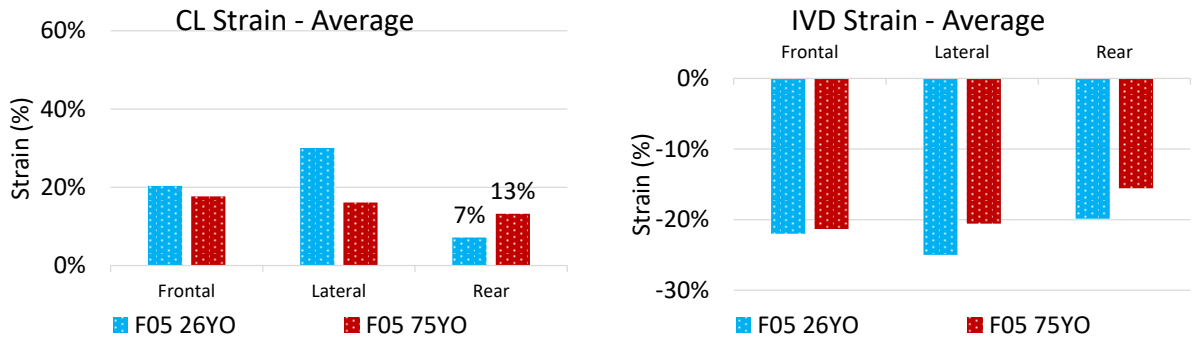

Figure 53: Female model average CL, and IVD space strain for frontal, lateral and rear impacts.

Considering the frontal impacts separating each impact severity and segment level, the $F05_{75YO}$ predicted less CL strain in general across all segment levels and impact severities compared to the $F05_{26YO}$. With regards to the IVD space strain, the $F05_{75YO}$ model predicted more strain in the upper segment levels (C23 to C45) while less in the lower segment levels (C56 and C67) than those of the $F05_{26YO}$ model (Figure 54).

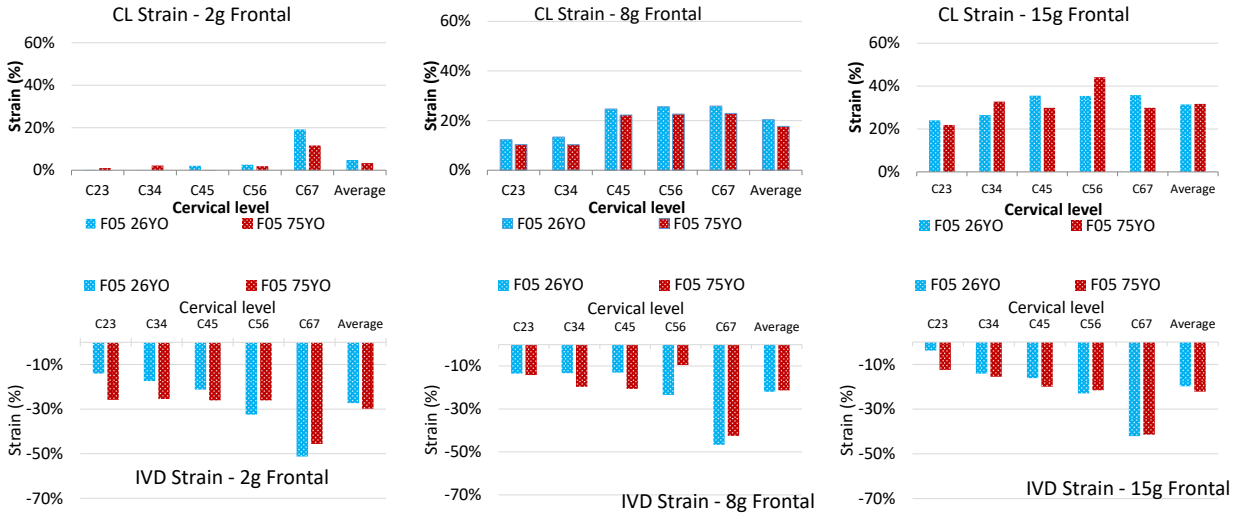

Figure 54: $F05_{75YO}$ and $F05_{26YO}$ capsular ligament (CL) and intervertebral disc (IVD) strain in the 2g, 8g, and 15g frontal impacts.

In lateral impacts, the $F05_{75YO}$ model predicted less CL and IVD space strain compared to the $F05_{26YO}$ model at most segment levels and impact severities (Figure 55). In the upper segments (C23 and C34), for the lateral 7g lateral impacts, the IVD space strain predicted by the $F05_{75YO}$ model was 4% higher than that of the $F05_{26YO}$.

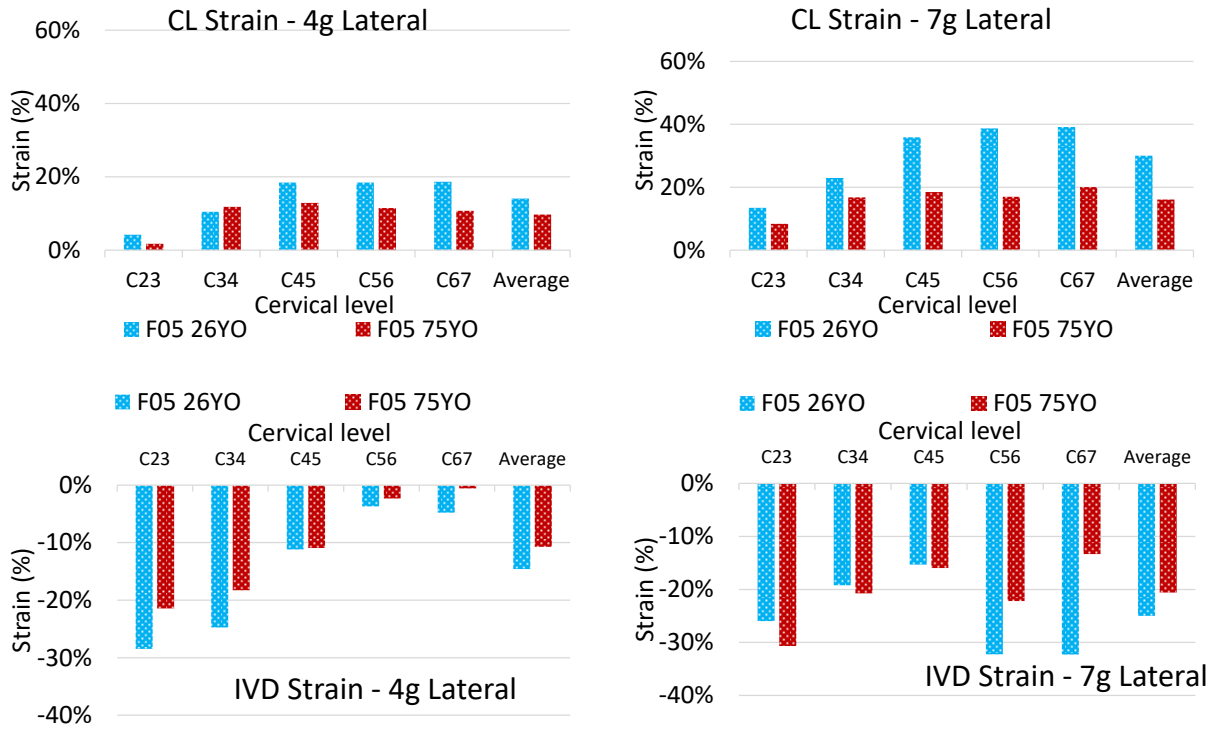

Figure 55: $F05_{75YO}$ and $F05_{26YO}$ capsular ligament (CL) and intervertebral disc (IVD) strain for the 4g and 7g lateral impacts.

In the rear impact, the $F05_{75YO}$ model predicted 6% more CL strain than that of the $F05_{26YO}$, but 4% less IVD space strain (Figure 56).

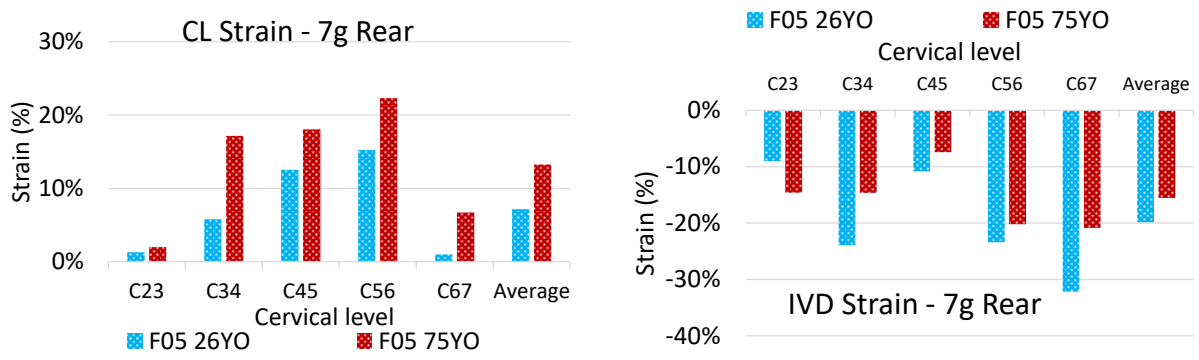

Figure 56: $F05_{75YO}$ and $F05_{26YO}$ capsular ligament (CL) and intervertebral disc (IVD) strain for the 7g rear impact.

4.4 Comparison of the Age Effects Between M50 Male and F05 Female Models

Considering head kinematics, the effect of the increased lordosis associated with age was similar between the small stature female and mid-size male models where the difference between young and aged was modest. The biggest difference was observed in the lateral impacts. The female models had lower CORA ratings (0.84 on average meaning "good" correlation) than the ratings of the male models (0.92 on average meaning "excellent" correlation). In both male and female models in the lateral impacts, the difference between the young and aged models head kinematic responses increased with increasing impact severity. The highest ratings corresponded to the rear impact in both males (0.97) and females (0.96) models. In frontal impacts, the male model had relatively low CORA ratings at low severities when compared to the ratings obtained at high severities. In contrast, this trend was not observed in the female model with similar ratings across all the impact severities (Figure 57).

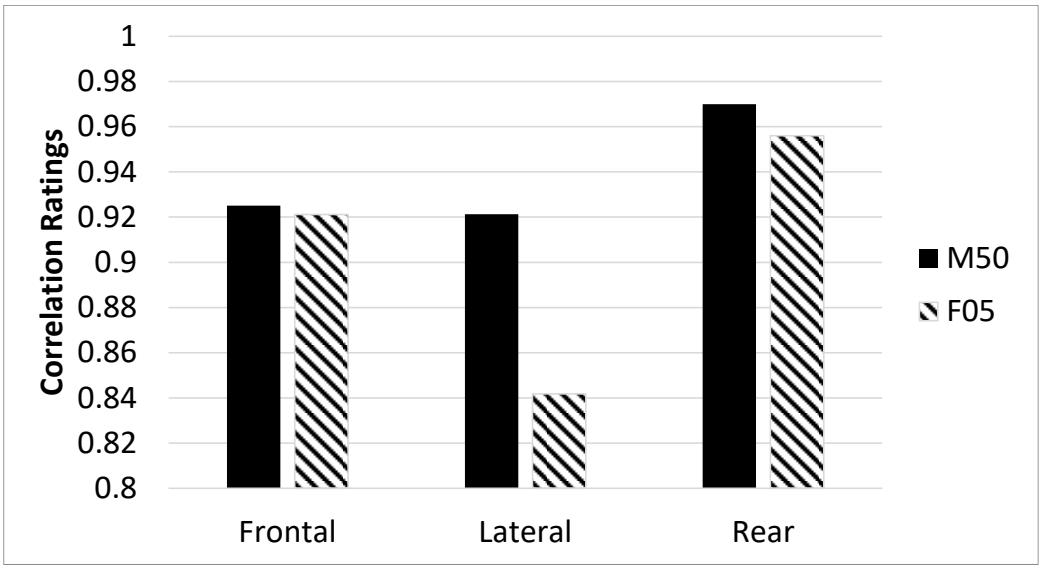

Figure 57: Average correlation ratings for the male (solid bars) and female (patterned bars) models based on head kinematics of the young and aged models.

The head kinematics curves of the four models had, in general, similar shapes and magnitudes. In the frontal impacts, the $M50_{75YO}$ model predicted hard tissue failure at the level C56 in the 8g+ impact severities that led to a spike in the head kinematics, creating a difference between models that was detectable at the head kinematics level (Figure 58). From the cross-correlation perspective, all four models were highly correlated, ranging from "good" to "excellent" correlation.

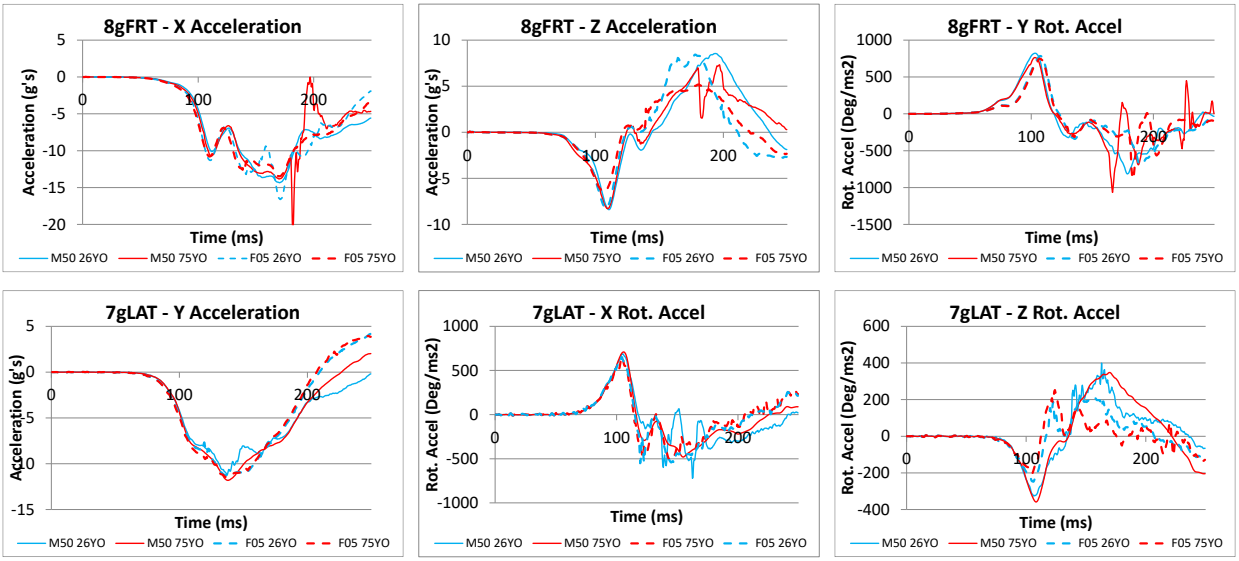

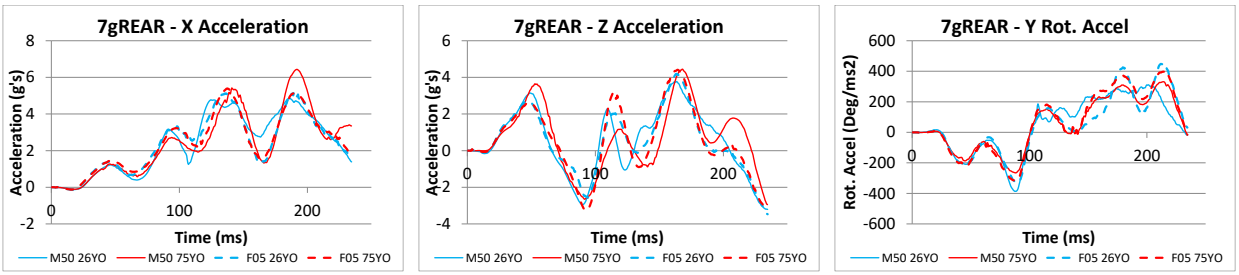

Figure 58: $M50_{26YO}$, $M50_{75YO}$, $F05_{26YO}$ and $F05_{75YO}$ head kinematics in an exemplar frontal (8g), lateral (7g) and rear (7g) impact.

When comparing the $M50_{26YO}$ and $F05_{26YO}$ at the soft tissue level, averaging impact severities and segment levels, the $F05_{26YO}$ model predicted less CL and IVD space strain in frontal, similar strains in lateral and more strains in rear impacts, compared to the $M50_{26YO}$ model. Similarly, when comparing the $F05_{75YO}$ and the $M50_{75YO}$ models, the $F05_{75YO}$ model predicted lower strains than the $M50_{75YO}$ in the frontal and lateral impacts but higher strains in the rear impact scenarios (Figure 59).

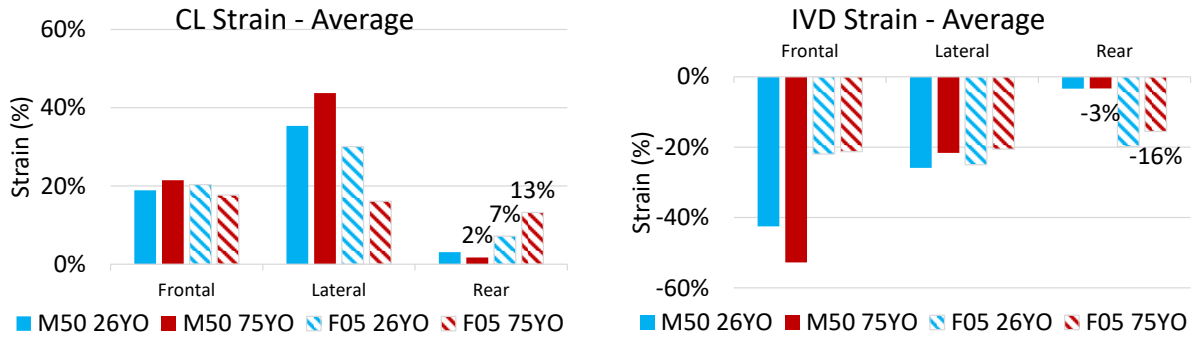

Figure 59: Average capsular ligament (CL) and intervertebral disc space (IVD) strains in the frontal, lateral and rear impacts for the male and female young and aged models.

In frontal impacts, the male model showed more sensitivity to the change in curvature compared to the female model. The IVD space strain changes were the major contrast between the male and female models, where the increased lordosis in the male model lead to an 18% more IVD space strain, with the ageing affecting more in the high severities than in the low severities. The effect of the aged curvature in the frontal impacts for the female model leads to 4% more IVD space strain (Figure 60). In frontal impacts, both male and female aged models predicted similar CL strains (Figure 60).

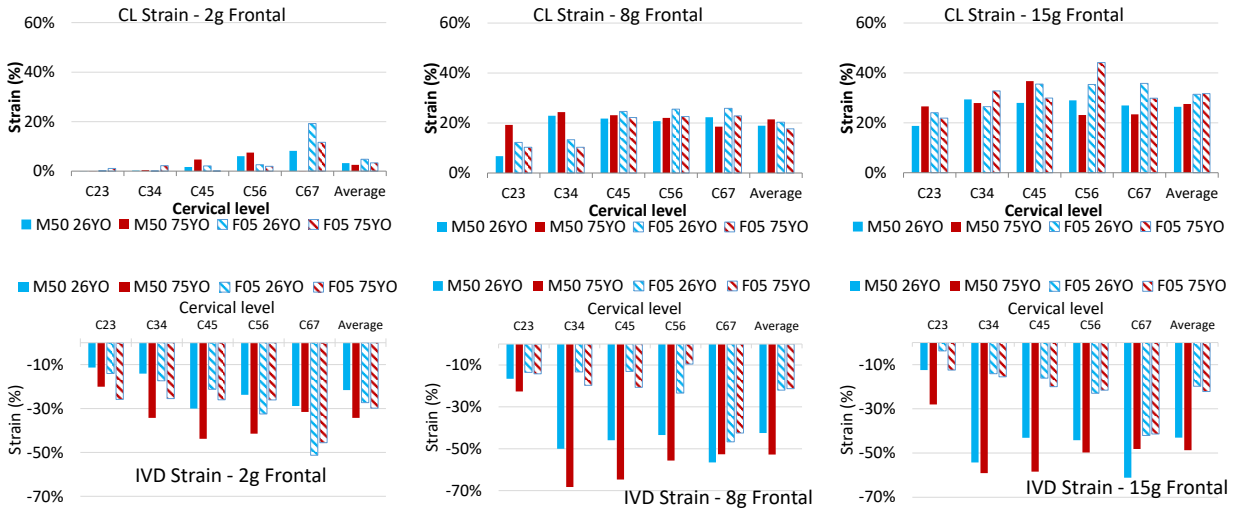

Figure 60: $M50_{26YO}$, $M50_{75YO}$, $F05_{26YO}$ and $F05_{75YO}$ capsular ligament (CL) and intervertebral disc (IVD) space strain in the 2g, 8g, and 15g frontal impacts.

In lateral impacts, the effect of the aged cervical curvature had a similar impact on the male and female models, with lower CL and IVD space strains in general. In the female model, the increased cervical curvature led to slightly more IVD space strain in the 4g lateral impact, while the opposite trend was observed for the male model (Figure 61).

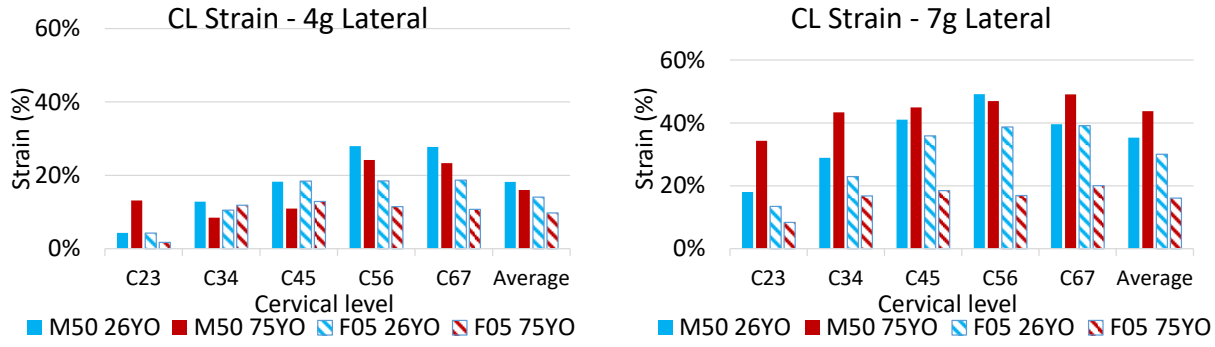

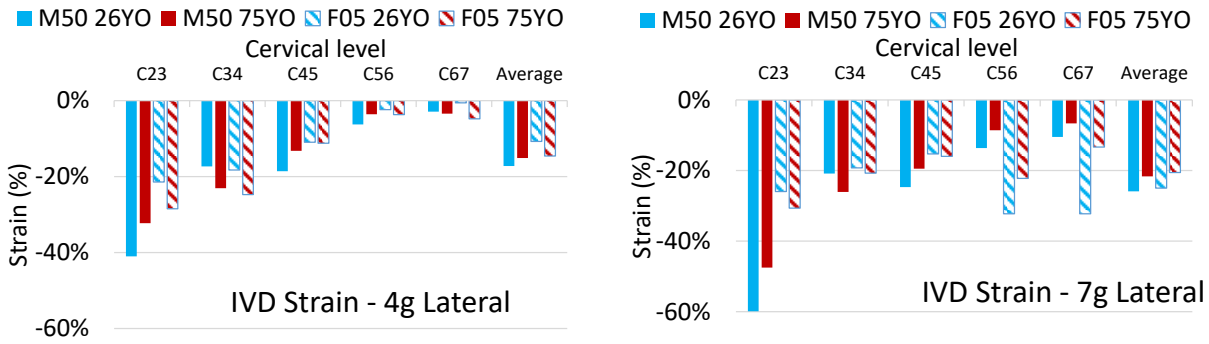

Figure 61: $M50_{26YO}$, $M50_{75YO}$, $F05_{26YO}$ and $F05_{75YO}$ capsular ligament (CL) and intervertebral disc (IVD) space strain for the 4g and 7g lateral impacts.

In the rear impact condition, the aged curvature in the female model leads to 5% more CL strain on average, whereas, in the male model, the average CL strain was 2% lower. In both male and female models, the aged curvature led to 5% less IVD space strain (Figure 62). Notably, the female models, $F05_{26YO}$ and $F05_{75YO}$, had higher CL and IVD space strains than the corresponding male models. In particular, the female models predicted CL strains 10% higher than those of the male models (Figure 62).

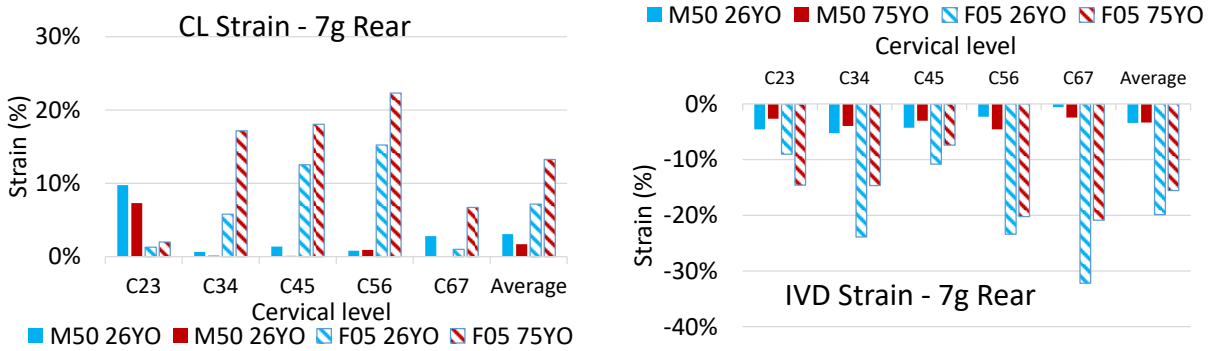

Figure 62: $M50_{26YO}$, $M50_{75YO}$, $F05_{26YO}$ and $F05_{75YO}$ capsular ligament (CL) and intervertebral disc (IVD) space strain for the 7g rear impact.

Chapter 5: Discussion

5.1.1 Model Anthropometrics and the Effect of Age in the Cervical Lordosis and Bone Morphology

The developed reposturing methodology was applied to create geometrically average 75 YO male and female neck models to investigate the effect of changing geometry on response and potential injury risk. This study was focused on explaining the increased susceptibility of the aged population to injury in crash scenarios as an effect of the geometrical changes associated with age. It is important to note that this work is based on two subject-specific models repostured to represent an average aged population. This is of importance, specifically in the male model, where it was shown in the current study that the neck length of the subject-specific model was higher than the average population in the literature. Although the subject selected for scanning met the average mass and stature requirements, differences in anthropometrics at the body region level could vary outside of the average for the target population. Interestingly, the $M50_{26YO}$ FE model curvature was straighter than the reported curvature of a 50^{th} percentile 26 YO male, but when accounting for the neck length, the curvature of the $M50_{26YO}$ model was in agreement with the literature (Reed and Jones, 2017). This effect was identified using literature that reports individual vertebral positions and is obscured when using literature that reports global metrics, such as Bezier angles, that depends more on the orientation, position, and shape of C7 and C2 with the mid-level vertebrae position and orientation having a lesser effect on them. Overall, the male neck model was closer to a 95^{th} percentile neck, based on the curvature and length. In contrast, the curvature and length of the female neck model were in agreement with the literature, falling within the reported range for the 5^{th} percentile female anthropometric group (Reed and Jones, 2017). The curvature of the young female model was straighter than the curvature of the young male model, and the change in lordosis due to age was more prominent than that in the male model. In addition, it was found that the facet angle in both male and female models was higher than the average reported in the literature (Parenteau et al., 2014). As a consequence, the aged facet angle was higher than is the average reported in the literature, but within two standard deviations of the average. The facet joint angle in females changes more with age than in males, suggesting that the change in facet angle might be related somehow to the change in curvature and head orientation with respect to the vertebrae.

Within the models, the cartilage geometry was updated to account for the non-linear distribution of the cartilage thickness and maximum thickness based on literature data (Womack et al., 2008). It was shown that the global kinematics (e.g. head kinematics) were insensitive to the proposed cartilage change;

however, the increased CORA ratings at the motion segment level suggested an improvement in the biofidelity of the facet joint. The proposed cartilage enhancement removed the interfacet gap present in the original models. However, simply closing the interfacet gap by linearly increasing the cartilage thickness could lead to an overly stiff cervical motion segment.

Geometrical variability in biological tissues is high. Importantly, the variability in anthropometrics greatly increases with age (Parenteau et al., 2014), and it might be a dominant factor in the increased incidence of injury in the aged population. In the present study, geometrical variability is not included. Variability of anthropometrics in the ageing process can be challenging to implement in HBMs, partially due to the difficulty of reposture models to a posture that might largely deviate from the original posture of the model. In addition, the relationship between local geometrical changes associated with age, such as facet angle, and the global changes, such as increased lordosis, is not clear.

5.1.2 Effect of Aged Posture on the Neck Model Response to Impact

From solely looking at the head kinematic response and the correlation ratings obtained by objectively comparing the head kinematic response of the young models to that of the aged models, it can be said that the effect of the postural changes associated with age was modest. Correlation ratings higher than 0.71 are often interpreted as a strong similarity between the compared responses and, therefore, models.

At the head kinematic level, the change in curvature associated with age had, in general, a similar effect in both the male and female models. In frontal impacts of high severity, the $M50_{75YO}$ model predicted hard tissue failure at the C4 level in contrast with the $F05_{75YO}$ model, which did not predict hard tissue failure in any impact loading. Higher compressive loads in the vertebral bodies of the $M50_{75YO}$ model, leading to hard tissue failure, compared to the $F05_{75YO}$ model, were attributed to the head mass of the $M50_{75YO}$ being more prominent than the head mass of the $F05_{75YO}$ model. The long neck of the male model led to a higher moment-arm that, together with the larger head mass, created higher compressive loads in regions of the vertebral bodies. Higher compressive loads were observed in the male models at all segment levels in the form of higher IVD space strain, compared to the female models. Another contributing factor could be the smaller cross-sectional area of the female neck model than that of the male model.

At the tissue level, the effects of the change in curvature with age were more pronounced compared to the head kinematics. For example, in the frontal impact for the male model, the aged posture led to 17% more IVD space strain in the C34 segment when compared to the young posture model. In contrast, in the

frontal impact for the female model, the aged posture led to similar IVD space strain regardless of both male and female models having similar correlation ratings (0.925 and 0.920, respectively).

The soft tissue response of the present study suggests that 50th males could be more prone to be affected by the morphological and postural changes associated with age than 5th percentile females in frontal and lateral impacts. Nevertheless, epidemiology studies conclude that the 5th percentile elderly female is at higher risk of injury under an impact scenario than its male counterpart (Bose et al., 2011). This hypothesis was not supported by the results of the present study for the frontal and lateral impacts when accounting for the change in curvature and facet angle using the same boundary conditions where the CL and IVD deformation were monitored. This can be attributed to a number of factors. First, the boundary conditions, based on resultant acceleration in the first thoracic (T1) vertebra of male subjects subjected to a sled pulse, were applied equally to both male and female models. However, it is possible that a sled pulse of 8g frontal, for example, could lead to different T1 kinematics in a small stature female than in a mid-size male. Secondly, the subject-specific nature of the models, where the male model was shown to have a longer than average neck.

In the rear impact, however, the female models (young and aged) predicted more CL and IVD space strain than their male counterparts. Importantly, the increased lordosis in the female model led to CL strain that exceeded the linear region of the CL (Shen, D,. 2020), suggesting an increased likelihood of injury with increasing age in the females, in agreement whit the epidemiology (Bose et al., 2011; Carlsson, 2012). The higher CL and IVD space strain in the females when compared to the male models in the rear impact was attributed to the more pronounced curvature in the females and to the musculature relevant in a rear impact. The volume of the anterior muscles, the relevant muscles in the rear impact, corresponds to 25% of the total neck muscle volume having a lesser contribution in an impact condition. The modest contribution of the musculature in a rear impact led to a higher sensitivity to geometrical and postural changes in the soft tissue response when compared to the frontal and lateral impact.

Essential aspects of the ageing process, such as changes in material properties or injury risk thresholds, were not considered in the present study that could potentially affect the results. Interestingly, the aged female model had slightly less CL and IVD deformations in frontal and lateral impacts than the young female model. The change in material properties and calcification of soft tissue (such as the IVD and CL) associated with age were not considered in the present study. It is a possibility that the change in curvature and morphology of the cervical spine is the response of the body to mitigate the change in material properties. Therefore, if only the morphology and posture are considered, less or similar soft

tissue strain can be observed in frontal and lateral impacts when compared to the young models. In addition, the muscle activation scheme was the same for both young and aged models. It is known that reaction time increase with age; this factor could further change the results of the comparison of age and sex groups under impact scenarios.

In general, the response of the aged posture models ($M50_{75YO}$ and $F05_{75YO}$) was similar to the young posture models ($M50_{26YO}$ and $F05_{26YO}$) concerning head kinematics with the main differences observed in the soft tissue metrics (CL and IVD deformation). In the rear impact condition, the female models had higher soft tissue strain than the male models, suggesting an increased likelihood of injury for the females in the rear impact in agreement with epidemiology data (Bose et al., 2011; Carlsson, 2012; Kahane J, 2013).

Chapter 6: Summary and Conclusions

The objective of this study was to develop 75 YO male and female neck models with average aged posture, based on existing young neck models. The motivation comes from epidemiology studies that suggest that the elderly are more susceptible to injury than the young population under similar loading conditions, potentially due to the different posture and hard tissue geometry, material properties, and/or exposure to different impact conditions. In addition, the elderly population is expected to increase over the next decade, especially in developed countries. Currently, there is no anthropometric test device (crash dummy) that represents this anthropometric group. Therefore, a tool to assess the efficacy of safety equipment on the elderly population is of interest. The aged population response associated with the morphological changes was assessed using human finite element models based on global response metrics (e.g. head kinematics) and local tissue measurements (e.g. capsular ligament strain).

A literature review to identify relevant geometrical factors that change with age was undertaken. The increased lordosis and facet angle were identified as important geometrical changes associated with increased age. A methodology to reposture and morph detailed human body models using a freely available reposturing package (PIPER) and a CAE tool (CATIA V5) was developed. The PIPER metadata developed in this research was made available to the research community through the PIPER community (www.piper-project.eu). The methodology was demonstrated to precisely reposture the male and female detailed neck models while retaining the mesh quality of the original models. The methods presented augments the reposturing capabilities in the field where other approaches have been used to morph, reposition and reposture HBMs by achieving targeted bone positions based on literature while retaining the mesh quality.

Female and male young subject-specific FE models were used (GHBMC F05-O v5.0 and M50-O v5.0 models) to investigate age and sex effects. The head and neck complex was extracted from the full-body models. Then, the capsular joint cartilage geometry (shape and thickness) of the two existing young models were enhanced based on literature data. The interfacet gap was closed as a consequence of the cartilage geometry modification, in agreement with imaging data. The models with the updated cartilage were then assessed at the full neck (in frontal, lateral and rear impacts) and motion segment (quasistatic extension, flexion, axial rotation, and lateral bending and dynamic extension-flexion loading) levels. The CORA ratings of the enhanced model improved over the original model at both the full neck and segment levels, suggesting that the facet joint cartilage plays a strong role in neck kinematics.

The updated models were repostured and morphed to represent an average aged version of their corresponding anthropometric groups using the available literature. The neck length and curvature of the young 50th male model were shown to be between that of a 50th percentile male and that of a 95th percentile male; as a result, the length of the aged model was larger, and the curvature was lower than those of a 50th percentile male as reported in the literature. The neck length and curvature of the young female model were in agreement with the literature data.

Then, to investigate the effect of the change in morphology and posture associated with age in males and females, the young and aged full neck models were evaluated under frontal, lateral and rear impacts with a variety of impact severities ranging from 2g to 15g. The head kinematics and the CL and IVD space strain were monitored and compared between models in frontal, lateral and rear impacts.

The effect of age was more evident in the male model than in the female model in the frontal impact. This was attributed to the combined effect of the head position and mass and to the longer than average neck. In aged models, both male and female, the head position was more anteriorly located than their young counterparts. Given that the male model had a higher mass head, a more anterior location induced more IVD space and CL strain in the frontal impacts. In the female model, the head mass was not enough to significantly affect the soft tissue response. Importantly, in the rear impact, the female model demonstrated higher CL and IVD space strain attributed to the modest contribution of the anterior muscles and to the greater curvature in the female models than in the male models. Such findings were in agreement with the literature that suggests that females are more susceptible to sustain injuries under rear impacts than males.

The trends observed in the CORA ratings were also observed in the soft tissue metrics, making the CORA ratings (or global metrics) potentially useful by giving the opportunity to quickly compare two models without the need to measure at the tissue level. For example, in the male models, the correlation ratings increased with increasing impact severity for the frontal impacts; this trend was also observed in the CL, and IVD space strain were at lower severities, the differences between young and aged were more pronounced than in the higher severities. Therefore, the common correlation rating thresholds used to define strong (> 0.71) similarity between curves might not be appropriate when comparing two computational models. Alternatively, correlation rating thresholds could be redefined in the context of the comparison of computational models, the likelihood of injury and soft tissue response given that general trends in CORA ratings are observed at the soft tissue level.

Differences in tissue response could be inferred based on head kinematics; however, it was shown in the present thesis that the direct measurements of deformation in the relevant tissues could better inform the differences in model response associated with geometrical changes consequence of the ageing process. Using global metrics to assess such effects could be insufficient to identify the effectiveness of safety equipment.

6.1.1 Limitations and Recommendations

Limitations of this study embed the limitations of the young FE neck models, in addition to the limitations introduced in the neck aged models. The material properties of the tissues through the model are based on experimental data, which often uses aged subjects and are not always in agreement with each other. That is, the age of the subjects used to test the cervical ligaments, for example, might not be the same age of the subjects used to test the passive muscle properties. Additional limitations include the lack of representation of some soft tissues (e.g. facet joint meniscoid and synovial fluid) that could potentially influence the soft tissue measurements presented in this study. In terms of the aged models, geometrically speaking, the growth of the hard tissue due to ossification was not implemented. The material properties, can change due to the ageing process, were not modified to reflect the aged population. It has been reported that the range of motion of the joints is reduced, and the bone strength reduces with age. Such changes could have a major effect on the neck tissue response under impact conditions. The muscle activation scheme was also not modified between the young and aged models. The neck models are symmetric in the sagittal plane; however, the vertebrae in a real human are highly non-symmetric. This asymmetry could be amplified with the ageing process, and, therefore, its effect is not captured in the present study. The muscle activation scheme in the aged population will likely be different than that of the young. The strength and reaction time of the neck muscles might decay with age, having an impact on the neck response.

In the current study, aged models that geometrically represent the average aged population were developed. However, the anthropometric variability dramatically increases with age; in the present study, variability was not accounted for. It is possible that the variability in posture has a more significant effect on the neck response than the average change in curvature. To understand the difference between sexes in neck response, in addition to the ageing process between males and females in the neck region, it would be desirable to develop a set of 4 models with the same middle arc length controlling the local neck length while varying the age and sex. A full set of material properties corresponding to a healthy 26 years old

subject could be of interest, given that the tissue testing used to populate the constitutive models is done using samples from subjects at different ages.

The full neck model has been validated against experimental data of young subjects using the head kinematic response using the T1 response as input; however, it would be ideal to have experiments of aged volunteers with data regarding vertebral kinematics to validate the aged models further using the T1 kinematics corresponding to an aged subject. Future work includes the assessment of the morphological changes associated with age together with material properties that represent this anthropometric group with the aim of better understanding the relationship between morphology and posture with material properties. In addition, the method to measure the soft tissue response needs more investigation. In the present study, IVD space and CL strain were used due to the implication of these tissues to injury; however, the interpretation of the tissue strain should be further investigated in order to better understand the implications of the ageing process in the soft tissue response.

Letter of Copyright Permissions

Copyright Clearance Center Marketplace™

Springer Nature BV - License Terms and Conditions

This is a License Agreement between Miguel Angel Corrales Fabre ("You") and Springer Nature BV ("Publisher") provided by Copyright Clearance Center ("CCC"). The license consists of your order details, the terms and conditions provided by Springer Nature BV, and the CCC terms and conditions.

All payments must be made in full to CCC.

Order Date	20-Aug-2020	Type of Use	Republish in a thesis/dissertation
Order license ID	1057096-1	Publisher	Kluwer Academic Publishers (Dordrecht)
ISSN	1573-9686	Portion	Image/photo/illustration

LICENSED CONTENT

Publication Title	Annals of biomedical engineering	Rightsholder	Springer Nature BV
Article Title	Cervical spine model to predict capsular ligament response in rear impact.	Publication Type	e-Journal
Author/Editor	American Institute of Physics., Biomedical Engineering Society.	Start Page	2152
Date	12/31/1971	End Page	2162
Language	English	Issue	8
Country	Netherlands	Volume	39

REQUEST DETAILS

Portion Type	Image/photo/illustration	Distribution	Worldwide
Number of images / photos / illustrations	1	Translation	Original language of publication
Format (select all that apply)	Print, Electronic	Copies for the disabled?	No
Who will republish the content?	Academic institution	Minor editing privileges?	No
Duration of Use	Life of current edition	Incidental promotional use?	No
Lifetime Unit Quantity	Up to 499	Currency	CAD
Rights Requested	Main product		

NEW WORK DETAILS

Title	Development of Elderly Posture Male and Female Finite Element Neck Models and Assessment of Tissue-Level Response Under Impact Loading.	**Institution name**	University of Waterloo
		Expected presentation date	2020-10-01
Instructor name	Duane S. Cronin		

ADDITIONAL DETAILS

The requesting person / organization to appear on the license	Miguel Angel Corrales Fabre

REUSE CONTENT DETAILS

Title, description or numeric reference of the portion(s)	Figure 1	**Title of the article/chapter the portion is from**	Cervical spine model to predict capsular ligament response in rear impact.
Editor of portion(s)	Jason, B., Fice; Duane, S., Cronin; Matthew, B., Panzer	**Author of portion(s)**	Jason, B., Fice; Duane, S., Cronin; Matthew, B., Panzer
Volume of serial or monograph	39	**Publication date of portion**	2011-04-30
Page or page range of portion	2152-2162		

PUBLISHER TERMS AND CONDITIONS

If you are placing a request on behalf of/for a corporate organization, please use RightsLink.For further information visit http://www.nature.com/reprints/permission-requests.html and https://www.springer.com/gp/rights-permissions/obtaining-permissions/882

CCC Republication Terms and Conditions

1. Description of Service; Defined Terms. This Republication License enables the User to obtain licenses for republication of one or more copyrighted works as described in detail on the relevant Order Confirmation (the "Work(s)"). Copyright Clearance Center, Inc. ("CCC") grants licenses through the Service on behalf of the rightsholder identified on the Order Confirmation (the "Rightsholder"). "Republication", as used herein, generally means the inclusion of a Work, in whole or in part, in a new work or works, also as described on the Order Confirmation. "User", as used herein, means the person or entity making such republication.

2. The terms set forth in the relevant Order Confirmation, and any terms set by the Rightsholder with respect to a particular Work, govern the terms of use of Works in connection with the Service. By using the Service, the person transacting for a republication license on behalf of the User represents and warrants that he/she/it (a) has been duly authorized by the User to accept, and hereby does accept, all such terms and conditions on behalf of User, and (b) shall inform User of all such terms and conditions. In the event such person is a "freelancer" or other third party independent of User and CCC, such party shall be deemed jointly a "User" for purposes of these terms and conditions. In any event, User shall be deemed to have accepted and agreed to all such terms and conditions if User republishes the Work in any fashion.

3. Scope of License; Limitations and Obligations.

   3.1. All Works and all rights therein, including copyright rights, remain the sole and exclusive property of the Rightsholder. The license created by the exchange of an Order Confirmation (and/or any invoice) and

payment by User of the full amount set forth on that document includes only those rights expressly set forth in the Order Confirmation and in these terms and conditions, and conveys no other rights in the Work(s) to User. All rights not expressly granted are hereby reserved.

3.2. General Payment Terms: You may pay by credit card or through an account with us payable at the end of the month. If you and we agree that you may establish a standing account with CCC, then the following terms apply: Remit Payment to: Copyright Clearance Center, 29118 Network Place, Chicago, IL 60673-1291. Payments Due: Invoices are payable upon their delivery to you (or upon our notice to you that they are available to you for downloading). After 30 days, outstanding amounts will be subject to a service charge of 1-1/2% per month or, if less, the maximum rate allowed by applicable law. Unless otherwise specifically set forth in the Order Confirmation or in a separate written agreement signed by CCC, invoices are due and payable on "net 30" terms. While User may exercise the rights licensed immediately upon issuance of the Order Confirmation, the license is automatically revoked and is null and void, as if it had never been issued, if complete payment for the license is not received on a timely basis either from User directly or through a payment agent, such as a credit card company.

3.3. Unless otherwise provided in the Order Confirmation, any grant of rights to User (i) is "one-time" (including the editions and product family specified in the license), (ii) is non-exclusive and non-transferable and (iii) is subject to any and all limitations and restrictions (such as, but not limited to, limitations on duration of use or circulation) included in the Order Confirmation or invoice and/or in these terms and conditions. Upon completion of the licensed use, User shall either secure a new permission for further use of the Work(s) or immediately cease any new use of the Work(s) and shall render inaccessible (such as by deleting or by removing or severing links or other locators) any further copies of the Work (except for copies printed on paper in accordance with this license and still in User's stock at the end of such period).

3.4. In the event that the material for which a republication license is sought includes third party materials (such as photographs, illustrations, graphs, inserts and similar materials) which are identified in such material as having been used by permission, User is responsible for identifying, and seeking separate licenses (under this Service or otherwise) for, any of such third party materials; without a separate license, such third party materials may not be used.

3.5. Use of proper copyright notice for a Work is required as a condition of any license granted under the Service. Unless otherwise provided in the Order Confirmation, a proper copyright notice will read substantially as follows: "Republished with permission of [Rightsholder's name], from [Work's title, author, volume, edition number and year of copyright]; permission conveyed through Copyright Clearance Center, Inc. " Such notice must be provided in a reasonably legible font size and must be placed either immediately adjacent to the Work as used (for example, as part of a by-line or footnote but not as a separate electronic link) or in the place where substantially all other credits or notices for the new work containing the republished Work are located. Failure to include the required notice results in loss to the Rightsholder and CCC, and the User shall be liable to pay liquidated damages for each such failure equal to twice the use fee specified in the Order Confirmation, in addition to the use fee itself and any other fees and charges specified.

3.6. User may only make alterations to the Work if and as expressly set forth in the Order Confirmation. No Work may be used in any way that is defamatory, violates the rights of third parties (including such third parties' rights of copyright, privacy, publicity, or other tangible or intangible property), or is otherwise illegal, sexually explicit or obscene. In addition, User may not conjoin a Work with any other material that may result in damage to the reputation of the Rightsholder. User agrees to inform CCC if it becomes aware of any infringement of any rights in a Work and to cooperate with any reasonable request of CCC or the Rightsholder in connection therewith.

4. Indemnity. User hereby indemnifies and agrees to defend the Rightsholder and CCC, and their respective employees and directors, against all claims, liability, damages, costs and expenses, including legal fees and expenses, arising out of any use of a Work beyond the scope of the rights granted herein, or any use of a Work which has been altered in any unauthorized way by User, including claims of defamation or infringement of rights of copyright, publicity, privacy or other tangible or intangible property.

5. Limitation of Liability. UNDER NO CIRCUMSTANCES WILL CCC OR THE RIGHTSHOLDER BE LIABLE FOR ANY DIRECT, INDIRECT, CONSEQUENTIAL OR INCIDENTAL DAMAGES (INCLUDING WITHOUT LIMITATION DAMAGES FOR LOSS OF BUSINESS PROFITS OR INFORMATION, OR FOR BUSINESS INTERRUPTION) ARISING OUT OF THE USE OR INABILITY TO USE A WORK, EVEN IF ONE OF THEM HAS BEEN ADVISED OF THE POSSIBILITY OF SUCH DAMAGES. In any event, the total liability of the Rightsholder and CCC (including their respective employees and directors) shall not exceed the total amount actually paid by User for this license. User assumes full liability for the actions and omissions of its principals, employees, agents, affiliates, successors and assigns.

6. Limited Warranties. THE WORK(S) AND RIGHT(S) ARE PROVIDED "AS IS". CCC HAS THE RIGHT TO GRANT TO USER THE RIGHTS GRANTED IN THE ORDER CONFIRMATION DOCUMENT. CCC AND THE RIGHTSHOLDER DISCLAIM ALL OTHER WARRANTIES RELATING TO THE WORK(S) AND RIGHT(S), EITHER EXPRESS OR IMPLIED, INCLUDING WITHOUT LIMITATION IMPLIED WARRANTIES OF MERCHANTABILITY OR FITNESS FOR A PARTICULAR PURPOSE. ADDITIONAL RIGHTS MAY BE REQUIRED TO USE ILLUSTRATIONS, GRAPHS, PHOTOGRAPHS, ABSTRACTS, INSERTS OR OTHER PORTIONS OF THE WORK (AS OPPOSED TO THE ENTIRE WORK) IN A MANNER CONTEMPLATED BY USER; USER UNDERSTANDS AND AGREES THAT NEITHER CCC NOR THE RIGHTSHOLDER MAY HAVE SUCH ADDITIONAL RIGHTS TO GRANT.

7. Effect of Breach. Any failure by User to pay any amount when due, or any use by User of a Work beyond the scope of the license set forth in the Order Confirmation and/or these terms and conditions, shall be a material breach of the license created by the Order Confirmation and these terms and conditions. Any breach not cured within 30 days of written notice thereof shall result in immediate termination of such license without further notice. Any unauthorized (but licensable) use of a Work that is terminated immediately upon notice thereof may be liquidated by payment of the Rightsholder's ordinary license price therefor; any unauthorized (and unlicensable) use that is not terminated immediately for any reason (including, for example, because materials containing the Work cannot reasonably be recalled) will be subject to all remedies available at law or in equity, but in no event to a payment of less than three times the Rightsholder's ordinary license price for the most closely analogous licensable use plus Rightsholder's and/or CCC's costs and expenses incurred in collecting such payment.

8. Miscellaneous.

    8.1. User acknowledges that CCC may, from time to time, make changes or additions to the Service or to these terms and conditions, and CCC reserves the right to send notice to the User by electronic mail or otherwise for the purposes of notifying User of such changes or additions; provided that any such changes or additions shall not apply to permissions already secured and paid for.

    8.2. Use of User-related information collected through the Service is governed by CCC's privacy policy, available online here:https://marketplace.copyright.com/rs-ui-web/mp/privacy-policy

    8.3. The licensing transaction described in the Order Confirmation is personal to User. Therefore, User may not assign or transfer to any other person (whether a natural person or an organization of any kind) the license created by the Order Confirmation and these terms and conditions or any rights granted hereunder; provided, however, that User may assign such license in its entirety on written notice to CCC in the event of a transfer of all or substantially all of User's rights in the new material which includes the Work(s) licensed under this Service.

    8.4. No amendment or waiver of any terms is binding unless set forth in writing and signed by the parties. The Rightsholder and CCC hereby object to any terms contained in any writing prepared by the User or its principals, employees, agents or affiliates and purporting to govern or otherwise relate to the licensing transaction described in the Order Confirmation, which terms are in any way inconsistent with any terms set forth in the Order Confirmation and/or in these terms and conditions or CCC's standard operating procedures, whether such writing is prepared prior to, simultaneously with or subsequent to the Order Confirmation, and whether such writing appears on a copy of the Order Confirmation or in a separate instrument.

    8.5. The licensing transaction described in the Order Confirmation document shall be governed by and

construed under the law of the State of New York, USA, without regard to the principles thereof of conflicts of law. Any case, controversy, suit, action, or proceeding arising out of, in connection with, or related to such licensing transaction shall be brought, at CCC's sole discretion, in any federal or state court located in the County of New York, State of New York, USA, or in any federal or state court whose geographical jurisdiction covers the location of the Rightsholder set forth in the Order Confirmation. The parties expressly submit to the personal jurisdiction and venue of each such federal or state court.If you have any comments or questions about the Service or Copyright Clearance Center, please contact us at 978-750-8400 or send an e-mail to support@copyright.com.

v 1.1

Copyright Clearance Center Marketplace™

Elsevier Science & Technology Journals - License Terms and Conditions

This is a License Agreement between Miguel Angel Corrales Fabre ("You") and Elsevier Science & Technology Journals ("Publisher") provided by Copyright Clearance Center ("CCC"). The license consists of your order details, the terms and conditions provided by Elsevier Science & Technology Journals, and the CCC terms and conditions.

All payments must be made in full to CCC.

Order Date	20-Aug-2020	**Type of Use**	Republish in a thesis/dissertation
Order license ID	1057096-2		
ISSN	1873-2380	**Publisher**	PERGAMON
		Portion	Image/photo/illustration

LICENSED CONTENT

Publication Title	Journal of biomechanics	**Rightsholder**	Elsevier Science & Technology Journals
Article Title	A female head-neck model for rear impact simulations.	**Publication Type**	e-Journal
		Start Page	49
Author/Editor	American Society of Biomechanics., European Society of Biomechanics., International Society of Biomechanics., Japanese Society for Clinical Biomechanics and Related Research., Australian and New Zealand Society of Biomechanics.	**End Page**	56
		Volume	51
		URL	http://www.sciencedirect.com/science/journal/00219290
Date	12/31/1967		
Language	English		
Country	United Kingdom of Great Britain and Northern Ireland		

REQUEST DETAILS

Portion Type	Image/photo/illustration	**Distribution**	Worldwide
Number of images / photos / illustrations	1	**Translation**	Original language of publication
Format (select all that apply)	Print, Electronic	**Copies for the disabled?**	No
		Minor editing privileges?	No
Who will republish the content?	Academic institution	**Incidental promotional use?**	No
Duration of Use	Life of current edition	**Currency**	CAD
Lifetime Unit Quantity	Up to 499		
Rights Requested	Main product		

NEW WORK DETAILS

Title	Development of Elderly Posture Male and Female Finite Element Neck Models and Assessment of Tissue-Level Response Under Impact Loading.	**Institution name**	University of Waterloo
		Expected presentation date	2020-10-01
Instructor name	Duane S, Cronin		

ADDITIONAL DETAILS

Order reference number	N/A	**The requesting person / organization to appear on the license**	Miguel Angel Corrales Fabre

REUSE CONTENT DETAILS

Title, description or numeric reference of the portion(s)	Figure 1	**Title of the article/chapter the portion is from**	A female head-neck model for rear impact simulations.
Editor of portion(s)	Östh, Jonas; Mendoza-Vazquez, Manuel; Sato, Fusako; Svensson, Mats Y.; Linder, Astrid; Brolin, Karin	**Author of portion(s)**	Östh, Jonas; Mendoza-Vazquez, Manuel; Sato, Fusako; Svensson, Mats Y.; Linder, Astrid; Brolin, Karin
Volume of serial or monograph	51	**Issue, if republishing an article from a serial**	N/A
Page or page range of portion	49-56	**Publication date of portion**	2016-11-25

PUBLISHER TERMS AND CONDITIONS

Elsevier publishes Open Access articles in both its Open Access journals and via its Open Access articles option in subscription journals, for which an author selects a user license permitting certain types of reuse without permission. Before proceeding please check if the article is Open Access on http://www.sciencedirect.com and refer to the user license for the individual article. Any reuse not included in the user license terms will require permission. You must always fully and appropriately credit the author and source. If any part of the material to be used (for example, figures) has appeared in the Elsevier publication for which you are seeking permission, with credit or acknowledgement to another source it is the responsibility of the user to ensure their reuse complies with the terms and conditions determined by the rights holder. Please contact permissions@elsevier.com with any queries.

CCC Republication Terms and Conditions

1. Description of Service; Defined Terms. This Republication License enables the User to obtain licenses for republication of one or more copyrighted works as described in detail on the relevant Order Confirmation (the "Work(s)"). Copyright Clearance Center, Inc. ("CCC") grants licenses through the Service on behalf of the rightsholder identified on the Order Confirmation (the "Rightsholder"). "Republication", as used herein, generally means the inclusion of a Work, in whole or in part, in a new work or works, also as described on the Order Confirmation. "User", as used herein, means the person or entity making such republication.

2. The terms set forth in the relevant Order Confirmation, and any terms set by the Rightsholder with respect to a particular Work, govern the terms of use of Works in connection with the Service. By using the Service, the person transacting for a republication license on behalf of the User represents and warrants that he/she/it (a) has been duly authorized by the User to accept, and hereby does accept, all such terms and conditions on behalf of User, and (b) shall inform User of all such terms and conditions. In the event such person is a "freelancer" or other third party independent of User and CCC, such party shall be deemed jointly a "User" for purposes of these terms and

conditions. In any event, User shall be deemed to have accepted and agreed to all such terms and conditions if User republishes the Work in any fashion.

3. Scope of License; Limitations and Obligations.

3.1. All Works and all rights therein, including copyright rights, remain the sole and exclusive property of the Rightsholder. The license created by the exchange of an Order Confirmation (and/or any invoice) and payment by User of the full amount set forth on that document includes only those rights expressly set forth in the Order Confirmation and in these terms and conditions, and conveys no other rights in the Work(s) to User. All rights not expressly granted are hereby reserved.

3.2. General Payment Terms: You may pay by credit card or through an account with us payable at the end of the month. If you and we agree that you may establish a standing account with CCC, then the following terms apply: Remit Payment to: Copyright Clearance Center, 29118 Network Place, Chicago, IL 60673-1291. Payments Due: Invoices are payable upon their delivery to you (or upon our notice to you that they are available to you for downloading). After 30 days, outstanding amounts will be subject to a service charge of 1-1/2% per month or, if less, the maximum rate allowed by applicable law. Unless otherwise specifically set forth in the Order Confirmation or in a separate written agreement signed by CCC, invoices are due and payable on "net 30" terms. While User may exercise the rights licensed immediately upon issuance of the Order Confirmation, the license is automatically revoked and is null and void, as if it had never been issued, if complete payment for the license is not received on a timely basis either from User directly or through a payment agent, such as a credit card company.

3.3. Unless otherwise provided in the Order Confirmation, any grant of rights to User (i) is "one-time" (including the editions and product family specified in the license), (ii) is non-exclusive and non-transferable and (iii) is subject to any and all limitations and restrictions (such as, but not limited to, limitations on duration of use or circulation) included in the Order Confirmation or invoice and/or in these terms and conditions. Upon completion of the licensed use, User shall either secure a new permission for further use of the Work(s) or immediately cease any new use of the Work(s) and shall render inaccessible (such as by deleting or by removing or severing links or other locators) any further copies of the Work (except for copies printed on paper in accordance with this license and still in User's stock at the end of such period).

3.4. In the event that the material for which a republication license is sought includes third party materials (such as photographs, illustrations, graphs, inserts and similar materials) which are identified in such material as having been used by permission, User is responsible for identifying, and seeking separate licenses (under this Service or otherwise) for, any of such third party materials; without a separate license, such third party materials may not be used.

3.5. Use of proper copyright notice for a Work is required as a condition of any license granted under the Service. Unless otherwise provided in the Order Confirmation, a proper copyright notice will read substantially as follows: "Republished with permission of [Rightsholder's name], from [Work's title, author, volume, edition number and year of copyright]; permission conveyed through Copyright Clearance Center, Inc. " Such notice must be provided in a reasonably legible font size and must be placed either immediately adjacent to the Work as used (for example, as part of a by-line or footnote but not as a separate electronic link) or in the place where substantially all other credits or notices for the new work containing the republished Work are located. Failure to include the required notice results in loss to the Rightsholder and CCC, and the User shall be liable to pay liquidated damages for each such failure equal to twice the use fee specified in the Order Confirmation, in addition to the use fee itself and any other fees and charges specified.

3.6. User may only make alterations to the Work if and as expressly set forth in the Order Confirmation. No Work may be used in any way that is defamatory, violates the rights of third parties (including such third parties' rights of copyright, privacy, publicity, or other tangible or intangible property), or is otherwise illegal, sexually explicit or obscene. In addition, User may not conjoin a Work with any other material that may result in damage to the reputation of the Rightsholder. User agrees to inform CCC if it becomes aware of any infringement of any rights in a Work and to cooperate with any reasonable request of CCC or the Rightsholder in connection therewith.

4. Indemnity. User hereby indemnifies and agrees to defend the Rightsholder and CCC, and their respective employees and directors, against all claims, liability, damages, costs and expenses, including legal fees and expenses, arising out of any use of a Work beyond the scope of the rights granted herein, or any use of a Work which has been altered in any unauthorized way by User, including claims of defamation or infringement of rights of copyright, publicity, privacy or other tangible or intangible property.

5. Limitation of Liability. UNDER NO CIRCUMSTANCES WILL CCC OR THE RIGHTSHOLDER BE LIABLE FOR ANY DIRECT, INDIRECT, CONSEQUENTIAL OR INCIDENTAL DAMAGES (INCLUDING WITHOUT LIMITATION DAMAGES FOR LOSS OF BUSINESS PROFITS OR INFORMATION, OR FOR BUSINESS INTERRUPTION) ARISING OUT OF THE USE OR INABILITY TO USE A WORK, EVEN IF ONE OF THEM HAS BEEN ADVISED OF THE POSSIBILITY OF SUCH DAMAGES. In any event, the total liability of the Rightsholder and CCC (including their respective employees and directors) shall not exceed the total amount actually paid by User for this license. User assumes full liability for the actions and omissions of its principals, employees, agents, affiliates, successors and assigns.

6. Limited Warranties. THE WORK(S) AND RIGHT(S) ARE PROVIDED "AS IS". CCC HAS THE RIGHT TO GRANT TO USER THE RIGHTS GRANTED IN THE ORDER CONFIRMATION DOCUMENT. CCC AND THE RIGHTSHOLDER DISCLAIM ALL OTHER WARRANTIES RELATING TO THE WORK(S) AND RIGHT(S), EITHER EXPRESS OR IMPLIED, INCLUDING WITHOUT LIMITATION IMPLIED WARRANTIES OF MERCHANTABILITY OR FITNESS FOR A PARTICULAR PURPOSE. ADDITIONAL RIGHTS MAY BE REQUIRED TO USE ILLUSTRATIONS, GRAPHS, PHOTOGRAPHS, ABSTRACTS, INSERTS OR OTHER PORTIONS OF THE WORK (AS OPPOSED TO THE ENTIRE WORK) IN A MANNER CONTEMPLATED BY USER; USER UNDERSTANDS AND AGREES THAT NEITHER CCC NOR THE RIGHTSHOLDER MAY HAVE SUCH ADDITIONAL RIGHTS TO GRANT.

7. Effect of Breach. Any failure by User to pay any amount when due, or any use by User of a Work beyond the scope of the license set forth in the Order Confirmation and/or these terms and conditions, shall be a material breach of the license created by the Order Confirmation and these terms and conditions. Any breach not cured within 30 days of written notice thereof shall result in immediate termination of such license without further notice. Any unauthorized (but licensable) use of a Work that is terminated immediately upon notice thereof may be liquidated by payment of the Rightsholder's ordinary license price therefor; any unauthorized (and unlicensable) use that is not terminated immediately for any reason (including, for example, because materials containing the Work cannot reasonably be recalled) will be subject to all remedies available at law or in equity, but in no event to a payment of less than three times the Rightsholder's ordinary license price for the most closely analogous licensable use plus Rightsholder's and/or CCC's costs and expenses incurred in collecting such payment.

8. Miscellaneous.

    8.1. User acknowledges that CCC may, from time to time, make changes or additions to the Service or to these terms and conditions, and CCC reserves the right to send notice to the User by electronic mail or otherwise for the purposes of notifying User of such changes or additions; provided that any such changes or additions shall not apply to permissions already secured and paid for.

    8.2. Use of User-related information collected through the Service is governed by CCC's privacy policy, available online here:https://marketplace.copyright.com/rs-ui-web/mp/privacy-policy

    8.3. The licensing transaction described in the Order Confirmation is personal to User. Therefore, User may not assign or transfer to any other person (whether a natural person or an organization of any kind) the license created by the Order Confirmation and these terms and conditions or any rights granted hereunder; provided, however, that User may assign such license in its entirety on written notice to CCC in the event of a transfer of all or substantially all of User's rights in the new material which includes the Work(s) licensed under this Service.

    8.4. No amendment or waiver of any terms is binding unless set forth in writing and signed by the parties. The Rightsholder and CCC hereby object to any terms contained in any writing prepared by the User or its principals, employees, agents or affiliates and purporting to govern or otherwise relate to the licensing

transaction described in the Order Confirmation, which terms are in any way inconsistent with any terms set forth in the Order Confirmation and/or in these terms and conditions or CCC's standard operating procedures, whether such writing is prepared prior to, simultaneously with or subsequent to the Order Confirmation, and whether such writing appears on a copy of the Order Confirmation or in a separate instrument.

8.5. The licensing transaction described in the Order Confirmation document shall be governed by and construed under the law of the State of New York, USA, without regard to the principles thereof of conflicts of law. Any case, controversy, suit, action, or proceeding arising out of, in connection with, or related to such licensing transaction shall be brought, at CCC's sole discretion, in any federal or state court located in the County of New York, State of New York, USA, or in any federal or state court whose geographical jurisdiction covers the location of the Rightsholder set forth in the Order Confirmation. The parties expressly submit to the personal jurisdiction and venue of each such federal or state court.If you have any comments or questions about the Service or Copyright Clearance Center, please contact us at 978-750-8400 or send an e-mail to support@copyright.com.

v 1.1

Bibliography

Barker, J.B., Cronin, D.S., 2020. Multi-Level Validation of a Male Neck Finite Element Model with Active Musculature. J. Biomech. Eng.

Barker, J.B., Cronin, D.S., Nightingale, R.W., 2017. Lower Cervical Spine Motion Segment Computational Model Validation: Kinematic and Kinetic Response for Quasi-Static and Dynamic Loading. J. Biomech. Eng. 139, 061009. https://doi.org/10.1115/1.4036464

Beillas, P., Berthet, F., 2017. An investigation of human body model morphing for the assessment of abdomen responses to impact against a population of test subjects. Traffic Inj. Prev. https://doi.org/10.1080/15389588.2017.1307971

Beillas, P., Petit, P., Kleiven, S., Kirscht, S., Chawla, A., Jolivet, E., Faure, F., Praxl, N., Bhaskar, A., 2015. Specifications of a Software Framework to Position and Personalise Human Body Models, in: IRCOBI 2015. pp. 594–595.

Boakye-Yiadom, S., Cronin, D.S., 2018. On the importance of retaining stresses and strains in repositioning computational biomechanical models of the cervical spine. Int. j. numer. method. biomed. eng. 34, 1–19. https://doi.org/10.1002/cnm.2905

Bogduk, N., Mercer, S., 2000. Biomechanics of the cervical spine. I: Normal kinematics. Clin. Biomech. https://doi.org/10.1016/S0268-0033(00)00034-6

Bose, D., Segui-Gomez, M., Crandall, J.R., 2011. Vulnerability of female drivers involved in motor vehicle crashes: An analysis of US population at risk. Am. J. Public Health. https://doi.org/10.2105/AJPH.2011.300275

Boyle, J.J.W., Milne, N., Singer, K.P., 2002. Influence of age on cervicothoracic spinal curvature: An ex vivo radiographic survey. Clin. Biomech. 17, 361–367. https://doi.org/10.1016/S0268-0033(02)00030-X

Burkhart, T.A., Andrews, D.M., Dunning, C.E., 2013. Finite element modeling mesh quality, energy balance and validation methods: A review with recommendations associated with the modeling of bone tissue. J. Biomech. https://doi.org/10.1016/j.jbiomech.2013.03.022

Camacho, D.L., Nightingale, R.W., Robinette, J.J., Vanguri, S.K., Coates, D.J., Myers, B.S., 1997. Experimental flexibility measurements for the development of a computational head-neck model

validated for near-vertex head impact. Most paper97334, 473–486. https://doi.org/10.4271/973345

Carlsson, A., 2012. Addressing Female Whiplash Injury Protection - A Step Towards 50th Percentile Female Rear Impact Occupant Models. Chalmers University of Technology.

Carlsson, A., Chang, F., Lemmen, P., Kullgren, A., Schmitt, K.U., Linder, A., Svensson, M.Y., 2014. Anthropometric Specifications, Development, and Evaluation of EvaRID-A 50th Percentile Female Rear Impact Finite Element Dummy Model. Traffic Inj. Prev. https://doi.org/10.1080/15389588.2014.885647

Cavanaugh, J.M., 2006. Pain Generation in Lumbar and Cervical Facet Joints. J. Bone Jt. Surg. https://doi.org/10.2106/jbjs.e.01411

Cesari, D., Compigne, S., Scherer, R., Xu, L., Takahashi, N., Page, M., Asakawa, K., Kostyniuk, G., Hautmann, E., Bortenschlager, K., Sakurai, M., Harigae, T., 2001. WorldSID Prototype Dummy Biomechanical Responses, in: SAE Technical Papers. https://doi.org/10.4271/2001-22-0013

Corrales, M.A., Cronin, D.S., 2019. Effect of Aged Neck Posture on Kinematics and Tissue-Level Response in Frontal Impact Conditions., in: International Research Council on the Biomechanics of Injury.

Correia, M.A., McLachlin, S.D., Cronin, D.S., 2020a. Optimization of muscle activation schemes in a finite element neck model simulating volunteer frontal impact scenarios. J. Biomech. https://doi.org/10.1016/j.jbiomech.2020.109754

Correia, M.A., McLachlin, S.D., Cronin, D.S., 2020b. Optimization of muscle activation schemes in a finite element neck model simulating volunteer frontal impact scenarios. J. Biomech. 104, 109754. https://doi.org/10.1016/j.jbiomech.2020.109754

Curatolo, M., Bogduk, N., Ivancic, P.C., McLean, S.A., Siegmund, G.P., Winkelstein, B.A., 2011. The role of tissue damage in whiplash-associated disorders. Spine (Phila. Pa. 1976). https://doi.org/10.1097/BRS.0b013e318238842a

Damas, S., Cordón, O., Ibáñez, O., 2020. Handbook on Craniofacial Superimposition, Handbook on Craniofacial Superimposition. https://doi.org/10.1007/978-3-319-11137-7

Davis, J., Kaufman, K.R., Lieber, R.L., 2003. Correlation between active and passive isometric force and intramuscular pressure in the isolated rabbit tibialis anterior muscle. J. Biomech. https://doi.org/10.1016/S0021-9290(02)00430-X

Deng, B., Begeman, P.C., Yang, K.H., Tashman, S., King, A.I., 2000. Kinematics of Human Cadaver Cervical Spine during Low Speed Rear-End Impacts, in: SAE Technical Papers. https://doi.org/10.4271/2000-01-SC13

Deng, Y.C., Li, X., Liu, Y., 1999. Modeling of the human cervical spine using finite element techniques, in: SAE Technical Papers. https://doi.org/10.4271/1999-01-1310

Denozière, G., Ku, D.N., 2006. Biomechanical comparison between fusion of two vertebrae and implantation of an artificial intervertebral disc. J. Biomech. https://doi.org/10.1016/j.jbiomech.2004.07.039

DeWit, J.A., Cronin, D.S., 2012. Cervical spine segment finite element model for traumatic injury prediction. J. Mech. Behav. Biomed. Mater. 10, 138–150. https://doi.org/10.1016/j.jmbbm.2012.02.015

DiSilvestro, M.R., Suh, J.K.F., 2001. A cross-validation of the biphasic poroviscoelastic model of articular cartilage in unconfined compression, indentation, and confined compression. J. Biomech. https://doi.org/10.1016/S0021-9290(00)00224-4

Ebara, S., Iatridis, J.C., Setton, L.A., Foster, R.J., Van Mow, C., Weidenbaum, M., 1996. Tensile properties of nondegenerate human lumbar anulus fibrosus. Spine (Phila. Pa. 1976). https://doi.org/10.1097/00007632-199602150-00009

Farrell, S.F., Osmotherly, P.G., Rivett, D.A., Cornwall, J., 2015. Can E12 sheet plastination be used to examine the presence and incidence of intra-articular spinal meniscoids? Anatomy. https://doi.org/10.2399/ana.14.046

Fice, J.B., Cronin, D.S., 2012. Investigation of whiplash injuries in the upper cervical spine using a detailed neck model. J. Biomech. https://doi.org/10.1016/j.jbiomech.2012.01.016

Fice, J.B., Cronin, D.S., Panzer, M.B., 2011. Cervical Spine Model to Predict Capsular Ligament Response in Rear Impact. Ann. Biomed. Eng. 39, 2152–2162. https://doi.org/10.1007/s10439-011-0315-4

Fon, G.J., Pitt, M.J., Thies, A.C., 1980. Thoracic kyphosis: Range in normal subjects. Am. J. Roentgenol. https://doi.org/10.2214/ajr.134.5.979

Fréchède, B., Bertholon, N., Le Coz, J.-Y., Lavaste, F., Skalli, W., 2005. Finite element model of the human neck during omni-directional impacts. Part I. Kinematics and injury. Rev. Eur. des éléments

finis. https://doi.org/10.3166/reef.14.463-485

Frechede, B., Bertholon, N., Saillant, G., Lavaste, F., Skalli, W., 2006. Finite element model of the human neck during omni-directional impacts. Part II: relation between cervical curvature and risk of injury. Comput. Methods Biomech. Biomed. Engin. 9, 379–86. https://doi.org/10.1080/10255840600980940

Frechede, B, Bertholon, N., Saillant, G., Lavaste, F., Skalli, W., 2006. Finite element model of the human neck during omni-directional impacts. Part II: relation between cervical curvature and risk of injury. Comput. Methods Biomech. Biomed. Engin. 9, 379–86. https://doi.org/10.1080/10255840600980940

Fujita, Y., Duncan, N.A., Lotz, J.C., 1997. Radial tensile properties of the lumbar annulus fibrosus are site and degeneration dependent. J. Orthop. Res. https://doi.org/10.1002/jor.1100150605

Gayzik, F.S., Moreno, D.P., Geer, C.P., Wuertzer, S.D., Martin, R.S., Stitzel, J.D., 2011. Development of a full body CAD dataset for computational modeling: A multi-modality approach. Ann. Biomed. Eng. 39, 2568–2583. https://doi.org/10.1007/s10439-011-0359-5

Gilad, I., Nissan, M., 1986. A study of vertebra and disc geometric relations of the human cervical and lumbar spine. Spine (Phila. Pa. 1976). https://doi.org/10.1097/00007632-198603000-00010

Gordon, C.C., Blackwell, C.L., Bradtmiller, B., Parham, J.L., Barrientos, P., Paquette, S.P., Corner, B.D., Carson, J.M., Venezia, J.C., Rockwell, B.M., Mucher, M., Kristensen, S., 2014. 2012 Anthropometric Survey of U.S. Army Personnel: Methods and Summary Statistics. Security.

Gordon, C.C., Churchill, T., Clauser, C.E., Bradtmiller, B., McConville, J.T., Tebbetts, I., Walker, R. a, 1989. 1988 Anthropometric Survey of U.S. Army Personnel: Pilot Summary Statistics. Security.

Hadjidakis, D.J., Androulakis, I.I., 2006. Bone remodeling, in: Annals of the New York Academy of Sciences. https://doi.org/10.1196/annals.1365.035

Happee, R., 1994. Inverse dynamic optimization including muscular dynamics, a new simulation method applied to goal directed movements. J. Biomech. 27, 953–960.

Hedenstierna, S., Halldin, P., Brolin, K., 2008. Evaluation of a combination of continuum and truss finite elements in a model of passive and active muscle tissue. Comput. Methods Biomech. Biomed. Engin. https://doi.org/10.1080/17474230802312516

Heinrich, D., Holzmann, C., Wagner, A., Fischer, A., Pfeifer, R., Graw, M., Schick, S., 2017. What are

the differences in injury patterns of young and elderly traffic accident fatalities considering death on scene and death in hospital? Int. J. Legal Med. https://doi.org/10.1007/s00414-017-1531-8

Hiroshi Yamada, 1971. Hiroshi Yamada. (1971). Strength of Biological Materials. Journal of anatomy (Vol. 108). http://doi.org/10.1016/0021-9290(71)90027-3Strength of Biological Materials. J. Anat. https://doi.org/10.1016/0021-9290(71)90027-3

Holzapfel, G.A., Schulze-Bauer, C.A.J., Feigl, G., Regitnig, P., 2005. Single lamellar mechanics of the human lumbar anulus fibrosus. Biomech. Model. Mechanobiol. https://doi.org/10.1007/s10237-004-0053-8

HOSOYA, N, 2002. Japanese anthropometric reference data 2001 (JARD 2001). Japanese J. Nutr. Assess. 19, 1–81.

Hu, J., Zhang, K., Reed, M.P., Wang, J.-T., Neal, M., Lin, C.-H., 2019. Frontal crash simulations using parametric human models representing a diverse population. Traffic Inj. Prev. 20, S97–S105. https://doi.org/10.1080/15389588.2019.1581926

Huang, J., Long, Y., Yan, Y., Hu, L., 2018. Development and validation of an age-specific lower extremity finite element model for simulating pedestrian accidents. Appl. Bionics Biomech. https://doi.org/10.1155/2018/5906987

Humzah, M.D., Soames, R.W., 1988. Human intervertebral disc: Structure and function. Anat. Rec. 220, 337–356.

Ivancic, P.C., Panjabi, M.M., Ito, S., Cripton, P.A., Wang, J.L., 2005. Biofidelic whole cervical spine model with muscle force replication for whiplash simulation. Eur. Spine J. https://doi.org/10.1007/s00586-004-0758-5

Iwamoto, M., Nakahira, Y., Kimpara, H., 2015. Development and Validation of the Total HUman Model for Safety (THUMS) Toward Further Understanding of Occupant Injury Mechanisms in Precrash and During Crash. Traffic Inj. Prev. https://doi.org/10.1080/15389588.2015.1015000

Janak, T., Lafon, Y., Petit, P., Beillas, P., 2018. Transformation Smoothing to use after Positioning of Finite Element Human Body Models, in: IRCOBI 2018. pp. 224–236.

Jaumard, N. V., Bauman, J.A., Weisshaar, C.L., Guarino, B.B., Welch, W.C., Winkelstein, B.A., 2011. Contact pressure in the facet joint during sagittal bending of the cadaveric cervical spine. J. Biomech. Eng. https://doi.org/10.1115/1.4004409

John, J.D., Arun, M.W.J., Saravanakumar, G., Yoganandan, N., 2017. Cervical spine finite element model with anatomically accurate asymmetric intervertebral discs, in: Summer Biomechanics, Bioengineering, and Biotransport Conference.

John, J.D., Yoganandan, N., Arun, M.W.J., Saravana Kumar, G., 2018. Influence of morphological variations on cervical spine segmental responses from inertial loading. Traffic Inj. Prev. https://doi.org/10.1080/15389588.2017.1403017

Kahane J, C., 2013. Injury Vulnerability and Effectiveness of Occupant Protection Technologies for Older Occupants and Women. Natl. Highw. Traffic Saf. Adm. https://doi.org/Report No. DOT HS 811 766

Kasra, M., Parnianpour, M., Shirazi-Adl, A., Wang, J.L., Grynpas, M.D., 2004. Effect of strain rate on tensile properties of sheep disc anulus fibrosus. Technol. Heal. Care. https://doi.org/10.3233/thc-2004-12405

Keaveny, T.M., Morgan, E.F., Niebur, G.L., Yeh, O.C., 2001. Biomechanics of Trabecular Bone. Annu. Rev. Biomed. Eng. https://doi.org/10.1146/annurev.bioeng.3.1.307

Kitagawa, Y., Yasuki, T., Hasegawa, J., 2008. Research study on neck injury lessening with active head restraint using human body FE model. Traffic Inj. Prev. https://doi.org/10.1080/15389580802381954

Kitagawa, Y., Yasuki, T., Hasegawa, J., 2006. A study of cervical spine kinematics and joint capsule strain in rear impacts using a human FE model. Stapp Car Crash J. https://doi.org/2006-22-0020 [pii]

Klinich, K.D., Ebert, S.M., Reed, M.P., 2012. Quantifying Cervical-Spine Curvature Using Bézier Splines. J. Biomech. Eng. 134, 114503. https://doi.org/10.1115/1.4007749

Klinich, K.D., Ebert, S.M., Van Ee, C.A., Flannagan, C.A.C., Prasad, M., Reed, M.P., Schneider, L.W., 2004. Cervical Spine Geometry in the Automotive Seated Posture: Variations with Age, Stature, and Gender. Stapp Car Crash J. 48, 301–330. https://doi.org/2004-22-00014 [pii]

Knaub, K., Myers, B.S., 1998. Cervical Spine Muscle. Natl. Highw. Traffic Saf. Adm. NHTSA-98-3.

Knupp, P.M., 2002. Algebraic mesh quality metrics. SIAM J. Sci. Comput. https://doi.org/10.1137/S1064827500371499

Kullgren, A., Stigson, H., Krafft, M., 2013. Development of whiplash associated disorders for male and

female car occupants in cars launched since the 80s in different impact directions, in: 2013 IRCOBI Conference Proceedings - International Research Council on the Biomechanics of Injury.

Langlois, J.A., Rutland-Brown, W., Wald, M.M., 2006. The Epidemiology and Impact of Traumatic Brain Injury A Brief Overview. J Head Trauma Rehabil. https://doi.org/00001199-200609000-00001 [pii]

Lindahl, O., 1976. Mechanical properties of dried defatted spongy bone. Acta Orthop. https://doi.org/10.3109/17453677608998966

Lomoschitz, F.M., Blackmore, C.C., Mirza, S.K., Mann, F.A., 2002. Cervical spine injuries in patients 65 years old and older: epidemiologic analysis regarding the effects of age and injury mechanism on distribution, type, and stability of injuries. AJR. Am. J. Roentgenol. https://doi.org/10.2214/ajr.178.3.1780573

Mattucci, S.F.E., Cronin, D.S., 2015. A method to characterize average cervical spine ligament response based on raw data sets for implementation into injury biomechanics models. J. Mech. Behav. Biomed. Mater. https://doi.org/10.1016/j.jmbbm.2014.09.023

Mattucci, S.F.E., Moulton, J.A., Chandrashekar, N., Cronin, D.S., 2012. Strain rate dependent properties of younger human cervical spine ligaments. J. Mech. Behav. Biomed. Mater. https://doi.org/10.1016/j.jmbbm.2012.02.004

McElhaney, J.H., 1966. Dynamic response of bone and muscle tissue. J. Appl. Physiol. https://doi.org/10.1152/jappl.1966.21.4.1231

Mertz, H.J., Irwin, A.L., Melvin, J.W., Stanaker, R.L., Beebe, M.S., 1989. Size, weight and biomechanical impact response requirements for adult size small female and large male dummies, in: SAE Technical Papers. https://doi.org/10.4271/890756

Meyer, F., Bourdet, N., Deck, C., Willinger, R., Raul, J.S., 2004. Human Neck Finite Element Model Development and Validation against Original Experimental Data, in: SAE Technical Papers. https://doi.org/10.4271/2004-22-0008

Moroney, S.P., Schultz, A.B., Miller, J.A.A., Andersson, G.B.J., 1988. Load-displacement properties of lower cervical spine motion segments. J. Biomech. 21, 769–779. https://doi.org/10.1016/0021-9290(88)90285-0

Ng, H.-W., Teo, E.-C., Lee, K.-K., Qiu, T.-X., 2003. Finite element analysis of cervical spinal instability

under physiologic loading. J. Spinal Disord. Tech.

Nightingale, R.W., Carol Chancey, V., Ottaviano, D., Luck, J.F., Tran, L., Prange, M., Myers, B.S., 2007a. Flexion and extension structural properties and strengths for male cervical spine segments. J. Biomech. 40, 535–542. https://doi.org/10.1016/j.jbiomech.2006.02.015

Nightingale, R.W., Carol Chancey, V., Ottaviano, D., Luck, J.F., Tran, L., Prange, M., Myers, B.S., 2007b. Flexion and extension structural properties and strengths for male cervical spine segments. J. Biomech. 40, 535–542. https://doi.org/10.1016/j.jbiomech.2006.02.015

Östh, J., Brolin, K., Svensson, M.Y., Linder, A., 2016. A Female Ligamentous Cervical Spine Finite Element Model Validated for Physiological Loads. J. Biomech. Eng. https://doi.org/10.1115/1.4032966

Östh, J., Mendoza-Vazquez, M., Sato, F., Svensson, M.Y., Linder, A., Brolin, K., 2017a. A female head–neck model for rear impact simulations. J. Biomech. https://doi.org/10.1016/j.jbiomech.2016.11.066

Östh, J., Mendoza-Vazquez, M., Sato, F., Svensson, M.Y., Linder, A., Brolin, K., 2017b. A female head–neck model for rear impact simulations. J. Biomech. 51, 49–56. https://doi.org/10.1016/J.JBIOMECH.2016.11.066

Panjabi, M.M., Crisco, J.J., Vasavada, A., Oda, T., Cholewicki, J., Nibu, K., Shin, E., 2001. Mechanical properties of the human cervical spine as shown by three-dimensional load-displacement curves. Spine (Phila. Pa. 1976). 26, 2692–2700. https://doi.org/10.1097/00007632-200112150-00012

Panjabi, Manohar M., Duranceau, J., Goel, V., Oxland, T., Takata, K., 1991a. Cervical human vertebrae: Quantitative three-dimensional anatomy of the middle and lower regions. Spine (Phila. Pa. 1976). https://doi.org/10.1097/00007632-199108000-00001

Panjabi, M.M., Oxland, T., Takata, K., Goel, V., Duranceau, J., Krag, M., 1993. Articular facets of the human spine. Quantitative three-dimensional anatomy. Spine (Phila. Pa. 1976). 18, 1298–310. https://doi.org/10.1097/00007632-199308000-00009

Panjabi, Manohar M, Oxland, T.R., Parks, E.H., 1991. Quantitative Anatomy of Cervical Spine Ligaments. Part II. Middle and Lower Cervical Spine. J. Spinal Disord. 4, 277–285. https://doi.org/10.1097/00002517-199109000-00004

Panjabi, Manohar M., Oxland, T.R., Parks, E.H., 1991b. Quantitative Anatomy of Cervical Spine Ligaments. Part I. Upper Cervical Spine. J. Spinal Disord. https://doi.org/10.1097/00002517-

199109000-00003

Panjabi, M M, Oxland, T.R., Parks, E.H., 1991c. Quantitative anatomy of cervical spine ligaments. Part II. Middle and lower cervical spine. J. Spinal Disord. https://doi.org/10.1097/00002517-199109000-00004

Panzer, M.B., Cronin, D.S., 2009. C4-C5 segment finite element model development, validation, and load-sharing investigation. J. Biomech. https://doi.org/10.1016/j.jbiomech.2008.11.036

Panzer, M.B., Fice, J.B., Cronin, D.S., 2011. Cervical spine response in frontal crash. Med. Eng. Phys. https://doi.org/10.1016/j.medengphy.2011.05.004

Parenteau, C.S., Wang, N.C., Zhang, P., Caird, M.S., Wang, S.C., 2014. Quantification of Pediatric and Adult Cervical Vertebra—Anatomical Characteristics by Age and Gender for Automotive Application. Traffic Inj. Prev. 15, 572–582. https://doi.org/10.1080/15389588.2013.843774

Park, J., Ebert, S.M., Reed, M.P., Hallman, J.J., 2016a. Statistical Models for Predicting Automobile Driving Postures for Men and Women Including Effects of Age. Hum. Factors 58, 261–278. https://doi.org/10.1177/0018720815610249

Park, J., Ebert, S.M., Reed, M.P., Hallman, J.J., 2016b. A statistical model including age to predict passenger postures in the rear seats of automobiles. Ergonomics 59, 796–805. https://doi.org/10.1080/00140139.2015.1088076

Pearson, A.M., Ivancic, P.C., Ito, S., Panjabi, M.M., 2004. Facet Joint Kinematics and Injury Mechanisms during Simulated Whiplash. Spine (Phila. Pa. 1976). https://doi.org/10.1097/01.BRS.0000090836.50508.F7

Pooni, J.S., Hukins, D.W.L., Harris, P.F., Hilton, R.C., Davies, K.E., 1986. Comparison of the structure of human intervertebral discs in the cervical, thoracic and lumbar regions of the spine. Surg. Radiol. Anat. https://doi.org/10.1007/BF02427846

Przybylski, G.J., Patel, P.R., Carlin, G.J., Woo, S.L.Y., 1998. Quantitative anthropometry of the subatlantal cervical longitudinal ligaments. Spine (Phila. Pa. 1976). https://doi.org/10.1097/00007632-199804150-00010

Putra, I.P.A., Iraeus, J., Thomson, R., Svensson, M.Y., Linder, A., Sato, F., 2019. Comparison of control strategies for the cervical muscles of an average female head-neck finite element model. Traffic Inj. Prev. https://doi.org/10.1080/15389588.2019.1670818

Pyttel, T., Floss, A., Thibaud, C., Goertz, C., 2007. Realistic simulation models for airbags and humans-new possibilities and limits of FE simulation. Int. J. Crashworthiness. https://doi.org/10.1080/13588260701483524

Quinn, K.P., Winkelstein, B.A., 2007. Cervical facet capsular ligament yield defines the threshold for injury and persistent joint-mediated neck pain. J. Biomech. https://doi.org/10.1016/j.jbiomech.2006.10.015

Reed, M.P., Jones, M.L.H., 2017. A Parametric Model of Cervical Spine Geometry and Posture A Parametric Model of Cervical Spine Geometry and Posture.

Reilly, D.T., Burstein, A.H., Frankel, V.H., 1974. The elastic modulus for bone. J. Biomech. https://doi.org/10.1016/0021-9290(74)90018-9

Schneider, L., Robbins, D., Pflüg, M., Snyder, R., 1983. Development of Anthropometrically Based Design Specifications for an Advanced Adult Anthropomorphic Dummy Family.

Schwartz, D., Guleyupoglu, B., Koya, B., Stitzel, J.D., Gayzik, F.S., 2015. Development of a Computationally Efficient Full Human Body Finite Element Model. Traffic Inj. Prev. https://doi.org/10.1080/15389588.2015.1021418

Schwer, L., 2006. Guide for verification and validation in computational solid mechanics. Am. Soc. Mech. Eng.

Shen, T.-W.D., n.d. Investigation of Whiplash Associated Disorders using Finite Element Neck Models with Active Musculature in Frontal, Rear and Lateral Impact. University of Waterloo.

Skaggs, D.L., Weidenbaum, M., Latridis, J.C., Ratcliffe, A., Mow, V.C., 1994. Regional variation in tensile properties and biochemical composition of the human lumbar anulus fibrosus. Spine (Phila. Pa. 1976). https://doi.org/10.1097/00007632-199406000-00002

Stemper, B.D., Yoganandan, N., Pintar, F.A., 2005. Effects of abnormal posture on capsular ligament elongations in a computational model subjected to whiplash loading. J. Biomech. https://doi.org/10.1016/j.jbiomech.2004.06.013

Takeshita, K., Peterson, E.T.K., Bylski-Austrow, D., Crawford, A.H., Nakamura, K., 2004. The nuchal ligament restrains cervical spine flexion. Spine (Phila. Pa. 1976).

Trajkovski, A., Omerović, S., Hribernik, M., Prebil, I., 2014. Failure properties and damage of cervical spine ligaments, experiments and modeling. J. Biomech. Eng. https://doi.org/10.1115/1.4026424

Wheeldon, J.A., Pintar, F.A., Knowles, S., Yoganandan, N., 2006. Experimental flexion/extension data corridors for validation of finite element models of the young, normal cervical spine. J. Biomech. 39, 375–380. https://doi.org/10.1016/j.jbiomech.2004.11.014

Winters, J.M., 1995. How detailed should muscle models be to understand multi-joint movement coordination? Hum. Mov. Sci. https://doi.org/10.1016/0167-9457(95)00023-6

Winters, J.M., 1990. Hill-Based Muscle Models: A Systems Engineering Perspective, in: Multiple Muscle Systems. https://doi.org/10.1007/978-1-4613-9030-5_5

Winters, J.M., Stark, L., 1988. Estimated mechanical properties of synergistic muscles involved in movements of a variety of human joints. J. Biomech. https://doi.org/10.1016/0021-9290(88)90249-7

Winters, J.M., Stark, L., 1985. Analysis of Fundamental Human Movement Patterns Through the Use of In-Depth Antagonistic Muscle Models. IEEE Trans. Biomed. Eng. https://doi.org/10.1109/TBME.1985.325498

Wismans, J., Philippens, M., Van Oorschot, E., Kallieris, D., Mattern, R., 1987. Comparison of human volunteer and cadaver head-neck response in frontal flexion, in: SAE Technical Papers. https://doi.org/10.4271/872194

Wismans, J., Spenny, C.H., 1983. Performance requirements for mechanical necks in lateral flexion, in: SAE Technical Papers. https://doi.org/10.4271/831613

Womack, W., Ayturk, U.M., Puttlitz, C.M., 2011. Cartilage Thickness Distribution Affects Computational Model Predictions of Cervical Spine Facet Contact Parameters. J. Biomech. Eng. 133, 011009. https://doi.org/10.1115/1.4002855

Womack, W., Woldtvedt, D., Puttlitz, C.M., 2008. Lower cervical spine facet cartilage thickness mapping. Osteoarthr. Cartil. 16, 1018–1023. https://doi.org/10.1016/j.joca.2008.01.007

Yang, K.H., 2017. Basic finite element method as applied to injury biomechanics, Basic Finite Element Method as Applied to Injury Biomechanics. https://doi.org/10.1016/c2015-0-06702-8

Yang, K.H., Kish, V.L., 1988. Compressibility measurement of human intervertebral nucleus pulposus. J. Biomech. https://doi.org/10.1016/0021-9290(88)90059-0

Yang, K.H., Zhu, F., Luan, F., Zhao, L., Begeman, P.C., Yang KH Luan F, et al, Z.F., 1998. Development of a Finite Element Model of the Human Neck. 42nd Stapp Car Crash Conf. https://doi.org/10.4271/983157.

Yoganandan, N., Cusick, J.F., Pintar, F.A., Rao, R.D., 2001. Whiplash injury determination with conventional spine imaging and cryomicrotomy, in: Spine. https://doi.org/10.1097/00007632-200111150-00010

Yoganandan, N., Knowles, S.A., Maiman, D.J., Pintar, F.A., 2003. Anatomic study of the morphology of human cervical facet joint. Spine (Phila. Pa. 1976). https://doi.org/10.1097/01.BRS.0000085356.89103.A5

Zhang, K., Cao, L., Fanta, A., Reed, M.P., Neal, M., Wang, J.T., Lin, C.H., Hu, J., 2017. An automated method to morph finite element whole-body human models with a wide range of stature and body shape for both men and women. J. Biomech. https://doi.org/10.1016/j.jbiomech.2017.06.015

Zhang, Q.H., Tan, S.H., Teo, E.C., 2008. Finite element analysis of head-neck kinematics under simulated rear impact at different accelerations. Proc. Inst. Mech. Eng. Part H J. Eng. Med. https://doi.org/10.1243/09544119JEIM209

Appendix 1: Segment Level Validation of the Updated Cartilage Geometry

Segment C34:

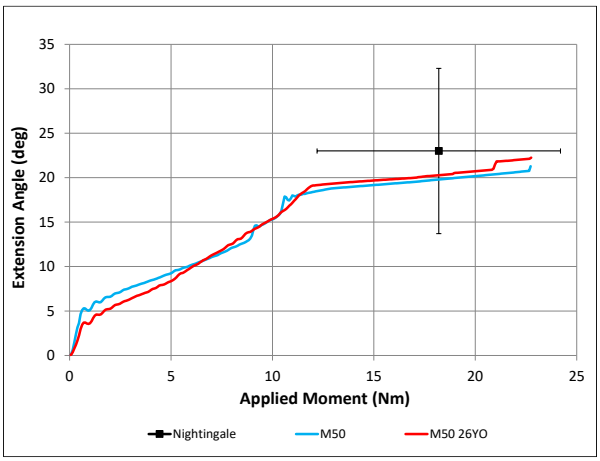

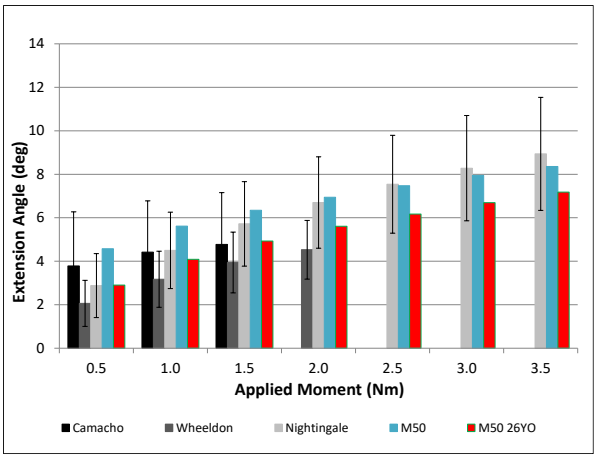

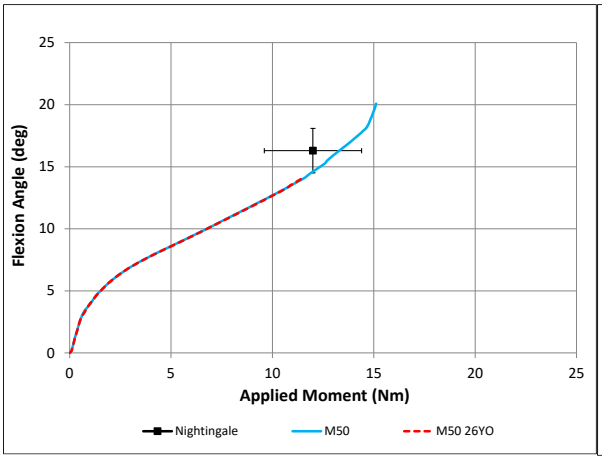

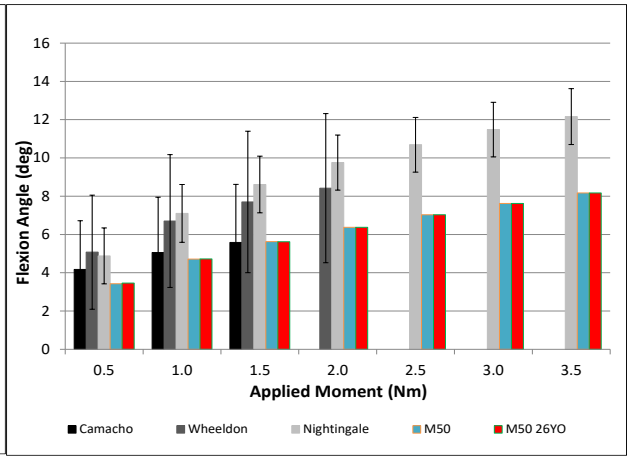

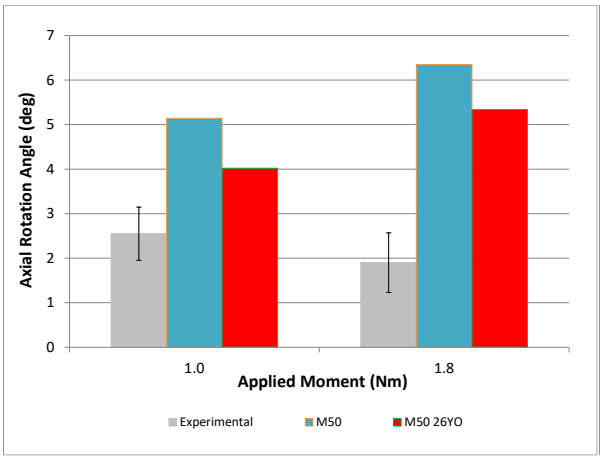
Axial Rotation Angle (deg)
0
1
2
3
4
5
6
7
1.0
1.8
Applied Moment (Nm)
Experimental
M50
M50 26YO

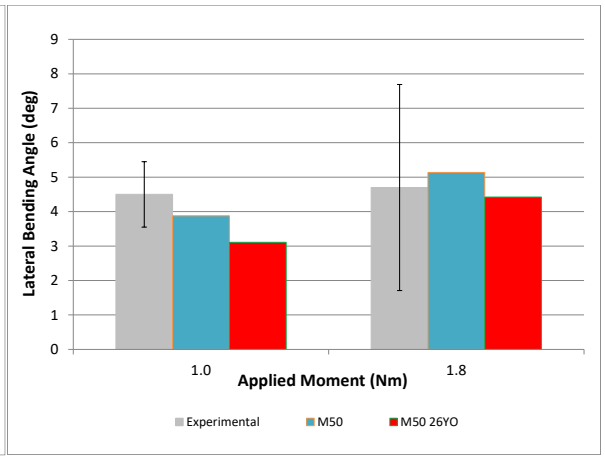
Lateral Bending Angle (deg)
0
1
2
3
4
5
6
7
8
9
1.0
1.8
Applied Moment (Nm)
Experimental
M50
M50 26YO

Segment C45:

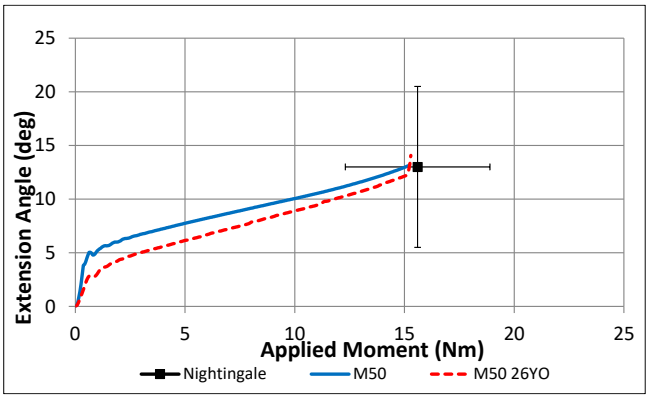
Extension Angle (deg)
0
5
10
15
20
25
0
5
10
15
20
25
Applied Moment (Nm)
Nightingale
M50
M50 26YO

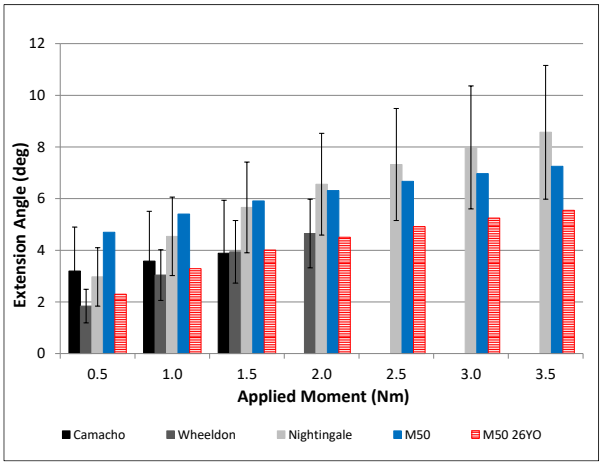
Extension Angle (deg)
0
2
4
6
8
10
12
0.5
1.0
1.5
2.0
2.5
3.0
3.5
Applied Moment (Nm)
Camacho
Wheeldon
Nightingale
M50
M50 26YO

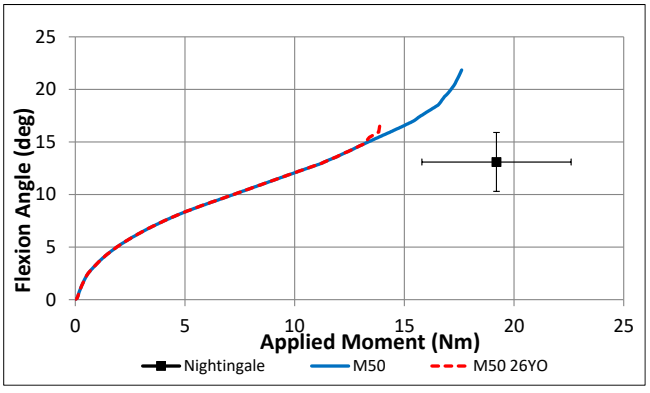
Flexion Angle (deg)
0
5
10
15
20
25
0
5
10
15
20
25
Applied Moment (Nm)
Nightingale
M50
M50 26YO

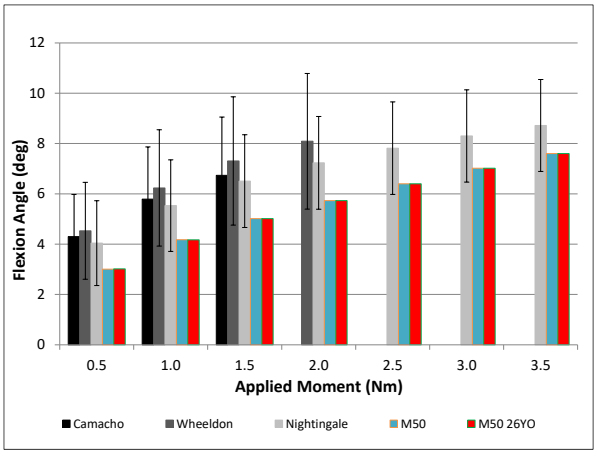
Flexion Angle (deg)
0
2
4
6
8
10
12
0.5
1.0
1.5
2.0
2.5
3.0
3.5
Applied Moment (Nm)
Camacho
Wheeldon
Nightingale
M50
M50 26YO

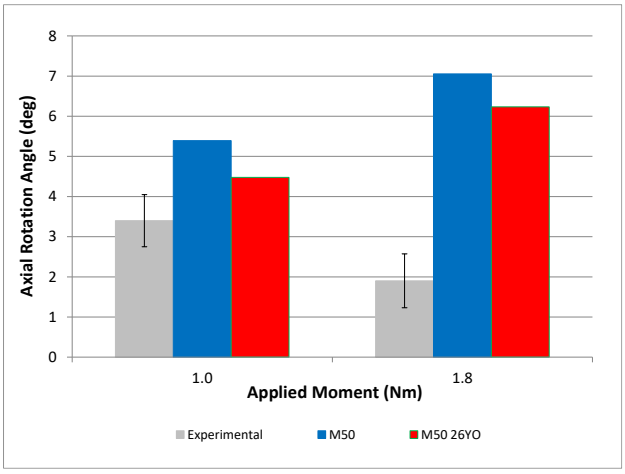
Axial Rotation Angle (deg)
Applied Moment (Nm)
1.0
1.8
Experimental
M50
M50 26YO

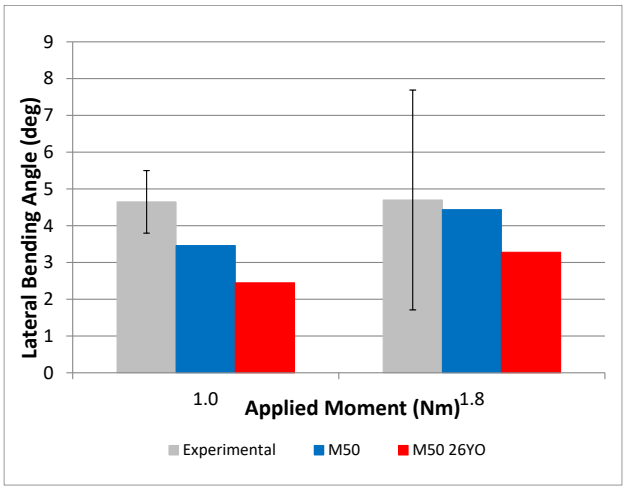
Lateral Bending Angle (deg)
Applied Moment (Nm)
1.0
1.8
Experimental
M50
M50 26YO

Segment C56

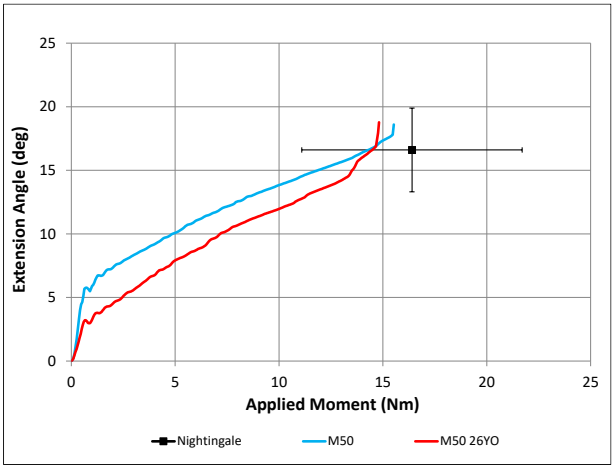
Extension Angle (deg)
Applied Moment (Nm)
Nightingale
M50
M50 26YO

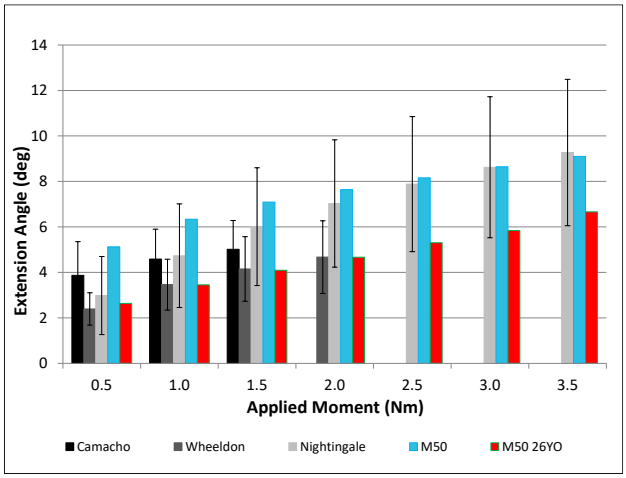
Extension Angle (deg)
Applied Moment (Nm)
Camacho
Wheeldon
Nightingale
M50
M50 26YO

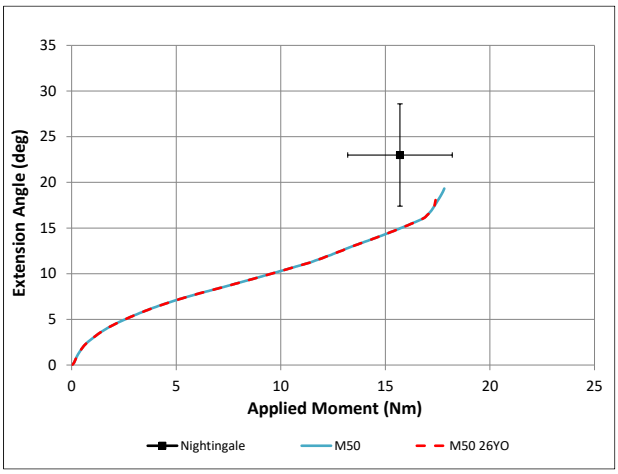
Extension Angle (deg)
Applied Moment (Nm)
Nightingale
M50
M50 26YO

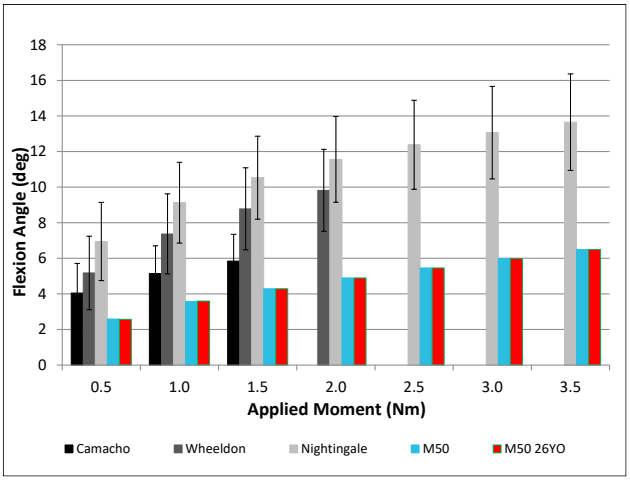
Flexion Angle (deg)
Applied Moment (Nm)
Camacho
Wheeldon
Nightingale
M50
M50 26YO

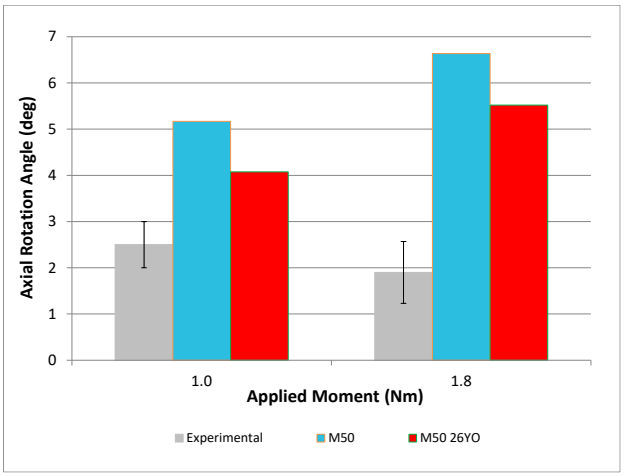
Axial Rotation Angle (deg)
0
1
2
3
4
5
6
7
1.0
1.8
Applied Moment (Nm)
Experimental
M50
M50 26YO

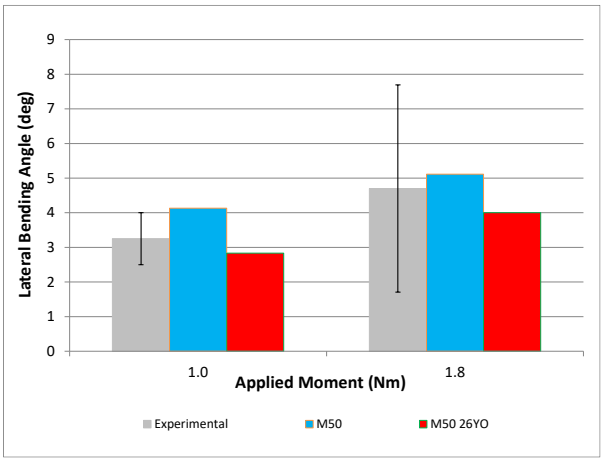
Lateral Bending Angle (deg)
0
1
2
3
4
5
6
7
8
9
1.0
1.8
Applied Moment (Nm)
Experimental
M50
M50 26YO

Segment C67:

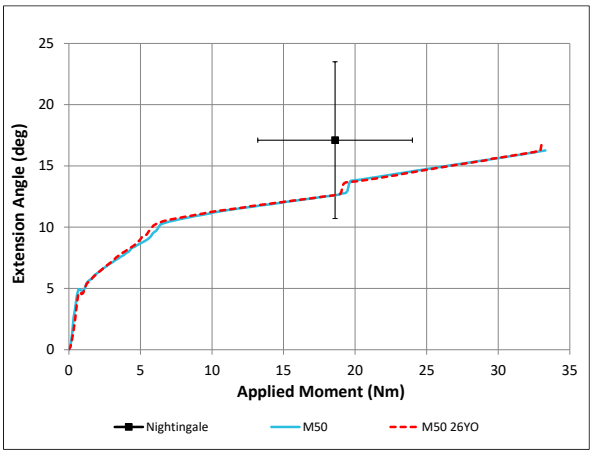
Extension Angle (deg)
0
5
10
15
20
25
0
5
10
15
20
25
30
35
Applied Moment (Nm)
Nightingale
M50
M50 26YO

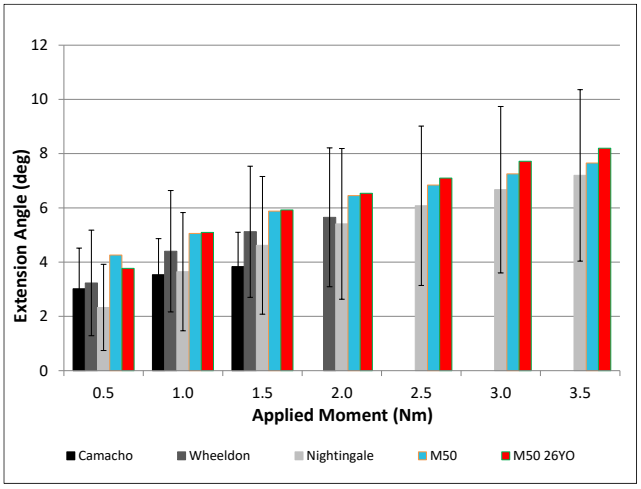
Extension Angle (deg)
0
2
4
6
8
10
12
0.5
1.0
1.5
2.0
2.5
3.0
3.5
Applied Moment (Nm)
Camacho
Wheeldon
Nightingale
M50
M50 26YO

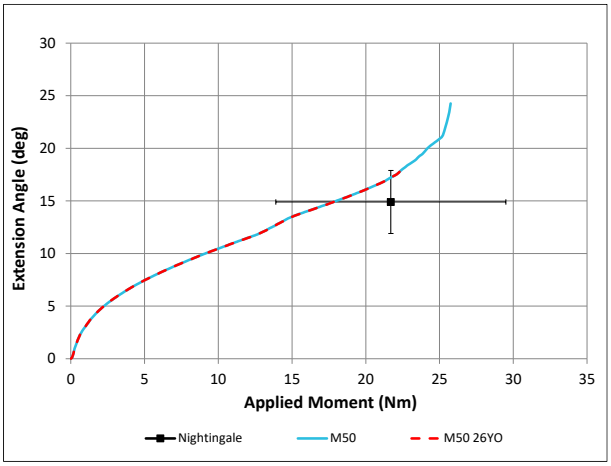
Extension Angle (deg)
0
5
10
15
20
25
30
0
5
10
15
20
25
30
35
Applied Moment (Nm)
Nightingale
M50
M50 26YO

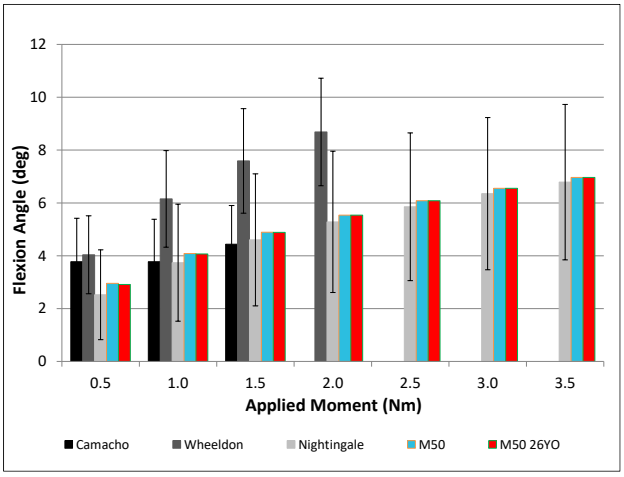
Flexion Angle (deg)
0
2
4
6
8
10
12
0.5
1.0
1.5
2.0
2.5
3.0
3.5
Applied Moment (Nm)
Camacho
Wheeldon
Nightingale
M50
M50 26YO

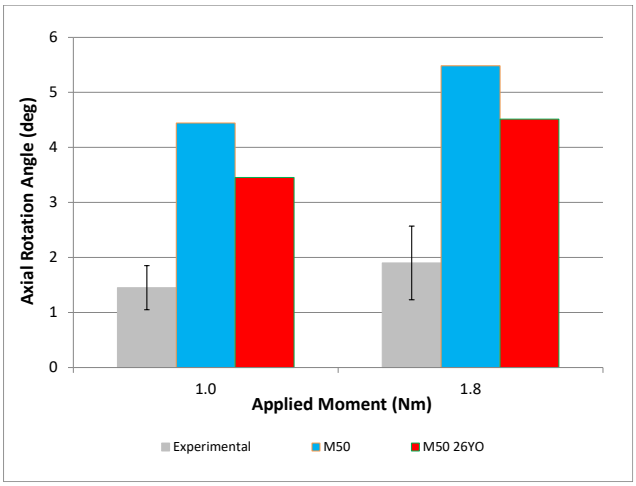
Axial Rotation Angle (deg)
6
5
4
3
2
1
0
1.0
1.8
Applied Moment (Nm)
Experimental
M50
M50 26YO

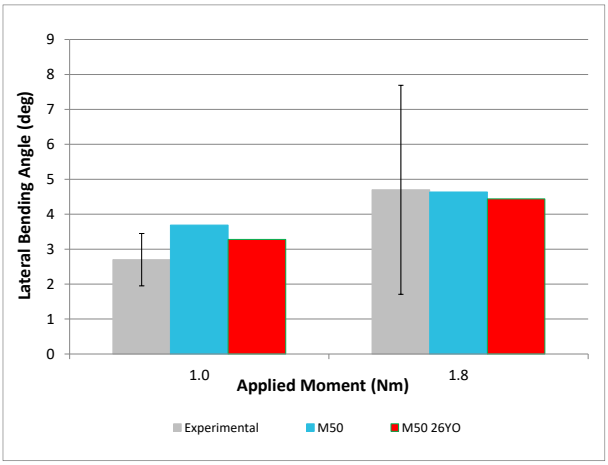
Lateral Bending Angle (deg)
9
8
7
6
5
4
3
2
1
0
1.0
1.8
Applied Moment (Nm)
Experimental
M50
M50 26YO

Appendix 2: Full Neck Level Validation of the Updated Cartilage Geometry

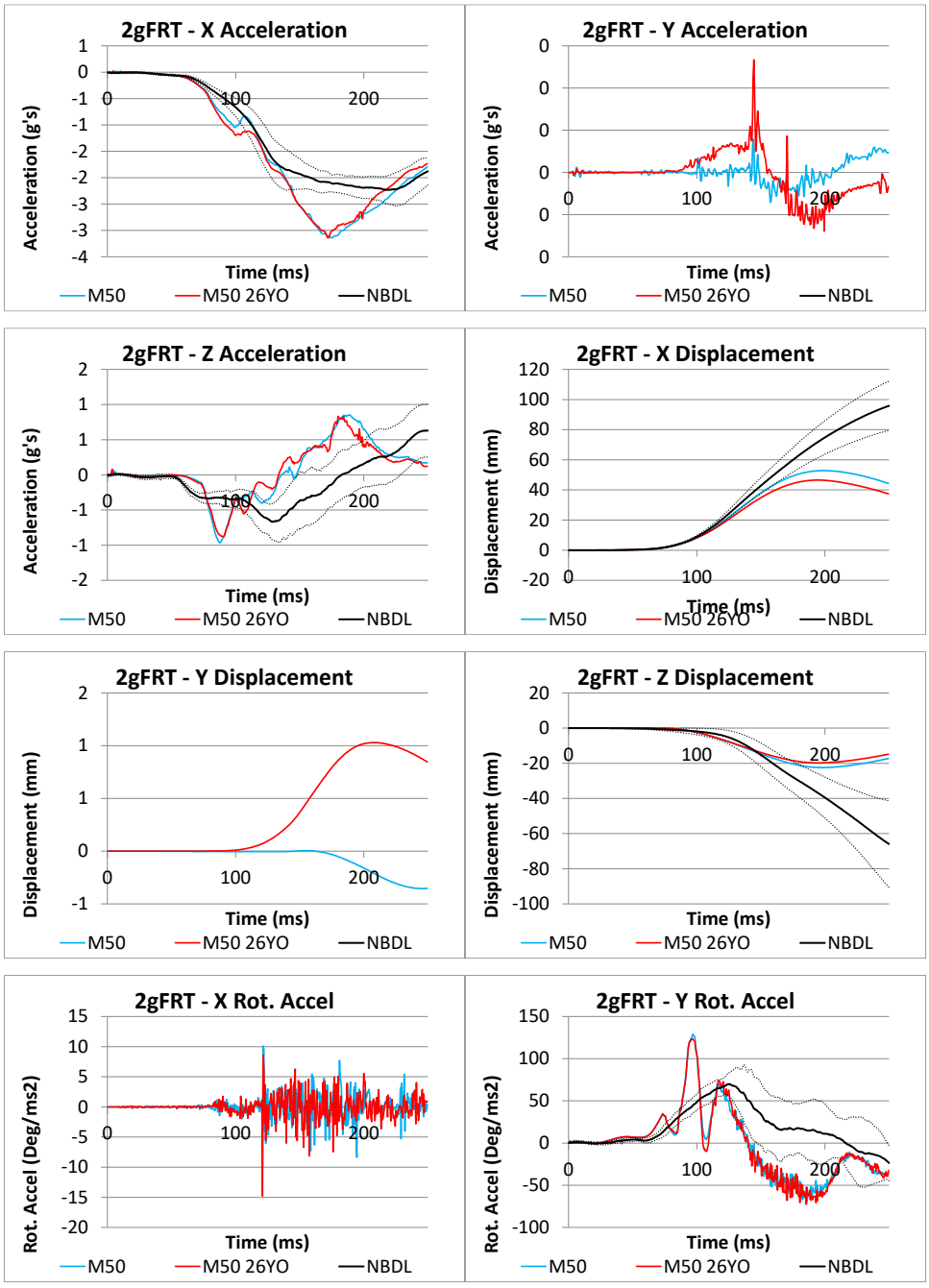

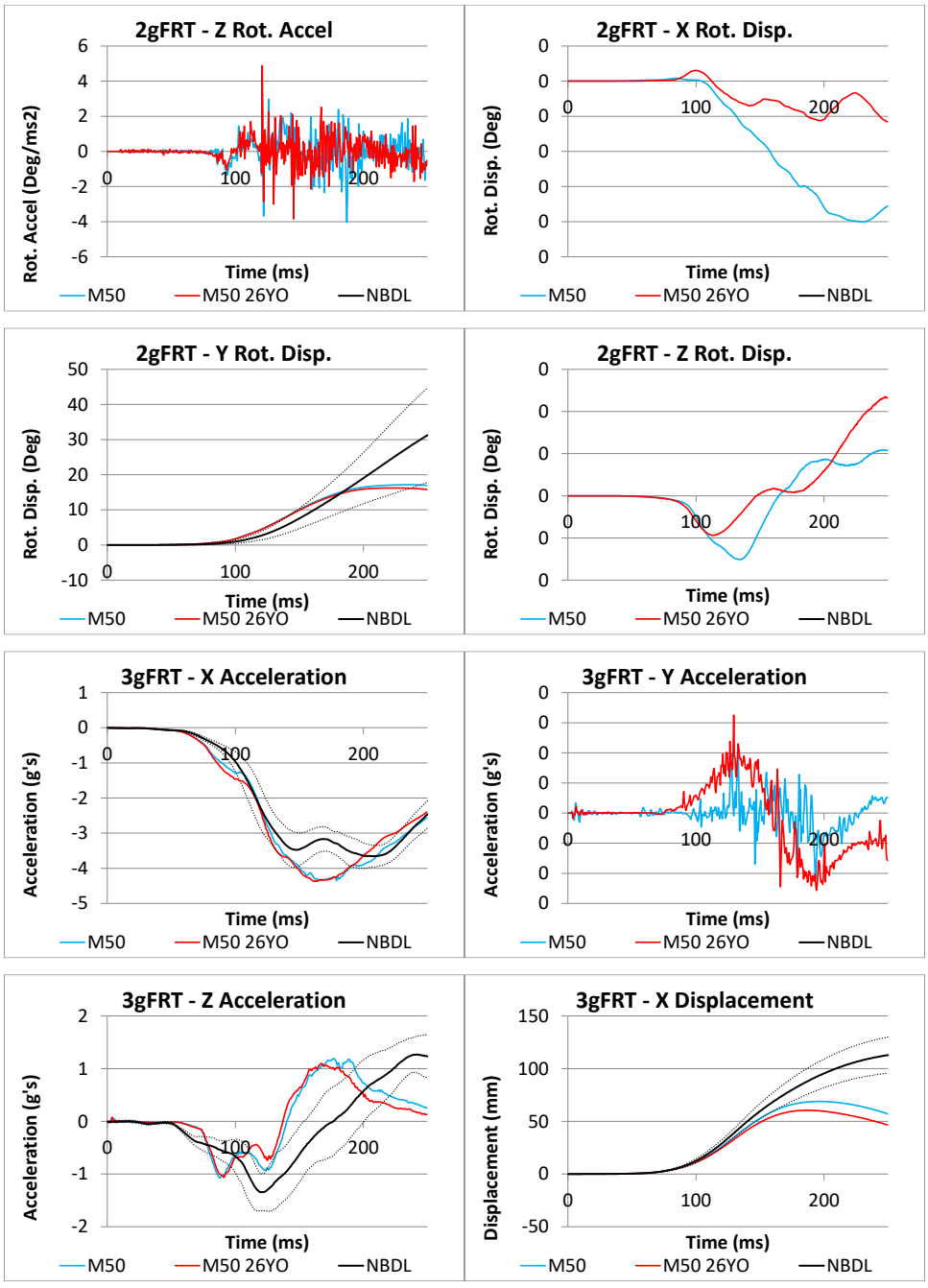
2gFRT - Z Rot. Accel
Rot. Accel (Deg/ms2)
Time (ms)
M50
M50 26YO
NBDL
2gFRT - X Rot. Disp.
Rot. Disp. (Deg)
Time (ms)
M50
M50 26YO
NBDL
2gFRT - Y Rot. Disp.
Rot. Disp. (Deg)
Time (ms)
M50
M50 26YO
NBDL
2gFRT - Z Rot. Disp.
Rot. Disp. (Deg)
Time (ms)
M50
M50 26YO
NBDL
3gFRT - X Acceleration
Acceleration (g's)
Time (ms)
M50
M50 26YO
NBDL
3gFRT - Y Acceleration
Acceleration (g's)
Time (ms)
M50
M50 26YO
NBDL
3gFRT - Z Acceleration
Acceleration (g's)
Time (ms)
M50
M50 26YO
NBDL
3gFRT - X Displacement
Displacement (mm)
Time (ms)
M50
M50 26YO
NBDL

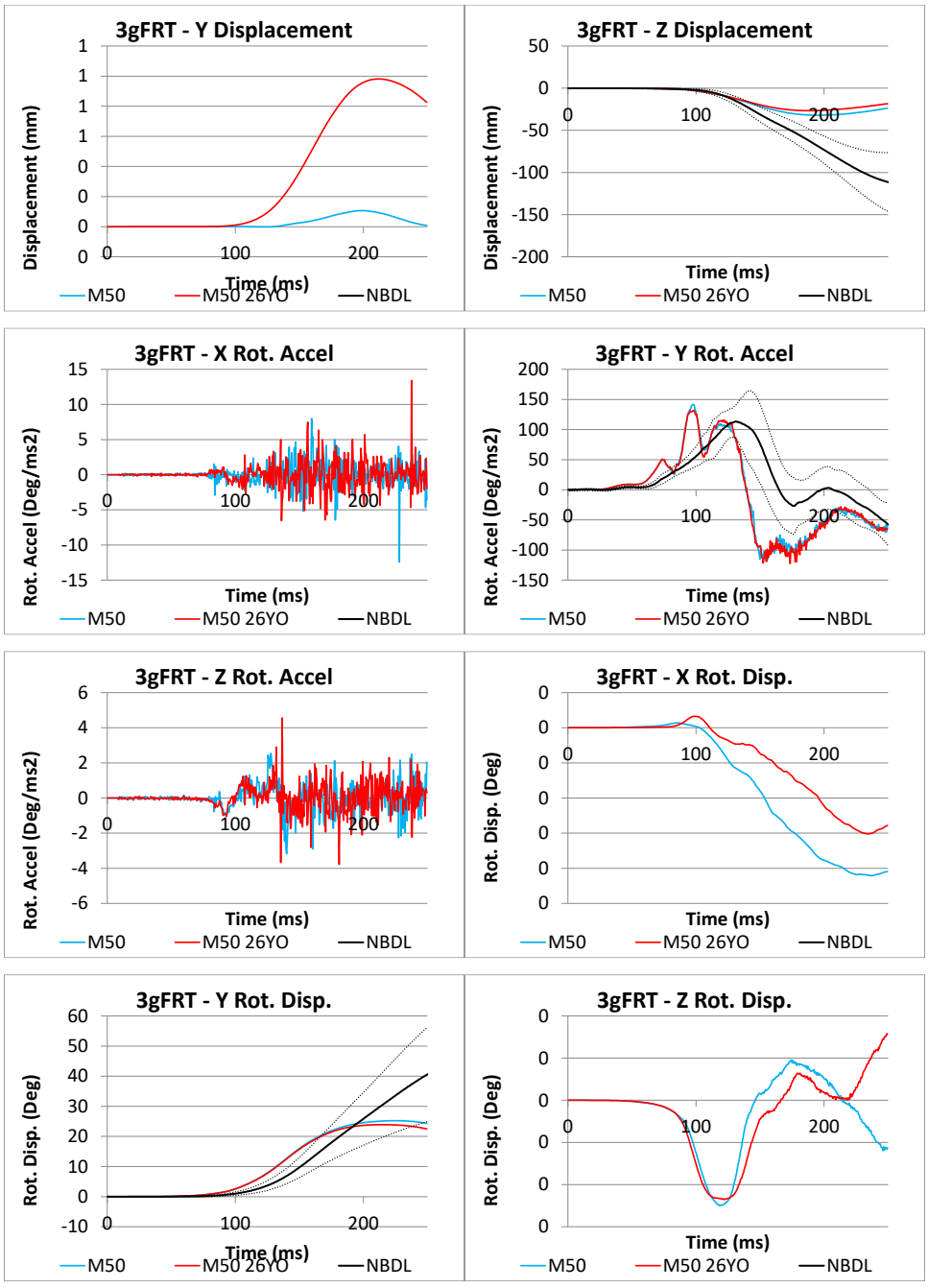
3gFRT - Y Displacement
Displacement (mm)
Time (ms)
M50
M50 26YO
NBDL
3gFRT - Z Displacement
Displacement (mm)
Time (ms)
M50
M50 26YO
NBDL
3gFRT - X Rot. Accel
Rot. Accel (Deg/ms2)
Time (ms)
M50
M50 26YO
NBDL
3gFRT - Y Rot. Accel
Rot. Accel (Deg/ms2)
Time (ms)
M50
M50 26YO
NBDL
3gFRT - Z Rot. Accel
Rot. Accel (Deg/ms2)
Time (ms)
M50
M50 26YO
NBDL
3gFRT - X Rot. Disp.
Rot. Disp. (Deg)
Time (ms)
M50
M50 26YO
NBDL
3gFRT - Y Rot. Disp.
Rot. Disp. (Deg)
Time (ms)
M50
M50 26YO
NBDL
3gFRT - Z Rot. Disp.
Rot. Disp. (Deg)
Time (ms)
M50
M50 26YO
NBDL

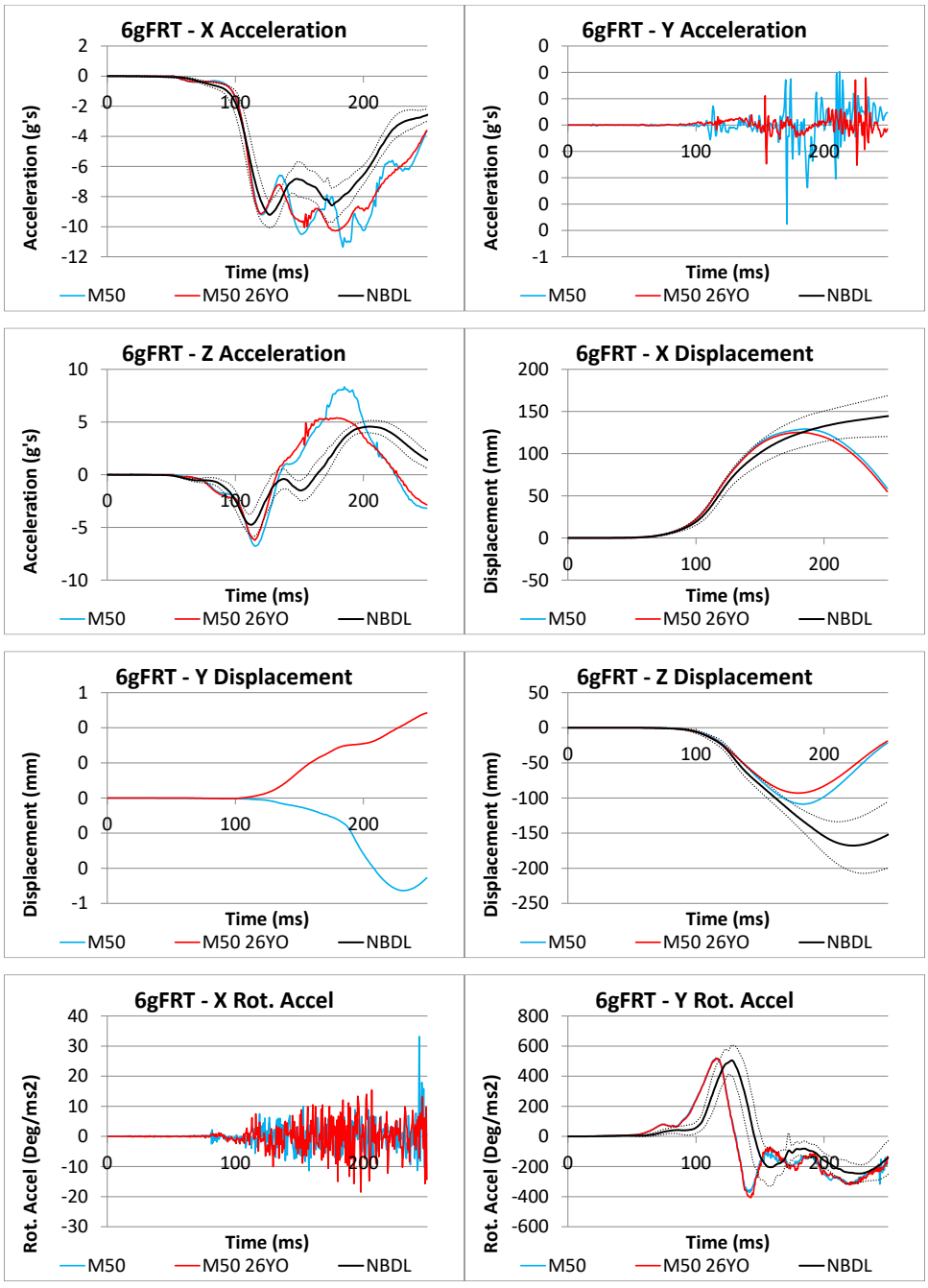
6gFRT - X Acceleration
Acceleration (g's)
Time (ms)
M50
M50 26YO
NBDL
6gFRT - Y Acceleration
Acceleration (g's)
Time (ms)
M50
M50 26YO
NBDL
6gFRT - Z Acceleration
Acceleration (g's)
Time (ms)
M50
M50 26YO
NBDL
6gFRT - X Displacement
Displacement (mm)
Time (ms)
M50
M50 26YO
NBDL
6gFRT - Y Displacement
Displacement (mm)
Time (ms)
M50
M50 26YO
NBDL
6gFRT - Z Displacement
Displacement (mm)
Time (ms)
M50
M50 26YO
NBDL
6gFRT - X Rot. Accel
Rot. Accel (Deg/ms2)
Time (ms)
M50
M50 26YO
NBDL
6gFRT - Y Rot. Accel
Rot. Accel (Deg/ms2)
Time (ms)
M50
M50 26YO
NBDL

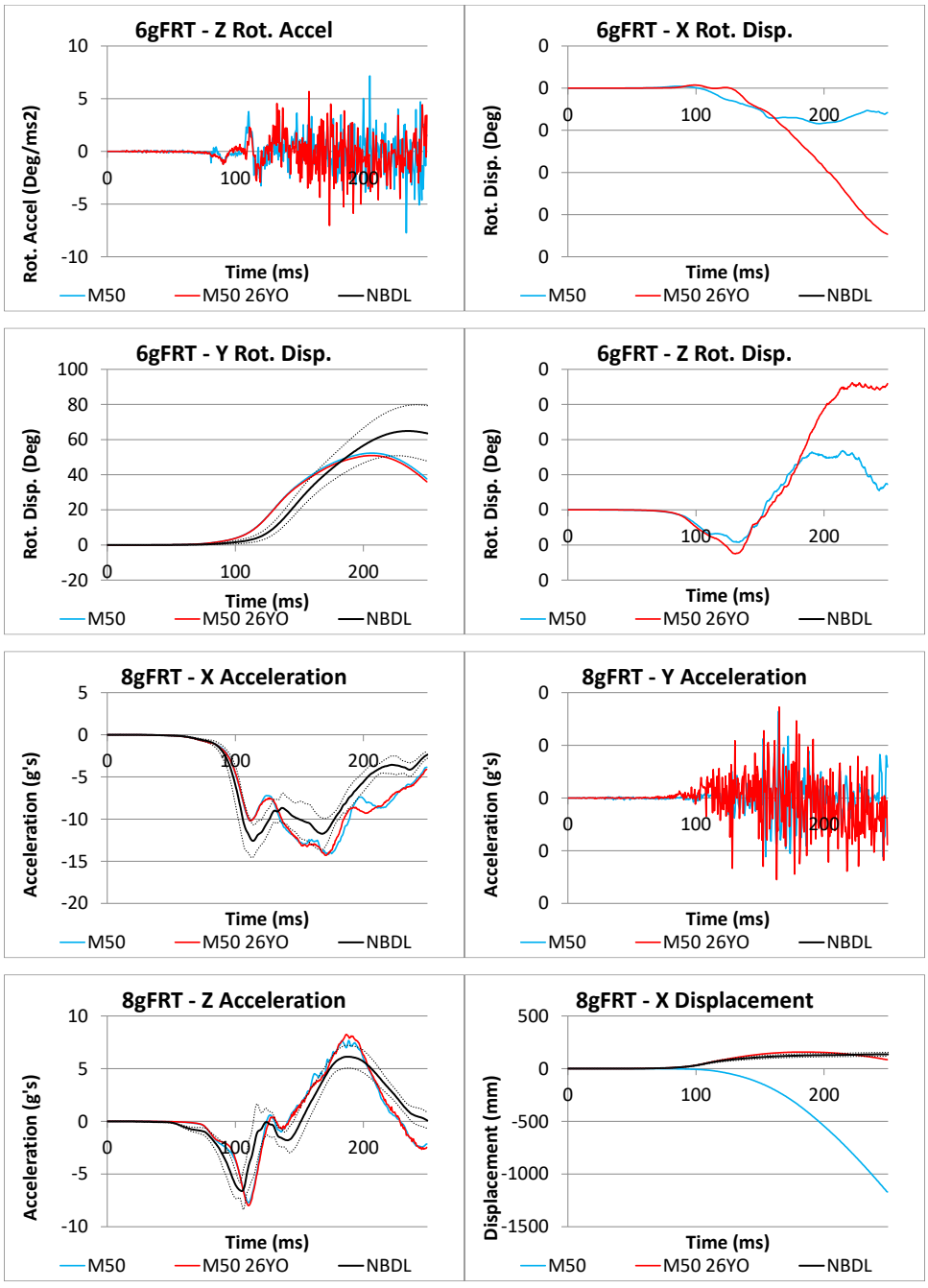
6gFRT - Z Rot. Accel
Rot. Accel (Deg/ms2)
Time (ms)
6gFRT - X Rot. Disp.
Rot. Disp. (Deg)
Time (ms)
6gFRT - Y Rot. Disp.
Rot. Disp. (Deg)
Time (ms)
6gFRT - Z Rot. Disp.
Rot. Disp. (Deg)
Time (ms)
8gFRT - X Acceleration
Acceleration (g's)
Time (ms)
8gFRT - Y Acceleration
Acceleration (g's)
Time (ms)
8gFRT - Z Acceleration
Acceleration (g's)
Time (ms)
8gFRT - X Displacement
Displacement (mm)
Time (ms)
M50
M50 26YO
NBDL

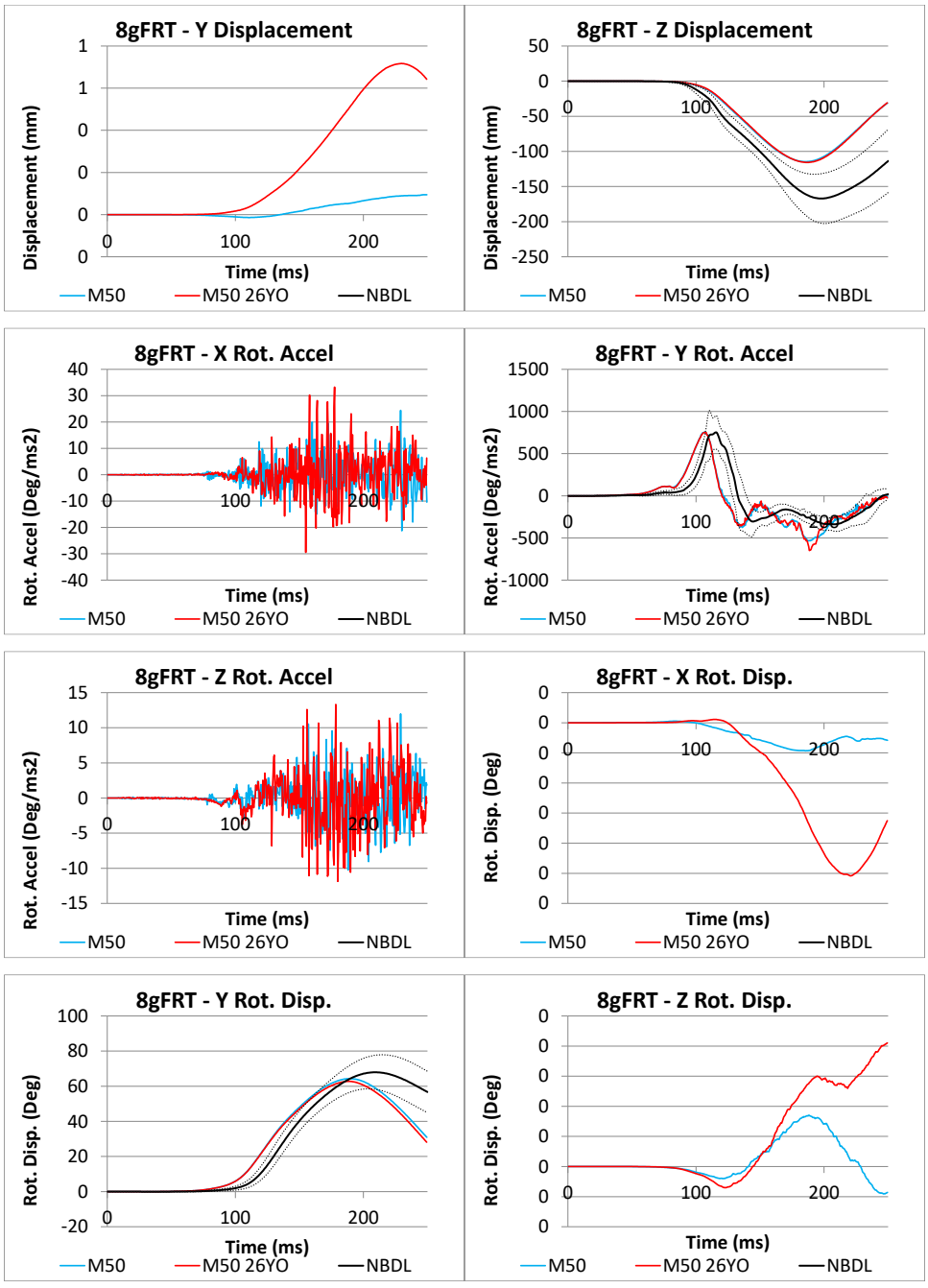
8gFRT - Y Displacement
Displacement (mm)
Time (ms)
M50
M50 26YO
NBDL
8gFRT - Z Displacement
Displacement (mm)
Time (ms)
M50
M50 26YO
NBDL
8gFRT - X Rot. Accel
Rot. Accel (Deg/ms2)
Time (ms)
M50
M50 26YO
NBDL
8gFRT - Y Rot. Accel
Rot. Accel (Deg/ms2)
Time (ms)
M50
M50 26YO
NBDL
8gFRT - Z Rot. Accel
Rot. Accel (Deg/ms2)
Time (ms)
M50
M50 26YO
NBDL
8gFRT - X Rot. Disp.
Rot. Disp. (Deg)
Time (ms)
M50
M50 26YO
NBDL
8gFRT - Y Rot. Disp.
Rot. Disp. (Deg)
Time (ms)
M50
M50 26YO
NBDL
8gFRT - Z Rot. Disp.
Rot. Disp. (Deg)
Time (ms)
M50
M50 26YO
NBDL

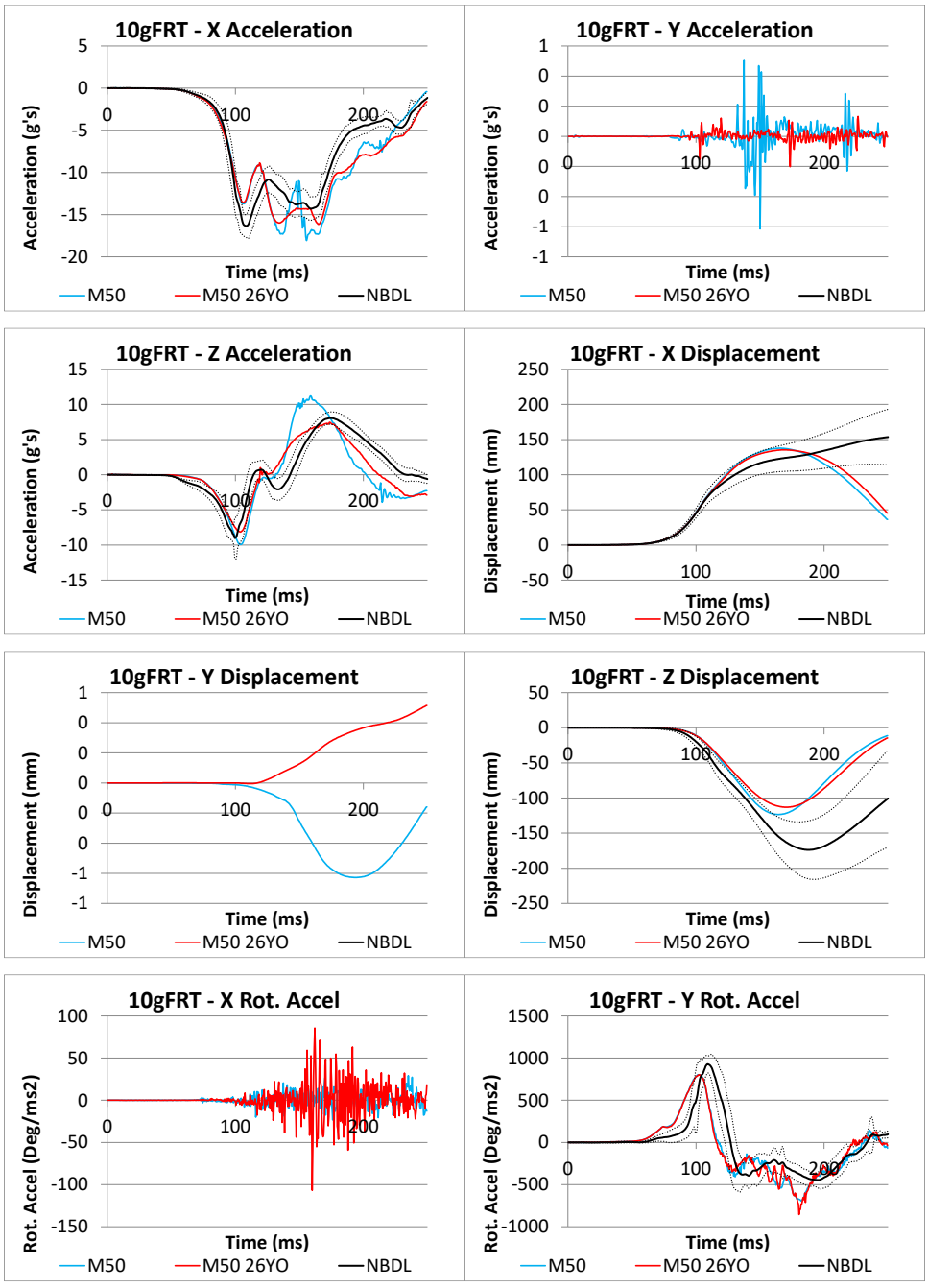
10gFRT - X Acceleration
Acceleration (g's)
Time (ms)
M50
M50 26YO
NBDL
10gFRT - Y Acceleration
Acceleration (g's)
Time (ms)
M50
M50 26YO
NBDL
10gFRT - Z Acceleration
Acceleration (g's)
Time (ms)
M50
M50 26YO
NBDL
10gFRT - X Displacement
Displacement (mm)
Time (ms)
M50
M50 26YO
NBDL
10gFRT - Y Displacement
Displacement (mm)
Time (ms)
M50
M50 26YO
NBDL
10gFRT - Z Displacement
Displacement (mm)
Time (ms)
M50
M50 26YO
NBDL
10gFRT - X Rot. Accel
Rot. Accel (Deg/ms2)
Time (ms)
M50
M50 26YO
NBDL
10gFRT - Y Rot. Accel
Rot. Accel (Deg/ms2)
Time (ms)
M50
M50 26YO
NBDL

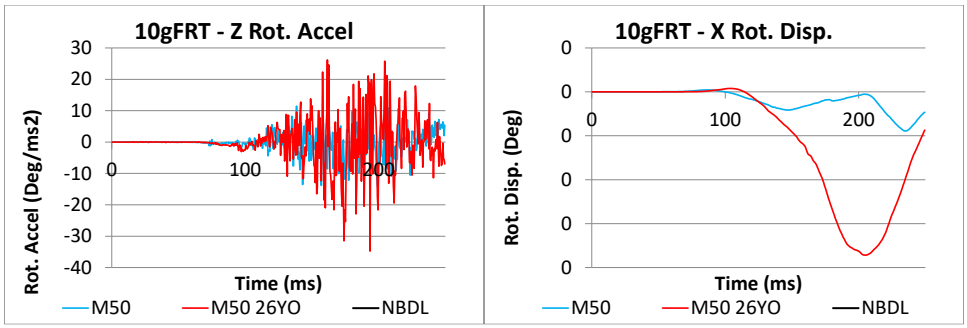
10gFRT - Z Rot. Accel
Rot. Accel (Deg/ms2)
Time (ms)
M50
M50 26YO
NBDL

10gFRT - X Rot. Disp.
Rot. Disp. (Deg)
Time (ms)
M50
M50 26YO
NBDL

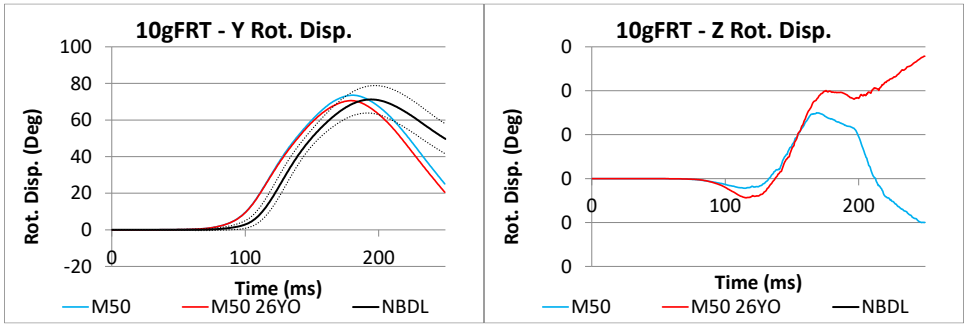
10gFRT - Y Rot. Disp.
Rot. Disp. (Deg)
Time (ms)
M50
M50 26YO
NBDL

10gFRT - Z Rot. Disp.
Rot. Disp. (Deg)
Time (ms)
M50
M50 26YO
NBDL

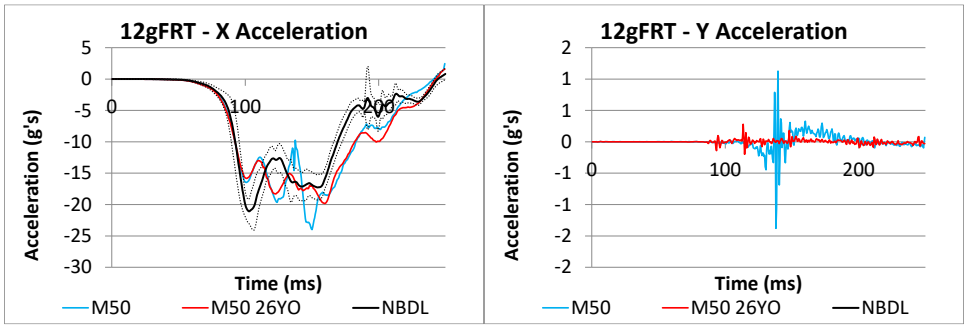
12gFRT - X Acceleration
Acceleration (g's)
Time (ms)
M50
M50 26YO
NBDL

12gFRT - Y Acceleration
Acceleration (g's)
Time (ms)
M50
M50 26YO
NBDL

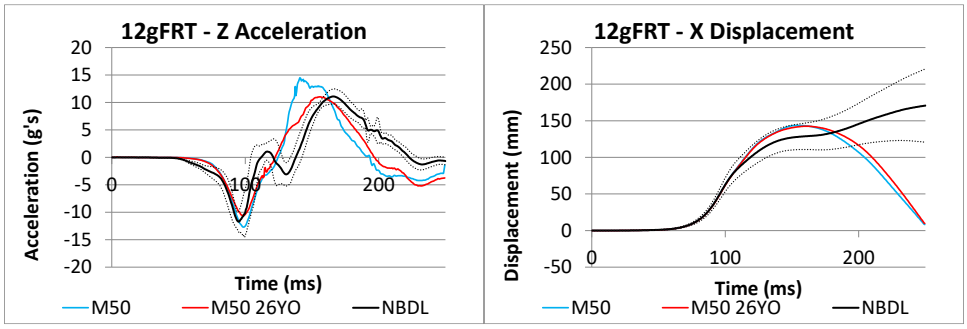
12gFRT - Z Acceleration
Acceleration (g's)
Time (ms)
M50
M50 26YO
NBDL

12gFRT - X Displacement
Displacement (mm)
Time (ms)
M50
M50 26YO
NBDL

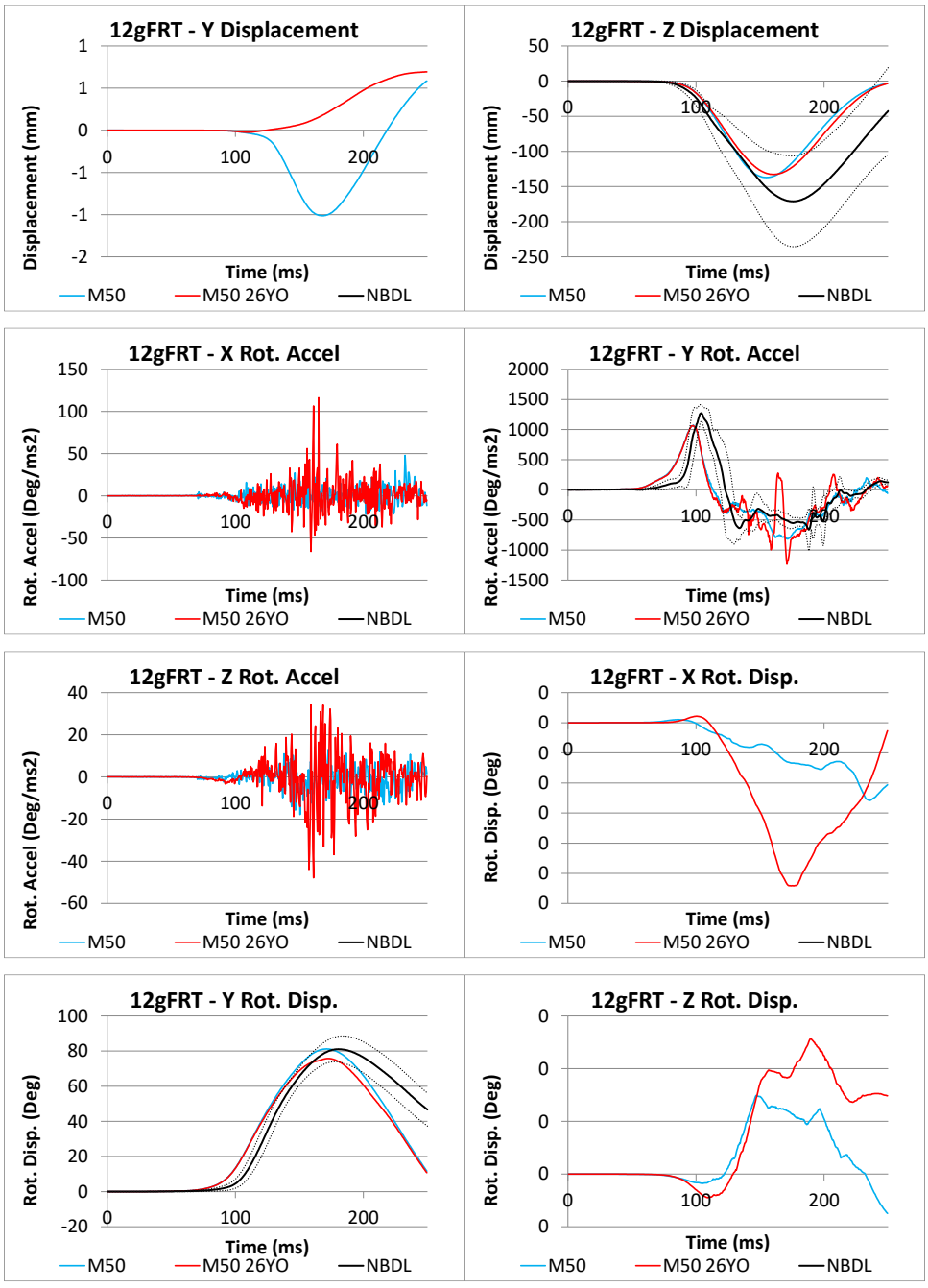
12gFRT - Y Displacement
Displacement (mm)
Time (ms)
M50
M50 26YO
NBDL
12gFRT - Z Displacement
Displacement (mm)
Time (ms)
M50
M50 26YO
NBDL
12gFRT - X Rot. Accel
Rot. Accel (Deg/ms2)
Time (ms)
M50
M50 26YO
NBDL
12gFRT - Y Rot. Accel
Rot. Accel (Deg/ms2)
Time (ms)
M50
M50 26YO
NBDL
12gFRT - Z Rot. Accel
Rot. Accel (Deg/ms2)
Time (ms)
M50
M50 26YO
NBDL
12gFRT - X Rot. Disp.
Rot. Disp. (Deg)
Time (ms)
M50
M50 26YO
NBDL
12gFRT - Y Rot. Disp.
Rot. Disp. (Deg)
Time (ms)
M50
M50 26YO
NBDL
12gFRT - Z Rot. Disp.
Rot. Disp. (Deg)
Time (ms)
M50
M50 26YO
NBDL

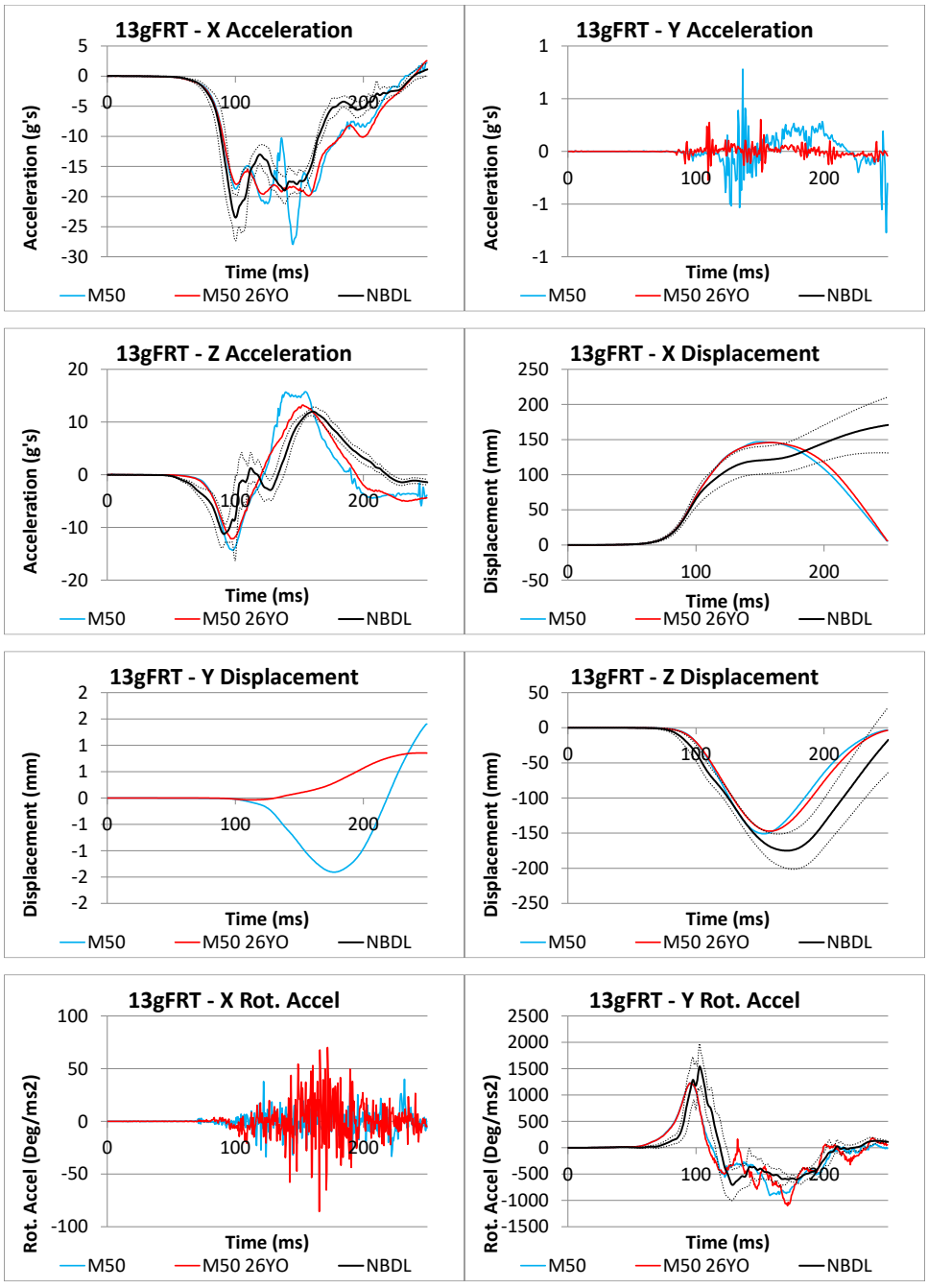
13gFRT - X Acceleration
Acceleration (g's)
Time (ms)
M50
M50 26YO
NBDL
13gFRT - Y Acceleration
Acceleration (g's)
Time (ms)
M50
M50 26YO
NBDL
13gFRT - Z Acceleration
Acceleration (g's)
Time (ms)
M50
M50 26YO
NBDL
13gFRT - X Displacement
Displacement (mm)
Time (ms)
M50
M50 26YO
NBDL
13gFRT - Y Displacement
Displacement (mm)
Time (ms)
M50
M50 26YO
NBDL
13gFRT - Z Displacement
Displacement (mm)
Time (ms)
M50
M50 26YO
NBDL
13gFRT - X Rot. Accel
Rot. Accel (Deg/ms2)
Time (ms)
M50
M50 26YO
NBDL
13gFRT - Y Rot. Accel
Rot. Accel (Deg/ms2)
Time (ms)
M50
M50 26YO
NBDL

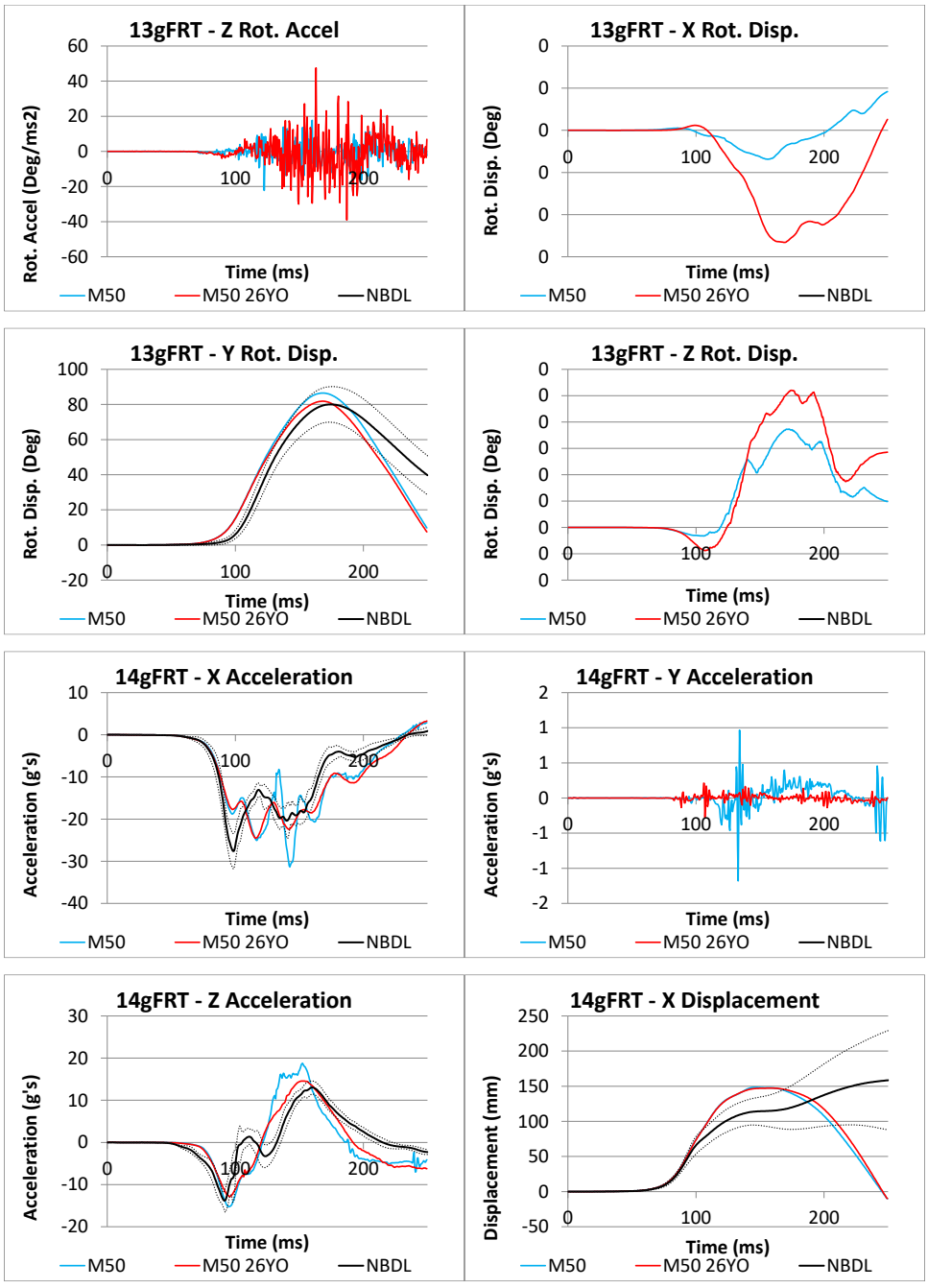
13gFRT - Z Rot. Accel
Rot. Accel (Deg/ms2)
60
40
20
0
-20
-40
-60
0
100
200
Time (ms)
M50
M50 26YO
NBDL
13gFRT - X Rot. Disp.
Rot. Disp. (Deg)
Time (ms)
M50
M50 26YO
NBDL
13gFRT - Y Rot. Disp.
Rot. Disp. (Deg)
100
80
60
40
20
0
-20
Time (ms)
M50
M50 26YO
NBDL
13gFRT - Z Rot. Disp.
Rot. Disp. (Deg)
Time (ms)
M50
M50 26YO
NBDL
14gFRT - X Acceleration
Acceleration (g's)
10
0
-10
-20
-30
-40
Time (ms)
M50
M50 26YO
NBDL
14gFRT - Y Acceleration
Acceleration (g's)
2
1
1
0
-1
-1
-2
Time (ms)
M50
M50 26YO
NBDL
14gFRT - Z Acceleration
Acceleration (g's)
30
20
10
0
-10
-20
Time (ms)
M50
M50 26YO
NBDL
14gFRT - X Displacement
Displacement (mm)
250
200
150
100
50
0
-50
Time (ms)
M50
M50 26YO
NBDL

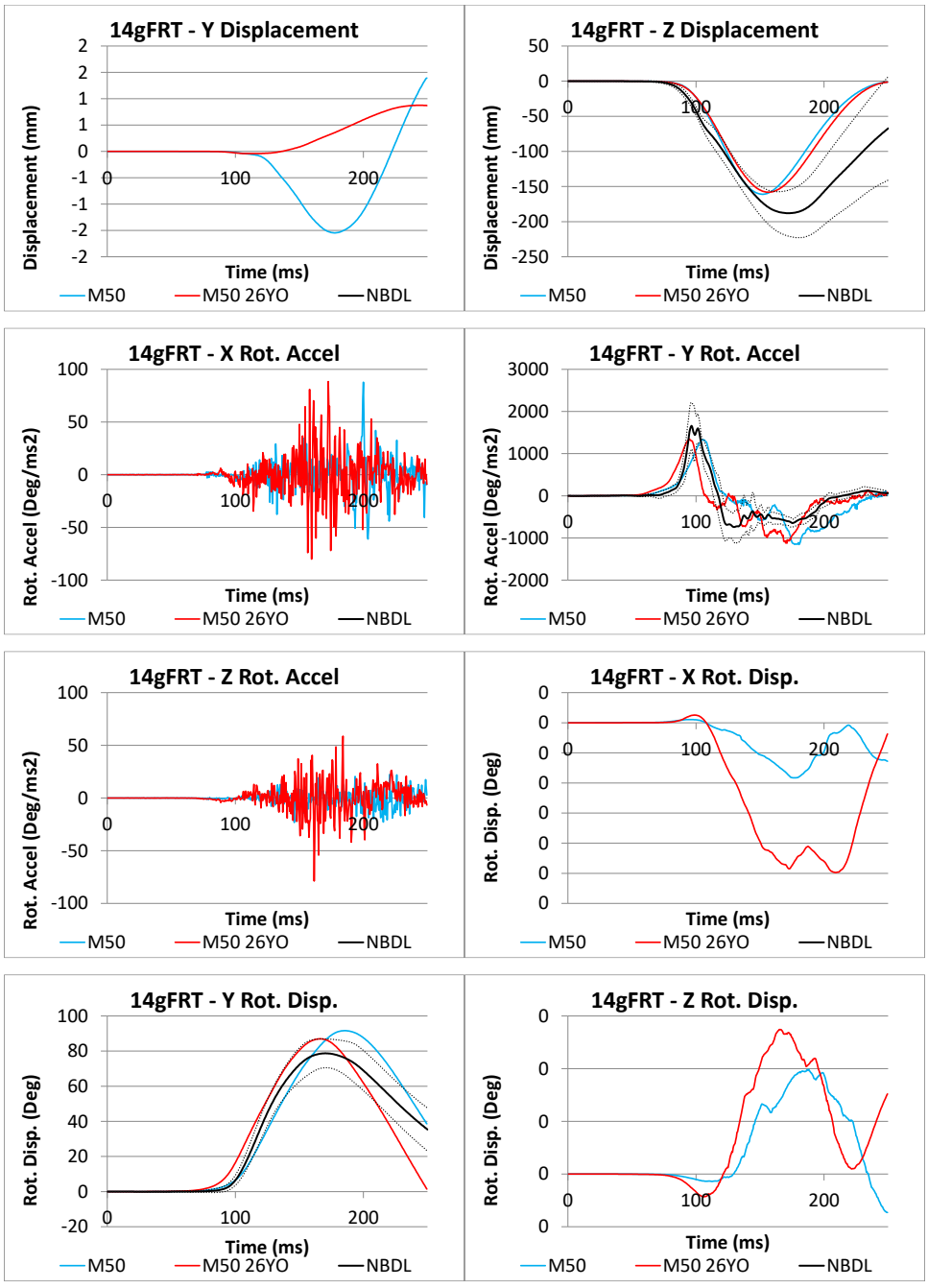
14gFRT - Y Displacement
Displacement (mm)
Time (ms)
M50
M50 26YO
NBDL
14gFRT - Z Displacement
Displacement (mm)
Time (ms)
M50
M50 26YO
NBDL
14gFRT - X Rot. Accel
Rot. Accel (Deg/ms2)
Time (ms)
M50
M50 26YO
NBDL
14gFRT - Y Rot. Accel
Rot. Accel (Deg/ms2)
Time (ms)
M50
M50 26YO
NBDL
14gFRT - Z Rot. Accel
Rot. Accel (Deg/ms2)
Time (ms)
M50
M50 26YO
NBDL
14gFRT - X Rot. Disp.
Rot. Disp. (Deg)
Time (ms)
M50
M50 26YO
NBDL
14gFRT - Y Rot. Disp.
Rot. Disp. (Deg)
Time (ms)
M50
M50 26YO
NBDL
14gFRT - Z Rot. Disp.
Rot. Disp. (Deg)
Time (ms)
M50
M50 26YO
NBDL

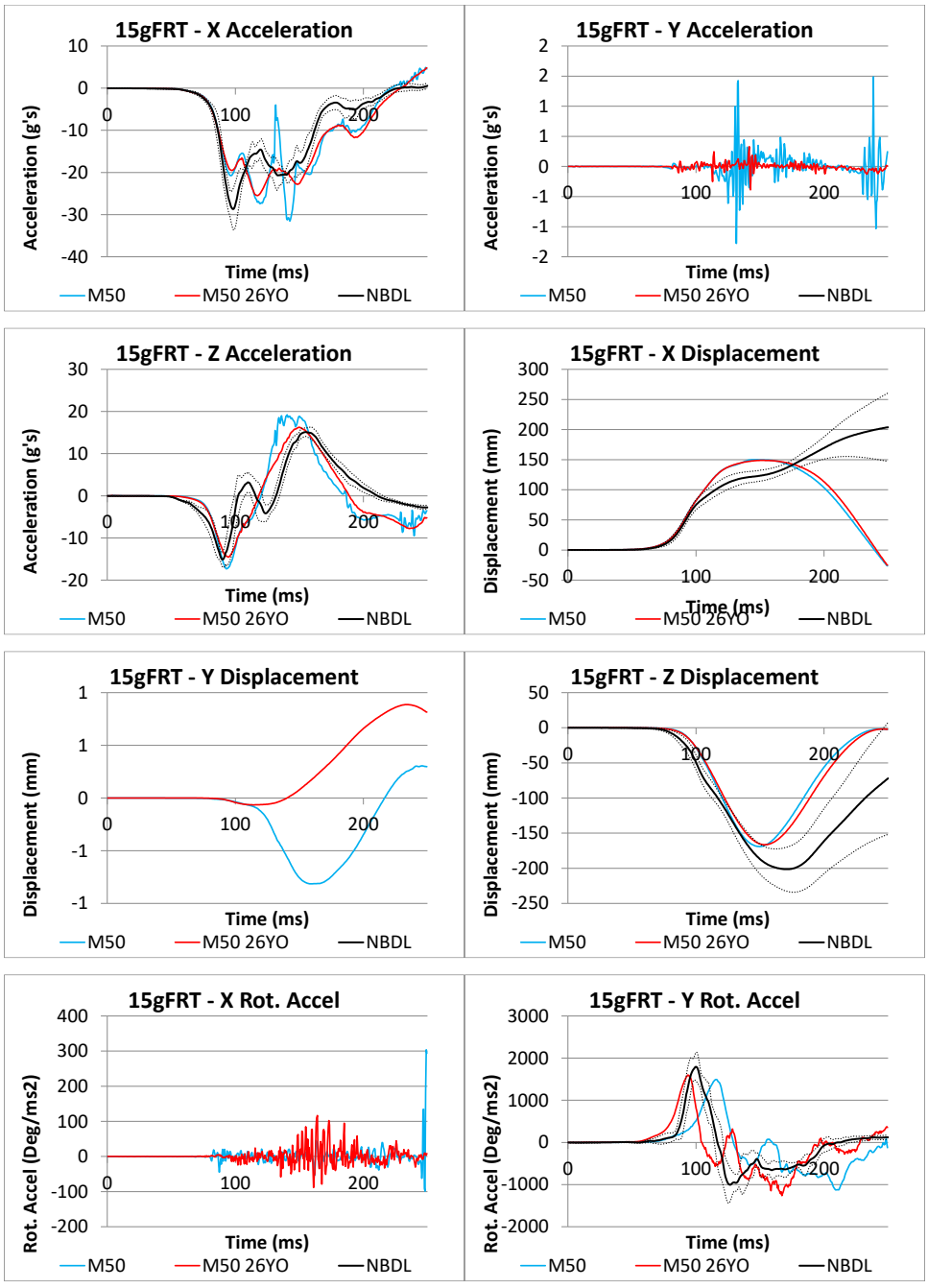
15gFRT - X Acceleration
Acceleration (g's)
Time (ms)
M50
M50 26YO
NBDL
15gFRT - Y Acceleration
Acceleration (g's)
Time (ms)
M50
M50 26YO
NBDL
15gFRT - Z Acceleration
Acceleration (g's)
Time (ms)
M50
M50 26YO
NBDL
15gFRT - X Displacement
Displacement (mm)
Time (ms)
M50
M50 26YO
NBDL
15gFRT - Y Displacement
Displacement (mm)
Time (ms)
M50
M50 26YO
NBDL
15gFRT - Z Displacement
Displacement (mm)
Time (ms)
M50
M50 26YO
NBDL
15gFRT - X Rot. Accel
Rot. Accel (Deg/ms2)
Time (ms)
M50
M50 26YO
NBDL
15gFRT - Y Rot. Accel
Rot. Accel (Deg/ms2)
Time (ms)
M50
M50 26YO
NBDL

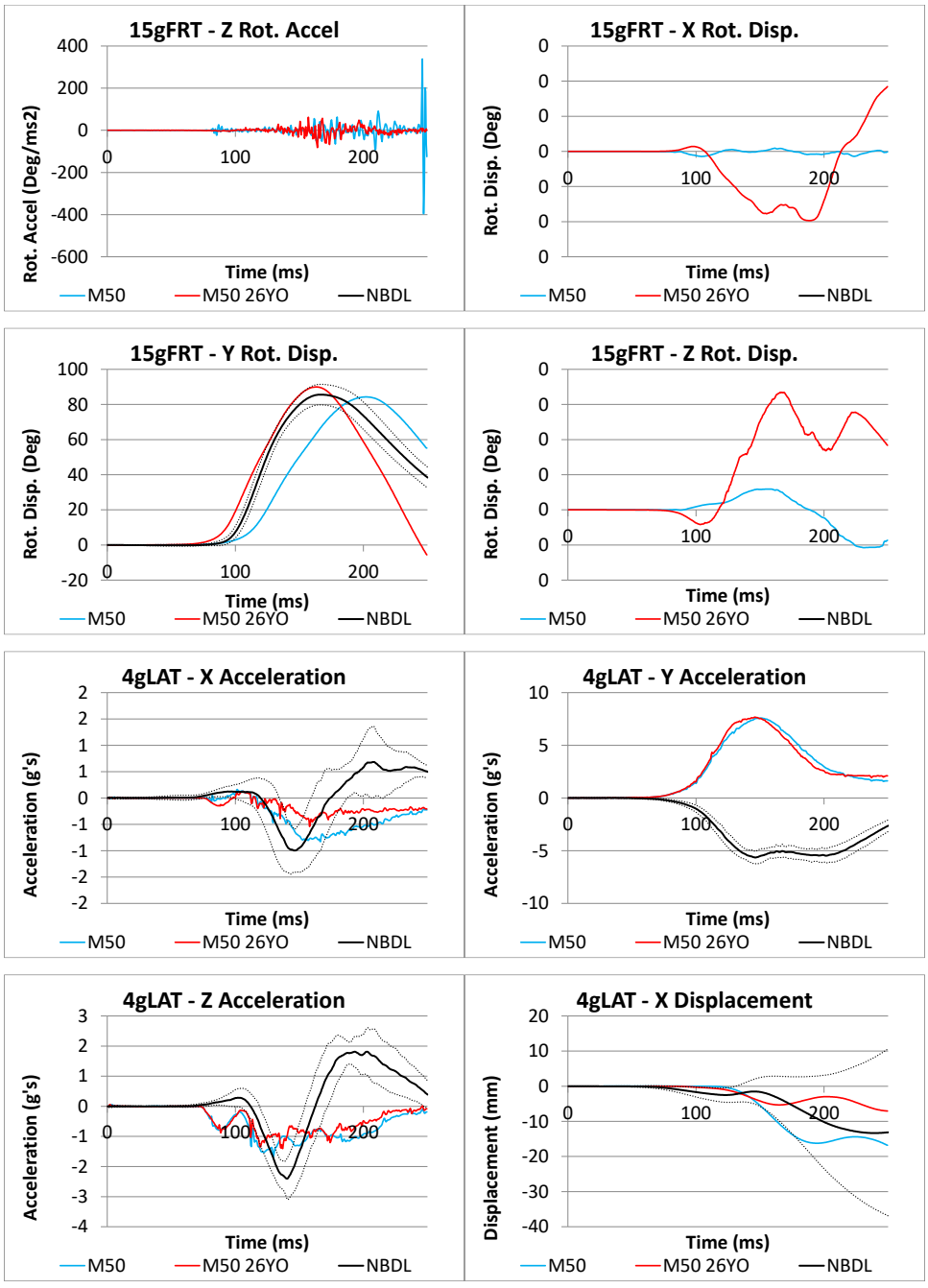
15gFRT - Z Rot. Accel
Rot. Accel (Deg/ms2)
400
200
0
-200
-400
-600
0
100
200
Time (ms)
M50
M50 26YO
NBDL
15gFRT - X Rot. Disp.
Rot. Disp. (Deg)
Time (ms)
M50
M50 26YO
NBDL
15gFRT - Y Rot. Disp.
Rot. Disp. (Deg)
100
80
60
40
20
0
-20
Time (ms)
M50
M50 26YO
NBDL
15gFRT - Z Rot. Disp.
Rot. Disp. (Deg)
Time (ms)
M50
M50 26YO
NBDL
4gLAT - X Acceleration
Acceleration (g's)
2
1
0
-1
-2
Time (ms)
M50
M50 26YO
NBDL
4gLAT - Y Acceleration
Acceleration (g's)
10
5
0
-5
-10
Time (ms)
M50
M50 26YO
NBDL
4gLAT - Z Acceleration
Acceleration (g's)
3
2
1
0
-1
-2
-3
-4
Time (ms)
M50
M50 26YO
NBDL
4gLAT - X Displacement
Displacement (mm)
20
10
0
-10
-20
-30
-40
Time (ms)
M50
M50 26YO
NBDL

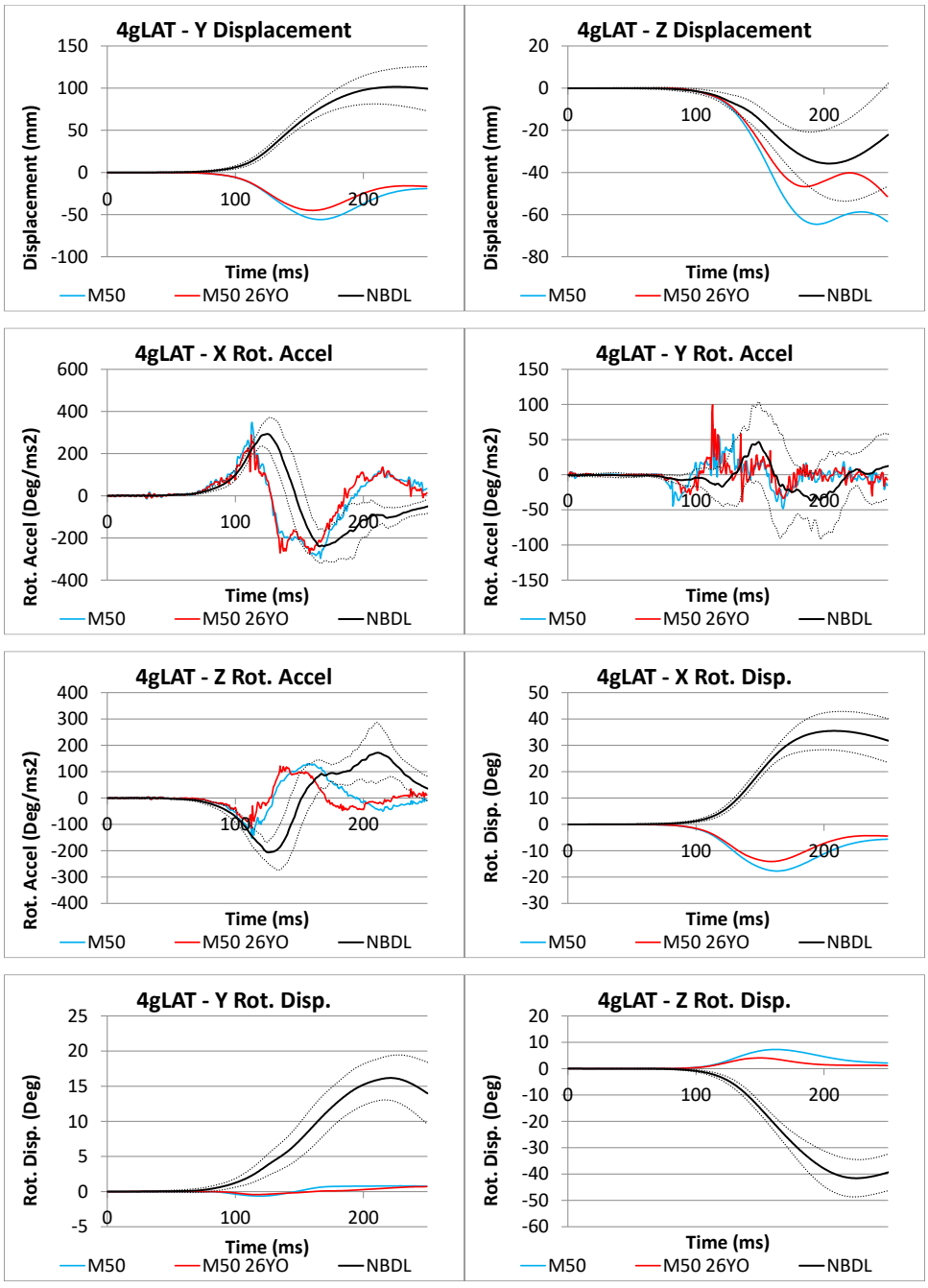
4gLAT - Y Displacement
Displacement (mm)
150
100
50
0
-50
-100
0
100
200
Time (ms)
M50
M50 26YO
NBDL
4gLAT - Z Displacement
Displacement (mm)
20
0
-20
-40
-60
-80
0
100
200
Time (ms)
M50
M50 26YO
NBDL
4gLAT - X Rot. Accel
Rot. Accel (Deg/ms2)
600
400
200
0
-200
-400
0
100
200
Time (ms)
M50
M50 26YO
NBDL
4gLAT - Y Rot. Accel
Rot. Accel (Deg/ms2)
150
100
50
0
-50
-100
-150
0
100
200
Time (ms)
M50
M50 26YO
NBDL
4gLAT - Z Rot. Accel
Rot. Accel (Deg/ms2)
400
300
200
100
0
-100
-200
-300
-400
0
100
200
Time (ms)
M50
M50 26YO
NBDL
4gLAT - X Rot. Disp.
Rot. Disp. (Deg)
50
40
30
20
10
0
-10
-20
-30
0
100
200
Time (ms)
M50
M50 26YO
NBDL
4gLAT - Y Rot. Disp.
Rot. Disp. (Deg)
25
20
15
10
5
0
-5
0
100
200
Time (ms)
M50
M50 26YO
NBDL
4gLAT - Z Rot. Disp.
Rot. Disp. (Deg)
20
10
0
-10
-20
-30
-40
-50
-60
0
100
200
Time (ms)
M50
M50 26YO
NBDL

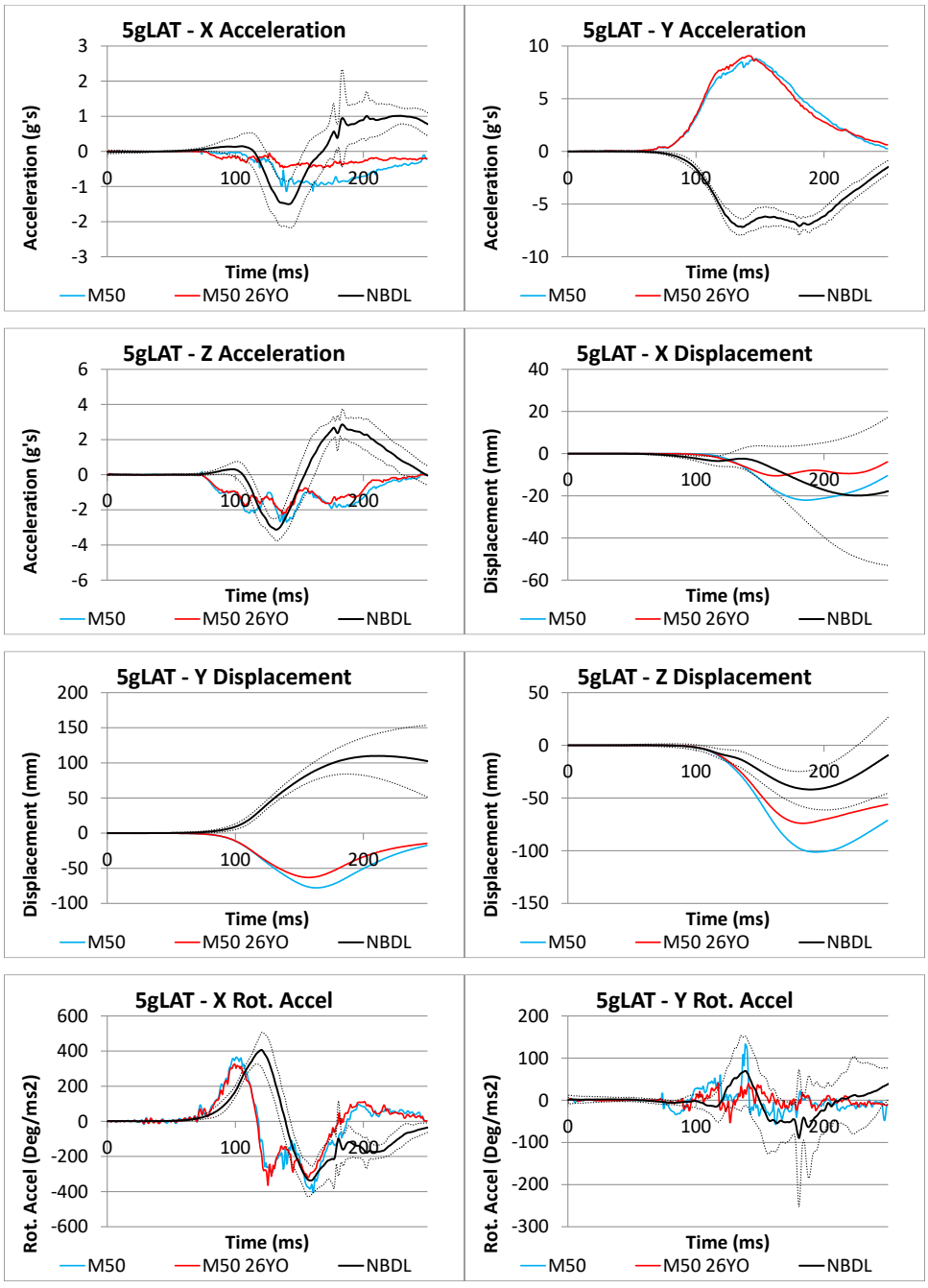
5gLAT - X Acceleration
Acceleration (g's)
Time (ms)
M50
M50 26YO
NBDL
5gLAT - Y Acceleration
Acceleration (g's)
Time (ms)
M50
M50 26YO
NBDL
5gLAT - Z Acceleration
Acceleration (g's)
Time (ms)
M50
M50 26YO
NBDL
5gLAT - X Displacement
Displacement (mm)
Time (ms)
M50
M50 26YO
NBDL
5gLAT - Y Displacement
Displacement (mm)
Time (ms)
M50
M50 26YO
NBDL
5gLAT - Z Displacement
Displacement (mm)
Time (ms)
M50
M50 26YO
NBDL
5gLAT - X Rot. Accel
Rot. Accel (Deg/ms2)
Time (ms)
M50
M50 26YO
NBDL
5gLAT - Y Rot. Accel
Rot. Accel (Deg/ms2)
Time (ms)
M50
M50 26YO
NBDL

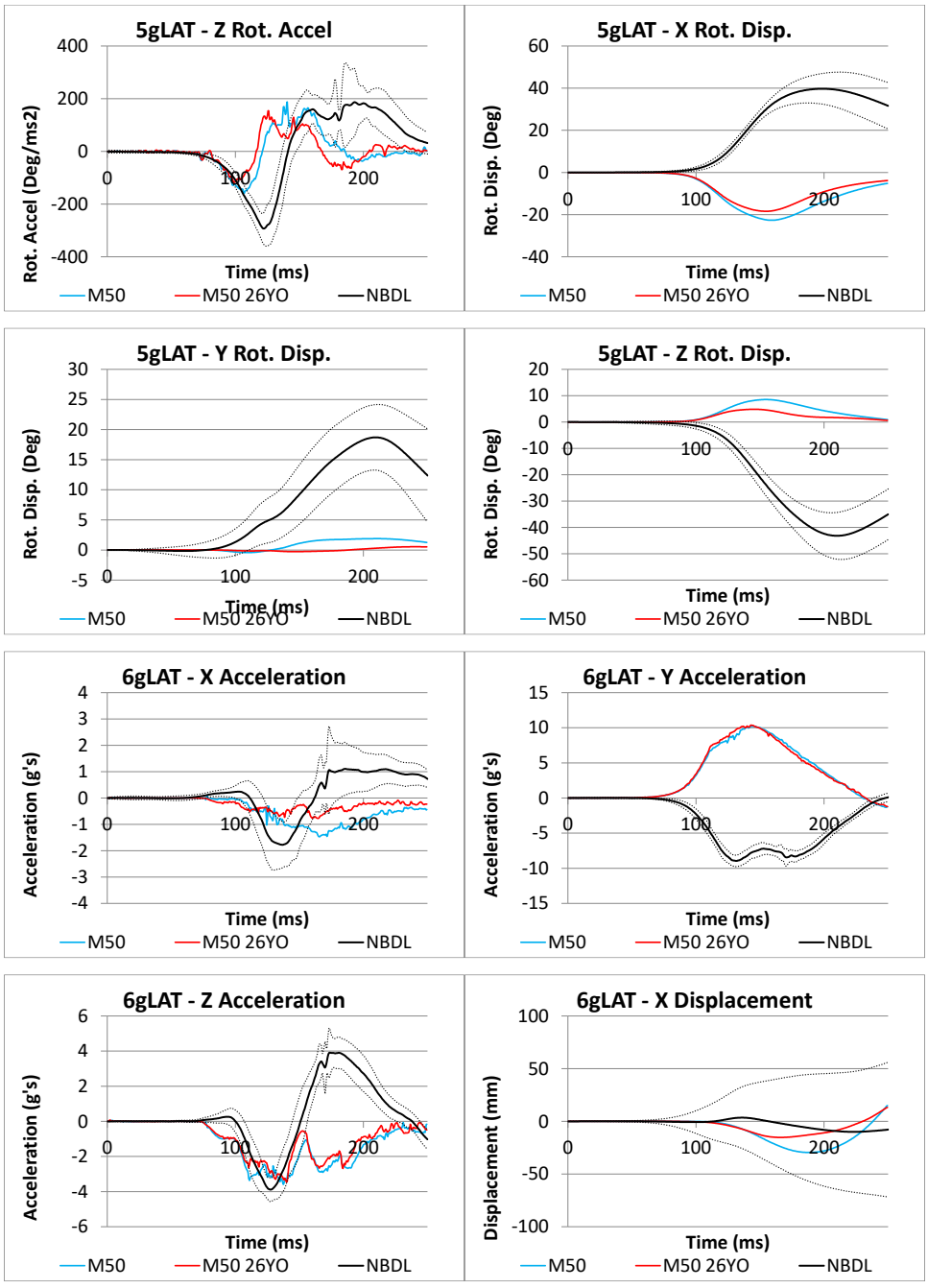
5gLAT - Z Rot. Accel
Rot. Accel (Deg/ms2)
400
200
0
-200
-400
0
100
200
Time (ms)
M50
M50 26YO
NBDL
5gLAT - X Rot. Disp.
Rot. Disp. (Deg)
60
40
20
0
-20
-40
0
100
200
Time (ms)
M50
M50 26YO
NBDL
5gLAT - Y Rot. Disp.
Rot. Disp. (Deg)
30
25
20
15
10
5
0
-5
0
100
200
Time (ms)
M50
M50 26YO
NBDL
5gLAT - Z Rot. Disp.
Rot. Disp. (Deg)
20
10
0
-10
-20
-30
-40
-50
-60
0
100
200
Time (ms)
M50
M50 26YO
NBDL
6gLAT - X Acceleration
Acceleration (g's)
4
3
2
1
0
-1
-2
-3
-4
0
100
200
Time (ms)
M50
M50 26YO
NBDL
6gLAT - Y Acceleration
Acceleration (g's)
15
10
5
0
-5
-10
-15
0
100
200
Time (ms)
M50
M50 26YO
NBDL
6gLAT - Z Acceleration
Acceleration (g's)
6
4
2
0
-2
-4
-6
0
100
200
Time (ms)
M50
M50 26YO
NBDL
6gLAT - X Displacement
Displacement (mm)
100
50
0
-50
-100
0
100
200
Time (ms)
M50
M50 26YO
NBDL

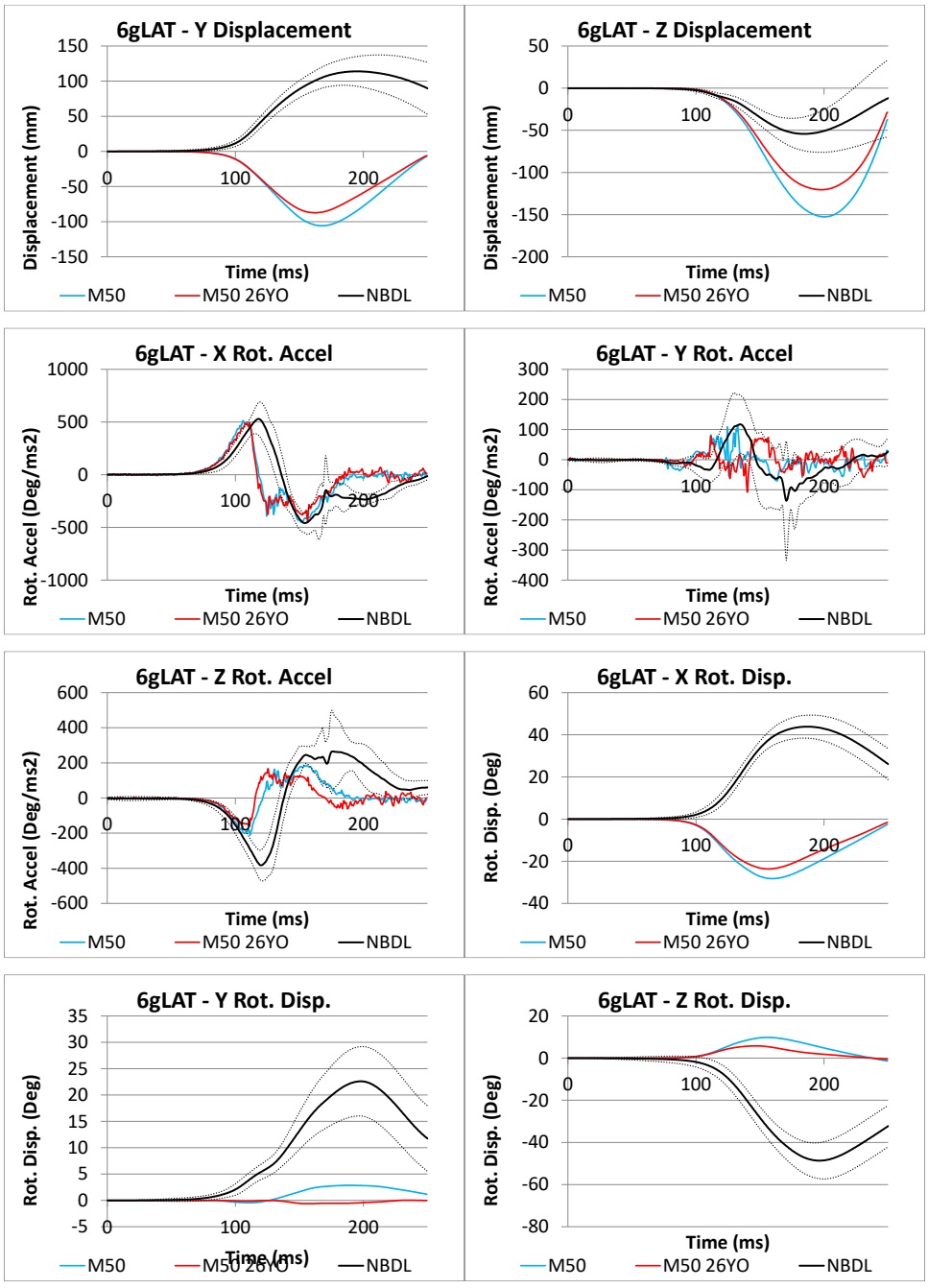
6gLAT - Y Displacement
Displacement (mm)
150
100
50
0
-50
-100
-150
0
100
200
Time (ms)
M50
M50 26YO
NBDL
6gLAT - Z Displacement
Displacement (mm)
50
0
-50
-100
-150
-200
0
100
200
Time (ms)
M50
M50 26YO
NBDL
6gLAT - X Rot. Accel
Rot. Accel (Deg/ms2)
1000
500
0
-500
-1000
0
100
200
Time (ms)
M50
M50 26YO
NBDL
6gLAT - Y Rot. Accel
Rot. Accel (Deg/ms2)
300
200
100
0
-100
-200
-300
-400
0
100
200
Time (ms)
M50
M50 26YO
NBDL
6gLAT - Z Rot. Accel
Rot. Accel (Deg/ms2)
600
400
200
0
-200
-400
-600
0
100
200
Time (ms)
M50
M50 26YO
NBDL
6gLAT - X Rot. Disp.
Rot. Disp. (Deg)
60
40
20
0
-20
-40
0
100
200
Time (ms)
M50
M50 26YO
NBDL
6gLAT - Y Rot. Disp.
Rot. Disp. (Deg)
35
30
25
20
15
10
5
0
-5
0
100
200
Time (ms)
M50
M50 26YO
NBDL
6gLAT - Z Rot. Disp.
Rot. Disp. (Deg)
20
0
-20
-40
-60
-80
0
100
200
Time (ms)
M50
M50 26YO
NBDL

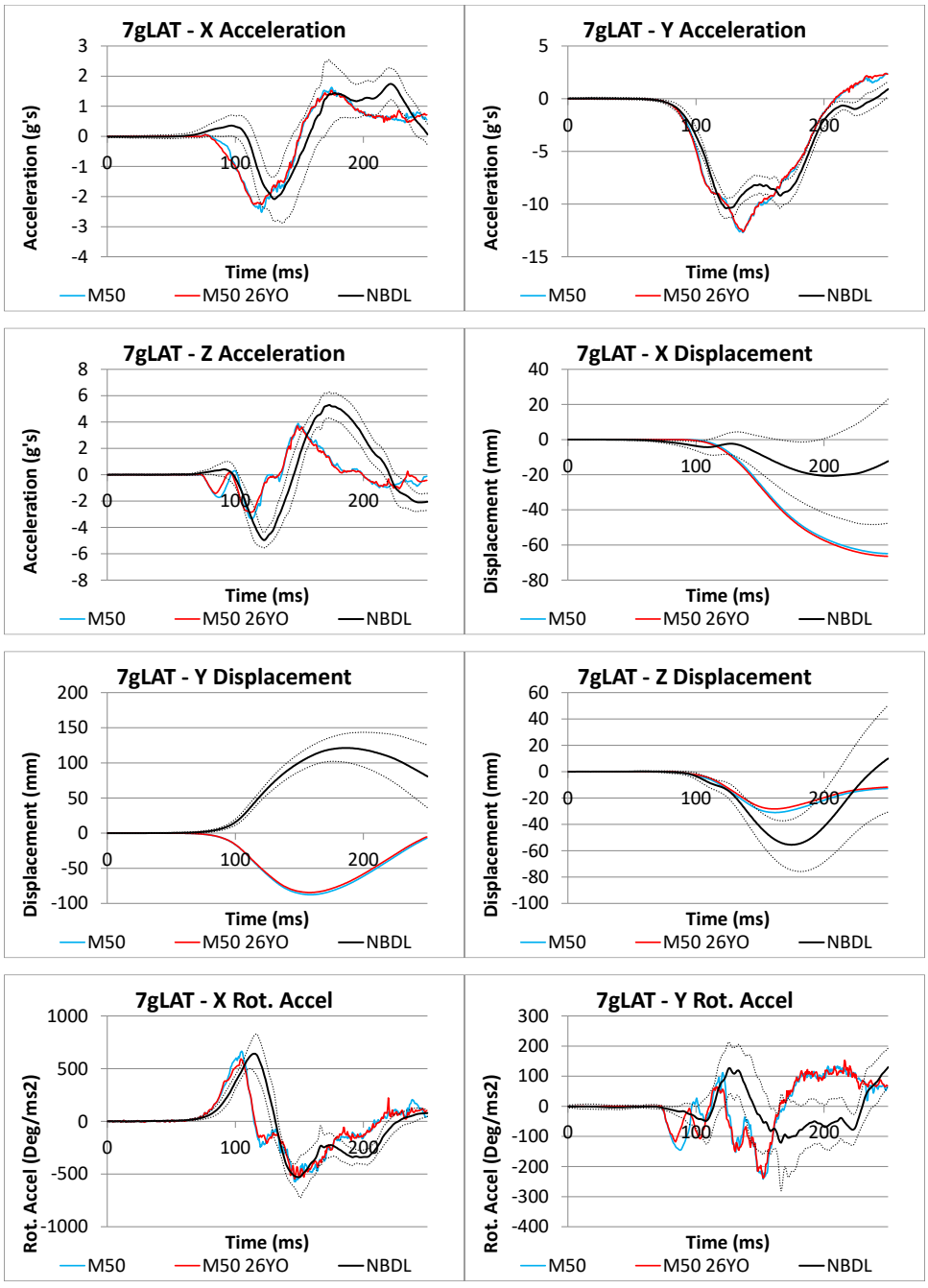
7gLAT - X Acceleration
Acceleration (g's)
Time (ms)
M50
M50 26YO
NBDL
7gLAT - Y Acceleration
Acceleration (g's)
Time (ms)
M50
M50 26YO
NBDL
7gLAT - Z Acceleration
Acceleration (g's)
Time (ms)
M50
M50 26YO
NBDL
7gLAT - X Displacement
Displacement (mm)
Time (ms)
M50
M50 26YO
NBDL
7gLAT - Y Displacement
Displacement (mm)
Time (ms)
M50
M50 26YO
NBDL
7gLAT - Z Displacement
Displacement (mm)
Time (ms)
M50
M50 26YO
NBDL
7gLAT - X Rot. Accel
Rot. Accel (Deg/ms2)
Time (ms)
M50
M50 26YO
NBDL
7gLAT - Y Rot. Accel
Rot. Accel (Deg/ms2)
Time (ms)
M50
M50 26YO
NBDL

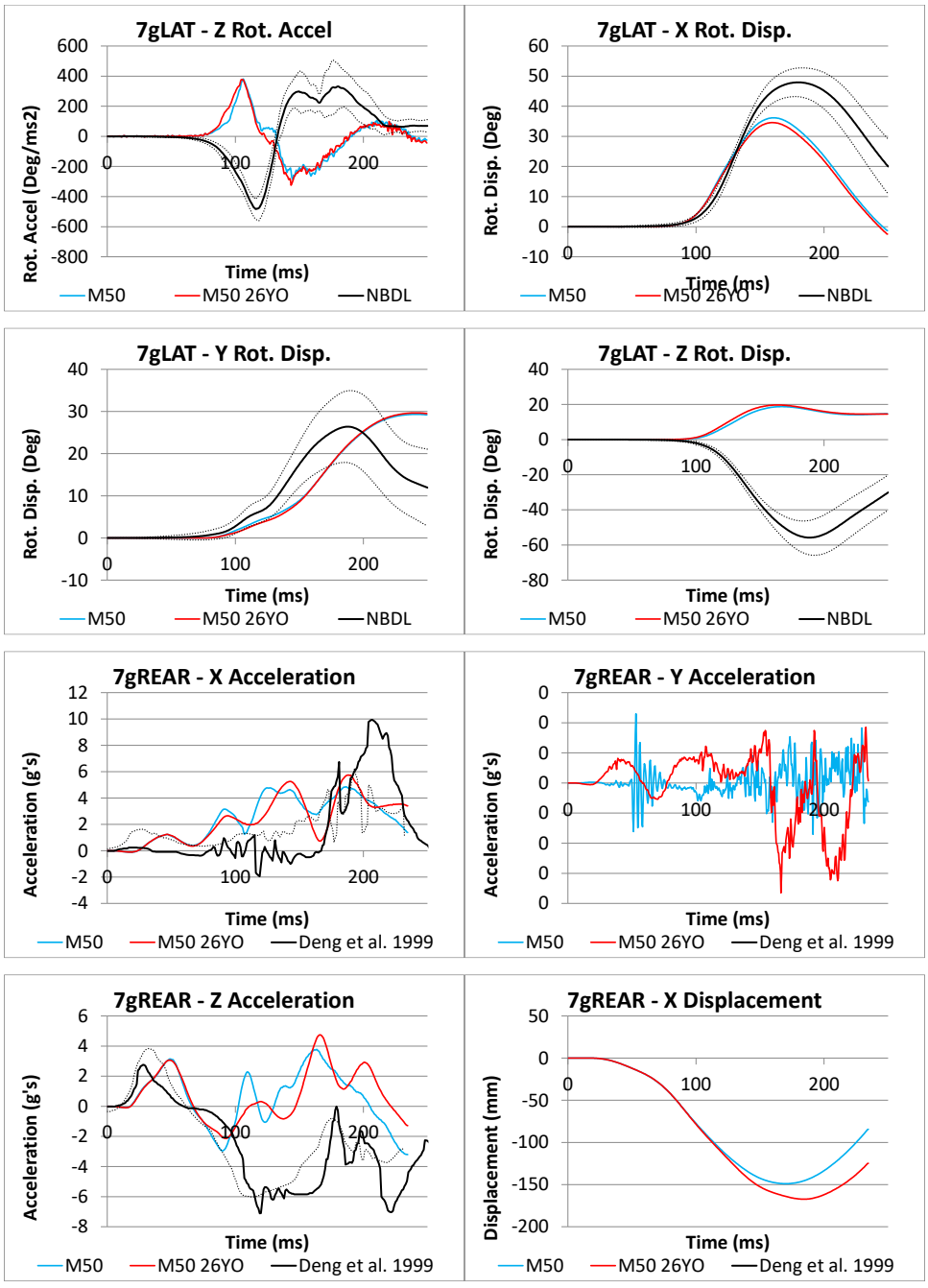
7gLAT - Z Rot. Accel
Rot. Accel (Deg/ms2)
600
400
200
0
-200
-400
-600
-800
0
100
200
Time (ms)
M50
M50 26YO
NBDL
7gLAT - X Rot. Disp.
Rot. Disp. (Deg)
60
50
40
30
20
10
0
-10
0
100
200
Time (ms)
M50
M50 26YO
NBDL
7gLAT - Y Rot. Disp.
Rot. Disp. (Deg)
40
30
20
10
0
-10
0
100
200
Time (ms)
M50
M50 26YO
NBDL
7gLAT - Z Rot. Disp.
Rot. Disp. (Deg)
40
20
0
-20
-40
-60
-80
0
100
200
Time (ms)
M50
M50 26YO
NBDL
7gREAR - X Acceleration
Acceleration (g's)
12
10
8
6
4
2
0
-2
-4
0
100
200
Time (ms)
M50
M50 26YO
Deng et al. 1999
7gREAR - Y Acceleration
Acceleration (g's)
0
0
0
0
0
0
0
0
0
100
200
Time (ms)
M50
M50 26YO
Deng et al. 1999
7gREAR - Z Acceleration
Acceleration (g's)
6
4
2
0
-2
-4
-6
-8
0
100
200
Time (ms)
M50
M50 26YO
Deng et al. 1999
7gREAR - X Displacement
Displacement (mm)
50
0
-50
-100
-150
-200
0
100
200
Time (ms)
M50
M50 26YO
Deng et al. 1999

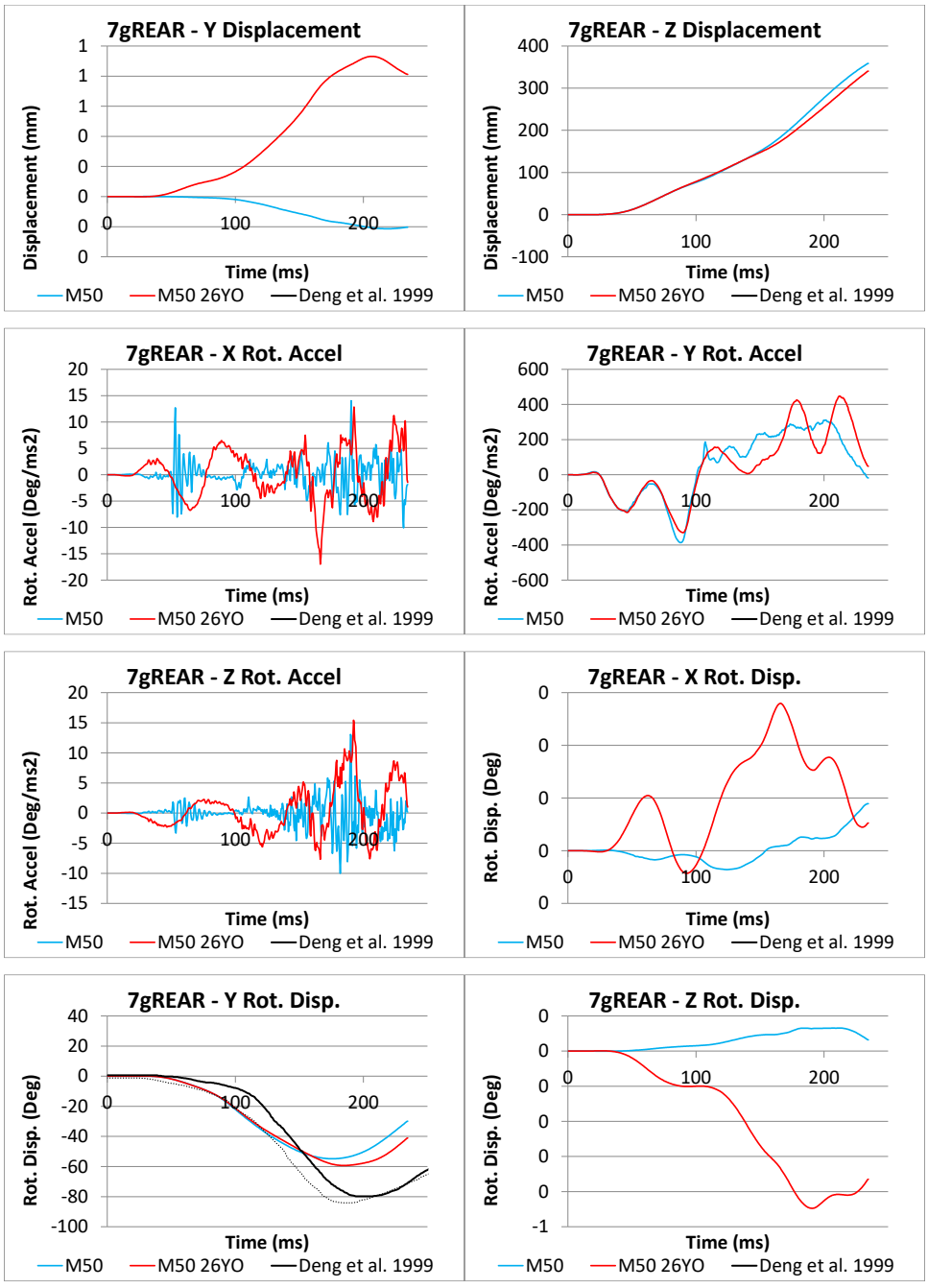
7gREAR - Y Displacement
Displacement (mm)
Time (ms)
M50
M50 26YO
Deng et al. 1999
7gREAR - Z Displacement
Displacement (mm)
Time (ms)
M50
M50 26YO
Deng et al. 1999
7gREAR - X Rot. Accel
Rot. Accel (Deg/ms2)
Time (ms)
M50
M50 26YO
Deng et al. 1999
7gREAR - Y Rot. Accel
Rot. Accel (Deg/ms2)
Time (ms)
M50
M50 26YO
Deng et al. 1999
7gREAR - Z Rot. Accel
Rot. Accel (Deg/ms2)
Time (ms)
M50
M50 26YO
Deng et al. 1999
7gREAR - X Rot. Disp.
Rot. Disp. (Deg)
Time (ms)
M50
M50 26YO
Deng et al. 1999
7gREAR - Y Rot. Disp.
Rot. Disp. (Deg)
Time (ms)
M50
M50 26YO
Deng et al. 1999
7gREAR - Z Rot. Disp.
Rot. Disp. (Deg)
Time (ms)
M50
M50 26YO
Deng et al. 1999

Appendix 3: $M50_{26YO}$ and $M50_{75YO}$ Time Histories of the Head Kinematic Response and Soft Tissue Metrics

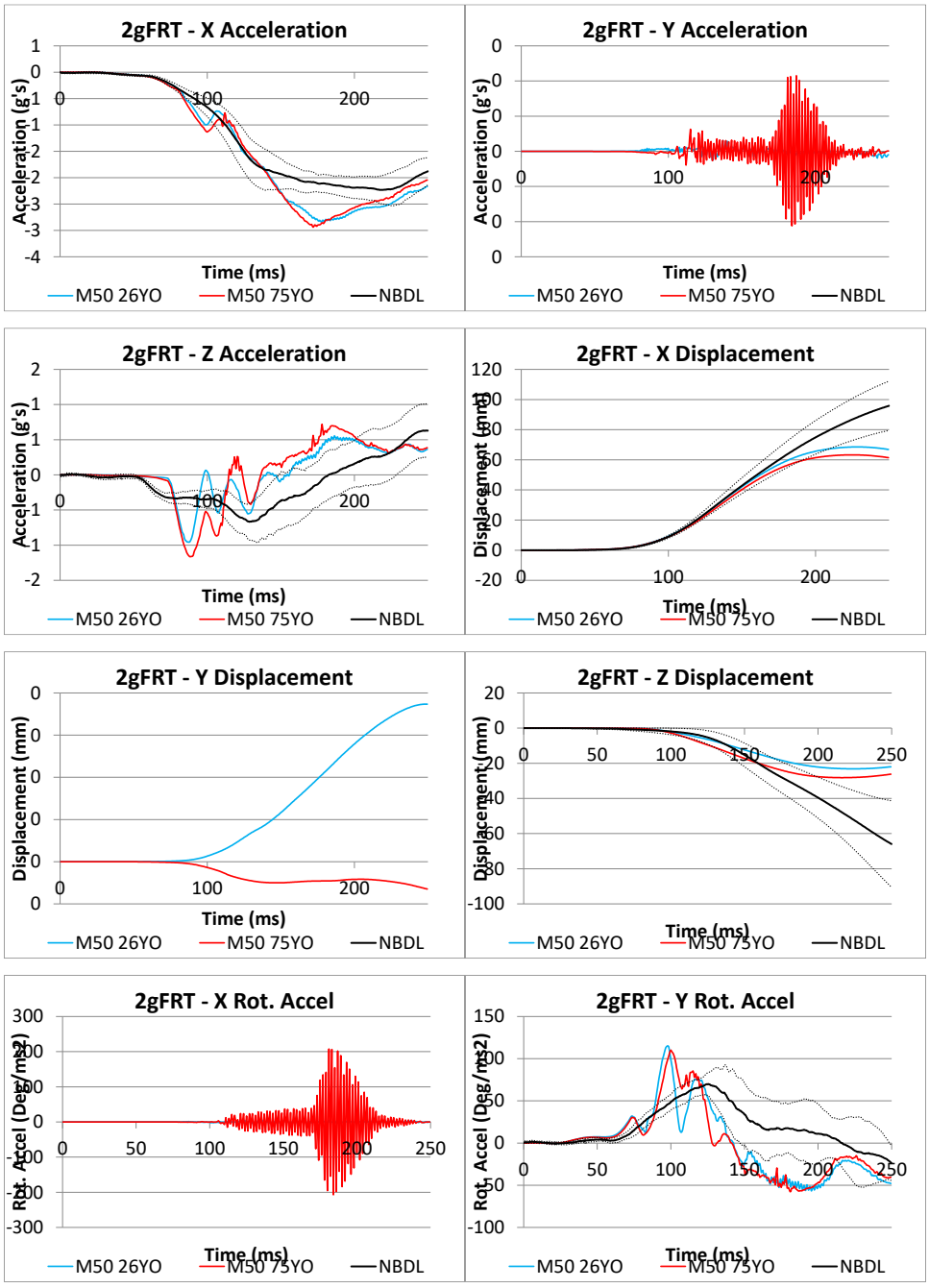

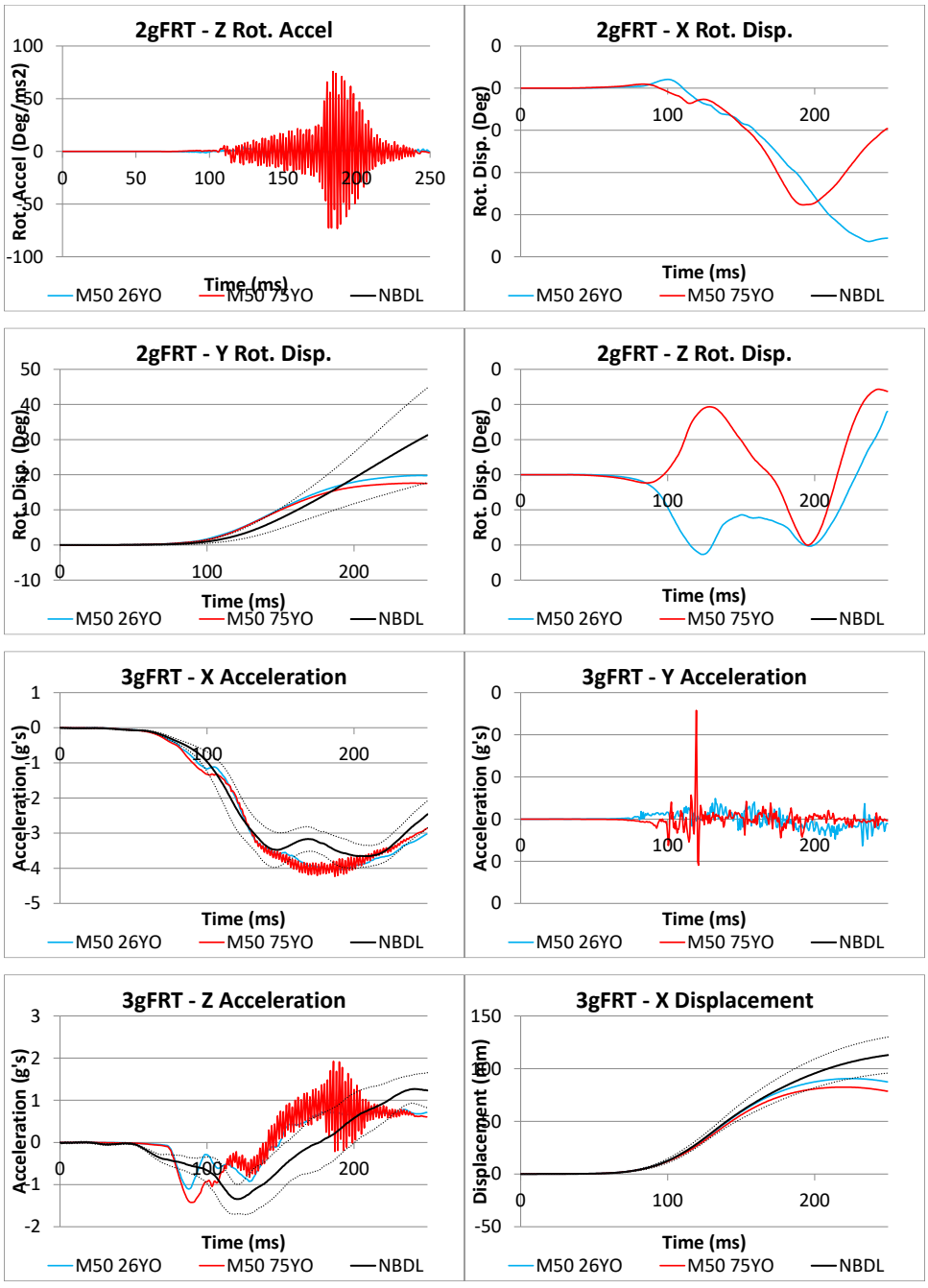
2gFRT - Z Rot. Accel
Rot. Accel (Deg/ms2)
Time (ms)
2gFRT - X Rot. Disp.
Rot. Disp. (Deg)
Time (ms)
2gFRT - Y Rot. Disp.
Rot. Disp. (Deg)
Time (ms)
2gFRT - Z Rot. Disp.
Rot. Disp. (Deg)
Time (ms)
3gFRT - X Acceleration
Acceleration (g's)
Time (ms)
3gFRT - Y Acceleration
Acceleration (g's)
Time (ms)
3gFRT - Z Acceleration
Acceleration (g's)
Time (ms)
3gFRT - X Displacement
Displacement (mm)
Time (ms)
M50 26YO
M50 75YO
NBDL

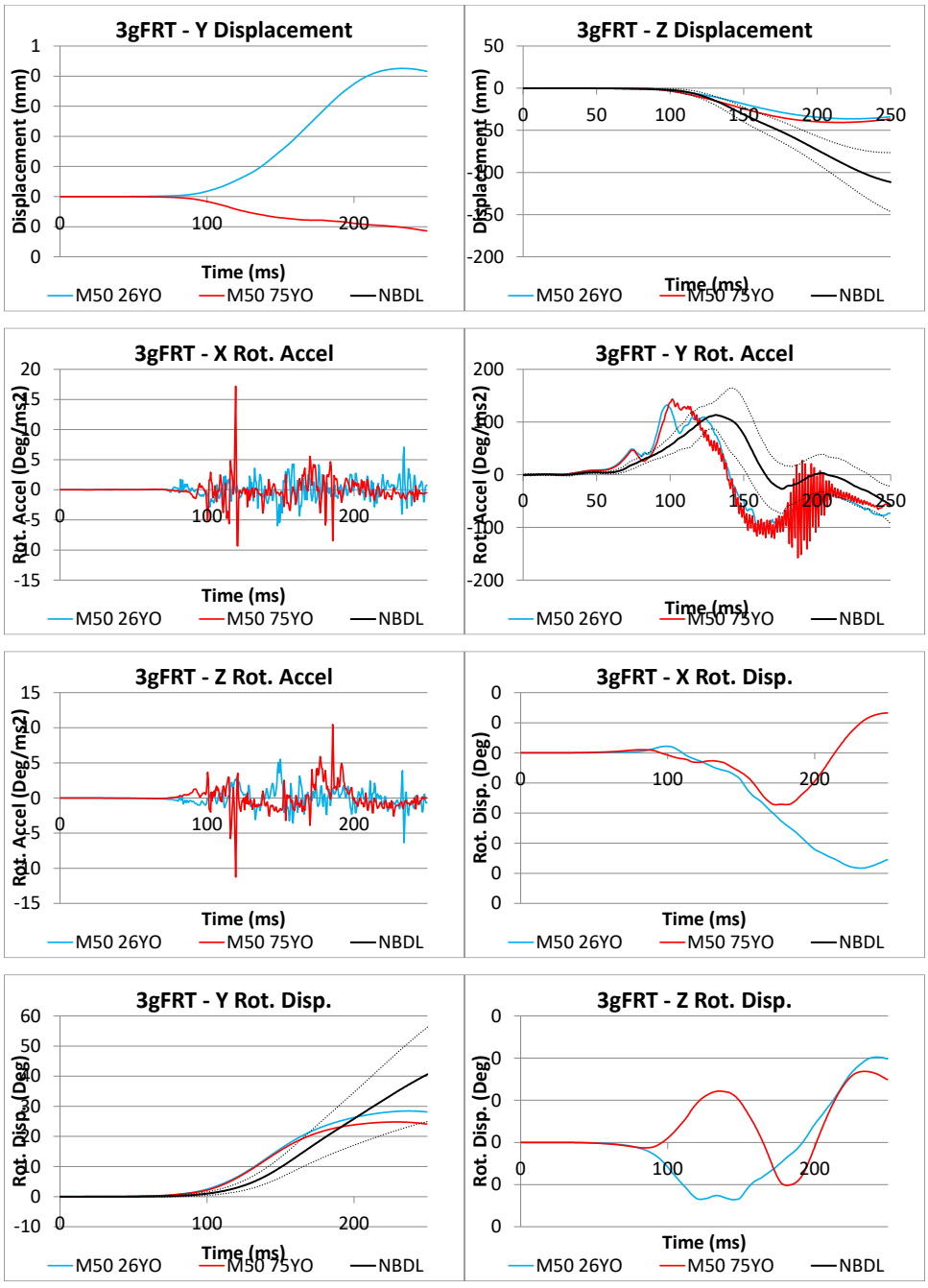
3gFRT - Y Displacement
Displacement (mm)
Time (ms)
M50 26YO
M50 75YO
NBDL
3gFRT - Z Displacement
Displacement (mm)
Time (ms)
M50 26YO
M50 75YO
NBDL
3gFRT - X Rot. Accel
Rot. Accel (Deg/ms2)
Time (ms)
M50 26YO
M50 75YO
NBDL
3gFRT - Y Rot. Accel
Rot. Accel (Deg/ms2)
Time (ms)
M50 26YO
M50 75YO
NBDL
3gFRT - Z Rot. Accel
Rot. Accel (Deg/ms2)
Time (ms)
M50 26YO
M50 75YO
NBDL
3gFRT - X Rot. Disp.
Rot. Disp. (Deg)
Time (ms)
M50 26YO
M50 75YO
NBDL
3gFRT - Y Rot. Disp.
Rot. Disp. (Deg)
Time (ms)
M50 26YO
M50 75YO
NBDL
3gFRT - Z Rot. Disp.
Rot. Disp. (Deg)
Time (ms)
M50 26YO
M50 75YO
NBDL

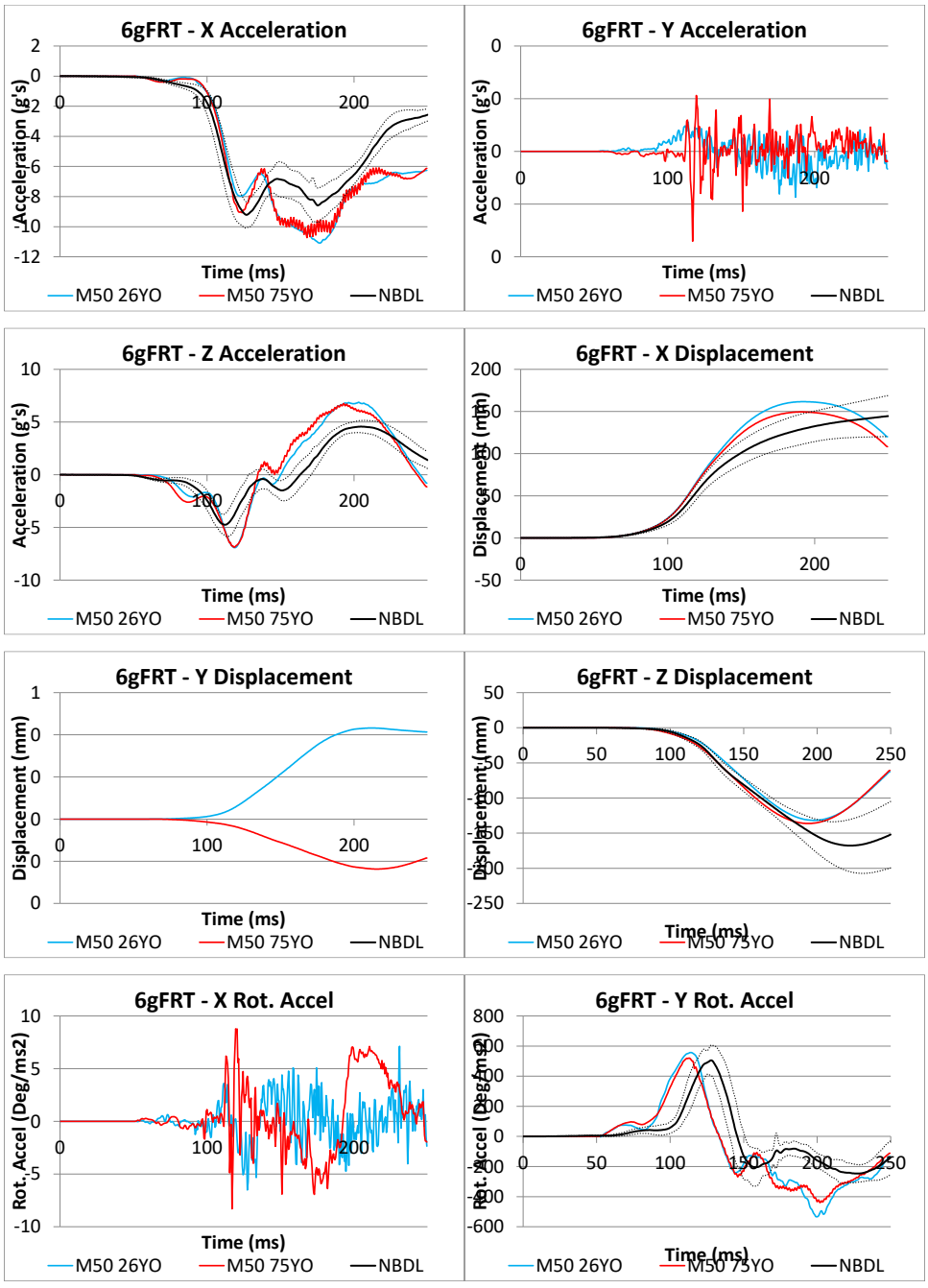
6gFRT - X Acceleration
Acceleration (g's)
Time (ms)
M50 26YO
M50 75YO
NBDL
6gFRT - Y Acceleration
Acceleration (g's)
Time (ms)
M50 26YO
M50 75YO
NBDL
6gFRT - Z Acceleration
Acceleration (g's)
Time (ms)
M50 26YO
M50 75YO
NBDL
6gFRT - X Displacement
Displacement (mm)
Time (ms)
M50 26YO
M50 75YO
NBDL
6gFRT - Y Displacement
Displacement (mm)
Time (ms)
M50 26YO
M50 75YO
NBDL
6gFRT - Z Displacement
Displacement (mm)
Time (ms)
M50 26YO
M50 75YO
NBDL
6gFRT - X Rot. Accel
Rot. Accel (Deg/ms2)
Time (ms)
M50 26YO
M50 75YO
NBDL
6gFRT - Y Rot. Accel
Rot. Accel (Deg/ms2)
Time (ms)
M50 26YO
M50 75YO
NBDL

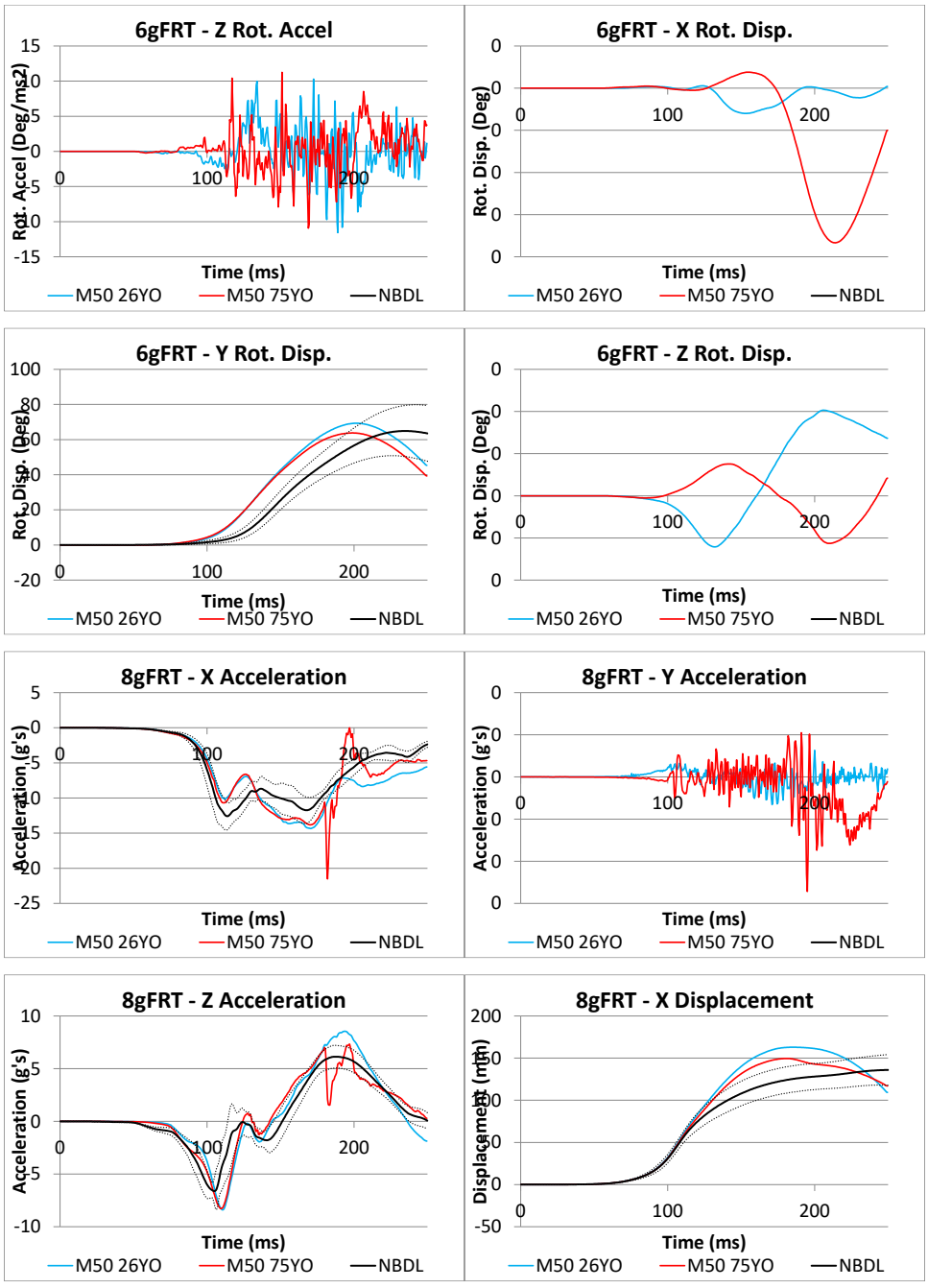
6gFRT - Z Rot. Accel
Rot. Accel (Deg/ms2)
Time (ms)
6gFRT - X Rot. Disp.
Rot. Disp. (Deg)
6gFRT - Y Rot. Disp.
6gFRT - Z Rot. Disp.
8gFRT - X Acceleration
Acceleration (g's)
8gFRT - Y Acceleration
8gFRT - Z Acceleration
8gFRT - X Displacement
Displacement (mm)
M50 26YO
M50 75YO
NBDL

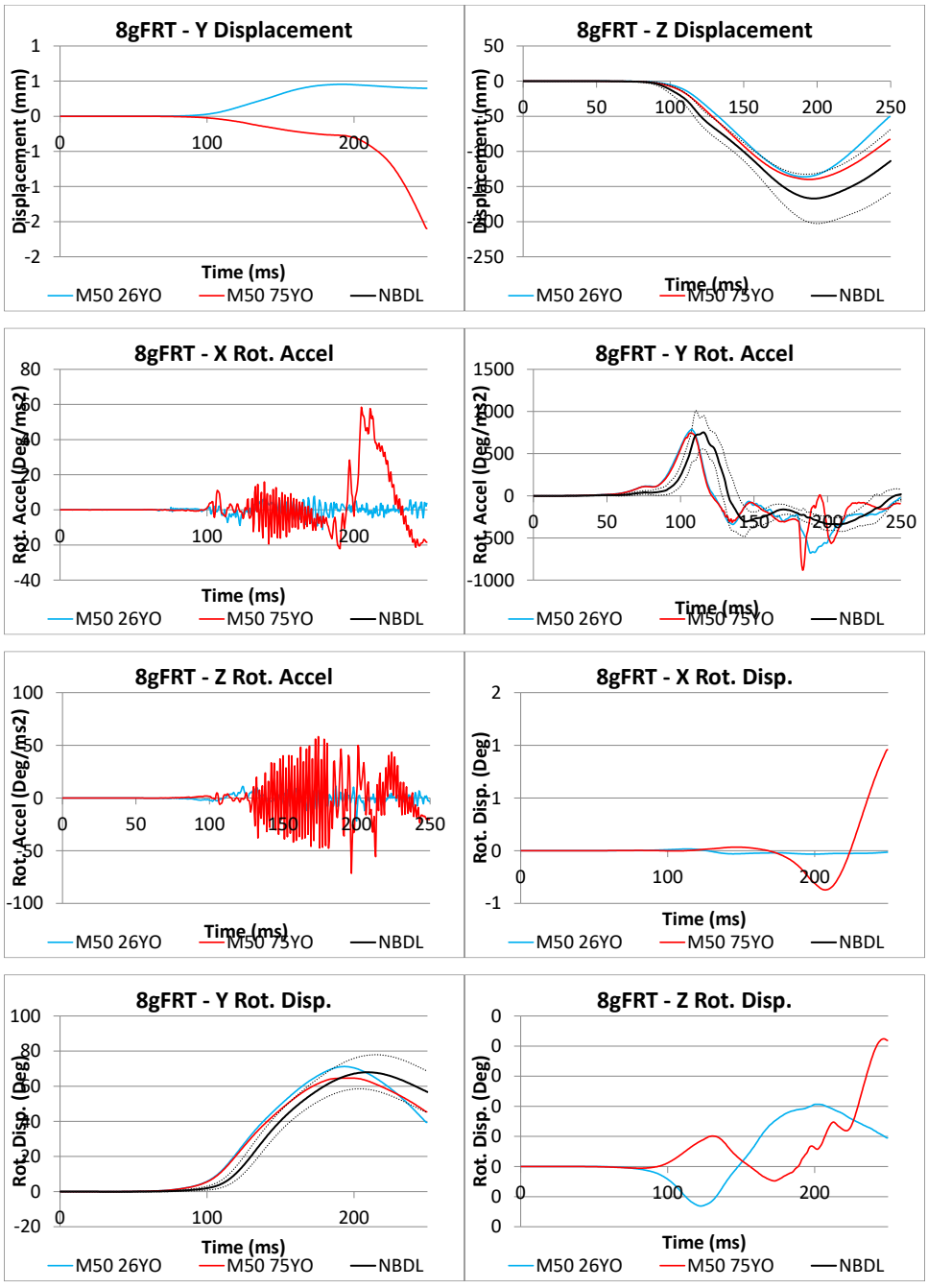
8gFRT - Y Displacement
Displacement (mm)
Time (ms)
M50 26YO
M50 75YO
NBDL
8gFRT - Z Displacement
Displacement (mm)
Time (ms)
M50 26YO
M50 75YO
NBDL
8gFRT - X Rot. Accel
Rot. Accel (Deg/ms2)
Time (ms)
M50 26YO
M50 75YO
NBDL
8gFRT - Y Rot. Accel
Rot. Accel (Deg/ms2)
Time (ms)
M50 26YO
M50 75YO
NBDL
8gFRT - Z Rot. Accel
Rot. Accel (Deg/ms2)
Time (ms)
M50 26YO
M50 75YO
NBDL
8gFRT - X Rot. Disp.
Rot. Disp. (Deg)
Time (ms)
M50 26YO
M50 75YO
NBDL
8gFRT - Y Rot. Disp.
Rot. Disp. (Deg)
Time (ms)
M50 26YO
M50 75YO
NBDL
8gFRT - Z Rot. Disp.
Rot. Disp. (Deg)
Time (ms)
M50 26YO
M50 75YO
NBDL

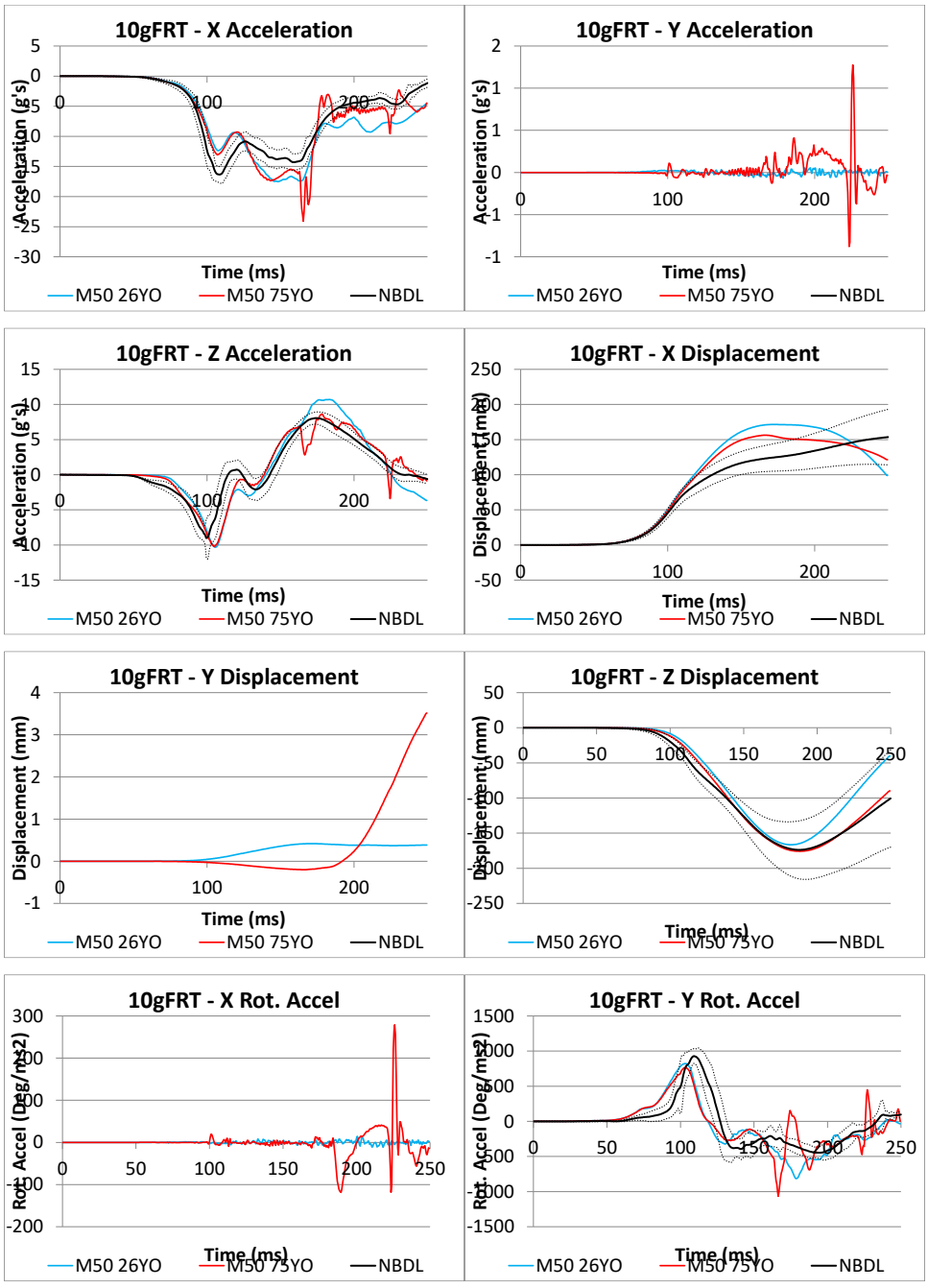
10gFRT - X Acceleration
Acceleration (g's)
Time (ms)
M50 26YO
M50 75YO
NBDL
10gFRT - Y Acceleration
Acceleration (g's)
Time (ms)
M50 26YO
M50 75YO
NBDL
10gFRT - Z Acceleration
Acceleration (g's)
Time (ms)
M50 26YO
M50 75YO
NBDL
10gFRT - X Displacement
Displacement (mm)
Time (ms)
M50 26YO
M50 75YO
NBDL
10gFRT - Y Displacement
Displacement (mm)
Time (ms)
M50 26YO
M50 75YO
NBDL
10gFRT - Z Displacement
Displacement (mm)
Time (ms)
M50 26YO
M50 75YO
NBDL
10gFRT - X Rot. Accel
Rot. Accel (Deg/ms2)
Time (ms)
M50 26YO
M50 75YO
NBDL
10gFRT - Y Rot. Accel
Rot. Accel (Deg/ms2)
Time (ms)
M50 26YO
M50 75YO
NBDL

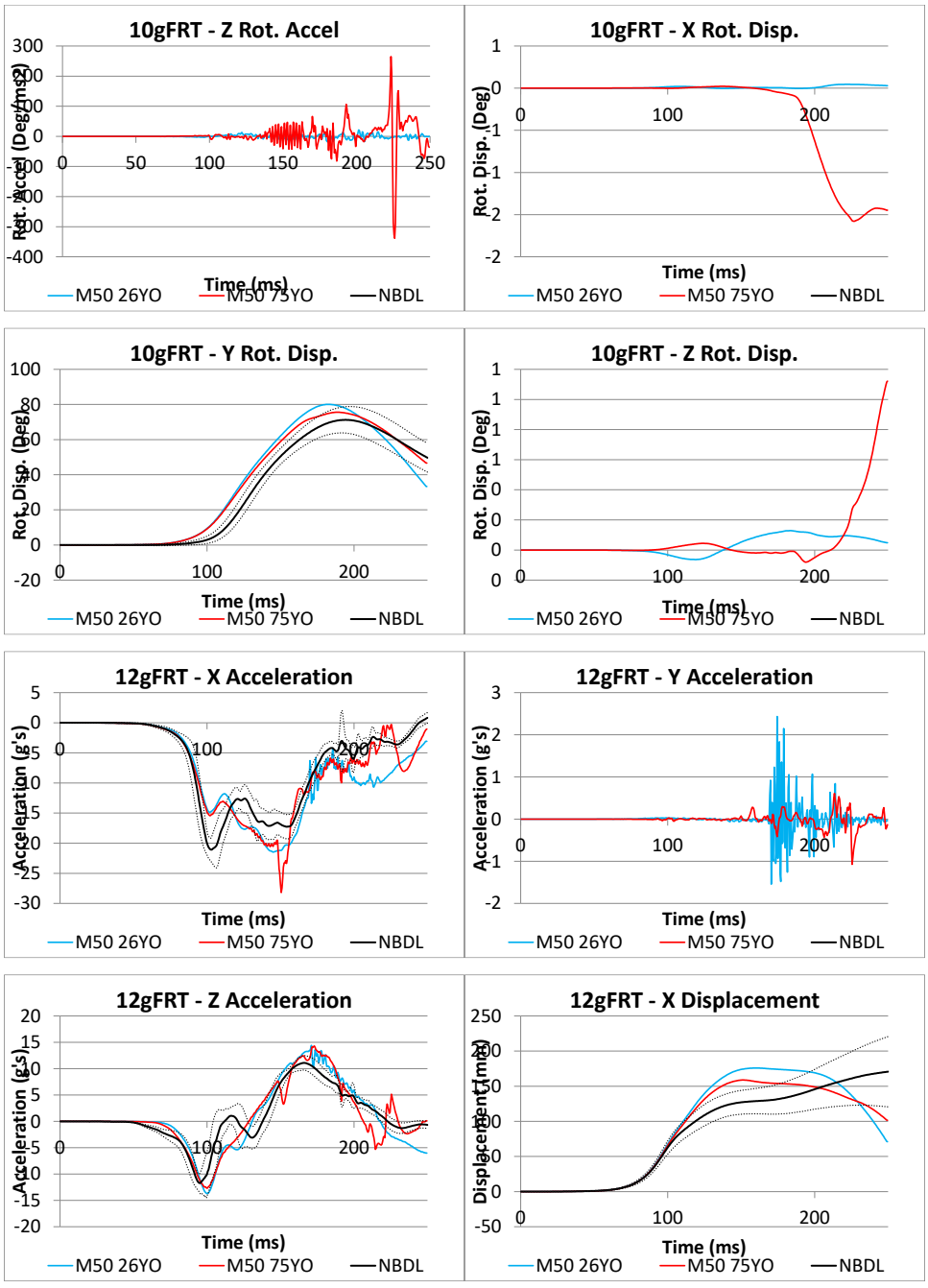
10gFRT - Z Rot. Accel
Rot. Accel (Deg/ms2)
Time (ms)
10gFRT - X Rot. Disp.
Rot. Disp. (Deg)
Time (ms)
10gFRT - Y Rot. Disp.
Rot. Disp. (Deg)
Time (ms)
10gFRT - Z Rot. Disp.
Rot. Disp. (Deg)
Time (ms)
12gFRT - X Acceleration
Acceleration (g's)
Time (ms)
12gFRT - Y Acceleration
Acceleration (g's)
Time (ms)
12gFRT - Z Acceleration
Acceleration (g's)
Time (ms)
12gFRT - X Displacement
Displacement (mm)
Time (ms)
M50 26YO
M50 75YO
NBDL

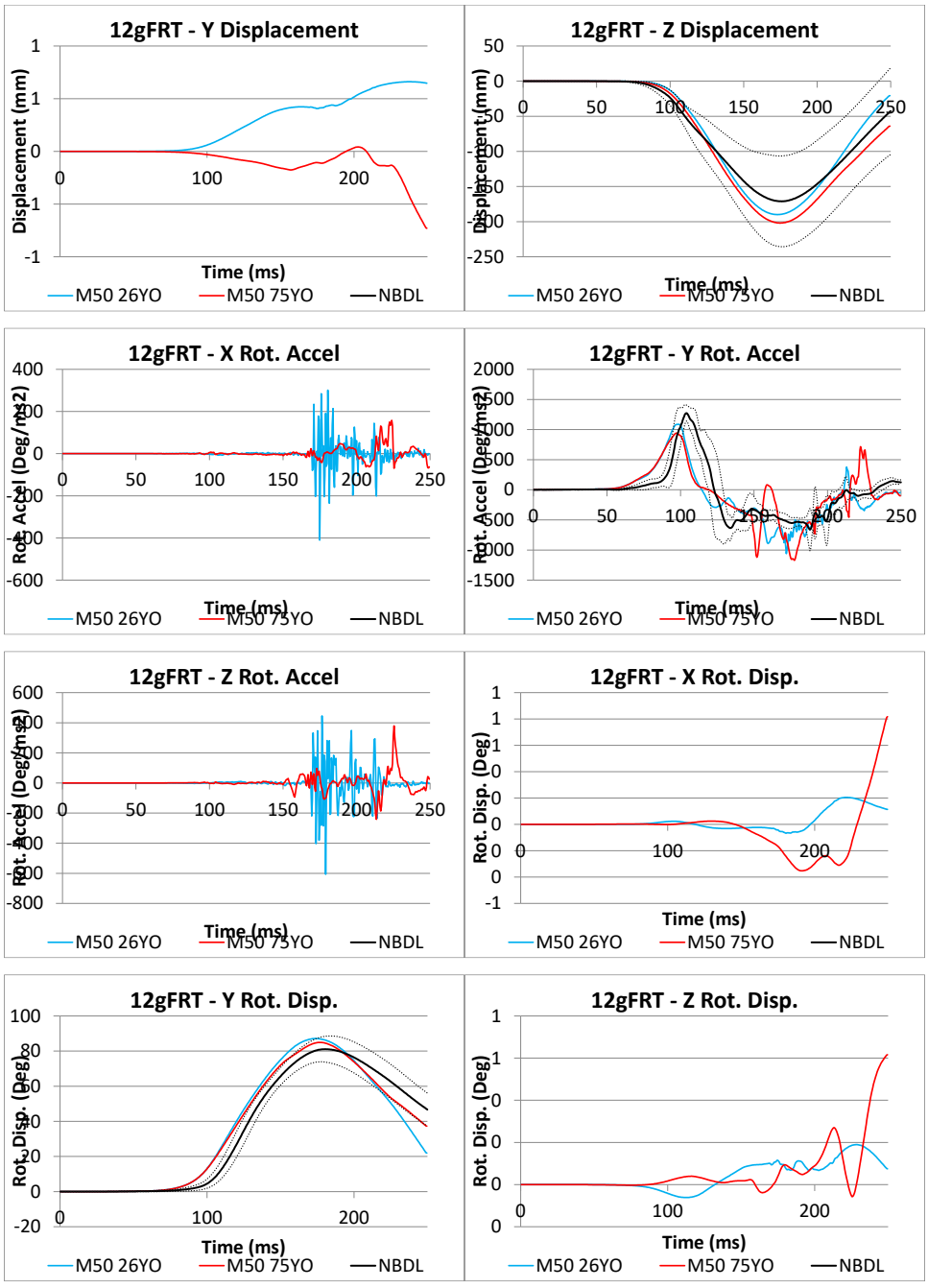
12gFRT - Y Displacement
Displacement (mm)
Time (ms)
M50 26YO
M50 75YO
NBDL
12gFRT - Z Displacement
Displacement (mm)
Time (ms)
M50 26YO
M50 75YO
NBDL
12gFRT - X Rot. Accel
Rot. Accel (Deg/ms2)
Time (ms)
M50 26YO
M50 75YO
NBDL
12gFRT - Y Rot. Accel
Rot. Accel (Deg/ms2)
Time (ms)
M50 26YO
M50 75YO
NBDL
12gFRT - Z Rot. Accel
Rot. Accel (Deg/ms2)
Time (ms)
M50 26YO
M50 75YO
NBDL
12gFRT - X Rot. Disp.
Rot. Disp. (Deg)
Time (ms)
M50 26YO
M50 75YO
NBDL
12gFRT - Y Rot. Disp.
Rot. Disp. (Deg)
Time (ms)
M50 26YO
M50 75YO
NBDL
12gFRT - Z Rot. Disp.
Rot. Disp. (Deg)
Time (ms)
M50 26YO
M50 75YO
NBDL

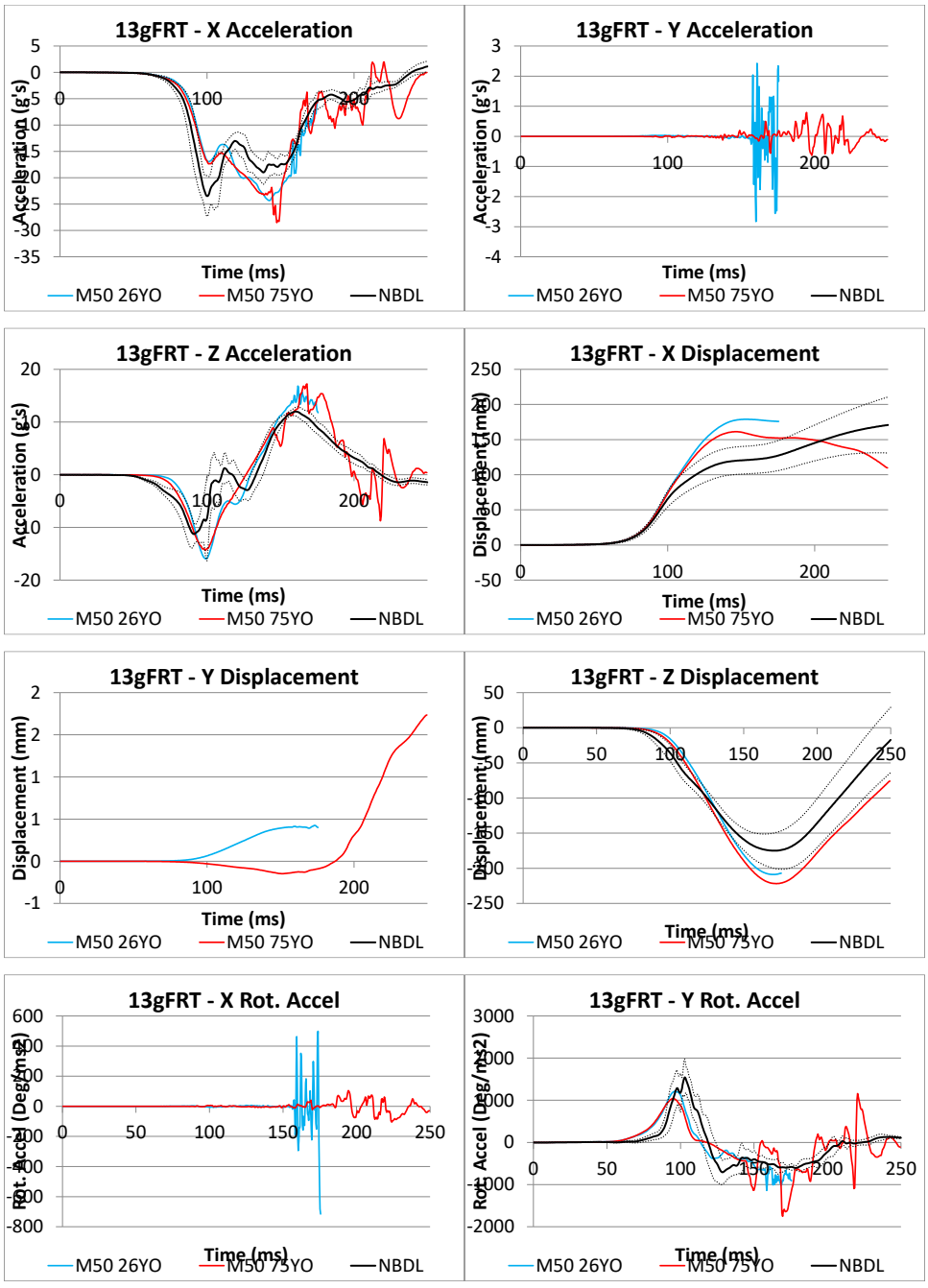
13gFRT - X Acceleration
Acceleration (g's)
Time (ms)
M50 26YO
M50 75YO
NBDL
13gFRT - Y Acceleration
Acceleration (g's)
Time (ms)
M50 26YO
M50 75YO
NBDL
13gFRT - Z Acceleration
Acceleration (g's)
Time (ms)
M50 26YO
M50 75YO
NBDL
13gFRT - X Displacement
Displacement (mm)
Time (ms)
M50 26YO
M50 75YO
NBDL
13gFRT - Y Displacement
Displacement (mm)
Time (ms)
M50 26YO
M50 75YO
NBDL
13gFRT - Z Displacement
Displacement (mm)
Time (ms)
M50 26YO
M50 75YO
NBDL
13gFRT - X Rot. Accel
Rot. Accel (Deg/(ms2)
Time (ms)
M50 26YO
M50 75YO
NBDL
13gFRT - Y Rot. Accel
Rot. Accel (Deg/(ms2)
Time (ms)
M50 26YO
M50 75YO
NBDL

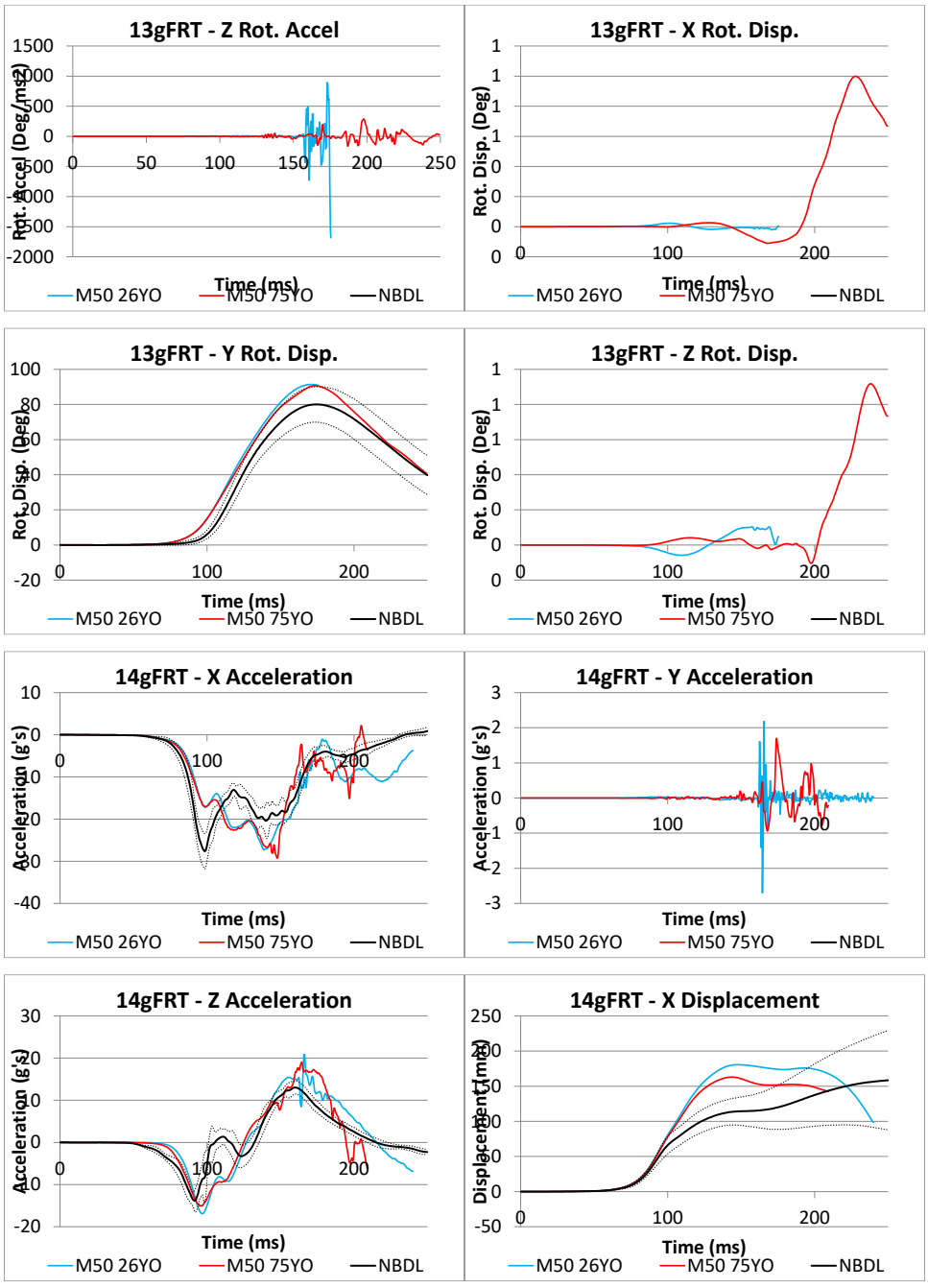
13gFRT - Z Rot. Accel
Rot. Accel (Deg/ms2)
Time (ms)
13gFRT - X Rot. Disp.
Rot. Disp. (Deg)
13gFRT - Y Rot. Disp.
13gFRT - Z Rot. Disp.
14gFRT - X Acceleration
Acceleration (g's)
14gFRT - Y Acceleration
14gFRT - Z Acceleration
14gFRT - X Displacement
Displacement (mm)
M50 26YO
M50 75YO
NBDL

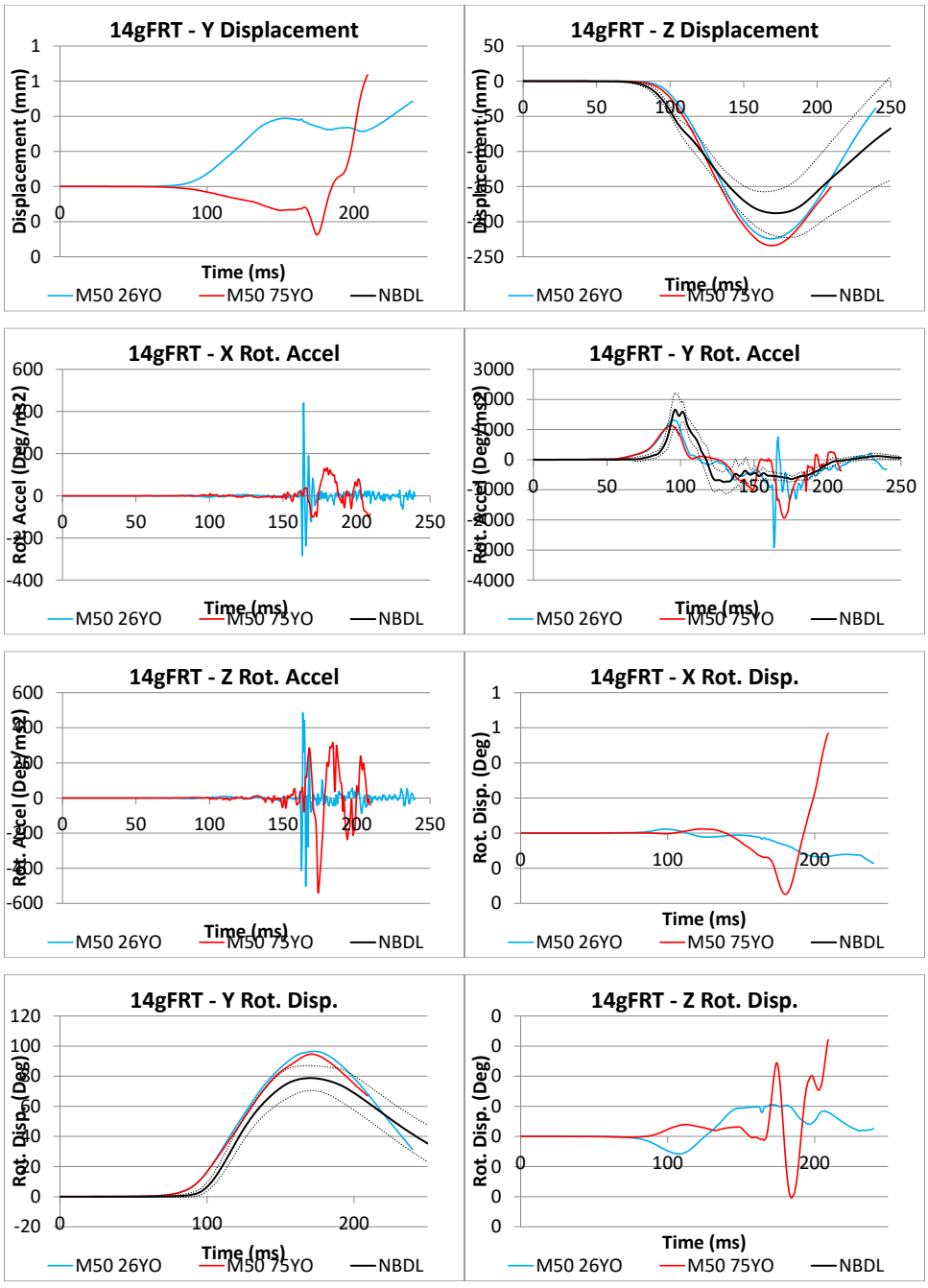
14gFRT - Y Displacement
Displacement (mm)
Time (ms)
M50 26YO
M50 75YO
NBDL
14gFRT - Z Displacement
Displacement (mm)
Time (ms)
M50 26YO
M50 75YO
NBDL
14gFRT - X Rot. Accel
Rot. Accel (Deg/ms2)
Time (ms)
M50 26YO
M50 75YO
NBDL
14gFRT - Y Rot. Accel
Rot. Accel (Deg/ms2)
Time (ms)
M50 26YO
M50 75YO
NBDL
14gFRT - Z Rot. Accel
Rot. Accel (Deg/ms2)
Time (ms)
M50 26YO
M50 75YO
NBDL
14gFRT - X Rot. Disp.
Rot. Disp. (Deg)
Time (ms)
M50 26YO
M50 75YO
NBDL
14gFRT - Y Rot. Disp.
Rot. Disp. (Deg)
Time (ms)
M50 26YO
M50 75YO
NBDL
14gFRT - Z Rot. Disp.
Rot. Disp. (Deg)
Time (ms)
M50 26YO
M50 75YO
NBDL

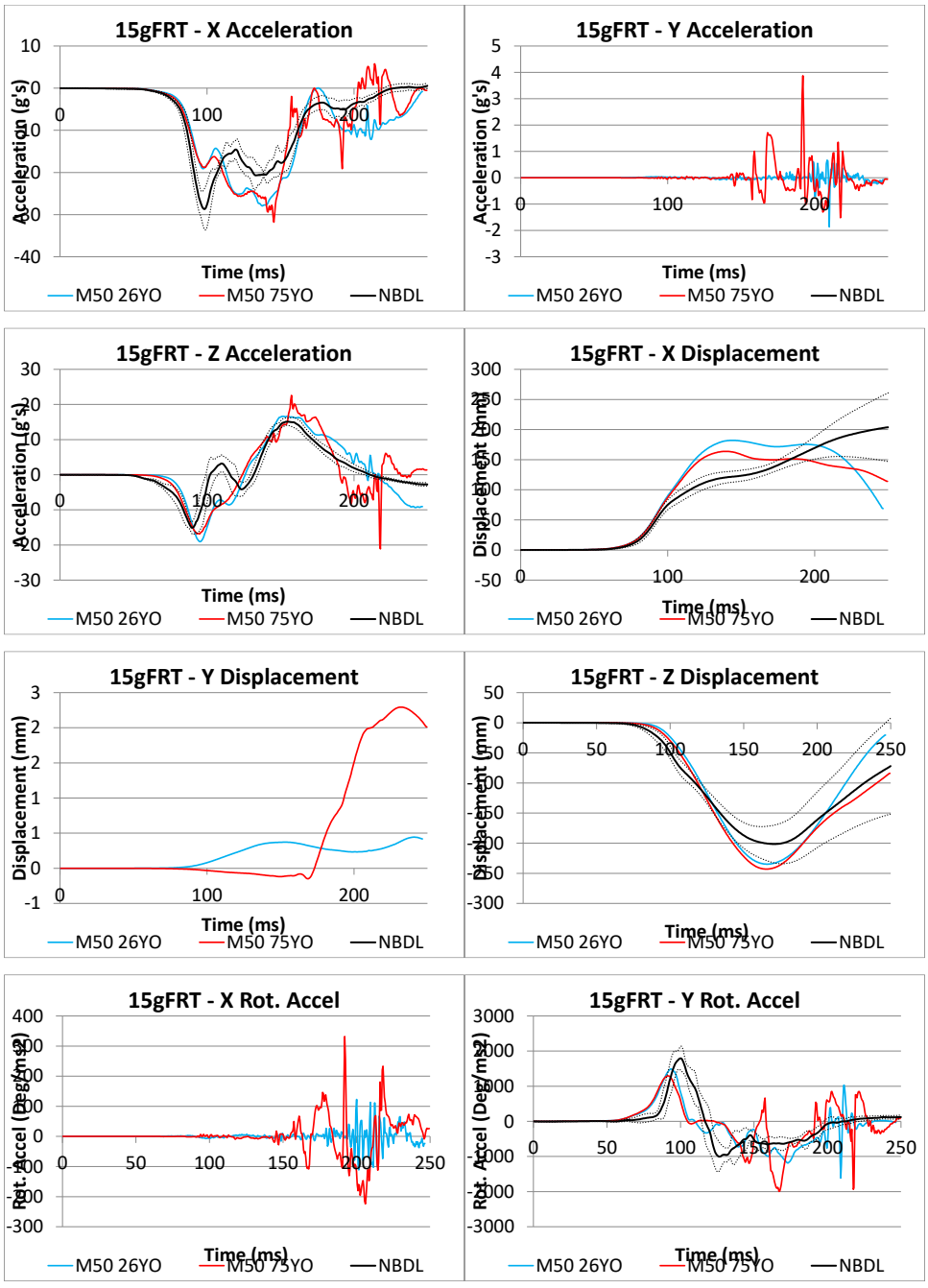
15gFRT - X Acceleration
Acceleration (g's)
Time (ms)
M50 26YO
M50 75YO
NBDL
15gFRT - Y Acceleration
Acceleration (g's)
Time (ms)
M50 26YO
M50 75YO
NBDL
15gFRT - Z Acceleration
Acceleration (g's)
Time (ms)
M50 26YO
M50 75YO
NBDL
15gFRT - X Displacement
Displacement (mm)
Time (ms)
M50 26YO
M50 75YO
NBDL
15gFRT - Y Displacement
Displacement (mm)
Time (ms)
M50 26YO
M50 75YO
NBDL
15gFRT - Z Displacement
Displacement (mm)
Time (ms)
M50 26YO
M50 75YO
NBDL
15gFRT - X Rot. Accel
Rot. Accel (Deg/ms2)
Time (ms)
M50 26YO
M50 75YO
NBDL
15gFRT - Y Rot. Accel
Rot. Accel (Deg/ms2)
Time (ms)
M50 26YO
M50 75YO
NBDL

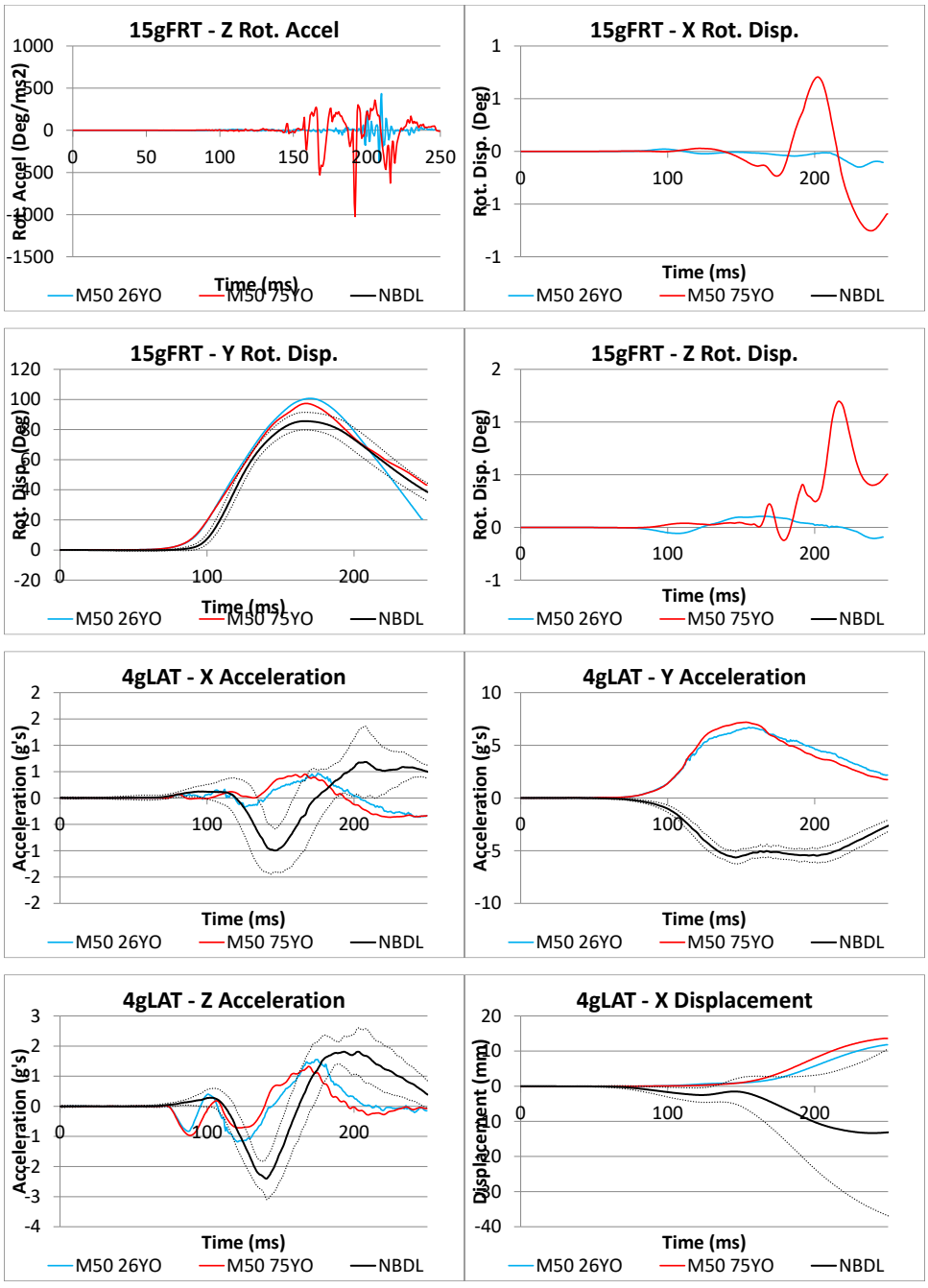
15gFRT - Z Rot. Accel
Rot. Accel (Deg/ms2)
Time (ms)
15gFRT - X Rot. Disp.
Rot. Disp. (Deg)
Time (ms)
15gFRT - Y Rot. Disp.
Rot. Disp. (Deg)
Time (ms)
15gFRT - Z Rot. Disp.
Rot. Disp. (Deg)
Time (ms)
4gLAT - X Acceleration
Acceleration (g's)
Time (ms)
4gLAT - Y Acceleration
Acceleration (g's)
Time (ms)
4gLAT - Z Acceleration
Acceleration (g's)
Time (ms)
4gLAT - X Displacement
Displacement (mm)
Time (ms)
M50 26YO
M50 75YO
NBDL

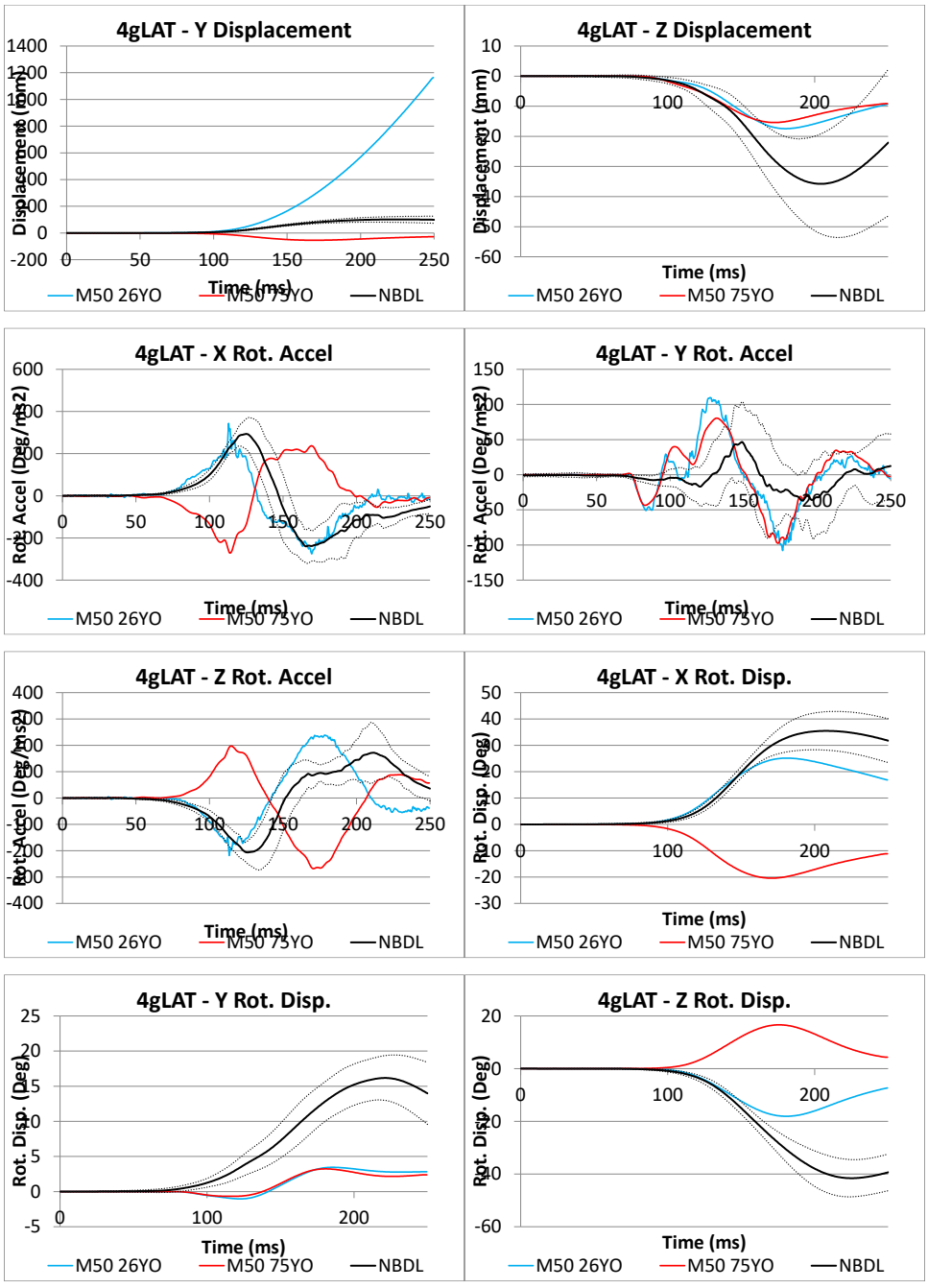
4gLAT - Y Displacement
Displacement (mm)
Time (ms)
M50 26YO
M50 75YO
NBDL
4gLAT - Z Displacement
Displacement (mm)
Time (ms)
M50 26YO
M50 75YO
NBDL
4gLAT - X Rot. Accel
Rot. Accel (Deg/ms2)
Time (ms)
M50 26YO
M50 75YO
NBDL
4gLAT - Y Rot. Accel
Rot. Accel (Deg/ms2)
Time (ms)
M50 26YO
M50 75YO
NBDL
4gLAT - Z Rot. Accel
Rot. Accel (Deg/ms2)
Time (ms)
M50 26YO
M50 75YO
NBDL
4gLAT - X Rot. Disp.
Rot. Disp. (Deg)
Time (ms)
M50 26YO
M50 75YO
NBDL
4gLAT - Y Rot. Disp.
Rot. Disp. (Deg)
Time (ms)
M50 26YO
M50 75YO
NBDL
4gLAT - Z Rot. Disp.
Rot. Disp. (Deg)
Time (ms)
M50 26YO
M50 75YO
NBDL

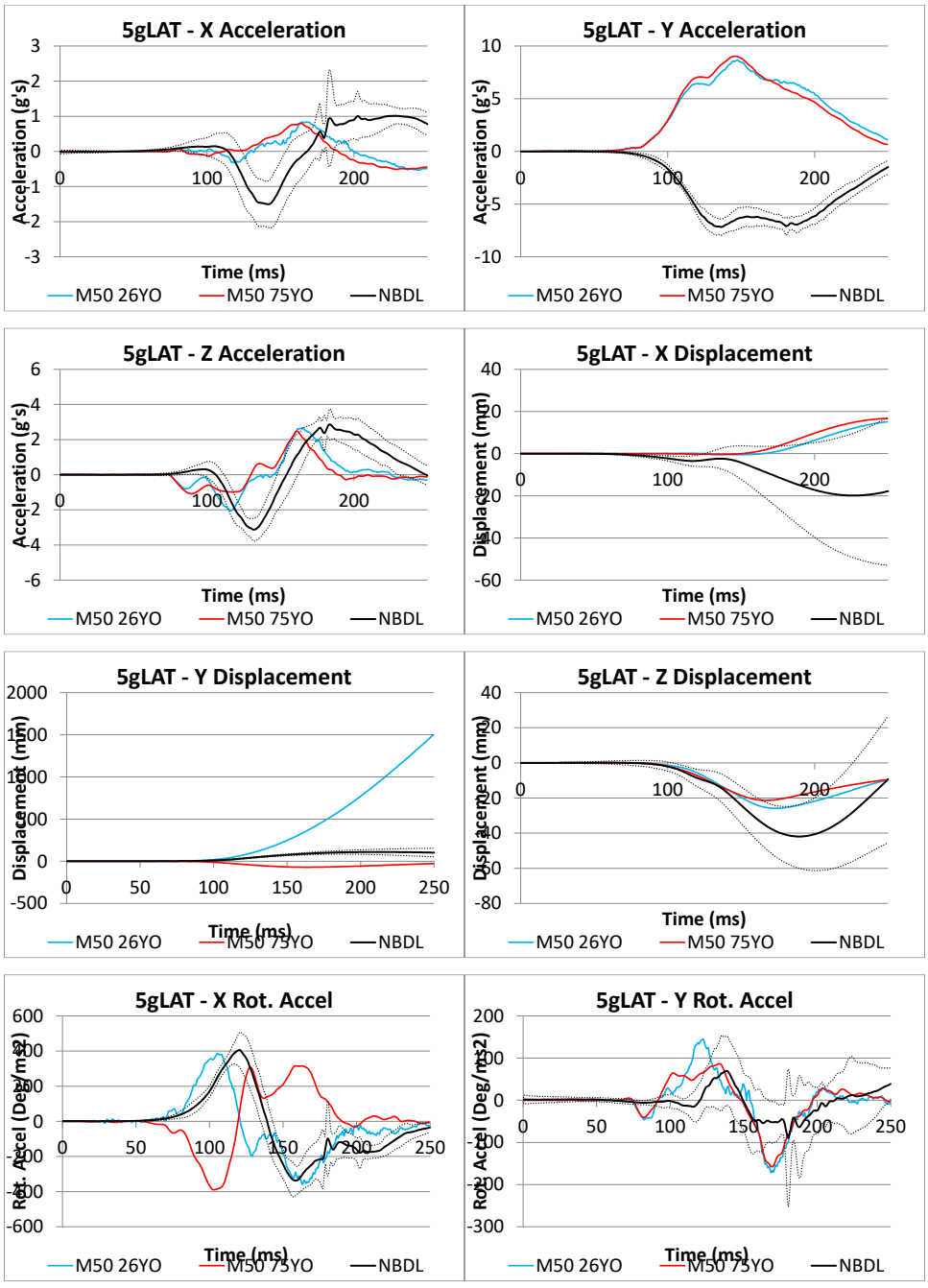
5gLAT - X Acceleration
Acceleration (g's)
Time (ms)
M50 26YO
M50 75YO
NBDL
5gLAT - Y Acceleration
Acceleration (g's)
Time (ms)
M50 26YO
M50 75YO
NBDL
5gLAT - Z Acceleration
Acceleration (g's)
Time (ms)
M50 26YO
M50 75YO
NBDL
5gLAT - X Displacement
Displacement (mm)
Time (ms)
M50 26YO
M50 75YO
NBDL
5gLAT - Y Displacement
Displacement (mm)
Time (ms)
M50 26YO
M50 75YO
NBDL
5gLAT - Z Displacement
Displacement (mm)
Time (ms)
M50 26YO
M50 75YO
NBDL
5gLAT - X Rot. Accel
Rot. Accel (Deg/ms2)
Time (ms)
M50 26YO
M50 75YO
NBDL
5gLAT - Y Rot. Accel
Rot. Accel (Deg/ms2)
Time (ms)
M50 26YO
M50 75YO
NBDL

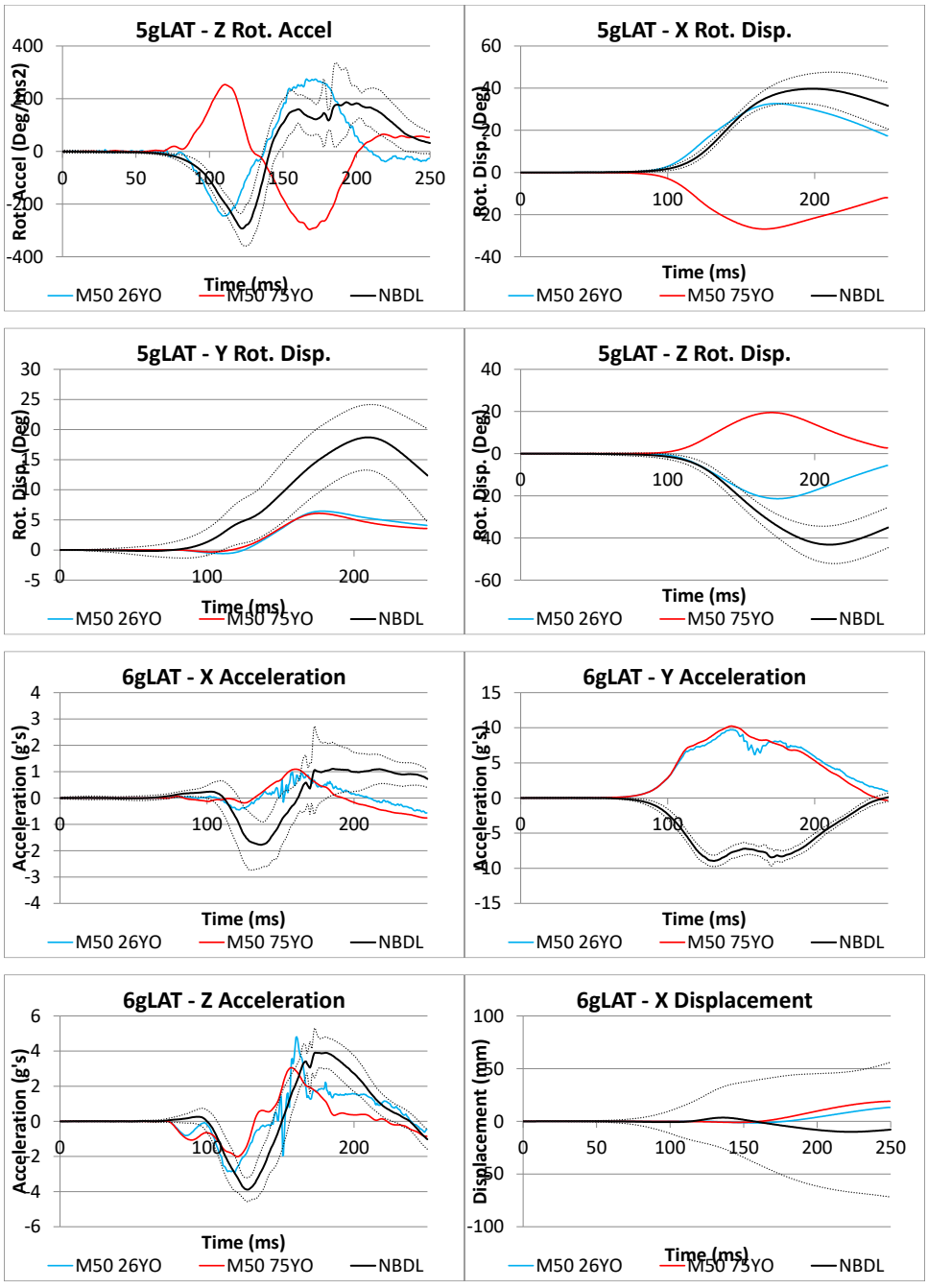
5gLAT - Z Rot. Accel
Rot. Accel (Deg./ms2)
Time (ms)
5gLAT - X Rot. Disp.
Rot. Disp. (Deg.)
Time (ms)
5gLAT - Y Rot. Disp.
Rot. Disp. (Deg.)
Time (ms)
5gLAT - Z Rot. Disp.
Rot. Disp. (Deg.)
Time (ms)
6gLAT - X Acceleration
Acceleration (g's)
Time (ms)
6gLAT - Y Acceleration
Acceleration (g's)
Time (ms)
6gLAT - Z Acceleration
Acceleration (g's)
Time (ms)
6gLAT - X Displacement
Displacement (mm)
Time (ms)
M50 26YO
M50 75YO
NBDL

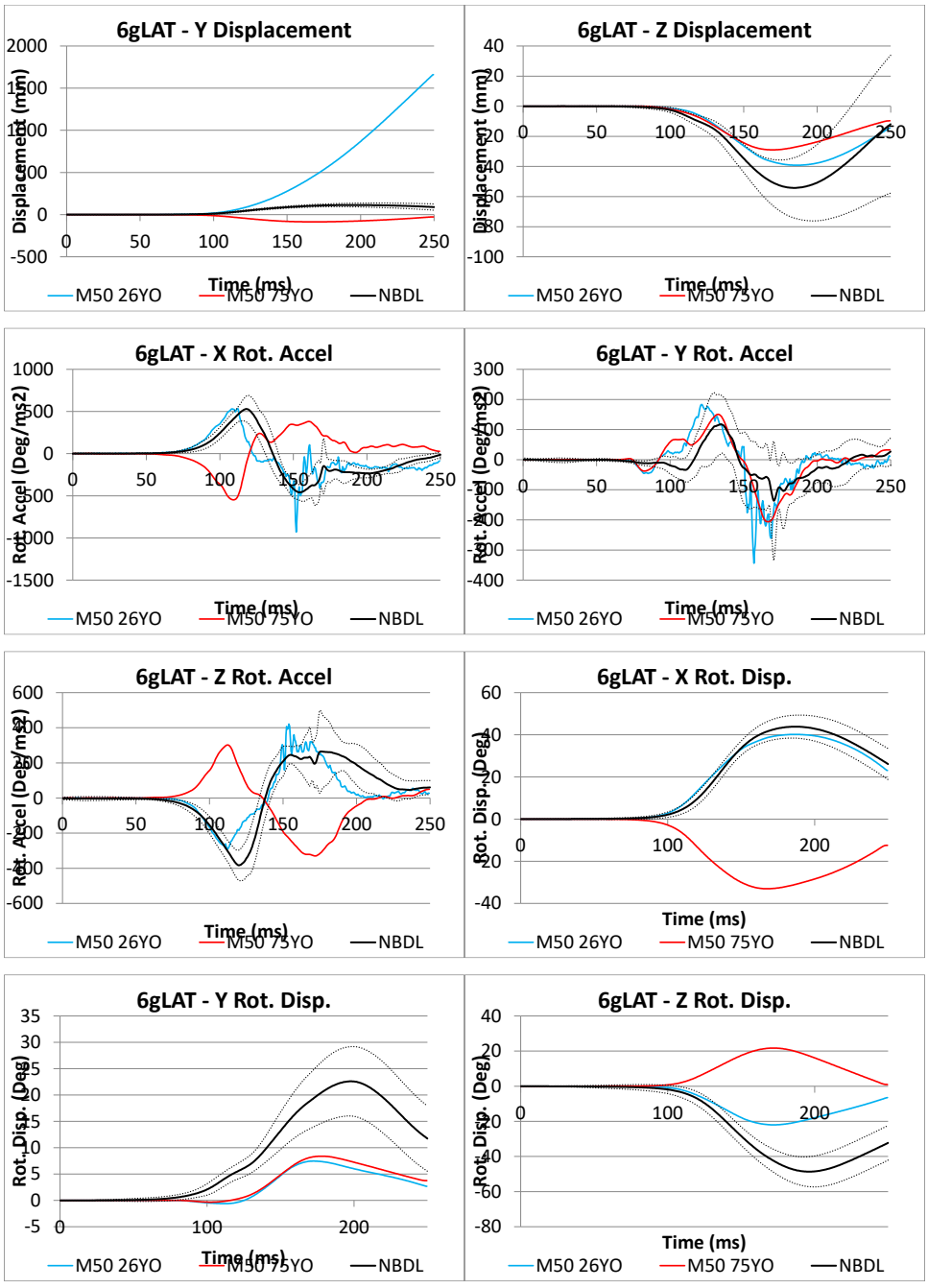
6gLAT - Y Displacement
Displacement (mm)
Time (ms)
6gLAT - Z Displacement
Displacement (mm)
Time (ms)
6gLAT - X Rot. Accel
Rot. Accel (Deg/ms2)
Time (ms)
6gLAT - Y Rot. Accel
Rot. Accel (Deg/ms2)
Time (ms)
6gLAT - Z Rot. Accel
Rot. Accel (Deg/ms2)
Time (ms)
6gLAT - X Rot. Disp.
Rot. Disp. (Deg.)
Time (ms)
6gLAT - Y Rot. Disp.
Rot. Disp. (Deg.)
Time (ms)
6gLAT - Z Rot. Disp.
Rot. Disp. (Deg.)
Time (ms)
M50 26YO
M50 75YO
NBDL

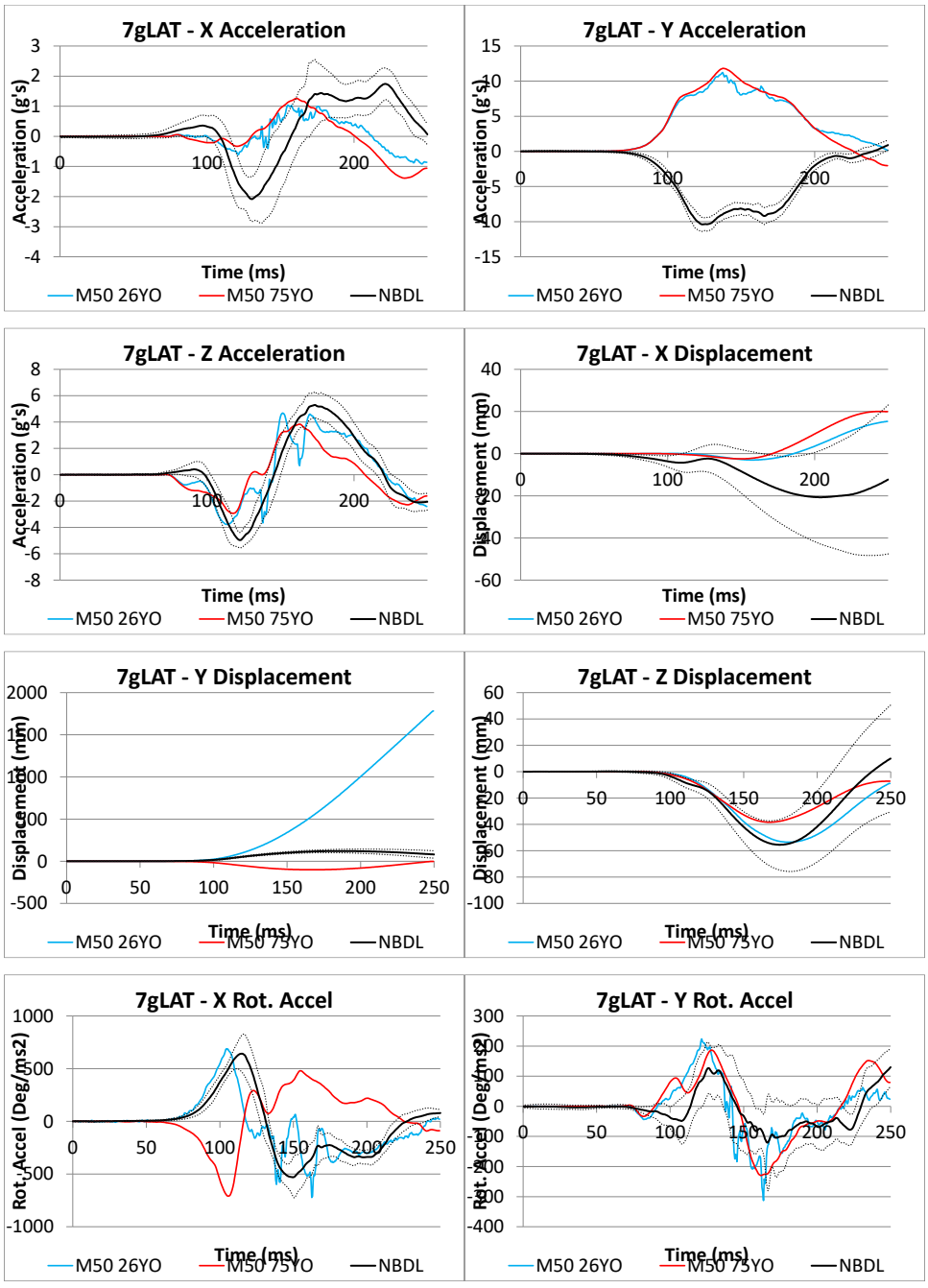
7gLAT - X Acceleration
Acceleration (g's)
Time (ms)
M50 26YO
M50 75YO
NBDL
7gLAT - Y Acceleration
Acceleration (g's)
Time (ms)
M50 26YO
M50 75YO
NBDL
7gLAT - Z Acceleration
Acceleration (g's)
Time (ms)
M50 26YO
M50 75YO
NBDL
7gLAT - X Displacement
Displacement (mm)
Time (ms)
M50 26YO
M50 75YO
NBDL
7gLAT - Y Displacement
Displacement (mm)
Time (ms)
M50 26YO
M50 75YO
NBDL
7gLAT - Z Displacement
Displacement (mm)
Time (ms)
M50 26YO
M50 75YO
NBDL
7gLAT - X Rot. Accel
Rot. Accel (Deg/ms2)
Time (ms)
M50 26YO
M50 75YO
NBDL
7gLAT - Y Rot. Accel
Rot. Accel (Deg/ms2)
Time (ms)
M50 26YO
M50 75YO
NBDL

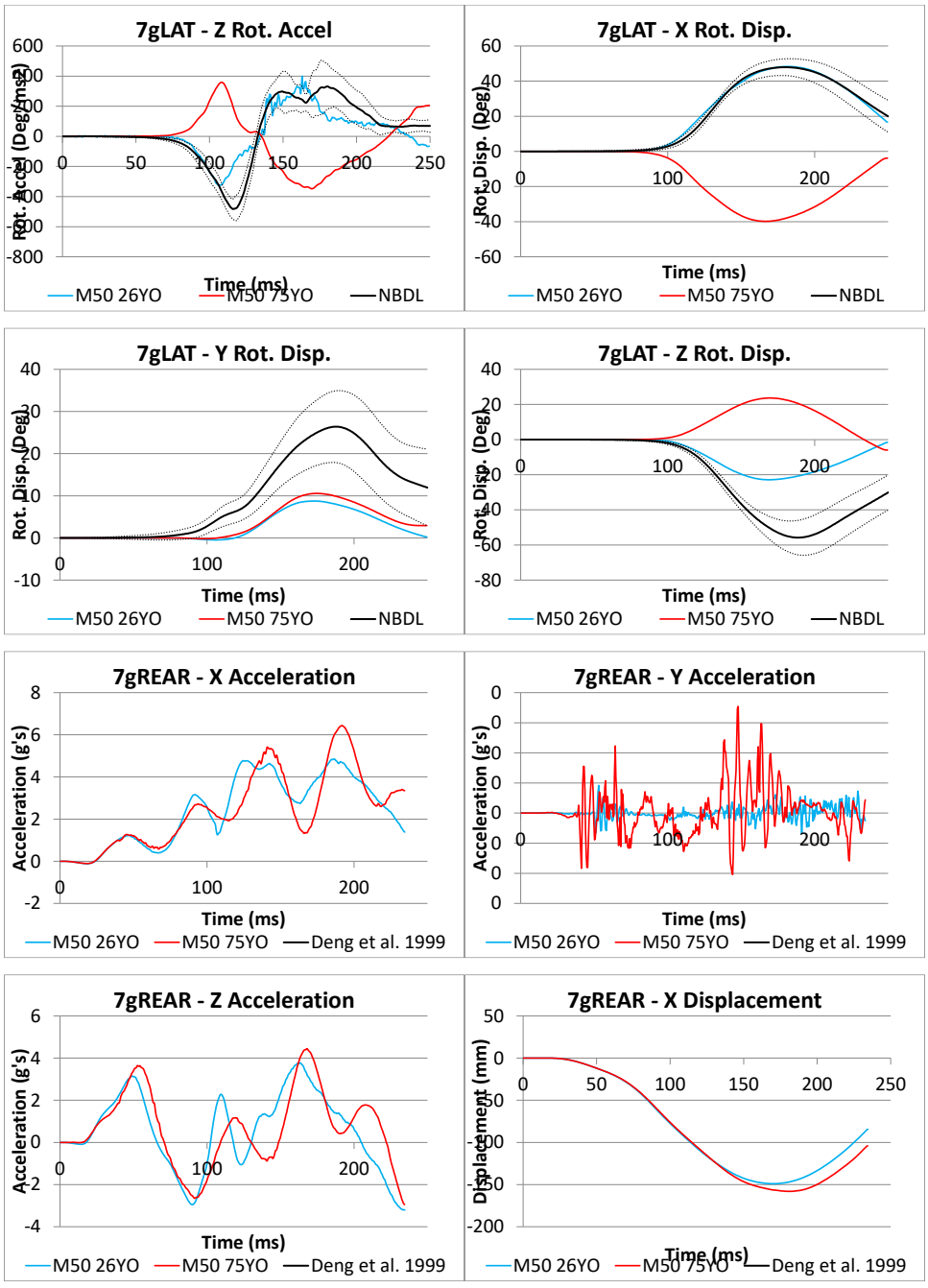
7gLAT - Z Rot. Accel
Rot. Accel (Deg/ms2)
Time (ms)
M50 26YO
M50 75YO
NBDL
7gLAT - X Rot. Disp.
Rot. Disp. (Deg.)
Time (ms)
M50 26YO
M50 75YO
NBDL
7gLAT - Y Rot. Disp.
Rot. Disp. (Deg.)
Time (ms)
M50 26YO
M50 75YO
NBDL
7gLAT - Z Rot. Disp.
Rot. Disp. (Deg.)
Time (ms)
M50 26YO
M50 75YO
NBDL
7gREAR - X Acceleration
Acceleration (g's)
Time (ms)
M50 26YO
M50 75YO
Deng et al. 1999
7gREAR - Y Acceleration
Acceleration (g's)
Time (ms)
M50 26YO
M50 75YO
Deng et al. 1999
7gREAR - Z Acceleration
Acceleration (g's)
Time (ms)
M50 26YO
M50 75YO
Deng et al. 1999
7gREAR - X Displacement
Displacement (mm)
Time (ms)
M50 26YO
M50 75YO
Deng et al. 1999

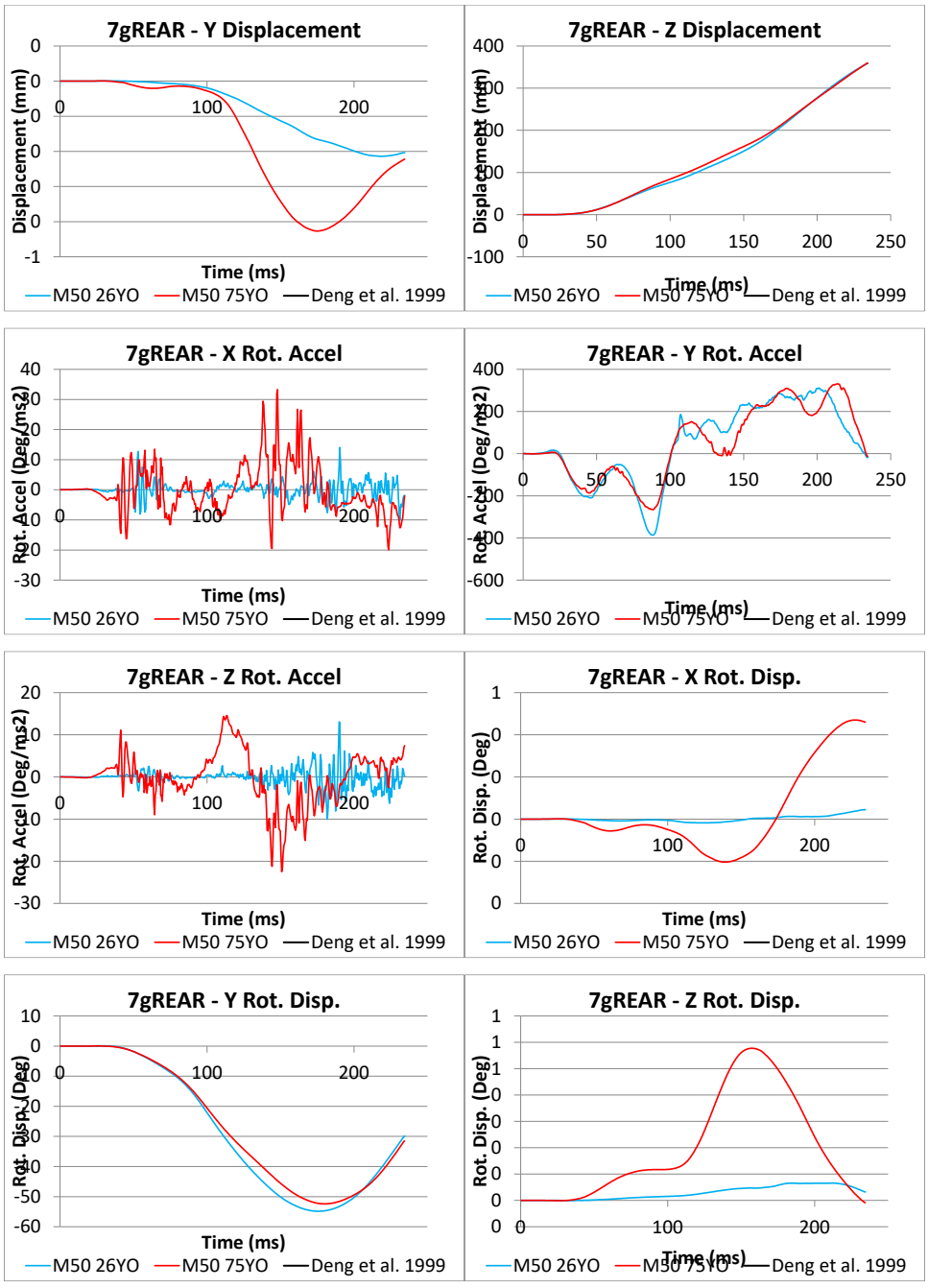
7gREAR - Y Displacement
Displacement (mm)
Time (ms)
7gREAR - Z Displacement
Displacement (mm)
Time (ms)
7gREAR - X Rot. Accel
Rot. Accel (Deg/ms2)
Time (ms)
7gREAR - Y Rot. Accel
Rot. Accel (Deg/ms2)
Time (ms)
7gREAR - Z Rot. Accel
Rot. Accel (Deg/ms2)
Time (ms)
7gREAR - X Rot. Disp.
Rot. Disp. (Deg)
Time (ms)
7gREAR - Y Rot. Disp.
Rot. Disp. (Deg)
Time (ms)
7gREAR - Z Rot. Disp.
Rot. Disp. (Deg)
Time (ms)
M50 26YO
M50 75YO
Deng et al. 1999

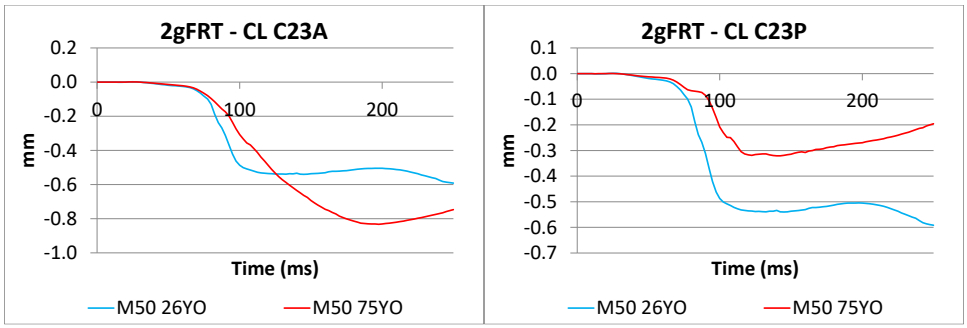
2gFRT - CL C23A
mm
Time (ms)
M50 26YO
M50 75YO

2gFRT - CL C23P
mm
Time (ms)
M50 26YO
M50 75YO

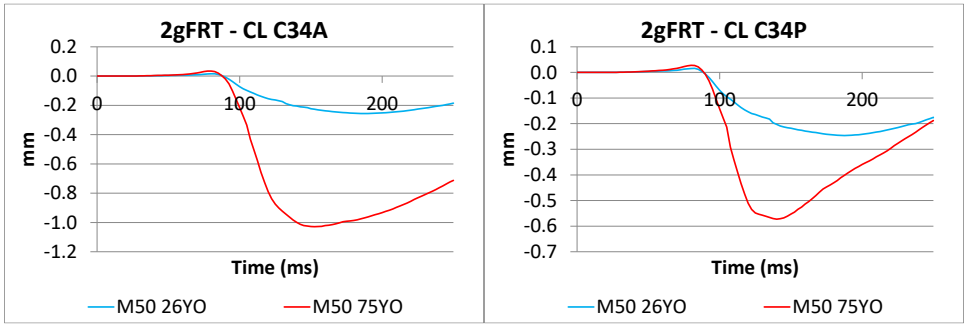
2gFRT - CL C34A
mm
Time (ms)
M50 26YO
M50 75YO

2gFRT - CL C34P
mm
Time (ms)
M50 26YO
M50 75YO

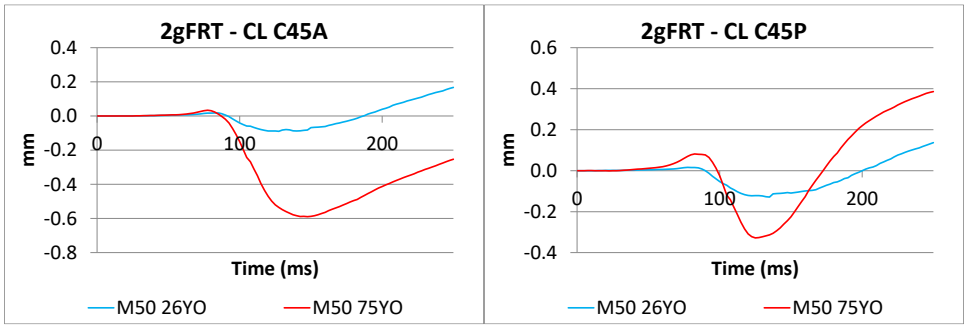
2gFRT - CL C45A
mm
Time (ms)
M50 26YO
M50 75YO

2gFRT - CL C45P
mm
Time (ms)
M50 26YO
M50 75YO

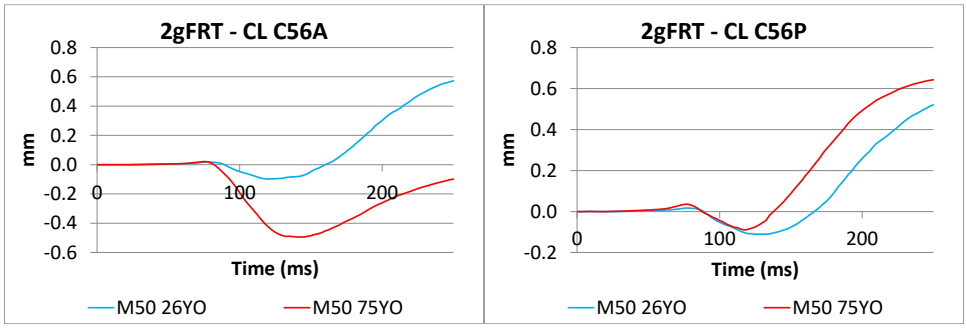
2gFRT - CL C56A
mm
Time (ms)
M50 26YO
M50 75YO

2gFRT - CL C56P
mm
Time (ms)
M50 26YO
M50 75YO

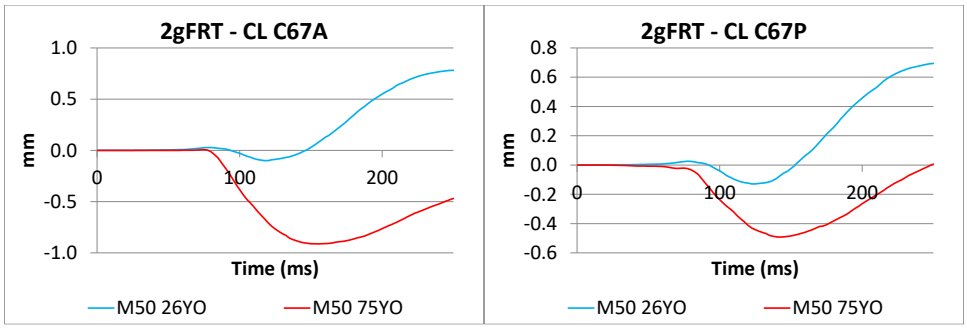
2gFRT - CL C67A
mm
Time (ms)
M50 26YO
M50 75YO

2gFRT - CL C67P
mm
Time (ms)
M50 26YO
M50 75YO

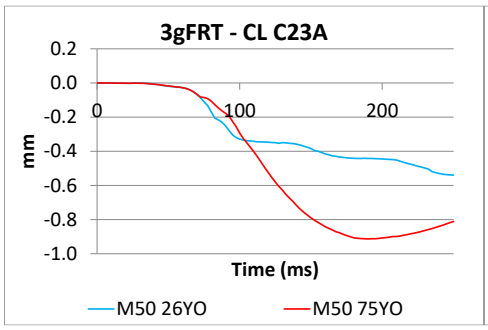
3gFRT - CL C23A
mm
Time (ms)
M50 26YO
M50 75YO

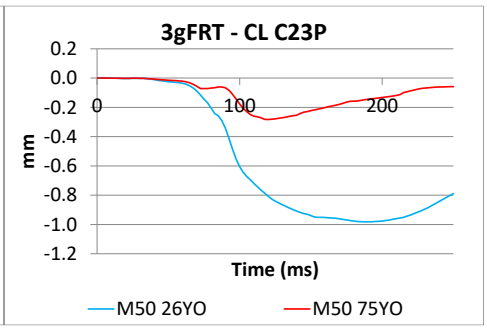
3gFRT - CL C23P
mm
Time (ms)
M50 26YO
M50 75YO

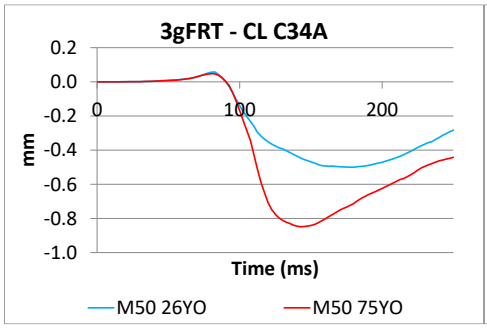
3gFRT - CL C34A
mm
Time (ms)
M50 26YO
M50 75YO

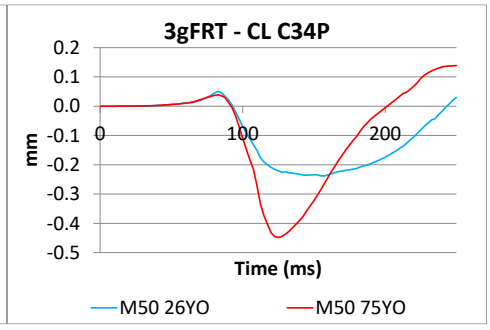
3gFRT - CL C34P
mm
Time (ms)
M50 26YO
M50 75YO

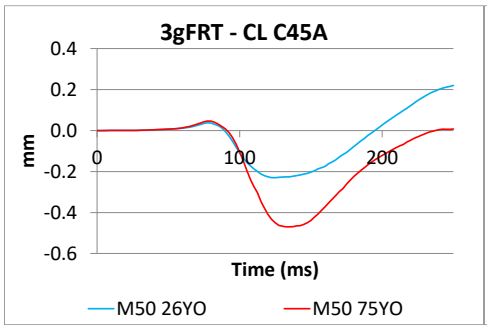
3gFRT - CL C45A
mm
Time (ms)
M50 26YO
M50 75YO

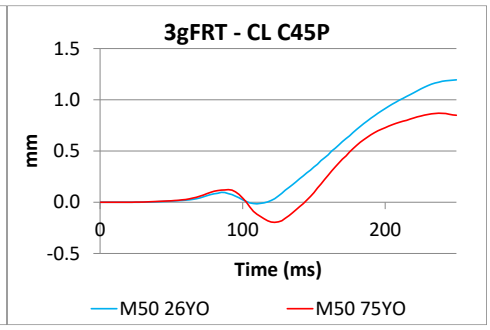
3gFRT - CL C45P
mm
Time (ms)
M50 26YO
M50 75YO

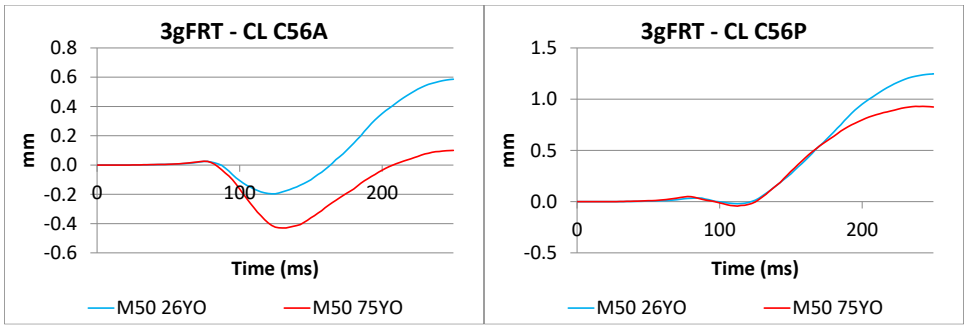
3gFRT - CL C56A
mm
Time (ms)
M50 26YO
M50 75YO

3gFRT - CL C56P
mm
Time (ms)
M50 26YO
M50 75YO

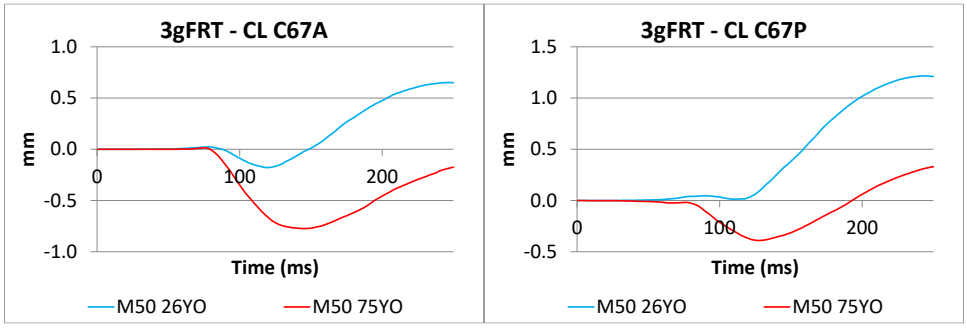
3gFRT - CL C67A
mm
Time (ms)
M50 26YO
M50 75YO

3gFRT - CL C67P
mm
Time (ms)
M50 26YO
M50 75YO

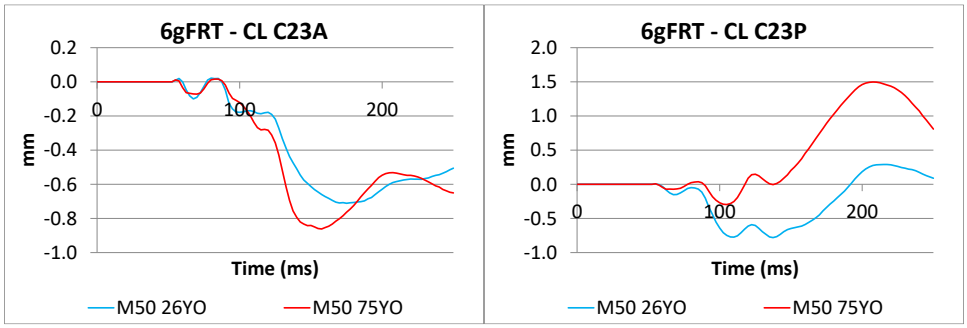
6gFRT - CL C23A
mm
Time (ms)
M50 26YO
M50 75YO

6gFRT - CL C23P
mm
Time (ms)
M50 26YO
M50 75YO

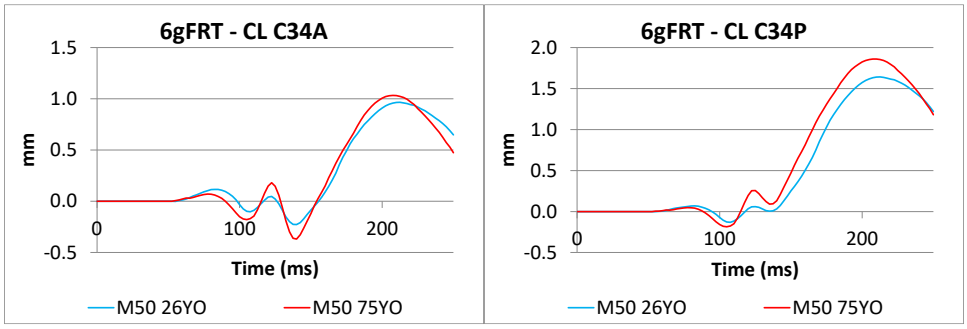
6gFRT - CL C34A
mm
Time (ms)
M50 26YO
M50 75YO

6gFRT - CL C34P
mm
Time (ms)
M50 26YO
M50 75YO

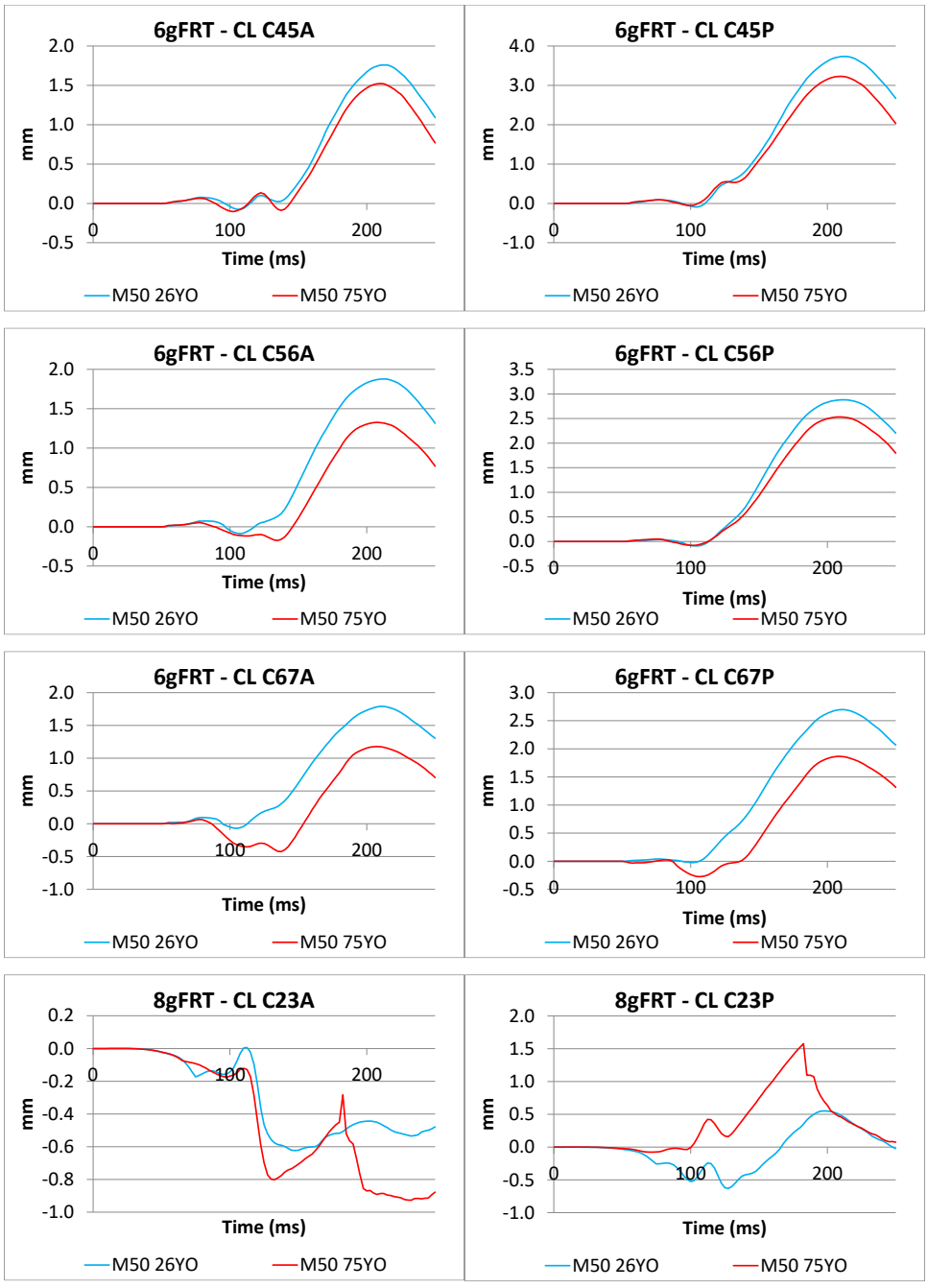
6gFRT - CL C45A
mm
Time (ms)
M50 26YO
M50 75YO
6gFRT - CL C45P
mm
Time (ms)
M50 26YO
M50 75YO
6gFRT - CL C56A
mm
Time (ms)
M50 26YO
M50 75YO
6gFRT - CL C56P
mm
Time (ms)
M50 26YO
M50 75YO
6gFRT - CL C67A
mm
Time (ms)
M50 26YO
M50 75YO
6gFRT - CL C67P
mm
Time (ms)
M50 26YO
M50 75YO
8gFRT - CL C23A
mm
Time (ms)
M50 26YO
M50 75YO
8gFRT - CL C23P
mm
Time (ms)
M50 26YO
M50 75YO

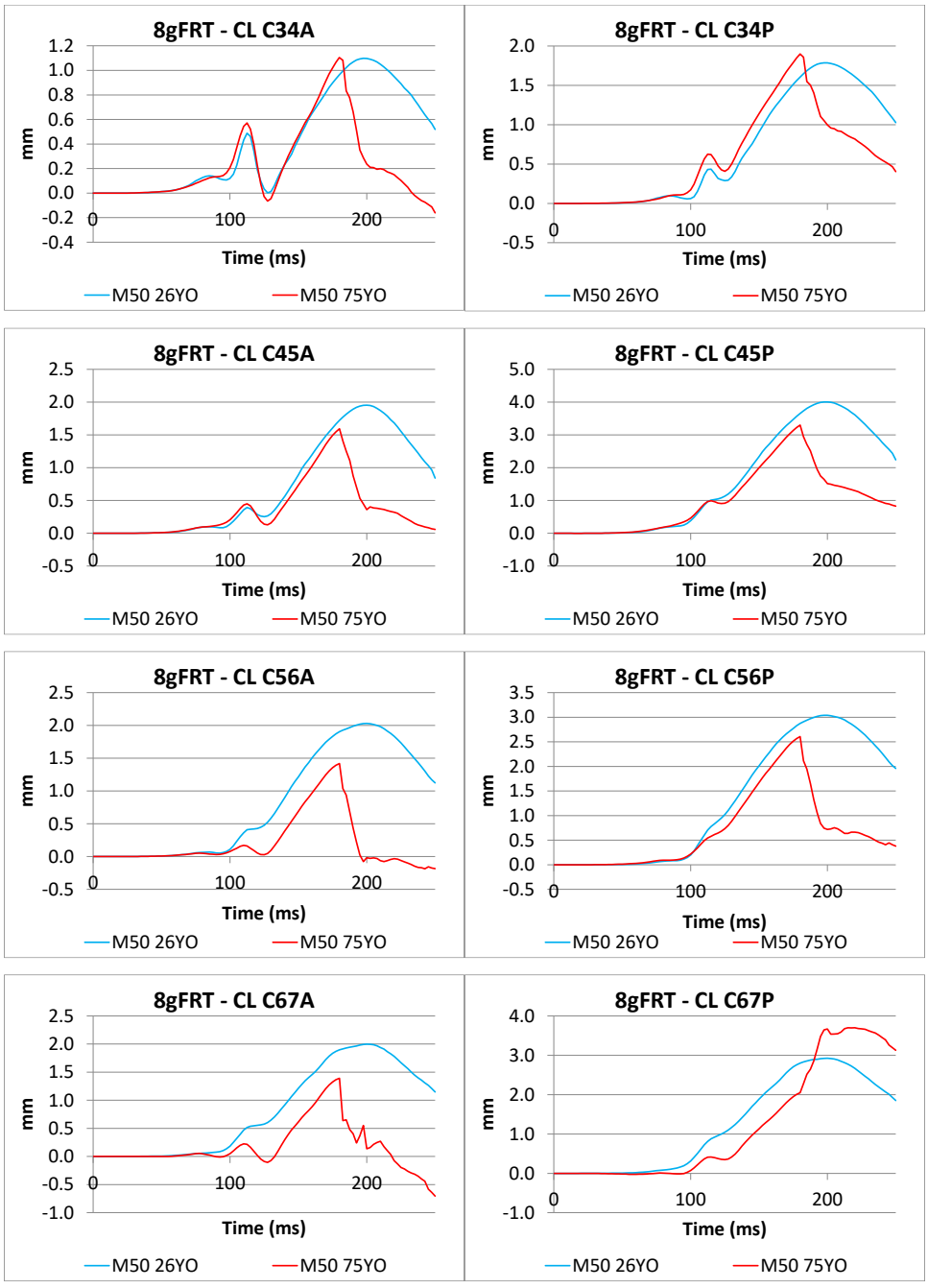
8gFRT - CL C34A
mm
Time (ms)
M50 26YO
M50 75YO
8gFRT - CL C34P
mm
Time (ms)
M50 26YO
M50 75YO
8gFRT - CL C45A
mm
Time (ms)
M50 26YO
M50 75YO
8gFRT - CL C45P
mm
Time (ms)
M50 26YO
M50 75YO
8gFRT - CL C56A
mm
Time (ms)
M50 26YO
M50 75YO
8gFRT - CL C56P
mm
Time (ms)
M50 26YO
M50 75YO
8gFRT - CL C67A
mm
Time (ms)
M50 26YO
M50 75YO
8gFRT - CL C67P
mm
Time (ms)
M50 26YO
M50 75YO

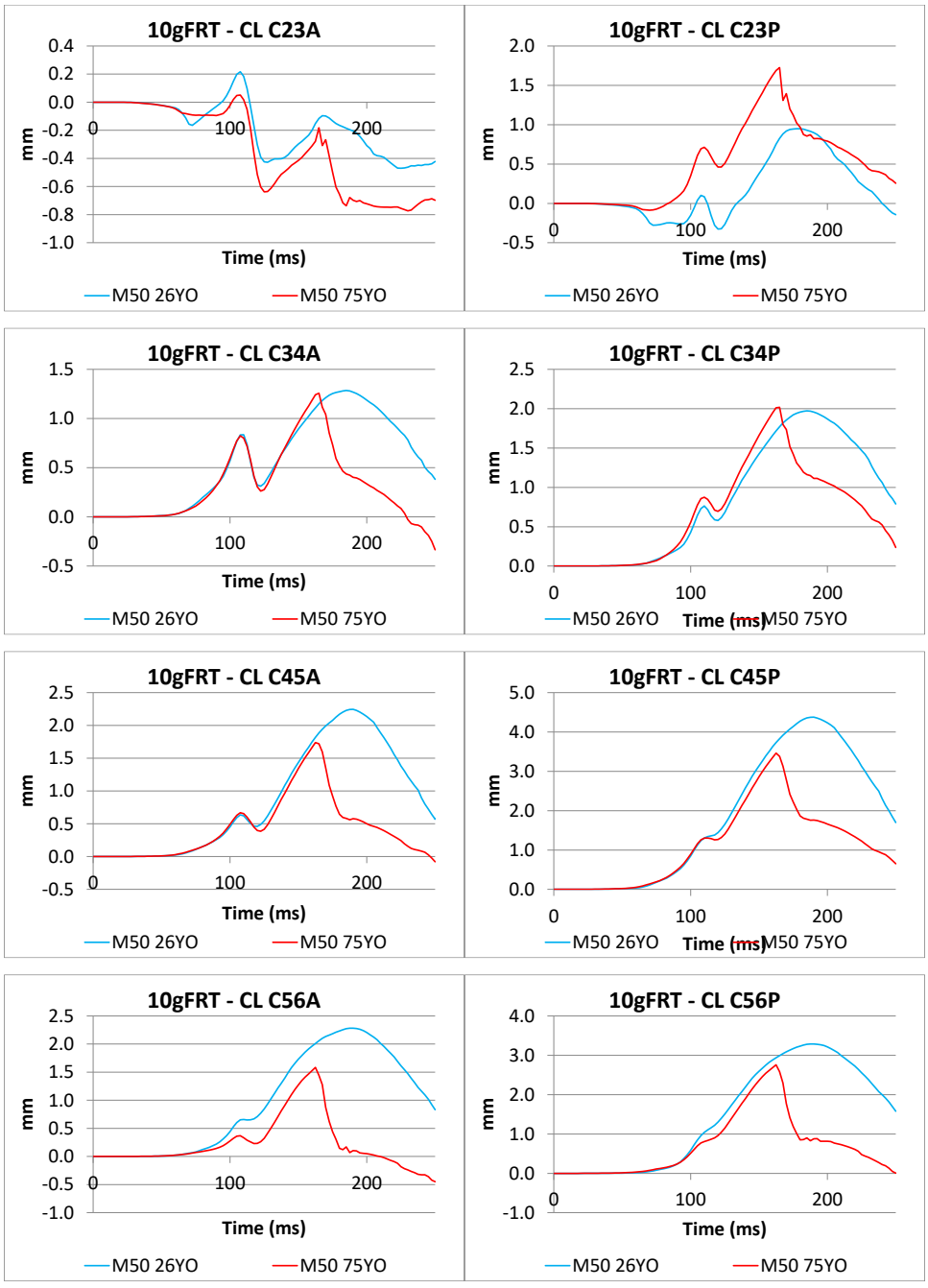
10gFRT - CL C23A
mm
Time (ms)
M50 26YO
M50 75YO
10gFRT - CL C23P
mm
Time (ms)
M50 26YO
M50 75YO
10gFRT - CL C34A
mm
Time (ms)
M50 26YO
M50 75YO
10gFRT - CL C34P
mm
Time (ms)
M50 26YO
M50 75YO
10gFRT - CL C45A
mm
Time (ms)
M50 26YO
M50 75YO
10gFRT - CL C45P
mm
Time (ms)
M50 26YO
M50 75YO
10gFRT - CL C56A
mm
Time (ms)
M50 26YO
M50 75YO
10gFRT - CL C56P
mm
Time (ms)
M50 26YO
M50 75YO

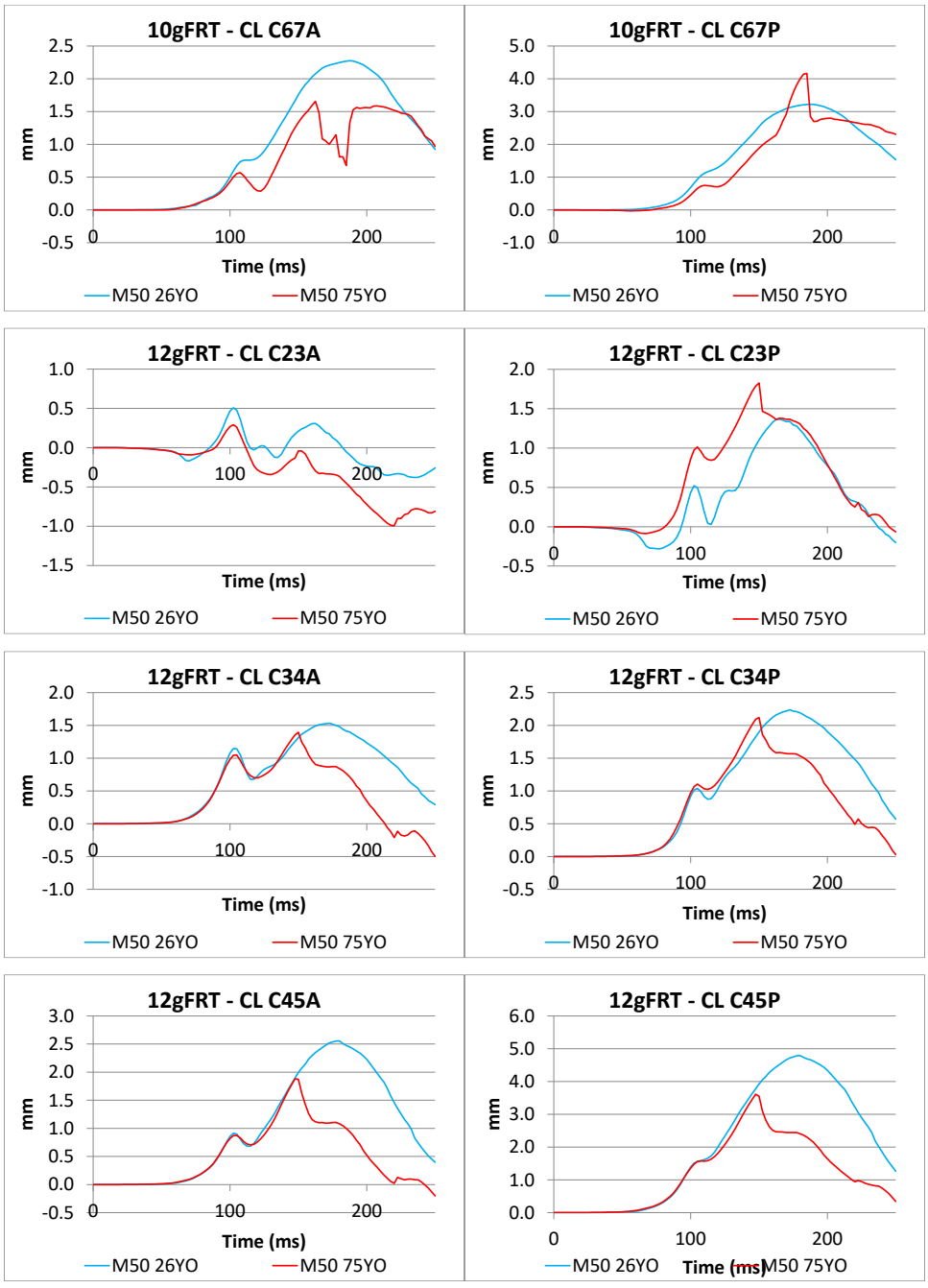
10gFRT - CL C67A
mm
Time (ms)
M50 26YO
M50 75YO
10gFRT - CL C67P
mm
Time (ms)
M50 26YO
M50 75YO
12gFRT - CL C23A
mm
Time (ms)
M50 26YO
M50 75YO
12gFRT - CL C23P
mm
Time (ms)
M50 26YO
M50 75YO
12gFRT - CL C34A
mm
Time (ms)
M50 26YO
M50 75YO
12gFRT - CL C34P
mm
Time (ms)
M50 26YO
M50 75YO
12gFRT - CL C45A
mm
Time (ms)
M50 26YO
M50 75YO
12gFRT - CL C45P
mm
Time (ms)
M50 26YO
M50 75YO

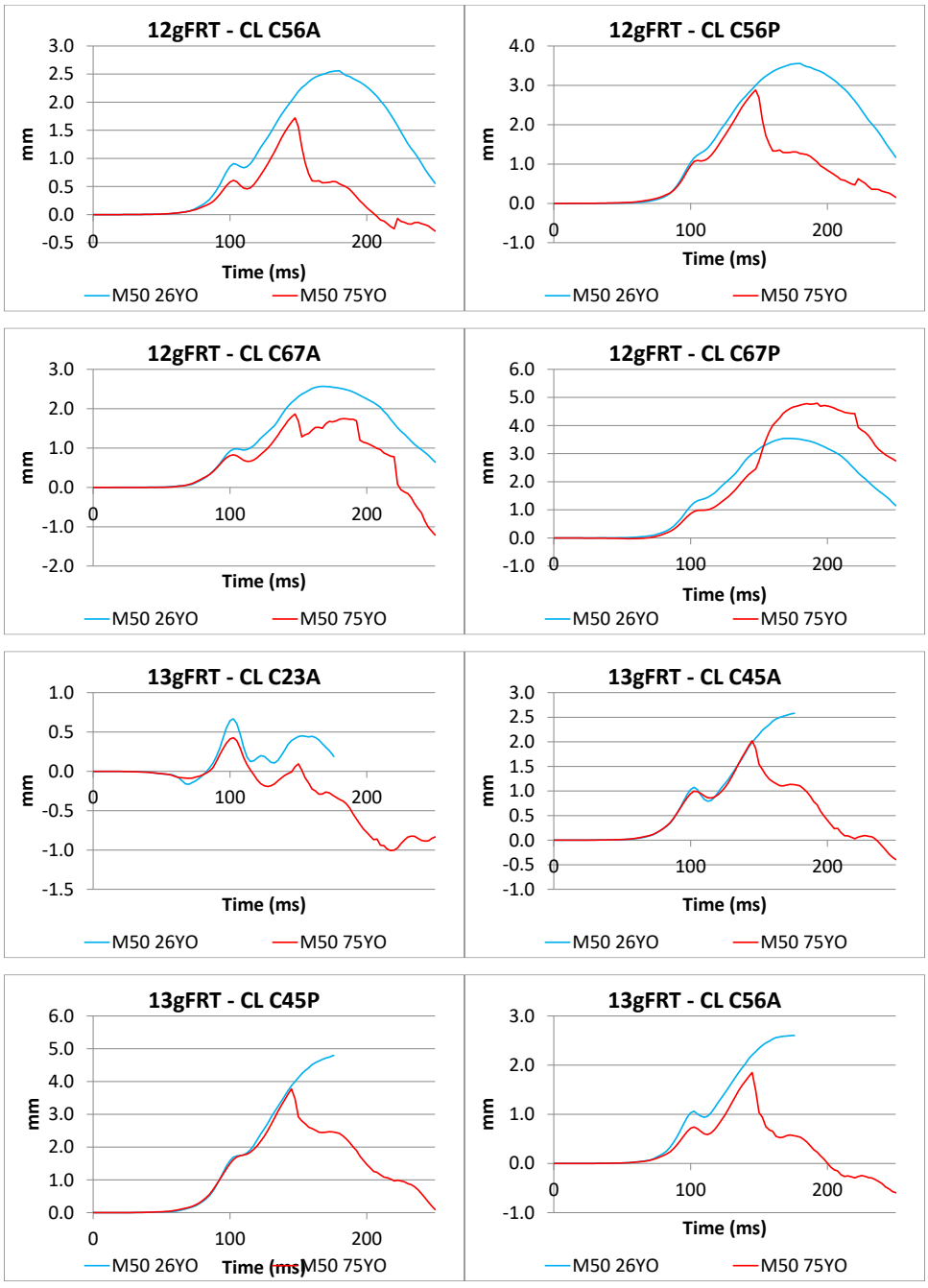
12gFRT - CL C56A
mm
Time (ms)
M50 26YO
M50 75YO
12gFRT - CL C56P
mm
Time (ms)
M50 26YO
M50 75YO
12gFRT - CL C67A
mm
Time (ms)
M50 26YO
M50 75YO
12gFRT - CL C67P
mm
Time (ms)
M50 26YO
M50 75YO
13gFRT - CL C23A
mm
Time (ms)
M50 26YO
M50 75YO
13gFRT - CL C45A
mm
Time (ms)
M50 26YO
M50 75YO
13gFRT - CL C45P
mm
Time (ms)
M50 26YO
M50 75YO
13gFRT - CL C56A
mm
Time (ms)
M50 26YO
M50 75YO

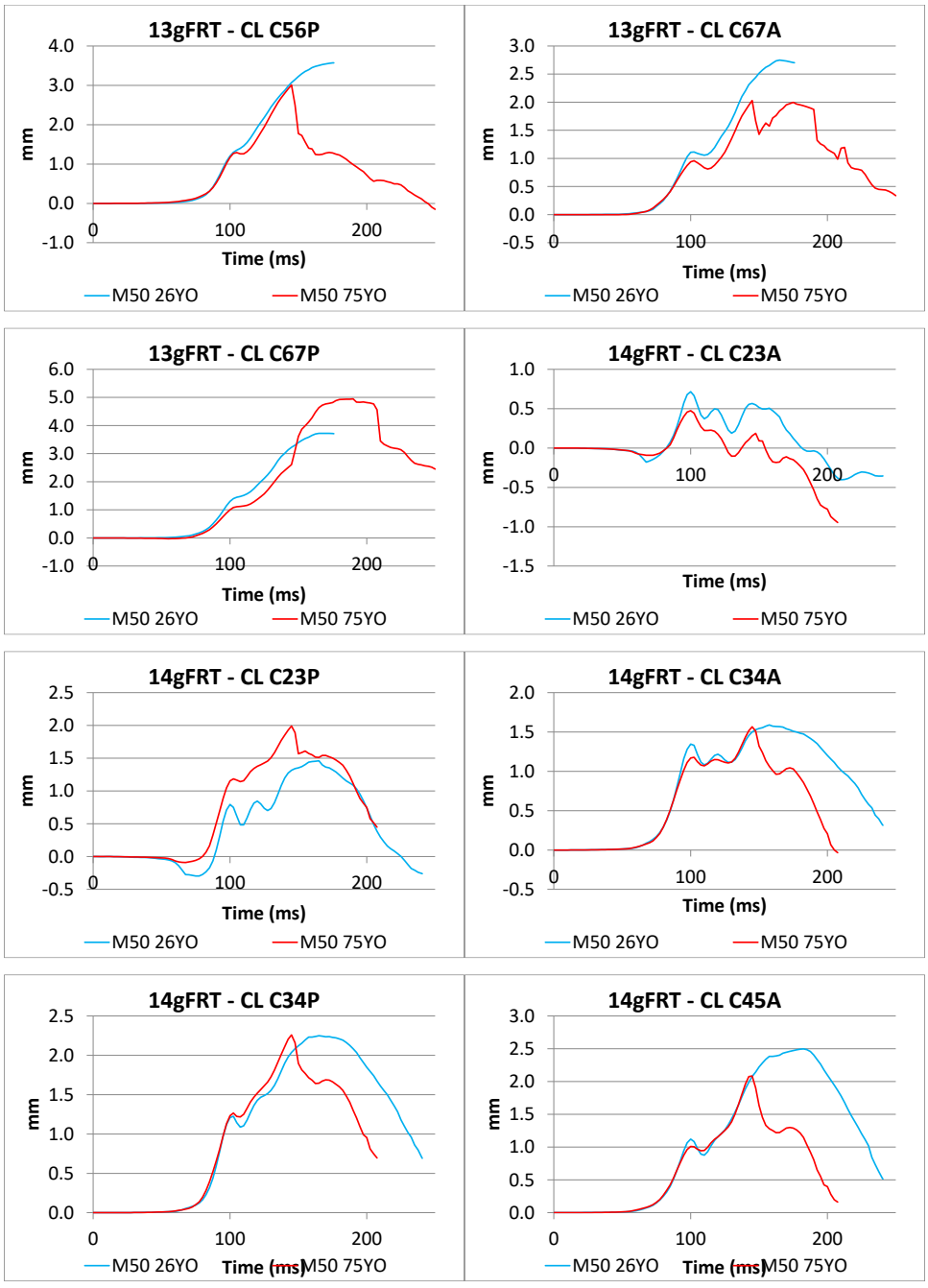
13gFRT - CL C56P
mm
Time (ms)
M50 26YO
M50 75YO
13gFRT - CL C67A
mm
Time (ms)
M50 26YO
M50 75YO
13gFRT - CL C67P
mm
Time (ms)
M50 26YO
M50 75YO
14gFRT - CL C23A
mm
Time (ms)
M50 26YO
M50 75YO
14gFRT - CL C23P
mm
Time (ms)
M50 26YO
M50 75YO
14gFRT - CL C34A
mm
Time (ms)
M50 26YO
M50 75YO
14gFRT - CL C34P
mm
Time (ms)
M50 26YO
M50 75YO
14gFRT - CL C45A
mm
Time (ms)
M50 26YO
M50 75YO

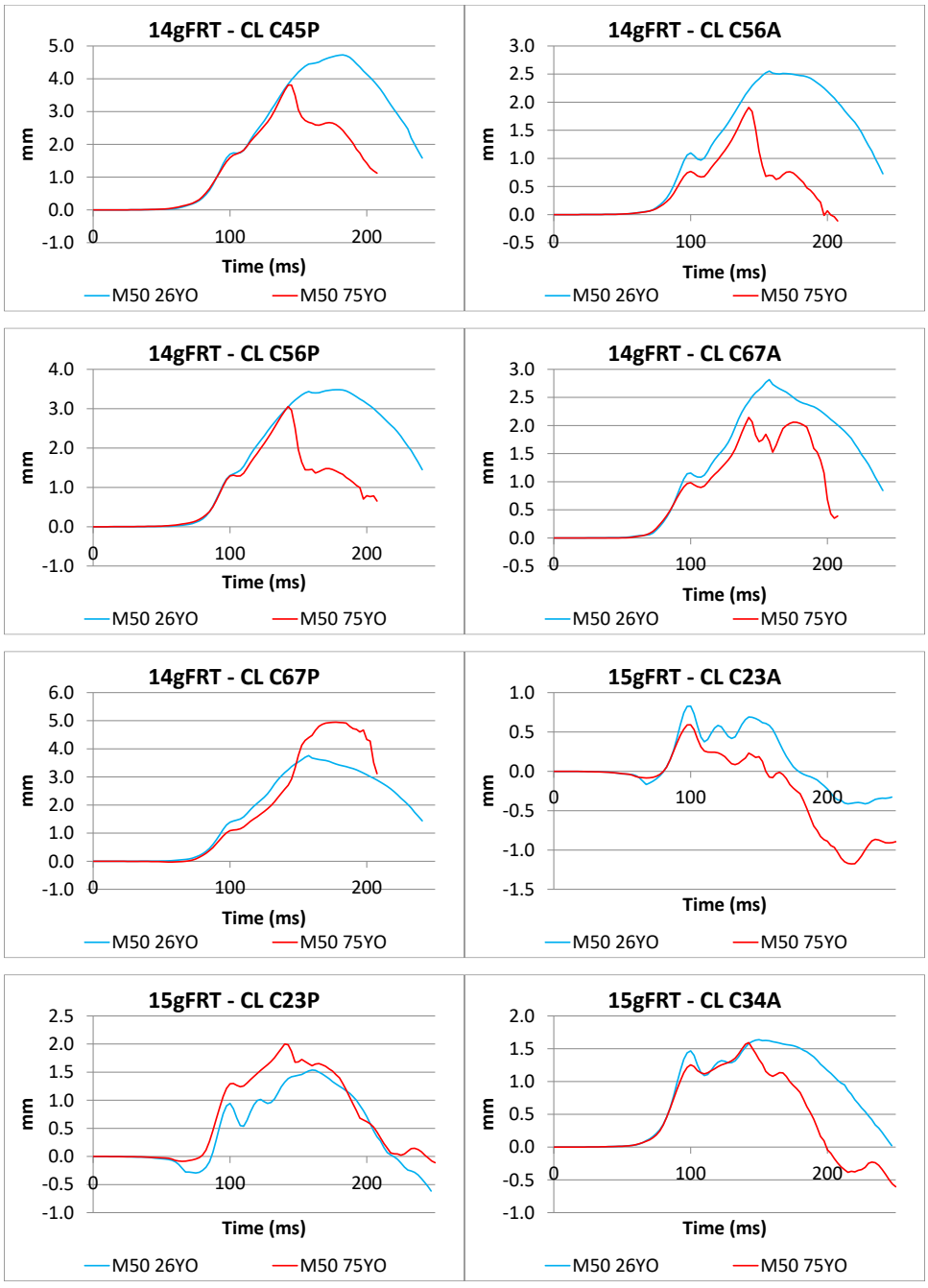
14gFRT - CL C45P
mm
Time (ms)
M50 26YO
M50 75YO
14gFRT - CL C56A
mm
Time (ms)
M50 26YO
M50 75YO
14gFRT - CL C56P
mm
Time (ms)
M50 26YO
M50 75YO
14gFRT - CL C67A
mm
Time (ms)
M50 26YO
M50 75YO
14gFRT - CL C67P
mm
Time (ms)
M50 26YO
M50 75YO
15gFRT - CL C23A
mm
Time (ms)
M50 26YO
M50 75YO
15gFRT - CL C23P
mm
Time (ms)
M50 26YO
M50 75YO
15gFRT - CL C34A
mm
Time (ms)
M50 26YO
M50 75YO

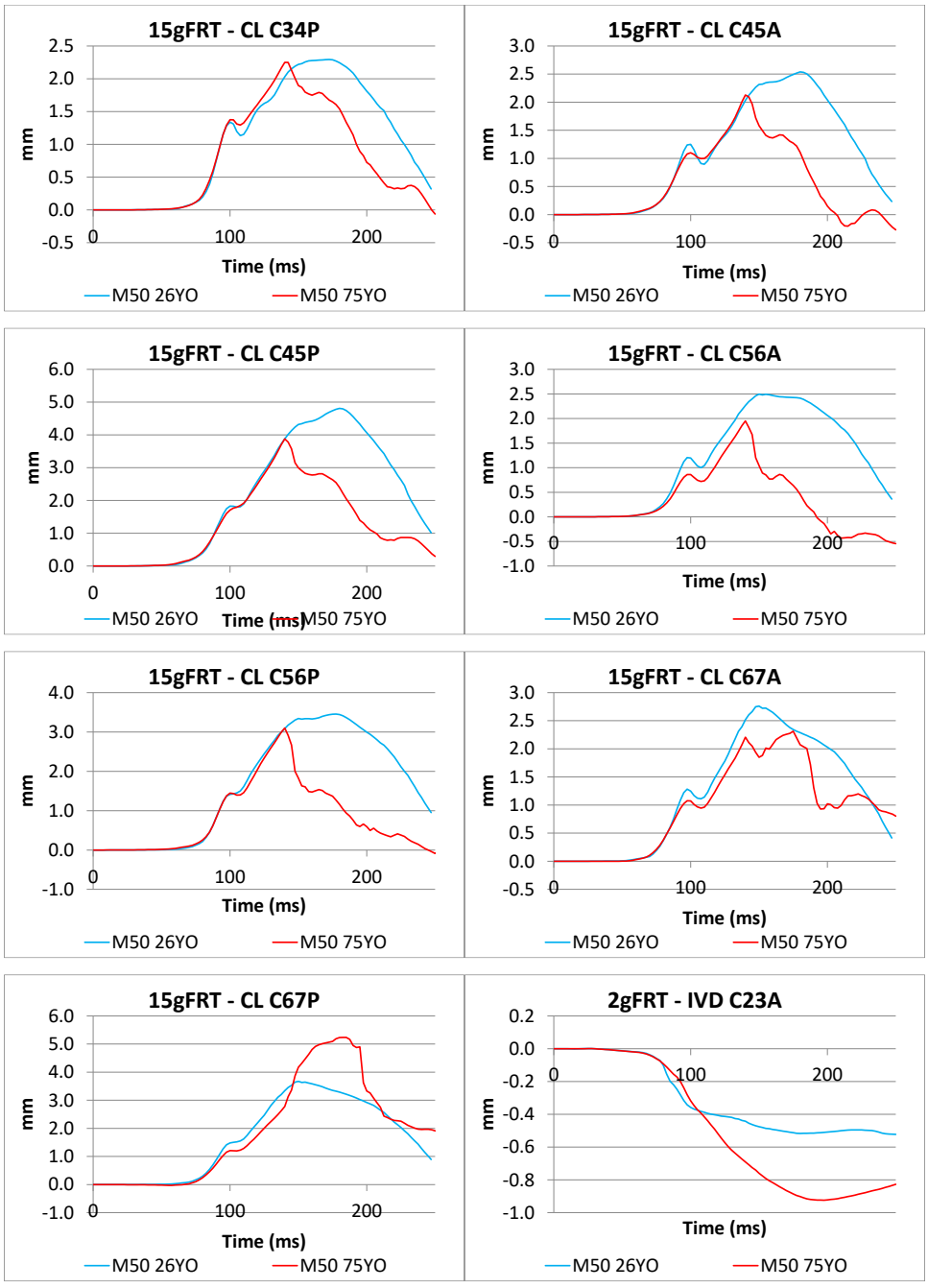
15gFRT - CL C34P
mm
Time (ms)
M50 26YO
M50 75YO
15gFRT - CL C45A
mm
Time (ms)
M50 26YO
M50 75YO
15gFRT - CL C45P
mm
Time (ms)
M50 26YO
M50 75YO
15gFRT - CL C56A
mm
Time (ms)
M50 26YO
M50 75YO
15gFRT - CL C56P
mm
Time (ms)
M50 26YO
M50 75YO
15gFRT - CL C67A
mm
Time (ms)
M50 26YO
M50 75YO
15gFRT - CL C67P
mm
Time (ms)
M50 26YO
M50 75YO
2gFRT - IVD C23A
mm
Time (ms)
M50 26YO
M50 75YO

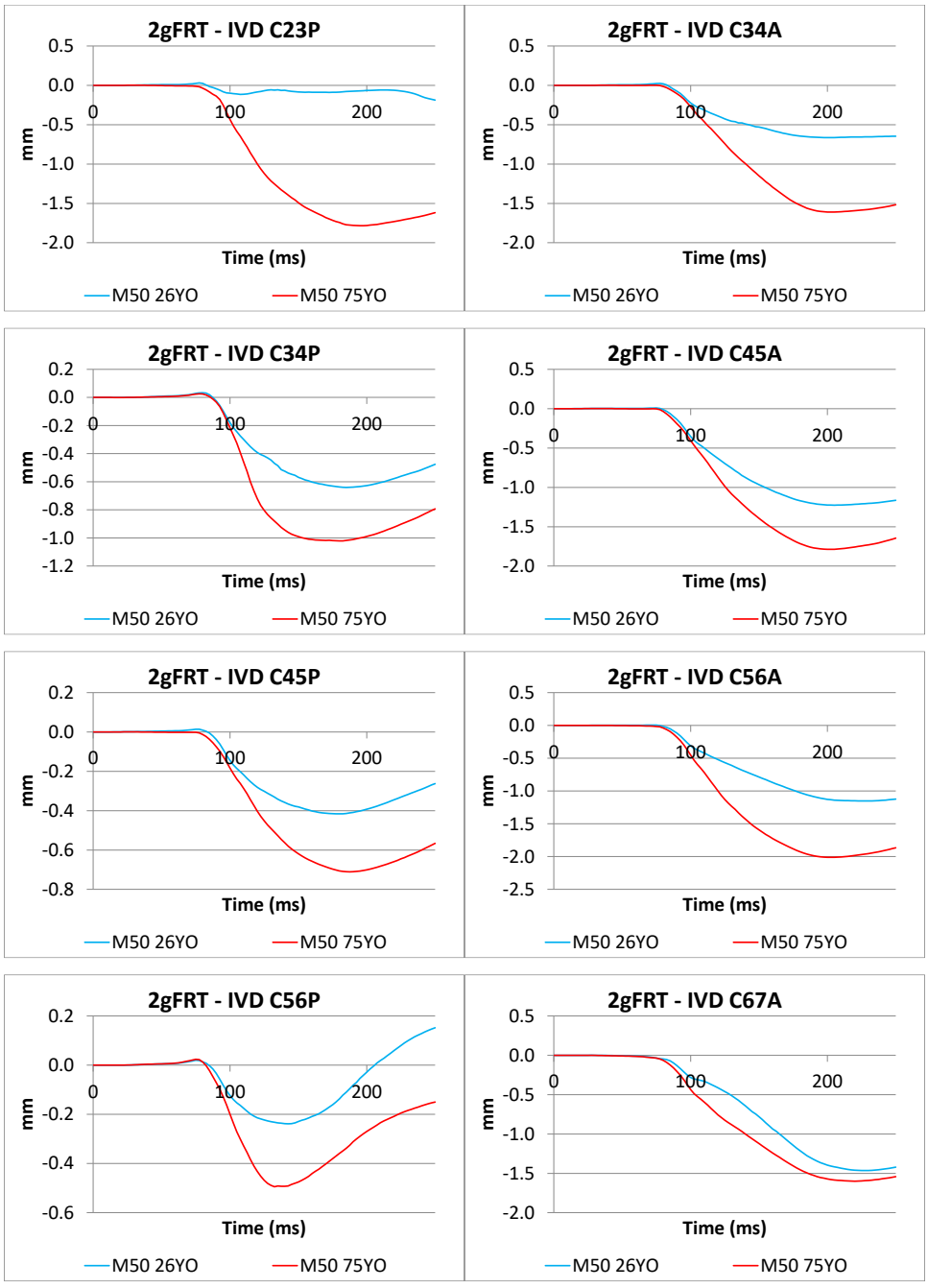
2gFRT - IVD C23P
0.5
0.0
-0.5
-1.0
-1.5
-2.0
mm
0
100
200
Time (ms)
M50 26YO
M50 75YO
2gFRT - IVD C34A
0.5
0.0
-0.5
-1.0
-1.5
-2.0
mm
0
100
200
Time (ms)
M50 26YO
M50 75YO
2gFRT - IVD C34P
0.2
0.0
-0.2
-0.4
-0.6
-0.8
-1.0
-1.2
mm
0
100
200
Time (ms)
M50 26YO
M50 75YO
2gFRT - IVD C45A
0.5
0.0
-0.5
-1.0
-1.5
-2.0
mm
0
100
200
Time (ms)
M50 26YO
M50 75YO
2gFRT - IVD C45P
0.2
0.0
-0.2
-0.4
-0.6
-0.8
mm
0
100
200
Time (ms)
M50 26YO
M50 75YO
2gFRT - IVD C56A
0.5
0.0
-0.5
-1.0
-1.5
-2.0
-2.5
mm
0
100
200
Time (ms)
M50 26YO
M50 75YO
2gFRT - IVD C56P
0.2
0.0
-0.2
-0.4
-0.6
mm
0
100
200
Time (ms)
M50 26YO
M50 75YO
2gFRT - IVD C67A
0.5
0.0
-0.5
-1.0
-1.5
-2.0
mm
0
100
200
Time (ms)
M50 26YO
M50 75YO

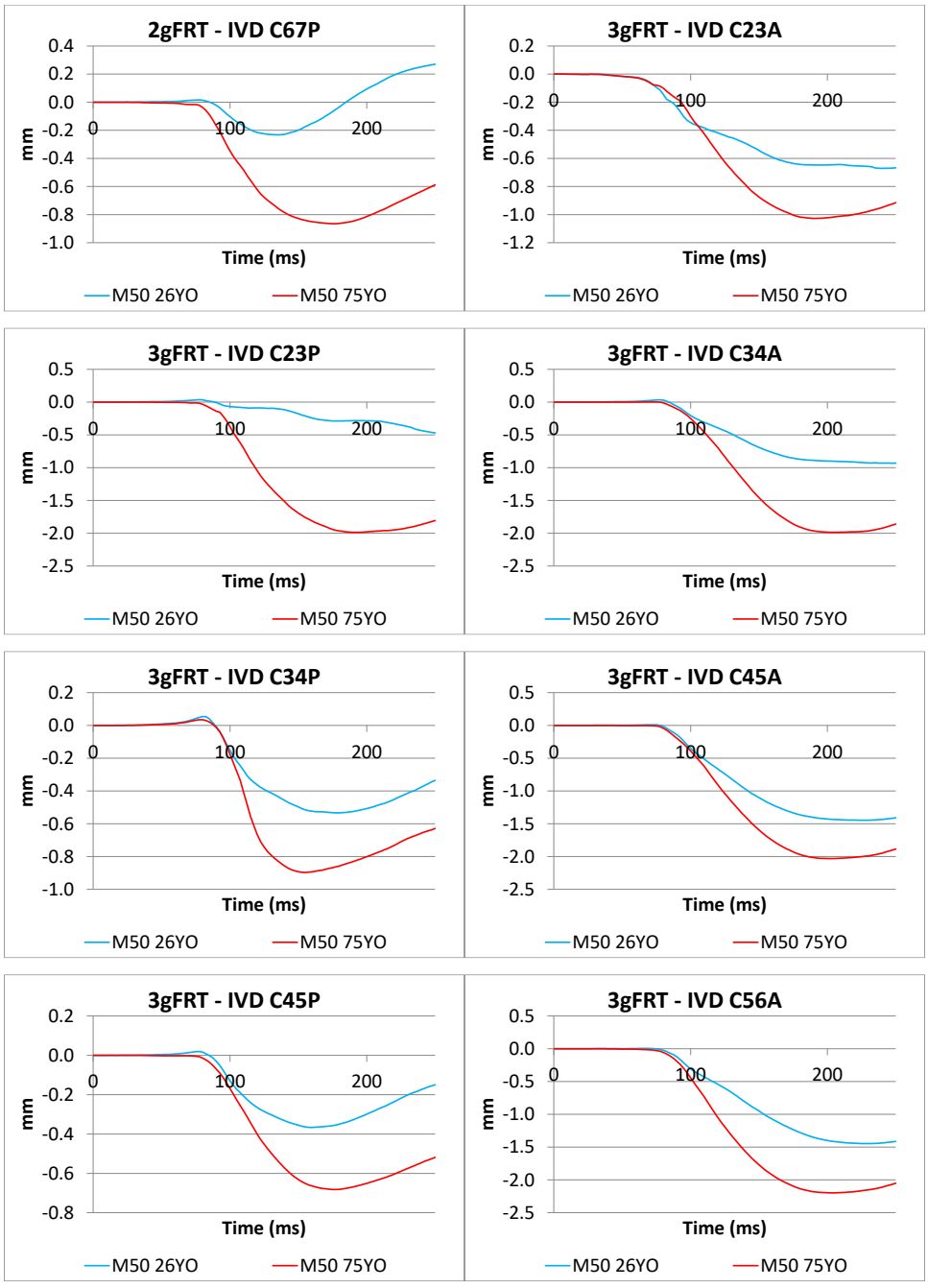
2gFRT - IVD C67P
3gFRT - IVD C23A
3gFRT - IVD C23P
3gFRT - IVD C34A
3gFRT - IVD C34P
3gFRT - IVD C45A
3gFRT - IVD C45P
3gFRT - IVD C56A
mm
Time (ms)
M50 26YO
M50 75YO

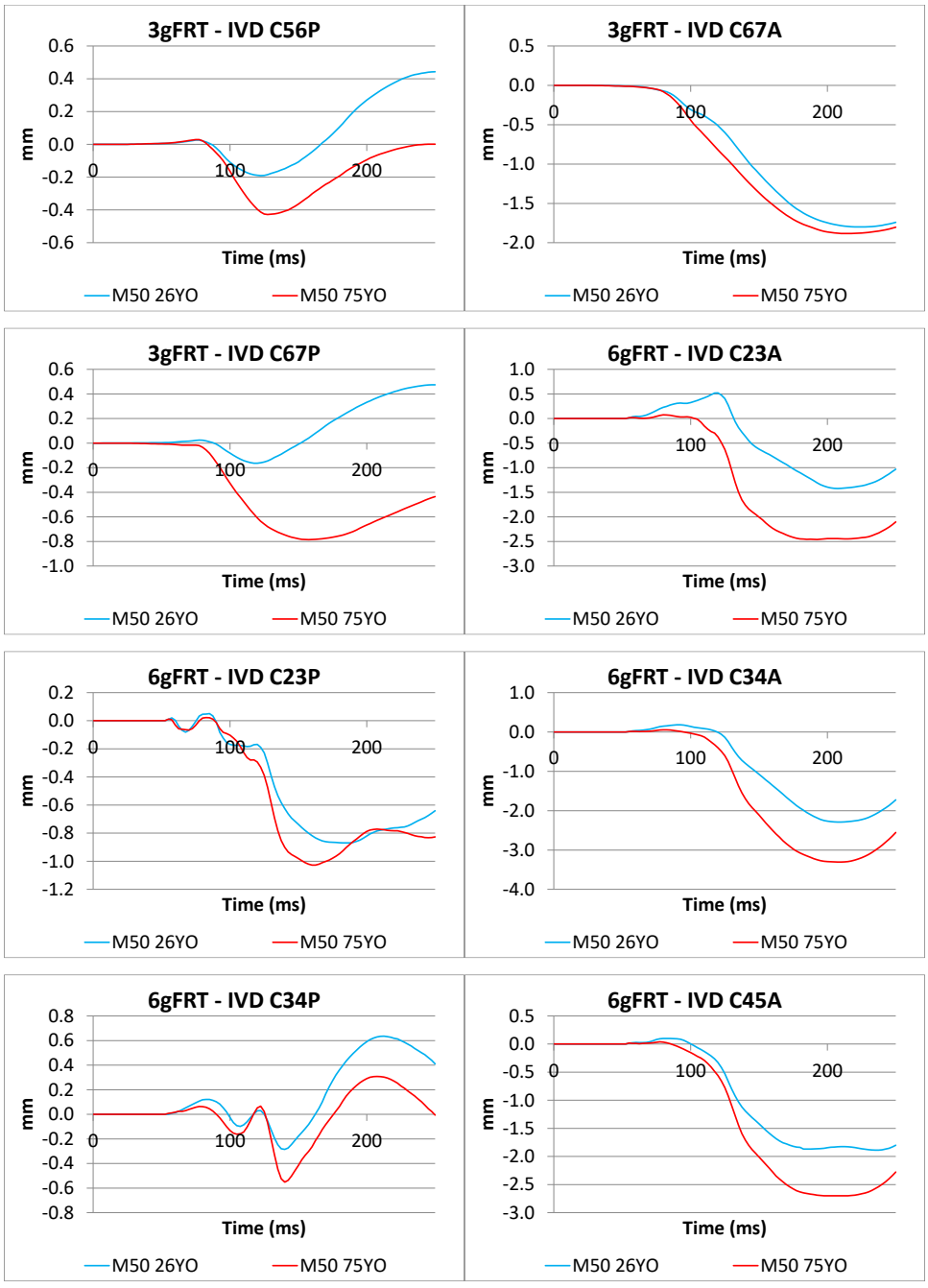
3gFRT - IVD C56P
mm
Time (ms)
M50 26YO
M50 75YO
3gFRT - IVD C67A
mm
Time (ms)
M50 26YO
M50 75YO
3gFRT - IVD C67P
mm
Time (ms)
M50 26YO
M50 75YO
6gFRT - IVD C23A
mm
Time (ms)
M50 26YO
M50 75YO
6gFRT - IVD C23P
mm
Time (ms)
M50 26YO
M50 75YO
6gFRT - IVD C34A
mm
Time (ms)
M50 26YO
M50 75YO
6gFRT - IVD C34P
mm
Time (ms)
M50 26YO
M50 75YO
6gFRT - IVD C45A
mm
Time (ms)
M50 26YO
M50 75YO

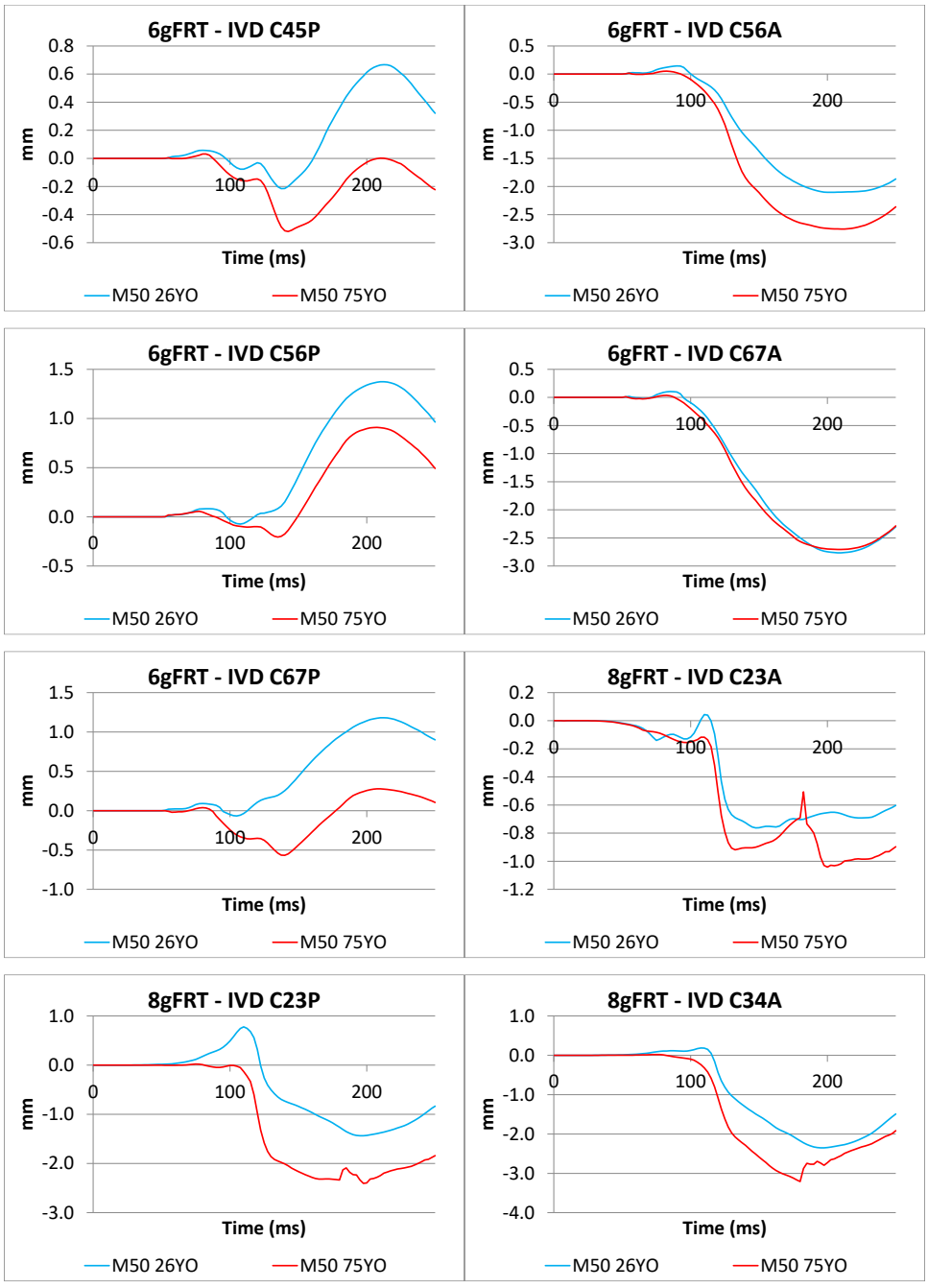
6gFRT - IVD C45P
mm
Time (ms)
M50 26YO
M50 75YO
6gFRT - IVD C56A
mm
Time (ms)
M50 26YO
M50 75YO
6gFRT - IVD C56P
mm
Time (ms)
M50 26YO
M50 75YO
6gFRT - IVD C67A
mm
Time (ms)
M50 26YO
M50 75YO
6gFRT - IVD C67P
mm
Time (ms)
M50 26YO
M50 75YO
8gFRT - IVD C23A
mm
Time (ms)
M50 26YO
M50 75YO
8gFRT - IVD C23P
mm
Time (ms)
M50 26YO
M50 75YO
8gFRT - IVD C34A
mm
Time (ms)
M50 26YO
M50 75YO

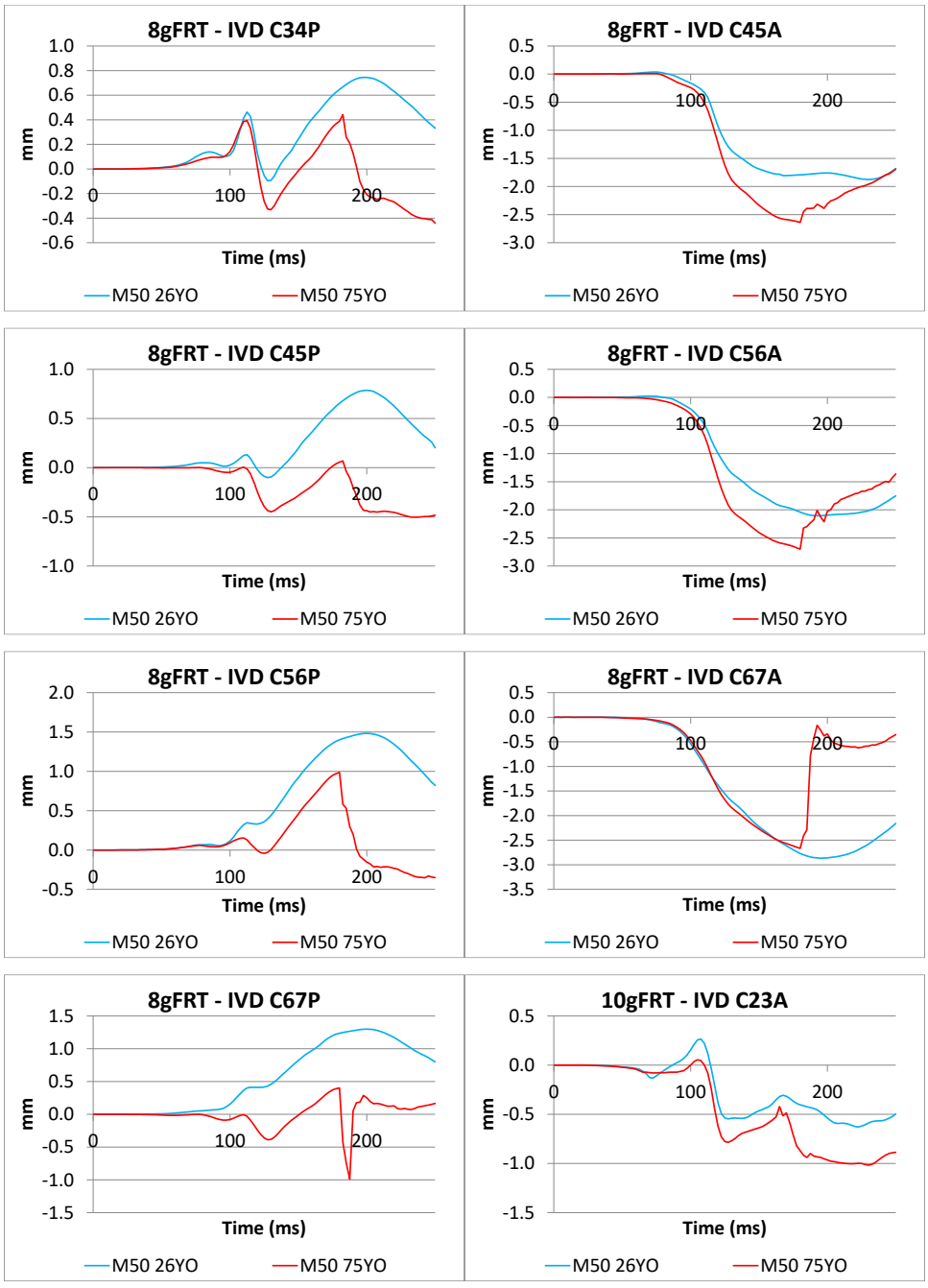
8gFRT - IVD C34P
mm
Time (ms)
M50 26YO
M50 75YO
8gFRT - IVD C45A
mm
Time (ms)
M50 26YO
M50 75YO
8gFRT - IVD C45P
mm
Time (ms)
M50 26YO
M50 75YO
8gFRT - IVD C56A
mm
Time (ms)
M50 26YO
M50 75YO
8gFRT - IVD C56P
mm
Time (ms)
M50 26YO
M50 75YO
8gFRT - IVD C67A
mm
Time (ms)
M50 26YO
M50 75YO
8gFRT - IVD C67P
mm
Time (ms)
M50 26YO
M50 75YO
10gFRT - IVD C23A
mm
Time (ms)
M50 26YO
M50 75YO

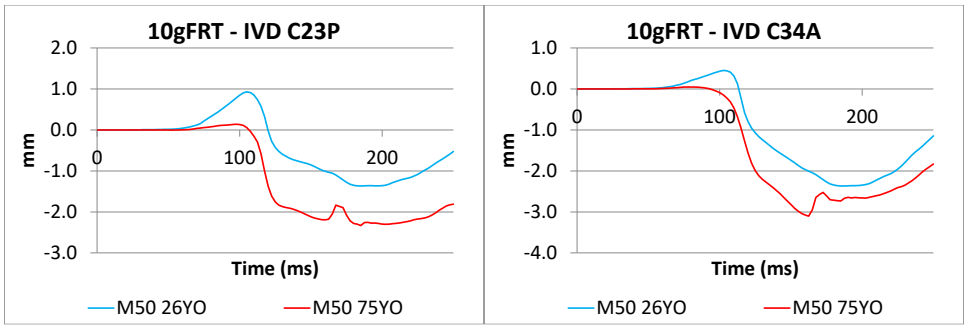
10gFRT - IVD C23P
mm
Time (ms)
M50 26YO
M50 75YO

10gFRT - IVD C34A
mm
Time (ms)
M50 26YO
M50 75YO

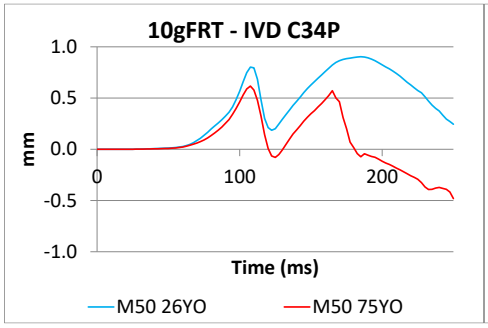
10gFRT - IVD C34P
mm
Time (ms)
M50 26YO
M50 75YO

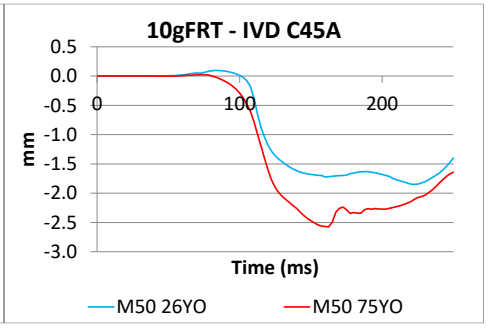
10gFRT - IVD C45A
mm
Time (ms)
M50 26YO
M50 75YO

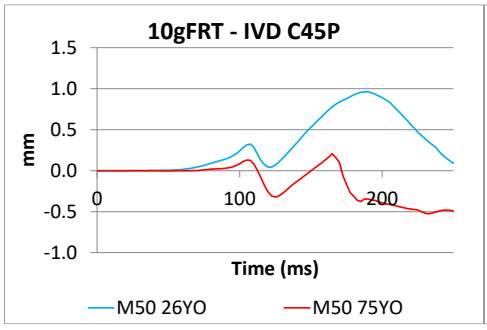
10gFRT - IVD C45P
mm
Time (ms)
M50 26YO
M50 75YO

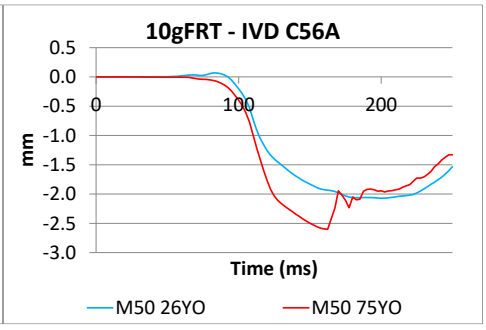
10gFRT - IVD C56A
mm
Time (ms)
M50 26YO
M50 75YO

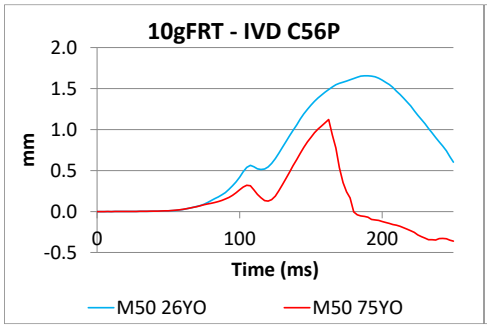
10gFRT - IVD C56P
mm
Time (ms)
M50 26YO
M50 75YO

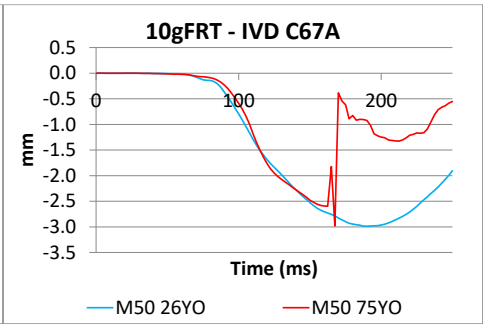
10gFRT - IVD C67A
mm
Time (ms)
M50 26YO
M50 75YO

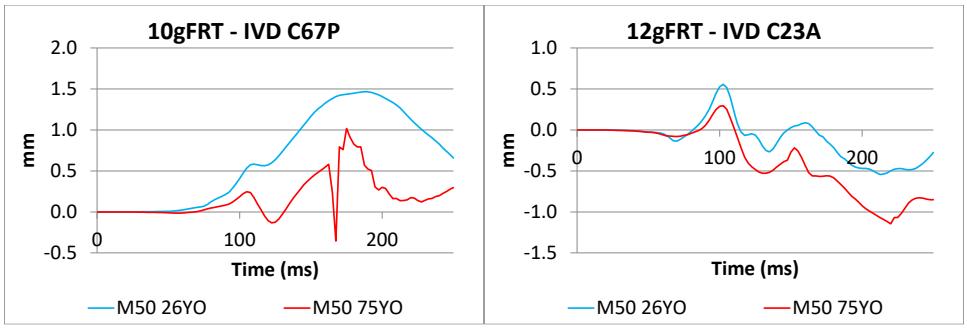
10gFRT - IVD C67P
mm
Time (ms)
M50 26YO
M50 75YO

12gFRT - IVD C23A
mm
Time (ms)
M50 26YO
M50 75YO

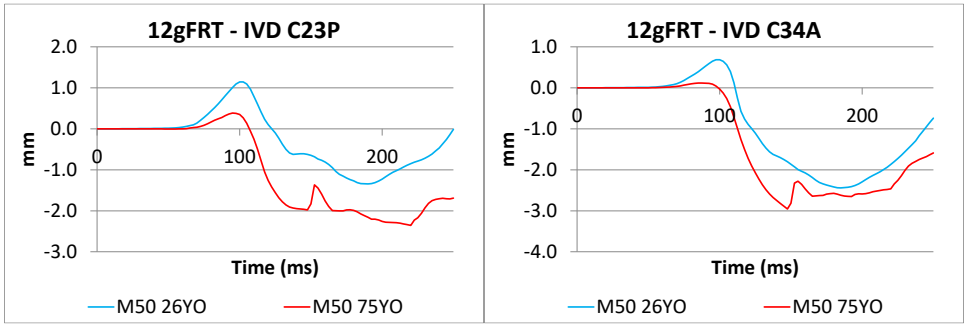
12gFRT - IVD C23P
mm
Time (ms)
M50 26YO
M50 75YO

12gFRT - IVD C34A
mm
Time (ms)
M50 26YO
M50 75YO

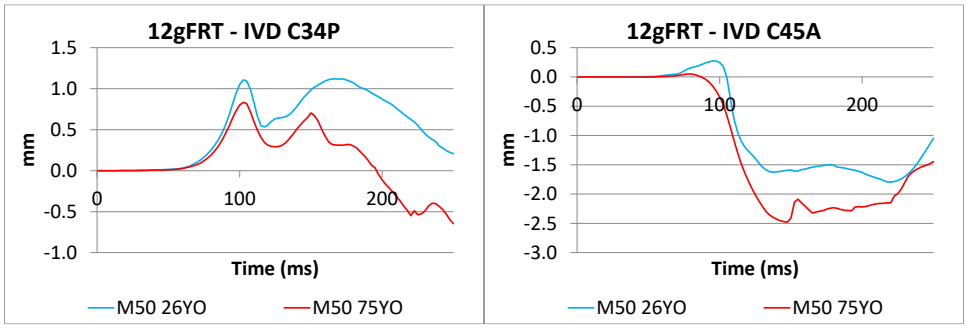
12gFRT - IVD C34P
mm
Time (ms)
M50 26YO
M50 75YO

12gFRT - IVD C45A
mm
Time (ms)
M50 26YO
M50 75YO

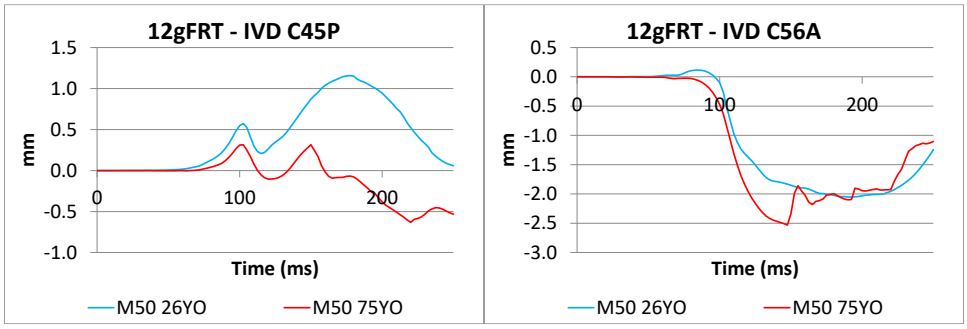
12gFRT - IVD C45P
mm
Time (ms)
M50 26YO
M50 75YO

12gFRT - IVD C56A
mm
Time (ms)
M50 26YO
M50 75YO

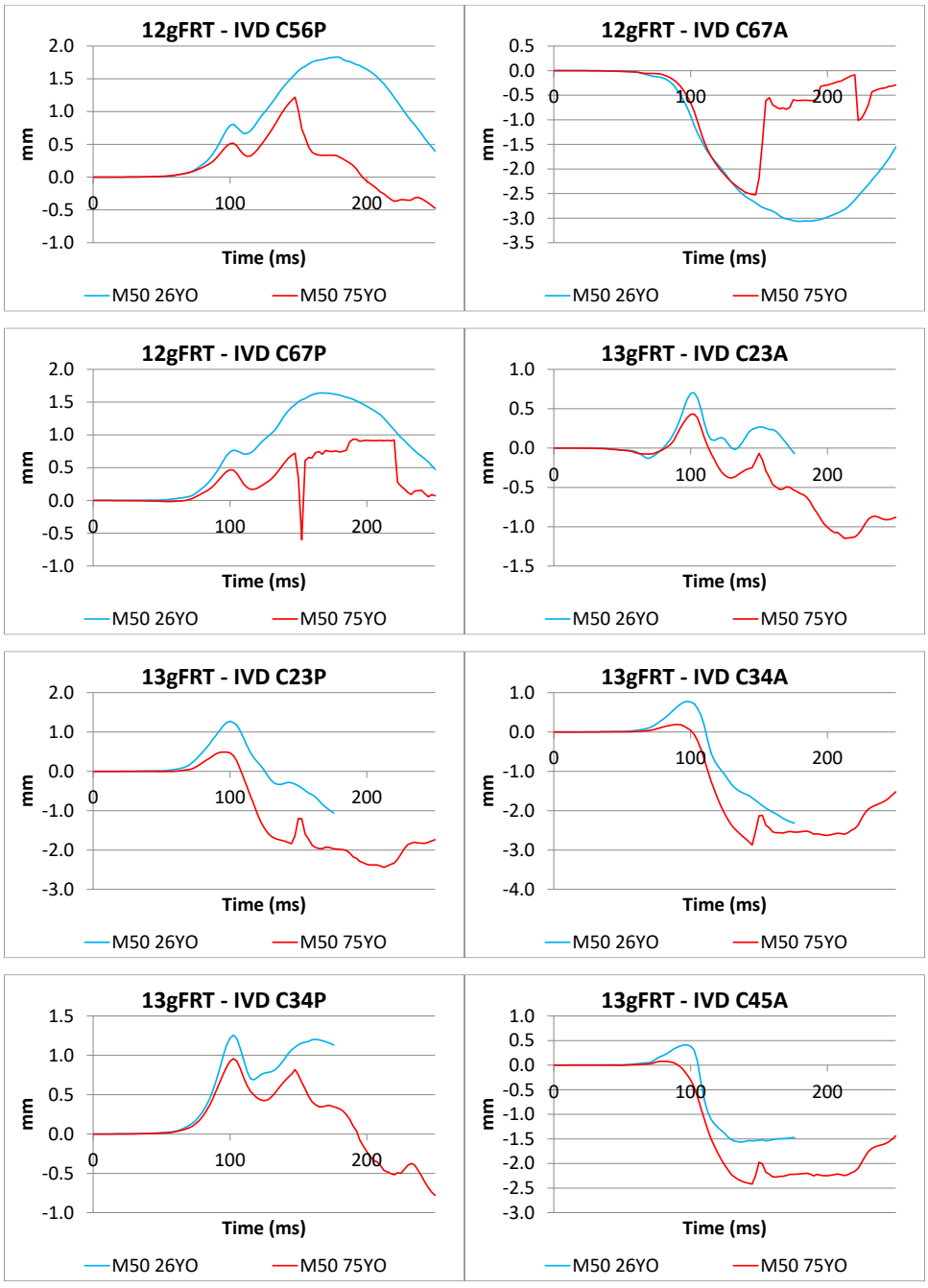
12gFRT - IVD C56P
12gFRT - IVD C67A
12gFRT - IVD C67P
13gFRT - IVD C23A
13gFRT - IVD C23P
13gFRT - IVD C34A
13gFRT - IVD C34P
13gFRT - IVD C45A
mm
Time (ms)
M50 26YO
M50 75YO

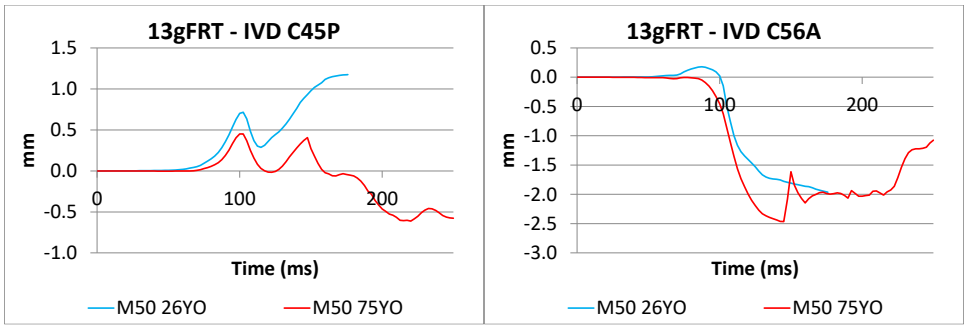
13gFRT - IVD C45P
mm
Time (ms)
M50 26YO
M50 75YO

13gFRT - IVD C56A
mm
Time (ms)
M50 26YO
M50 75YO

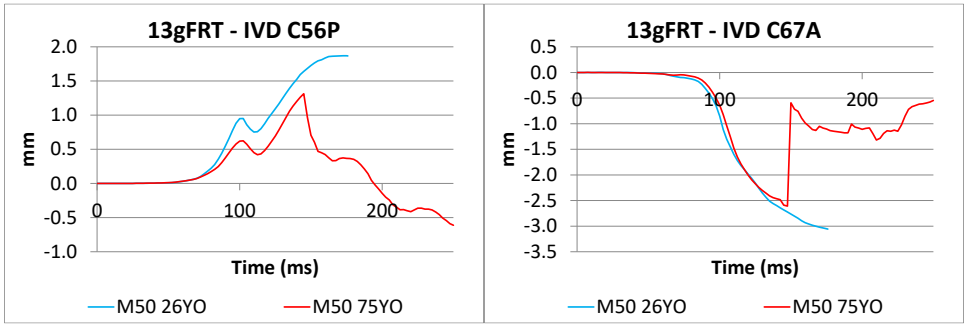
13gFRT - IVD C56P
mm
Time (ms)
M50 26YO
M50 75YO

13gFRT - IVD C67A
mm
Time (ms)
M50 26YO
M50 75YO

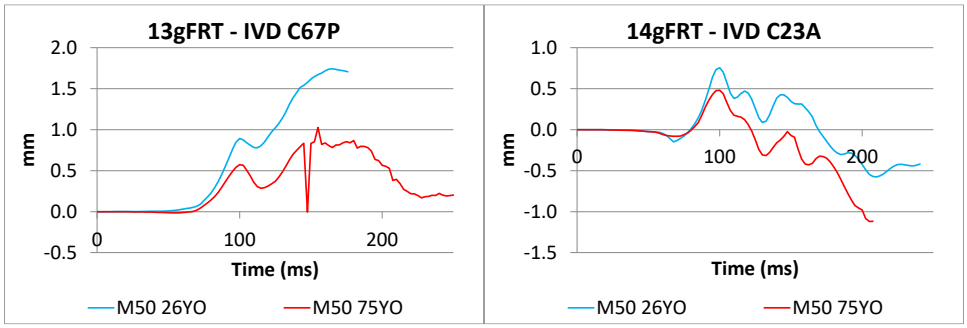
13gFRT - IVD C67P
mm
Time (ms)
M50 26YO
M50 75YO

14gFRT - IVD C23A
mm
Time (ms)
M50 26YO
M50 75YO

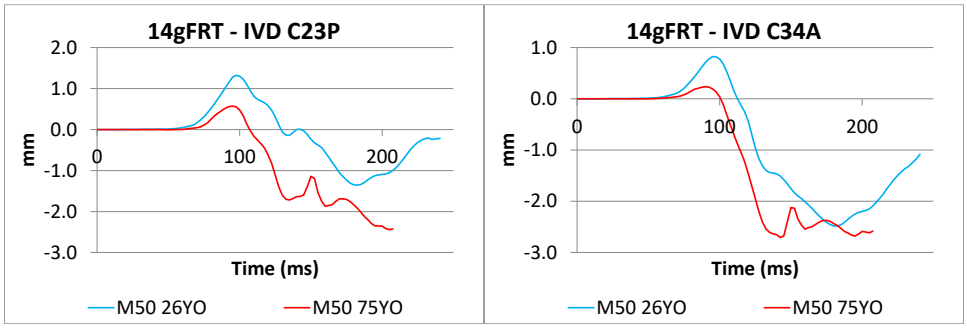
14gFRT - IVD C23P
mm
Time (ms)
M50 26YO
M50 75YO

14gFRT - IVD C34A
mm
Time (ms)
M50 26YO
M50 75YO

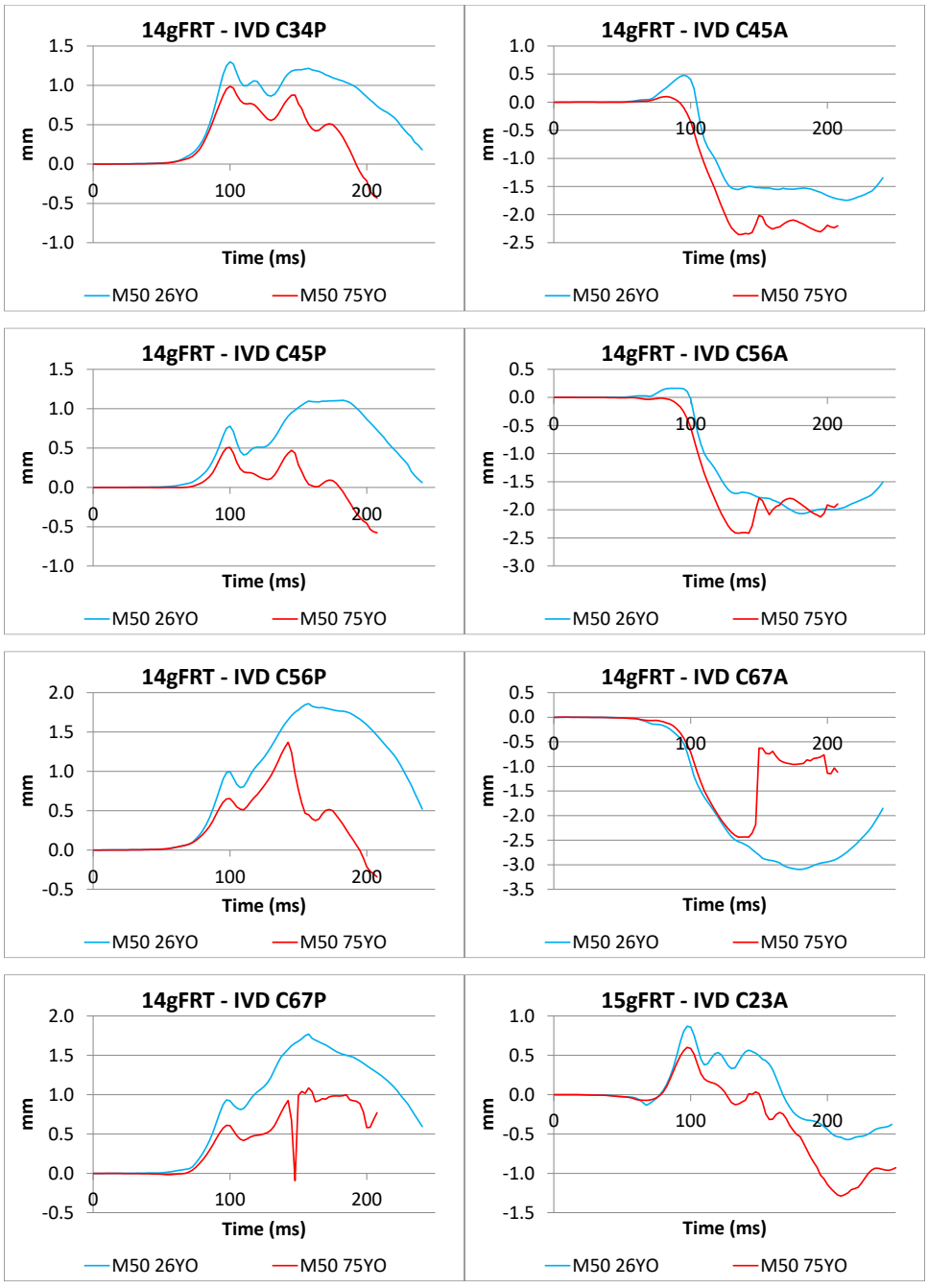
14gFRT - IVD C34P
14gFRT - IVD C45A
14gFRT - IVD C45P
14gFRT - IVD C56A
14gFRT - IVD C56P
14gFRT - IVD C67A
14gFRT - IVD C67P
15gFRT - IVD C23A
mm
Time (ms)
M50 26YO
M50 75YO

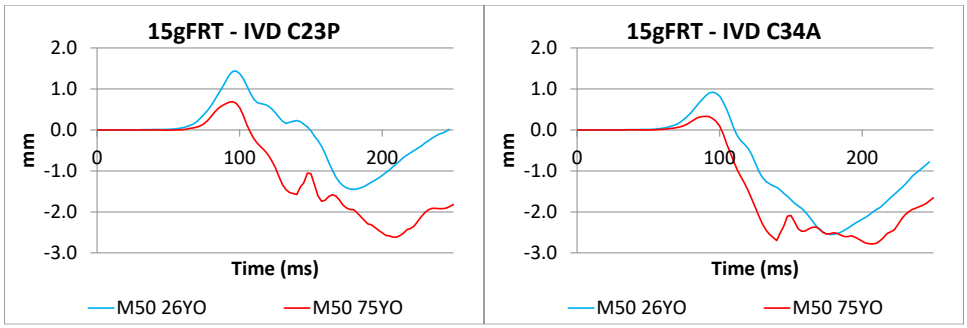
15gFRT - IVD C23P
mm
Time (ms)
M50 26YO
M50 75YO

15gFRT - IVD C34A
mm
Time (ms)
M50 26YO
M50 75YO

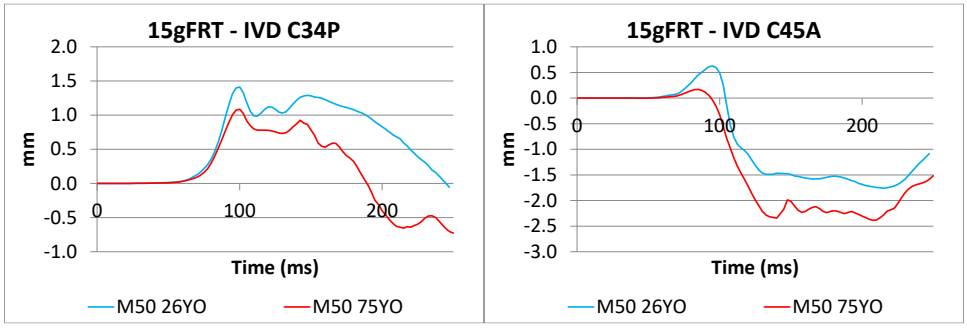
15gFRT - IVD C34P
mm
Time (ms)
M50 26YO
M50 75YO

15gFRT - IVD C45A
mm
Time (ms)
M50 26YO
M50 75YO

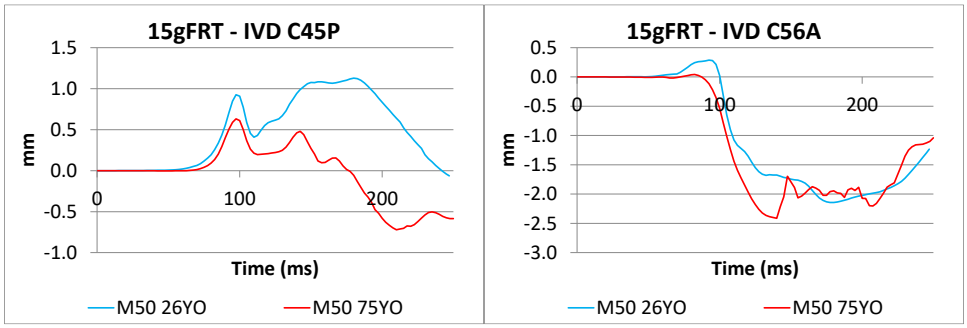
15gFRT - IVD C45P
mm
Time (ms)
M50 26YO
M50 75YO

15gFRT - IVD C56A
mm
Time (ms)
M50 26YO
M50 75YO

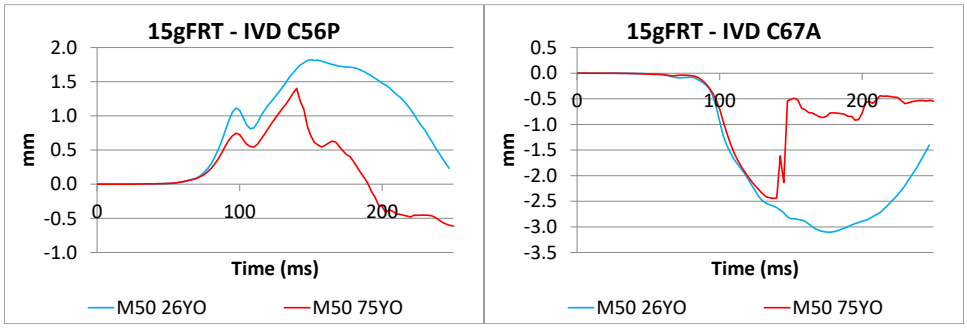
15gFRT - IVD C56P
mm
Time (ms)
M50 26YO
M50 75YO

15gFRT - IVD C67A
mm
Time (ms)
M50 26YO
M50 75YO

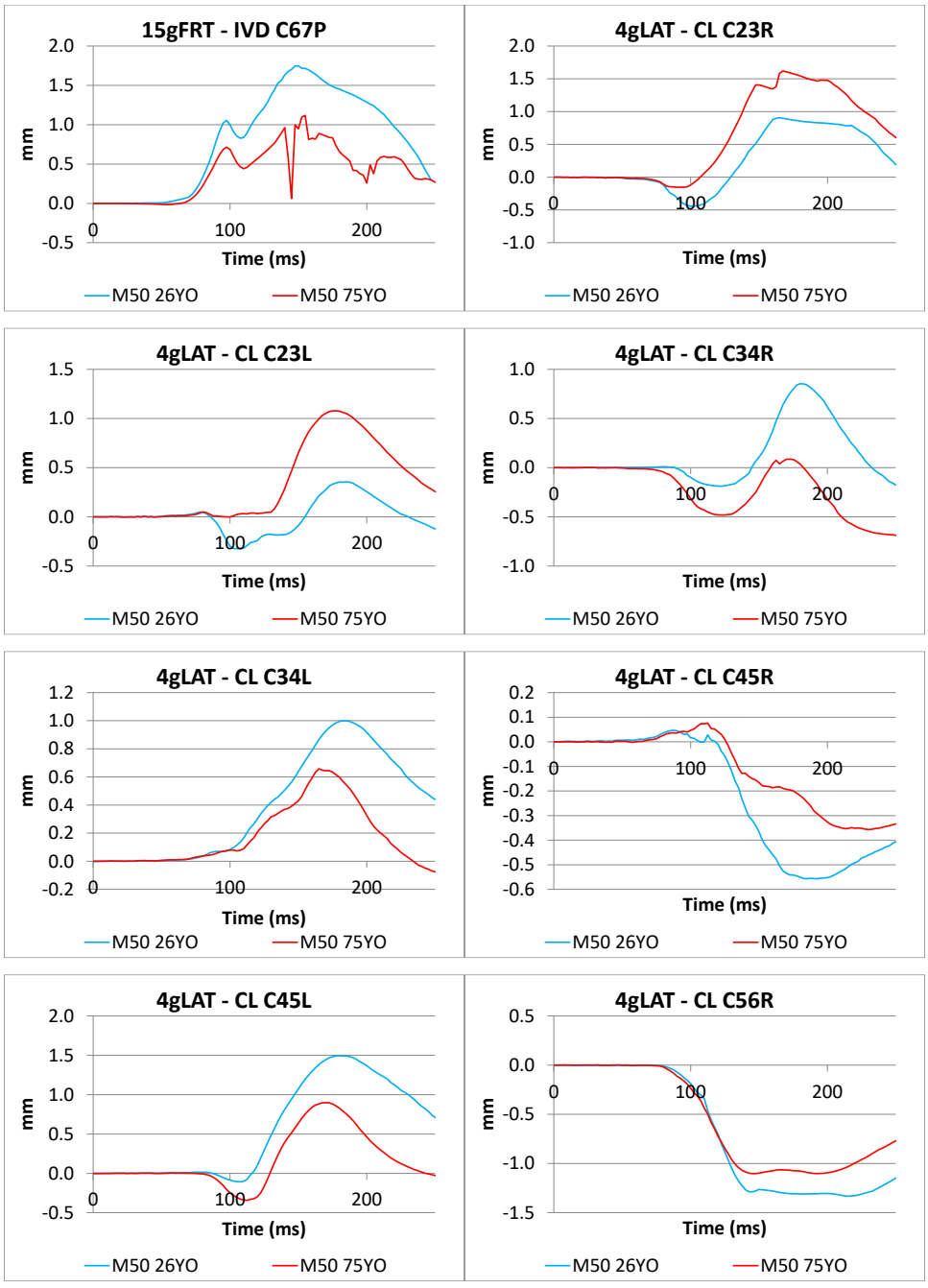
15gFRT - IVD C67P
4gLAT - CL C23R
4gLAT - CL C23L
4gLAT - CL C34R
4gLAT - CL C34L
4gLAT - CL C45R
4gLAT - CL C45L
4gLAT - CL C56R
mm
Time (ms)
M50 26YO
M50 75YO

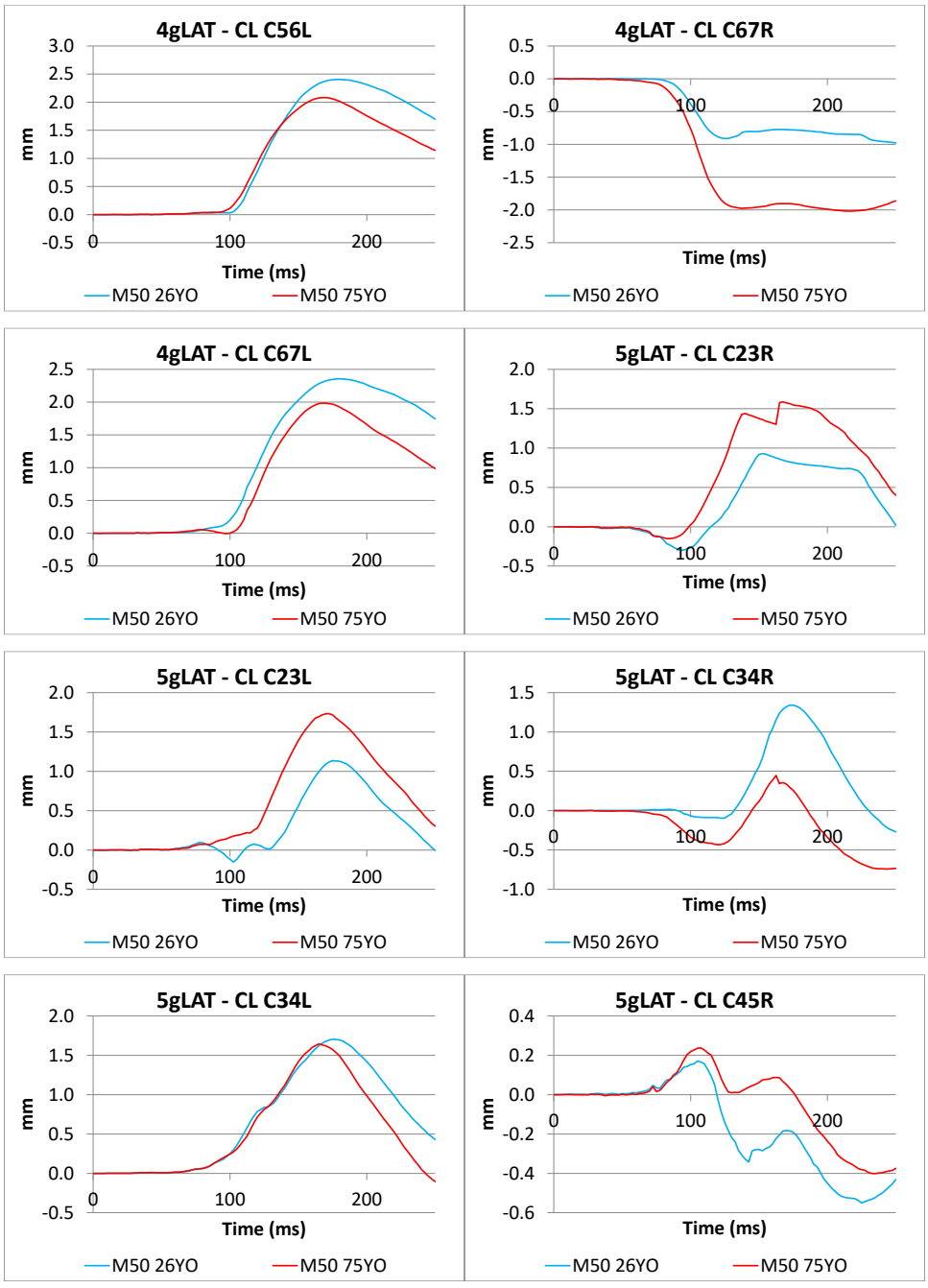
4gLAT - CL C56L
mm
Time (ms)
M50 26YO
M50 75YO
4gLAT - CL C67R
mm
Time (ms)
M50 26YO
M50 75YO
4gLAT - CL C67L
mm
Time (ms)
M50 26YO
M50 75YO
5gLAT - CL C23R
mm
Time (ms)
M50 26YO
M50 75YO
5gLAT - CL C23L
mm
Time (ms)
M50 26YO
M50 75YO
5gLAT - CL C34R
mm
Time (ms)
M50 26YO
M50 75YO
5gLAT - CL C34L
mm
Time (ms)
M50 26YO
M50 75YO
5gLAT - CL C45R
mm
Time (ms)
M50 26YO
M50 75YO

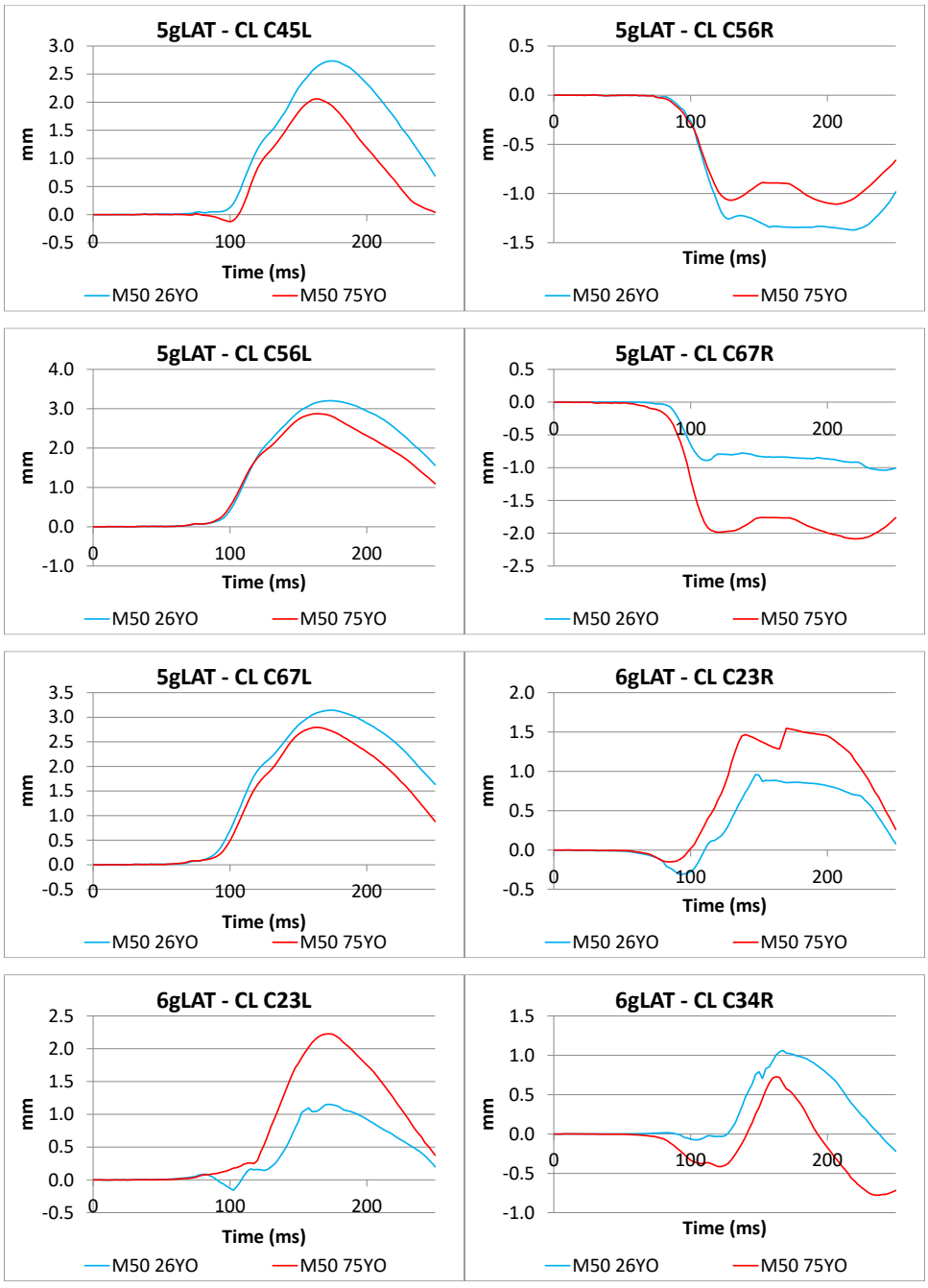
5gLAT - CL C45L
mm
Time (ms)
M50 26YO
M50 75YO
5gLAT - CL C56R
mm
Time (ms)
M50 26YO
M50 75YO
5gLAT - CL C56L
mm
Time (ms)
M50 26YO
M50 75YO
5gLAT - CL C67R
mm
Time (ms)
M50 26YO
M50 75YO
5gLAT - CL C67L
mm
Time (ms)
M50 26YO
M50 75YO
6gLAT - CL C23R
mm
Time (ms)
M50 26YO
M50 75YO
6gLAT - CL C23L
mm
Time (ms)
M50 26YO
M50 75YO
6gLAT - CL C34R
mm
Time (ms)
M50 26YO
M50 75YO

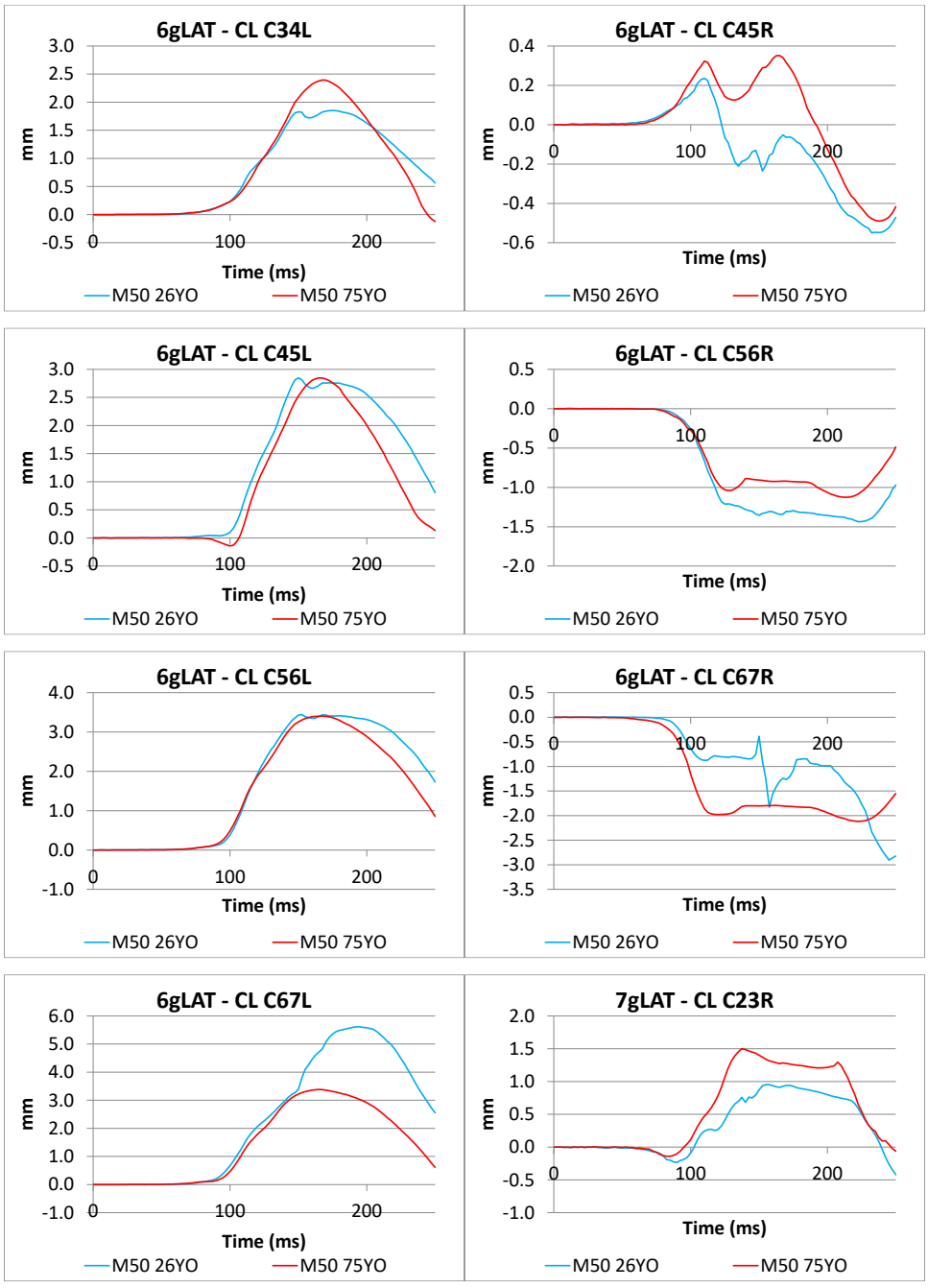
6gLAT - CL C34L
mm
Time (ms)
M50 26YO
M50 75YO
6gLAT - CL C45R
mm
Time (ms)
M50 26YO
M50 75YO
6gLAT - CL C45L
mm
Time (ms)
M50 26YO
M50 75YO
6gLAT - CL C56R
mm
Time (ms)
M50 26YO
M50 75YO
6gLAT - CL C56L
mm
Time (ms)
M50 26YO
M50 75YO
6gLAT - CL C67R
mm
Time (ms)
M50 26YO
M50 75YO
6gLAT - CL C67L
mm
Time (ms)
M50 26YO
M50 75YO
7gLAT - CL C23R
mm
Time (ms)
M50 26YO
M50 75YO

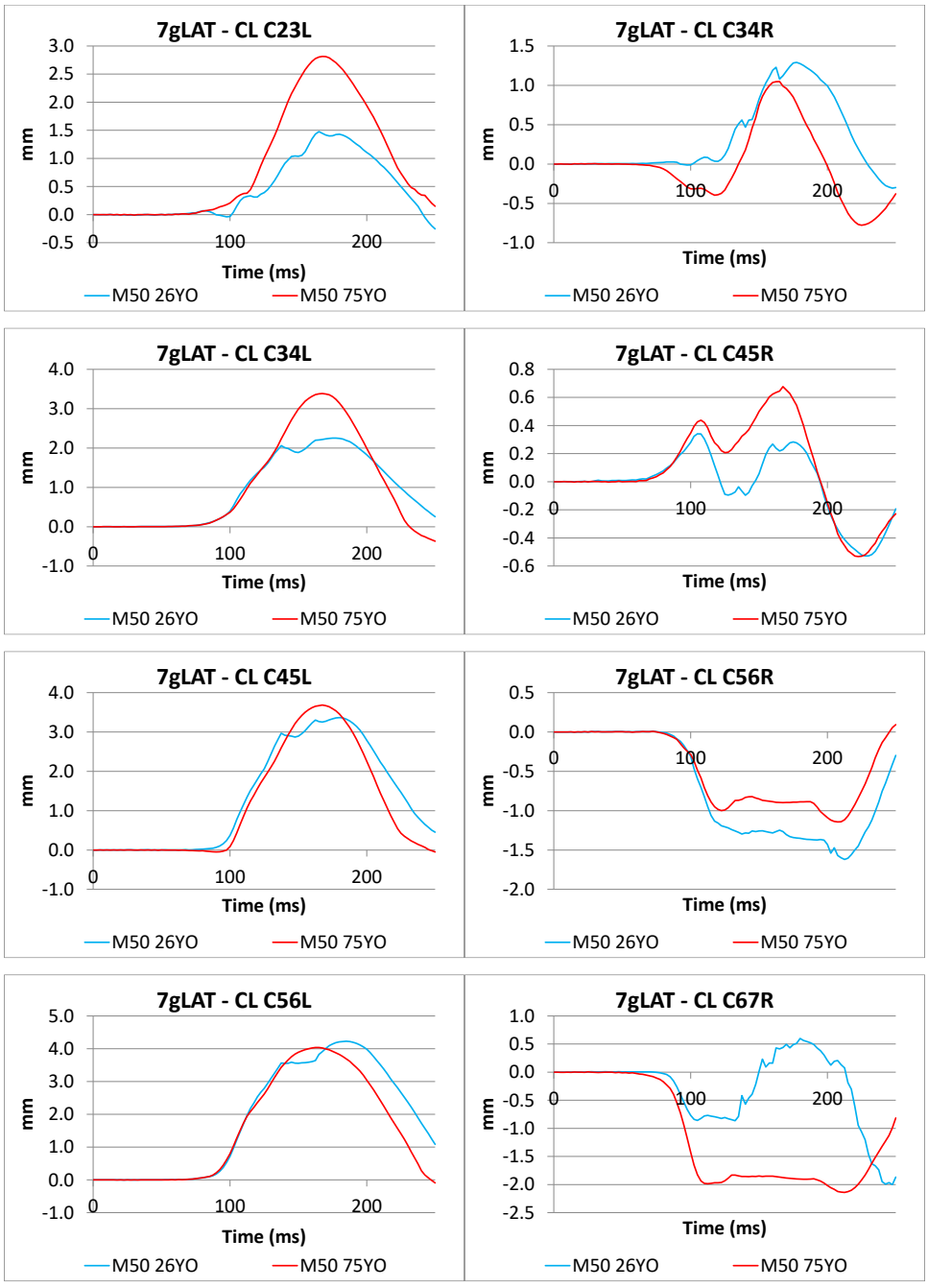
7gLAT - CL C23L
mm
Time (ms)
M50 26YO
M50 75YO
7gLAT - CL C34R
mm
Time (ms)
M50 26YO
M50 75YO
7gLAT - CL C34L
mm
Time (ms)
M50 26YO
M50 75YO
7gLAT - CL C45R
mm
Time (ms)
M50 26YO
M50 75YO
7gLAT - CL C45L
mm
Time (ms)
M50 26YO
M50 75YO
7gLAT - CL C56R
mm
Time (ms)
M50 26YO
M50 75YO
7gLAT - CL C56L
mm
Time (ms)
M50 26YO
M50 75YO
7gLAT - CL C67R
mm
Time (ms)
M50 26YO
M50 75YO

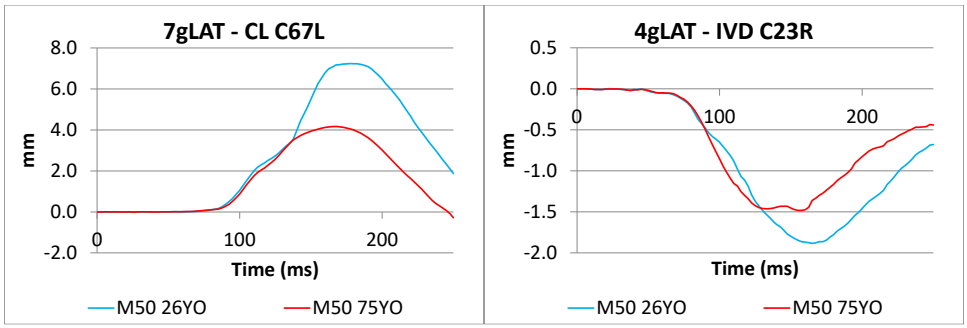
7gLAT - CL C67L
mm
Time (ms)
M50 26YO
M50 75YO

4gLAT - IVD C23R
mm
Time (ms)
M50 26YO
M50 75YO

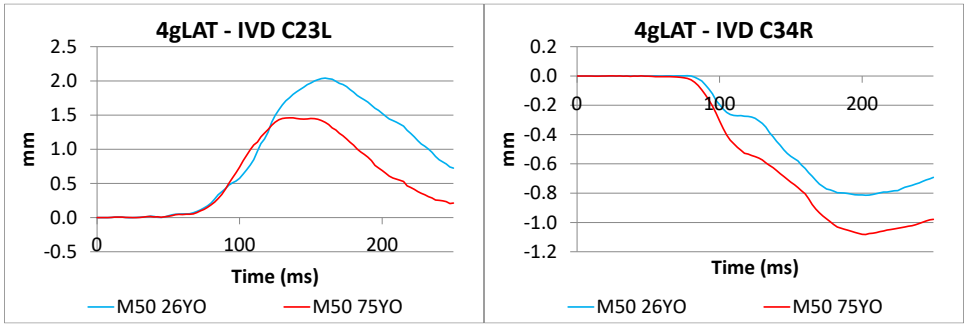
4gLAT - IVD C23L
mm
Time (ms)
M50 26YO
M50 75YO

4gLAT - IVD C34R
mm
Time (ms)
M50 26YO
M50 75YO

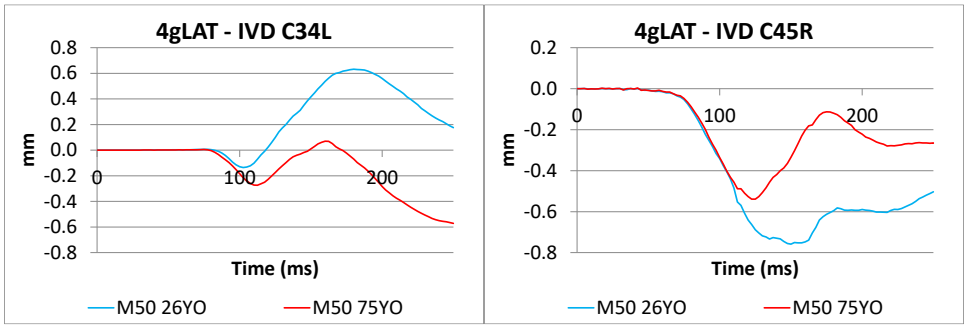
4gLAT - IVD C34L
mm
Time (ms)
M50 26YO
M50 75YO

4gLAT - IVD C45R
mm
Time (ms)
M50 26YO
M50 75YO

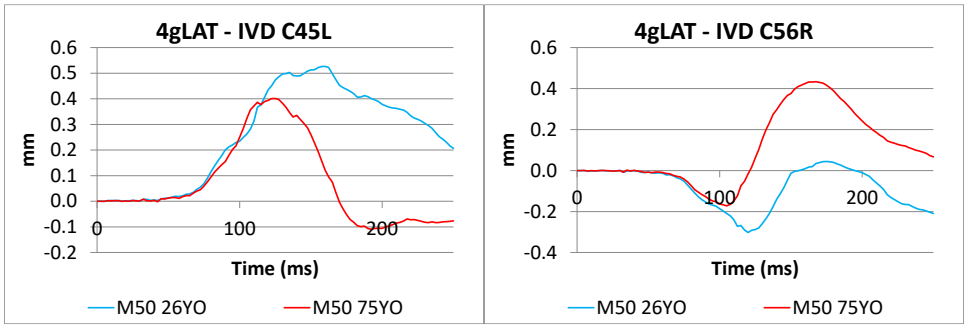
4gLAT - IVD C45L
mm
Time (ms)
M50 26YO
M50 75YO

4gLAT - IVD C56R
mm
Time (ms)
M50 26YO
M50 75YO

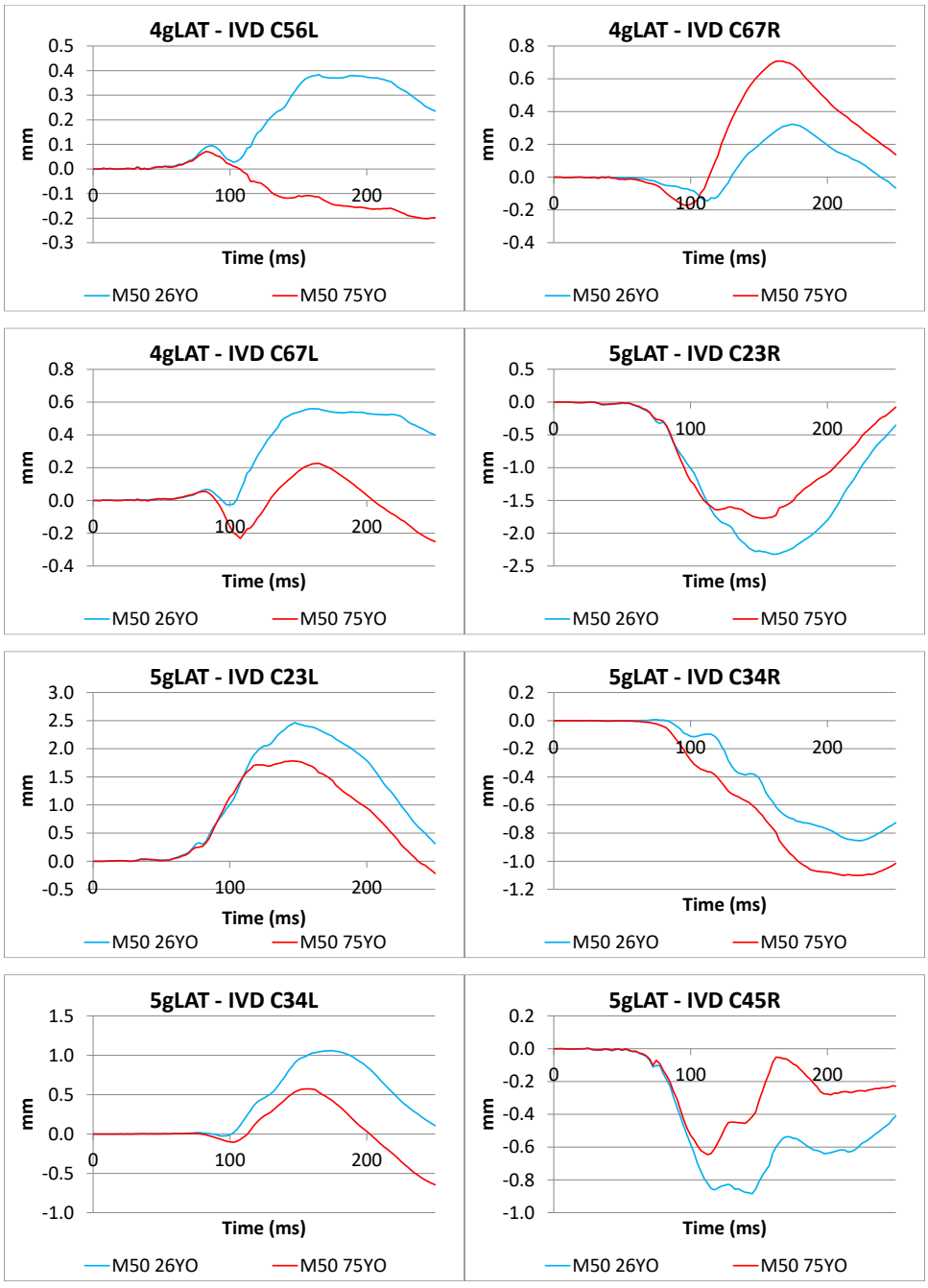
4gLAT - IVD C56L
mm
Time (ms)
M50 26YO
M50 75YO
4gLAT - IVD C67R
mm
Time (ms)
M50 26YO
M50 75YO
4gLAT - IVD C67L
mm
Time (ms)
M50 26YO
M50 75YO
5gLAT - IVD C23R
mm
Time (ms)
M50 26YO
M50 75YO
5gLAT - IVD C23L
mm
Time (ms)
M50 26YO
M50 75YO
5gLAT - IVD C34R
mm
Time (ms)
M50 26YO
M50 75YO
5gLAT - IVD C34L
mm
Time (ms)
M50 26YO
M50 75YO
5gLAT - IVD C45R
mm
Time (ms)
M50 26YO
M50 75YO

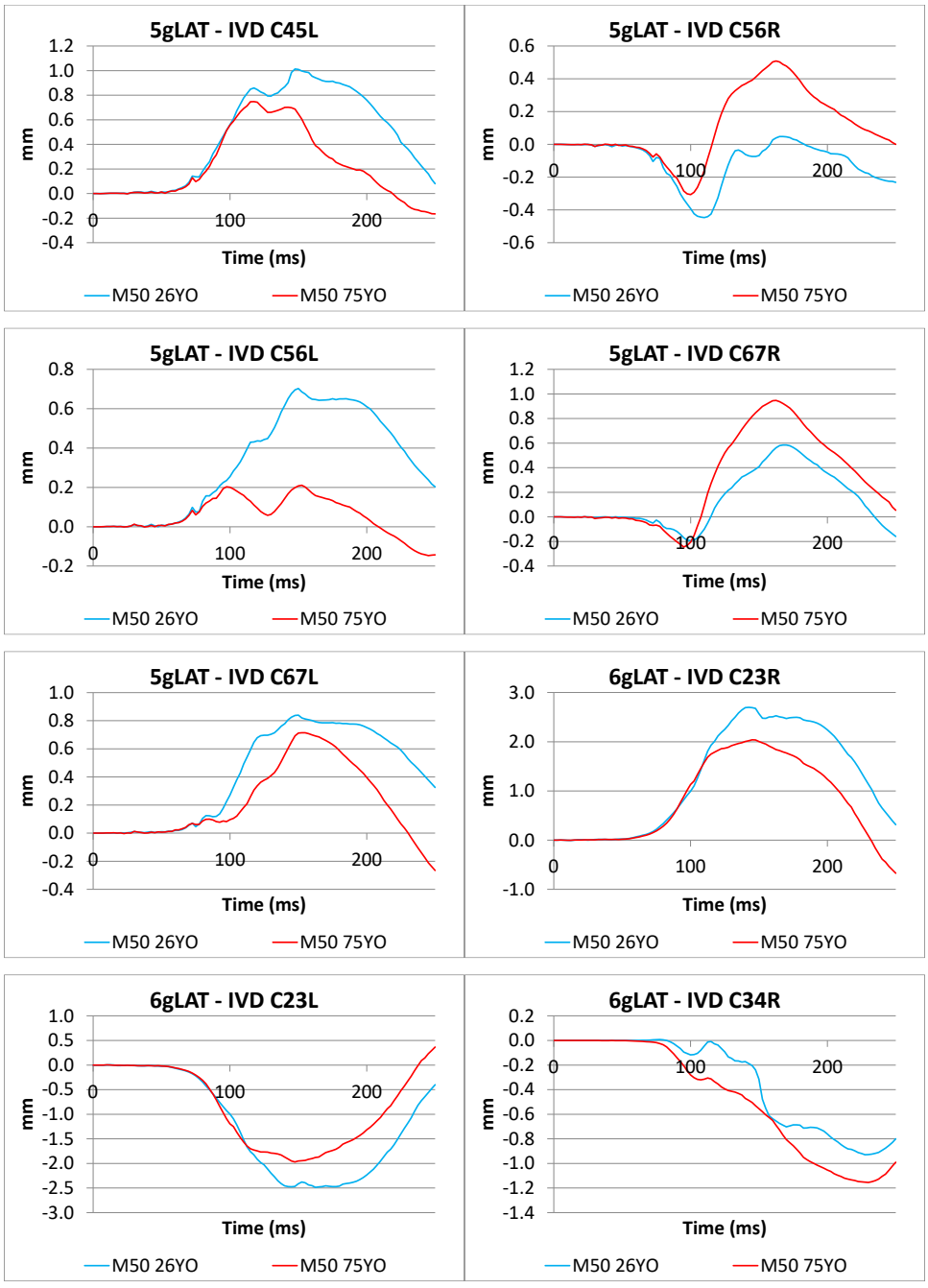
5gLAT - IVD C45L
mm
Time (ms)
M50 26YO
M50 75YO
5gLAT - IVD C56R
mm
Time (ms)
M50 26YO
M50 75YO
5gLAT - IVD C56L
mm
Time (ms)
M50 26YO
M50 75YO
5gLAT - IVD C67R
mm
Time (ms)
M50 26YO
M50 75YO
5gLAT - IVD C67L
mm
Time (ms)
M50 26YO
M50 75YO
6gLAT - IVD C23R
mm
Time (ms)
M50 26YO
M50 75YO
6gLAT - IVD C23L
mm
Time (ms)
M50 26YO
M50 75YO
6gLAT - IVD C34R
mm
Time (ms)
M50 26YO
M50 75YO

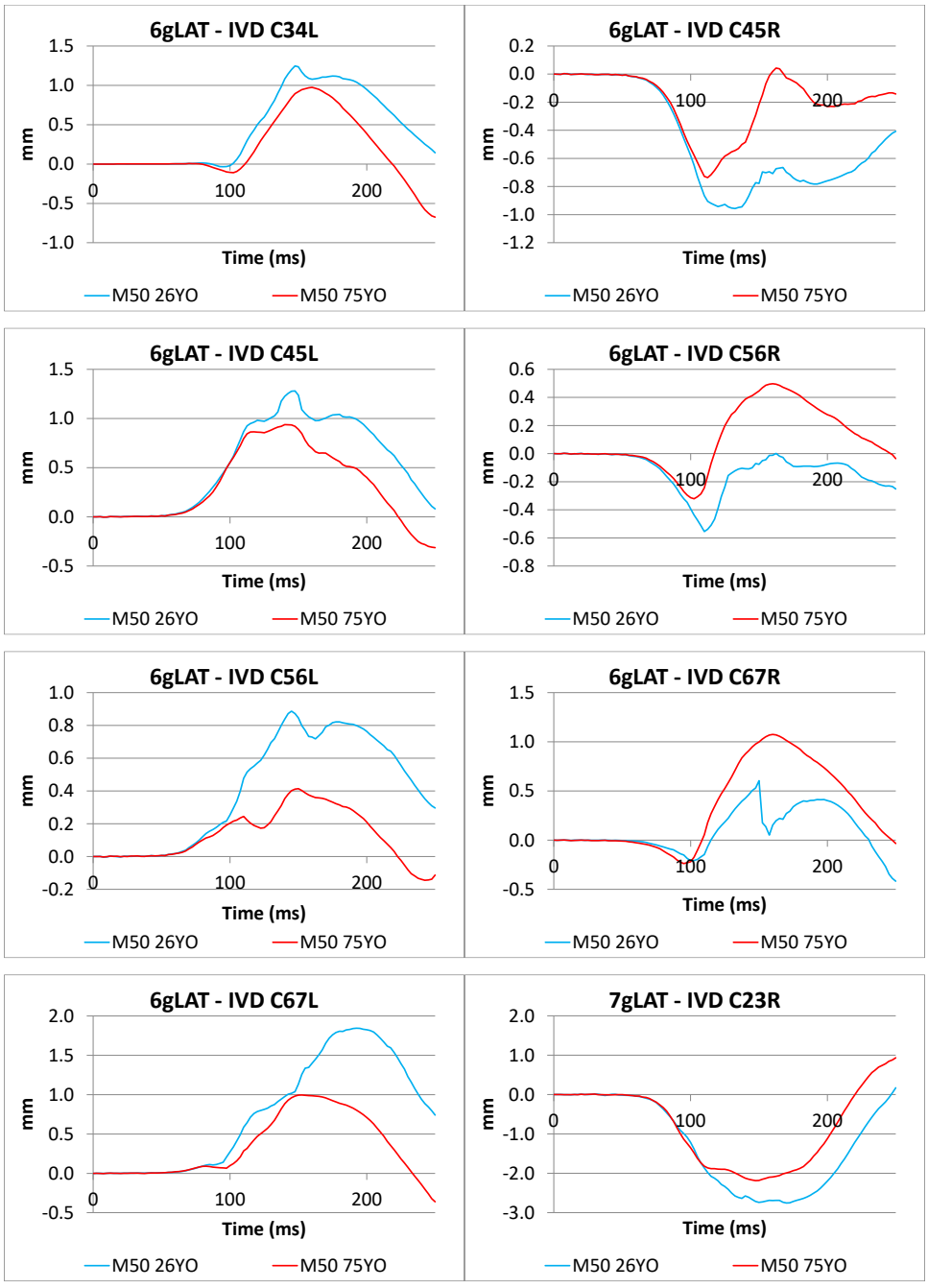
6gLAT - IVD C34L
mm
Time (ms)
M50 26YO
M50 75YO
6gLAT - IVD C45R
mm
Time (ms)
M50 26YO
M50 75YO
6gLAT - IVD C45L
mm
Time (ms)
M50 26YO
M50 75YO
6gLAT - IVD C56R
mm
Time (ms)
M50 26YO
M50 75YO
6gLAT - IVD C56L
mm
Time (ms)
M50 26YO
M50 75YO
6gLAT - IVD C67R
mm
Time (ms)
M50 26YO
M50 75YO
6gLAT - IVD C67L
mm
Time (ms)
M50 26YO
M50 75YO
7gLAT - IVD C23R
mm
Time (ms)
M50 26YO
M50 75YO

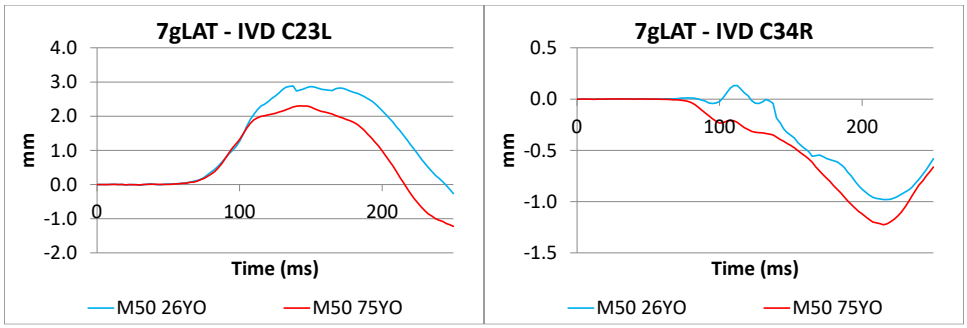
7gLAT - IVD C23L
mm
Time (ms)
M50 26YO
M50 75YO

7gLAT - IVD C34R
mm
Time (ms)
M50 26YO
M50 75YO

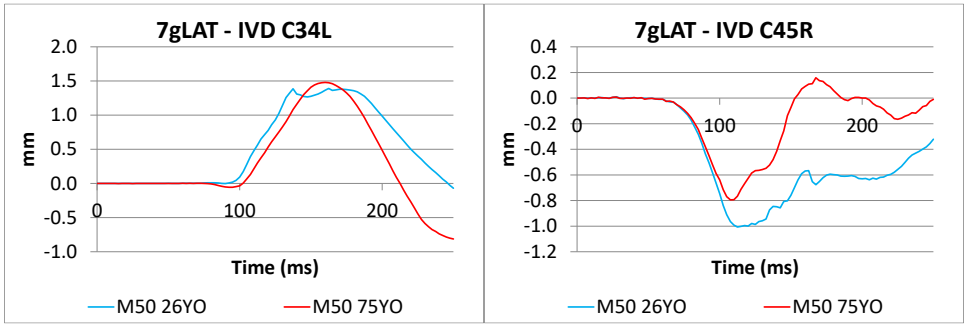
7gLAT - IVD C34L
mm
Time (ms)
M50 26YO
M50 75YO

7gLAT - IVD C45R
mm
Time (ms)
M50 26YO
M50 75YO

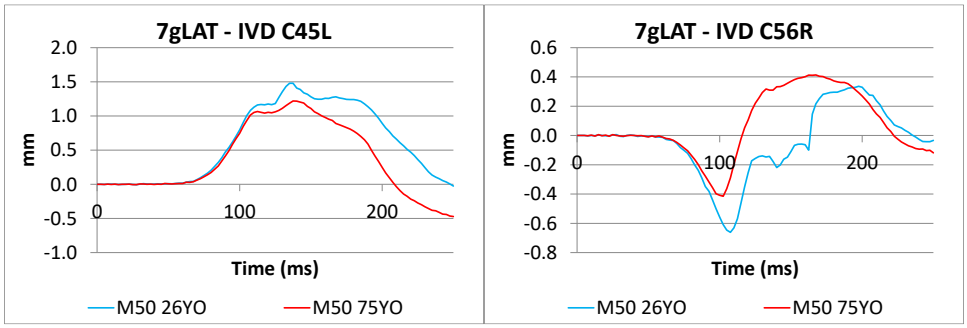
7gLAT - IVD C45L
mm
Time (ms)
M50 26YO
M50 75YO

7gLAT - IVD C56R
mm
Time (ms)
M50 26YO
M50 75YO

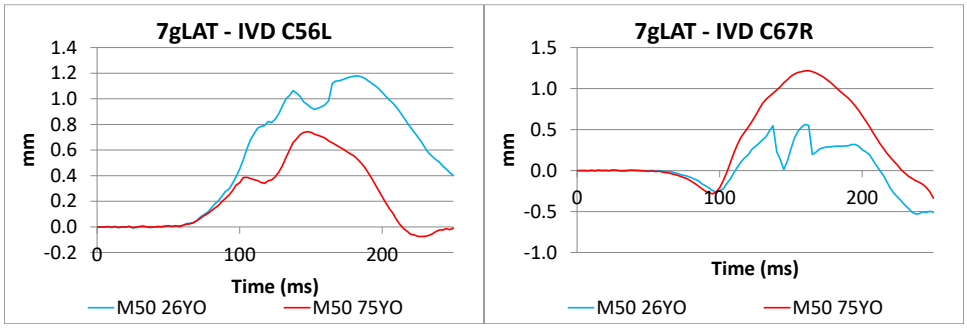
7gLAT - IVD C56L
mm
Time (ms)
M50 26YO
M50 75YO

7gLAT - IVD C67R
mm
Time (ms)
M50 26YO
M50 75YO

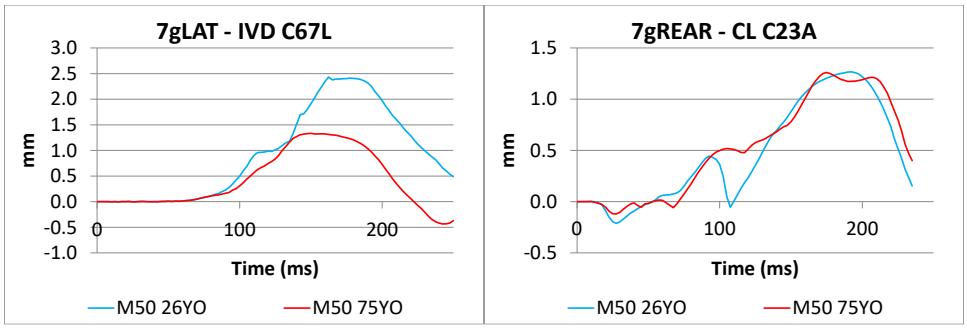
7gLAT - IVD C67L
mm
Time (ms)
M50 26YO
M50 75YO

7gREAR - CL C23A
mm
Time (ms)
M50 26YO
M50 75YO

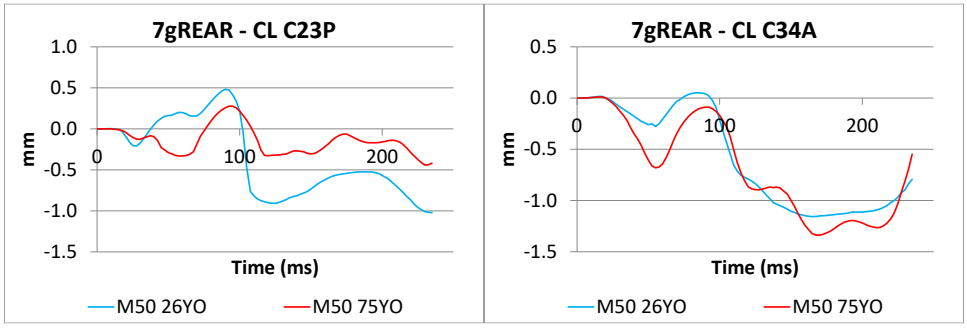
7gREAR - CL C23P
mm
Time (ms)
M50 26YO
M50 75YO

7gREAR - CL C34A
mm
Time (ms)
M50 26YO
M50 75YO

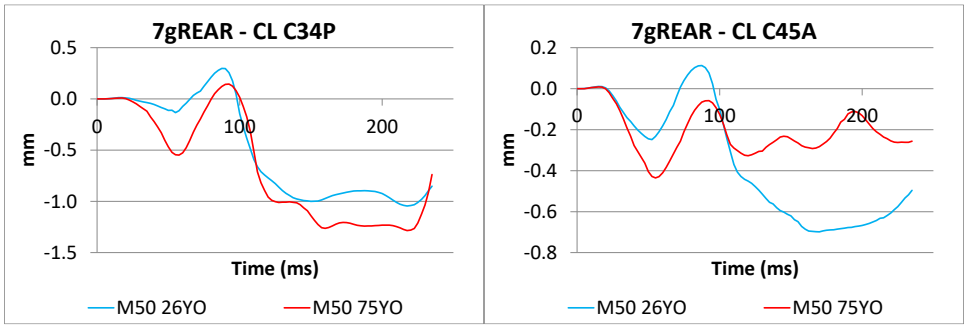
7gREAR - CL C34P
mm
Time (ms)
M50 26YO
M50 75YO

7gREAR - CL C45A
mm
Time (ms)
M50 26YO
M50 75YO

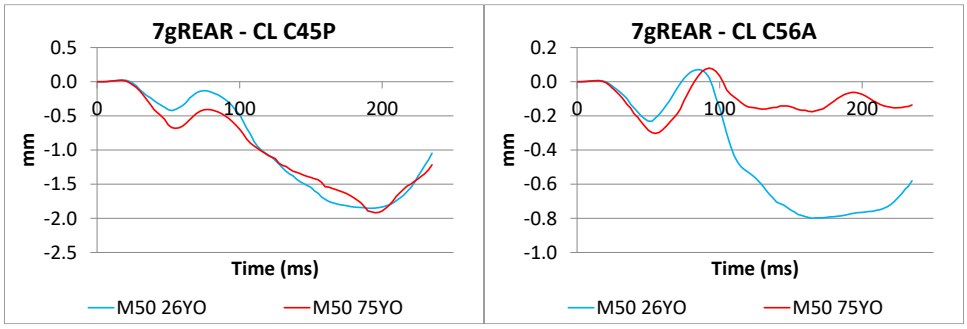
7gREAR - CL C45P
mm
Time (ms)
M50 26YO
M50 75YO

7gREAR - CL C56A
mm
Time (ms)
M50 26YO
M50 75YO

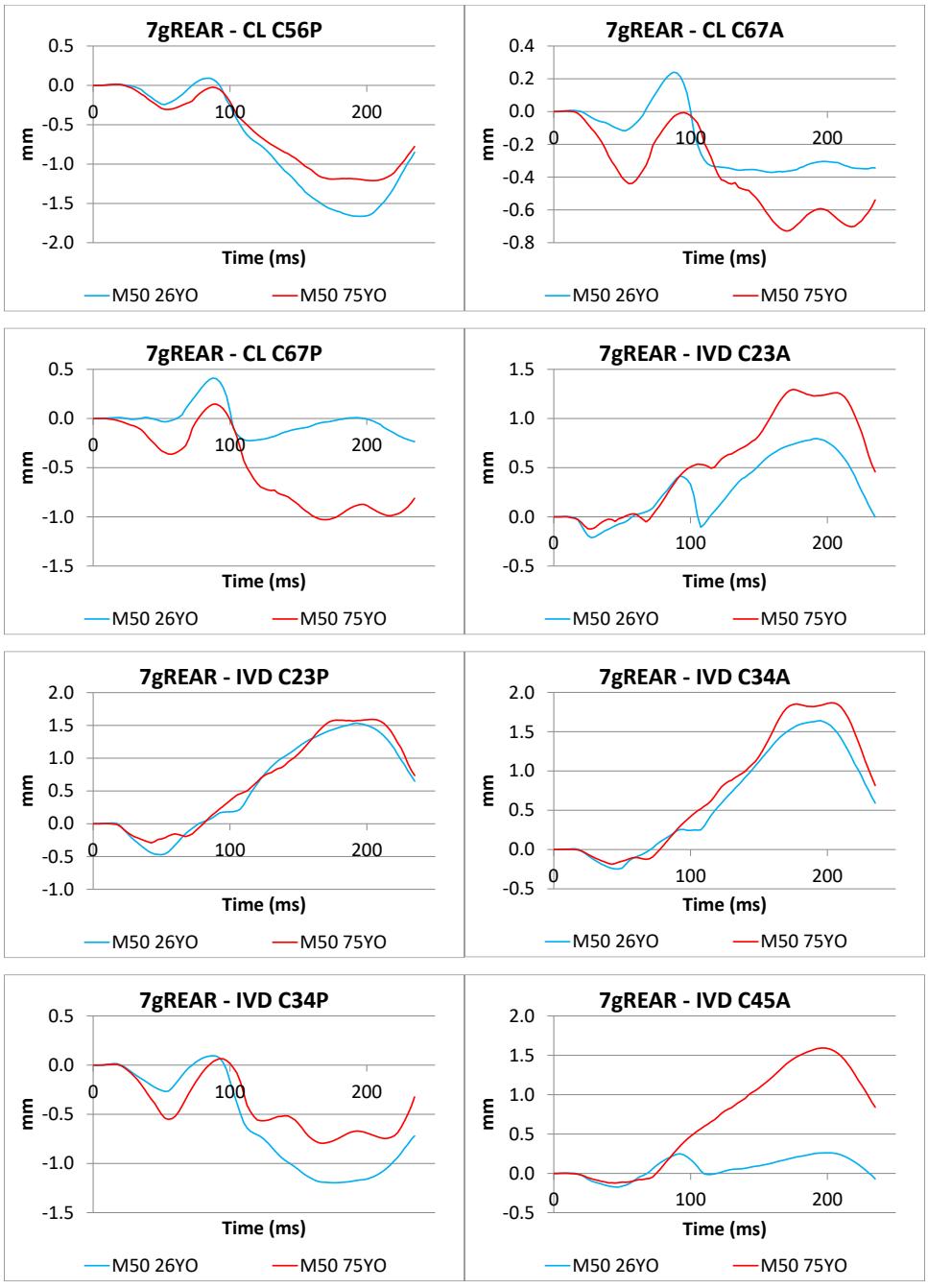
7gREAR - CL C56P
0.5
0.0
-0.5
-1.0
-1.5
-2.0
mm
0
100
200
Time (ms)
M50 26YO
M50 75YO
7gREAR - CL C67A
0.4
0.2
0.0
-0.2
-0.4
-0.6
-0.8
mm
0
100
200
Time (ms)
M50 26YO
M50 75YO
7gREAR - CL C67P
0.5
0.0
-0.5
-1.0
-1.5
mm
0
100
200
Time (ms)
M50 26YO
M50 75YO
7gREAR - IVD C23A
1.5
1.0
0.5
0.0
-0.5
mm
0
100
200
Time (ms)
M50 26YO
M50 75YO
7gREAR - IVD C23P
2.0
1.5
1.0
0.5
0.0
-0.5
-1.0
mm
0
100
200
Time (ms)
M50 26YO
M50 75YO
7gREAR - IVD C34A
2.0
1.5
1.0
0.5
0.0
-0.5
mm
0
100
200
Time (ms)
M50 26YO
M50 75YO
7gREAR - IVD C34P
0.5
0.0
-0.5
-1.0
-1.5
mm
0
100
200
Time (ms)
M50 26YO
M50 75YO
7gREAR - IVD C45A
2.0
1.5
1.0
0.5
0.0
-0.5
mm
0
100
200
Time (ms)
M50 26YO
M50 75YO

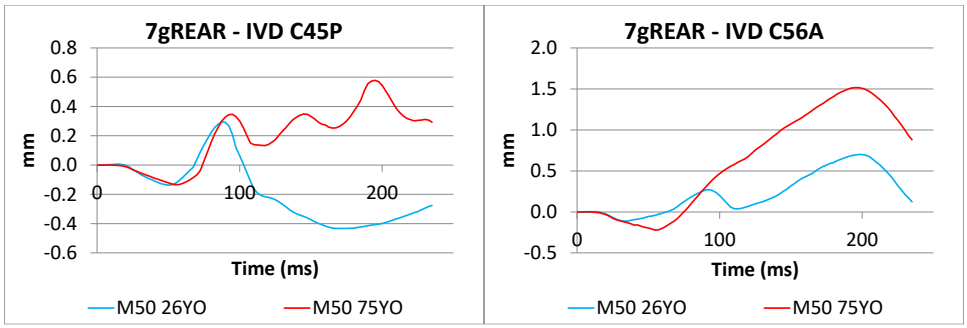
7gREAR - IVD C45P
0.8
0.6
0.4
0.2
0.0
-0.2
-0.4
-0.6
mm
0
100
200
Time (ms)
M50 26YO
M50 75YO

7gREAR - IVD C56A
2.0
1.5
1.0
0.5
0.0
-0.5
mm
0
100
200
Time (ms)
M50 26YO
M50 75YO

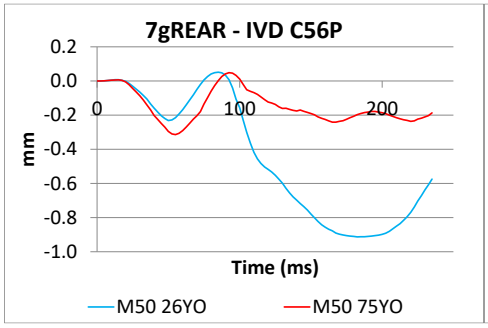
7gREAR - IVD C56P
0.2
0.0
-0.2
-0.4
-0.6
-0.8
-1.0
mm
0
100
200
Time (ms)
M50 26YO
M50 75YO

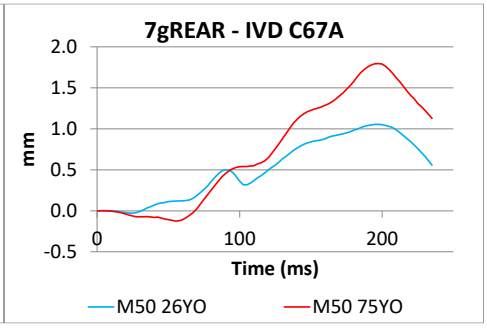
7gREAR - IVD C67A
2.0
1.5
1.0
0.5
0.0
-0.5
mm
0
100
200
Time (ms)
M50 26YO
M50 75YO

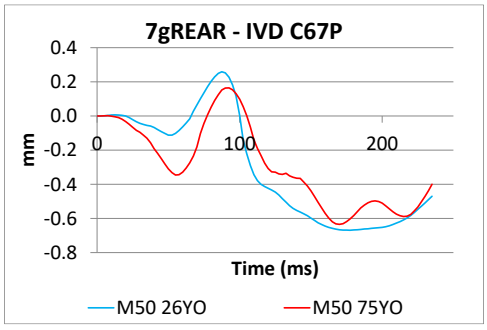
7gREAR - IVD C67P
0.4
0.2
0.0
-0.2
-0.4
-0.6
-0.8
mm
0
100
200
Time (ms)
M50 26YO
M50 75YO

Appendix 4: $F05_{26YO}$ and $F05_{75YO}$ Time Histories of the Head Kinematic Response and Soft Tissue Metrics

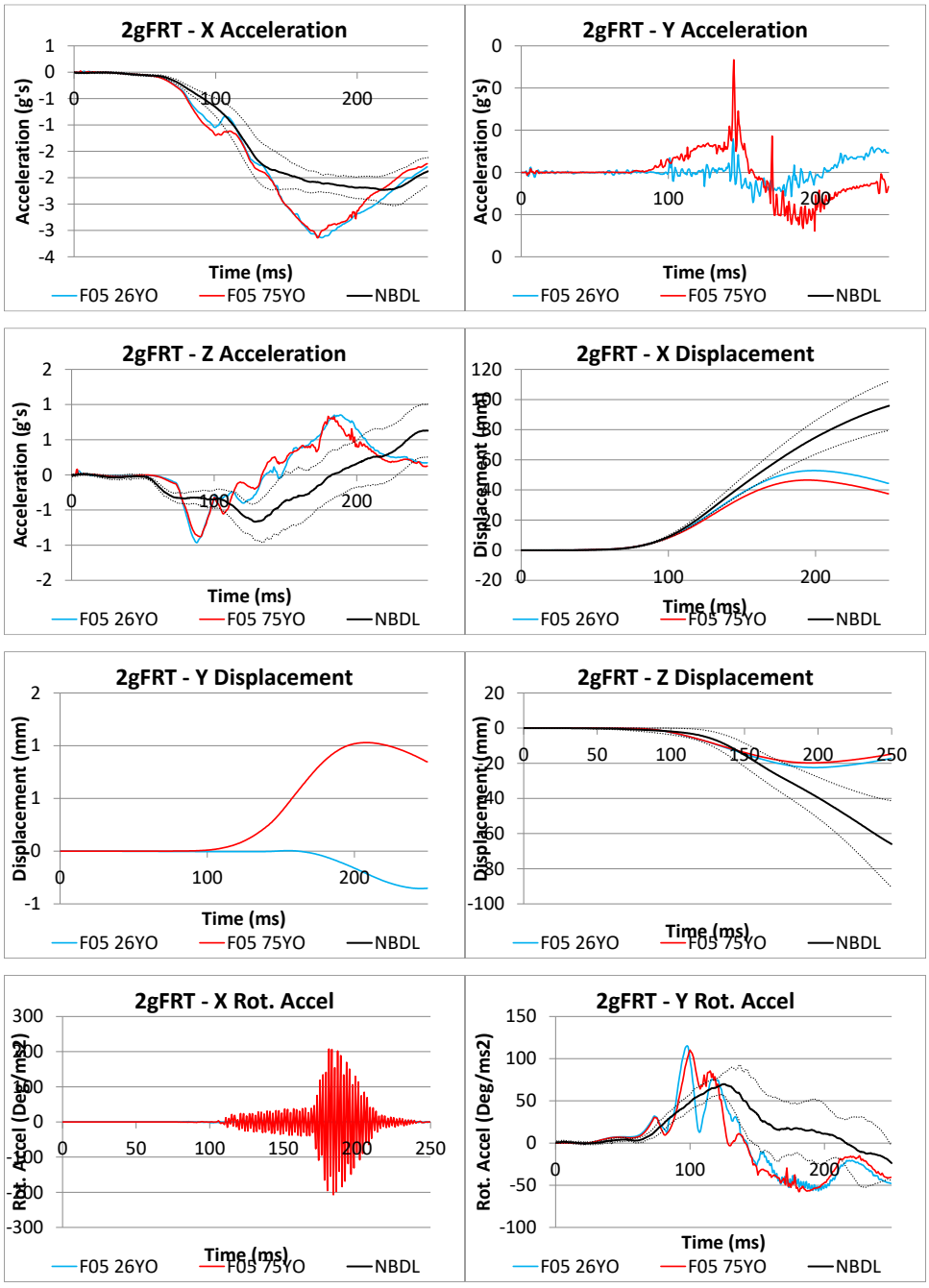

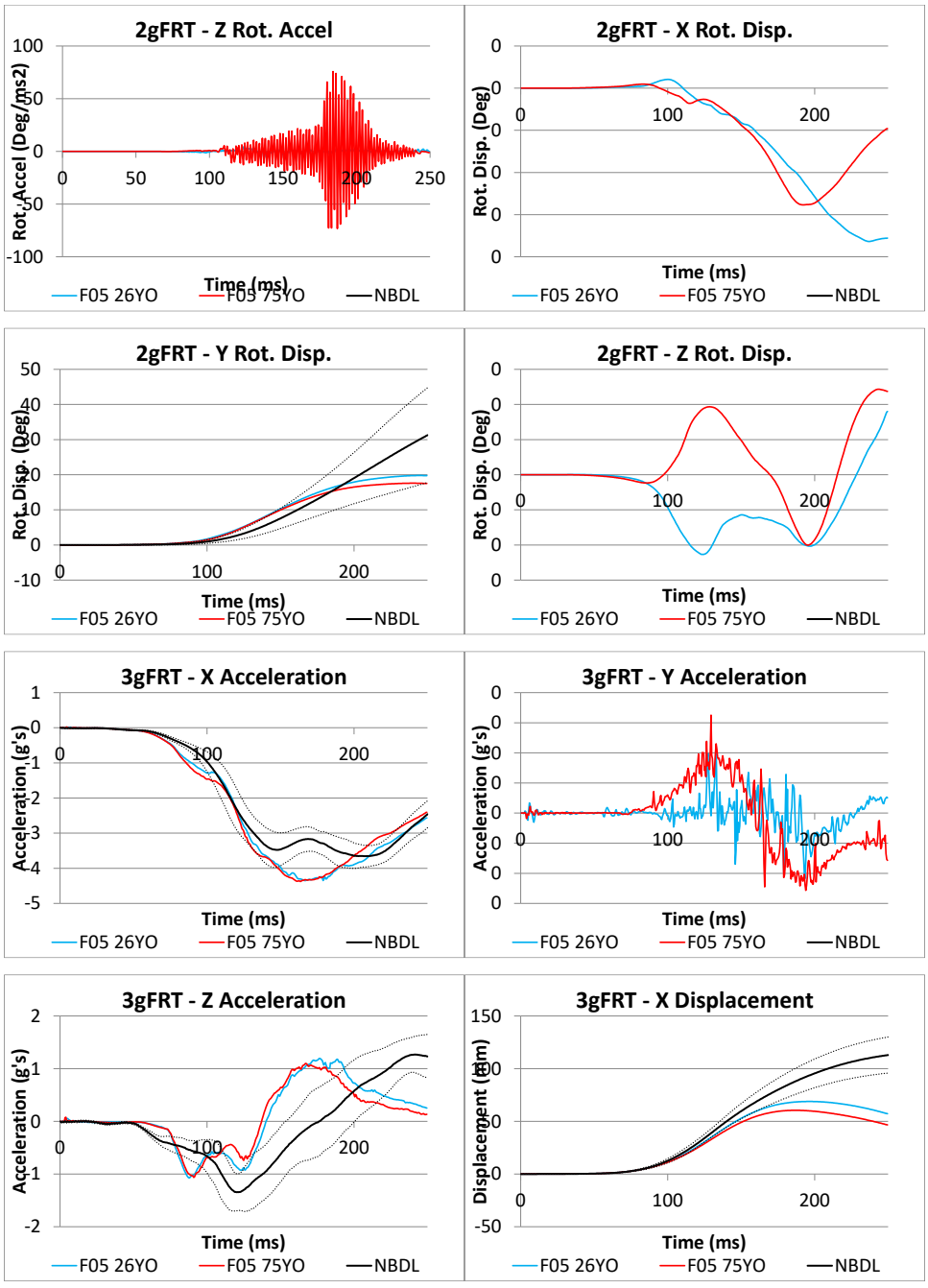
2gFRT - Z Rot. Accel
Rot. Accel (Deg/ms2)
Time (ms)
2gFRT - X Rot. Disp.
Rot. Disp. (Deg)
Time (ms)
2gFRT - Y Rot. Disp.
Rot. Disp. (Deg)
Time (ms)
2gFRT - Z Rot. Disp.
Rot. Disp. (Deg)
Time (ms)
3gFRT - X Acceleration
Acceleration (g's)
Time (ms)
3gFRT - Y Acceleration
Acceleration (g's)
Time (ms)
3gFRT - Z Acceleration
Acceleration (g's)
Time (ms)
3gFRT - X Displacement
Displacement (mm)
Time (ms)
F05 26YO
F05 75YO
NBDL

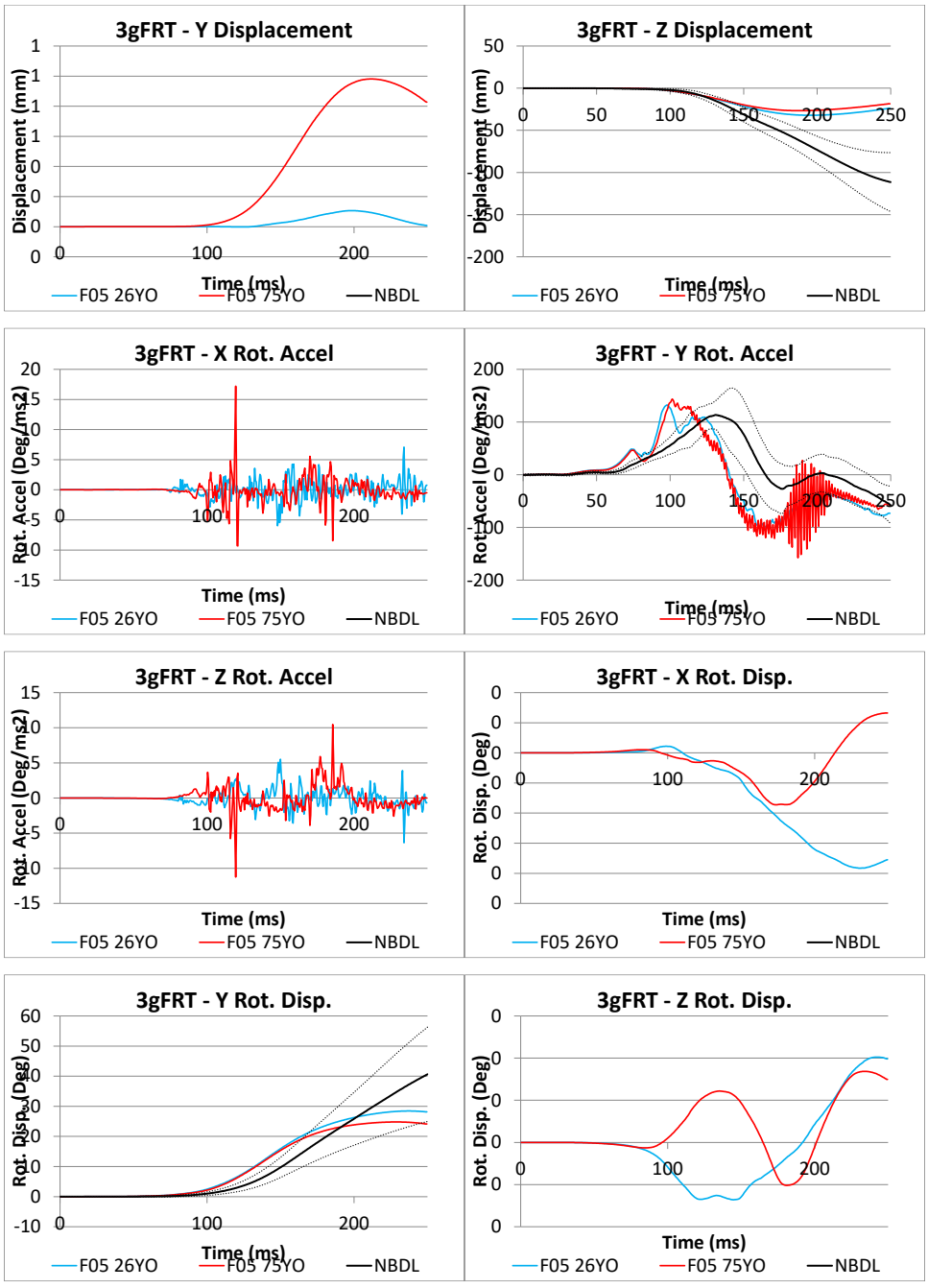
3gFRT - Y Displacement
Displacement (mm)
Time (ms)
F05 26YO
F05 75YO
NBDL
3gFRT - Z Displacement
Displacement (mm)
Time (ms)
F05 26YO
F05 75YO
NBDL
3gFRT - X Rot. Accel
Rot. Accel (Deg/ms2)
Time (ms)
F05 26YO
F05 75YO
NBDL
3gFRT - Y Rot. Accel
Rot. Accel (Deg/ms2)
Time (ms)
F05 26YO
F05 75YO
NBDL
3gFRT - Z Rot. Accel
Rot. Accel (Deg/ms2)
Time (ms)
F05 26YO
F05 75YO
NBDL
3gFRT - X Rot. Disp.
Rot. Disp. (Deg)
Time (ms)
F05 26YO
F05 75YO
NBDL
3gFRT - Y Rot. Disp.
Rot. Disp. (Deg)
Time (ms)
F05 26YO
F05 75YO
NBDL
3gFRT - Z Rot. Disp.
Rot. Disp. (Deg)
Time (ms)
F05 26YO
F05 75YO
NBDL

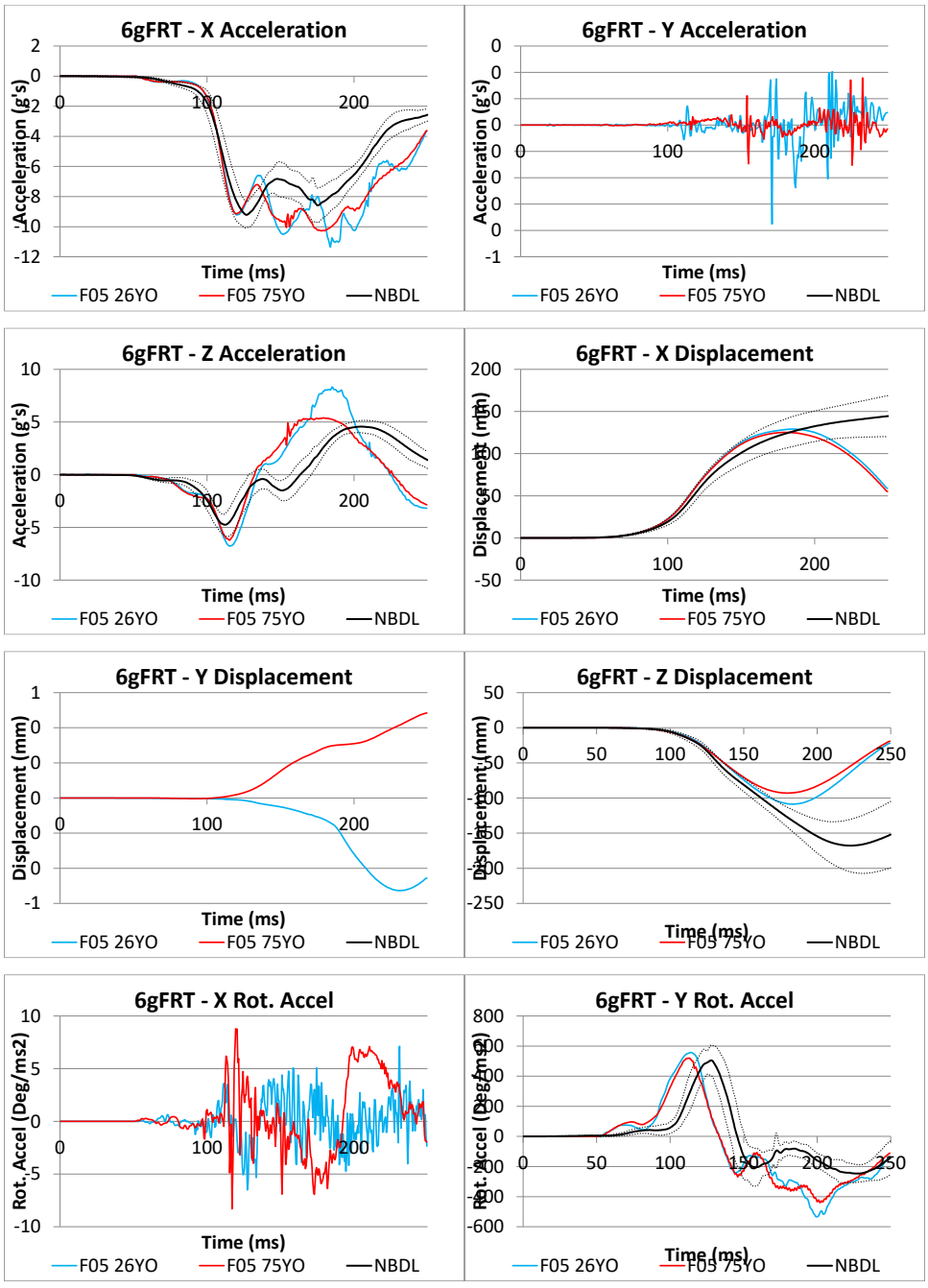
6gFRT - X Acceleration
Acceleration (g's)
Time (ms)
F05 26YO
F05 75YO
NBDL
6gFRT - Y Acceleration
Acceleration (g's)
Time (ms)
F05 26YO
F05 75YO
NBDL
6gFRT - Z Acceleration
Acceleration (g's)
Time (ms)
F05 26YO
F05 75YO
NBDL
6gFRT - X Displacement
Displacement (mm)
Time (ms)
F05 26YO
F05 75YO
NBDL
6gFRT - Y Displacement
Displacement (mm)
Time (ms)
F05 26YO
F05 75YO
NBDL
6gFRT - Z Displacement
Displacement (mm)
Time (ms)
F05 26YO
F05 75YO
NBDL
6gFRT - X Rot. Accel
Rot. Accel (Deg/ms2)
Time (ms)
F05 26YO
F05 75YO
NBDL
6gFRT - Y Rot. Accel
Rot. Accel (Deg/ms2)
Time (ms)
F05 26YO
F05 75YO
NBDL

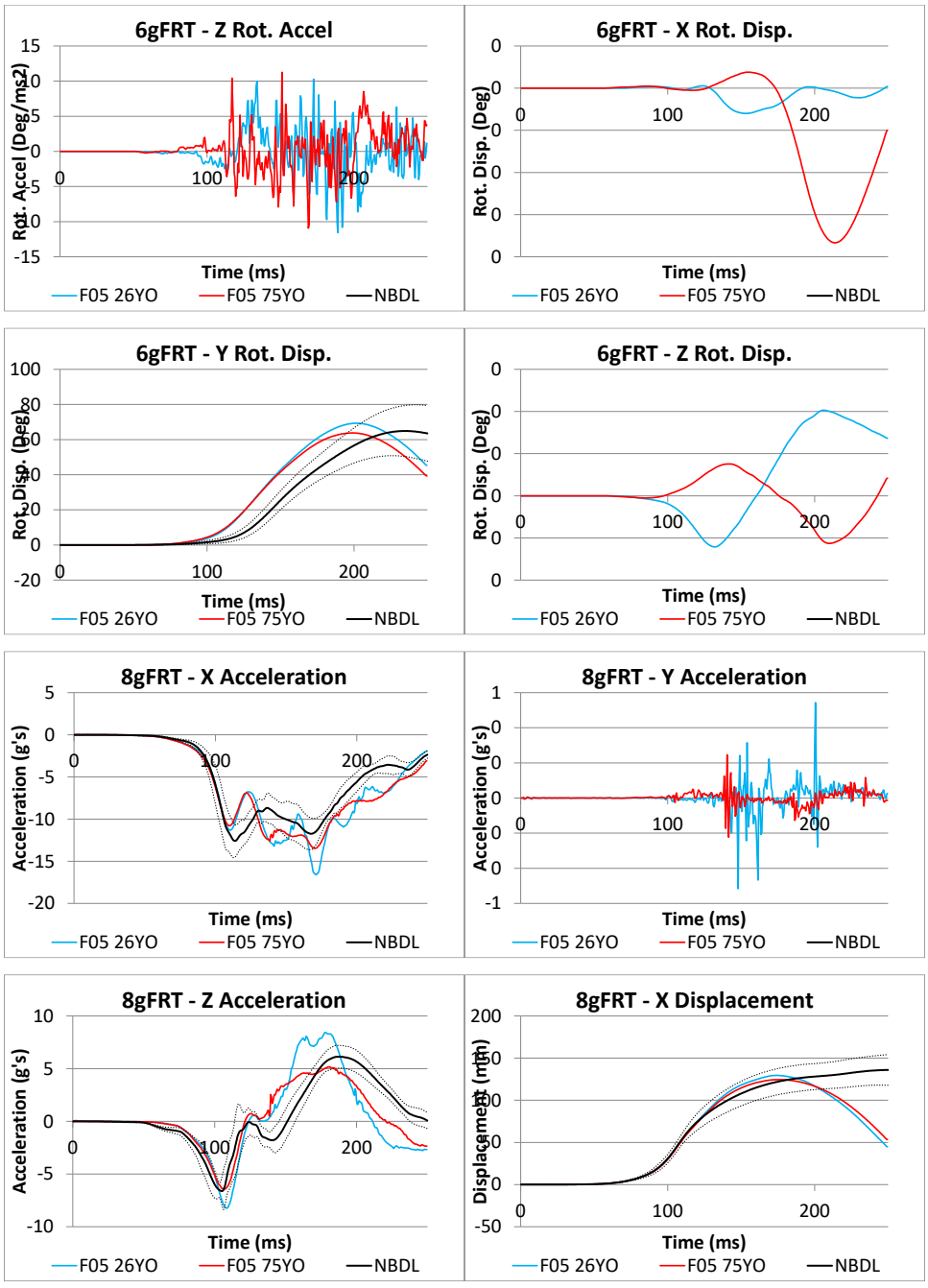
6gFRT - Z Rot. Accel
Rot. Accel (Deg/ms2)
Time (ms)
F05 26YO
F05 75YO
NBDL
6gFRT - X Rot. Disp.
Rot. Disp. (Deg)
Time (ms)
F05 26YO
F05 75YO
NBDL
6gFRT - Y Rot. Disp.
Rot. Disp. (Deg)
Time (ms)
F05 26YO
F05 75YO
NBDL
6gFRT - Z Rot. Disp.
Rot. Disp. (Deg)
Time (ms)
F05 26YO
F05 75YO
NBDL
8gFRT - X Acceleration
Acceleration (g's)
Time (ms)
F05 26YO
F05 75YO
NBDL
8gFRT - Y Acceleration
Acceleration (g's)
Time (ms)
F05 26YO
F05 75YO
NBDL
8gFRT - Z Acceleration
Acceleration (g's)
Time (ms)
F05 26YO
F05 75YO
NBDL
8gFRT - X Displacement
Displacement (mm)
Time (ms)
F05 26YO
F05 75YO
NBDL

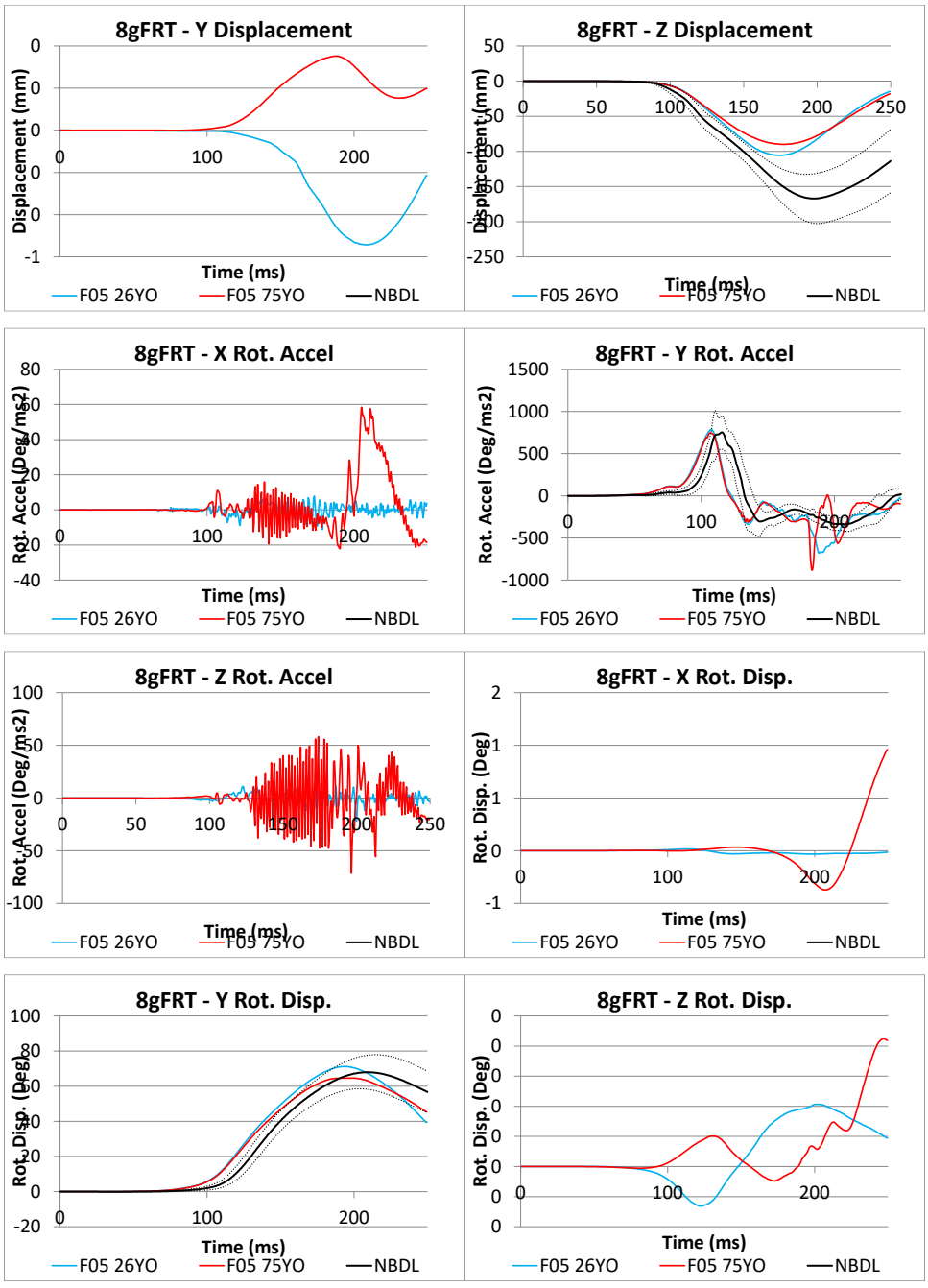
8gFRT - Y Displacement
Displacement (mm)
Time (ms)
F05 26YO
F05 75YO
NBDL
8gFRT - Z Displacement
Displacement (mm)
Time (ms)
F05 26YO
F05 75YO
NBDL
8gFRT - X Rot. Accel
Rot. Accel (Deg/ms2)
Time (ms)
F05 26YO
F05 75YO
NBDL
8gFRT - Y Rot. Accel
Rot. Accel (Deg/ms2)
Time (ms)
F05 26YO
F05 75YO
NBDL
8gFRT - Z Rot. Accel
Rot. Accel (Deg/ms2)
Time (ms)
F05 26YO
F05 75YO
NBDL
8gFRT - X Rot. Disp.
Rot. Disp. (Deg)
Time (ms)
F05 26YO
F05 75YO
NBDL
8gFRT - Y Rot. Disp.
Rot. Disp. (Deg)
Time (ms)
F05 26YO
F05 75YO
NBDL
8gFRT - Z Rot. Disp.
Rot. Disp. (Deg)
Time (ms)
F05 26YO
F05 75YO
NBDL

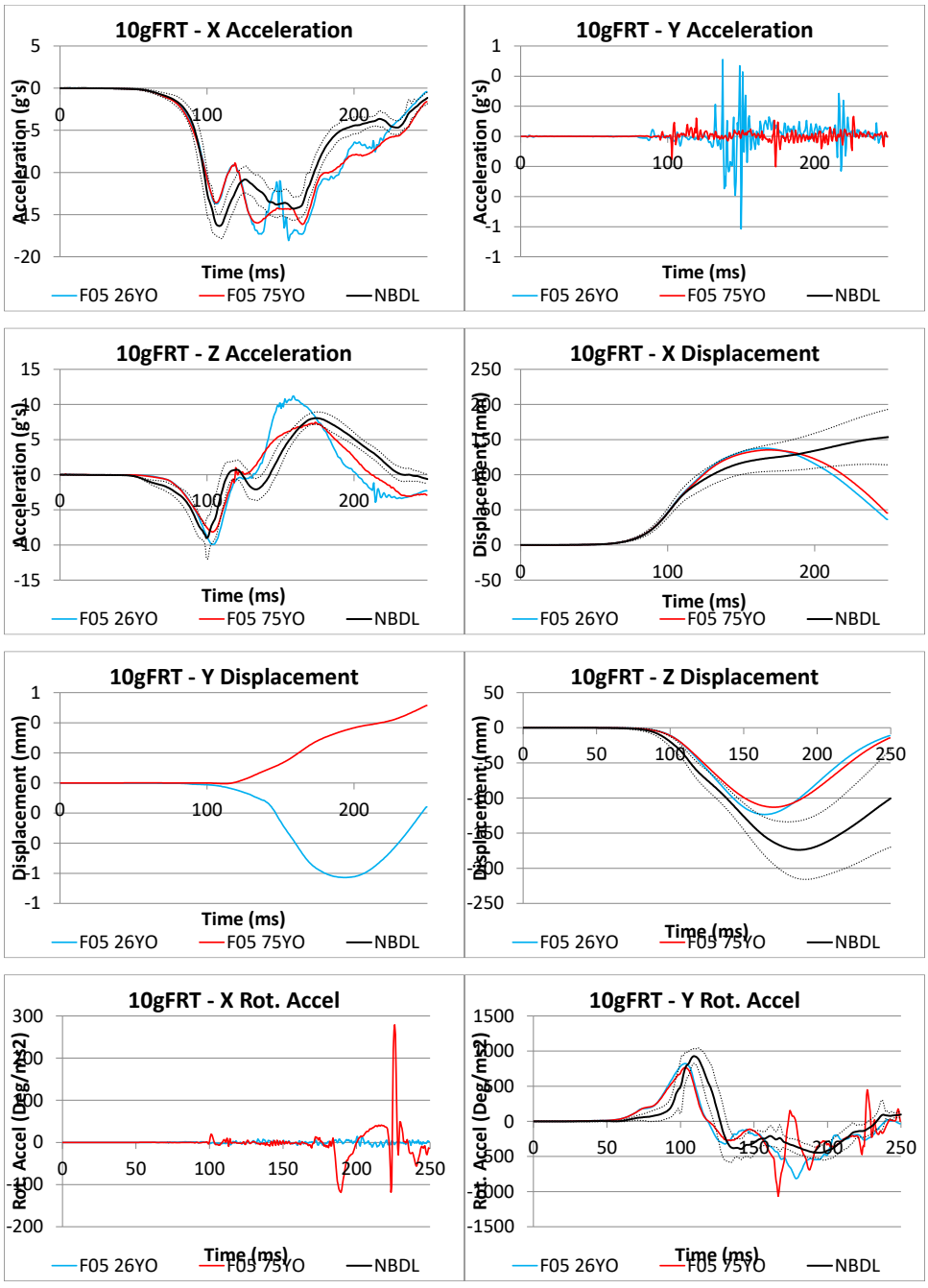
10gFRT - X Acceleration
Acceleration (g's)
Time (ms)
F05 26YO
F05 75YO
NBDL
10gFRT - Y Acceleration
Acceleration (g's)
Time (ms)
F05 26YO
F05 75YO
NBDL
10gFRT - Z Acceleration
Acceleration (g's)
Time (ms)
F05 26YO
F05 75YO
NBDL
10gFRT - X Displacement
Displacement (mm)
Time (ms)
F05 26YO
F05 75YO
NBDL
10gFRT - Y Displacement
Displacement (mm)
Time (ms)
F05 26YO
F05 75YO
NBDL
10gFRT - Z Displacement
Displacement (mm)
Time (ms)
F05 26YO
F05 75YO
NBDL
10gFRT - X Rot. Accel
Rot. Accel (Deg/sec2)
Time (ms)
F05 26YO
F05 75YO
NBDL
10gFRT - Y Rot. Accel
Rot. Accel (Deg/sec2)
Time (ms)
F05 26YO
F05 75YO
NBDL

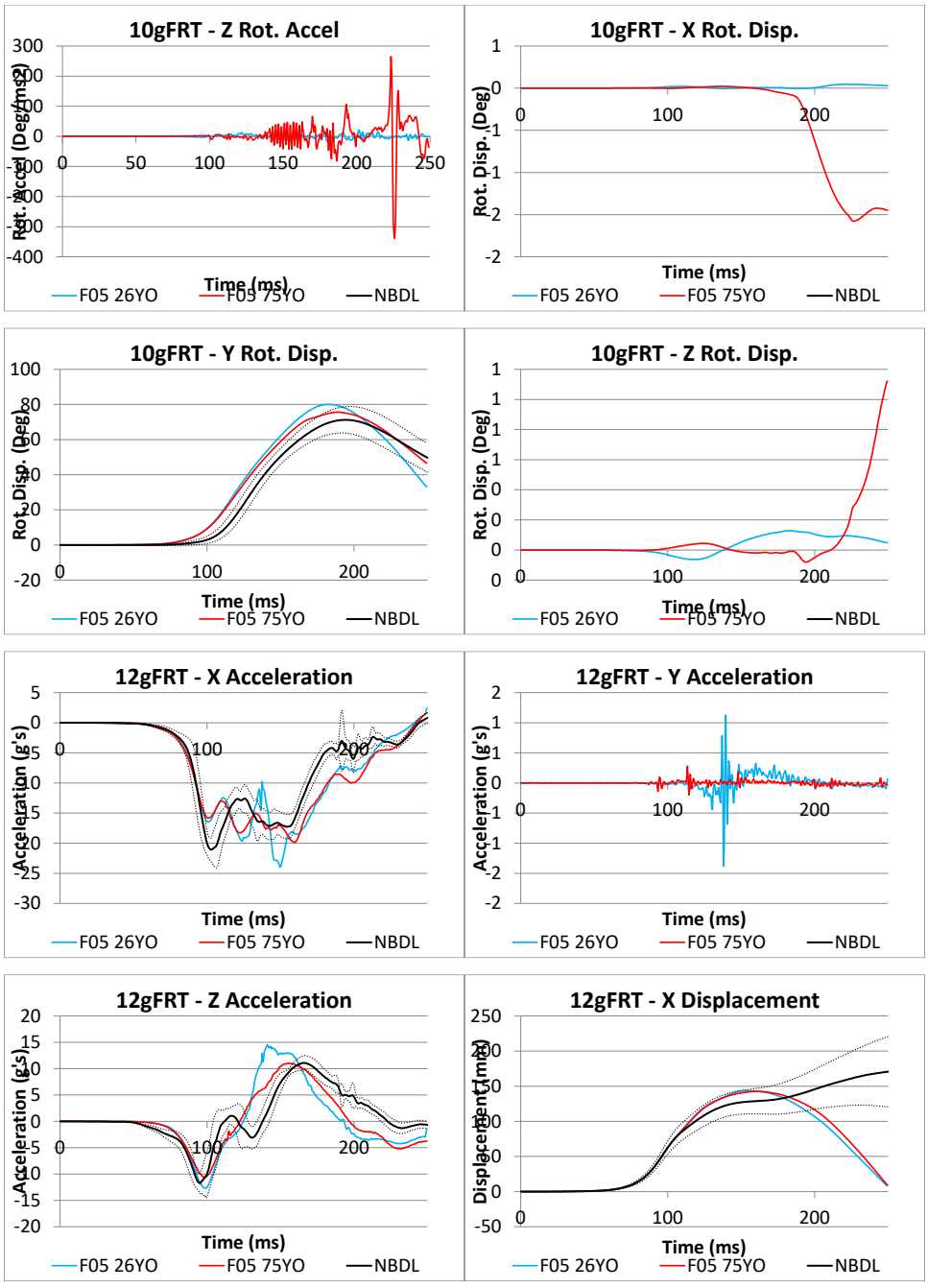
10gFRT - Z Rot. Accel
Rot. Accel (Deg/ms2)
Time (ms)
10gFRT - X Rot. Disp.
Rot. Disp. (Deg)
Time (ms)
10gFRT - Y Rot. Disp.
Rot. Disp. (Deg)
Time (ms)
10gFRT - Z Rot. Disp.
Rot. Disp. (Deg)
Time (ms)
12gFRT - X Acceleration
Acceleration (g's)
Time (ms)
12gFRT - Y Acceleration
Acceleration (g's)
Time (ms)
12gFRT - Z Acceleration
Acceleration (g's)
Time (ms)
12gFRT - X Displacement
Displacement (mm)
Time (ms)
F05 26YO
F05 75YO
NBDL

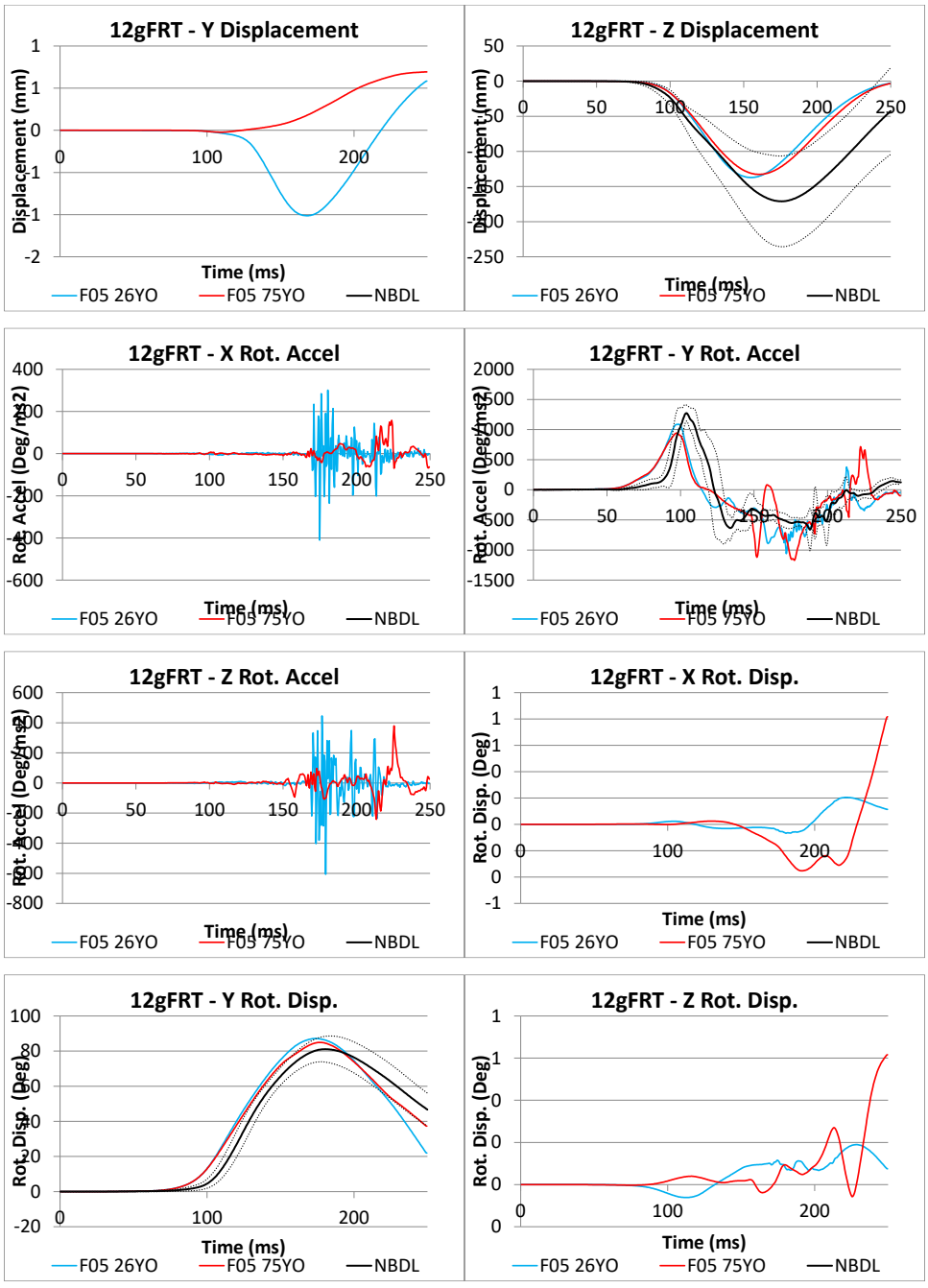
12gFRT - Y Displacement
Displacement (mm)
Time (ms)
F05 26YO
F05 75YO
NBDL
12gFRT - Z Displacement
Displacement (mm)
Time (ms)
F05 26YO
F05 75YO
NBDL
12gFRT - X Rot. Accel
Rot. Accel (Deg/ms2)
Time (ms)
F05 26YO
F05 75YO
NBDL
12gFRT - Y Rot. Accel
Rot. Accel (Deg/ms2)
Time (ms)
F05 26YO
F05 75YO
NBDL
12gFRT - Z Rot. Accel
Rot. Accel (Deg/ms2)
Time (ms)
F05 26YO
F05 75YO
NBDL
12gFRT - X Rot. Disp.
Rot. Disp. (Deg)
Time (ms)
F05 26YO
F05 75YO
NBDL
12gFRT - Y Rot. Disp.
Rot. Disp. (Deg)
Time (ms)
F05 26YO
F05 75YO
NBDL
12gFRT - Z Rot. Disp.
Rot. Disp. (Deg)
Time (ms)
F05 26YO
F05 75YO
NBDL

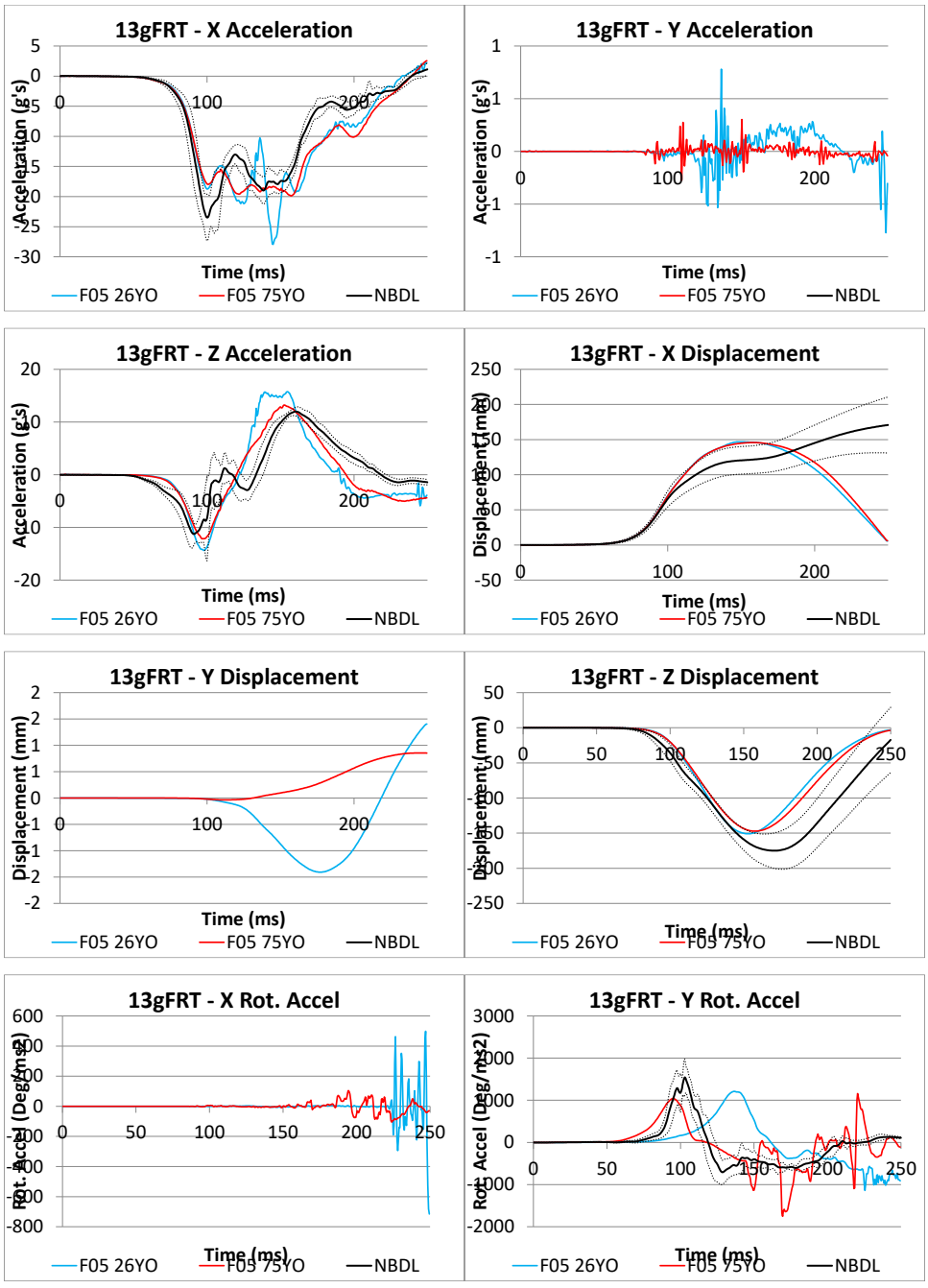
13gFRT - X Acceleration
Acceleration (g's)
Time (ms)
F05 26YO
F05 75YO
NBDL
13gFRT - Y Acceleration
Acceleration (g's)
Time (ms)
F05 26YO
F05 75YO
NBDL
13gFRT - Z Acceleration
Acceleration (g's)
Time (ms)
F05 26YO
F05 75YO
NBDL
13gFRT - X Displacement
Displacement (mm)
Time (ms)
F05 26YO
F05 75YO
NBDL
13gFRT - Y Displacement
Displacement (mm)
Time (ms)
F05 26YO
F05 75YO
NBDL
13gFRT - Z Displacement
Displacement (mm)
Time (ms)
F05 26YO
F05 75YO
NBDL
13gFRT - X Rot. Accel
Rot. Accel (Deg/(ms2)
Time (ms)
F05 26YO
F05 75YO
NBDL
13gFRT - Y Rot. Accel
Rot. Accel (Deg/(ms2)
Time (ms)
F05 26YO
F05 75YO
NBDL

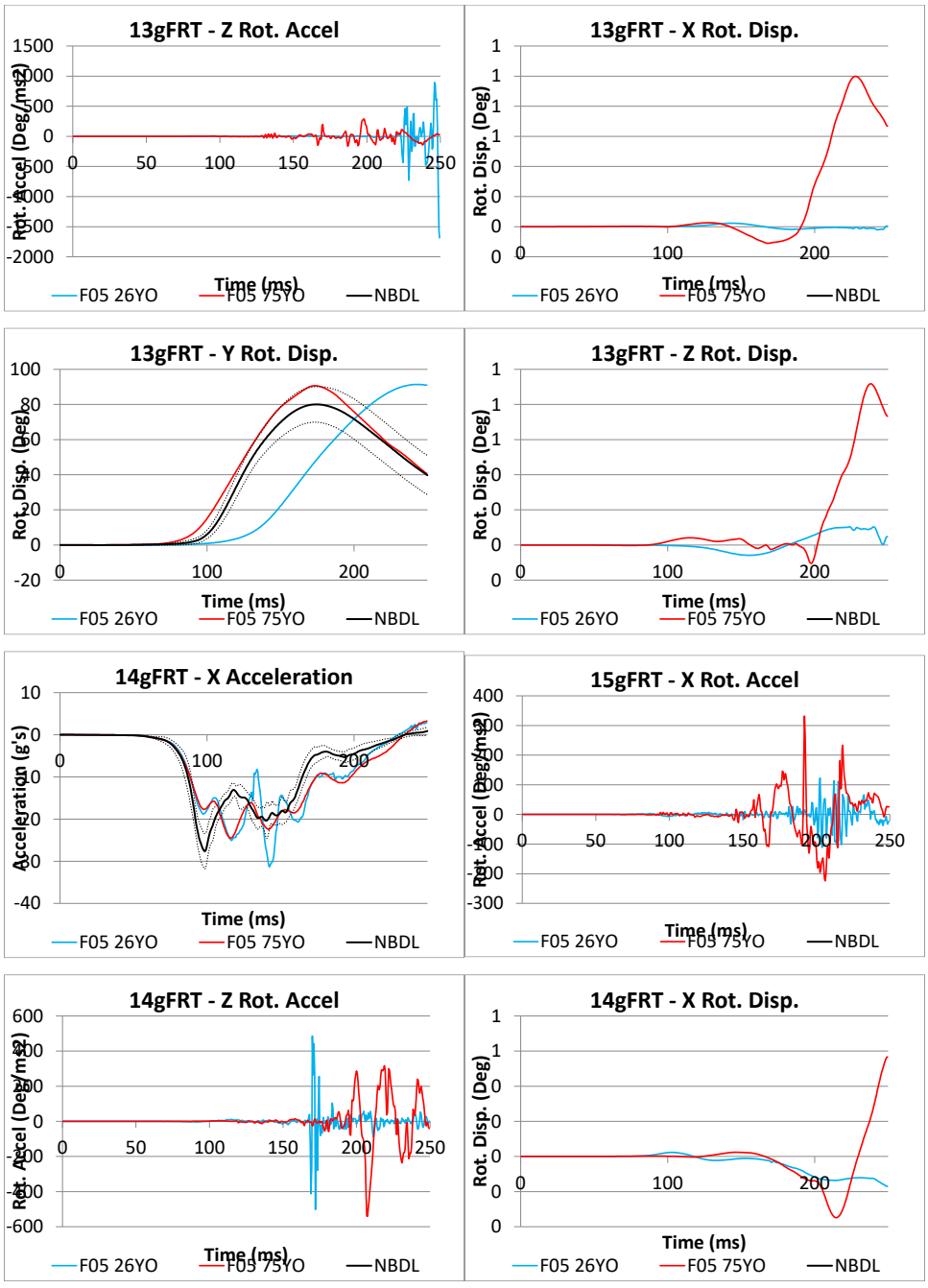
13gFRT - Z Rot. Accel
Rot. Accel (Deg/ms2)
Time (ms)
F05 26YO
F05 75YO
NBDL
13gFRT - X Rot. Disp.
Rot. Disp. (Deg)
Time (ms)
F05 26YO
F05 75YO
NBDL
13gFRT - Y Rot. Disp.
Rot. Disp. (Deg)
Time (ms)
F05 26YO
F05 75YO
NBDL
13gFRT - Z Rot. Disp.
Rot. Disp. (Deg)
Time (ms)
F05 26YO
F05 75YO
NBDL
14gFRT - X Acceleration
Acceleration (g's)
Time (ms)
F05 26YO
F05 75YO
NBDL
15gFRT - X Rot. Accel
Rot. Accel (Deg/ms2)
Time (ms)
F05 26YO
F05 75YO
NBDL
14gFRT - Z Rot. Accel
Rot. Accel (Deg/ms2)
Time (ms)
F05 26YO
F05 75YO
NBDL
14gFRT - X Rot. Disp.
Rot. Disp. (Deg)
Time (ms)
F05 26YO
F05 75YO
NBDL

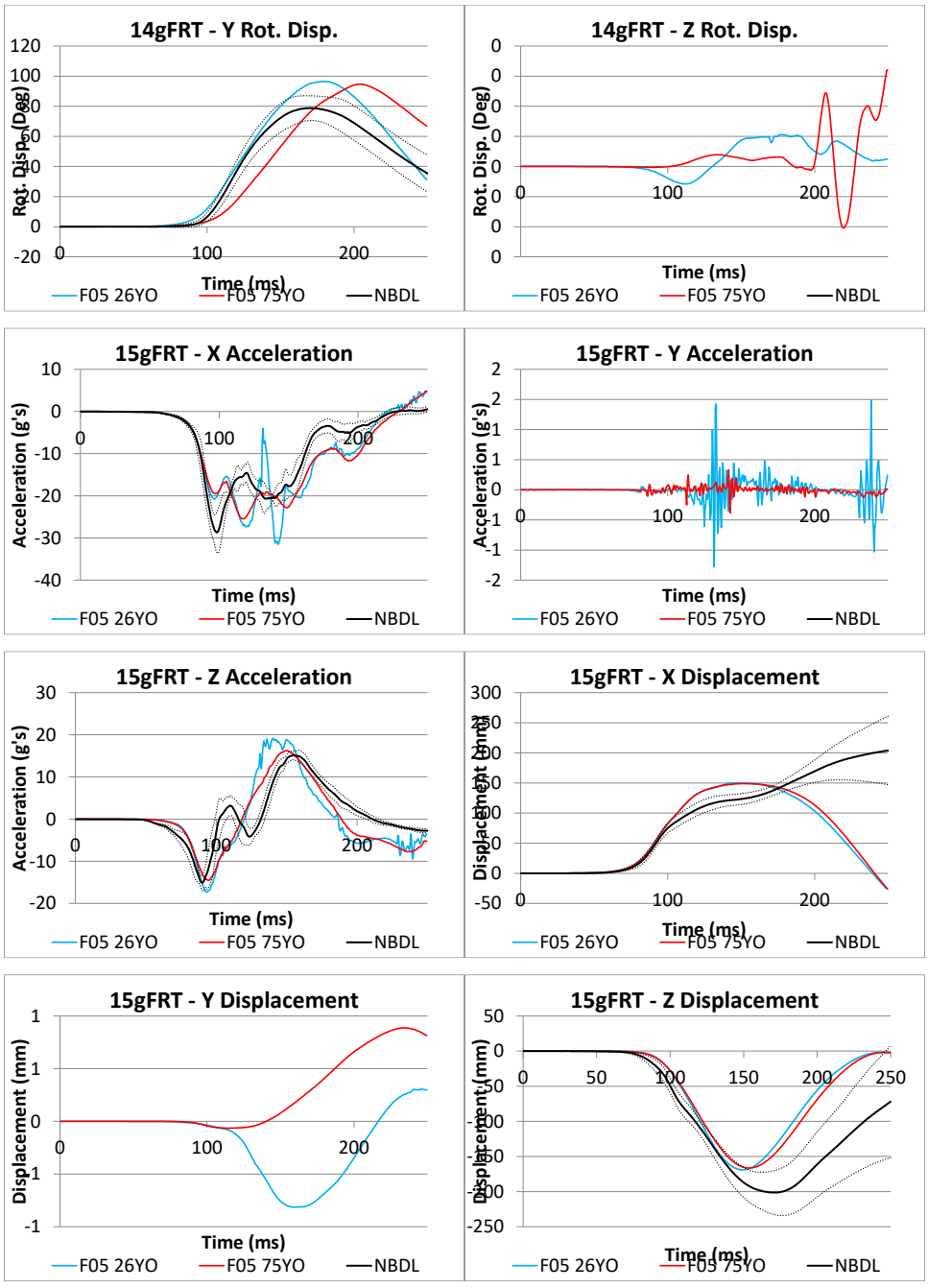
14gFRT - Y Rot. Disp.
Rot. Disp. (Deg)
Time (ms)
14gFRT - Z Rot. Disp.
Rot. Disp. (Deg)
Time (ms)
15gFRT - X Acceleration
Acceleration (g's)
Time (ms)
15gFRT - Y Acceleration
Acceleration (g's)
Time (ms)
15gFRT - Z Acceleration
Acceleration (g's)
Time (ms)
15gFRT - X Displacement
Displacement (mm)
Time (ms)
15gFRT - Y Displacement
Displacement (mm)
Time (ms)
15gFRT - Z Displacement
Displacement (mm)
Time (ms)
F05 26YO
F05 75YO
NBDL

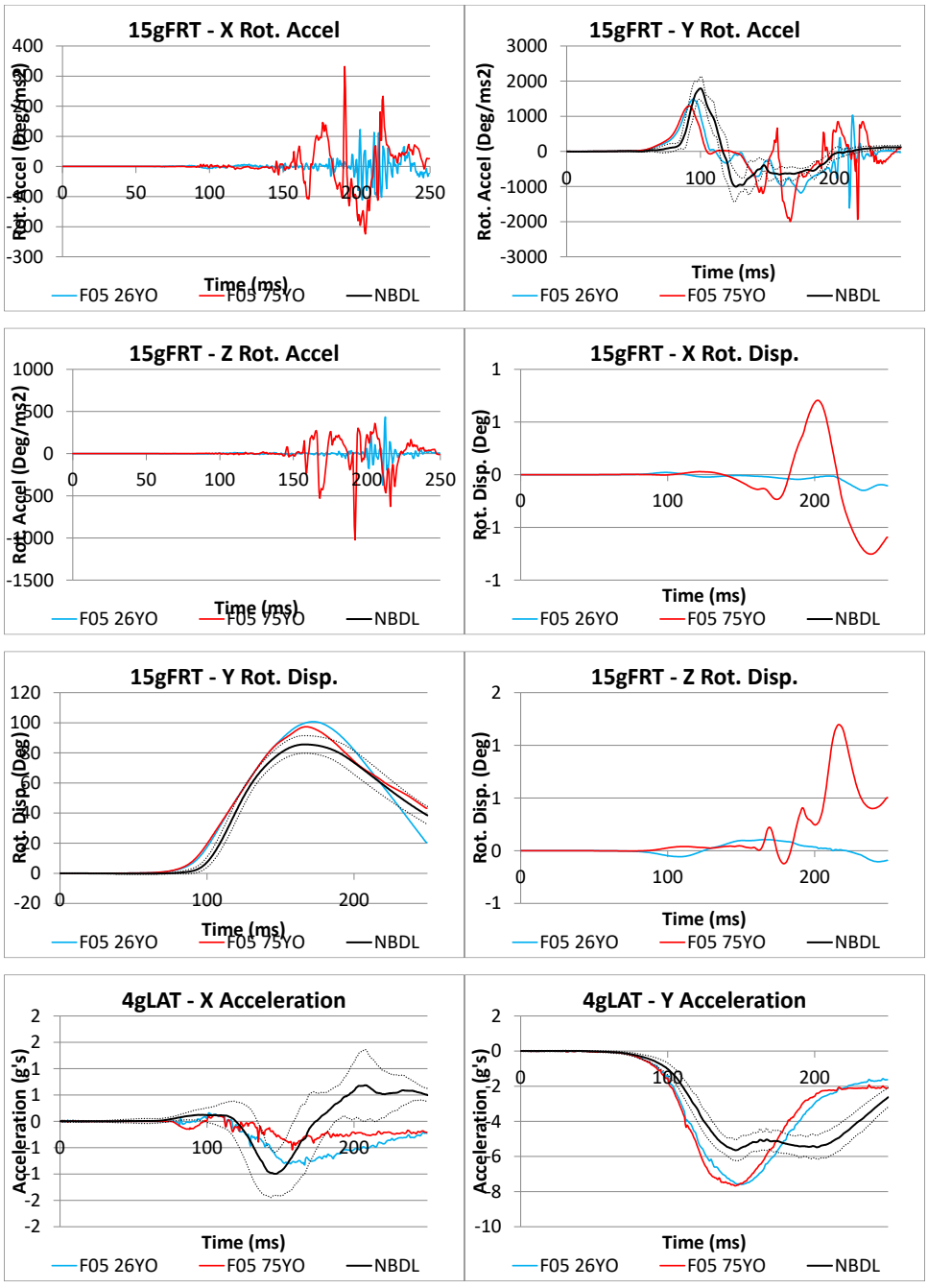
15gFRT - X Rot. Accel
Rot. Accel (Deg/ms2)
Time (ms)
F05 26YO
F05 75YO
NBDL
15gFRT - Y Rot. Accel
Rot. Accel (Deg/ms2)
Time (ms)
F05 26YO
F05 75YO
NBDL
15gFRT - Z Rot. Accel
Rot. Accel (Deg/ms2)
Time (ms)
F05 26YO
F05 75YO
NBDL
15gFRT - X Rot. Disp.
Rot. Disp. (Deg)
Time (ms)
F05 26YO
F05 75YO
NBDL
15gFRT - Y Rot. Disp.
Rot. Disp. (Deg)
Time (ms)
F05 26YO
F05 75YO
NBDL
15gFRT - Z Rot. Disp.
Rot. Disp. (Deg)
Time (ms)
F05 26YO
F05 75YO
NBDL
4gLAT - X Acceleration
Acceleration (g's)
Time (ms)
F05 26YO
F05 75YO
NBDL
4gLAT - Y Acceleration
Acceleration (g's)
Time (ms)
F05 26YO
F05 75YO
NBDL

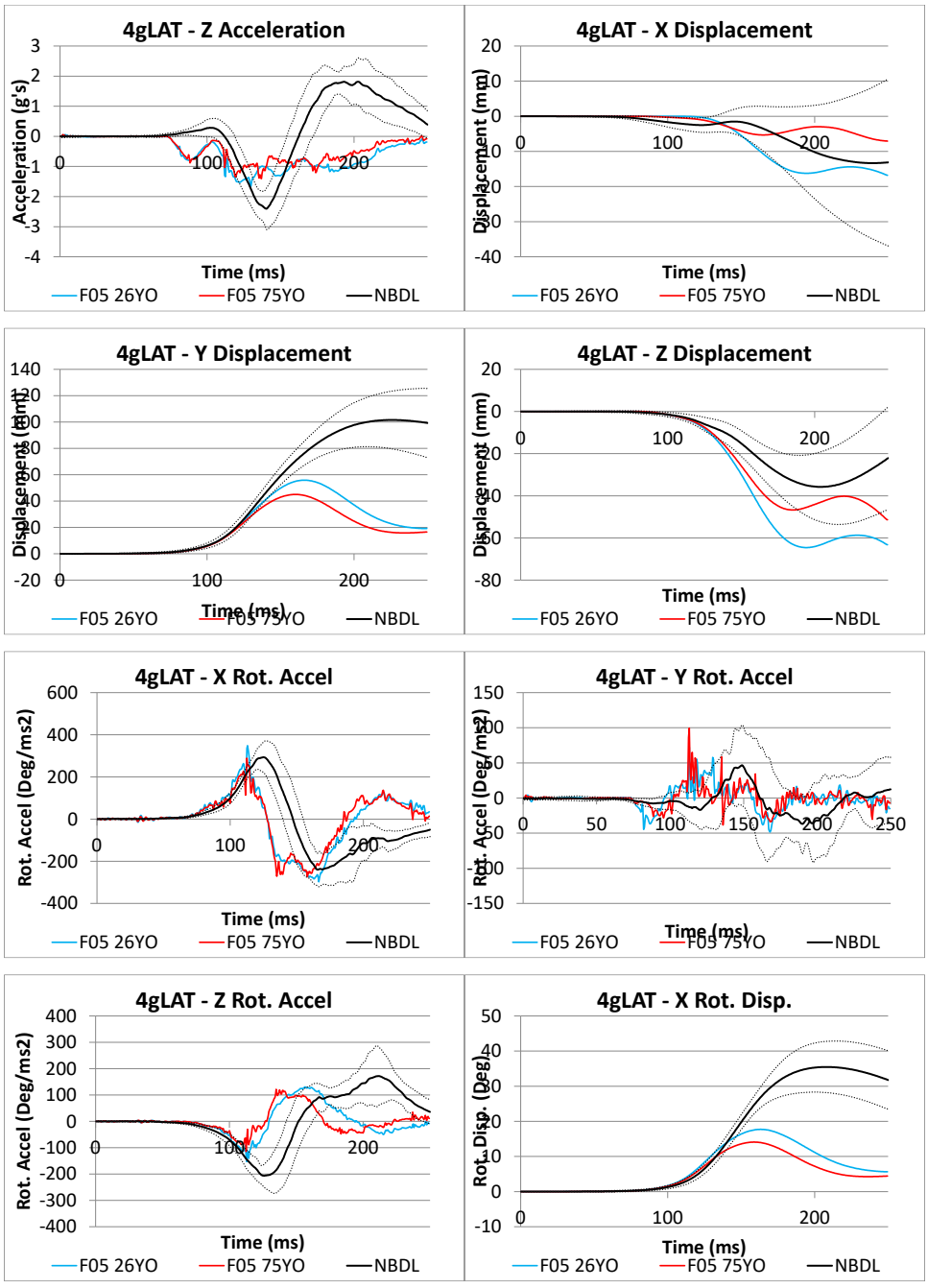
4gLAT - Z Acceleration
Acceleration (g's)
Time (ms)
4gLAT - X Displacement
Displacement (mm)
Time (ms)
4gLAT - Y Displacement
Displacement (mm)
Time (ms)
4gLAT - Z Displacement
Displacement (mm)
Time (ms)
4gLAT - X Rot. Accel
Rot. Accel (Deg/ms2)
Time (ms)
4gLAT - Y Rot. Accel
Rot. Accel (Deg/ms2)
Time (ms)
4gLAT - Z Rot. Accel
Rot. Accel (Deg/ms2)
Time (ms)
4gLAT - X Rot. Disp.
Rot. Disp. (Deg)
Time (ms)
F05 26YO
F05 75YO
NBDL

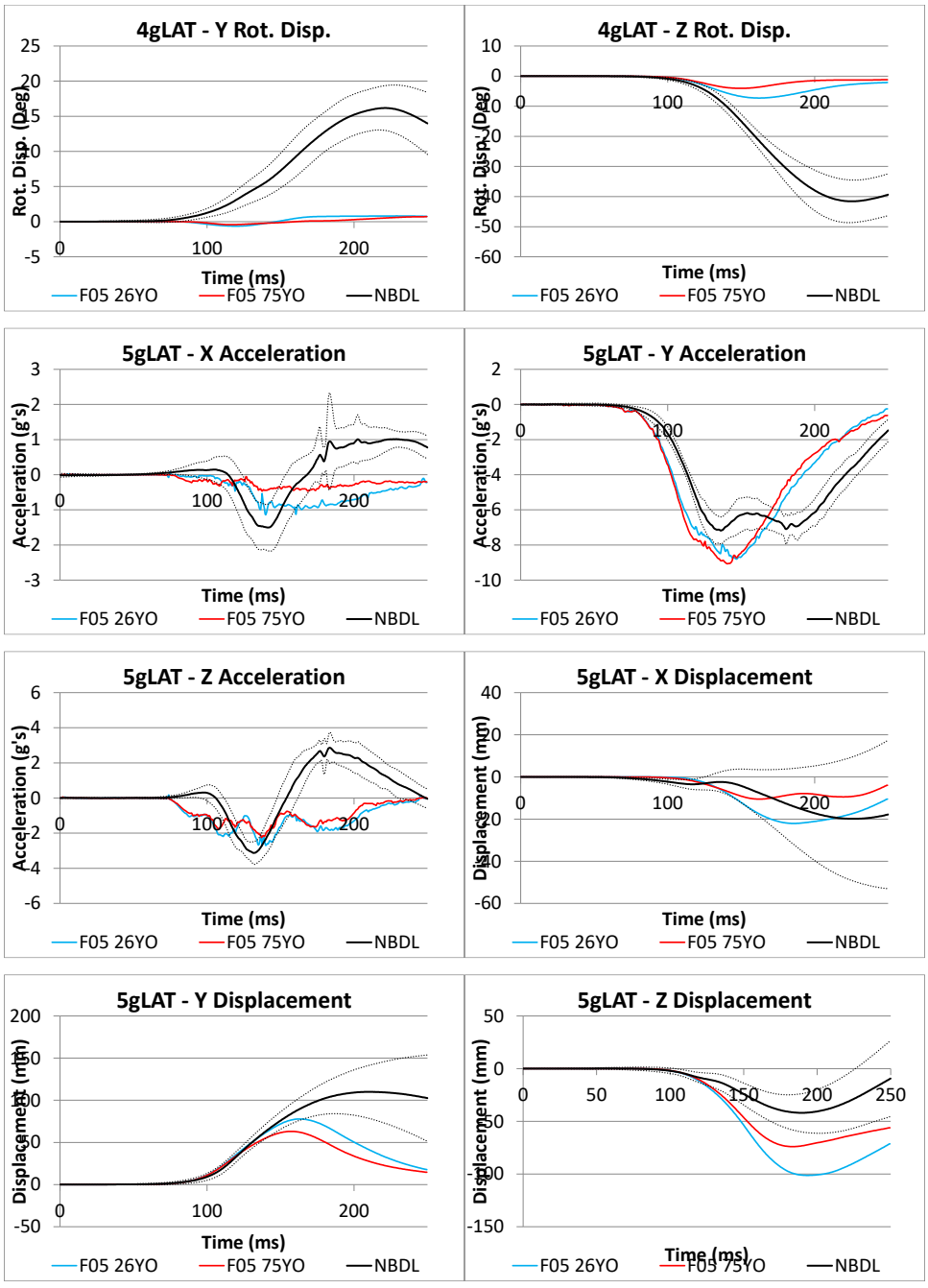
4gLAT - Y Rot. Disp.
Rot. Disp. (Deg.)
Time (ms)
F05 26YO
F05 75YO
NBDL
4gLAT - Z Rot. Disp.
Rot. Disp. (Deg.)
Time (ms)
F05 26YO
F05 75YO
NBDL
5gLAT - X Acceleration
Acceleration (g's)
Time (ms)
F05 26YO
F05 75YO
NBDL
5gLAT - Y Acceleration
Acceleration (g's)
Time (ms)
F05 26YO
F05 75YO
NBDL
5gLAT - Z Acceleration
Acceleration (g's)
Time (ms)
F05 26YO
F05 75YO
NBDL
5gLAT - X Displacement
Displacement (mm)
Time (ms)
F05 26YO
F05 75YO
NBDL
5gLAT - Y Displacement
Displacement (mm)
Time (ms)
F05 26YO
F05 75YO
NBDL
5gLAT - Z Displacement
Displacement (mm)
Time (ms)
F05 26YO
F05 75YO
NBDL

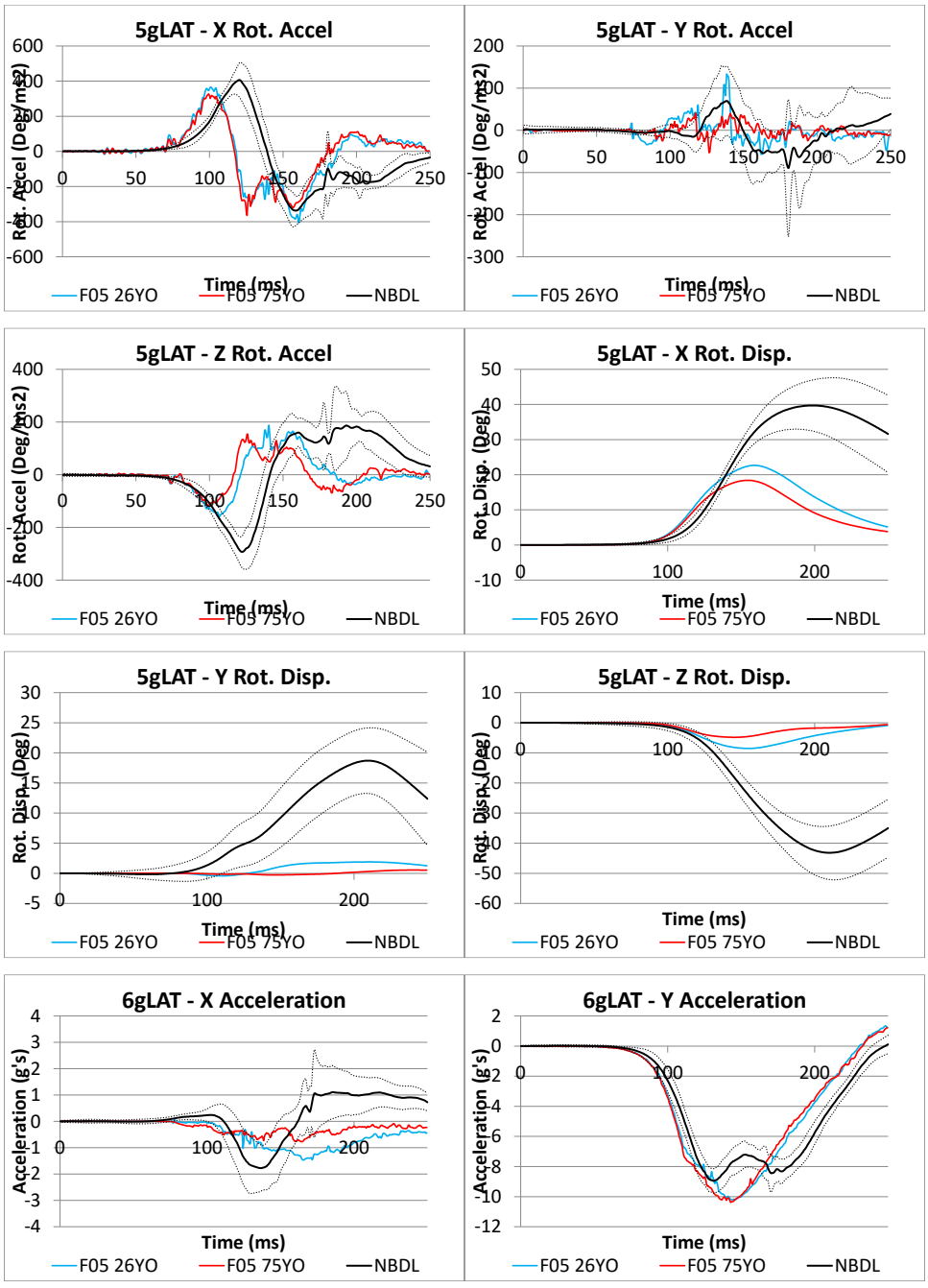
5gLAT - X Rot. Accel
Rot. Accel (Deg/ms2)
Time (ms)
F05 26YO
F05 75YO
NBDL
5gLAT - Y Rot. Accel
Rot. Accel (Deg/ms2)
Time (ms)
F05 26YO
F05 75YO
NBDL
5gLAT - Z Rot. Accel
Rot. Accel (Deg/ms2)
Time (ms)
F05 26YO
F05 75YO
NBDL
5gLAT - X Rot. Disp.
Rot. Disp. (Deg)
Time (ms)
F05 26YO
F05 75YO
NBDL
5gLAT - Y Rot. Disp.
Rot. Disp. (Deg)
Time (ms)
F05 26YO
F05 75YO
NBDL
5gLAT - Z Rot. Disp.
Rot. Disp. (Deg)
Time (ms)
F05 26YO
F05 75YO
NBDL
6gLAT - X Acceleration
Acceleration (g's)
Time (ms)
F05 26YO
F05 75YO
NBDL
6gLAT - Y Acceleration
Acceleration (g's)
Time (ms)
F05 26YO
F05 75YO
NBDL

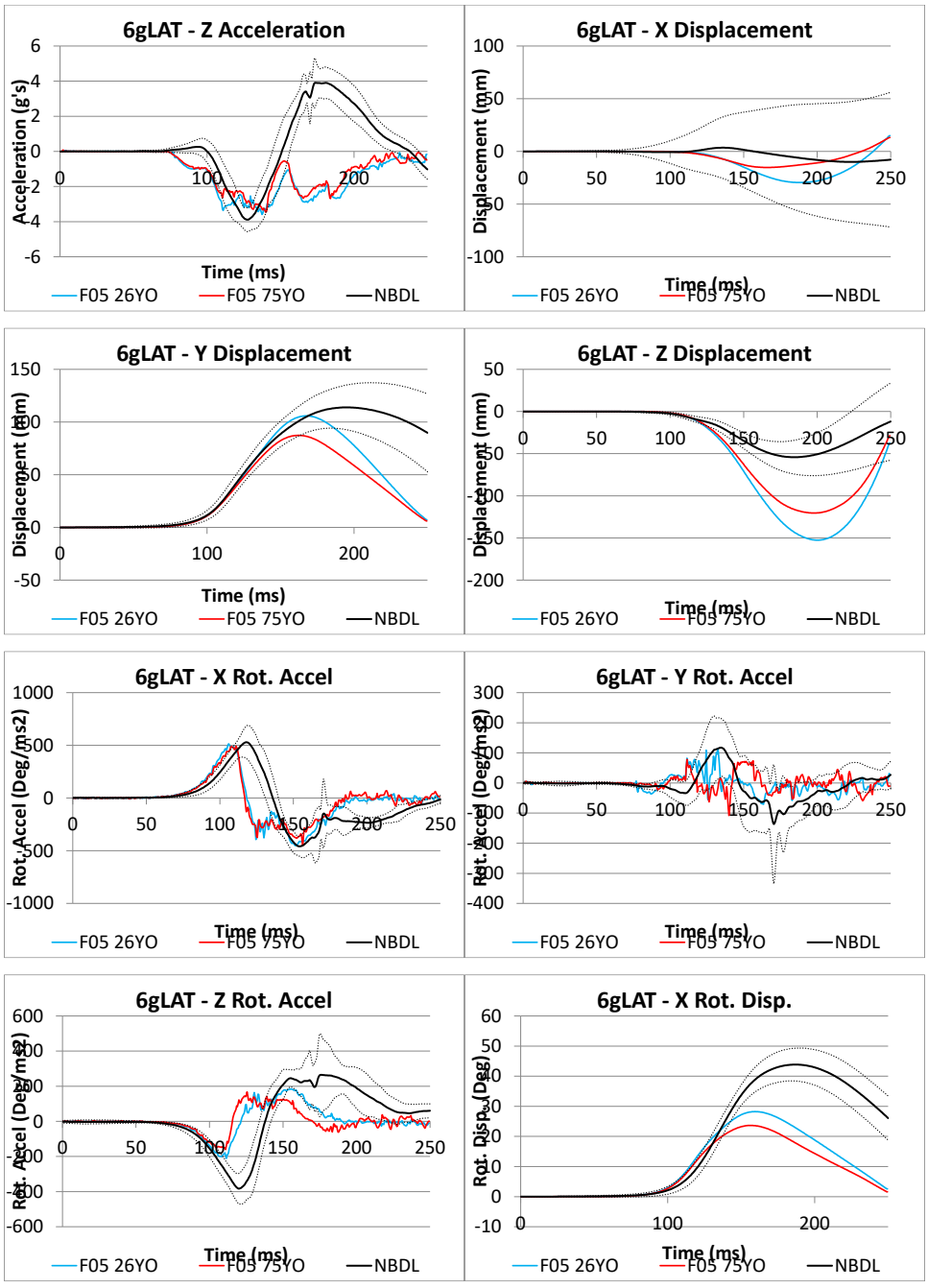
6gLAT - Z Acceleration
Acceleration (g's)
Time (ms)
6gLAT - X Displacement
Displacement (mm)
Time (ms)
6gLAT - Y Displacement
Displacement (mm)
Time (ms)
6gLAT - Z Displacement
Displacement (mm)
Time (ms)
6gLAT - X Rot. Accel
Rot. Accel (Deg/ms2)
Time (ms)
6gLAT - Y Rot. Accel
Rot. Accel (Deg/ms2)
Time (ms)
6gLAT - Z Rot. Accel
Rot. Accel (Deg/ms2)
Time (ms)
6gLAT - X Rot. Disp.
Rot. Disp. (Deg)
Time (ms)
F05 26YO
F05 75YO
NBDL

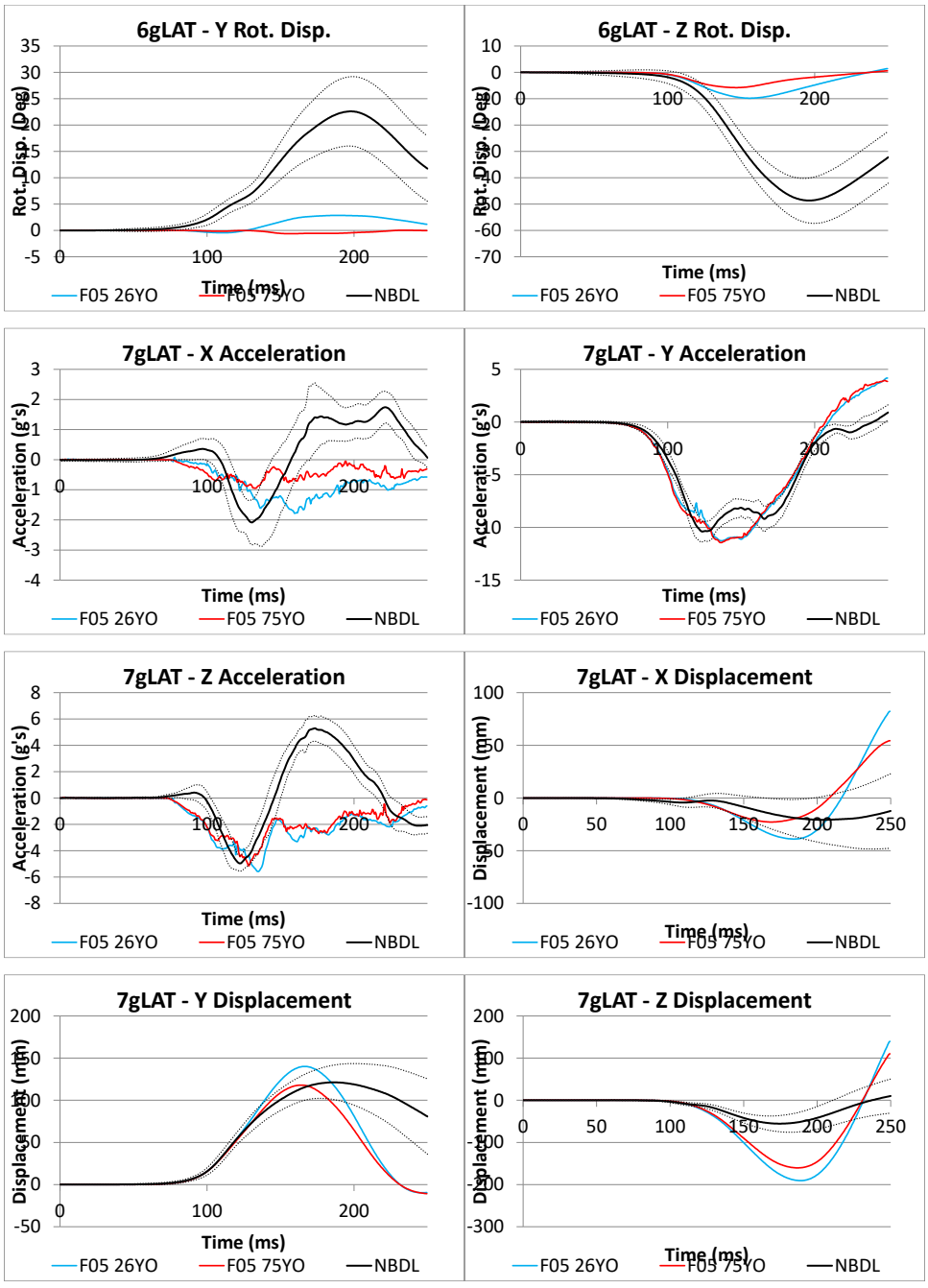
6gLAT - Y Rot. Disp.
Rot. Disp. (Deg)
Time (ms)
F05 26YO
F05 75YO
NBDL
6gLAT - Z Rot. Disp.
Rot. Disp. (Deg)
Time (ms)
F05 26YO
F05 75YO
NBDL
7gLAT - X Acceleration
Acceleration (g's)
Time (ms)
F05 26YO
F05 75YO
NBDL
7gLAT - Y Acceleration
Acceleration (g's)
Time (ms)
F05 26YO
F05 75YO
NBDL
7gLAT - Z Acceleration
Acceleration (g's)
Time (ms)
F05 26YO
F05 75YO
NBDL
7gLAT - X Displacement
Displacement (mm)
Time (ms)
F05 26YO
F05 75YO
NBDL
7gLAT - Y Displacement
Displacement (mm)
Time (ms)
F05 26YO
F05 75YO
NBDL
7gLAT - Z Displacement
Displacement (mm)
Time (ms)
F05 26YO
F05 75YO
NBDL

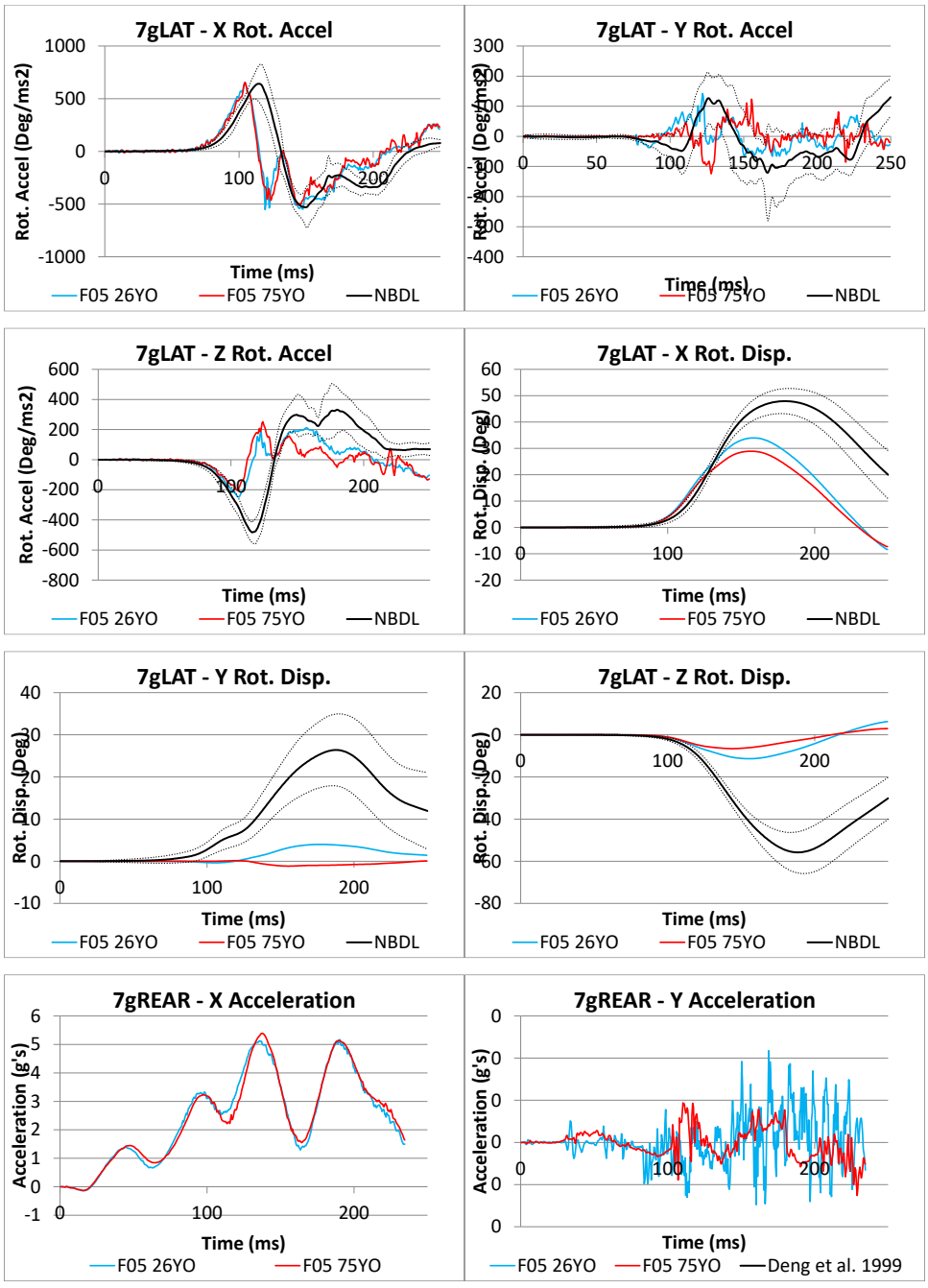
7gLAT - X Rot. Accel
Rot. Accel (Deg/ms2)
Time (ms)
F05 26YO
F05 75YO
NBDL
7gLAT - Y Rot. Accel
Rot. Accel (Deg/ms2)
Time (ms)
F05 26YO
F05 75YO
NBDL
7gLAT - Z Rot. Accel
Rot. Accel (Deg/ms2)
Time (ms)
F05 26YO
F05 75YO
NBDL
7gLAT - X Rot. Disp.
Rot. Disp. (Deg)
Time (ms)
F05 26YO
F05 75YO
NBDL
7gLAT - Y Rot. Disp.
Rot. Disp. (Deg)
Time (ms)
F05 26YO
F05 75YO
NBDL
7gLAT - Z Rot. Disp.
Rot. Disp. (Deg)
Time (ms)
F05 26YO
F05 75YO
NBDL
7gREAR - X Acceleration
Acceleration (g's)
Time (ms)
F05 26YO
F05 75YO
7gREAR - Y Acceleration
Acceleration (g's)
Time (ms)
F05 26YO
F05 75YO
Deng et al. 1999

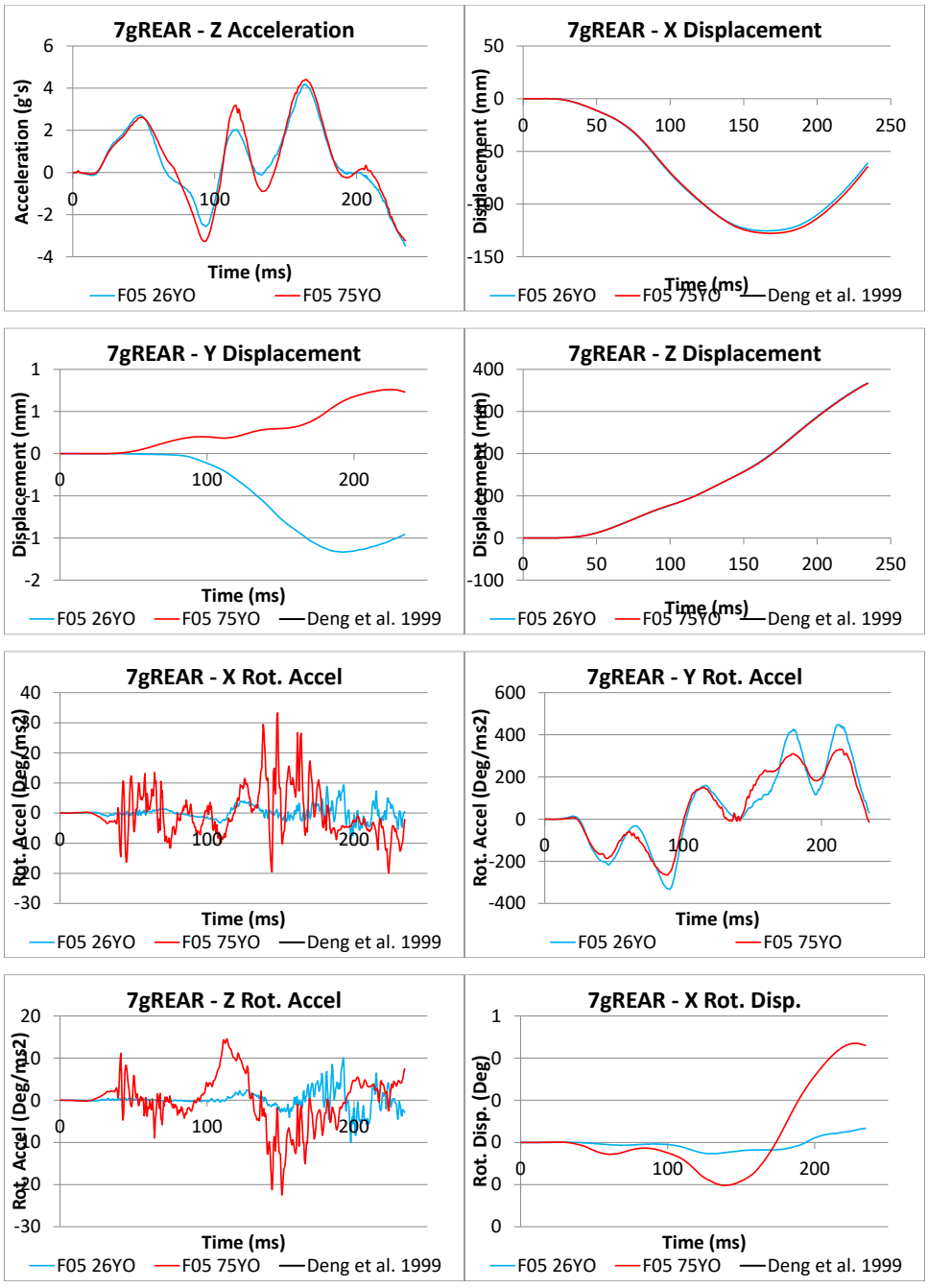
7gREAR - Z Acceleration
Acceleration (g's)
Time (ms)
F05 26YO
F05 75YO
7gREAR - X Displacement
Displacement (mm)
Time (ms)
F05 26YO
F05 75YO
Deng et al. 1999
7gREAR - Y Displacement
Displacement (mm)
Time (ms)
F05 26YO
F05 75YO
Deng et al. 1999
7gREAR - Z Displacement
Displacement (mm)
Time (ms)
F05 26YO
F05 75YO
Deng et al. 1999
7gREAR - X Rot. Accel
Rot. Accel (Deg/ms2)
Time (ms)
F05 26YO
F05 75YO
Deng et al. 1999
7gREAR - Y Rot. Accel
Rot. Accel (Deg/ms2)
Time (ms)
F05 26YO
F05 75YO
7gREAR - Z Rot. Accel
Rot. Accel (Deg/ms2)
Time (ms)
F05 26YO
F05 75YO
Deng et al. 1999
7gREAR - X Rot. Disp.
Rot. Disp. (Deg)
Time (ms)
F05 26YO
F05 75YO
Deng et al. 1999

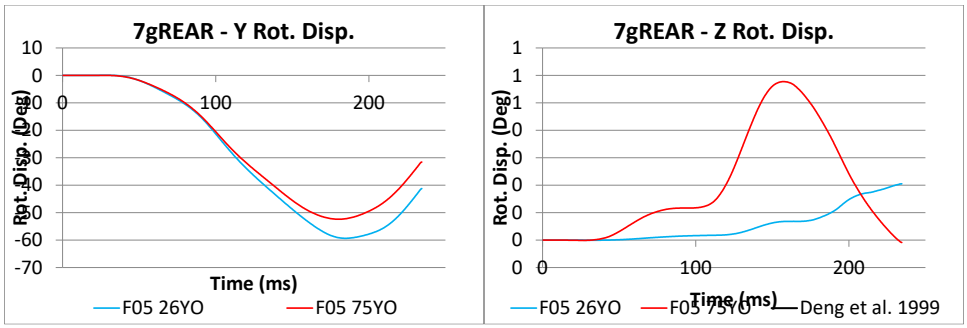
7gREAR - Y Rot. Disp.
Rot. Disp. (Deg)
Time (ms)
F05 26YO
F05 75YO

7gREAR - Z Rot. Disp.
Rot. Disp. (Deg)
Time (ms)
F05 26YO
F05 75YO
Deng et al. 1999

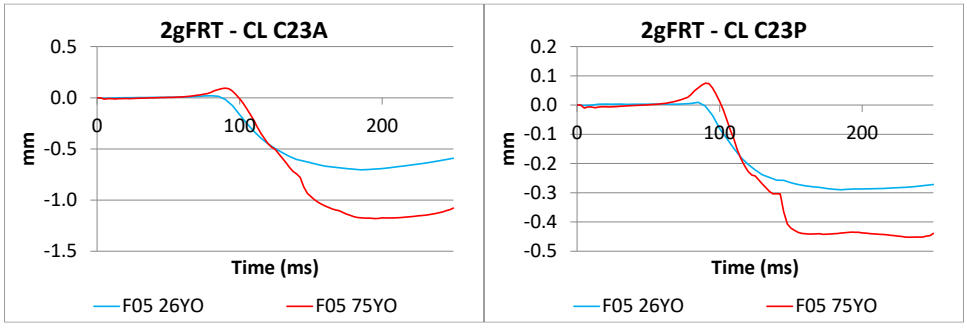
2gFRT - CL C23A
mm
Time (ms)
F05 26YO
F05 75YO

2gFRT - CL C23P
mm
Time (ms)
F05 26YO
F05 75YO

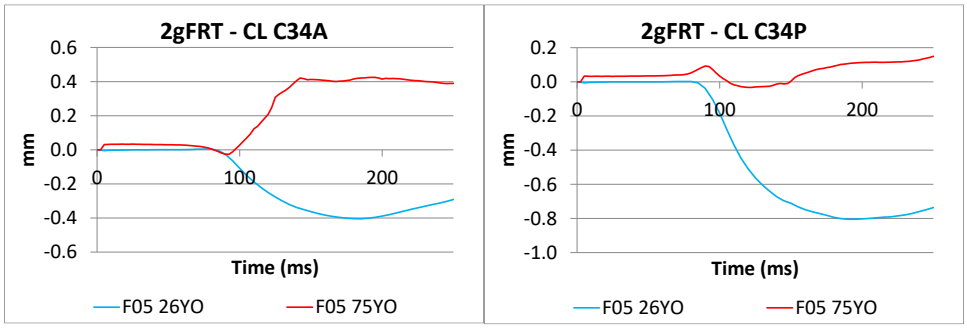
2gFRT - CL C34A
mm
Time (ms)
F05 26YO
F05 75YO

2gFRT - CL C34P
mm
Time (ms)
F05 26YO
F05 75YO

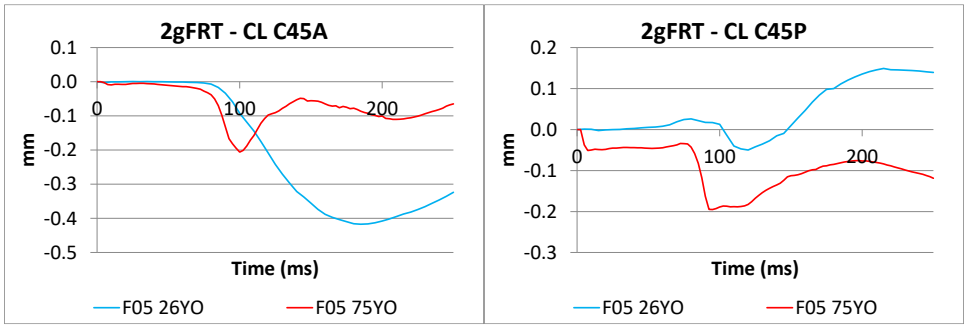
2gFRT - CL C45A
mm
Time (ms)
F05 26YO
F05 75YO

2gFRT - CL C45P
mm
Time (ms)
F05 26YO
F05 75YO

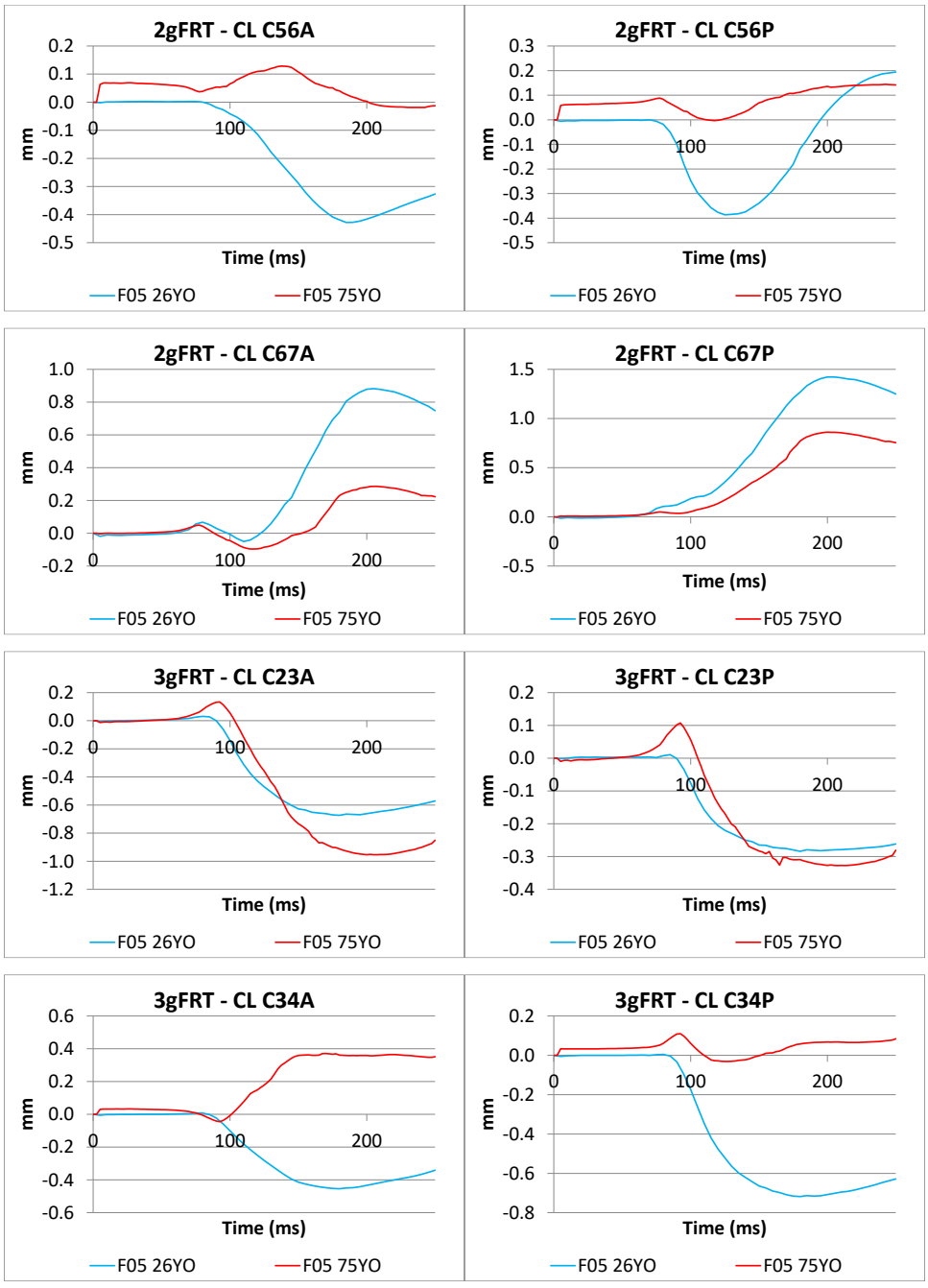
2gFRT - CL C56A
mm
Time (ms)
F05 26YO
F05 75YO
2gFRT - CL C56P
mm
Time (ms)
F05 26YO
F05 75YO
2gFRT - CL C67A
mm
Time (ms)
F05 26YO
F05 75YO
2gFRT - CL C67P
mm
Time (ms)
F05 26YO
F05 75YO
3gFRT - CL C23A
mm
Time (ms)
F05 26YO
F05 75YO
3gFRT - CL C23P
mm
Time (ms)
F05 26YO
F05 75YO
3gFRT - CL C34A
mm
Time (ms)
F05 26YO
F05 75YO
3gFRT - CL C34P
mm
Time (ms)
F05 26YO
F05 75YO

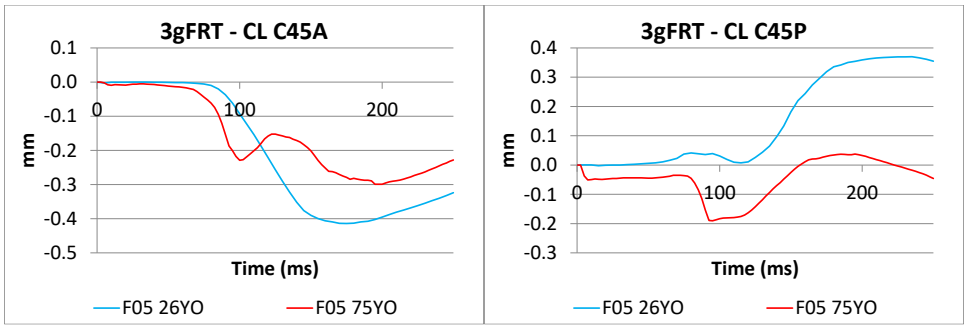
3gFRT - CL C45A
mm
Time (ms)
F05 26YO
F05 75YO

3gFRT - CL C45P
mm
Time (ms)
F05 26YO
F05 75YO

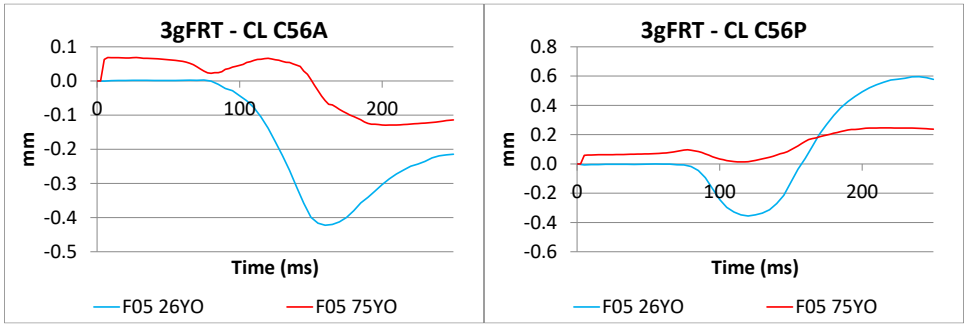
3gFRT - CL C56A
mm
Time (ms)
F05 26YO
F05 75YO

3gFRT - CL C56P
mm
Time (ms)
F05 26YO
F05 75YO

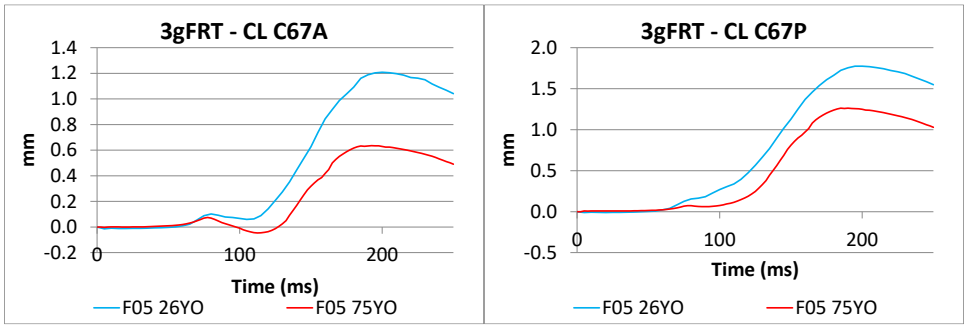
3gFRT - CL C67A
mm
Time (ms)
F05 26YO
F05 75YO

3gFRT - CL C67P
mm
Time (ms)
F05 26YO
F05 75YO

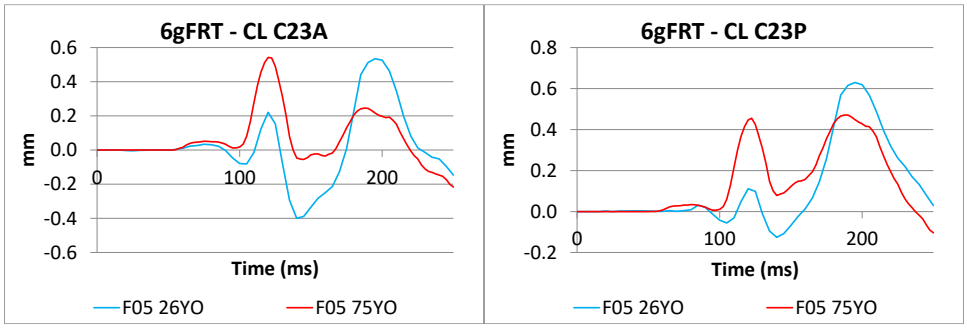
6gFRT - CL C23A
mm
Time (ms)
F05 26YO
F05 75YO

6gFRT - CL C23P
mm
Time (ms)
F05 26YO
F05 75YO

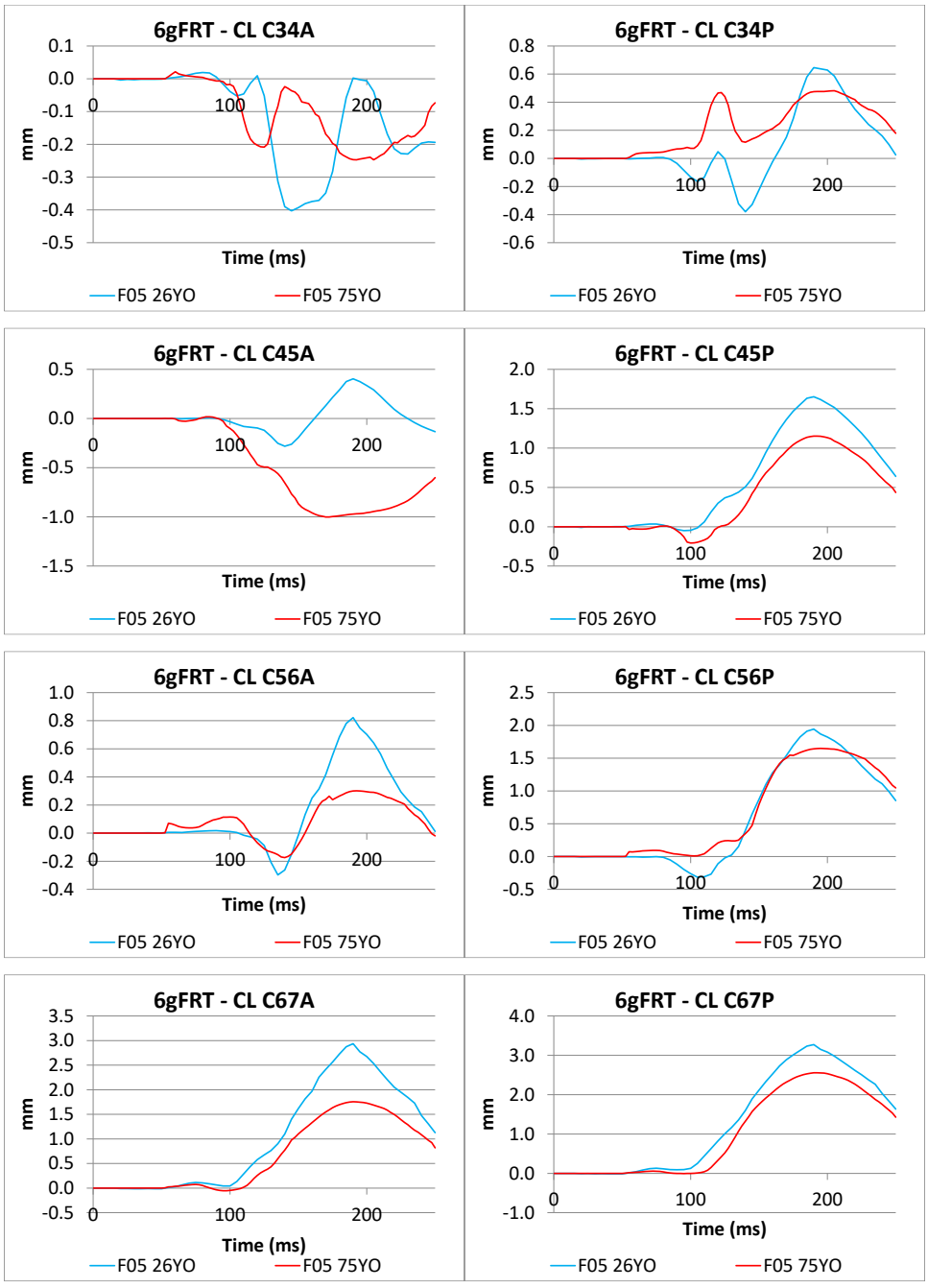
6gFRT - CL C34A
mm
Time (ms)
F05 26YO
F05 75YO
6gFRT - CL C34P
mm
Time (ms)
F05 26YO
F05 75YO
6gFRT - CL C45A
mm
Time (ms)
F05 26YO
F05 75YO
6gFRT - CL C45P
mm
Time (ms)
F05 26YO
F05 75YO
6gFRT - CL C56A
mm
Time (ms)
F05 26YO
F05 75YO
6gFRT - CL C56P
mm
Time (ms)
F05 26YO
F05 75YO
6gFRT - CL C67A
mm
Time (ms)
F05 26YO
F05 75YO
6gFRT - CL C67P
mm
Time (ms)
F05 26YO
F05 75YO

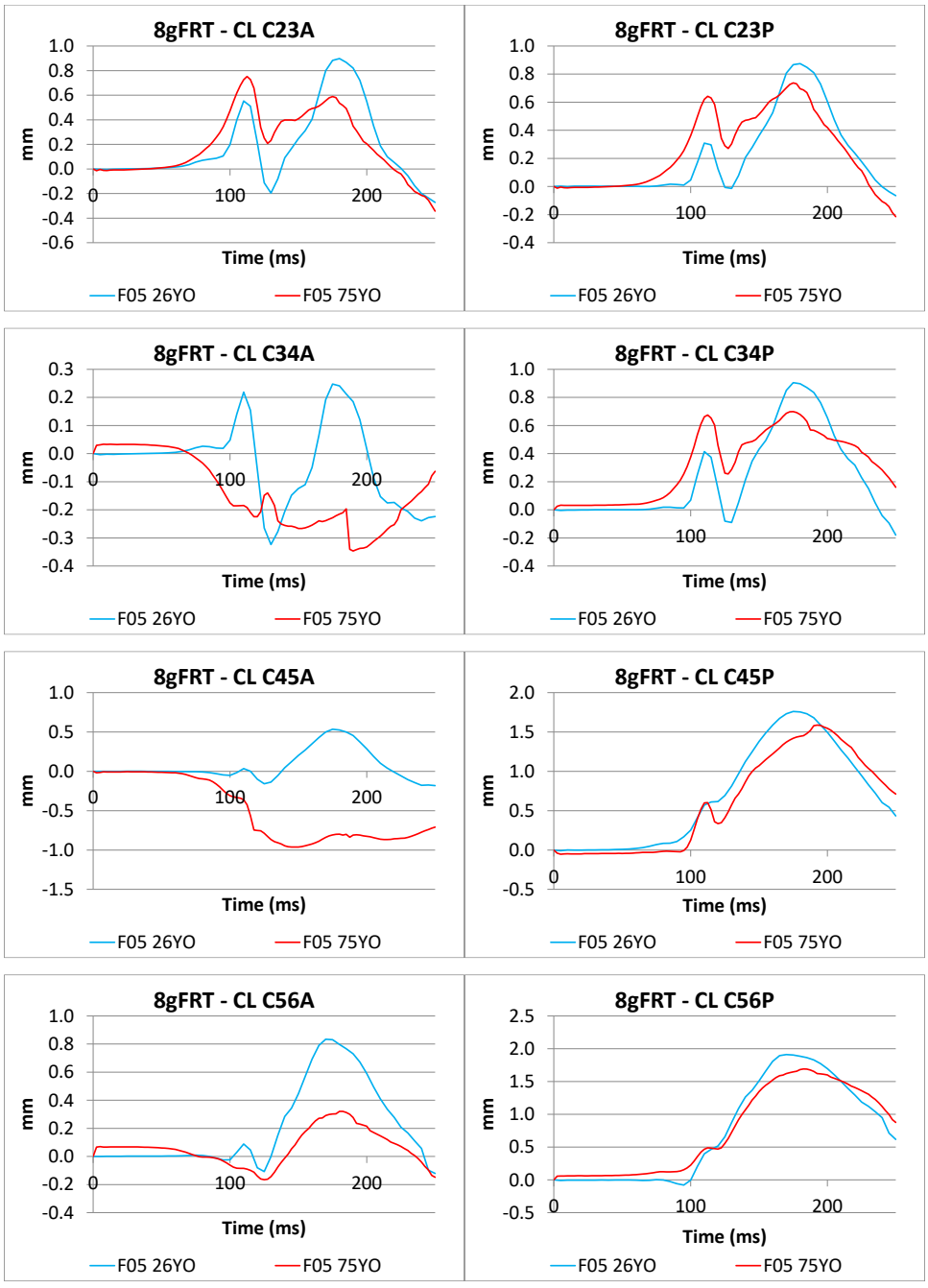
8gFRT - CL C23A
mm
Time (ms)
F05 26YO
F05 75YO
8gFRT - CL C23P
mm
Time (ms)
F05 26YO
F05 75YO
8gFRT - CL C34A
mm
Time (ms)
F05 26YO
F05 75YO
8gFRT - CL C34P
mm
Time (ms)
F05 26YO
F05 75YO
8gFRT - CL C45A
mm
Time (ms)
F05 26YO
F05 75YO
8gFRT - CL C45P
mm
Time (ms)
F05 26YO
F05 75YO
8gFRT - CL C56A
mm
Time (ms)
F05 26YO
F05 75YO
8gFRT - CL C56P
mm
Time (ms)
F05 26YO
F05 75YO

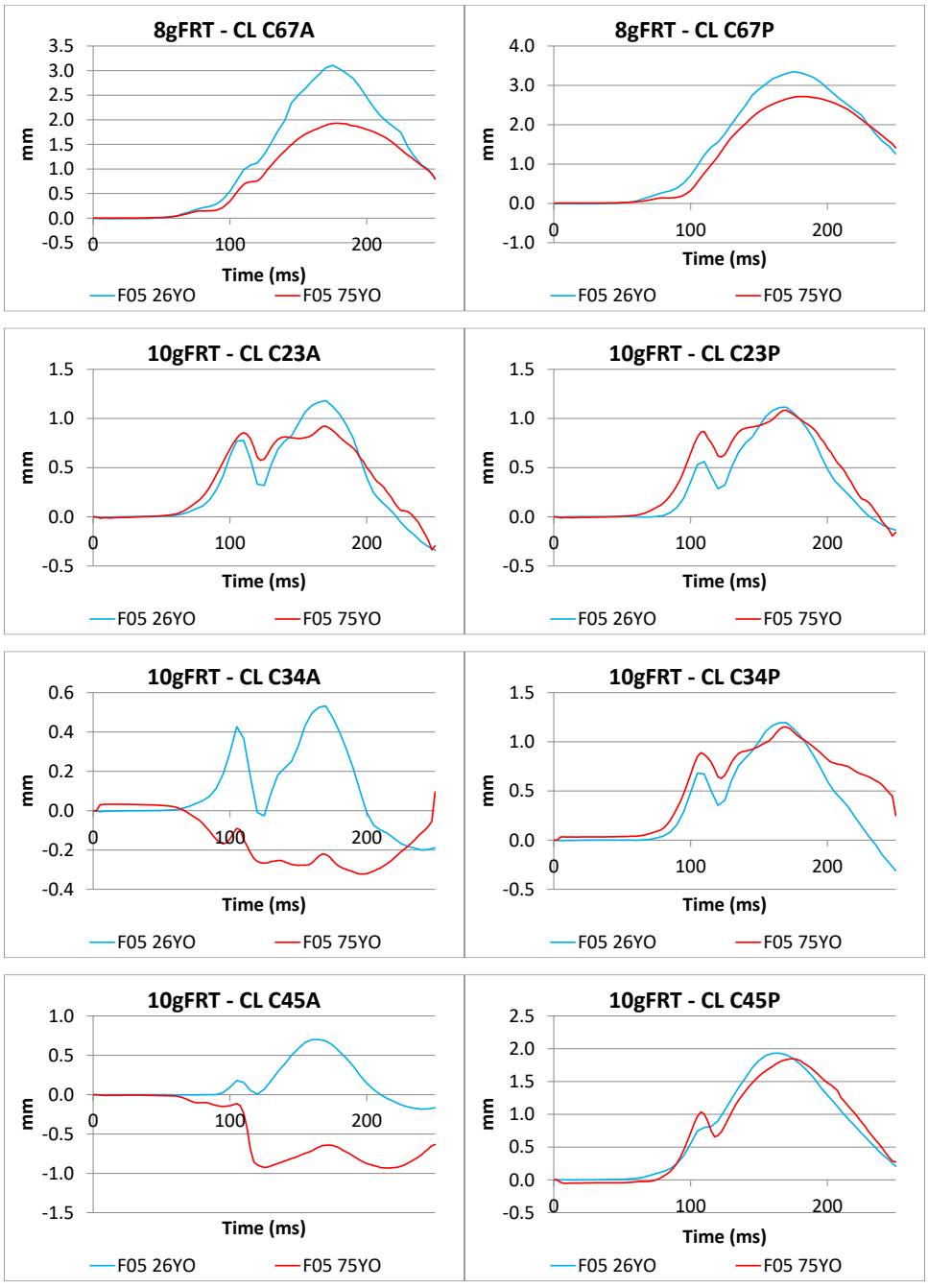
8gFRT - CL C67A
mm
Time (ms)
F05 26YO
F05 75YO
8gFRT - CL C67P
mm
Time (ms)
F05 26YO
F05 75YO
10gFRT - CL C23A
mm
Time (ms)
F05 26YO
F05 75YO
10gFRT - CL C23P
mm
Time (ms)
F05 26YO
F05 75YO
10gFRT - CL C34A
mm
Time (ms)
F05 26YO
F05 75YO
10gFRT - CL C34P
mm
Time (ms)
F05 26YO
F05 75YO
10gFRT - CL C45A
mm
Time (ms)
F05 26YO
F05 75YO
10gFRT - CL C45P
mm
Time (ms)
F05 26YO
F05 75YO

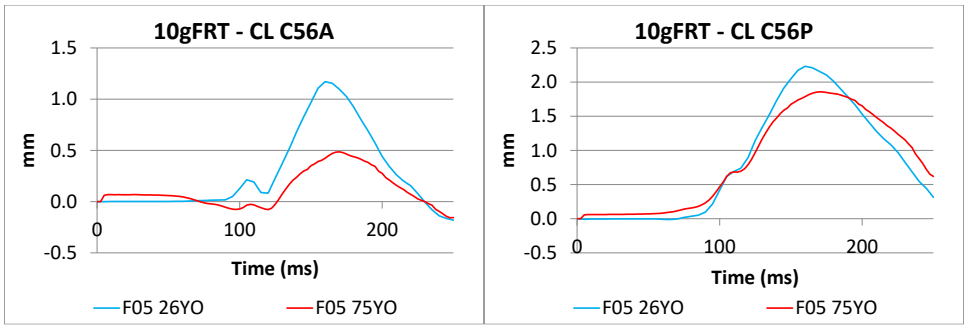
10gFRT - CL C56A
mm
Time (ms)
F05 26YO
F05 75YO

10gFRT - CL C56P
mm
Time (ms)
F05 26YO
F05 75YO

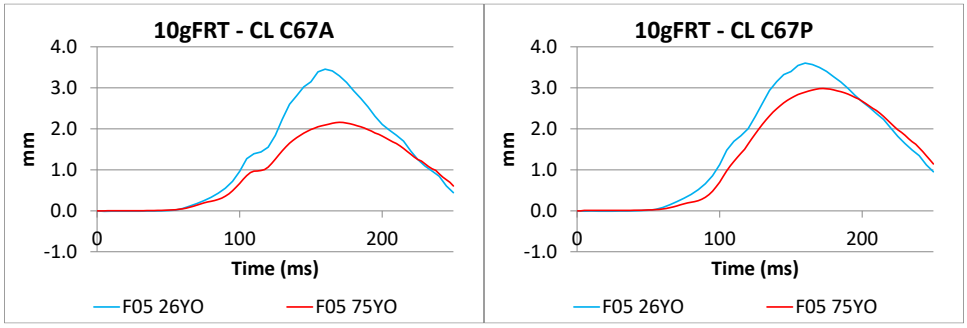
10gFRT - CL C67A
mm
Time (ms)
F05 26YO
F05 75YO

10gFRT - CL C67P
mm
Time (ms)
F05 26YO
F05 75YO

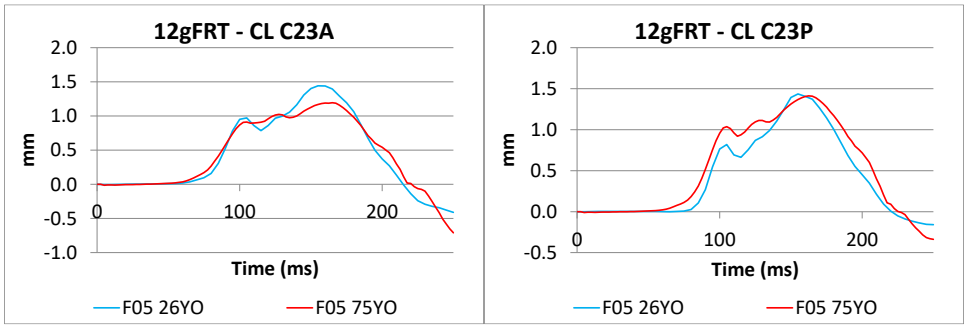
12gFRT - CL C23A
mm
Time (ms)
F05 26YO
F05 75YO

12gFRT - CL C23P
mm
Time (ms)
F05 26YO
F05 75YO

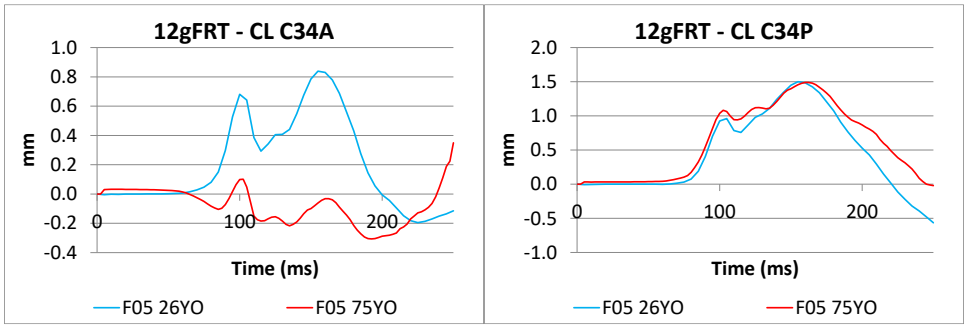
12gFRT - CL C34A
mm
Time (ms)
F05 26YO
F05 75YO

12gFRT - CL C34P
mm
Time (ms)
F05 26YO
F05 75YO

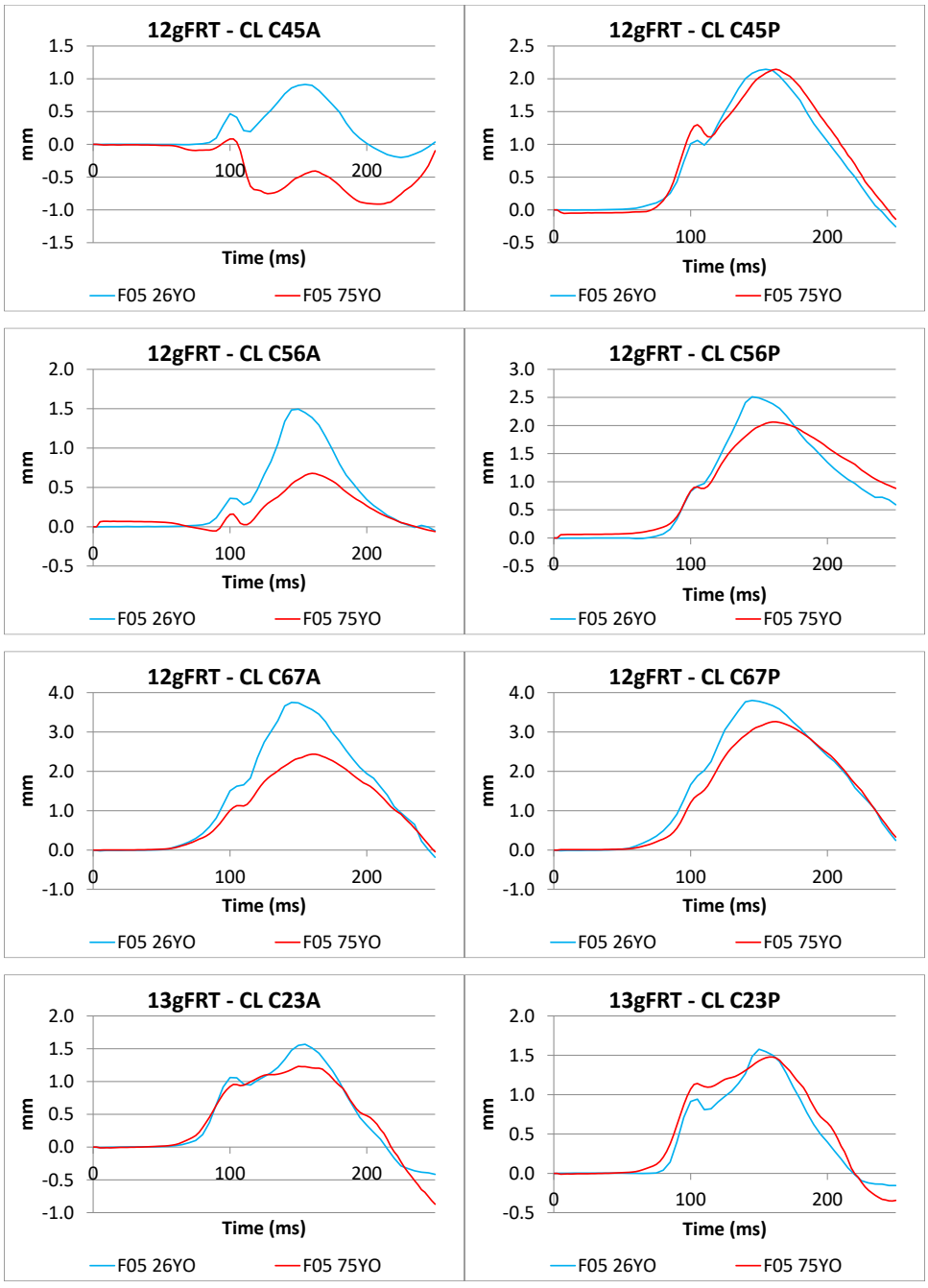
12gFRT - CL C45A
mm
Time (ms)
F05 26YO
F05 75YO
12gFRT - CL C45P
mm
Time (ms)
F05 26YO
F05 75YO
12gFRT - CL C56A
mm
Time (ms)
F05 26YO
F05 75YO
12gFRT - CL C56P
mm
Time (ms)
F05 26YO
F05 75YO
12gFRT - CL C67A
mm
Time (ms)
F05 26YO
F05 75YO
12gFRT - CL C67P
mm
Time (ms)
F05 26YO
F05 75YO
13gFRT - CL C23A
mm
Time (ms)
F05 26YO
F05 75YO
13gFRT - CL C23P
mm
Time (ms)
F05 26YO
F05 75YO

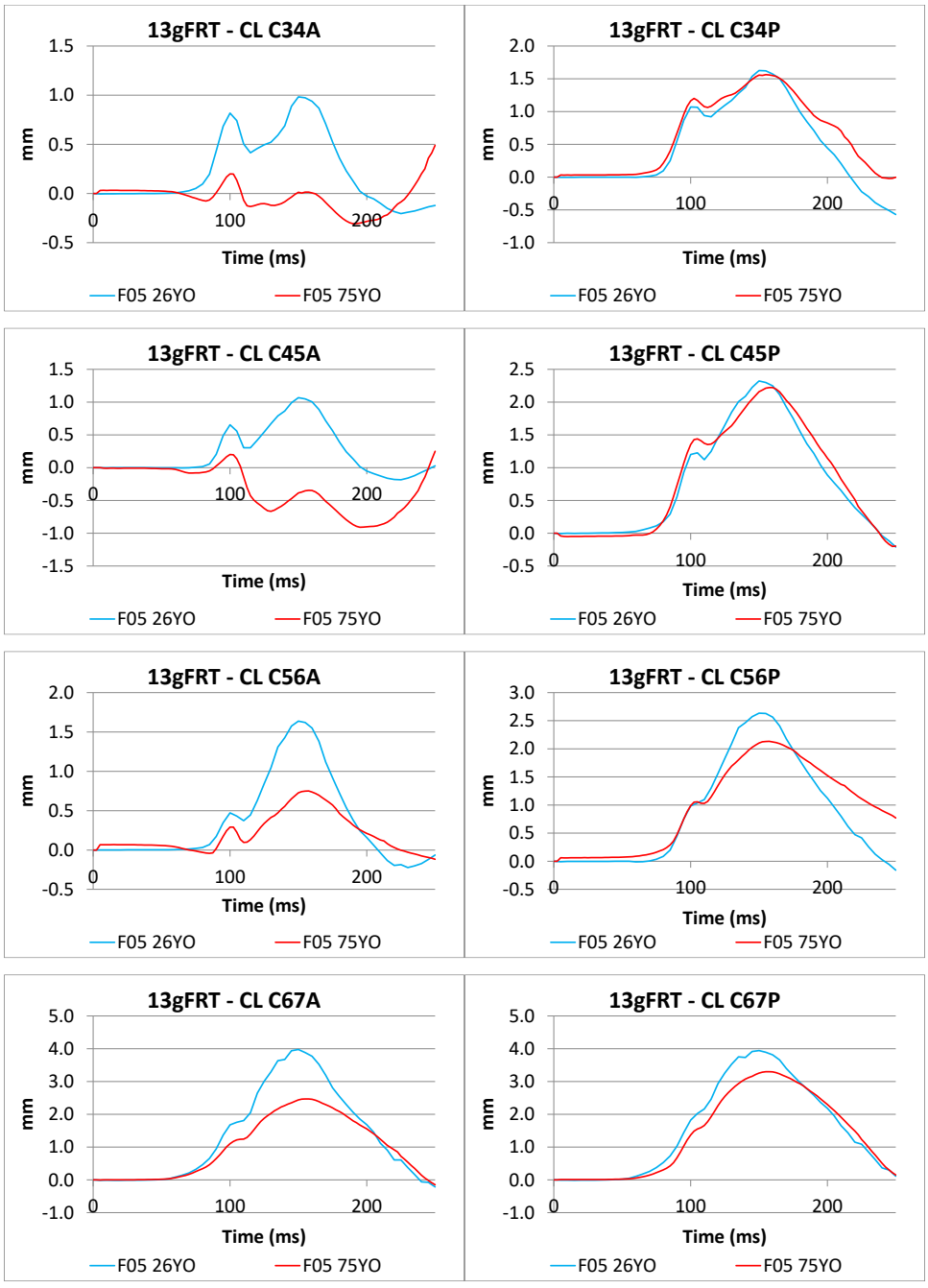
13gFRT - CL C34A
mm
Time (ms)
F05 26YO
F05 75YO
13gFRT - CL C34P
mm
Time (ms)
F05 26YO
F05 75YO
13gFRT - CL C45A
mm
Time (ms)
F05 26YO
F05 75YO
13gFRT - CL C45P
mm
Time (ms)
F05 26YO
F05 75YO
13gFRT - CL C56A
mm
Time (ms)
F05 26YO
F05 75YO
13gFRT - CL C56P
mm
Time (ms)
F05 26YO
F05 75YO
13gFRT - CL C67A
mm
Time (ms)
F05 26YO
F05 75YO
13gFRT - CL C67P
mm
Time (ms)
F05 26YO
F05 75YO

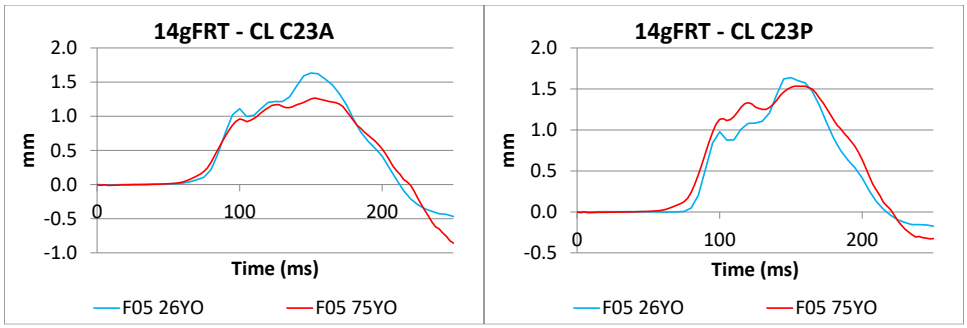
14gFRT - CL C23A
mm
Time (ms)
F05 26YO
F05 75YO

14gFRT - CL C23P
mm
Time (ms)
F05 26YO
F05 75YO

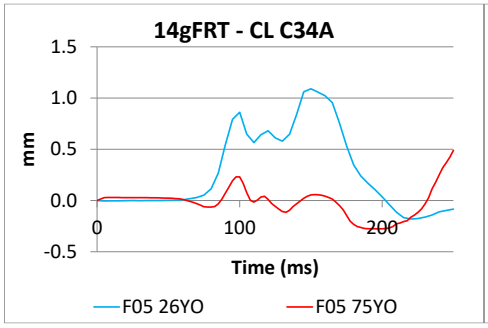
14gFRT - CL C34A
mm
Time (ms)
F05 26YO
F05 75YO

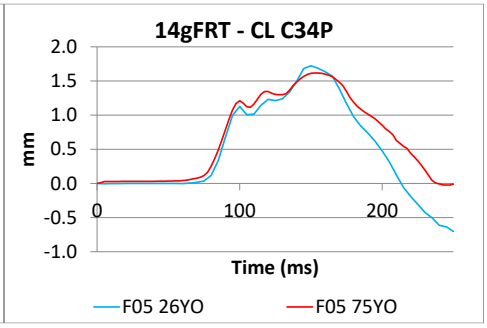
14gFRT - CL C34P
mm
Time (ms)
F05 26YO
F05 75YO

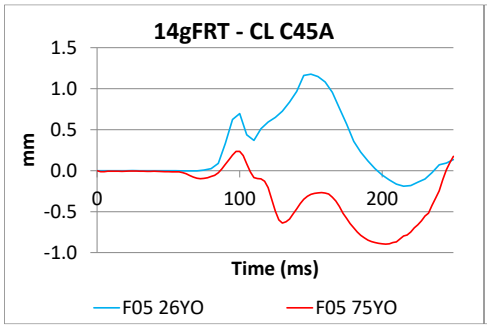
14gFRT - CL C45A
mm
Time (ms)
F05 26YO
F05 75YO

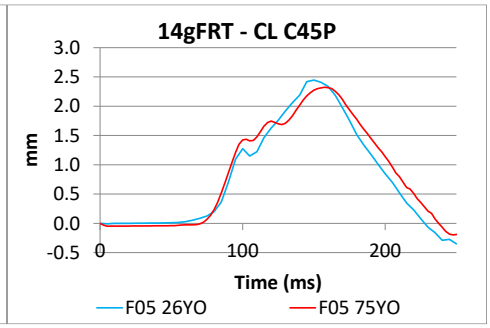
14gFRT - CL C45P
mm
Time (ms)
F05 26YO
F05 75YO

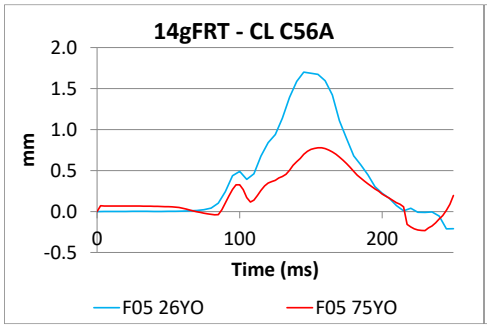
14gFRT - CL C56A
mm
Time (ms)
F05 26YO
F05 75YO

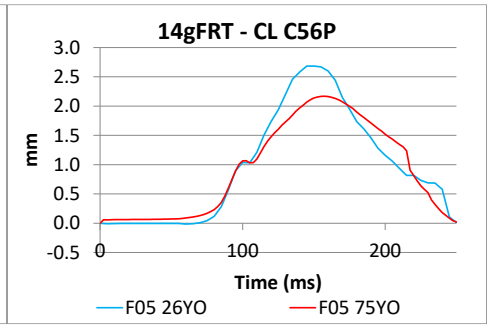
14gFRT - CL C56P
mm
Time (ms)
F05 26YO
F05 75YO

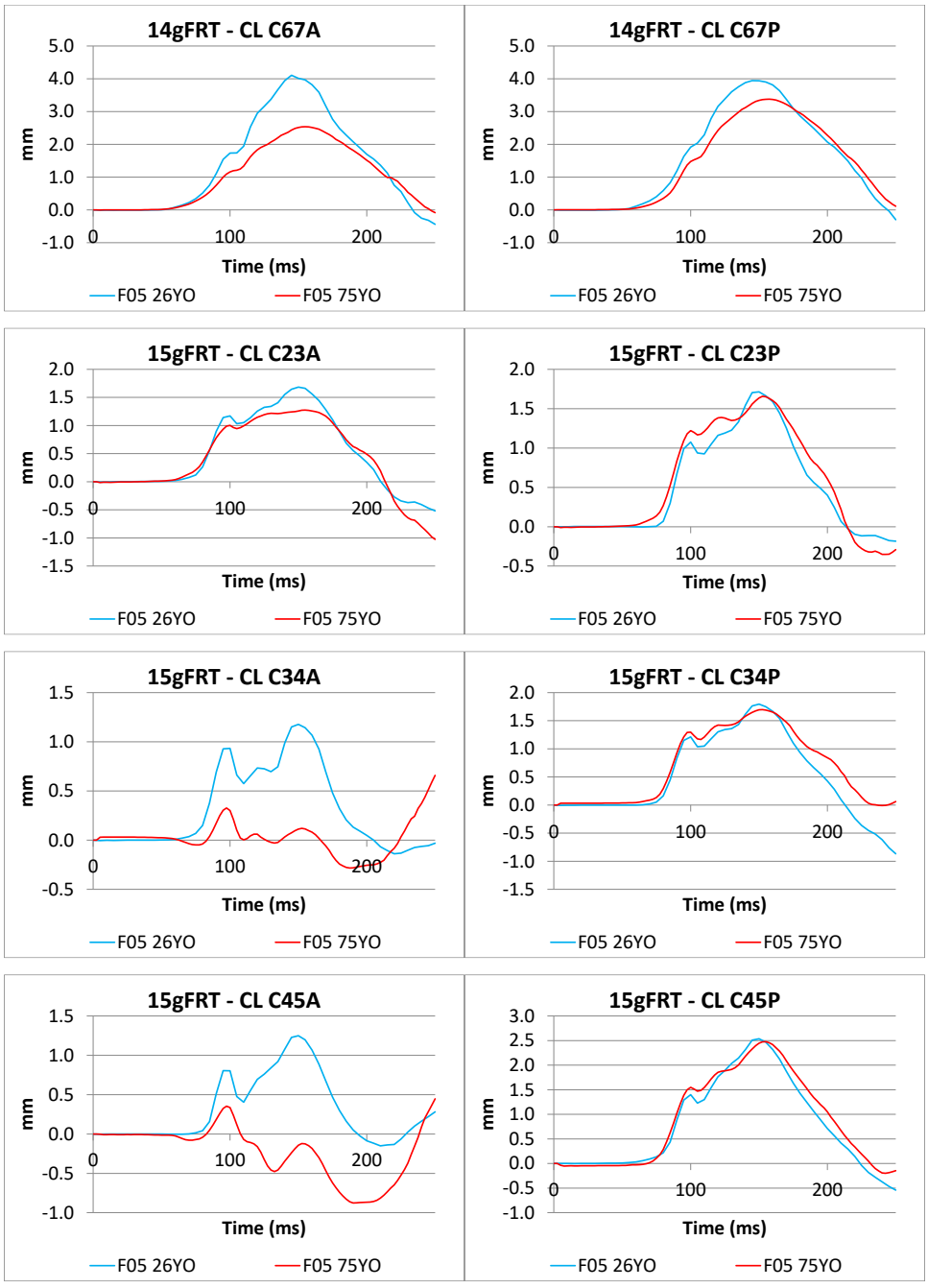
14gFRT - CL C67A
14gFRT - CL C67P
15gFRT - CL C23A
15gFRT - CL C23P
15gFRT - CL C34A
15gFRT - CL C34P
15gFRT - CL C45A
15gFRT - CL C45P
mm
Time (ms)
F05 26YO
F05 75YO

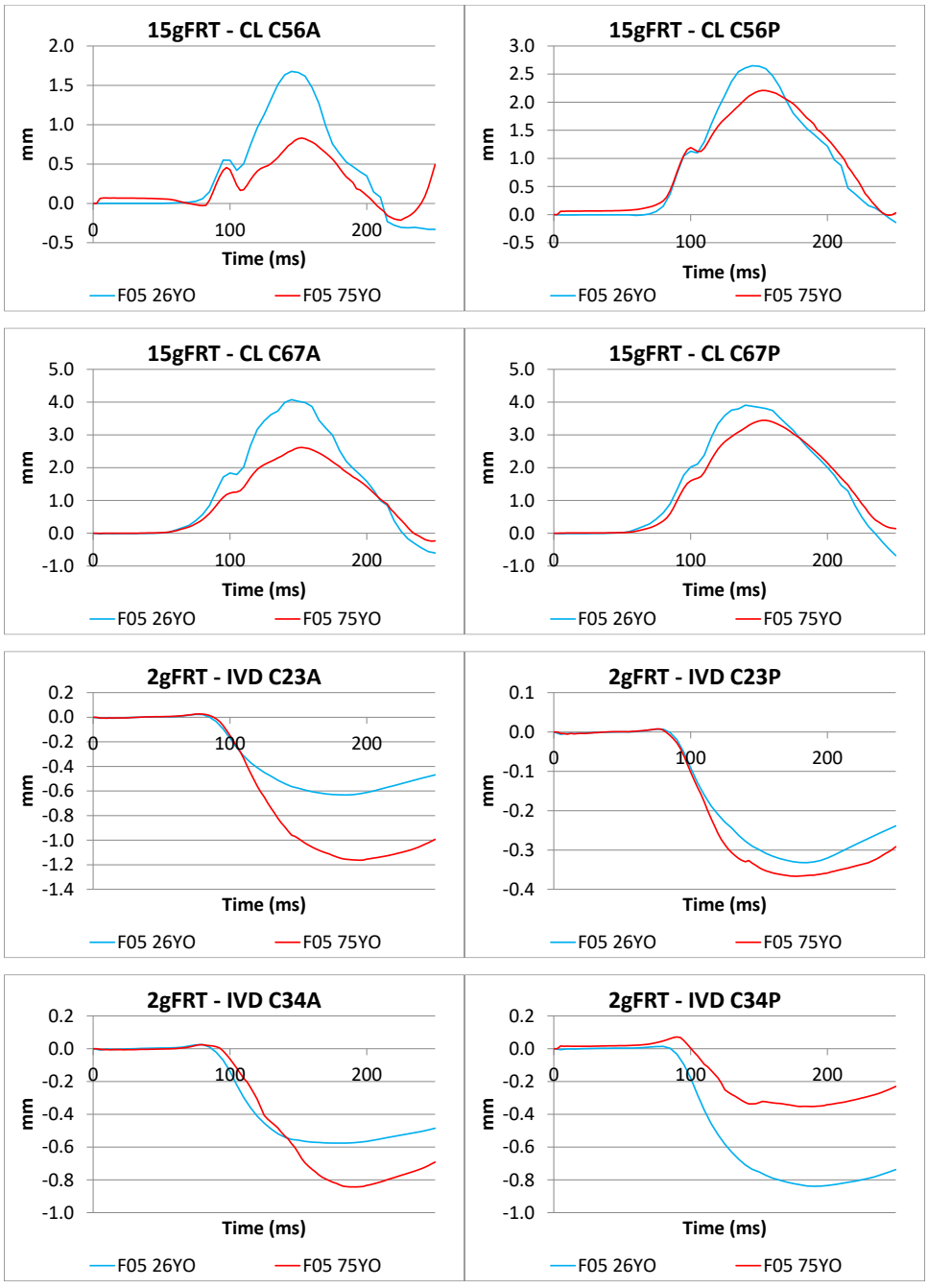
15gFRT - CL C56A
mm
Time (ms)
F05 26YO
F05 75YO
15gFRT - CL C56P
mm
Time (ms)
F05 26YO
F05 75YO
15gFRT - CL C67A
mm
Time (ms)
F05 26YO
F05 75YO
15gFRT - CL C67P
mm
Time (ms)
F05 26YO
F05 75YO
2gFRT - IVD C23A
mm
Time (ms)
F05 26YO
F05 75YO
2gFRT - IVD C23P
mm
Time (ms)
F05 26YO
F05 75YO
2gFRT - IVD C34A
mm
Time (ms)
F05 26YO
F05 75YO
2gFRT - IVD C34P
mm
Time (ms)
F05 26YO
F05 75YO

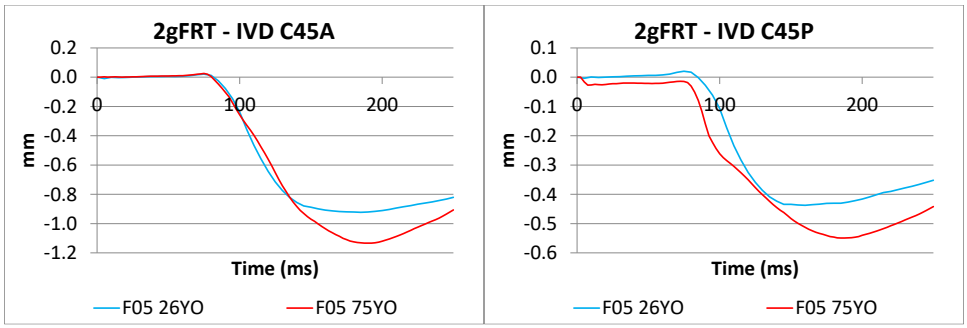
2gFRT - IVD C45A
mm
Time (ms)
F05 26YO
F05 75YO

2gFRT - IVD C45P
mm
Time (ms)
F05 26YO
F05 75YO

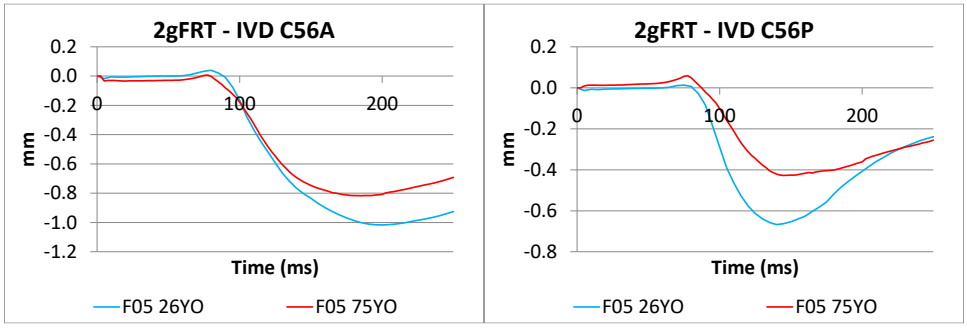
2gFRT - IVD C56A
mm
Time (ms)
F05 26YO
F05 75YO

2gFRT - IVD C56P
mm
Time (ms)
F05 26YO
F05 75YO

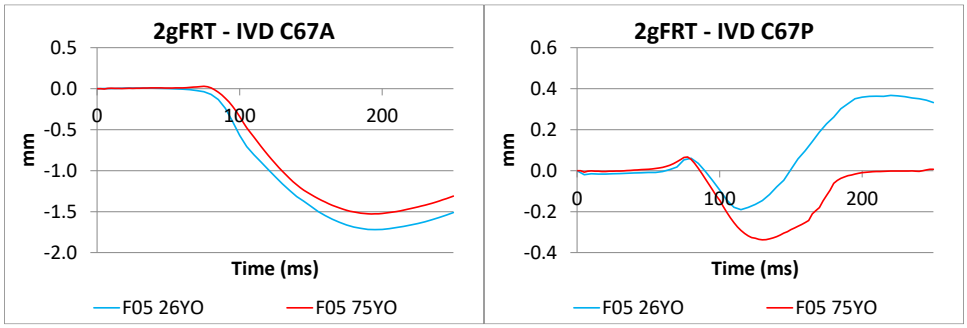
2gFRT - IVD C67A
mm
Time (ms)
F05 26YO
F05 75YO

2gFRT - IVD C67P
mm
Time (ms)
F05 26YO
F05 75YO

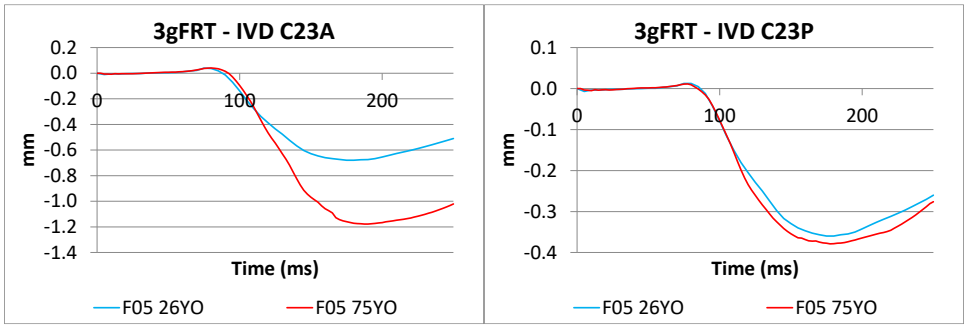
3gFRT - IVD C23A
mm
Time (ms)
F05 26YO
F05 75YO

3gFRT - IVD C23P
mm
Time (ms)
F05 26YO
F05 75YO

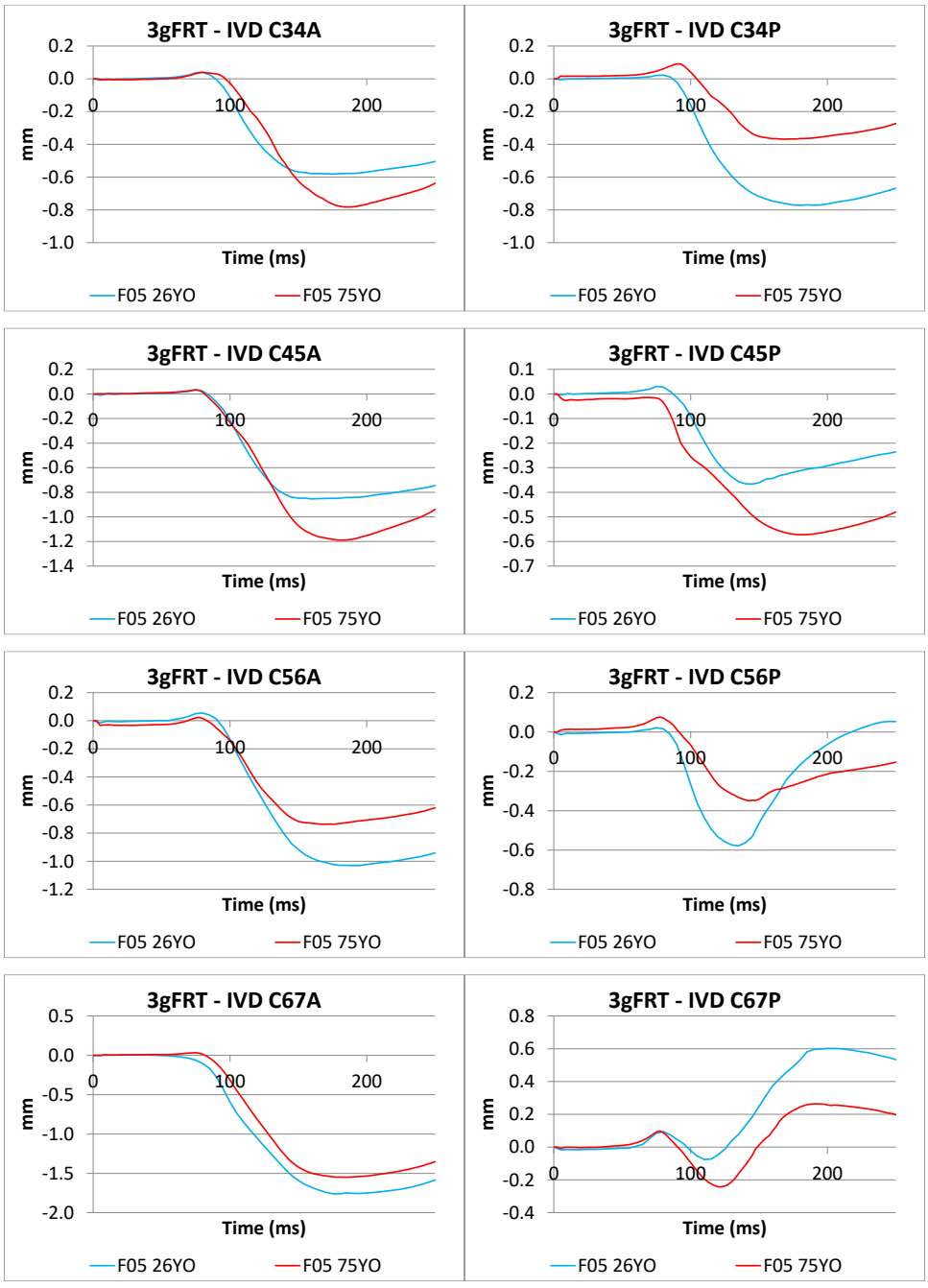
3gFRT - IVD C34A
0.2
0.0
-0.2
-0.4
-0.6
-0.8
-1.0
mm
0
100
200
Time (ms)
F05 26YO
F05 75YO
3gFRT - IVD C34P
0.2
0.0
-0.2
-0.4
-0.6
-0.8
-1.0
mm
0
100
200
Time (ms)
F05 26YO
F05 75YO
3gFRT - IVD C45A
0.2
0.0
-0.2
-0.4
-0.6
-0.8
-1.0
-1.2
-1.4
mm
0
100
200
Time (ms)
F05 26YO
F05 75YO
3gFRT - IVD C45P
0.1
0.0
-0.1
-0.2
-0.3
-0.4
-0.5
-0.6
-0.7
mm
0
100
200
Time (ms)
F05 26YO
F05 75YO
3gFRT - IVD C56A
0.2
0.0
-0.2
-0.4
-0.6
-0.8
-1.0
-1.2
mm
0
100
200
Time (ms)
F05 26YO
F05 75YO
3gFRT - IVD C56P
0.2
0.0
-0.2
-0.4
-0.6
-0.8
mm
0
100
200
Time (ms)
F05 26YO
F05 75YO
3gFRT - IVD C67A
0.5
0.0
-0.5
-1.0
-1.5
-2.0
mm
0
100
200
Time (ms)
F05 26YO
F05 75YO
3gFRT - IVD C67P
0.8
0.6
0.4
0.2
0.0
-0.2
-0.4
mm
0
100
200
Time (ms)
F05 26YO
F05 75YO

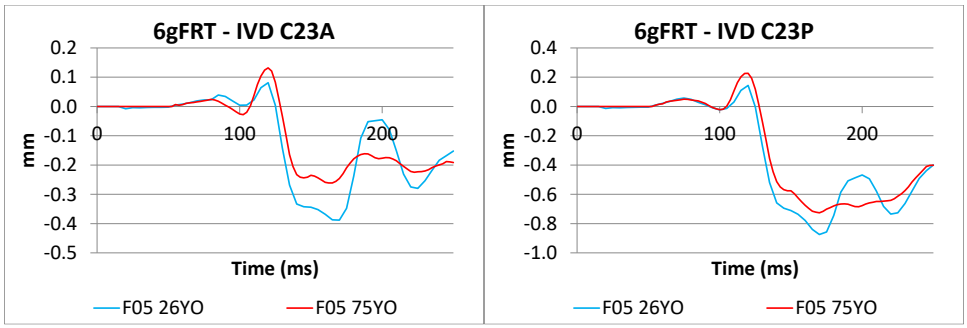
6gFRT - IVD C23A
mm
Time (ms)
F05 26YO
F05 75YO

6gFRT - IVD C23P
mm
Time (ms)
F05 26YO
F05 75YO

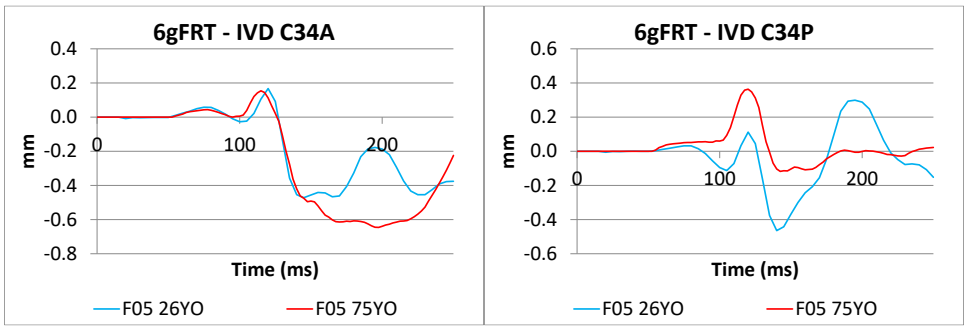
6gFRT - IVD C34A
mm
Time (ms)
F05 26YO
F05 75YO

6gFRT - IVD C34P
mm
Time (ms)
F05 26YO
F05 75YO

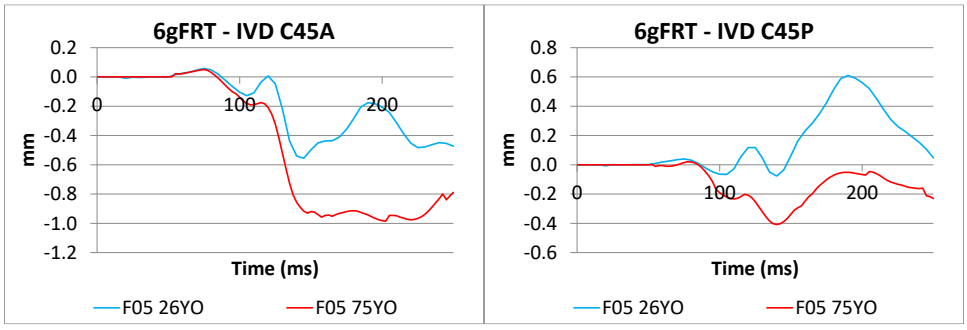
6gFRT - IVD C45A
mm
Time (ms)
F05 26YO
F05 75YO

6gFRT - IVD C45P
mm
Time (ms)
F05 26YO
F05 75YO

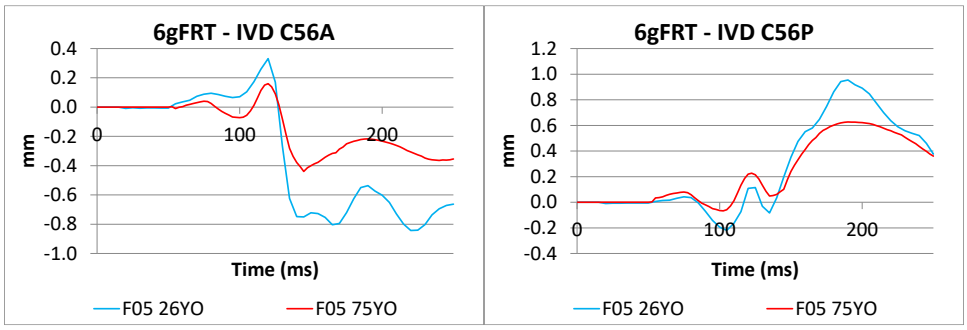
6gFRT - IVD C56A
mm
Time (ms)
F05 26YO
F05 75YO

6gFRT - IVD C56P
mm
Time (ms)
F05 26YO
F05 75YO

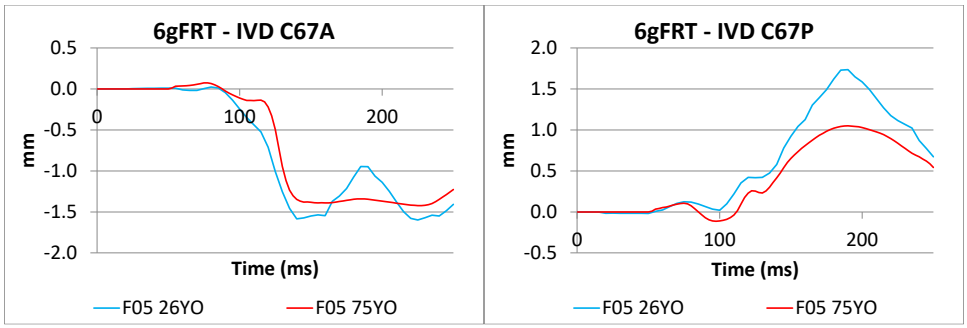
6gFRT - IVD C67A
mm
Time (ms)
F05 26YO
F05 75YO

6gFRT - IVD C67P
mm
Time (ms)
F05 26YO
F05 75YO

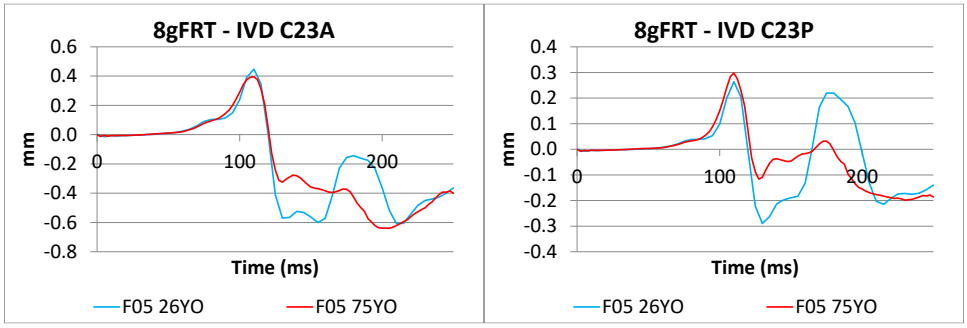
8gFRT - IVD C23A
mm
Time (ms)
F05 26YO
F05 75YO

8gFRT - IVD C23P
mm
Time (ms)
F05 26YO
F05 75YO

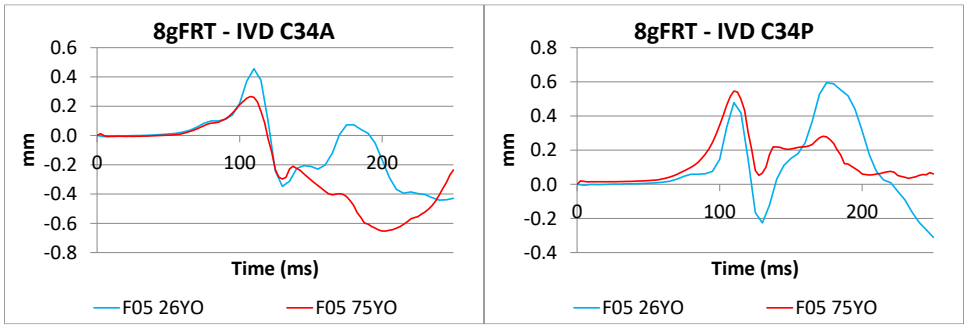
8gFRT - IVD C34A
mm
Time (ms)
F05 26YO
F05 75YO

8gFRT - IVD C34P
mm
Time (ms)
F05 26YO
F05 75YO

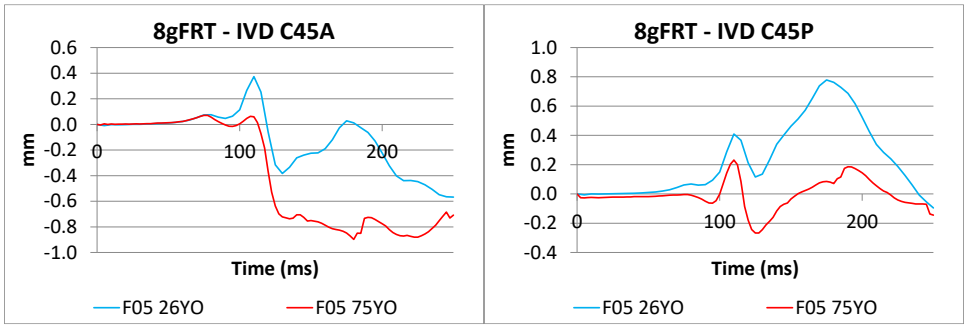
8gFRT - IVD C45A
mm
Time (ms)
F05 26YO
F05 75YO

8gFRT - IVD C45P
mm
Time (ms)
F05 26YO
F05 75YO

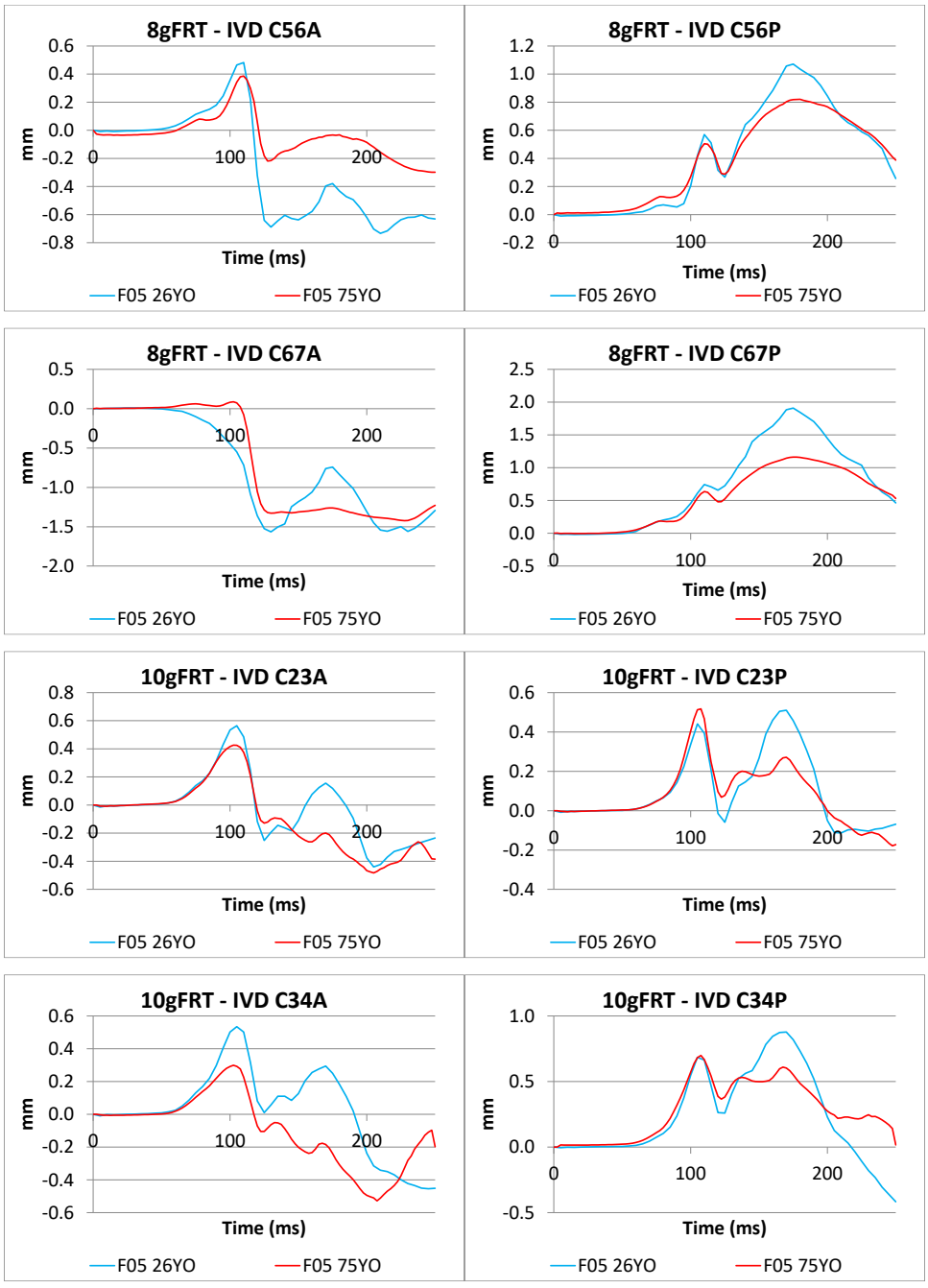
8gFRT - IVD C56A
mm
Time (ms)
F05 26YO
F05 75YO
8gFRT - IVD C56P
mm
Time (ms)
F05 26YO
F05 75YO
8gFRT - IVD C67A
mm
Time (ms)
F05 26YO
F05 75YO
8gFRT - IVD C67P
mm
Time (ms)
F05 26YO
F05 75YO
10gFRT - IVD C23A
mm
Time (ms)
F05 26YO
F05 75YO
10gFRT - IVD C23P
mm
Time (ms)
F05 26YO
F05 75YO
10gFRT - IVD C34A
mm
Time (ms)
F05 26YO
F05 75YO
10gFRT - IVD C34P
mm
Time (ms)
F05 26YO
F05 75YO

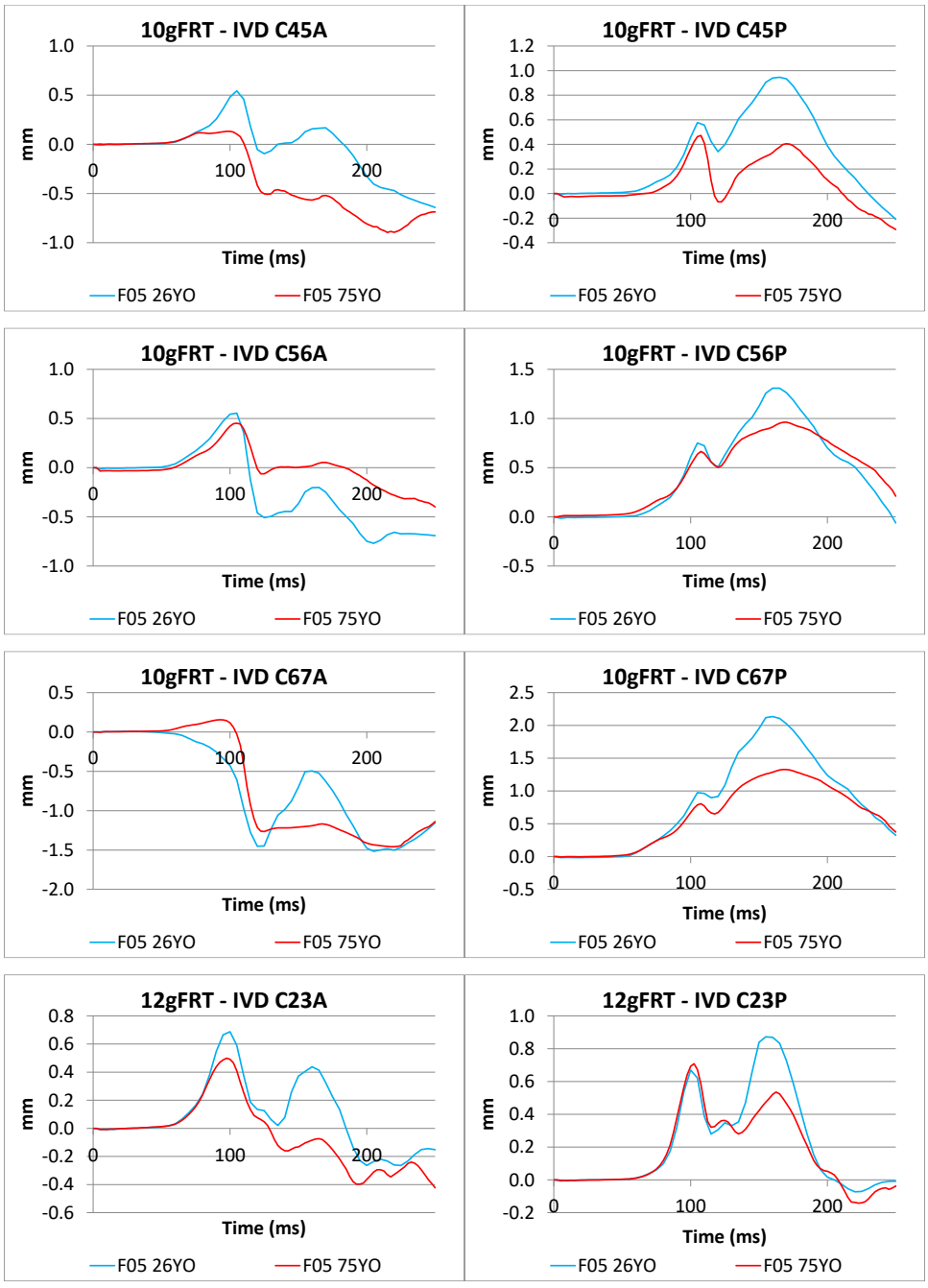
10gFRT - IVD C45A
mm
Time (ms)
F05 26YO
F05 75YO
10gFRT - IVD C45P
mm
Time (ms)
F05 26YO
F05 75YO
10gFRT - IVD C56A
mm
Time (ms)
F05 26YO
F05 75YO
10gFRT - IVD C56P
mm
Time (ms)
F05 26YO
F05 75YO
10gFRT - IVD C67A
mm
Time (ms)
F05 26YO
F05 75YO
10gFRT - IVD C67P
mm
Time (ms)
F05 26YO
F05 75YO
12gFRT - IVD C23A
mm
Time (ms)
F05 26YO
F05 75YO
12gFRT - IVD C23P
mm
Time (ms)
F05 26YO
F05 75YO

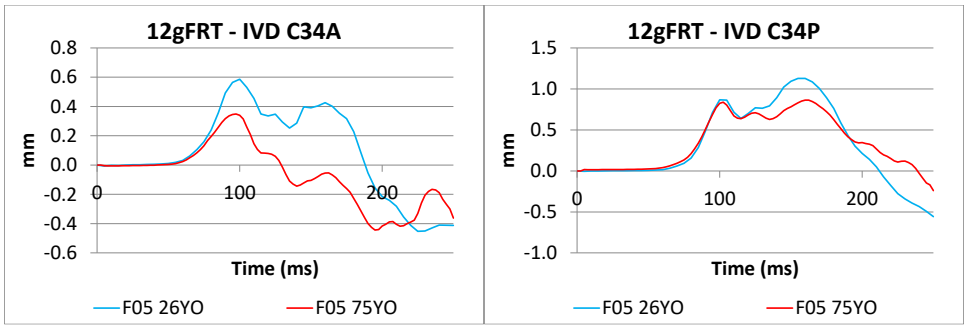
12gFRT - IVD C34A
mm
Time (ms)
F05 26YO
F05 75YO

12gFRT - IVD C34P
mm
Time (ms)
F05 26YO
F05 75YO

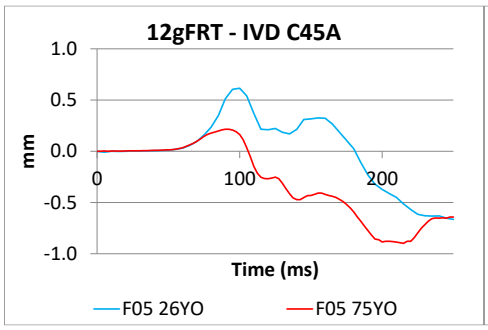
12gFRT - IVD C45A
mm
Time (ms)
F05 26YO
F05 75YO

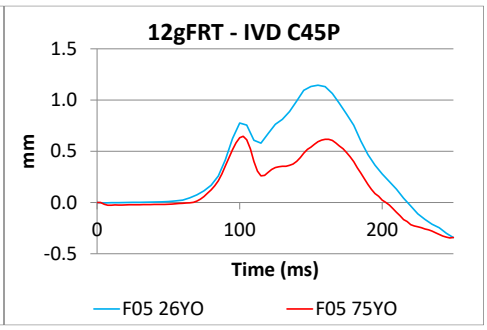
12gFRT - IVD C45P
mm
Time (ms)
F05 26YO
F05 75YO

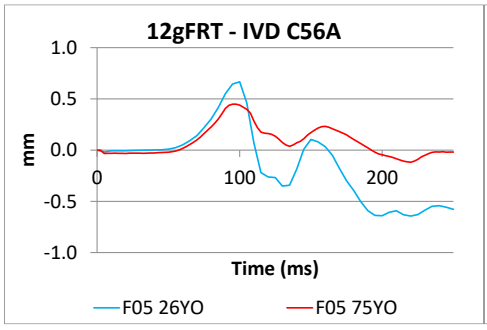
12gFRT - IVD C56A
mm
Time (ms)
F05 26YO
F05 75YO

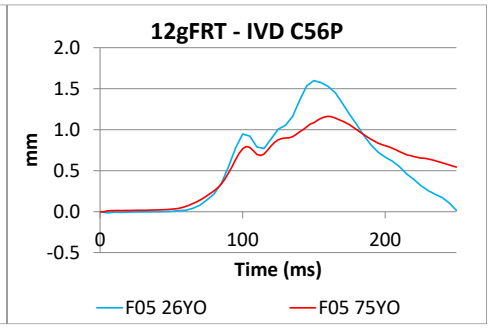
12gFRT - IVD C56P
mm
Time (ms)
F05 26YO
F05 75YO

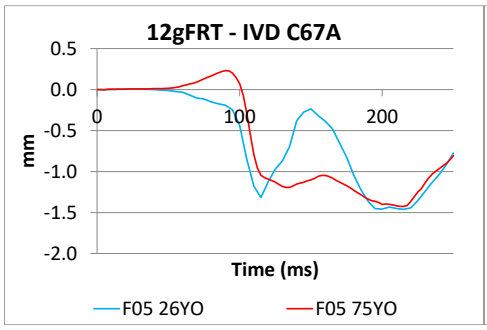
12gFRT - IVD C67A
mm
Time (ms)
F05 26YO
F05 75YO

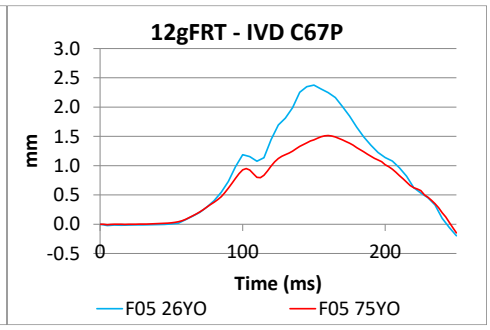
12gFRT - IVD C67P
mm
Time (ms)
F05 26YO
F05 75YO

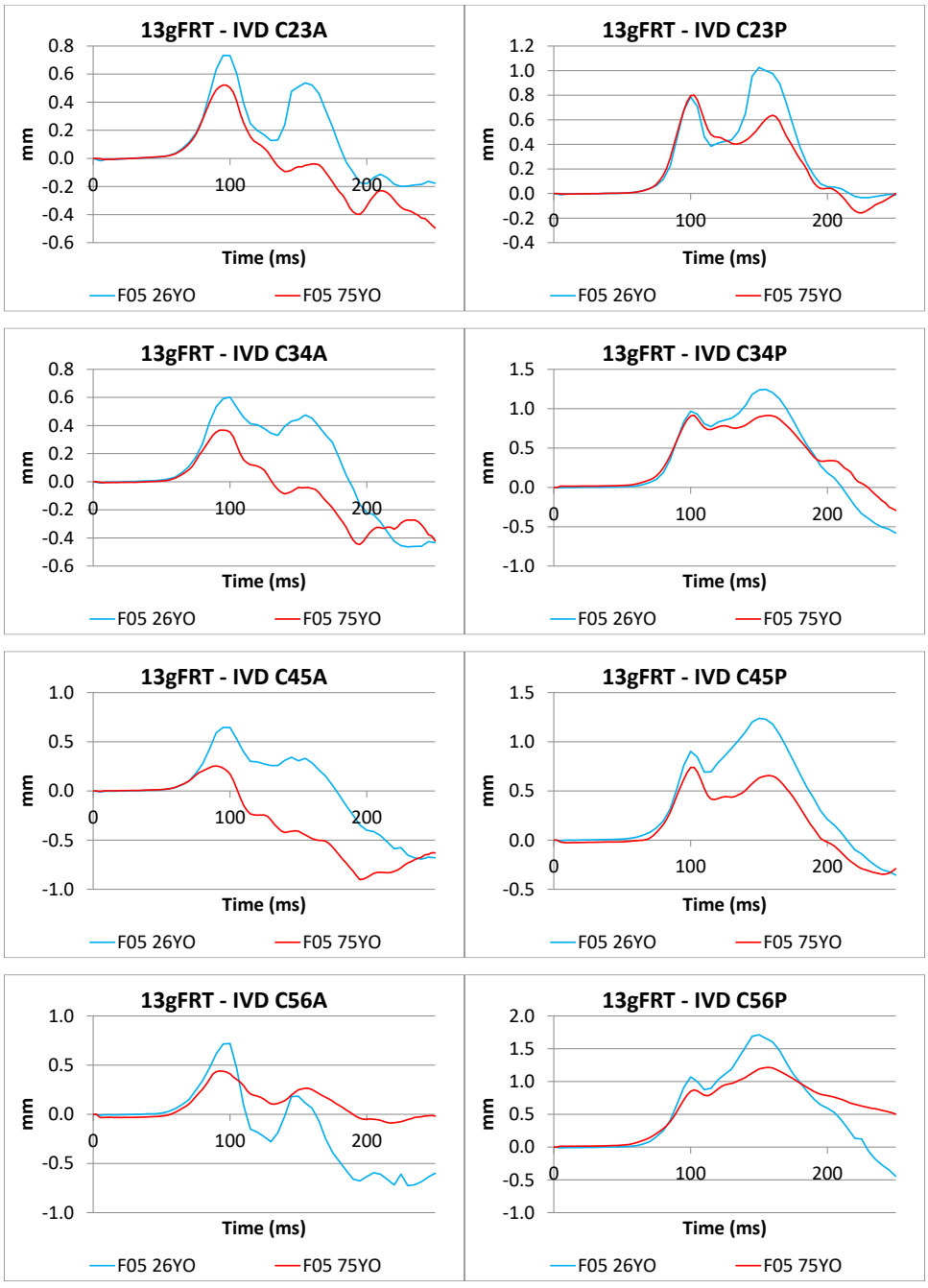
13gFRT - IVD C23A
mm
Time (ms)
F05 26YO
F05 75YO
13gFRT - IVD C23P
mm
Time (ms)
F05 26YO
F05 75YO
13gFRT - IVD C34A
mm
Time (ms)
F05 26YO
F05 75YO
13gFRT - IVD C34P
mm
Time (ms)
F05 26YO
F05 75YO
13gFRT - IVD C45A
mm
Time (ms)
F05 26YO
F05 75YO
13gFRT - IVD C45P
mm
Time (ms)
F05 26YO
F05 75YO
13gFRT - IVD C56A
mm
Time (ms)
F05 26YO
F05 75YO
13gFRT - IVD C56P
mm
Time (ms)
F05 26YO
F05 75YO

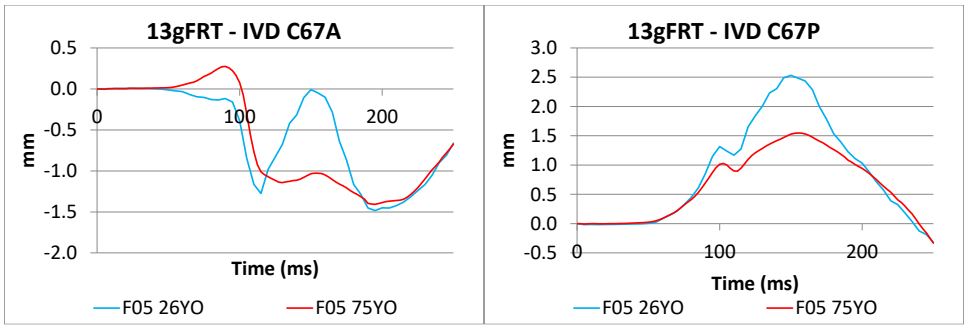
13gFRT - IVD C67A
mm
Time (ms)
F05 26YO
F05 75YO

13gFRT - IVD C67P
mm
Time (ms)
F05 26YO
F05 75YO

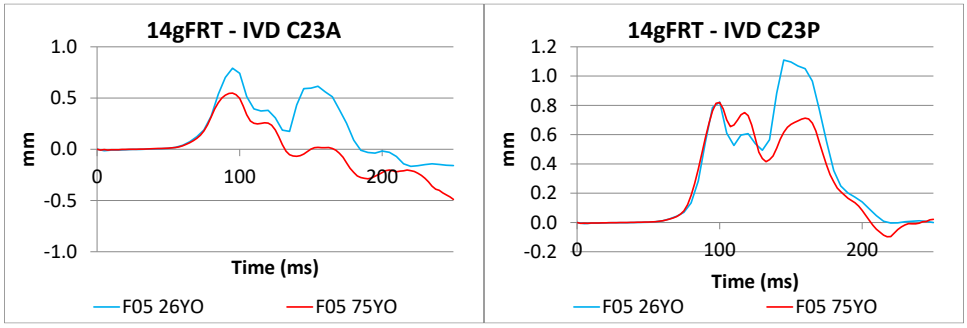
14gFRT - IVD C23A
mm
Time (ms)
F05 26YO
F05 75YO

14gFRT - IVD C23P
mm
Time (ms)
F05 26YO
F05 75YO

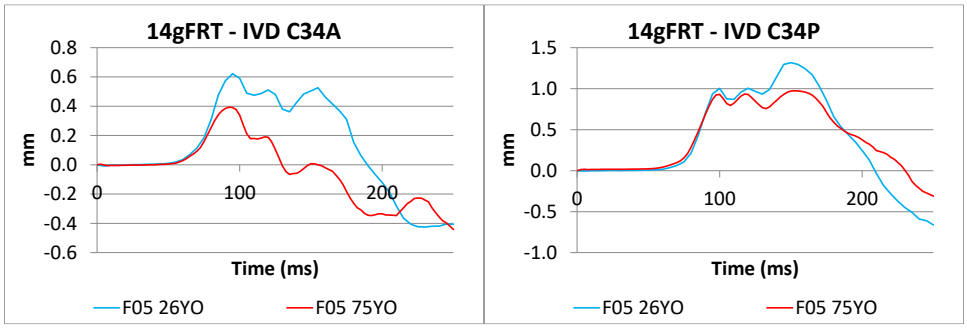
14gFRT - IVD C34A
mm
Time (ms)
F05 26YO
F05 75YO

14gFRT - IVD C34P
mm
Time (ms)
F05 26YO
F05 75YO

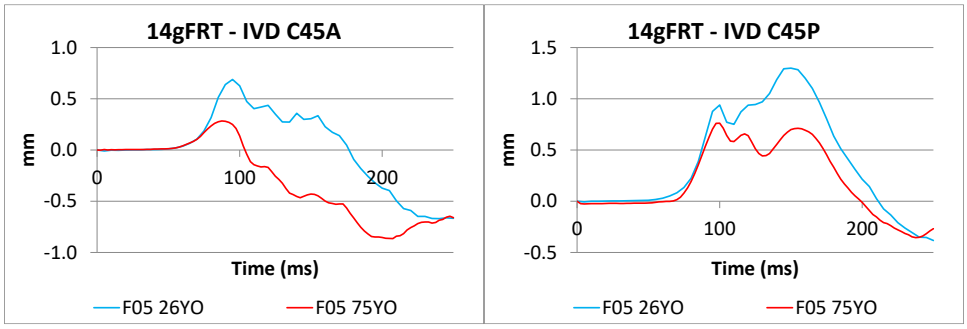
14gFRT - IVD C45A
mm
Time (ms)
F05 26YO
F05 75YO

14gFRT - IVD C45P
mm
Time (ms)
F05 26YO
F05 75YO

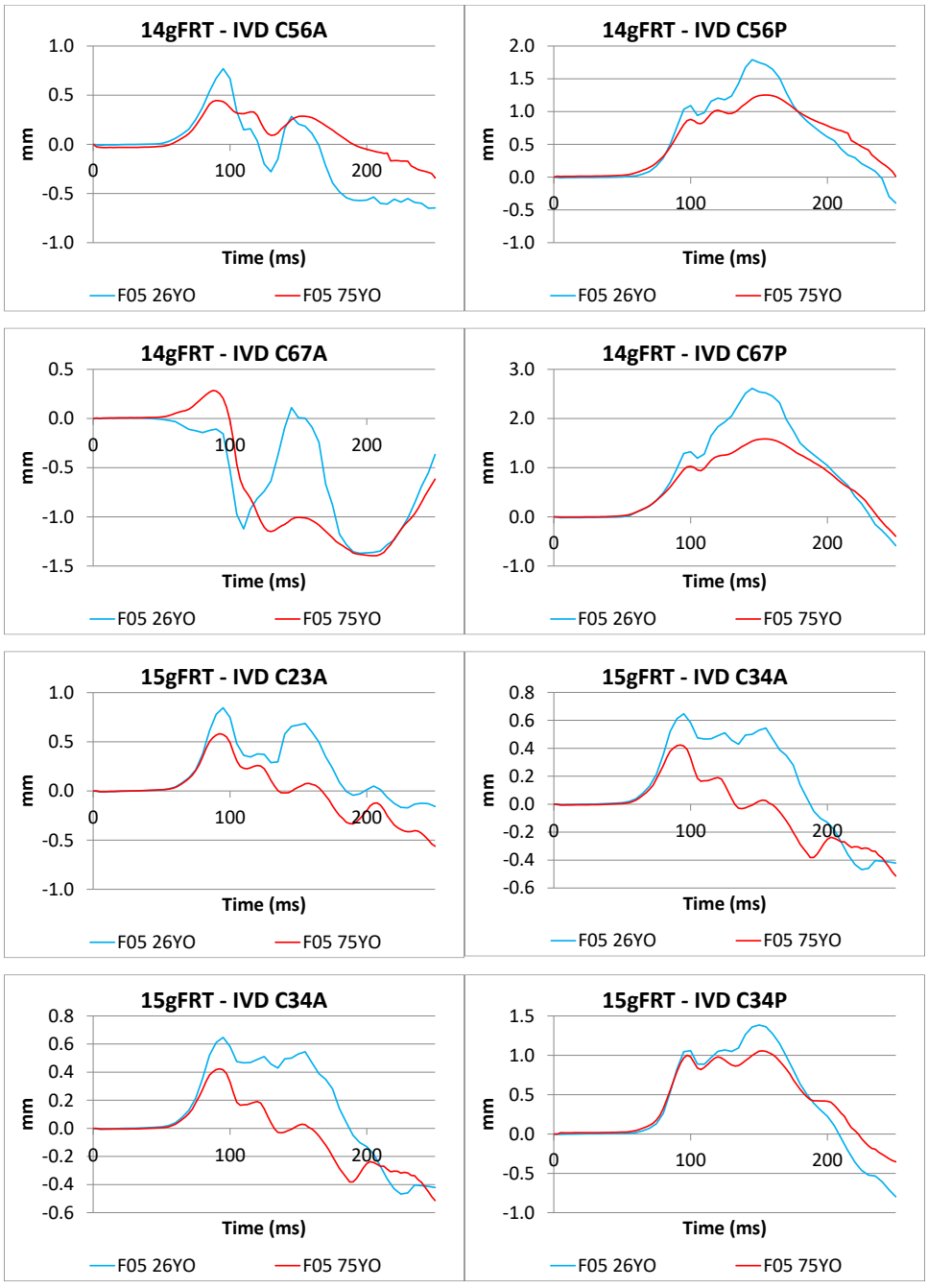
14gFRT - IVD C56A
mm
Time (ms)
F05 26YO
F05 75YO
14gFRT - IVD C56P
mm
Time (ms)
F05 26YO
F05 75YO
14gFRT - IVD C67A
mm
Time (ms)
F05 26YO
F05 75YO
14gFRT - IVD C67P
mm
Time (ms)
F05 26YO
F05 75YO
15gFRT - IVD C23A
mm
Time (ms)
F05 26YO
F05 75YO
15gFRT - IVD C34A
mm
Time (ms)
F05 26YO
F05 75YO
15gFRT - IVD C34A
mm
Time (ms)
F05 26YO
F05 75YO
15gFRT - IVD C34P
mm
Time (ms)
F05 26YO
F05 75YO

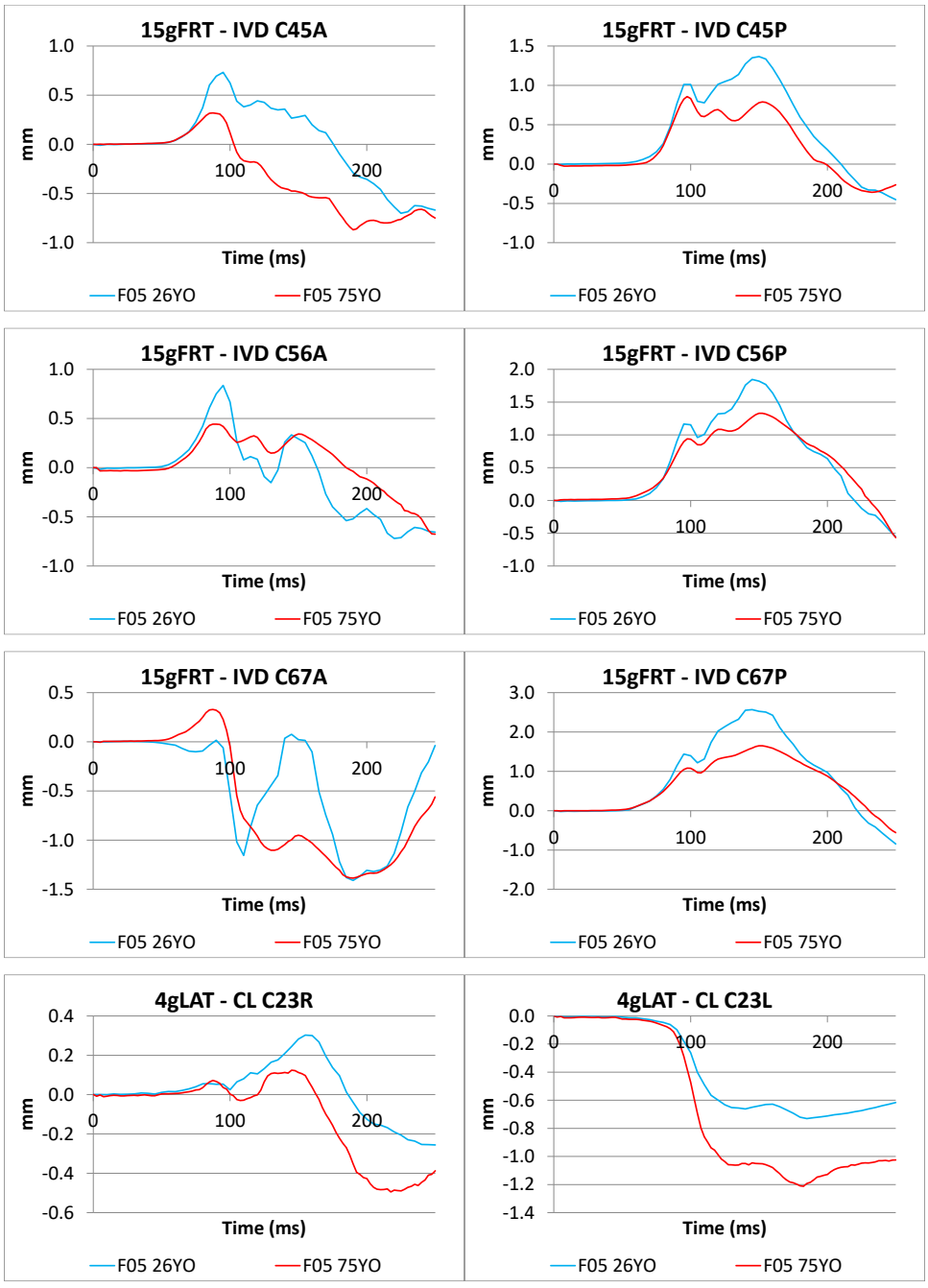
15gFRT - IVD C45A
mm
Time (ms)
F05 26YO
F05 75YO
15gFRT - IVD C45P
mm
Time (ms)
F05 26YO
F05 75YO
15gFRT - IVD C56A
mm
Time (ms)
F05 26YO
F05 75YO
15gFRT - IVD C56P
mm
Time (ms)
F05 26YO
F05 75YO
15gFRT - IVD C67A
mm
Time (ms)
F05 26YO
F05 75YO
15gFRT - IVD C67P
mm
Time (ms)
F05 26YO
F05 75YO
4gLAT - CL C23R
mm
Time (ms)
F05 26YO
F05 75YO
4gLAT - CL C23L
mm
Time (ms)
F05 26YO
F05 75YO

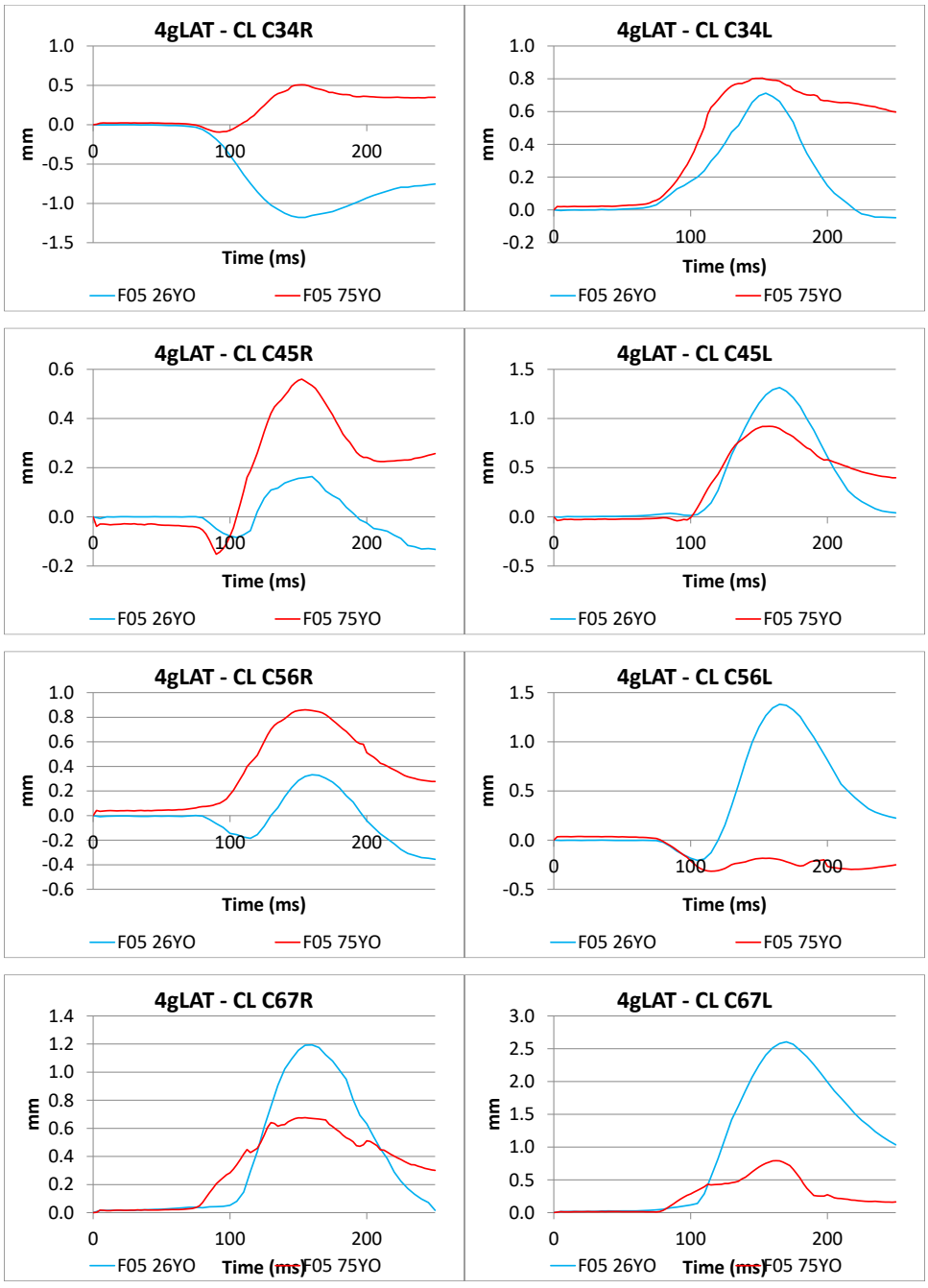
4gLAT - CL C34R
mm
Time (ms)
F05 26YO
F05 75YO
4gLAT - CL C34L
mm
Time (ms)
F05 26YO
F05 75YO
4gLAT - CL C45R
mm
Time (ms)
F05 26YO
F05 75YO
4gLAT - CL C45L
mm
Time (ms)
F05 26YO
F05 75YO
4gLAT - CL C56R
mm
Time (ms)
F05 26YO
F05 75YO
4gLAT - CL C56L
mm
Time (ms)
F05 26YO
F05 75YO
4gLAT - CL C67R
mm
Time (ms)
F05 26YO
F05 75YO
4gLAT - CL C67L
mm
Time (ms)
F05 26YO
F05 75YO

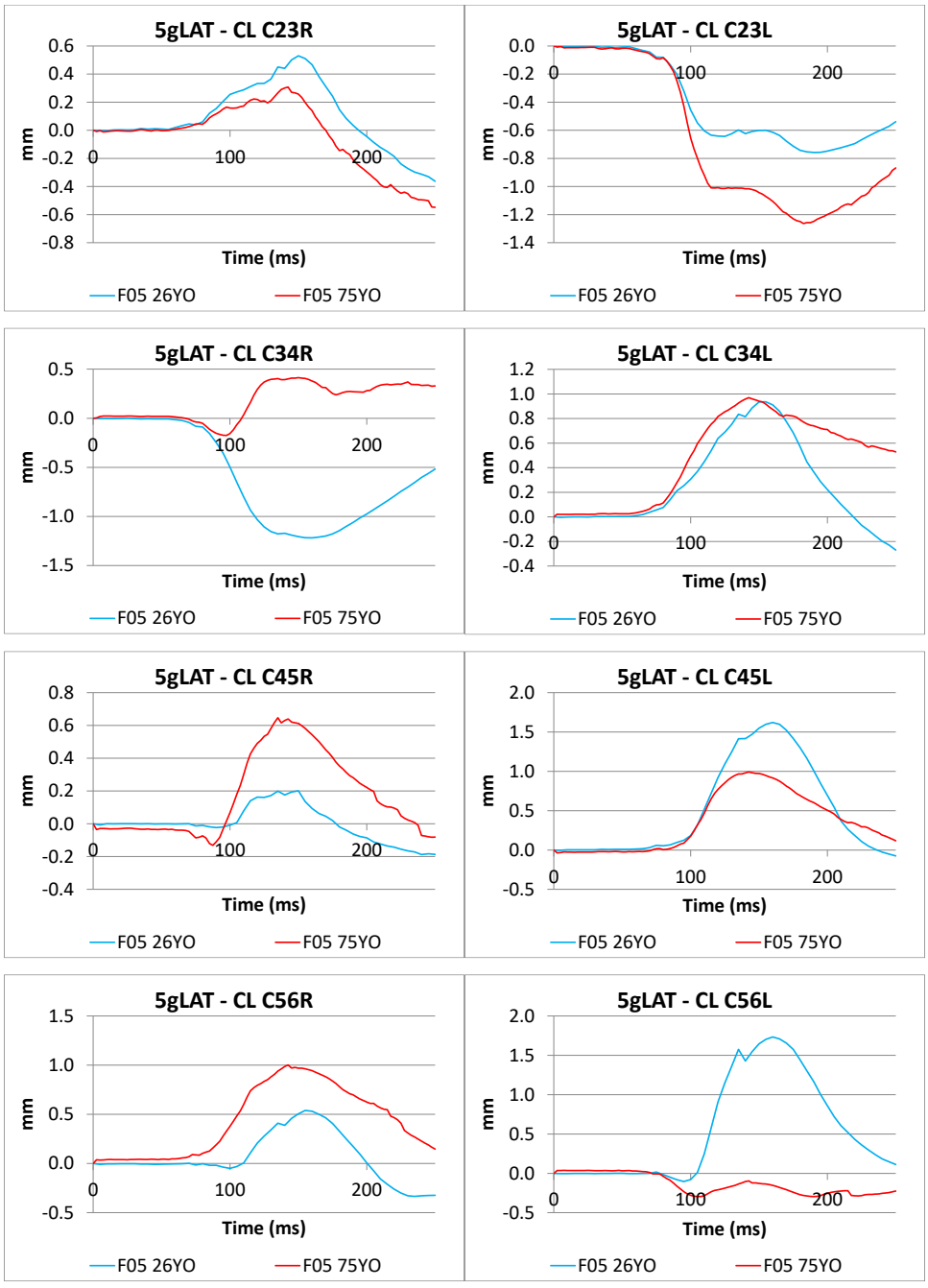
5gLAT - CL C23R
mm
Time (ms)
F05 26YO
F05 75YO
5gLAT - CL C23L
mm
Time (ms)
F05 26YO
F05 75YO
5gLAT - CL C34R
mm
Time (ms)
F05 26YO
F05 75YO
5gLAT - CL C34L
mm
Time (ms)
F05 26YO
F05 75YO
5gLAT - CL C45R
mm
Time (ms)
F05 26YO
F05 75YO
5gLAT - CL C45L
mm
Time (ms)
F05 26YO
F05 75YO
5gLAT - CL C56R
mm
Time (ms)
F05 26YO
F05 75YO
5gLAT - CL C56L
mm
Time (ms)
F05 26YO
F05 75YO

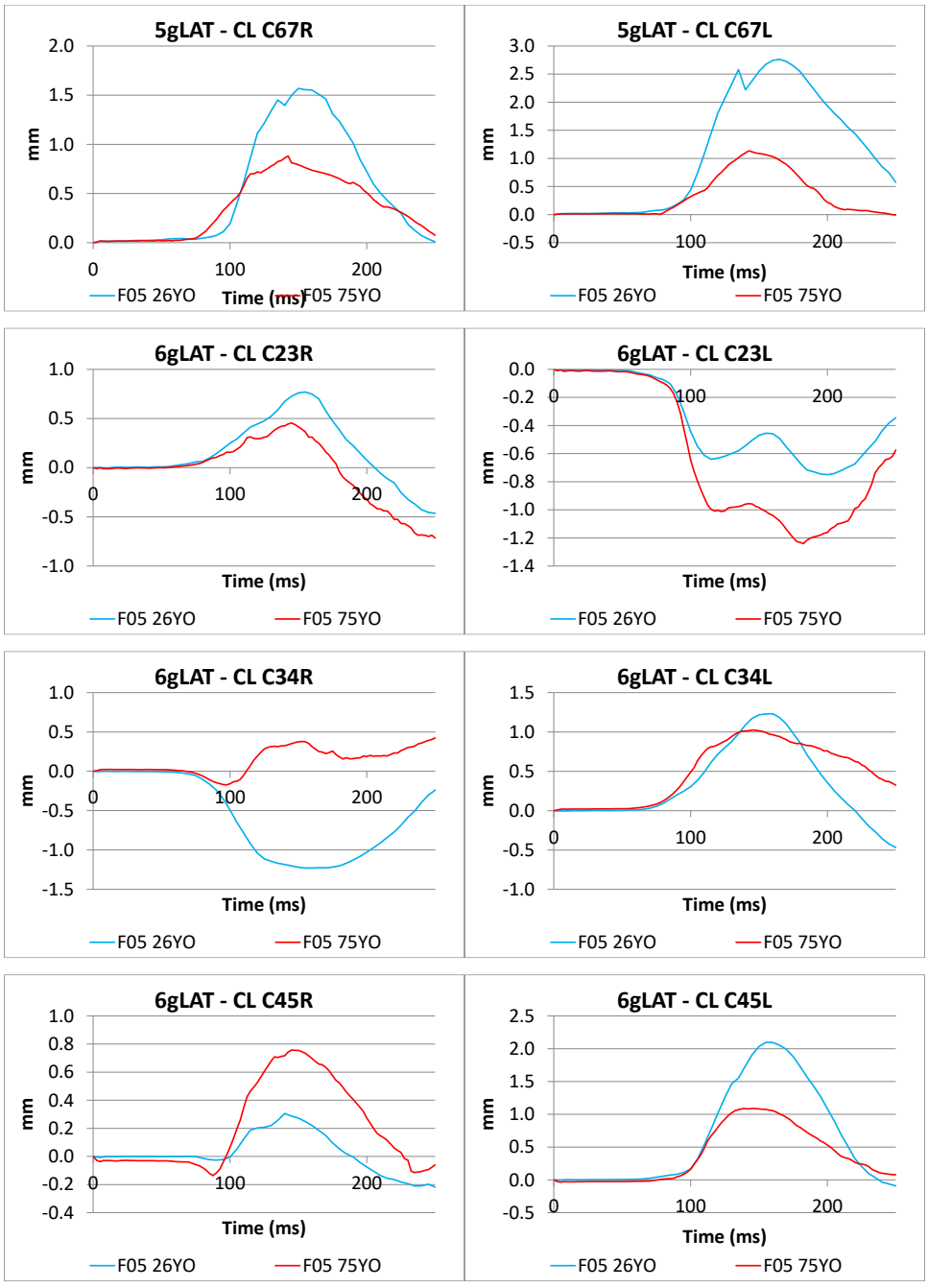
5gLAT - CL C67R
mm
Time (ms)
F05 26YO
F05 75YO
5gLAT - CL C67L
mm
Time (ms)
F05 26YO
F05 75YO
6gLAT - CL C23R
mm
Time (ms)
F05 26YO
F05 75YO
6gLAT - CL C23L
mm
Time (ms)
F05 26YO
F05 75YO
6gLAT - CL C34R
mm
Time (ms)
F05 26YO
F05 75YO
6gLAT - CL C34L
mm
Time (ms)
F05 26YO
F05 75YO
6gLAT - CL C45R
mm
Time (ms)
F05 26YO
F05 75YO
6gLAT - CL C45L
mm
Time (ms)
F05 26YO
F05 75YO

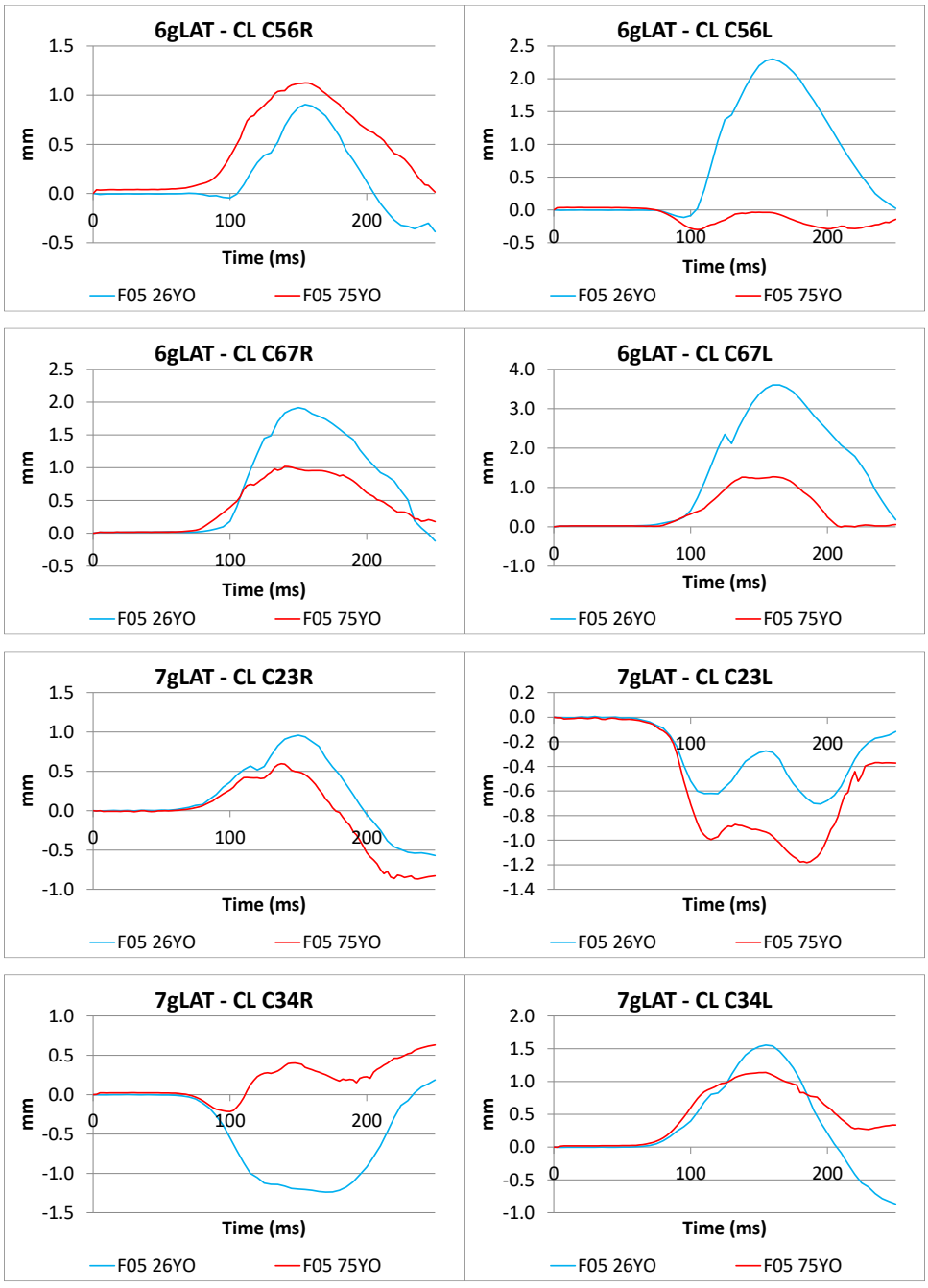
6gLAT - CL C56R
mm
Time (ms)
F05 26YO
F05 75YO
6gLAT - CL C56L
mm
Time (ms)
F05 26YO
F05 75YO
6gLAT - CL C67R
mm
Time (ms)
F05 26YO
F05 75YO
6gLAT - CL C67L
mm
Time (ms)
F05 26YO
F05 75YO
7gLAT - CL C23R
mm
Time (ms)
F05 26YO
F05 75YO
7gLAT - CL C23L
mm
Time (ms)
F05 26YO
F05 75YO
7gLAT - CL C34R
mm
Time (ms)
F05 26YO
F05 75YO
7gLAT - CL C34L
mm
Time (ms)
F05 26YO
F05 75YO

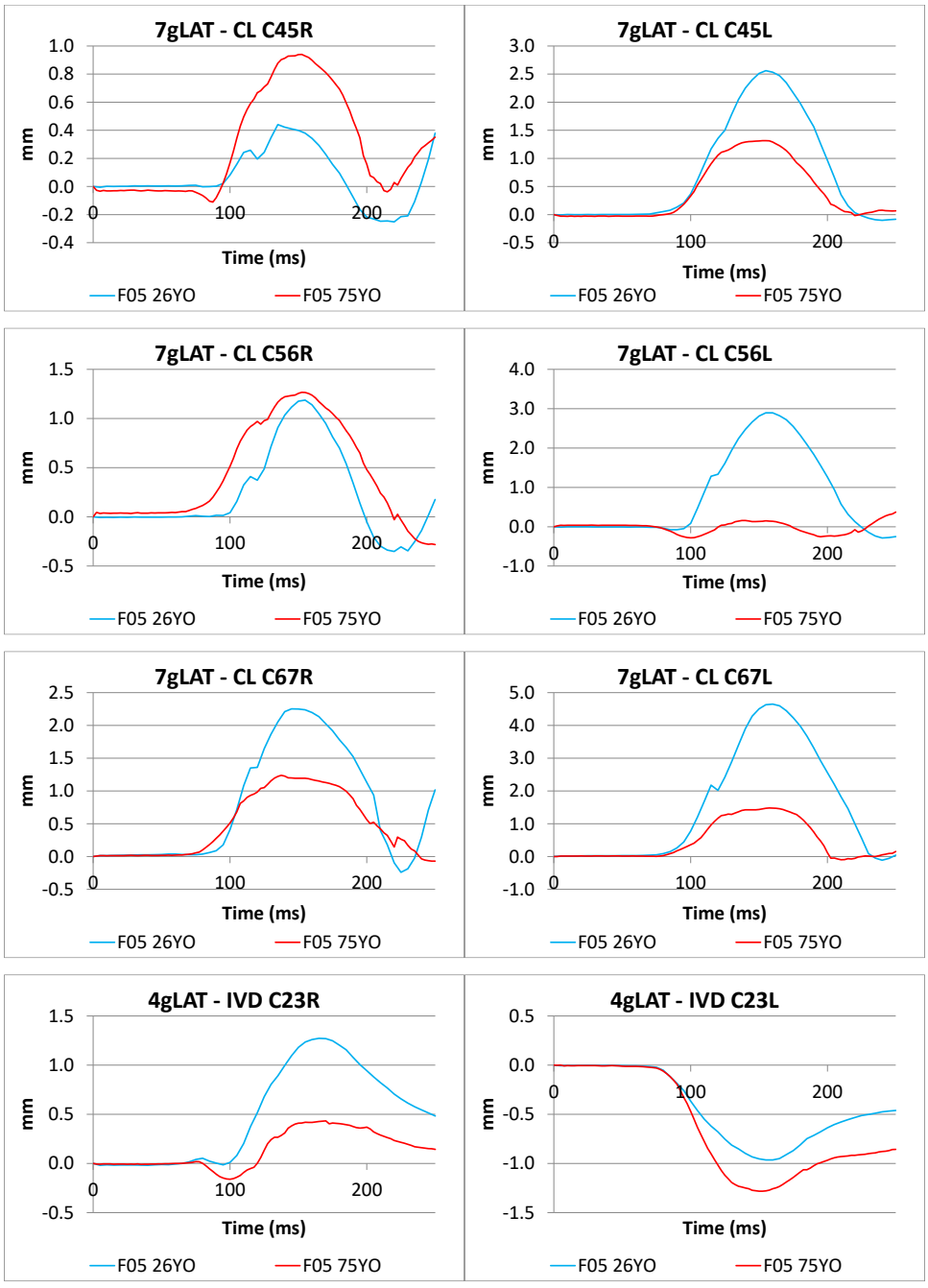
7gLAT - CL C45R
mm
Time (ms)
F05 26YO
F05 75YO
7gLAT - CL C45L
mm
Time (ms)
F05 26YO
F05 75YO
7gLAT - CL C56R
mm
Time (ms)
F05 26YO
F05 75YO
7gLAT - CL C56L
mm
Time (ms)
F05 26YO
F05 75YO
7gLAT - CL C67R
mm
Time (ms)
F05 26YO
F05 75YO
7gLAT - CL C67L
mm
Time (ms)
F05 26YO
F05 75YO
4gLAT - IVD C23R
mm
Time (ms)
F05 26YO
F05 75YO
4gLAT - IVD C23L
mm
Time (ms)
F05 26YO
F05 75YO

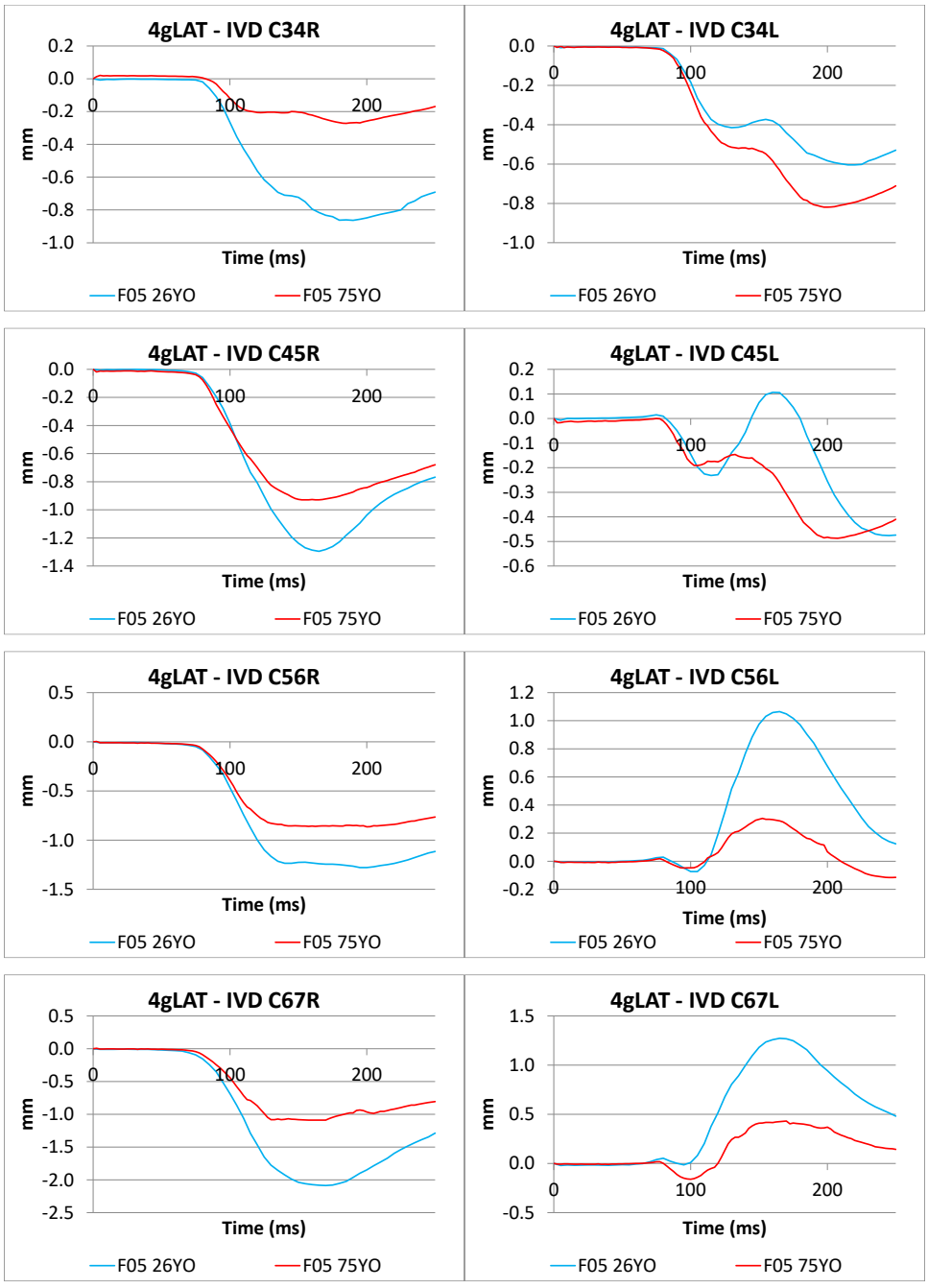
4gLAT - IVD C34R
0.2
0.0
-0.2
-0.4
-0.6
-0.8
-1.0
mm
0
100
200
Time (ms)
F05 26YO
F05 75YO
4gLAT - IVD C34L
0.0
-0.2
-0.4
-0.6
-0.8
-1.0
mm
0
100
200
Time (ms)
F05 26YO
F05 75YO
4gLAT - IVD C45R
0.0
-0.2
-0.4
-0.6
-0.8
-1.0
-1.2
-1.4
mm
0
100
200
Time (ms)
F05 26YO
F05 75YO
4gLAT - IVD C45L
0.2
0.1
0.0
-0.1
-0.2
-0.3
-0.4
-0.5
-0.6
mm
0
100
200
Time (ms)
F05 26YO
F05 75YO
4gLAT - IVD C56R
0.5
0.0
-0.5
-1.0
-1.5
mm
0
100
200
Time (ms)
F05 26YO
F05 75YO
4gLAT - IVD C56L
1.2
1.0
0.8
0.6
0.4
0.2
0.0
-0.2
mm
0
100
200
Time (ms)
F05 26YO
F05 75YO
4gLAT - IVD C67R
0.5
0.0
-0.5
-1.0
-1.5
-2.0
-2.5
mm
0
100
200
Time (ms)
F05 26YO
F05 75YO
4gLAT - IVD C67L
1.5
1.0
0.5
0.0
-0.5
mm
0
100
200
Time (ms)
F05 26YO
F05 75YO

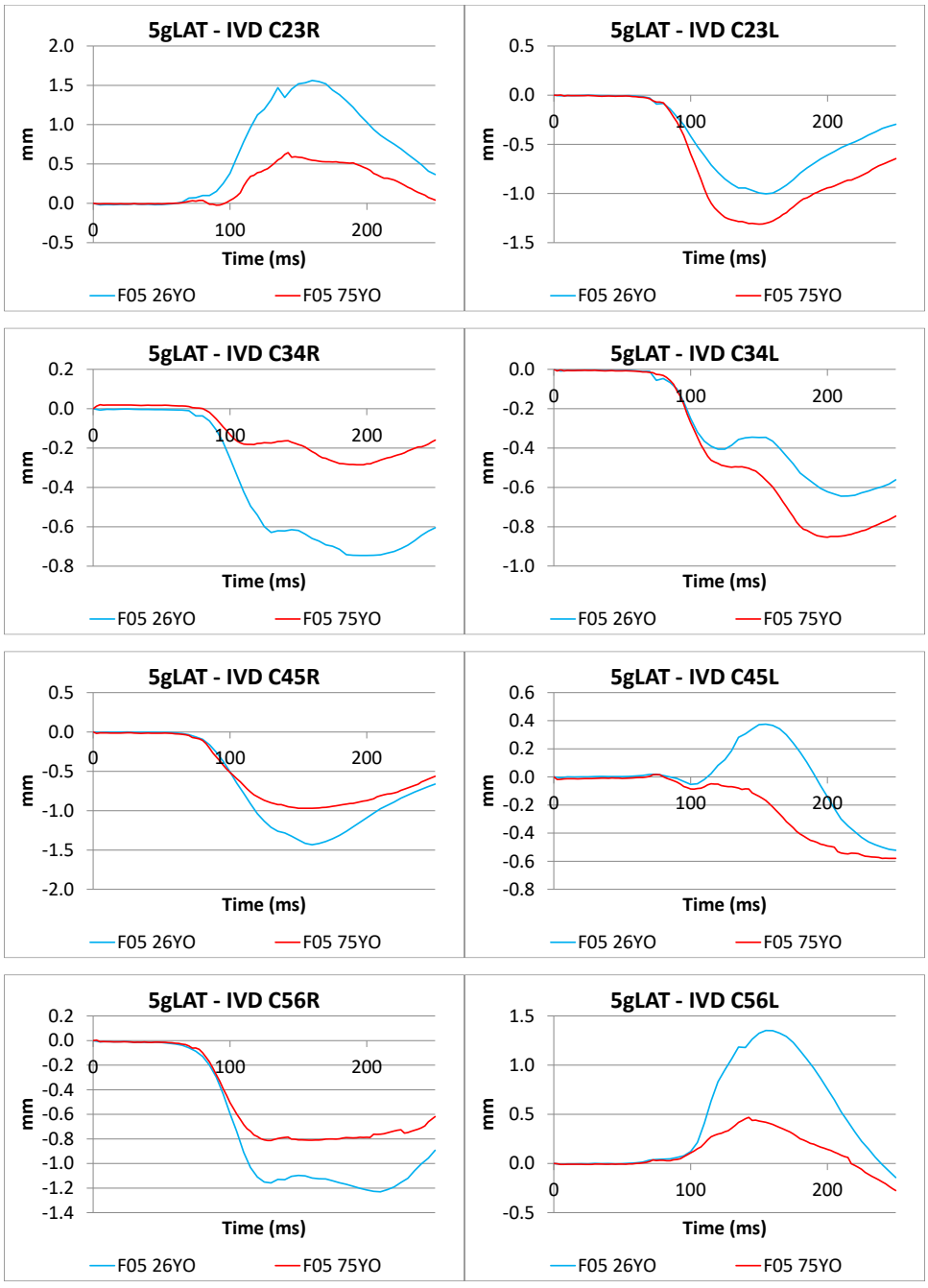
5gLAT - IVD C23R
mm
Time (ms)
F05 26YO
F05 75YO
5gLAT - IVD C23L
mm
Time (ms)
F05 26YO
F05 75YO
5gLAT - IVD C34R
mm
Time (ms)
F05 26YO
F05 75YO
5gLAT - IVD C34L
mm
Time (ms)
F05 26YO
F05 75YO
5gLAT - IVD C45R
mm
Time (ms)
F05 26YO
F05 75YO
5gLAT - IVD C45L
mm
Time (ms)
F05 26YO
F05 75YO
5gLAT - IVD C56R
mm
Time (ms)
F05 26YO
F05 75YO
5gLAT - IVD C56L
mm
Time (ms)
F05 26YO
F05 75YO

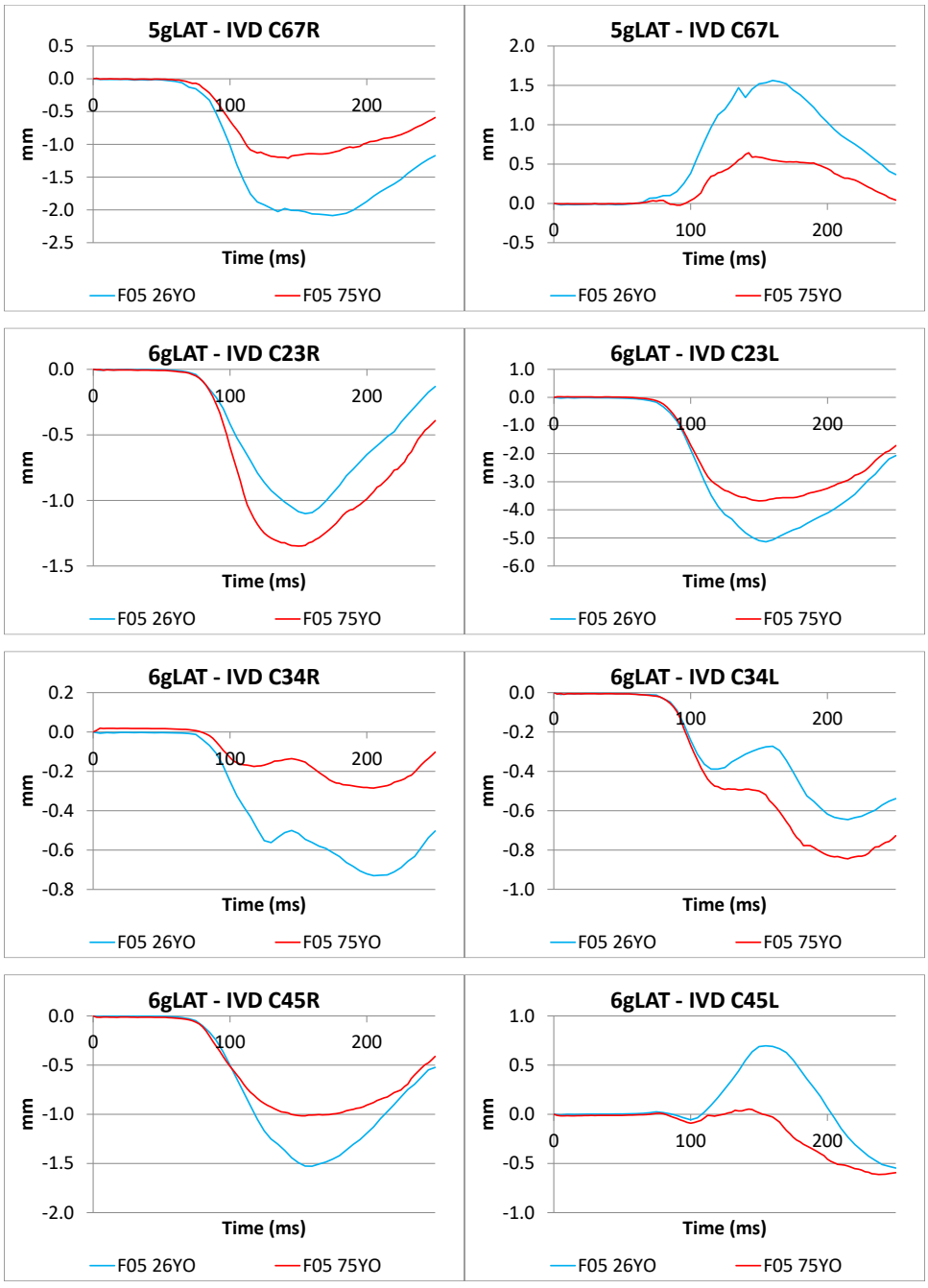
5gLAT - IVD C67R
mm
Time (ms)
F05 26YO
F05 75YO
5gLAT - IVD C67L
mm
Time (ms)
F05 26YO
F05 75YO
6gLAT - IVD C23R
mm
Time (ms)
F05 26YO
F05 75YO
6gLAT - IVD C23L
mm
Time (ms)
F05 26YO
F05 75YO
6gLAT - IVD C34R
mm
Time (ms)
F05 26YO
F05 75YO
6gLAT - IVD C34L
mm
Time (ms)
F05 26YO
F05 75YO
6gLAT - IVD C45R
mm
Time (ms)
F05 26YO
F05 75YO
6gLAT - IVD C45L
mm
Time (ms)
F05 26YO
F05 75YO

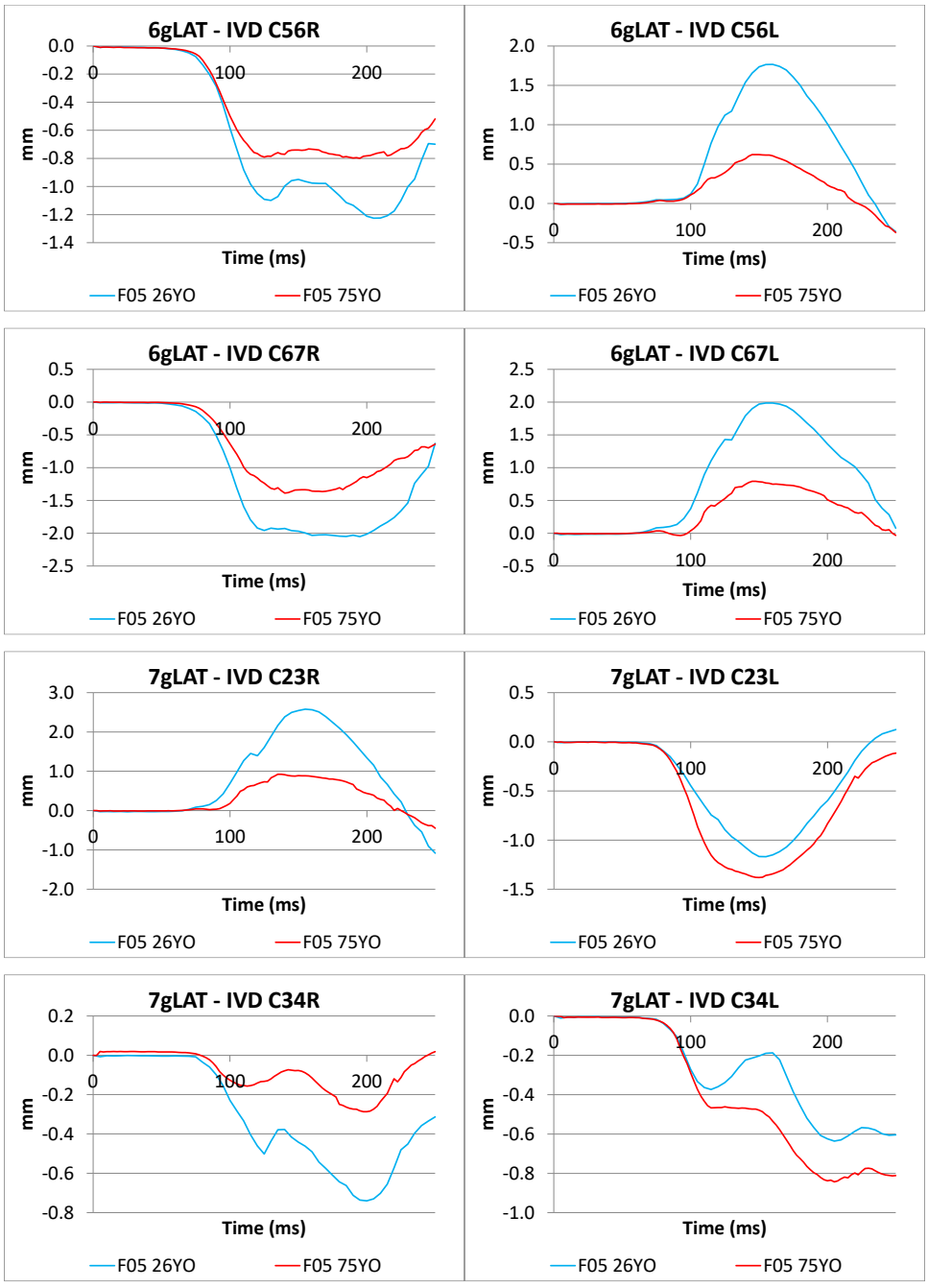
6gLAT - IVD C56R
0.0
-0.2
-0.4
-0.6
-0.8
-1.0
-1.2
-1.4
mm
0
100
200
Time (ms)
F05 26YO
F05 75YO
6gLAT - IVD C56L
2.0
1.5
1.0
0.5
0.0
-0.5
mm
0
100
200
Time (ms)
F05 26YO
F05 75YO
6gLAT - IVD C67R
0.5
0.0
-0.5
-1.0
-1.5
-2.0
-2.5
mm
0
100
200
Time (ms)
F05 26YO
F05 75YO
6gLAT - IVD C67L
2.5
2.0
1.5
1.0
0.5
0.0
-0.5
mm
0
100
200
Time (ms)
F05 26YO
F05 75YO
7gLAT - IVD C23R
3.0
2.0
1.0
0.0
-1.0
-2.0
mm
0
100
200
Time (ms)
F05 26YO
F05 75YO
7gLAT - IVD C23L
0.5
0.0
-0.5
-1.0
-1.5
mm
0
100
200
Time (ms)
F05 26YO
F05 75YO
7gLAT - IVD C34R
0.2
0.0
-0.2
-0.4
-0.6
-0.8
mm
0
100
200
Time (ms)
F05 26YO
F05 75YO
7gLAT - IVD C34L
0.0
-0.2
-0.4
-0.6
-0.8
-1.0
mm
0
100
200
Time (ms)
F05 26YO
F05 75YO

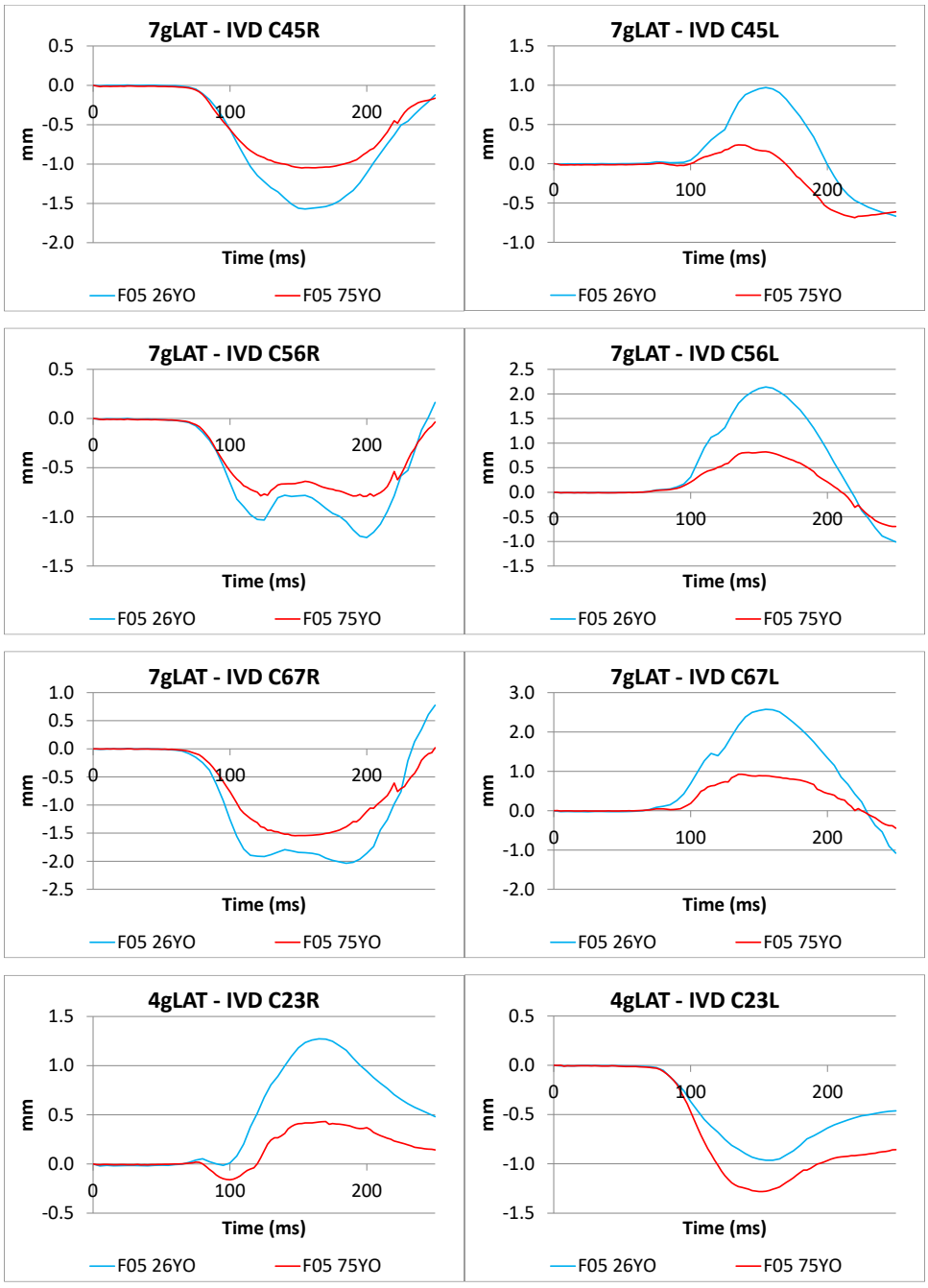
7gLAT - IVD C45R
mm
Time (ms)
F05 26YO
F05 75YO
7gLAT - IVD C45L
mm
Time (ms)
F05 26YO
F05 75YO
7gLAT - IVD C56R
mm
Time (ms)
F05 26YO
F05 75YO
7gLAT - IVD C56L
mm
Time (ms)
F05 26YO
F05 75YO
7gLAT - IVD C67R
mm
Time (ms)
F05 26YO
F05 75YO
7gLAT - IVD C67L
mm
Time (ms)
F05 26YO
F05 75YO
4gLAT - IVD C23R
mm
Time (ms)
F05 26YO
F05 75YO
4gLAT - IVD C23L
mm
Time (ms)
F05 26YO
F05 75YO

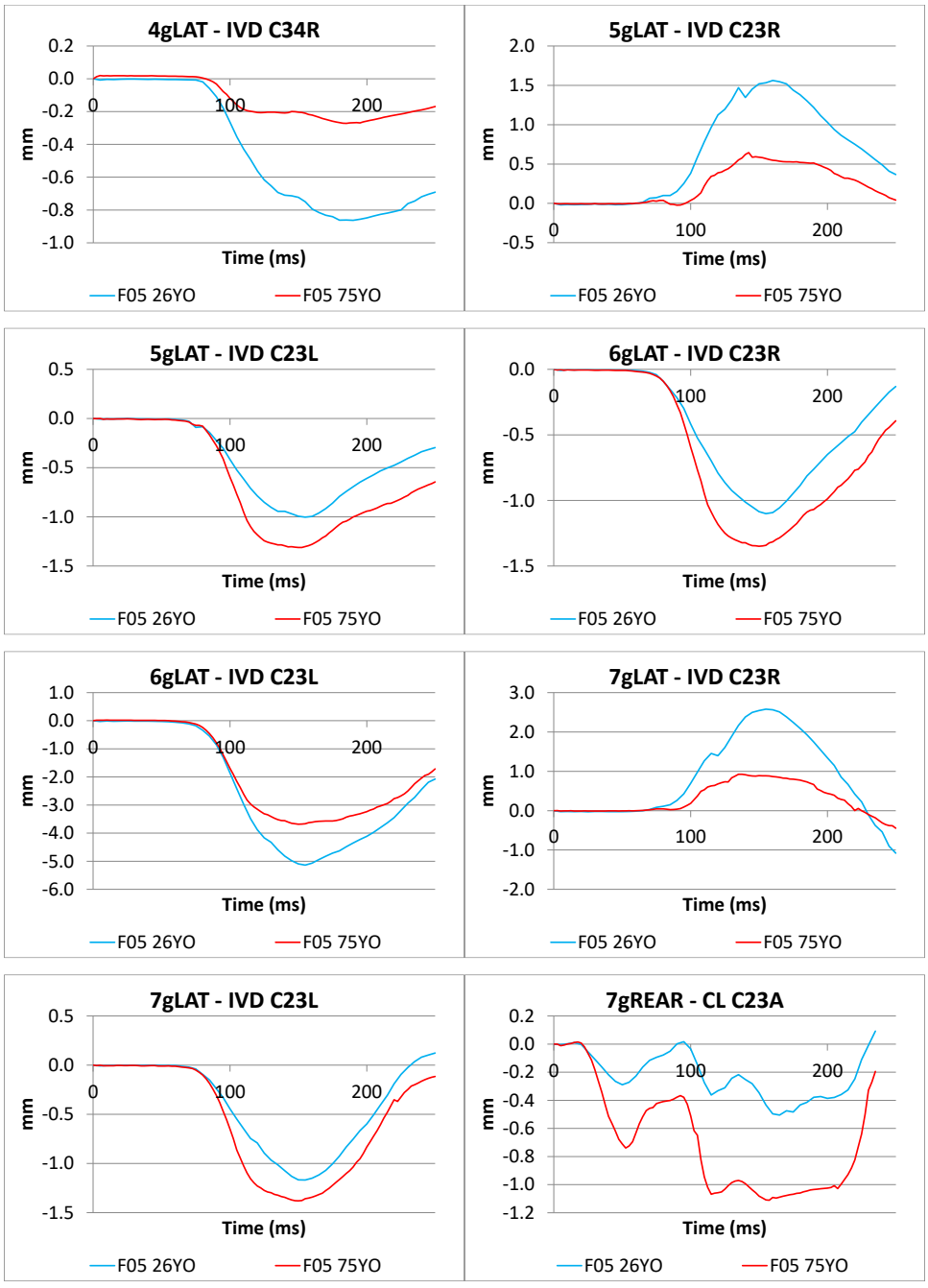
4gLAT - IVD C34R
0.2
0.0
-0.2
-0.4
-0.6
-0.8
-1.0
mm
0
100
200
Time (ms)
F05 26YO
F05 75YO
5gLAT - IVD C23R
2.0
1.5
1.0
0.5
0.0
-0.5
mm
0
100
200
Time (ms)
F05 26YO
F05 75YO
5gLAT - IVD C23L
0.5
0.0
-0.5
-1.0
-1.5
mm
0
100
200
Time (ms)
F05 26YO
F05 75YO
6gLAT - IVD C23R
0.0
-0.5
-1.0
-1.5
mm
0
100
200
Time (ms)
F05 26YO
F05 75YO
6gLAT - IVD C23L
1.0
0.0
-1.0
-2.0
-3.0
-4.0
-5.0
-6.0
mm
0
100
200
Time (ms)
F05 26YO
F05 75YO
7gLAT - IVD C23R
3.0
2.0
1.0
0.0
-1.0
-2.0
mm
0
100
200
Time (ms)
F05 26YO
F05 75YO
7gLAT - IVD C23L
0.5
0.0
-0.5
-1.0
-1.5
mm
0
100
200
Time (ms)
F05 26YO
F05 75YO
7gREAR - CL C23A
0.2
0.0
-0.2
-0.4
-0.6
-0.8
-1.0
-1.2
mm
0
100
200
Time (ms)
F05 26YO
F05 75YO

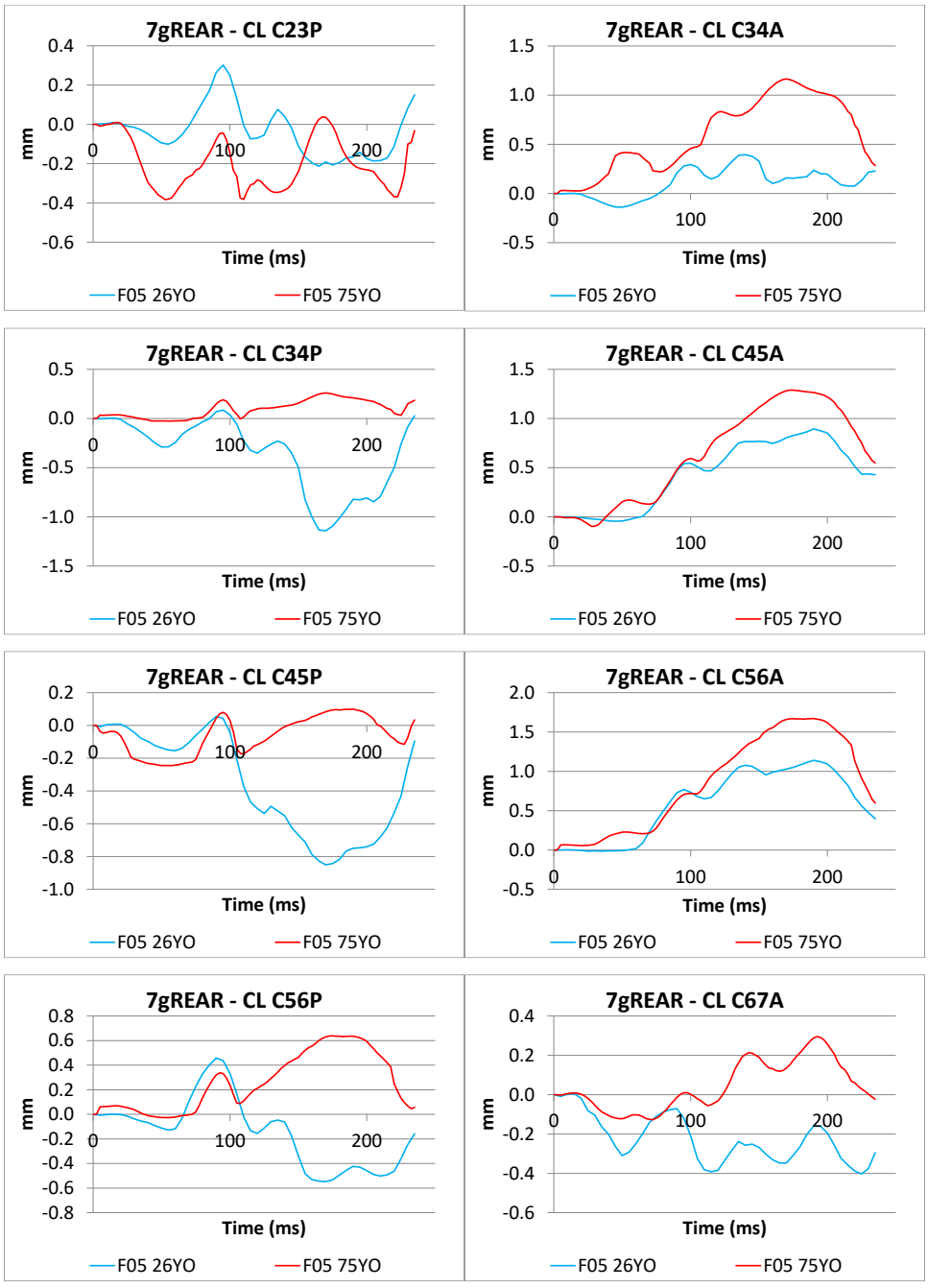
7gREAR - CL C23P
0.4
0.2
0.0
-0.2
-0.4
-0.6
mm
0
100
200
Time (ms)
F05 26YO
F05 75YO
7gREAR - CL C34A
1.5
1.0
0.5
0.0
-0.5
mm
0
100
200
Time (ms)
F05 26YO
F05 75YO
7gREAR - CL C34P
0.5
0.0
-0.5
-1.0
-1.5
mm
0
100
200
Time (ms)
F05 26YO
F05 75YO
7gREAR - CL C45A
1.5
1.0
0.5
0.0
-0.5
mm
0
100
200
Time (ms)
F05 26YO
F05 75YO
7gREAR - CL C45P
0.2
0.0
-0.2
-0.4
-0.6
-0.8
-1.0
mm
0
100
200
Time (ms)
F05 26YO
F05 75YO
7gREAR - CL C56A
2.0
1.5
1.0
0.5
0.0
-0.5
mm
0
100
200
Time (ms)
F05 26YO
F05 75YO
7gREAR - CL C56P
0.8
0.6
0.4
0.2
0.0
-0.2
-0.4
-0.6
-0.8
mm
0
100
200
Time (ms)
F05 26YO
F05 75YO
7gREAR - CL C67A
0.4
0.2
0.0
-0.2
-0.4
-0.6
mm
0
100
200
Time (ms)
F05 26YO
F05 75YO

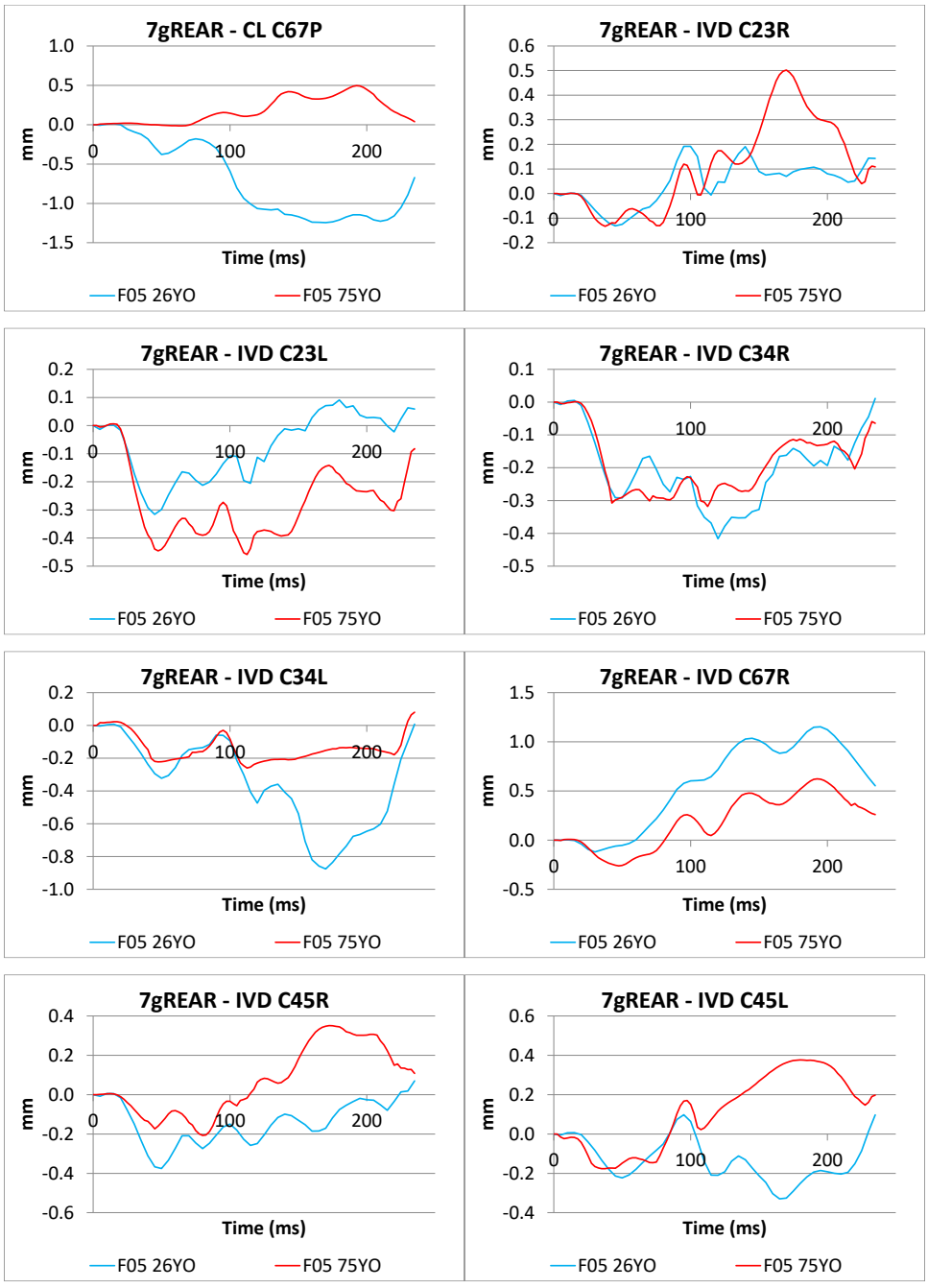
7gREAR - CL C67P
mm
Time (ms)
F05 26YO
F05 75YO
7gREAR - IVD C23R
mm
Time (ms)
F05 26YO
F05 75YO
7gREAR - IVD C23L
mm
Time (ms)
F05 26YO
F05 75YO
7gREAR - IVD C34R
mm
Time (ms)
F05 26YO
F05 75YO
7gREAR - IVD C34L
mm
Time (ms)
F05 26YO
F05 75YO
7gREAR - IVD C67R
mm
Time (ms)
F05 26YO
F05 75YO
7gREAR - IVD C45R
mm
Time (ms)
F05 26YO
F05 75YO
7gREAR - IVD C45L
mm
Time (ms)
F05 26YO
F05 75YO

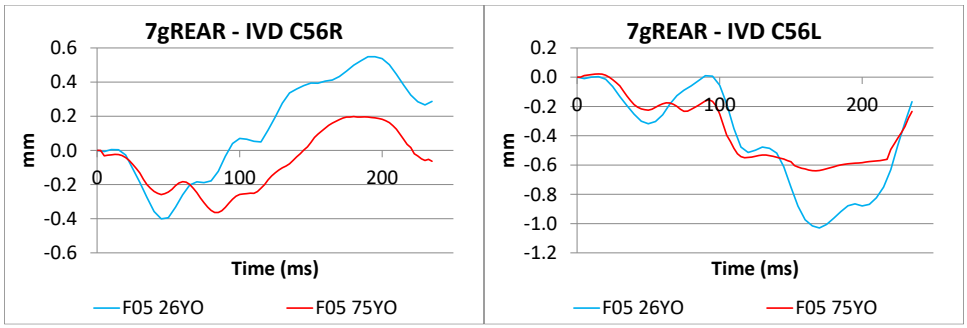
7gREAR - IVD C56R
0.6
0.4
0.2
0.0
-0.2
-0.4
-0.6
mm
0
100
200
Time (ms)
F05 26YO
F05 75YO

7gREAR - IVD C56L
0.2
0.0
-0.2
-0.4
-0.6
-0.8
-1.0
-1.2
mm
0
100
200
Time (ms)
F05 26YO
F05 75YO

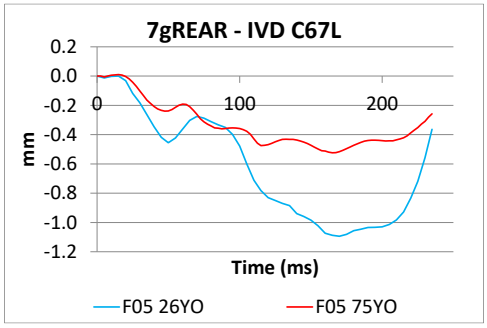
7gREAR - IVD C67L
0.2
0.0
-0.2
-0.4
-0.6
-0.8
-1.0
-1.2
mm
0
100
200
Time (ms)
F05 26YO
F05 75YO